

Loughborough University  
Institutional Repository

---

*Enhancing nucleic acid  
detection using inductively  
coupled plasma mass  
spectrometry, by means of  
metal and nano-particle  
labelling*

This item was submitted to Loughborough University's Institutional Repository by the/an author.

**Additional Information:**

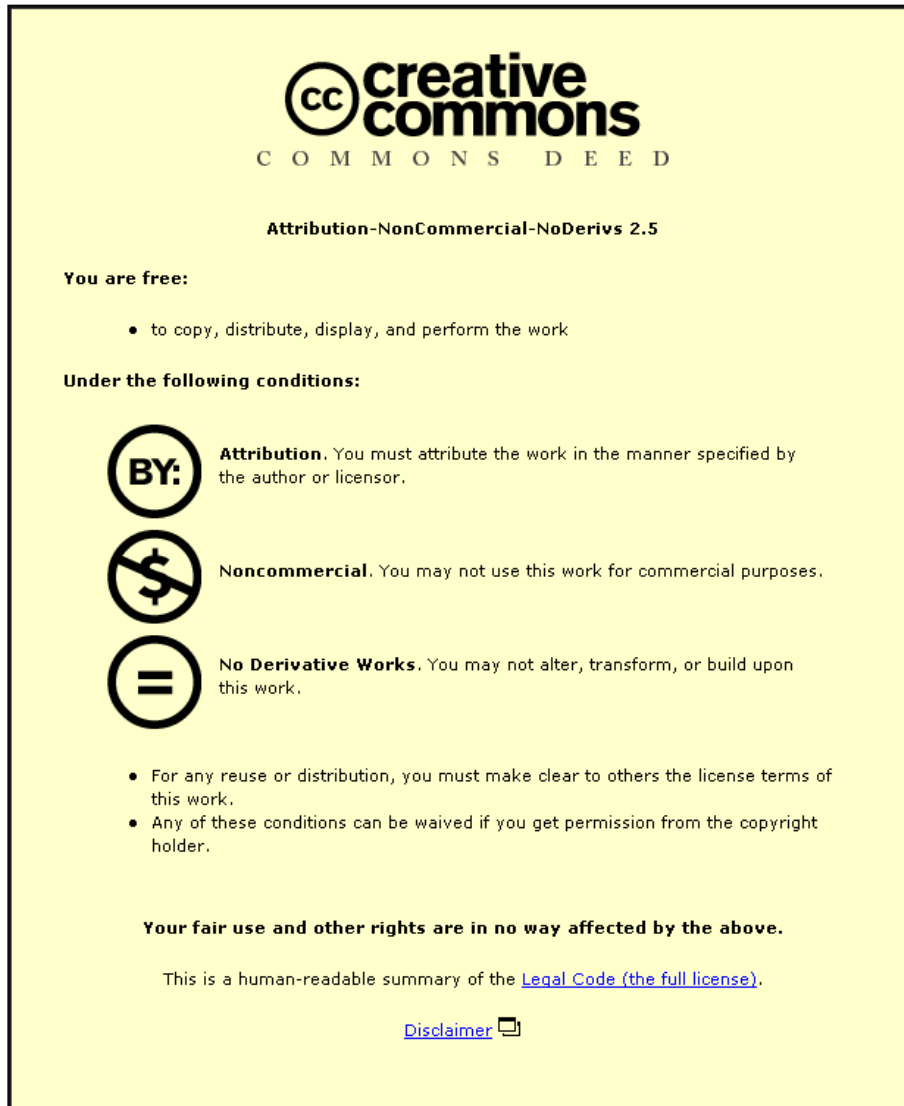
- A Doctoral Thesis submitted in partial fulfilment of the requirements for the award of degree of Doctor of Philosophy of Loughborough University.

**Metadata Record:** <https://dspace.lboro.ac.uk/2134/4641>

**Publisher:** © Samantha Louise Kerr

Please cite the published version.

This item was submitted to Loughborough's Institutional Repository (<https://dspace.lboro.ac.uk/>) by the author and is made available under the following Creative Commons Licence conditions.



**CC creative commons**  
COMMONS DEED

**Attribution-NonCommercial-NoDerivs 2.5**

**You are free:**

- to copy, distribute, display, and perform the work

**Under the following conditions:**

**BY:** **Attribution.** You must attribute the work in the manner specified by the author or licensor.


**Noncommercial.** You may not use this work for commercial purposes.

**No Derivative Works.** You may not alter, transform, or build upon this work.

- For any reuse or distribution, you must make clear to others the license terms of this work.
- Any of these conditions can be waived if you get permission from the copyright holder.

**Your fair use and other rights are in no way affected by the above.**

This is a human-readable summary of the [Legal Code \(the full license\)](#).

[Disclaimer](#) 

For the full text of this licence, please go to:  
<http://creativecommons.org/licenses/by-nc-nd/2.5/>

**Enhancing Nucleic Acid Detection Using  
Inductively Coupled Plasma Mass Spectrometry,  
by Means of Metal and Nano-particle Labelling**

**Samantha Louise Kerr**

**A Doctoral Thesis**

**Submitted in partial fulfilment of the requirements for the  
award of degree of Doctor of Philosophy of Loughborough  
University**

**© Samantha Kerr 2008**

# Table of Contents

Table of Contents .....	2
List of Figures.....	5
List of Tables.....	12
Acknowledgements .....	13
Abstract .....	14
Glossary of Terms .....	16
1. Introduction.....	19
1.1 Objectives.....	19
1.2 Genomics.....	24
1.2.1 Structure of DNA.....	24
1.2.2 DNA Function.....	28
1.2.3 DNA Replication .....	28
1.2.4 Protein Synthesis.....	33
1.2.4.1 Transcription .....	34
1.2.4.2 Translation .....	37
1.3 Inductively Coupled Plasma Mass Spectrometry .....	42
1.3.1 Instrumentation .....	42
1.3.1.1 The Sample Introduction System .....	43
1.3.1.2 The Plasma.....	44
1.3.1.3 The Interface Region.....	45
1.3.1.4 Mass Analyser and Detectors .....	46
1.3.2 Application of ICP-MS to Genomics Research .....	47
1.3.2.1 Cool Plasma .....	49
1.3.2.2 Collision/Reaction Cells.....	49
1.3.2.3 High Resolution ICP-MS .....	53
1.4 Linear Ion Trap Mass Spectrometry .....	62
1.4.1 Instrumentation .....	63
1.4.1.1 Ionisation.....	63
1.4.1.2 Interface .....	65
1.4.1.3 Ion Guides and Optics .....	65
1.4.1.4 Quadrupole Linear Ion Trap Mass Analyser .....	66
1.4.1.5 Detector.....	70
1.4.2 Scanning Modes.....	70
1.4.2.1 Full Scan .....	71
1.4.2.2 Selected Ion Monitoring (SIM).....	71
1.4.2.3 Selected Reaction Monitoring (SRM).....	71
1.4.2.4 Consecutive Reaction Monitoring (CRM) .....	71
1.4.2.5 Zoom Scan .....	72
1.4.3 Experiment Modes.....	72
1.4.3.1 MS and MS <sup>n</sup> .....	73
1.4.3.2 Data Dependent Experiments .....	73
1.4.3.3 Other Experiment Types .....	74
2 Elemental Labelling .....	76
2.1 Introduction .....	76
2.2 Instruments and Reagents.....	79
2.3 Monomaleimido Nanogold Labelling of Sulfhydryl Modified DNA .....	83
2.3.1 Introduction to Monomaleimido Nanogold labelling.....	83
2.3.2 Sulfhydryl Derivatisation of DNA .....	84
2.3.3 Method of Labelling .....	92
2.3.3.1 Labelling of Di-nucleotides.....	92
2.3.3.2 Labelling of 25 mer Oligonucleotides.....	94
2.4 Results of Monomaleimido Nanogold Labelling.....	97
2.4.1 Sulfhydryl Derivatisation.....	97

2.4.2	Labelling Results .....	111
2.4.2.1	Labelling of Di-nucleotides.....	111
2.4.2.2	Labelling of 25 mer Oligonucleotides.....	118
2.4.3	Monomaleimido Nanogold Labelling Summary.....	130
2.5	Streptavidin FluoroNanogold Labelling of Biotinylated DNA.....	132
2.5.1	Introduction to Streptavidin FluoroNangold Labelling.....	132
2.5.2	Biotinylation of DNA .....	133
2.5.3	Method of Labelling .....	135
2.5.4	Methods of Separation .....	135
2.5.4.1	Gel Filtration .....	135
2.5.4.2	Anion Exchange HPLC.....	137
2.5.4.3	Immobilised Metal Affinity Chromatography.....	139
2.5.4.4	Reversed Phase HPLC .....	140
2.6	Results of Streptavidin FluoroNanogold Labelling .....	143
2.6.1	Methods of Separation .....	143
2.6.1.1	Gel Filtration.....	143
2.6.1.2	Anion Exchange HPLC.....	144
2.6.1.3	Immobilised Metal Affinity Chromatography.....	147
2.6.1.4	Reversed Phase HPLC .....	151
2.6.2	Summary.....	179
3	Platinum Metallodrugs.....	182
3.1	Introduction .....	182
3.1.1	Cisplatin.....	183
3.1.2	Oxaliplatin .....	185
3.1.3	Metallodrug Detection .....	186
3.2	Quantifying Pt adduct Formation by ICP-MS .....	190
3.2.1	Introduction.....	190
3.2.2	Instrument Parameters.....	192
3.2.2.1	Analysis of Whole ctDNA .....	193
3.2.2.2	Analysis of Digested DNA.....	194
3.2.3	Results.....	195
3.2.3.1	Analysis of Whole ctDNA .....	195
3.2.3.2	Analysis of Digested DNA.....	211
3.2.4	Summary.....	219
4	Investigation of Oxaliplatin Interactions with DNA Nucleobases by means of Organic Mass Spectrometry.....	221
4.1	Introduction .....	221
4.2	Instrumentation and Reagents .....	222
4.3	Results .....	225
4.3.1	Oxaliplatin Analysis.....	225
4.3.2	Evidence of Adduct Formation .....	228
4.3.2.1	Oxaliplatin-Adenine Adduct Fragmentation .....	230
4.3.2.2	Oxaliplatin-Guanine Adduct Fragmentation .....	233
4.3.2.3	Oxaliplatin-Thymine Adduct Fragmentation .....	236
4.3.2.4	Oxaliplatin-Cytosine Adduct Fragmentation .....	239
4.3.2.5	Branching Diagrams.....	242
4.3.3	Isobaric Interferences.....	245
4.3.4	Oxaliplatin Binding in the Presence of all Four Nucleobases.....	248
4.3.5	Preferential Binding Studies .....	251
4.4	Summary .....	255
5	Anion Exchange HPLC-ICP-MS of Single Nucleotide Polymorphisms (SNPs).....	257
5.1	Introduction .....	257
5.2	Instrumentation and Reagents .....	258
5.2.1	Collision Cell .....	260
5.2.2	Cool Plasma .....	261
5.3	Results .....	261

5.3.1	Collision Cell .....	261
5.3.2	Cool Plasma .....	269
5.4	Summary for Anion Exchange HPLC-ICP-MS of SNP's .....	271
6	Conclusions.....	273
6.1	Further Research.....	274
6.1.1	Improving Existing Methodologies.....	274
6.1.2	Combining Elemental Labelling with Pt-DNA Adduct Detection.....	275
6.1.2.1	Elemental Labelling with the Post Labelling Assay.....	276
6.1.2.2	Elemental Labelling of Adduct Recognition Antibodies.....	277
7	References.....	279
8	Appendix 1: TSKgel-DNA-NPR Phase .....	290
9	Appendix 2: LTQ Data from oxaliplatin-DNA adducts.....	291
9.1	Appendix 2.1: Oxaliplatin Mass Spectrometry Data (in the absence of nucleobase).....	291
9.2	Appendix 2.2: Mass Spectrometry Data from Oxaliplatin Mono-Nucleobase Solutions.....	293
	Oxaliplatin-Adenine Mass Spectra .....	293
	Oxaliplatin-Guanine Mass Spectra .....	297
	Oxaliplatin-Thymine Mass Spectra.....	302
	Oxaliplatin-Cytosine Mass Spectrometry Data.....	304
	Hydrated Complexes of Guanine .....	306
9.3	Appendix 2.3: Oxaliplatin mixture containing A, C, G and T in equal-molar proportions .....	308
9.4	Appendix 2.4: Oxaliplatin mixture containing A, C, G and T with an excess of oxaliplatin .....	316
9.5	Appendix 2.5: Fragmentation of the Pt-AG adduct.....	320
10	Appendix 3: Continued Professional Development Record .....	323
11	Published Material.....	325

## List of Figures

FIGURE 1:1: ANALYTICAL METHODS AVAILABLE FOR BIOMOLECULE ANALYSIS .....	20
FIGURE 1:2: SCHEMATIC SHOWING THE VARIOUS METHODS OF DETECTING DNA BY ELEMENTAL MASS SPECTROMETRY. ....	23
FIGURE 1:3: STRUCTURES OF DEOXYRIBOSE SUGAR, NUCLEOSIDE AND NUCLEOTIDE.....	24
FIGURE 1:4: PHOSPHODIESTER BOND FORMATION BETWEEN NUCLEOTIDES. ....	25
FIGURE 1:5: STRUCTURES OF THE PURINE AND PYRIMIDINE DNA BASES. ....	26
FIGURE 1:6: BASE PAIRING OF DNA.....	27
FIGURE 1:7: DNA REPLICATION.....	29
FIGURE 1:8: ADDITION OF FREE DNTP ONTO A GROWING DNA CHAIN. ....	31
FIGURE 1:9: CONVERSION OF PYROPHOSPHATE.....	32
FIGURE 1:10: STRUCTURE OF RIBOSE SUGAR AND URACIL.....	34
FIGURE 1:11: RIBOSOME COMPLEX.....	39
FIGURE 1:12: STRUCTURE OF tRNA. ....	40
FIGURE 1:13: SCHEMATIC SHOWING THE PROCESS OF ELONGATION. ....	41
FIGURE 1:14: SCHEMATIC DIAGRAM OF A TYPICAL ICP-MS INSTRUMENT. ....	43
FIGURE 1:15: CONCENTRIC NEBULISER, REPRINTED WITH PERMISSION OF MEINHARD GLASS PRODUCTS (COLORADO, USA).....	44
FIGURE 1:16: RF COIL AND TORCH ARRANGEMENT.....	45
FIGURE 1:17: THE INTERFACE REGION.....	46
FIGURE 1:18: SCHEMATIC OF A REVERSE NIER-JOHNSON MAGNETIC SECTOR INSTRUMENT.....	55
FIGURE 1:19: APPROXIMATE SIGNAL INTENSITY AND CONCENTRATION RANGE OF EACH DETECTOR FOR THE ELEMENT 2XR. <sup>68</sup> .....	57
FIGURE 1:20: MAGNET CYCLE DURING MASS ACCURACY SCAN. ....	60
FIGURE 1:21: MAGNET CYCLE DURING SPEED SCANNING.....	61
FIGURE 1:22: SCHEMATIC SHOWING THE LINEAR ION TRAP INSTRUMENTATION OF A THERMO FINNIGAN LTQ.....	62
FIGURE 1:23: ESI PROCESS IN POSITIVE ION MODE. ....	64
FIGURE 1:24: ION STORAGE. ....	67
FIGURE 1:25: ION ISOLATION.....	68
FIGURE 1:26 PARENT ION FRAGMENTATION.....	68
FIGURE 1:27: PRODUCT ION SCAN OUT FROM THE LINEAR ION TRAP. ....	69
FIGURE 1:28: SCANNING MODES AVAILABLE FOR THE LINEAR ION TRAP.....	72
FIGURE 1:29: A SUMMARY OF THE PROCESSES OCCURRING WITHIN THE LINEAR ION TRAP DURING A DATA DEPENDANT EXPERIMENT. ....	74
FIGURE 2:1: MONOMALEIMIDO NANOGOLD.....	83
FIGURE 2:2: REACTION BETWEEN SULFHYDRYL MODIFIED DNA AND MMN.....	84
FIGURE 2:3: STAGE 1 OF THE SULFHYDRYL DERIVATISATION REACTION.....	85
FIGURE 2:4: STAGE 2 OF THE SULFHYDRYL DERIVATISATION REACTION.....	85
FIGURE 2:5: INSTRUMENT SET UP.....	87
FIGURE 2:6: ANION EXCHANGE SPE SEPARATION METHOD FOR MODIFIED OLIGONUCLEOTIDES.....	88
FIGURE 2:7: A) TCEP STRUCTURE AND B) MECHANISM FOR DISULFIDE REDUCTION. <sup>110</sup> .....	89
FIGURE 2:8: MECHANISM OF ELLMAN'S ASSAY. <sup>111</sup> .....	91
FIGURE 2:9: A) <sup>31</sup> P <sup>16</sup> O SIGNAL INTENSITY AND B) <sup>32</sup> S <sup>16</sup> O SIGNAL INTENSITY DURING THE STAGE 1 (OLIGONUCLEOTIDE-CYSTAMINE SPECIES) GEL FILTRATION PURIFICATION STEP. ELUTED WITH 0.15 M AMMONIUM CHLORIDE AND 1 mM EDTA, pH ~6.3, 200 µL INJECTION VOLUME. ....	98
FIGURE 2:10: UV CHROMATOGRAM DURING THE STAGE 1 (OLIGONUCLEOTIDE-CYSTAMINE SPECIES) GEL FILTRATION PURIFICATION STEP. ELUTED WITH 0.15 M AMMONIUM CHLORIDE AND 1 mM EDTA, pH ~6.3, 50 µL INJECTION VOLUME, 25 PMOLES OF OLIGONUCLEOTIDE. ....	100
FIGURE 2:11: CHROMATOGRAM AT 260 NM OF THE STAGE 1 PRODUCT (OLIGONUCLEOTIDE-CYSTAMINE SPECIES) IN ABSENCE OF EDC DURING GEL FILTRATION SEPARATION. ELUTED WITH 0.15 M AMMONIUM CHLORIDE AND 1 mM EDTA, pH ~6.3, 50 µL INJECTION VOLUME, 25 PMOLES OLIGONUCLEOTIDE.....	101
FIGURE 2:12: A) <sup>31</sup> P <sup>16</sup> O SIGNAL INTENSITY AND B) <sup>32</sup> S <sup>16</sup> O SIGNAL INTENSITY DURING THE GEL FILTRATION PURIFICATION OF THE STAGE 2 PRODUCT (SULFHYDRYL MODIFIED OLIGONUCLEOTIDE). ELUTED WITH 0.15 M AMMONIUM CHLORIDE AND 1 mM EDTA, pH ~6.3.....	103

FIGURE 2:13: UV CHROMATOGRAM AT 260 NM OF STAGE 2 (SULFHYDRYL MODIFIED OLIGONUCLEOTIDE) GEL FILTRATION PURIFICATION. 0.15 M AMMONIUM CHLORIDE AND 1 mM EDTA, PH ~ 6.3. ....	105
FIGURE 2:14: UV CHROMATOGRAM AT 260 NM OF THE STAGE 2 (SULFHYDRYL MODIFIED OLIGONUCLEOTIDE) REACTION MIXTURE AFTER REDUCTION WITH DTT AT PH 8. ....	106
FIGURE 2:15: OVERLAID UV SPECTRA OF COLUMN ELUENTS DURING VARIOUS STAGES OF A 25 MER OLIGONUCLEOTIDE ANION EXCHANGE SPE SEPARATION. ....	107
FIGURE 2:16: OVERLAID UV SPECTRA OF COLUMN ELUENTS DURING VARIOUS STAGES OF ANION EXCHANGE SPE OF THE STAGE 1 PRODUCT (OLIGONUCLEOTIDE-CYSTAMINE SPECIES), DNA CONCENTRATION ~9 $\mu$ M. ....	109
FIGURE 2:17: OVERLAID UV SPECTRA OF COLUMN ELUENTS DURING VARIOUS STAGES OF ANION EXCHANGE SPE OF THE STAGE 2 PRODUCT, DNA CONCENTRATION ~2 $\mu$ M. ....	110
FIGURE 2:18: $^{197}\text{Au}$ AND $^{31}\text{P}^{16}\text{O}$ SIGNAL INTENSITY DURING SEPARATION OF THE MMN-DI-NUCLEOTIDE TAGGING REACTION MIXTURE. TSKGEL-DNA-NPR 7.5 CM X 4.6 MM COLUMN, MOBILE PHASE A = 20 MM TRIS-HCL, PH 9, B = 20 MM TRIS + 0.3 M CITRATE AND 0.1 AMMONIUM CHLORIDE, PH 9. 0 MINS = 0% B, 2 MIN = 0% B, 15 MIN = 100% B, 17 MIN = 100% B. FLOW RATE = 0.7 ML MIN <sup>-1</sup> , 10 $\mu$ L INJECTION VOLUME. ....	112
FIGURE 2:19: $^{31}\text{P}^{16}\text{O}$ AND $^{32}\text{S}^{16}\text{O}$ SIGNAL INTENSITY DURING THE GEL FILTRATION SEPARATION OF SULFHYDRYL MODIFIED DI-NUCLEOTIDE AND DTT. ....	113
FIGURE 2:20: ICP-MS DATA FOR THE MMN-DI-NUCLEOTIDE TAGGING REACTION MIXTURE. TSKGEL-DNA-NPR 7.5 CM X 4.6 MM COLUMN. MOBILE PHASE A = 5 mM TRIS-HCL, PH 9 B = 5 mM TRIS + 0.1 M AMMONIUM CHLORIDE, PH 9. 0 MIN = 0% B, 3 MIN = 0% B, 15 MIN = 100% B. FLOW RATE = 0.5 ML MIN <sup>-1</sup> . 10 $\mu$ L INJECTION VOLUME. ....	115
FIGURE 2:21: A) AU SIGNAL DURING THE INJECTION OF THE MMN RETENTION TIME MARKER. B) AU SIGNAL INTENSITY DURING SEPARATION OF THE MMN-DI-NUCLEOTIDE TAGGING REACTION MIXTURE. BICINE WAS EMPLOYED AS AN ELUENT FOR BOTH INJECTIONS. ....	117
FIGURE 2:22: A) UNBOUND MMN (3 $\mu$ M). B) UNLABELLED AND UNMODIFIED 25 MER OLIGONUCLEOTIDE (10 $\mu$ M). BOTH SAMPLES ELUTED FROM A TSKGEL-DNA-NPR GUARD COLUMN WITH 20 MM TRIS-HCL, PH 9 (A) AND 20 MM TRIS + 0.3 M CITRATE AND 0.1 M AMMONIUM CHLORIDE, PH 9 (B). GRADIENT = 10% B AT 0 MIN, 90% B AT 10 MIN AND 90% B AT 12 MIN. FLOW RATE = 1 ML MIN <sup>-1</sup> . WAVELENGTH = 260 NM. ....	119
FIGURE 2:23: CHROMATOGRAM OF THE MMN-25 MER TAGGING REACTION MIXTURE ELUTED FROM A TSKGEL-DNA-NPR GUARD COLUMN WITH 20 MM TRIS-HCL, PH 9 (A) AND 20 MM TRIS + 0.3 M CITRATE AND 0.1 M AMMONIUM CHLORIDE, PH 9 (B). GRADIENT = 10% B AT 0 MIN, 90% B AT 10 MIN AND 90% B AT 12 MIN. FLOW RATE = 1 ML MIN <sup>-1</sup> . WAVELENGTH = 260 NM. ....	120
FIGURE 2:24: MMN LABELLING EFFICIENCY WITH TIME. ....	128
FIGURE 2:25: ALEXA FLUOR - 488 STREPTAVIDIN FLUORONANOGOLD. ....	132
FIGURE 2:26: STREPTAVIDIN FLUORONANOGOLD LABELLING OF BIOTINYLATED DNA. ....	133
FIGURE 2:27: BIOTINYLATED DNA 5' PHOSPHATE. ....	134
FIGURE 2:28: A) 10 $\mu$ M 25 MER OLIGONUCLEOTIDE SPECTRUM BEFORE IMAC SEPARATION. B) SFNG SPECTRUM BEFORE IMAC SEPARATION (0.18 $\mu$ M NANOGOLD AND ~ 0.85 $\mu$ M ALEXA FLUOR-488). ....	148
FIGURE 2:29: OVERLAID SPECTRA OF THE THREE SODIUM HYDROXIDE ELUTION STEPS FOR DNA ELUTION FROM THE IMAC PHASE. ....	149
FIGURE 2:30: OVERLAID SPECTRA FOR THE THREE SODIUM HYDROXIDE ELUTION STEPS OF SFNG FROM IMAC PHASE. ....	150
FIGURE 2:31: A) 5' BIOTINYLATED 24 MER RETENTION TIME MARKER. B) SFNG RETENTION TIME MARKER. BOTH SPECIES ELUTED FROM A HYPERSIL C18 COLUMN (250 MM X 4.6 MM) WITH 35% METHANOL ISOCRATIC ELUTION. FLOW RATE = 0.6 ML MIN <sup>-1</sup> , 10 $\mu$ L INJECTION VOLUME. 260 NM DETECTION WAVELENGTH. ....	152
FIGURE 2:32: CHROMTOGRAM OF THE SFNG-BIOTINYLATED DNA REACTION MIXTURE, ELUTED FROM A HYPERSIL C18 COLUMN (250 MM X 4.6 MM) WITH 35 % METHANOL, ISOCRATIC ELUTION, 0.6 ML MIN <sup>-1</sup> FLOW RATE, 10 $\mu$ L INJECTION VOLUME. 260 NM DETECTION WAVELENGTH. ....	154
FIGURE 2:33: SCHEMATIC SHOWING THE COUPLING OF A HPLC COLUMN TO A NEBULISER WITH THE AID OF A FLOW SPLITTER. ....	158
FIGURE 2:34: A) $^{197}\text{Au}$ CHROMATOGRAM OF UNBOUND SFNG CONTAINING 21.12 NG ML <sup>-1</sup> AU. B) $^{197}\text{Au}$ CHROMATOGRAM OF SFNG-DNA REACTION MIXTURE CONTAINING 14.8 NG ML <sup>-1</sup> AU. BOTH SAMPLES	



WERE ELUTED FROM A WATERS $\mu$ BONDAPAK C18 COLUMN (300 MM X 3.9 MM, 10 $\mu$ M) WITH 5% METHANOL ISOCRATIC MOBILE PHASE. 10 $\mu$ L INJECTION VOLUME. ....	159
FIGURE 2:35: $^{197}$ AU CHROMATOGRAM OF SFNG CONTROL REACTION CONTAINING 3.6 FOLD MOLAR EXCESS OF BINDING SITES AND UNMODIFIED 25 MER. ELUTED FROM A WATERS $\mu$ BONDAPAK C18 COLUMN (300 MM X 3.9 MM, 10 $\mu$ M) WITH 5% METHANOL ISOCRATIC MOBILE PHASE. 10 $\mu$ L INJECTION VOLUME. ....	164
FIGURE 2:36: $^{197}$ AU SIGNAL INTENSITY DURING INJECTION OF A DEIONISED WATER BLANK. ELUTED FROM A WATERS $\mu$ BONDAPAK C18 COLUMN (300 MM X 3.9 MM) WITH 5% METHANOL ISOCRATIC ELUTION AT 1 ML MIN <sup>-1</sup> , 10 $\mu$ L INJECTION VOLUME. ....	165
FIGURE 2:37: A) $^{197}$ AU SIGNAL INTENSITY DURING INJECTION OF 1:1 DNA:BIOTIN BINDING SITE REACTION. B) $^{197}$ AU SIGNAL INTENSITY DURING INJECTION OF THE 1:2 DNA:BIOTIN BINDING SITE REACTION. BOTH SAMPLES ELUTED FROM A WATERS BONDAPAK C18 COLUMN (300 MM X 3.9 MM) WITH 5% METHANOL ISOCRATIC ELUTION AT 1 ML MIN <sup>-1</sup> , 10 $\mu$ L INJECTION VOLUME. ....	167
FIGURE 2:38: $^{197}$ AU SIGNAL INTENSITY DURING INJECTION OF DEIONISED WATER BLANK. ELUTED FROM A WATERS BONDAPAK C18 COLUMN (300 MM X 3.9 MM) WITH 5% METHANOL ISOCRATIC ELUTION AT 1 ML MIN <sup>-1</sup> , 10 $\mu$ L INJECTION VOLUME. ....	168
FIGURE 2:39: A) $^{197}$ AU SIGNAL INTENSITY DURING INJECTION OF A SFNG STANDARD CONTAINING 9.34 NG ML <sup>-1</sup> AU. B) $^{197}$ AU SIGNAL INTENSITY DURING INJECTION THE EQUAL MOLAR BIOTIN BINDING SITE REACTION. BOTH SAMPLES ELUTED FROM A WATERS $\mu$ BONDAPAK C18 COLUMN (300 MM X 3.9 MM) WITH 5% METHANOL ISOCRATIC ELUTION AT 1 ML MIN <sup>-1</sup> , 10 $\mu$ L INJECTION VOLUME. ....	172
FIGURE 2:40: A) $^{197}$ AU SIGNAL INTENSITY DURING INJECTION OF THE 1:1 DNA:BIOTIN BINDING SITE REACTION MIXTURE. B) $^{197}$ AU SIGNAL INTENSITY DURING INJECTION OF THE 1:7.5 DNA:BIOTIN BINDING SITE REACTION MIXTURE. BOTH SAMPLES ELUTED FROM A WATERS $\mu$ BONDAPAK C18 COLUMN (300 MM X 3.9 MM) WITH 5% METHANOL ISOCRATIC ELUTION AT 1 ML MIN <sup>-1</sup> , 10 $\mu$ L INJECTION VOLUME. ....	175
FIGURE 3:1: EXAMPLES OF COMMON THERAPEUTIC METALLODRUGS. ....	183
FIGURE 3:2: CISPLATIN LIGAND EXCHANGE AND DNA ADDUCT FORMATION. ....	184
FIGURE 3:3: INTRA-STRANDED AND INTER-STRANDED PT-ADDUCTS FORMED WITH DNA. NOTE, LIGAND R REFERS TO THE NON-LEAVING GROUP, WHICH IS DIAMINOCYCLOHEXANE IN THE CASE OF OXALIPLATIN AND AMMONIA IN THE CASE OF CISPLATIN. ....	186
FIGURE 3:4: THE POST LABELLING ASSAY. ....	188
FIGURE 3:5: $^{31}$ P SIGNAL INTENSITY AGAINST CTDNA CONCENTRATION. ....	196
FIGURE 3:6: $^{31}$ P SIGNAL INTENSITY AGAINST CTDNA CONCENTRATION (0.1-0.5 MG ML <sup>-1</sup> CTDNA). ....	197
FIGURE 3:7: NUMBER OF OXALIPLATIN ADDUCTS PER LITRE AGAINST NUMBER OF OXALIPLATIN PER NUCLEOTIDE (0.25 MG CTDNA). ....	202
FIGURE 3:8: PT/P CONCENTRATION RATIO AGAINST NUMBER OF NUCLEOTIDES PER OXALIPLATIN MOLECULE (0.25 MG CTDNA). ....	203
FIGURE 3:9: NUMBER OF CISPLATIN AND OXALIPLATIN ADDUCTS PER LITRE FORMED AGAINST NUMBER PT MOLECULES PER NUCLEOTIDE (0.25 MG CTDNA). ....	207
FIGURE 3:10: PT/P RATIO AGAINST THE NUMBER OF DRUG MOLECULES PER NUCLEOTIDE (0.25 MG CTDNA). ....	208
FIGURE 3:11: PT CALIBRATION CURVES IN A 2% HYDROCHLORIC ACID AND 0.25 MG ML <sup>-1</sup> CTDNA MATRIX. ....	210
FIGURE 3:12: PT SIGNAL INTENSITY FOR DIGESTED DNA SAMPLES AND PT STANDARDS IN HYDROCHLORIC ACID AND DNA MATRIX. ....	212
FIGURE 3:13: RELATIONSHIP BETWEEN PT SIGNAL AND THE NUMBER OF PT ATOMS PER NUCLEOTIDE FOR BOTH CISPLATIN AND OXALIPLATIN FOLLOWING DIGESTION WITH NITRIC ACID AND HYDROGEN PEROXIDE. ...	214
FIGURE 3:14: RELATIONSHIP BETWEEN THE NUMBER OF ADDUCTS FORMED AND THE NUMBER OF DRUG MOLECULES PER NUCLEOTIDE FOR CISPLATIN TREATED CTDNA DIGESTED WITH NITRIC ACID AND HYDROGEN PEROXIDE. ....	216
FIGURE 3:15: THE RELATIONSHIP BETWEEN NUMBER OF PT-DNA ADDUCTS FORMED AND THE NUMBER OF DRUG MOLECULES PER NUCLEOTIDE, FOR BOTH CISPLATIN AND OXALIPLATIN TREATED CTDNA DIGESTED WITH NITRIC ACID/HYDROGEN PEROXIDE. APPROXIMATELY 12 $\mu$ G OF CTDNA DIGESTED. ....	218
FIGURE 3:16: PT/P RATIO AGAINST THE NUMBER OF DRUG MOLECULES PER NUCLEOTIDE FOR BOTH CISPLATIN AND OXALIPLATIN TREATED CTDNA DIGESTED WITH NITRIC ACID/HYDROGEN PEROXIDE. APPROXIMATELY 12 $\mu$ G OF CTDNA DIGESTED. ....	218
FIGURE 4:1: FULL SCAN MASS SPECTRUM OF 3.3 mM OXALIPLATIN. ....	225
FIGURE 4:2: MS/MS SPECTRUM OF PRODUCT IONS OBTAINED BY CID OF THE OXALIPLATIN PARENT ION AT M/Z 398, COLLISION ENERGY = 20 eV, ISOLATION WIDTH = 10 DA. ....	227
FIGURE 4:3: OXALIPLATIN FRAGMENTATION ION TREE. ....	228

FIGURE 4:4: MS/MS SPECTRUM OF PRODUCT IONS OBTAINED BY CID OF: A) $^{194}\text{Pt-AA}$ ADDUCT AT $m/z$ 577, COLLISION ENERGY = 20 eV, ISOLATION WIDTH = 1 DA. B) $^{194}\text{Pt-A}$ ADDUCT AT $m/z$ 442, COLLISION ENERGY = 20 eV, ISOLATION WIDTH = 1 DA. ....	231
FIGURE 4:5: PROPOSED FRAGMENTATION PATHWAY FOR $^{194}\text{Pt-ADENINE}$ ADDUCTS. ....	232
FIGURE 4:6: MS <sup>3</sup> SPECTRUM OF PRODUCT IONS OBTAINED BY CID OF THE $^{194}\text{Pt-G}$ ADDUCT AT $m/z$ 458, WHICH WAS OBTAINED THROUGH CID OF THE $^{194}\text{Pt-GG}$ ION AT $m/z$ 609. COLLISION ENERGY = 15 eV, ISOLATION WIDTH = 1 DA. ....	234
FIGURE 4:7: FRAGMENTATION PATHWAY OF OXALIPLATIN-GUANINE ADDUCTS. ....	235
FIGURE 4:8: MS/MS SPECTRUM OF PRODUCT IONS OBTAINED FROM CID OF THE $^{194}\text{Pt-T}$ ADDUCT AT $m/z$ 433, COLLISION ENERGY = 20 eV, ISOLATION WIDTH = 1 DA. ....	237
FIGURE 4:9: FRAGMENTATION PATHWAY FOR OXALIPLATIN-THYMINE ADDUCTS. ....	238
FIGURE 4:10: MS/MS SPECTRUM OF PRODUCT IONS OBTAINED BY CID OF: A) $^{195}\text{Pt-CC}$ ADDUCT AT $m/z$ 530, COLLISION ENERGY = 10 eV, ISOLATION WIDTH = 10 DA. B) $^{195}\text{Pt-C}$ ION AT $m/z$ 419, COLLISION ENERGY = 20 eV, ISOLATION WIDTH = 1 DA. ....	240
FIGURE 4:11: FRAGMENTATION PATHWAY OF THE OXALIPLATIN-CYTOSINE ADDUCTS. ....	241
FIGURE 4:12: BRANCHING DIAGRAMS SUMMARISING THE FRAGMENTATION OF OXALIPLATIN NUCLEOBASE ADDUCTS. ....	244
FIGURE 4:13: MASS SPECTRUM OF PRODUCT IONS FROM THE OXALIPLATIN SOLUTION CONTAINING ALL FOUR NUCLEOBASES AND AN EXCESS OF DRUG, WITH THE PT-G AND PT-A(H <sub>2</sub> O) ISOTOPES LABELLED. ....	246
FIGURE 4:14: MASS SPECTRUM (EXPANDED SCALE) OF PRODUCT IONS OBTAINED FROM THE OXALIPLATIN-GUANINE MONO-BASE SOLUTION, SHOWING THE PT-G AND PT-G(H <sub>2</sub> O) ISOTOPES. ....	247
FIGURE 4:15: FULL SCAN MASS SPECTRUM OF THE OXALIPLATIN SOLUTION CONTAINING A, C, G AND T. THE OXALIPLATIN WAS PRESENT IN A NEAR EQUAL MOLAR CONCENTRATION TO EACH OF THE BASES. ....	249
FIGURE 4:16: FULL SCAN MASS SPECTRUM OF OXALIPLATIN SOLUTION CONTAINING EXCESS DRUG WITH ALL FOUR NUCLEOBASES. ....	250
FIGURE 4:17: FULL POSITIVE ION SCAN OF THE ADENINE, GUANINE AND OXALIPLATIN SOLUTION. ....	252
FIGURE 4:18: BRANCHING DIAGRAM SUMMARISING THE FRAGMENTATION OF THE PT-AG ADDUCT. ....	253
FIGURE 4:19: RELATIVE SIGNAL INTENSITIES OF THE PT-AG ADDUCT ( $m/z$ 594) AND THE PRODUCT IONS, PT-G ( $m/z$ 459) AND PT-A ( $m/z$ 443) DURING INCREASING COLLISION ENERGIES. ....	254
FIGURE 5:1: SCHEMATIC SHOWING THE HPLC AND ICP-MS COUPLING. ....	260
FIGURE 5:2: UV CHROMATOGRAM OF 25 MER 1 (10 $\mu\text{M}$ ) ELUTED FROM A TSKGEL-DNA-NPR COLUMN (7.5 CM X 4.6 MM), 40%B AT 0 MINS, 100%B AT 15 MINS AND 100% B AT 20 MINS, 0.7 ML MIN <sup>-1</sup> , 5 $\mu\text{L}$ INJECTION VOLUME, 260 NM DETECTION WAVELENGTH. ....	262
FIGURE 5:3: A) UV CHROMATOGRAM CORRESPONDING TO 25 MER 2 (10 $\mu\text{M}$ ), 260 NM DETECTION WAVELENGTH. B) ICP-MS $^{47}\text{PO}$ SIGNAL INTENSITY DURING ELUTION OF 25 MER 2. OLIGONUCLEOTIDE ELUTED FROM A TSKGEL-DNA-NPR COLUMN (7.5 CM X 4.6 MM), 40%B AT 0 MINS, 100%B AT 15 MINS AND 100% B AT 20 MINS, 0.7 ML MIN <sup>-1</sup> , 5 $\mu\text{L}$ INJECTION VOLUME. ....	263
FIGURE 5:4: A) UV CHROMATOGRAM CORRESPONDING THE OLIGONUCLEOTIDE MIXTURE CONTAINING 25 MER 1 AND 2, EACH AT A CONCENTRATION OF 10 $\mu\text{M}$ , 260 NM DETECTION WAVELENGTH. B) ICP-MS $^{47}\text{PO}$ SIGNAL INTENSITY DURING ELUTION OF THE OLIGONUCLEOTIDE MIXTURE, ELUTED FROM A TSKGEL-DNA-NPR COLUMN (7.5 CM X 4.6 MM), 40%B AT 0 MINS, 100%B AT 15 MINS AND 100% B AT 20 MINS, 0.7 ML MIN <sup>-1</sup> , 5 $\mu\text{L}$ INJECTION VOLUME. ....	265
FIGURE 5:5: A) UV CHROMATOGRAM CORRESPONDING TO 25 MER 1 AND 2 EACH AT A CONCENTRATION OF 10 $\mu\text{M}$ , 260 NM DETECTION WAVELENGTH. B) ICP-MS $^{47}\text{PO}$ SIGNAL INTENSITY DURING ELUTION OF 25 MER 1 AND 2 MIXTURE. OLIGONUCLEOTIDE ELUTED FROM A TSKGEL-DNA-NPR COLUMN (7.5 CM X 4.6 MM), 50%B AT 0 MIN, 80%B AT 30 MIN, 0.7 ML MIN <sup>-1</sup> , 5 $\mu\text{L}$ INJECTION VOLUME. ....	268
FIGURE 5:6: ICP-MS $^{31}\text{P}^{16}\text{O}$ SIGNAL INTENSITY DURING ELUTION OF 25 MER 1 AND 2 MIXTURE (10 $\mu\text{M}$ ). OLIGONUCLEOTIDE ELUTED FROM A TSKGEL-DNA-NPR COLUMN (7.5 CM X 4.6 MM), 40%B AT 0 MINS, 100%B AT 15 MINS AND 100% B AT 20 MINS, 0.7 ML MIN <sup>-1</sup> , 5 $\mu\text{L}$ INJECTION VOLUME. ....	270
FIGURE 6:1: SITE SPECIFIC NANOGOLD LABELLING OF PT ADDUCTS USING THE PLA. ....	277
FIGURE 6:2: POTENTIAL METAL NANO-PARTICLE IMMUNOLOGICAL ASSAY COMBINED WITH ICP-MS FOR CISPLATIN-DNA ADDUCT DETECTION. ....	278
FIGURE 8:1: STRUCTURE OF THE DEAE PHASE. ....	290
FIGURE 9:1: MS/MS SPECTRUM OF PRODUCT IONS OBTAINED BY CID OF OXALIPLATIN PARENT ION AT $m/z$ 397, COLLISION ENERGY = 20 eV AND ISOLATION WIDTH = 1 DA. ....	291

FIGURE 9:2: MS/MS SPECTRUM OF PRODUCT IONS OBTAINED BY CID OF OXALIPLATIN PARENT ION AT $m/z$ 398, COLLISION ENERGY = 20 eV AND ISOLATION WIDTH = 1 Da. ....	292
FIGURE 9:3: MS/MS SPECTRUM OF PRODUCT IONS OBTAINED BY CID OF OXALIPLATIN PARENT ION AT $m/z$ 399, COLLISION ENERGY = 20 eV AND ISOLATION WIDTH = 1 Da. ....	292
FIGURE 9:4: FULL SCAN MASS SPECTRUM OF OXALIPLATIN-ADENINE MONO-BASE SOLUTION. ....	293
FIGURE 9:5: MS/MS OF PRODUCT IONS OBTAINED BY CID OF THE $^{195}\text{Pt}$ -A ADDUCT AT $m/z$ 443 TO YIELD THE FREE Pt DRUG AT $m/z$ 304-308 AND FREE ADENINE BASE AT $m/z$ 136. COLLISION ENERGY = 20 eV AND ISOLATION WIDTH = 1 Da. ....	294
FIGURE 9:6: MS/MS OF PRODUCT IONS OBTAINED BY CID OF THE $^{196}\text{Pt}$ -A ADDUCT AT $m/z$ 444 TO YIELD THE FREE Pt DRUG AT $m/z$ 309 AND FREE ADENINE BASE AT $m/z$ 136. COLLISION ENERGY = 15 eV AND ISOLATION WIDTH = 1 Da. ....	294
FIGURE 9:7: MS/MS SPECTRUM OF PRODUCT IONS OBTAINED BY CID OF THE $^{195}\text{Pt}$ -AA ADDUCT AT $m/z$ 578 TO YIELD THE $^{195}\text{Pt}$ -A ADDUCT AT $m/z$ 443. COLLISION ENERGY = 20 eV AND ISOLATION WIDTH = 10 Da. ....	295
FIGURE 9:8: MS/MS SPECTRUM OF PRODUCT IONS OBTAINED BY CID OF THE $^{196}\text{Pt}$ -AA ADDUCT AT $m/z$ 579 TO YIELD THE Pt-A ADDUCT AT $m/z$ 444. COLLISION ENERGY = 20 eV AND ISOLATION WIDTH = 1 Da. ....	295
FIGURE 9:9: $\text{MS}^3$ SPECTRUM OF PRODUCT IONS OBTAINED BY CID OF THE $^{195}\text{Pt}$ -A ADDUCT AT $m/z$ 443 (COLLISION ENERGY = 15 eV), WHICH WAS OBTAINED BY CID OF THE $^{195}\text{Pt}$ -AA ADDUCT AT $m/z$ 578 USING COLLISION ENERGY OF 20 eV. ....	296
FIGURE 9:10: FULL SCAN MASS SPECTRUM OF THE OXALIPLATIN-GUANINE MONO-BASE SOLUTION. ....	297
FIGURE 9:11: MS/MS SPECTRUM OF PRODUCT IONS OBTAINED BY CID OF THE $^{195}\text{Pt}$ -G ADDUCT AT $m/z$ 459 TO YIELD THE FREE Pt DRUG AT $m/z$ 306 AND FREE GUANINE BASE AT $m/z$ 152. COLLISION ENERGY = 20 eV AND ISOLATION WIDTH = 1 Da. ....	298
FIGURE 9:12: MS/MS SPECTRUM OF PRODUCT IONS OBTAINED BY CID OF THE $^{196}\text{Pt}$ -G AT $m/z$ 460 TO YIELD THE FREE Pt DRUG AT $m/z$ 307 AND FREE GUANINE BASE AT $m/z$ 152. COLLISION ENERGY = 20 eV AND ISOLATION WIDTH = 1 Da. ....	298
FIGURE 9:13: MS/MS SPECTRUM OF PRODUCT IONS OBTAINED BY CID OF THE $^{194}\text{Pt}$ -GG ADDUCT AT $m/z$ 609 TO YIELD THE Pt-G ADDUCT AT $m/z$ 458. COLLISION ENERGY = 20 eV AND ISOLATION WIDTH = 1 Da. ....	299
FIGURE 9:14: MS/MS SPECTRUM OF PRODUCT IONS OBTAINED BY CID OF THE $^{195}\text{Pt}$ -GG ADDUCT AT $m/z$ 610 TO YIELD THE $^{195}\text{Pt}$ -G ADDUCT AT $m/z$ 459. COLLISION ENERGY = 15 eV AND ISOLATION WIDTH = 10 Da. ....	299
FIGURE 9:15: MS/MS SPECTRUM OF PRODUCT IONS OBTAINED BY CID OF THE $^{196}\text{Pt}$ -GG ADDUCT AT $m/z$ 611 TO YIELD THE $^{196}\text{Pt}$ -G ADDUCT AT $m/z$ 460. COLLISION ENERGY = 20 eV AND ISOLATION WIDTH = 1 Da. ....	300
FIGURE 9:16: $\text{MS}^3$ SPECTRUM OF PRODUCT IONS OBTAINED BY CID OF THE $^{195}\text{Pt}$ -G ADDUCT AT $m/z$ 459 (COLLISION ENERGY = 15 eV), WHICH WAS OBTAINED BY CID OF THE $^{195}\text{Pt}$ -GG ADDUCT AT $m/z$ 610 (COLLISION ENERGY = 20 eV). ....	300
FIGURE 9:17: $\text{MS}^3$ SPECTRUM OF PRODUCT IONS OBTAINED BY CID OF THE $^{196}\text{Pt}$ -G ADDUCT AT $m/z$ 460 (COLLISION ENERGY = 15 eV), WHICH WAS OBTAINED BY CID OF THE $^{196}\text{Pt}$ -GG ADDUCT AT $m/z$ 611 (COLLISION ENERGY = 20 eV). ....	301
FIGURE 9:18: FULL SCAN MASS SPECTRUM OF OXALIPLATIN-THYMINE MONO-BASE SOLUTION. ....	302
FIGURE 9:19: MS/MS SPECTRUM OF PRODUCT IONS OBTAINED BY CID OF THE $^{195}\text{Pt}$ -T ADDUCT AT $m/z$ 434 TO YIELD THE FREE DRUG AT $m/z$ 306. COLLISION ENERGY = 20 eV AND ISOLATION WIDTH = 1 Da. ....	303
FIGURE 9:20: MS/MS SPECTRUM OF PRODUCT IONS OBTAINED BY CID OF THE $^{196}\text{Pt}$ -T ADDUCT AT $m/z$ 435 TO YIELD THE FREE DRUG AT $m/z$ 307. COLLISION ENERGY = 20 eV AND ISOLATION WIDTH = 1 Da. ....	303
FIGURE 9:21: FULL SCAN MASS SPECTRUM OF THE OXALIPLATIN-CYTOSINE MONO-BASE SOLUTION. ....	304
FIGURE 9:22: MS/MS SPECTRUM OF PRODUCT IONS OBTAINED BY CID OF THE $^{196}\text{Pt}$ -C ADDUCT AT $m/z$ 420 TO YIELD THE FREE DRUG AT $m/z$ 307. COLLISION ENERGY = 20 eV AND ISOLATION WIDTH = 1 Da. ....	305
FIGURE 9:23: MS/MS SPECTRUM OF PRODUCT IONS OBTAINED BY CID OF THE $^{195}\text{Pt}$ -CC ADDUCT AT $m/z$ 530 TO YIELD THE MONO-ADDUCT, COLLISION ENERGY = 20 eV AND ISOLATION WIDTH = 10 Da. ....	305
FIGURE 9:24: $\text{MS}^3$ SPECTRUM OF PRODUCT IONS OBTAINED BY CID OF THE $^{194}\text{Pt}$ -G ADDUCT AT $m/z$ 458, (COLLISION ENERGY = 20 eV) WHICH WAS OBTAINED BY CID OF THE $^{194}\text{Pt}$ -G( $\text{H}_2\text{O}$ ) ADDUCT AT $m/z$ 476. COLLISION ENERGY OF 15 eV. ....	306
FIGURE 9:25: $\text{MS}^3$ SPECTRUM OF PRODUCT IONS OBTAINED BY CID OF THE $^{195}\text{Pt}$ -G ADDUCT AT $m/z$ 459, (COLLISION ENERGY = 15 eV) WHICH WAS OBTAINED BY CID OF THE $^{195}\text{Pt}$ -G( $\text{H}_2\text{O}$ ) ADDUCT AT $m/z$ 477. COLLISION ENERGY OF 20 eV. ....	307
FIGURE 9:26: $\text{MS}^3$ SPECTRUM OF PRODUCT IONS OBTAINED BY CID OF THE $^{196}\text{Pt}$ -G ADDUCT AT $m/z$ 460, (COLLISION ENERGY = 20 eV) WHICH WAS OBTAINED BY CID OF THE $^{196}\text{Pt}$ -G( $\text{H}_2\text{O}$ ) ADDUCT AT $m/z$ 478, COLLISION ENERGY = 15 eV. ....	307

FIGURE 9:27: MS/MS SPECTRUM OF PRODUCT IONS OBTAINED BY CID OF THE <sup>196</sup> Pt-C ADDUCT AT <i>m/z</i> 420 TO YIELD THE FREE DRUG AT <i>m/z</i> 305. COLLISION ENERGY = 15 eV AND ISOLATION WIDTH = 10 Da. ....	308
FIGURE 9:28: MS/MS SPECTRUM OF PRODUCT IONS OBTAINED BY CID OF THE <sup>196</sup> Pt-C ADDUCT AT <i>m/z</i> 420 TO YIELD THE FREE DRUG AT <i>m/z</i> 306. COLLISION ENERGY = 20 eV AND ISOLATION WIDTH = 1 Da. ....	309
FIGURE 9:29: MS/MS OF SPECTRUM OF PRODUCT IONS OBTAINED BY CID OF THE Pt-A ADDUCT AT <i>m/z</i> 441 TO YIELD THE FREE DRUG AT <i>m/z</i> 307. COLLISION ENERGY = 15 eV AND ISOLATION WIDTH = 10 Da. ....	309
FIGURE 9:30: MS/MS SPECTRUM OF PRODUCT IONS OBTAINED BY CID OF THE <sup>195</sup> Pt-A ADDUCT AT <i>m/z</i> 443 TO YIELD THE FREE Pt DRUG AT <i>m/z</i> 308 AND FREE ADENINE BASE AT <i>m/z</i> 136. COLLISION ENERGY = 20 eV AND ISOLATION WIDTH = 1 Da. ....	310
FIGURE 9:31: MS/MS SPECTRUM OF PRODUCT IONS OBTAINED BY CID OF THE <sup>194</sup> Pt-G ADDUCT AT <i>m/z</i> 458 TO YIELD THE FREE Pt DRUG AT <i>m/z</i> 307. COLLISION ENERGY = 15 eV AND ISOLATION WIDTH = 10 Da. ...	310
FIGURE 9:32: MS/MS SPECTRUM OF PRODUCT IONS OBTAINED BY CID OF THE <sup>195</sup> Pt-G ADDUCT AT <i>m/z</i> 459 TO YIELD THE FREE Pt DRUG AT <i>m/z</i> 306 AND FREE GUANINE BASE AT <i>m/z</i> 152. COLLISION ENERGY = 20 eV AND ISOLATION WIDTH = 1 Da. ....	311
FIGURE 9:33: MS/MS SPECTRUM OF PRODUCT IONS OBTAINED BY CID OF THE <sup>195</sup> Pt-AA ADDUCT AT <i>m/z</i> 578 TO YIELD THE Pt-A ADDUCT AT <i>m/z</i> 443. COLLISION ENERGY = 15 eV AND ISOLATION WIDTH = 10 Da. ...	311
FIGURE 9:34: MS/MS SPECTRUM OF PRODUCT IONS OBTAINED BY CID OF THE <sup>196</sup> Pt-AA ADDUCT AT <i>m/z</i> 579 TO YIELD THE <sup>196</sup> Pt-A ADDUCT AT <i>m/z</i> 444. COLLISION ENERGY = 20 eV AND ISOLATION WIDTH = 1 Da. .	312
FIGURE 9:35: MS <sup>3</sup> SPECTRUM OF PRODUCT IONS OBTAINED BY CID OF THE <sup>196</sup> Pt-A ADDUCT AT <i>m/z</i> 444 (COLLISION ENERGY = 20 eV AND ISOLATION WIDTH = 1 Da), WHICH WERE OBTAINED THROUGH CID OF <sup>196</sup> Pt-AA ADDUCT AT <i>m/z</i> 579 (COLLISION ENERGY = 20 eV AND ISOLATION WIDTH = 1). ....	312
FIGURE 9:36: MS/MS SPECTRUM OF PRODUCT IONS OBTAINED BY CID OF THE <sup>195</sup> Pt-GG ADDUCT AT <i>m/z</i> 610 TO YIELD THE Pt-G ADDUCT AT <i>m/z</i> 459. COLLISION ENERGY = 15 eV AND ISOLATION WIDTH = 10 Da. ...	313
FIGURE 9:37: MS/MS SPECTRUM OF PRODUCT IONS OBTAINED BY CID OF THE <sup>196</sup> Pt-GG ADDUCT AT <i>m/z</i> 611 TO YIELD THE <sup>196</sup> Pt-G ADDUCT AT <i>m/z</i> 460. COLLISION ENERGY = 20 eV AND ISOLATION WIDTH = 1 Da. .	313
FIGURE 9:38: MS/MS SPECTRUM OF PRODUCT IONS OBTAINED BY CID OF THE Pt-AG ADDUCT AT <i>m/z</i> 592 TO YIELD THE Pt-G AND Pt-A ADDUCT AT <i>m/z</i> 459 AND 443 RESPECTIVELY. COLLISION ENERGY = 20 eV AND ISOLATION WIDTH = 10 Da. ....	314
FIGURE 9:39: MS/MS SPECTRUM OF PRODUCT IONS OBTAINED BY CID OF THE <sup>195</sup> Pt-AG ADDUCT AT <i>m/z</i> 594 TO YIELD THE <sup>195</sup> Pt-A AND <sup>195</sup> Pt-G ADDUCTS AT <i>m/z</i> 443 AND 459 RESPECTIVELY. COLLISION ENERGY = 20 eV AND ISOLATION WIDTH = 1 Da. ....	314
FIGURE 9:40: MS <sup>3</sup> SPECTRUM OF PRODUCT IONS OBTAINED BY CID OF THE Pt-G ADDUCT AT <i>m/z</i> 459 (COLLISION ENERGY = 20 eV AND ISOLATION WIDTH = 10), WHICH WAS OBTAINED BY CID OF THE Pt-AG ADDUCT AT <i>m/z</i> 594 (COLLISION ENERGY = 15 eV AND ISOLATION WIDTH = 10 Da). ....	315
FIGURE 9:41: MS <sup>3</sup> SPECTRUM OF PRODUCT IONS OBTAINED BY CID OF THE Pt-A ADDUCT AT <i>m/z</i> 443 (COLLISION ENERGY = 15 eV), WHICH WAS OBTAINED BY CID OF THE Pt-AG ADDUCT AT <i>m/z</i> 594 (COLLISION ENERGY = 20 eV AND ISOLATION WIDTH = 10 Da). ....	315
FIGURE 9:42: MS/MS SPECTRUM OF PRODUCT IONS OBTAINED BY CID OF THE <sup>196</sup> Pt-C ADDUCT AT <i>m/z</i> 420 TO YIELD THE FREE Pt DRUG AT <i>m/z</i> 307. COLLISION ENERGY = 20 eV AND ISOLATION WIDTH = 1 Da. ....	316
FIGURE 9:43: MS/MS SPECTRUM OF PRODUCT IONS OBTAINED BY CID OF THE <sup>195</sup> Pt-T ADDUCT AT <i>m/z</i> 434 TO YIELD THE FREE Pt DRUG AT <i>m/z</i> 306. COLLISION ENERGY = 20 eV AND ISOLATION WIDTH = 1 Da. ....	317
FIGURE 9:44: MS/MS SPECTRUM OF PRODUCT IONS OBTAINED BY CID OF THE <sup>195</sup> Pt-A ADDUCT AT <i>m/z</i> 443 TO OBTAIN THE FREE Pt DRUG AT <i>m/z</i> 308 AND FREE ADENINE BASE AT <i>m/z</i> 136. COLLISION ENERGY = 20 eV AND ISOLATION WIDTH = 1 Da. ....	317
FIGURE 9:45: MS/MS SPECTRUM OF PRODUCT IONS OBTAINED BY CID OF THE <sup>194</sup> Pt-G ADDUCT AT <i>m/z</i> 458 TO YIELD THE FREE Pt DRUG AT <i>m/z</i> 305 AND FREE GUANINE BASE AT <i>m/z</i> 152. COLLISION ENERGY = 20 eV AND ISOLATION WIDTH = 1 Da. ....	318
FIGURE 9:46: MS/MS SPECTRUM OF PRODUCT IONS OBTAINED BY CID OF <sup>195</sup> Pt-G(H <sub>2</sub> O) ADDUCT AT <i>m/z</i> 477 TO OBTAIN THE <sup>195</sup> Pt-G ADDUCT AT <i>m/z</i> 459. COLLISION ENERGY = 20 eV AND ISOLATION WIDTH = 1 Da. ....	318
FIGURE 9:47: MS <sup>3</sup> SPECTRUM OF PRODUCT IONS FORMED BY CID OF THE <sup>195</sup> Pt-G ADDUCT AT <i>m/z</i> 459 (COLLISION ENERGY = 20 eV), WHICH WAS OBTAINED BY CID OF THE <sup>195</sup> Pt-G(H <sub>2</sub> O) ADDUCT AT <i>m/z</i> 477 (COLLISION ENERGY = 20 eV AND ISOLATION WIDTH = 1). ....	319
FIGURE 9:48: MS/MS SPECTRUM OF PRODUCT IONS OBTAINED BY CID OF THE Pt-AG ADDUCT AT <i>m/z</i> 594 TO YIELD THE Pt-G AND Pt-A ADDUCTS AT <i>m/z</i> 459 AND 443 RESPECTIVELY. COLLISION ENERGY = 20 eV AND ISOLATION WIDTH = 10 Da. ....	320

FIGURE 9:49: MS/MS SPECTRUM OF PRODUCT IONS OBTAINED BY CID OF THE <sup>194</sup> PT-AG ADDUCT AT <i>M/Z</i> 593 TO YIELD THE <sup>194</sup> PT-A ADDUCT AND <sup>194</sup> PT-G ADDUCT AT <i>M/Z</i> 442 AND 458 RESPECTIVELY. COLLISION ENERGY = 20 eV AND ISOLATION WIDTH = 1 Da.....	321
FIGURE 9:50: MS <sup>3</sup> SPECTRUM OF PRODUCT IONS OBTAINED BY CID OF THE PT-A ADDUCT AT <i>M/Z</i> 443 (COLLISION ENERGY = 20 eV AND ISOLATION WIDTH = 10 Da), WHICH WERE OBTAINED BY CID OF PT-AG ADDUCT AT <i>M/Z</i> 593 (COLLISION ENERGY = 20 eV AND ISOLATION WIDTH = 10 Da).....	321
FIGURE 9:51: MS <sup>3</sup> SPECTRUM OF PRODUCT IONS OBTAINED BY CID OF THE PT-G ADDUCT AT <i>M/Z</i> 458 (COLLISION ENERGY = 20 eV AND ISOLATION WIDTH = 10), WHICH WERE OBTAINED BY CID OF THE PT-AG ADDUCT AT <i>M/Z</i> 593 (COLLISION ENERGY = 20 eV AND ISOLATION WIDTH = 10 Da).....	322
FIGURE 9:52: MS <sup>3</sup> SPECTRUM OF PRODUCT IONS OBTAINED BY CID OF THE <sup>194</sup> PT-G ADDUCT AT <i>M/Z</i> 458 (COLLISION ENERGY = 20 eV AND ISOLATION WIDTH = 1 Da), WHICH WAS OBTAINED BY CID OF THE <sup>194</sup> PT-AG ADDUCT AT <i>M/Z</i> 593 (COLLISION ENERGY = 20 eV AND ISOLATION WIDTH = 1 Da). .....	322

## List of Tables

TABLE 1:1: FUNCTIONS OF DNA POLYMERASE ENZYMES. <sup>20</sup> .....	32
TABLE 1:2: DIFFERENCES BETWEEN DNA AND RNA .....	33
TABLE 1:3: THE TYPES OF RNA AND THEIR CORRESPONDING RNA POLYMERASE REQUIRED FOR FORMATION. <sup>24</sup> .....	36
TABLE 1:4: ELEMENTS CONTAINED IN TYPICAL METALLOPROTEINS. <sup>50</sup> .....	48
TABLE 1:5: IONISATION POTENTIAL AND COMMON INTERFERENCES FOR P AND S .....	49
TABLE 1:6: COMMERCIALY AVAILABLE COLLISION/REACTION CELLS. <sup>52</sup> .....	51
TABLE 1:7: RESOLUTION REQUIRED TO SEPARATE P AND S FROM THEIR COMMON INTERFERENCES. <sup>27, 64</sup> .....	54
TABLE 1:8: DC POTENTIALS OF THE LINEAR ION TRAP DURING POSITIVE ION STORAGE AND TRANSMISSION. <sup>78</sup> .....	66
TABLE 2:1: PQ EXCELL OPERATING PARAMETERS .....	80
TABLE 2:2: ELEMENT 2XR OPERATING PARAMETERS .....	80
TABLE 2:3: OLIGONUCLEOTIDE SEQUENCES .....	82
TABLE 2:4: INSTRUMENT OPERATING CONDITIONS FOR DI-NUCLEOTIDE DESALTING .....	93
TABLE 2:5: HPLC CONDITIONS USED IN THE PURIFICATION OF DI-NUCLEOTIDE-AU CONJUGATES .....	94
TABLE 2:6: MMN-25 MER CONJUGATE SEPARATION METHOD .....	95
TABLE 2:7: SUMMARISED ICP-MS DATA FOR HPLC FRACTIONS COLLECTED DURING ELUTION OF THE MMN-25 MER SAMPLES .....	121
TABLE 2:8: <sup>197</sup> AU SIGNAL INTENSITY FOR THE MMN OPTIMISATION REACTIONS .....	124
TABLE 2:9: REACTION OPTIMISATION RESULTS AND CORRESPONDING REACTION EFFICIENCIES .....	127
TABLE 2:10: MOLECULAR WEIGHT OF SFNG, BIOTINYLATED OLIGONUCLEOTIDES AND SFNG CONJUGATES .....	136
TABLE 2:11: HPLC PARAMETERS EMPLOYED FOR THE ANION EXCHANGE SEPARATION OF THE SFNG AND SFNG-DNA CONJUGATES .....	138
TABLE 2:12: BASIC HPLC OPERATING PARAMETERS FOR THE C18 SEPARATION OF SFNG AND SFNG-DNA CONJUGATES .....	142
TABLE 2:13: AU CONCENTRATIONS IN SEPARATED FRACTIONS .....	155
TABLE 3:1: THERAPEUTIC FUNCTIONS OF SOME METAL COMPLEXES .....	182
TABLE 3:2: ELEMENT 2XR INSTRUMENT PARAMETERS .....	192
TABLE 3:3: OXALIPLATIN DATA FROM TREATED CTDNA (0.5 MG ML <sup>-1</sup> CTDNA MATRIX) .....	200
TABLE 3:4: OXALIPLATIN DATA FROM TREATED CTDNA (0.25 MG ML <sup>-1</sup> CTDNA MATRIX) .....	205
TABLE 3:5: CISPLATIN DATA FROM TREATED CTDNA (0.25 MG ML <sup>-1</sup> CTDNA MATRIX) .....	205
TABLE 3:6: PT SIGNAL INTENSITY AND CONCENTRATION IN DIGESTED CISPLATIN TREATED SAMPLES .....	213
TABLE 3:7: PT SIGNAL INTENSITY AND CONCENTRATION IN DIGESTED OXALIPLATIN TREATED SAMPLES .....	213
TABLE 4:1: ESI-MS OPERATING CONDITIONS .....	223
TABLE 4:2: CONCENTRATION OF OXALIPLATIN AND NUCLEOBASE IN INDIVIDUAL AND MIXED BASE SOLUTIONS. .....	224
TABLE 4:3: OXALIPLATIN ADDUCTS FORMED WITH INDIVIDUAL DNA NUCLEOBASES .....	229
TABLE 5:1: OLIGONUCLEOTIDE BASE SEQUENCES .....	258
TABLE 5:2: HPLC PARAMETERS FOR THE SEPARATION OF SNPs .....	259
TABLE 5:3: ICP-MS OPERATING PARAMETERS FOR THE COLLISION CELL METHOD .....	260
TABLE 5:4: SHALLOW GRADIENT USED FOR THE HPLC-ICP-MS OF SNPs, IN AN ATTEMPT TO REDUCE THE RISING BASELINE .....	267
TABLE 8:1: PROPERTIES OF THE TSKGEL-DEAE-NPR STATIONARY PHASE .....	290

## **Acknowledgements**

There are many people who I would like to thank and for a variety of reasons. Firstly I would like to thank Dr Barry Sharp who gave me this opportunity, and provided the research group with first class laboratory facilities. In addition, I would like to thank my former colleagues who include; Dr Monica Felipe Sotelo, Dr Helen Reid, Dr Peter Winship, Dr Ciaran O'Connor, Dr Mark Landon and Mr Dhinesh Asogan. An additional thank you is also reserved for Dr Barry Sharp and Dr Mark Landon for their comments and suggestions during the preparation of this document.

The technical staff at Loughborough University were always supportive and made life easier, thus I would like to acknowledge Dave Wilson, Trevor Brown, John Spray and Stuart Pinkney. In addition to Loughborough University staff, I would like to thank our collaborators, namely; Dr Chris Harrington, Dr Don Jones and Dr Rachel LePla from Leicester University and Dr Tamer Shoeib from the British University of Egypt, who provided a lot of support and advice.

On a more personal note, I would like to thank my parents for supporting me throughout my seven years at Loughborough University. Lastly, but no means least, I would like to thank my partner Mr Mark Walton, who I believe had the most difficult job of not only having to live with me, but gave me an immense amount of support and encouragement, especially when things got tough. If it were not for this support, this document certainly would not exist.

## Abstract

The application of ICP-MS to the fields of proteomics and genomics has arisen in part due to its ability to detect and quantify trace levels of S and P, which are major constituents in proteins and nucleic acids respectively. The development of collision/reaction cell technology and high resolution instruments has enabled these biologically important elements to be measured and quantified at the pg - ng ml<sup>-1</sup> level. Despite these advances, the detection limits of P and S are still inferior compared to other elements.

Oligonucleotides containing biotin functionality were labelled with Au nano-particles attached to a streptavidin protein to achieve site specific labelling, with 100% labelling efficiency. Each nano-particle contained ~86 Au atoms, resulting in an 882 fold signal enhancement for 24 base length oligonucleotides. However, this enhancement factor was only observed when one oligonucleotide bound to one nano-particle in a 1:1 ratio. Much lower Au labelling efficiencies and signal enhancements were observed when thiolated oligonucleotides were labelled with maleimide functionalised gold nano-particles. This was attributed to the extensive and difficult sample preparation steps that were required prior to labelling.

The detection and quantification of adducts formed between DNA and the Pt anti-cancer drugs cisplatin and oxaliplatin were also investigated with ICP-MS. Acid digestion of the carbon based DNA matrix enabled Pt adducts to be quantified at low dose rates of 1 Pt atom per 1 500 000 nucleotides in ~12 µg DNA. Such sensitive mass spectrometric determinations could be employed in clinical tests to detect and quantify low level adducts formed in patients *in-vivo*. To complement ICP-MS analysis, electrospray ionisation linear ion trap mass spectrometry was employed to study the interaction of oxaliplatin with the four DNA nucleobases. Multiple stage mass spectrometry enabled detailed Pt-nucleobase adduct fragmentation pathways to be established.

The method of DNA detection using P in conjunction with the collision cell, or cool plasma to form PO<sup>+</sup> was also demonstrated and the limitations of the method, namely, polyatomic interferences and severe matrix effects were highlighted.



**Keywords;** Oligonucleotides, DNA, Phosphorus, Gold, Nano-particles, Labelling, ICP-MS, Collision/reaction cell, HPLC-ICP-MS, ESI-MS, Platinum, Metallo drugs, Cisplatin, Oxaliplatin.

## Glossary of Terms

AC	Alternating current
APCI	Atmospheric pressure chemical ionisation
APPI	Atmospheric pressure photoionisation
AU	Absorbance units
BSA	Bovine serum albumin
CCT	Collision cell technology
CD	Circular dichromism
CID	Collision induced dissociation
CPS	Counts per second
CRM	Consecutive reaction monitoring
ctDNA	Calf thymus deoxyribonucleic acid
Da	Daltons
Dach	Diaminocyclohexane
DEAE	Diethylaminoethane
DNA	Deoxyribonucleic acid
DNase 1	DNA nuclease 1
dNMP	Deoxyribonucleotide monophosphate
dNTP	Deoxyribonucleotide triphosphate
DTNB	5,5'-dithiolbis(2-nitrobenzoic acid)
DTT	Dithiothreitol
DVB	Divinylbenzene
EDC	N-ethyl- <i>N'</i> -(3-dimethylaminopropyl)carbodiimide
EDT	Ethanedithiol
EDTA	Ethylenediaminetetraacetic acid
ESA	Electrostatic analyser
ESI	Electrospray ionisation
ESI-MS	Electrospray ionisation-mass spectrometry
GMP	Guanine monophosphate
hnRNA	Heterogeneous nuclear ribonucleic acid

HPLC	High performance liquid chromatography
HR-ICP-MS	High resolution inductively coupled plasma mass spectrometry
ICP-MS	Inductively coupled plasma mass spectrometry
IKEE	Ion kinetic energy effect
IMAC	Immobilised metal affinity chromatography
KED	Kinetic energy discrimination
LA	Laser ablation
LOD	Limits of detection
MALDI	Matrix-assisted laser desorption ionisation
MMN	Monomaleimido nanogold
mRNA	Messenger ribonucleic acid
MS	Mass spectrometry
MS <sup>n</sup>	Mass spectrometry to the n <sup>th</sup>
MS/MS	Tandem mass spectrometry
NDP	Nucleotide diphosphate
NMP	Nucleotide monophosphate
NMR	Nuclear magnetic resonance
NP1	Nuclease P1
NPR	Non porous resin
NSI	Nanospray ionisation
NTA	Nitrolotriacetic acid
NTP	Nucleotide triphosphate
PAGE	Polyacrylamide electrophoresis
PBS	Phosphorus buffered saline
PCR	Polymerase chain reaction
PEEK	Polyetheretherketone
PFA	Perfluoroalkoxy
pI	Isoelectric point
PLA	Post labelling assay
PS-DVB	Polystyrene divinylbenzene
RF	Radio frequency

RNA	Ribonucleic acid
RP-HPLC	Reversed phase high performance liquid chromatography
rNMP	Ribonucleotide monophosphate
rNTP	Ribonucleotide triphosphate
rRNA	Ribosomal ribonucleic acid
SAP	Shrimp alkaline phosphatase
SE	Standard error
SEM	Secondary electron multiplier
SERRS	Surface enhanced resonance raman scattering
SFNG	Alexa fluor-488 Streptavidin fluoronanogold
SIM	Selected ion monitoring
SNP	Single nucleotide polymorphism
SRM	Selected reaction monitoring
snRNA	Small nuclear ribonucleic acids
snRNP	Small nuclear ribonucleoproteins
SPE	Solid phase extraction
SVPD	Snake venom phosphodiesterase
T4PNK	T4 Polynucleotide kinase
TCEP	Tris(carboxyethyl)phosphine
TMACl	Tetramethyl ammonium chloride
TMAH	Tetramethyl ammonium hydroxide
TNB	Thio-bis-(2-nitrobenzoic acid)
TOF	Time of flight
TRA	Time resolved analysis
Tris	Tris(hydroxymethyl)aminomethane
tRNA	Transfer ribonucleic acid
UV	Ultra violet

# 1. Introduction

## 1.1 Objectives

Inductively coupled plasma mass spectrometry (ICP-MS) is the most sensitive and versatile analytical technique in elemental and isotopic analysis. Most elements in the periodic table can be ionised in the ICP source including biologically important elements such as P and S. As a result, biomolecules such as nucleic acids and proteins can be detected by their P and S content respectively.<sup>1-3</sup> Further, proteins containing metallic components such as Zn and Mn can be analysed by ICP-MS due to the detectable ions. Such developments have resulted in the increased use of ICP-MS in the analysis of biomolecules.

The traditional organic mass spectrometry methods based on electrospray ionisation (ESI) and matrix assisted laser desorption ionisation (MALDI) mass spectrometry, provide structural information and good powers of detection, but quantification can be problematic. ICP-MS provides complementary information to conventional organic mass spectrometry and has many additional advantages.<sup>4-6</sup> Firstly, ICP-MS offers very low limits of detection, which generally range from  $\text{pg l}^{-1}$ - $\mu\text{g l}^{-1}$  depending on the analyte. Calibration and quantification are much easier and only require inorganic elemental standard solutions. In addition, because ICP-MS measures the total concentration of an element regardless of chemical form, it facilitates mass balance calculations, which are vital for establishing analyte recovery and method validation. Although the ICP is a hard ionisation source and molecular information is destroyed, it can be employed as a selective detector when coupled to various separation techniques, providing a means of separating molecular species prior to elemental detection.<sup>6,7</sup> These factors have helped increase the popularity of ICP-MS in biological analysis. Figure 1:1 summarises the main analytical techniques available for obtaining both molecular and elemental information from biomolecules.

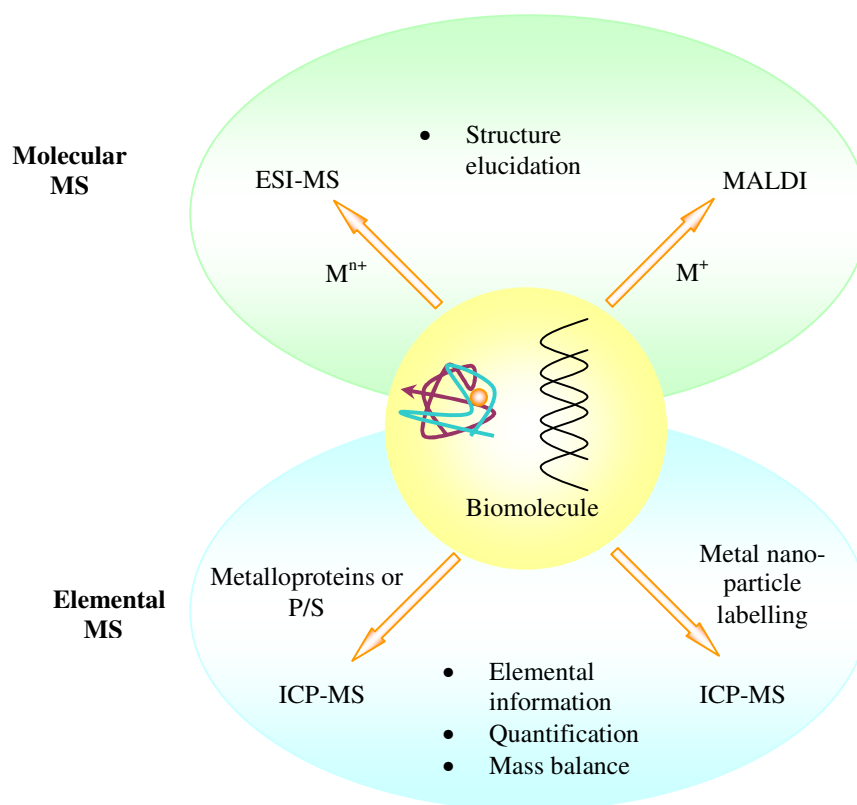


**Figure 1:1: Analytical methods available for biomolecule analysis.**

Despite the advantages of ICP-MS, P and S are problematic elements because they have high first ionisation potentials (10.5 and 10.4 eV respectively), which results in incomplete ionisation (~35% and 15% for P and S respectively)<sup>8</sup> and they suffer from polyatomic interferences at  $m/z$  31 and 32, which are derived from atmospheric gases and the sample solvent.<sup>9</sup> The advancements in collision/reaction cell<sup>1,9-11</sup> and high resolution instruments<sup>3, 11, 12</sup> has made it possible to remove or resolve the analyte ions from their interferences, but whilst metallic elements can readily be detected at  $\text{pg l}^{-1}$  levels, the detection limits for these elements are much higher. These problems can be avoided and the biomolecule signal enhanced if the biomolecule is labelled with a metallic element or a metal nano-particle, which is measured instead of P or S.<sup>13-16</sup> Since the sensitivity of ICP-MS increases with increasing number of similar isotopes in the sample, the incorporation of metal nano-particles, which contain multiple copies of the same isotope,

would allow for quantification at very low levels and avoids the problems encountered with P and S measurement, providing the metal label does not suffer any interferences.

Apart from avoiding the problems associated with P and S detection, metal or nano-particle labelling of biological molecules has additional advantages:

- Biomolecule structure and configuration does not necessarily have to be maintained, since only the elemental label will be detected and not the biomolecule directly. Thus, the sample does not have to be analysed immediately after sample preparation or stored in specialised conditions to prevent degradation.<sup>10, 16</sup>
- Reduced interferences, since a more favourable region of the mass spectrum is measured.
- More than one elemental label can be used simultaneously if there is more than one target molecule to study.<sup>10, 13</sup>
- Easy calibration and therefore quantitative analysis.
- Mass balance determinations.<sup>17</sup>

The primary aim of this thesis is to develop improved methods of biomolecule detection by using metal/nano-particle labelling coupled with analysis by ICP-MS.

This introduction will discuss the structure and function of DNA, whilst highlighting its importance in living systems. The analytical methods currently used for DNA detection will be briefly reviewed. The first aspect of the investigation will then be discussed, which involves improving DNA detection using elemental mass spectrometry by means of metal nano-particle labelling, where each nano-particle contained approximately 86 Au atoms. Gold has lower first ionisation potential than P and does not suffer the same interferences, resulting in improved sensitivity when bound to nucleic acids. More importantly, because each nano-particle contained ~86 Au atoms, a greater enhancement in sensitivity can be obtained to achieve ultra sensitive detection of nucleic acids. Two nanogold labelling routes were developed; both methods resulted in site specific labelling on the nucleic acid allowing for easy quantification. The methods of modifying DNA, the labelling procedure and the methods of purifying and detecting the conjugates will be discussed in detail.

The second aspect of this thesis concentrates on the ICP-MS analysis of DNA that had been treated with cisplatin or oxaliplatin anti-cancer drugs. These Pt containing complexes are known to interact with DNA *in-vivo* and *in-vitro*. Pt does not suffer from the same problems as P, hence the incorporation of Pt into the DNA molecule provides an additional label that can be employed for the ICP-MS analysis of DNA.<sup>18</sup> The total platinum concentration associated with DNA treated with varying doses of these drugs was determined. The ultimate aim was to develop a clinical test to detect and quantify the low level adducts formed in patients *in-vivo*, and to identify patients who are not responding well to the selected treatment. In addition to elemental mass spectrometry, the interaction of oxaliplatin with DNA nucleobases was investigated with ESI linear ion trap mass spectrometry. Detailed fragmentation pathways were established, whilst proposed product ion structures were presented, highlighting the complementary nature of elemental and molecular mass spectrometry techniques.

Finally, DNA detection by measuring the P signal associated with the sugar phosphate backbone will be discussed. The practical problems and limitations of P detection by ICP-MS will be highlighted. Figure 1:2 summarises the various routes by which nucleic acids have been detected and quantified in this thesis using ICP-MS.



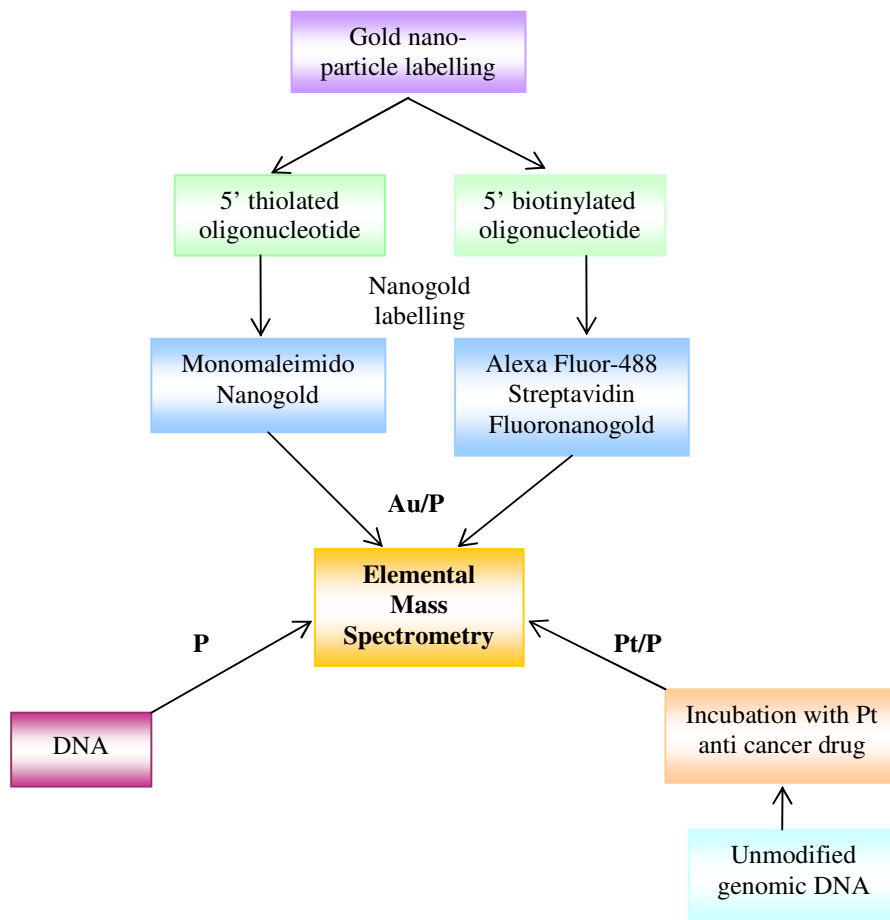


Figure 1:2: Schematic showing the various methods of detecting DNA by elemental mass spectrometry.

## 1.2 Genomics

### 1.2.1 Structure of DNA

Deoxyribonucleic acid (DNA) contains the chemical instructions required to create and sustain a living organism. All physical and biochemical characteristics of an organism are determined by the set of chemical instructions contained within DNA. The vast quantity and complexity of information stored in this genetic material provides the basis of genomic research. But remarkably only three main ingredients constitute DNA:

- Pentose sugar
- Nitrogen containing base
- Phosphate group

All three of the above ingredients are combined to form the basic sub-units required to create a DNA strand. The carbon atoms comprising the pentose sugar are numbered 1' to 5' as illustrated in Figure 1:3. The 2' carbon of the pentose sugar in DNA is not oxygenated, hence the term 'deoxyribonucleic acid'. A nucleoside is formed upon addition of a nitrogen-containing base to the 1' carbon atom of the pentose sugar. Further, the nucleoside becomes a nucleotide upon addition of a phosphate group on the 5' pentose carbon.<sup>19,20</sup> The structures of deoxyribose sugar, nucleoside and nucleotide are illustrated in Figure 1:3.

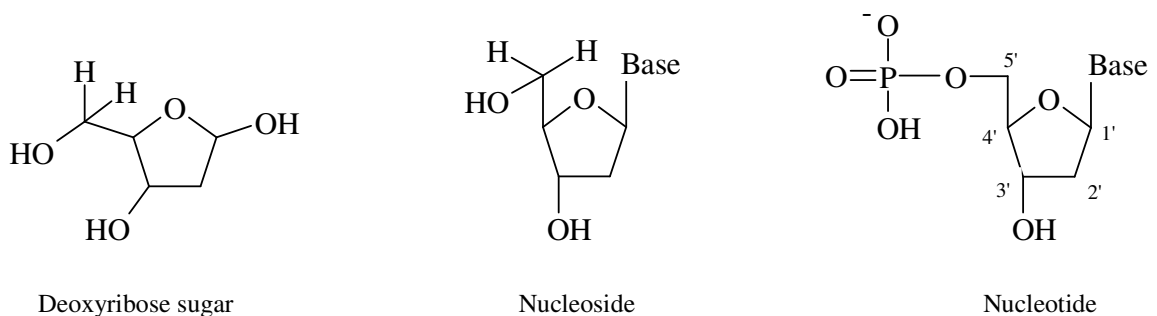


**Figure 1:3: Structures of deoxyribose sugar, nucleoside and nucleotide.**

The hydroxyl group on the 3' pentose carbon can form a phosphodiester bond with the 5' phosphate group of another nucleotide. The formation of such phosphodiester bonds between nucleotides results in a polynucleotide chain.<sup>20</sup> DNA is essentially a polymer of nucleotides, which are bonded together through these ester bonds. The first nucleotide in

the nucleic acid chain has a triphosphate group located on the 5' carbon of the pentose sugar. The reason for the presence of a triphosphate group on the first nucleotide in the chain will be explained in subsequent sections. The position of the phosphate group on the sugar is called the C5 position, which is also called the 5' end. The last nucleotide in the nucleic acid chain always has a hydroxyl group (-OH) at the C3 position on the pentose sugar. Hence, the hydroxyl group position is called the 3' end. Thus, nucleotides are joined together by the 5' end of one nucleotide forming a phosphodiester bond with the 3' end of another nucleotide.<sup>19, 20</sup> Figure 1:4 illustrates the phosphodiester bond along with the 3' and 5' positions on the nucleotide.

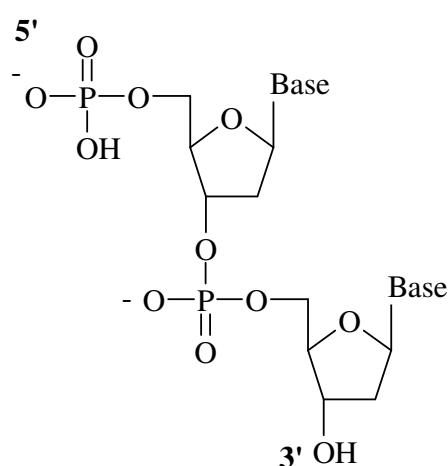
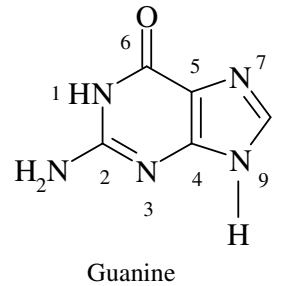
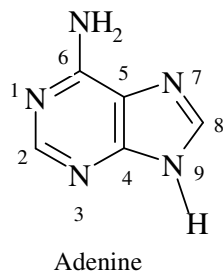


**Figure 1:4: Phosphodiester bond formation between nucleotides.**

One of four nitrogen bases can be incorporated onto the 1' carbon of a nucleoside, namely; adenine (A), cytosine (C), guanine (G) or thymine (T). The structures of the bases can be seen in Figure 1:5 and can be separated into two groups; purines and pyrimidines. Pyrimidine bases consist of one aromatic ring, whereas, purines are composed of two fused rings. Like in the case of the ribose sugar, the carbon and nitrogen atoms within the nucleobases are numbered as shown below. This ring numbering system has important implications in subsequent chapters when the interactions of nucleobases with metallodrugs are discussed.

Purine bases:



Pyrimidine bases:

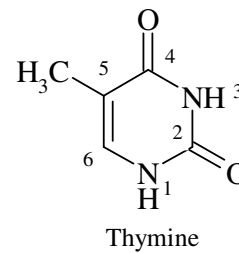
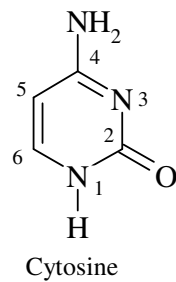


**Figure 1:5: Structures of the purine and pyrimidine DNA bases.**

Genomic DNA is arranged into two polynucleotide strands to form a helix, which is commonly known as the double helix. For the double helix to form, the bases on one strand form hydrogen bonds with bases on the neighbouring strand. This is known as complementary base pairing. However, the base pairing process is not random, but specific with only adenine and thymine pairing and also guanine and cytosine pairing. Two hydrogen bonds are formed between adenine and thymine, whilst three hydrogen bonds form between guanine and cytosine. This coupling of bases is known as complementary base pairing, thus, a complementary base pair consists of a purine and a pyrimidine.<sup>20</sup>

Adenine can only bind to thymine, and cytosine can only bond to guanine. The reasons for this can be explained by two factors. Firstly, the size of the bases has to be considered. The internal diameter of the double helix (1.1 nm wide) is not sufficient to allow adenine and guanine to pair.<sup>20</sup> Conversely, cytosine and thymine are not wide enough to fit within the sugar phosphate backbone and form a stable hydrogen bond, since the strength of hydrogen

bonds diminishes rapidly with distance. For these reasons a base pair has to be composed of a purine and a pyrimidine.

However, adenine and cytosine are not complementary base pairs, neither are guanine and thymine, yet both these pairs contain a purine and pyrimidine. This brings about the second factor that has to be considered, which is hydrogen bonding. Hydrogen bonds hold the two complementary base pairs together and ultimately help form the double helix. For a stable hydrogen bond to form the base pairs must have the appropriate hydrogen bond donor and acceptor atoms, along with a short distance between the base pairs. Although adenine-cytosine and guanine-thymine have a distance between them that could sustain a stable hydrogen bond, the hydrogen bond donors and acceptors are not properly matched, thus the DNA helix would have to distort to allow for this base pair combination.<sup>21</sup> For these reasons the complementary DNA base pairs are: adenine-thymine and guanine-cytosine. This strict pairing of bases helps minimise errors in the replication of DNA. Figure 1:6 shows how the bases are arranged in double stranded DNA. Note, that one DNA strand runs in the 5'→3' direction and the complementary strand is parallel but in the 3'→5' direction.

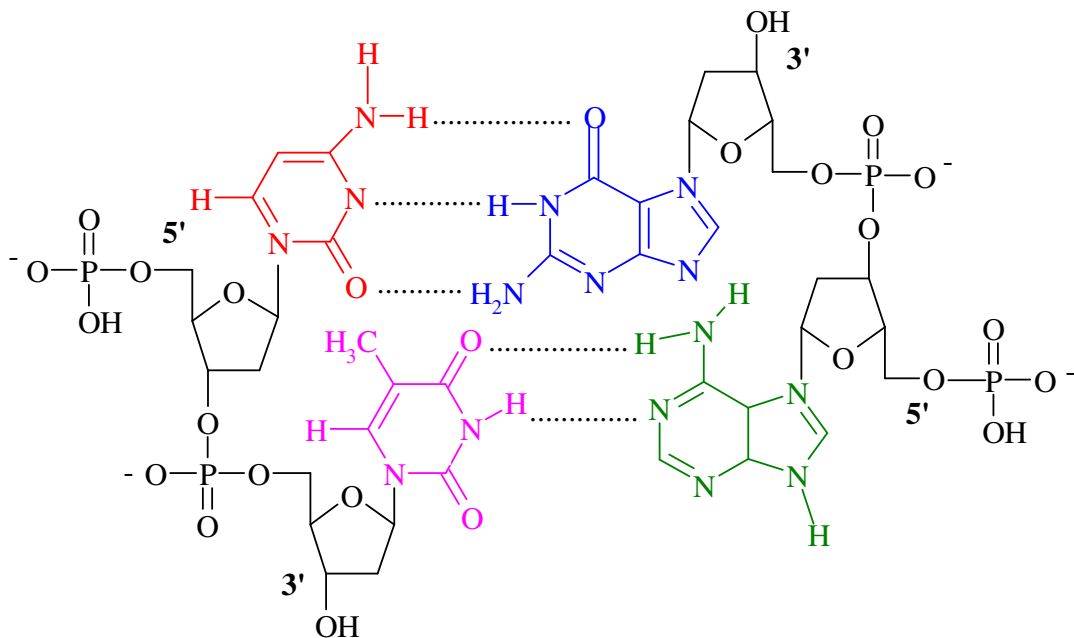


**Figure 1:6: Base pairing of DNA.**

The pentose sugars and phosphate groups alternate along the outside of the DNA helix to form the sugar phosphate backbone, whilst the base pairs are inside the helix holding the two polynucleotide strands together by hydrogen bonding. The width of the DNA molecule is 2 nm (outer diameter) and the length is approximately 1.8 m.<sup>19</sup> Each base pair is 3.4 Å apart and one complete turn contains 10 base pairs, therefore one turn is 34 Å in length.<sup>20</sup>

The external sugar phosphate backbone results in DNA carrying a net negative charge, which allows water molecules to pack around the outside of the DNA molecule to create hydration spheres around the sugar phosphate backbone.<sup>22</sup> Cations are also attracted to the exterior of the DNA molecule; thus, DNA can act as a cation exchange medium. Many other molecules within biological systems can also interact with DNA, as will be discussed later.

### **1.2.2 DNA Function**

DNA has two main functions which include; the replication of itself so genetic material can be passed onto new cells and ultimately offspring. The second function of DNA is protein synthesis. The DNA molecule contains regions of base pairs that code for specific proteins, these areas are called genes. Genes are decoded and proteins are synthesised by two processes known as transcription and translation. Both these processes will be discussed in detail in following sections. The discussion of DNA replication and protein synthesis are relevant to eukaryotic organisms.

### **1.2.3 DNA Replication**

DNA has the function of storing all the genetic information of an organism and to pass this genetic code onto new cells and ultimately offspring. As mentioned in the previous section, the complementary base pairing of DNA bases minimises the chances of errors occurring during DNA replication, hence the correct genetic code is passed on to new cells and offspring. DNA is stored in the cell nucleus where replication takes place. The nucleus helps protect DNA, as certain chemicals and radiation can easily damage it. If DNA were

stored in the cytoplasm, it would almost certainly be damaged leading to mutations.<sup>19</sup> The replication process is referred to as semi-conservative and is exhibited by all organisms.<sup>20</sup> The term ‘semi-conservative’ will become apparent during discussion.

The first stage of replication requires the DNA double helix to unwind, which is aided with the enzyme helicase. The origin of replication is where the two DNA strands unwind; this forms two exposed DNA strands known as the replication forks. The replication bubble is the name given to the regions of newly synthesised DNA.<sup>20</sup> The relative positions of the replication fork and bubble are shown in Figure 1:7. The replication bubble increases in size as the replication fork works its way along the DNA molecule and the new DNA chain grows.<sup>20, 23</sup>

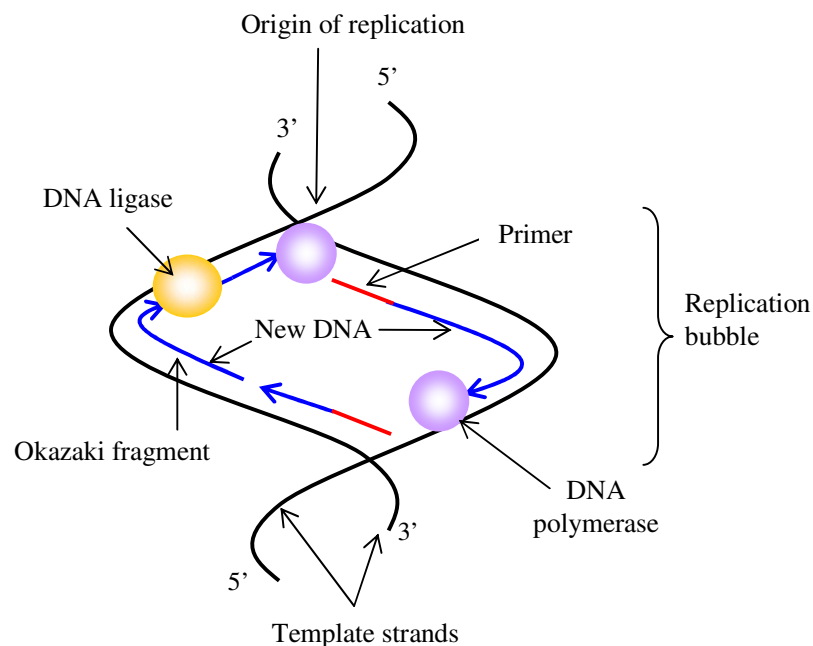


**Figure 1:7: DNA Replication.**

Short chain ribonucleic acids (RNA), known as primers mark the point where DNA replication is to begin. As a result, the base sequence of primers is complementary to the DNA base sequence where replication begins. The RNA primers anneal to the DNA with the help of an enzyme called RNA primase.<sup>19</sup> A covalent bond is then formed between the 3' (hydroxyl) end of the RNA primer and the 5' end of the newly synthesised DNA strand.<sup>20</sup> As the DNA helix unwinds, the base pairs become exposed and free surrounding

deoxynucleotide triphosphates (dNTP) bond to their complementary bases on the partially unwound DNA.

Both DNA strands act as templates for the formation of the new DNA (see Figure 1:7). Since one template strand will be exposed in the 3'→5' direction and the other strand exposed in the 5'→3' direction, the DNA replication forks of the two DNA template strands work in opposite directions.<sup>20</sup> The template strand, which is exposed in the 3'→5' direction, is copied continuously and the new DNA is formed in the 5'→3' direction; this is known as the leading strand. However, the other strand, which was exposed in the 5'→3' direction is copied discontinuously, but the new DNA is also formed in the 5'→3' direction and is known as the lagging strand. The discontinuous nature of replication on the lagging strand forms segments of new DNA called Okazaki fragments.<sup>20, 23</sup> The replication of the two anti-parallel strands occurs simultaneously.

As the free dNTP bond to their complementary bases on the unwound template DNA strands, they are hydrolysed to form deoxynucleotide monophosphates (dNMP) as they are added onto the growing DNA strand. Figure 1:8 illustrates the addition and hydrolysis of free dNTP's. Since the dNTP's are converted to dNMP's, two phosphate groups are removed, which is known as pyrophosphate and is subsequently converted to phosphate as shown in Figure 1:9.



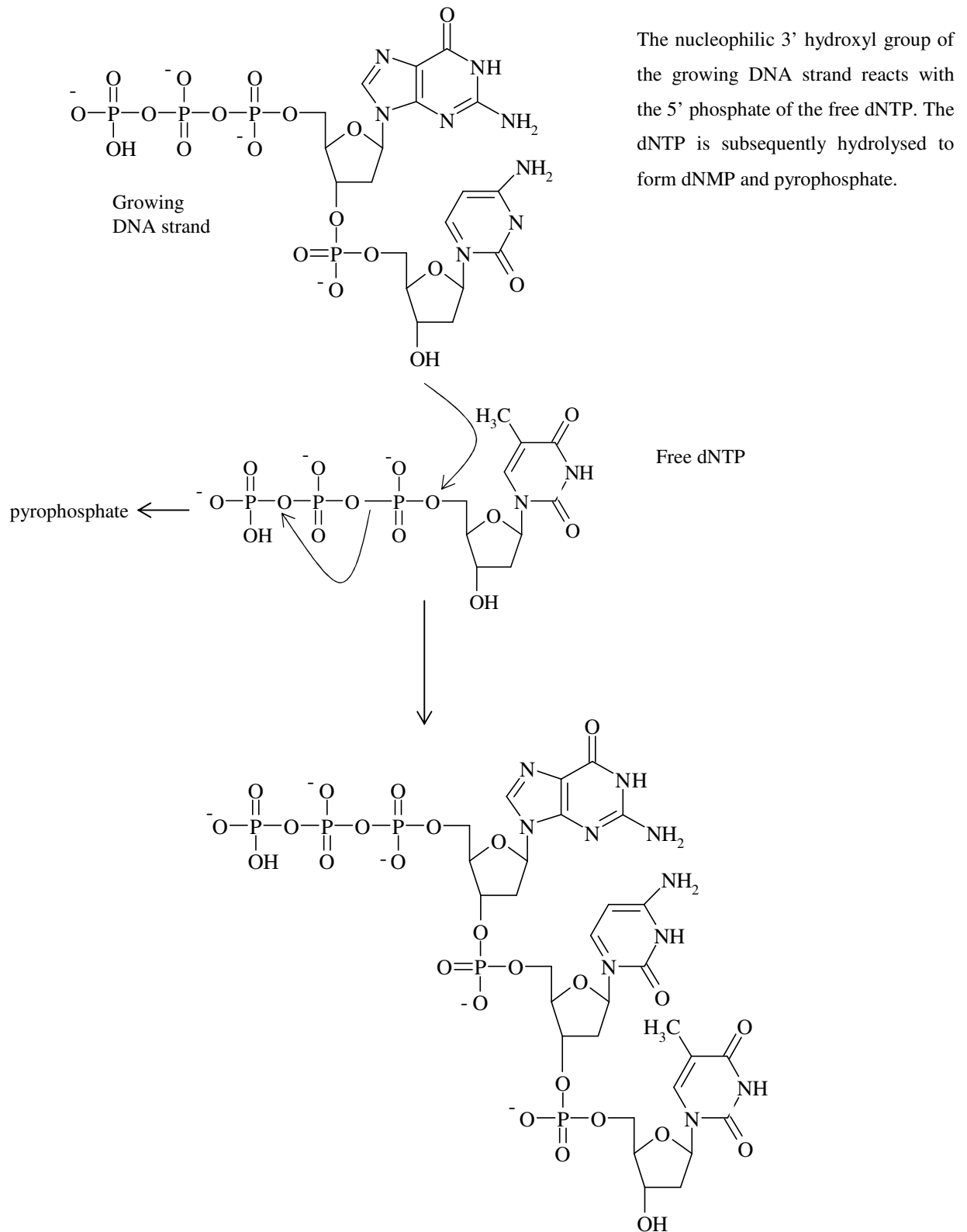


**Figure 1:8: Addition of free dNTP onto a growing DNA chain.**

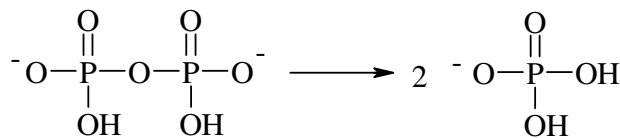


**Figure 1:9: Conversion of pyrophosphate.**

The pyrophosphate side product is converted to phosphate in a reaction that ensures dNTP is hydrolysed to dNMP and DNA polymerisation is irreversible.<sup>24</sup> DNA polymerase  $\alpha$  catalyses the formation of hydrogen bonds between the free nucleotides and the exposed DNA bases. This enzyme is also responsible for the formation of the phosphodiester bonds between neighbouring nucleotides. There are three types of DNA polymerase, the roles of these enzymes are summarised in Table 1:1.

**Table 1:1: Functions of DNA Polymerase Enzymes.<sup>20</sup>**

Polymerase	Function
DNA Polymerase $\alpha$	Polymerisation enzyme
DNA Polymerase $\beta$	Repair enzyme
DNA Polymerase $\gamma$	DNA replication in mitochondria

The newly formed DNA strands are complementary to their corresponding template strand, but it is important to note that the template DNA and new DNA strands are not identical, due to the complementary nature of base pairing. The two strands are said to be anti-parallel.<sup>19</sup> The Okazaki fragments that are formed as a result of discontinuous replication on the lagging strand (Figure 1:7) are joined together with DNA ligase to create a continuous complementary strand. This enzyme inserts the missing phosphodiester bonds between the Okazaki fragments to complete the sugar phosphate backbone.<sup>19</sup>

The final stage of replication involves the enzyme DNA polymerase, which removes the RNA primers that marked the starting points for DNA replication, and replaces the primers with new deoxynucleotides.<sup>19</sup> Methylating agents such as methionine, methylates the new DNA at various points along the strand. This acts as a protection mechanism for the DNA by preventing endonucleases destroying the organism's own genetic information.<sup>24</sup>

The whole process of replication is known as semi-conservative, since both DNA strands act as templates for the formation of new DNA. When replication is complete, two helices are present, each helix contains a DNA template strand (old DNA) and a new DNA strand.

### 1.2.4 Protein Synthesis

Protein synthesis is another vital role of DNA and is imperative for the sustainability of all living organisms. DNA contains sections of sequential nucleotides called genes that code for specific proteins. Each gene along the genome contains the genetic instructions for protein synthesis. There are two main stages in the production of proteins; transcription and translation.

DNA is not the only important component in protein synthesis; there is a group of nucleic acids called ribonucleic acids (RNA) that are vital for the production of proteins. RNA like DNA is composed of a pentose sugar, nitrogen containing bases and phosphate groups. However there are differences between the two nucleic acids, namely, the RNA ribose sugar is oxygenated at the 2' carbon, whereas in DNA this carbon position is deoxygenated. In addition, thymine is absent in RNA, but uracil is present instead. These subtle differences between the two nucleic acids are summarised in Table 1:2 and Figure 1:10.<sup>19</sup>

**Table 1:2: Differences between DNA and RNA.**

	<b>DNA</b>	<b>RNA</b>
<b>Pentose Sugar</b>	Deoxyribose sugar	Ribose sugar
<b>Bases</b>	A, C, G and T	A, C, G and U
<b>Size</b>	1.8 m in length	Various lengths, but significantly smaller than DNA.
<b>Number of Strands</b>	Double stranded	Usually single stranded however there are some double stranded forms of RNA.

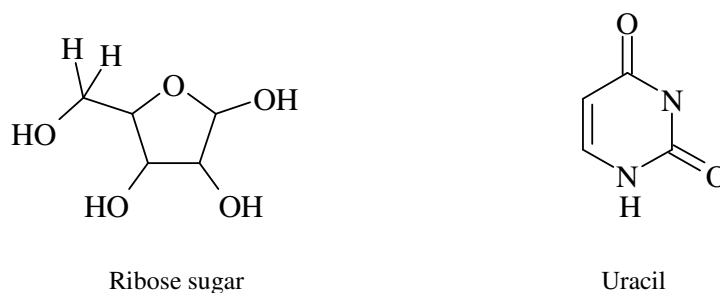


**Figure 1:10: Structure of ribose sugar and uracil.**

The process of protein synthesis requires the genetic information contained in DNA to be decoded. Transcription is responsible for transferring the genetic code from DNA into an RNA molecule, whilst translation uses the transcribed genetic code to build amino acid chains.<sup>19</sup> There are many types of RNA all of which have a specialised role in protein synthesis. Each type of RNA will be defined as the transcription and translation processes are discussed.

#### 1.2.4.1 Transcription

The genetic information contained in genes is transcribed into an RNA molecule called messenger RNA (mRNA), which is the product of transcription. The transcribed mRNA can be transported out of the nucleus to the cytoplasm, where proteins are produced.<sup>19</sup> Messenger RNA is therefore the carrier or messenger containing the genetic code required for protein synthesis.

The first step in transcription requires part of the DNA double helix to unwind, which is again aided by the helicase enzyme. Once the DNA has unwound the DNA bases are exposed and can be used as a template for mRNA production, analogous to DNA replication.<sup>19</sup> The enzyme RNA polymerase helps in the initiation of transcription by binding to the part of the DNA molecule where transcription is to begin. This specific site on the DNA molecule is known as the promoter, which determines which DNA strand is to be transcribed. Specific proteins known as transcription factors help RNA polymerase recognise the promoter site. The combination of all these components is known as the initiation complex.<sup>24</sup>

The anti-sense DNA strand is used as a template during transcription; the resulting mRNA molecule therefore has a base sequence, which is identical to the sense strand and complementary to the anti-sense strand. However, it must be noted that uracil is present in mRNA instead of thymine and the ribose sugar is oxygenated at the 2' carbon.<sup>19</sup>

RNA primers mark the section of DNA to be transcribed and just like DNA replication; the primers have a base sequence complementary to the start and end points of the gene to be transcribed. Once the DNA bases are exposed, free ribonucleotide bases can bind to the exposed DNA bases by complementary base pairing. RNA polymerase catalyses the formation of hydrogen bonds between the complementary DNA-RNA bases, as well as catalysing the growth of the RNA strand. The free ribonucleotide triphosphates (rNTP) are converted to ribonucleotide monophosphates (rNMP) as they are added to the growing RNA molecule. The pyrophosphate side product is again formed during mRNA formation and the polymerisation reaction is made irreversible by the conversion of pyrophosphate to phosphate (Figure 1:9).<sup>24</sup> Transcription along the DNA molecule occurs in the 3'→5' direction, so the resulting mRNA molecule grows in the 5'→3' direction.

RNA polymerase moves along the DNA strand catalysing the growth of the mRNA molecule. The energy released during the hydrolysis of rNTP is sufficient to allow the RNA polymerase to move along the DNA molecule. Many genes along the genome may be transcribed simultaneously, which in turn requires many RNA polymerase enzymes.<sup>24</sup> The portion of DNA that is transcribed is called the transcription unit. Once the transcription unit has been transcribed, the DNA double helix reforms and the newly formed mRNA molecule is removed from the DNA template.

There are three main types of RNA polymerase; each is responsible for the formation of different RNA molecules. RNA polymerase II is responsible for the formation of mRNA during transcription. Table 1:3 summarises the types of RNA and the corresponding RNA polymerase required for synthesis.

**Table 1:3: The types of RNA and their corresponding RNA polymerase required for formation.<sup>24</sup>**

RNA Polymerase	RNA Production
RNA Polymerase I	rRNA
RNA Polymerase II	mRNA and snRNA
RNA Polymerase III	Low molecular weight RNA molecules and tRNA

Once transcription is complete the resulting mRNA molecule undergoes some modifications before it is ready to leave the nucleus for protein synthesis. The unmodified mRNA is called pre-mRNA or the primary transcript and is much longer than the modified or mature mRNA that is employed during translation.<sup>24</sup> There are regions of bases within genes that do not code for proteins. These regions are known as intervening sequences or introns and are transcribed into the pre-mRNA, but need to be removed prior to translation. Exon is the name given to the useful parts of the transcribed gene that are required for translation.<sup>24</sup> There are numerous mechanisms which enable these transcribed introns to be removed from the pre-mRNA for mature mRNA production. Heterogeneous nuclear RNA (hnRNA) is another name given to the mRNA precursor. Pre-mRNA or hnRNA molecules are contained in the nucleus and have a half-life as short as a few minutes.<sup>24</sup>

Introns are removed from the hnRNA by a method called RNA splicing. Splicing has to be highly accurate, since additional bases or missing bases in the mature mRNA molecule would effect the transcription process, hence the translated protein may not contain the correct amino acid sequence.<sup>24</sup> Breaks or splice sites have to be introduced into the pre-mRNA molecule. These splice sites contain specific base sequences. Specific sequences also occur in exons, which promote the recognition of introns; these sites are known as exonic enhancers.<sup>24</sup> Splicing requires another type of RNA called small nuclear RNA (snRNA), which is found in the nucleus. SnRNA combines with specific proteins to create complexes called splicosomes. The pre-mRNA and splicosomes associate to form a macromolecular complex that removes introns from the pre-mRNA.<sup>24</sup>

In addition to splicing, the 5' end of the pre-mRNA molecule has a methylguanosine cap incorporated. It was discussed in the DNA replication section that the first nucleotide in a nucleic acid sequence is a triphosphate, since the first nucleotide is not hydrolysed to

rNMP. In the case of mRNA, this triphosphate is converted to a diphosphate by enzymatic action, then guanine monophosphate (GMP) is added to the diphosphate nucleotide *via* its 5' phosphate group. Thus, a triphosphate bridge links the first two nucleosides in the mRNA molecule. Both the terminal guanine and the neighbouring nucleotide in the mRNA chain are methylated. Methylation prevents endonucleases recognising and destroying the polynucleotide chain.<sup>24</sup> The modified mRNA molecule also has an adenosine polymer attached to its 3' end.<sup>24</sup> The adenosine polymer is added to the mRNA with the help of the enzyme, poly (A) polymerase and does not require a DNA template for the addition of the adenosine tail. The poly A tail also prevents the mRNA being degraded by nucleases.<sup>24</sup> The release of the mRNA from the nucleus is also aided by the capped 5' end.<sup>24</sup>

#### **1.2.4.2 Translation**

The second stage of protein synthesis translates the genetic code contained in mRNA into a string of amino acids, which are subsequently used in the formation of proteins. Translation employs a range of RNA molecules, each having their own specialised functions.

The modified or mature mRNA complete with the 3' and 5' modifications has to be transported out of the nucleus, through the cytoplasm to structures called ribosomes, where translation takes place. Ribosomes consist of proteins and another type of RNA called ribosomal RNA (rRNA). There are vast numbers of rRNA in cells for protein synthesis, for this reason the gene coding for rRNA is repeated throughout the genome many times.<sup>24</sup> Ribosomes can be found in the cytoplasm or situated on the surface of organelles known as the endoplasmic reticulum, which are also located in the cytoplasm of the cell. The ribosomes consist of two units; the large sub-unit and the small sub-unit, which are composed of four types of rRNA; 5S, 5.8S, 18S and 28S along with ribosomal proteins. The larger the rRNA molecule the higher the S value associated with it (the S value is called the Sedimentation Coefficient).<sup>24</sup> The large sub-unit contains three of the four types of rRNA; 5S, 5.8S and 28S. Hence, the small sub-unit contains the 18S rRNA.<sup>24</sup>

Translation consists of three distinct stages; initiation, elongation and termination. Each of these three stages has a different sequence of events that are involved in the decoding of genetic information.

### **Initiation**

Three adjacent bases along the mRNA chain are called codons and code for a particular amino acid. However, some codons also code for the initiation or termination of the transcription process. The triplet code is another name given to three adjacent bases that are involved in the decoding of genetic information on mRNA. Once the mRNA is transported to the ribosomes, the small ribosome sub-unit binds to the mRNA chain *via* the first codon, which is the initiator codon AUG. The large sub-unit then binds to the mRNA in preparation for amino acid assembly.<sup>24</sup>

There are three regions in the ribosome complex; Exit site (E site), Peptidyl site (P site) and the Aminoacyl site (A site). Each of the three-ribosome sites has important functions during the elongation process.<sup>24</sup> The first codon (AUG) in the mRNA molecule is held in the P site, and the next codon along is held at the A site, as shown in Figure 1:11. Many protein initiation factors are involved in the initiation of translation. The decoding of genetic information is thought to take place in the small ribosome sub-unit and the catalysis of peptide bonds between neighbouring amino acids takes place in the large ribosome sub-unit.<sup>24</sup>



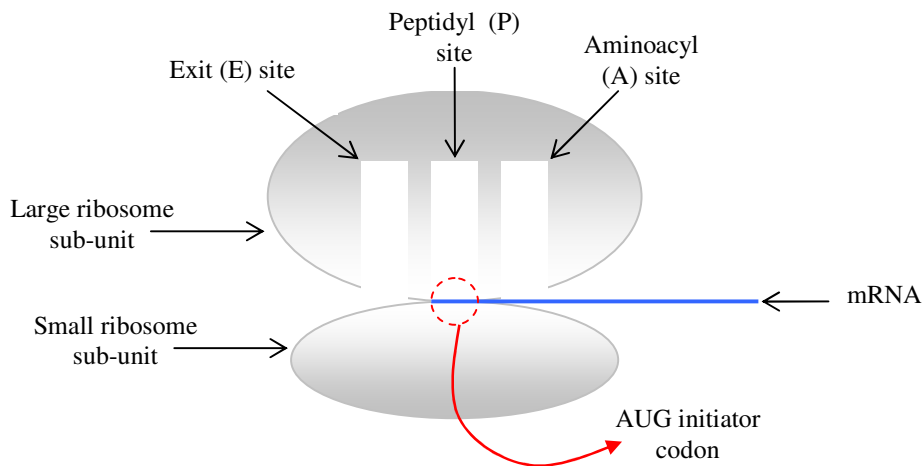


**Figure 1:11: Ribosome Complex.**

### **Elongation**

Another form of RNA known as transfer RNA (tRNA) is involved in translation and is responsible for transporting the correct amino acid to the mRNA molecule, and hence stringing the correct amino acid sequence together. There are approximately 50 types of tRNA; each is coded for by genes within the genome. RNA polymerase III is responsible for tRNA formation.<sup>24</sup>

The translation of the genetic code contained in mRNA into a protein is achieved by decoding the triplet codes or codons, which are contained within mRNA. As already stated; three sequential nucleotide bases along the mRNA code for an amino acid. Since there are four bases (A, U, G and C) and three bases code for an amino acid, there are 64 ( $4^3 = 64$ ) possible codons, allowing for 64 amino acids to be coded for. Since there are only 20 amino acids; each amino acid is normally coded by more than one codon. In addition, there are three triplets that do not code for any amino acids, but act as initiation or stop functions along the mRNA chain.<sup>24</sup>

Transfer RNA molecules are relatively large, containing between ~70-90 nucleotides. These molecules adopt distinctive configurations containing double stranded or folded regions known as stems. Stems are formed where the tRNA nucleotide sequence contains regions, which are complementary to other portions of the molecule, thus the

complementary regions of the tRNA molecule bind through hydrogen bonding. Loops are also found in the molecule due to lack of hydrogen bonding between other tRNA regions.<sup>24</sup> Figure 1:12 illustrates the distinctive ‘clover leaf’ configurations adopted by tRNA, due to the stems and loops.

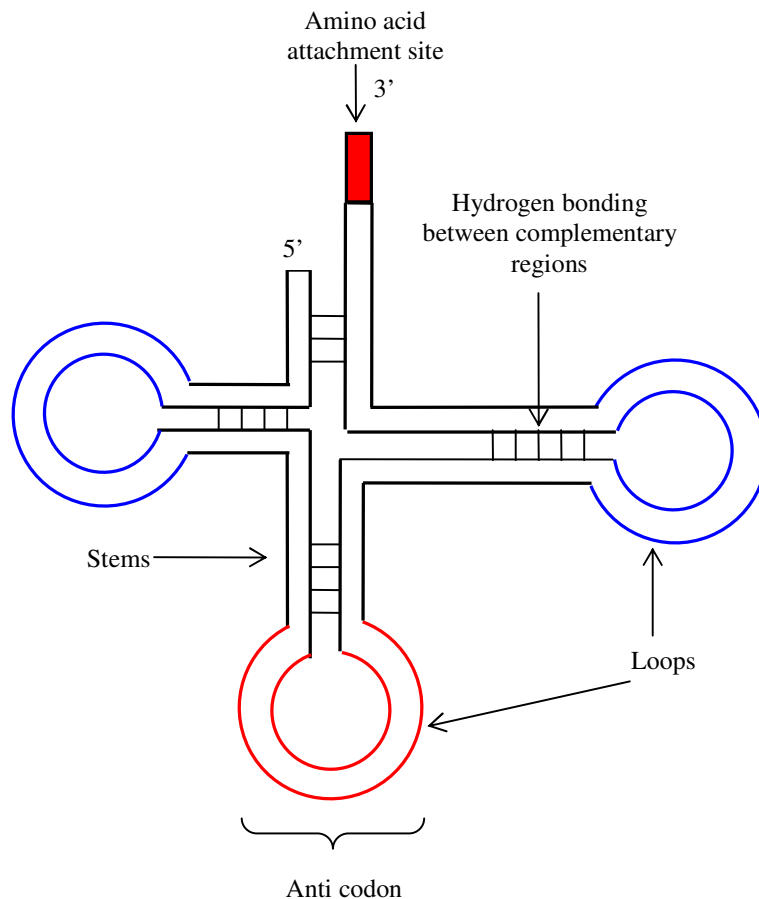


**Figure 1:12: Structure of tRNA.**

The 3' end of the tRNA molecule always contains the base adenine, which reacts with an amino acid and thus acts as the attachment site. The middle loop in the tRNA has a sequence of three bases called an anticodon. The anticodon is directly opposite the amino acid binding site on the tRNA molecule and must be complementary to an mRNA codon for an amino acid to be added to the new peptide chain.<sup>24</sup>

A tRNA molecule with an anticodon complementary to the first codon on the mRNA chain will bind to the ribosome at the P site (Figure 1:13). A second tRNA molecule with an

anticodon complementary to the second codon along the mRNA strand, will bind at the A site on the ribosome. Peptidyl transferase then catalyses the formation of peptide bonds between the amino acid at the A site and the amino acid at the P site.<sup>19, 23, 24</sup> The tRNA at the P site is then transferred to the E site as the ribosome moves along the mRNA, exposing the next codon on the mRNA molecule.<sup>24</sup> The amino acid at the A site is now located at the P site and contains two amino acids bound by a peptide bond. Another tRNA molecule with the correct anticodon sequence binds to the exposed A site. A peptide bond then forms between the amino acid at the A site and the amino acid dimer at the P site. Once the peptide bond is formed, the tRNA molecule at the P site moves to the E site on the ribosome and the neighbouring tRNA molecule which now contains three amino acids bonded together by peptide bonds, moves to the P site.<sup>24</sup> This process repeats itself until all the appropriate amino acids are added to the growing peptide chain. The exit site is the actual site where the tRNA molecules are released from the ribosome complex.<sup>24</sup> The process of elongation is summarised in Figure 1:13.

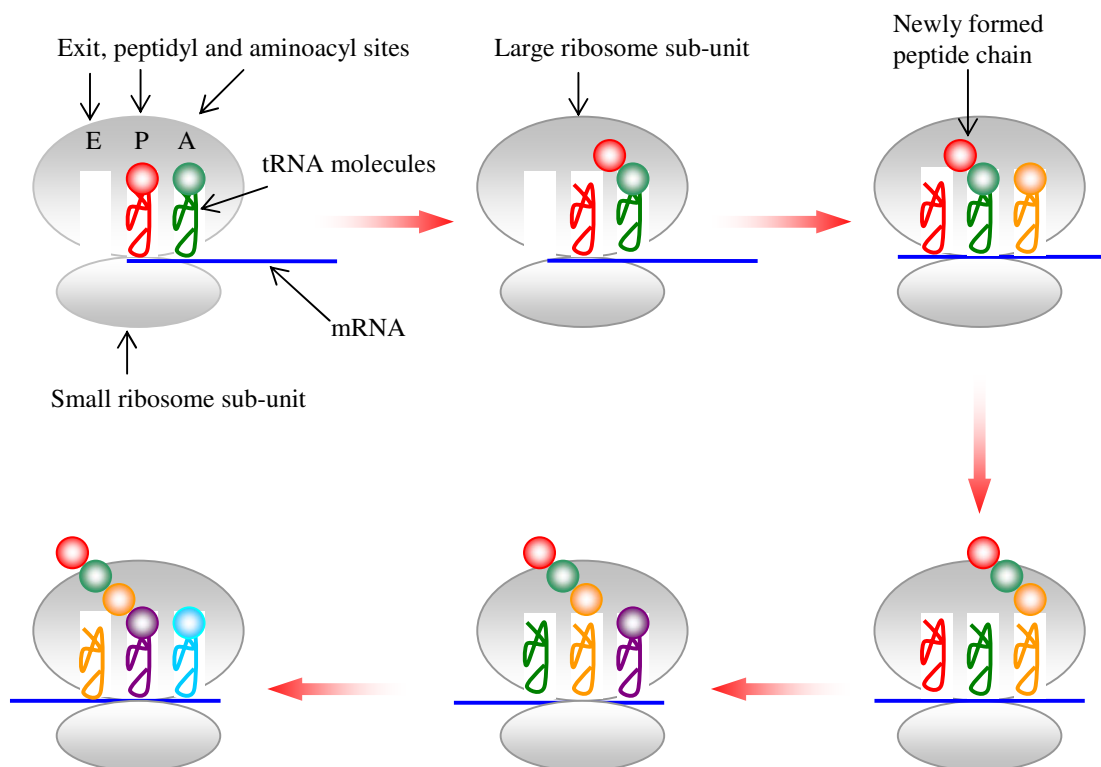


**Figure 1:13: Schematic showing the process of elongation.**

Translocation is the name given to the process where the ribosome moves along the mRNA chain, releasing the tRNA held at the E site and exposing the next available codon on the mRNA molecule. The translation of mRNA occurs in the 5'→3' direction.<sup>19, 24</sup>

### **Termination**

The elongation process is stopped once the ribosome reaches one of the stop codons (UAA, UGA and UAG) on the mRNA molecule.<sup>19</sup> These codons do not code for an amino acid, but ensures translation stops and the newly synthesised protein chain can be released from the tRNA by releasing factors.<sup>24</sup> The fate of the mRNA molecule depends on how much protein is required. Re-translation of mRNA can occur if the protein is in high demand.<sup>19</sup>

## **1.3 Inductively Coupled Plasma Mass Spectrometry**

Inductively coupled plasma mass spectrometry (ICP-MS) provides elemental and isotopic information and is capable of detecting most elements in the periodic table owing to its efficient ionisation source. This method is highly sensitive, selective, quantitative and exhibits a large linear range.<sup>10, 25</sup> This technique also boasts the capability of multi-elemental analysis, high sample throughput and isotope ratio measurements.<sup>12, 26-28</sup> In addition, numerous methods of sampling are available including; solution sample introduction, laser ablation<sup>15, 29, 30</sup> and the coupling of chromatographic techniques.<sup>28, 31-33</sup> For these reasons ICP-MS is an attractive alternative to traditional organic mass spectrometry techniques for detecting biomolecules.<sup>34-36</sup> ICP-MS instrumentation will be briefly discussed in the following section and then the applications in bioanalysis will be reviewed.

### **1.3.1 Instrumentation**

The instrumentation will be briefly discussed, although further sources of information will be referenced where appropriate. For simplicity, ICP-MS instrumentation will be broken down into five main sub-units, which are listed below, whilst the relative position of these sub-units in a conventional instrument are shown in Figure 1:14.

- Sample introduction system
- The plasma – ionisation
- The interface
- The mass analyser
- The detector

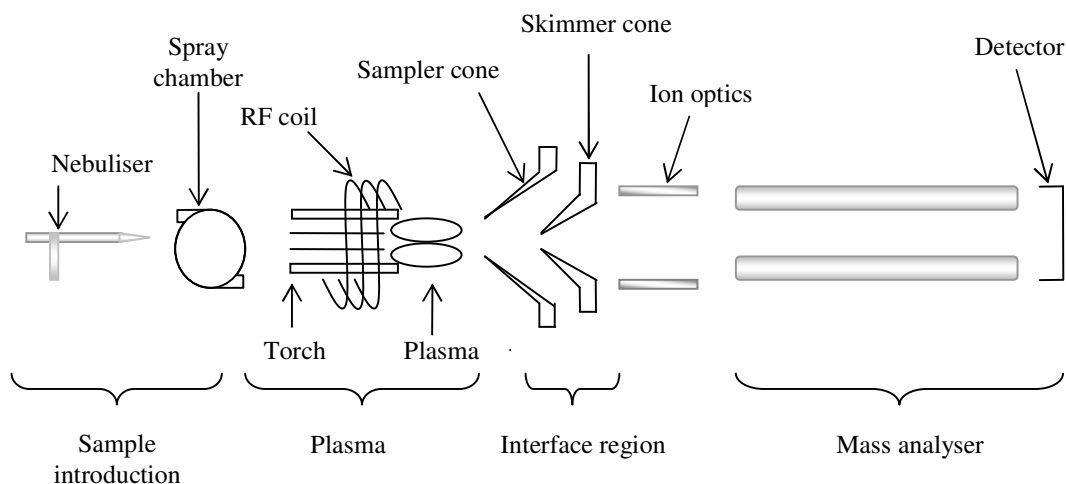


**Figure 1:14: Schematic diagram of a typical ICP-MS instrument.**

### 1.3.1.1 The Sample Introduction System

The standard way of introducing samples into the ICP ionisation source is through solution nebulisation. There are many types of commercially available nebuliser,<sup>27</sup> the most common being the concentric nebuliser, which is shown in Figure 1:15. The liquid sample is introduced through the central capillary, whilst a stream of argon gas is introduced at a right angle to the sample. As the sample and argon meet at the tip of the nebuliser, the sample is broken up into droplets due to the pneumatic action of the gas. A typical nebuliser uptake rate is approximately 1 ml min<sup>-1</sup>, although microflow nebulisers with uptake rates of between 20-600 µl min<sup>-1</sup> have gained popularity. The main advantage of low flow nebulisers is that only small sample volumes are required for analysis, this is particularly important in the biological field, where only limited sample may be available. Microflow nebulisers are available from a wide range of manufacturers' and are available in a wide range of materials to suit the application. Traditionally, nebulisers were

constructed of glass, however; other materials such as PFA, quartz and polyimide are also available to suit the application. For example, PFA nebulisers have the advantage of being inert and resistant to acids, bases and solvents.

The liquid droplets formed in the nebuliser aerosol vary in size. Only the small droplets, typically those  $<6\ \mu\text{m}$  in size are efficiently ionised in the plasma. Therefore, large droplets are removed with the aid of spray chambers. Like nebulisers, there are many types of spray chamber, but they all carry out the same function of excluding large aerosol droplets and allowing the smaller droplets to go through to the plasma.

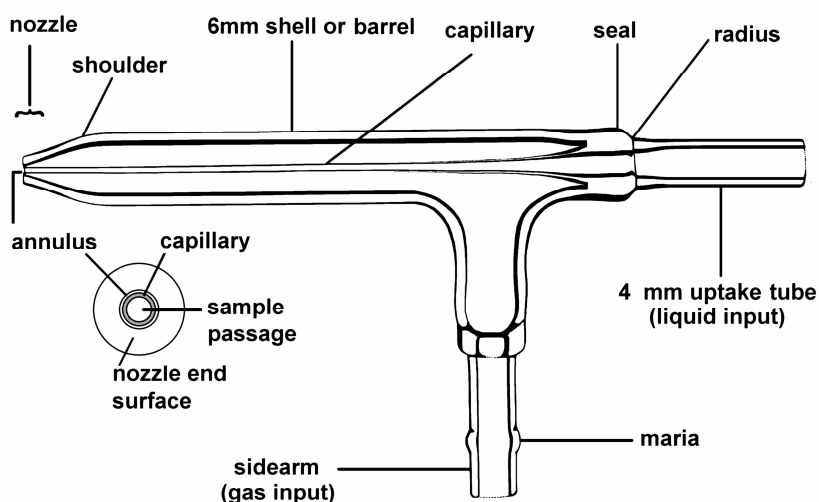


**Figure 1:15: Concentric nebuliser, reprinted with permission of Meinhard Glass Products (Colorado, USA).**

### 1.3.1.2 The Plasma

A mass spectrometric method requires the analyte to be ionised, which is achieved here using the plasma. A plasma is a partially or fully ionised gas, which in the case of the ICP is formed at atmospheric pressure. Argon gas, a torch, radio frequency (RF) coil and a RF generator are required for plasma generation.<sup>37</sup> The torch is usually made from quartz and consists of three concentric tubes; sample injector, outer and middle tube, as illustrated in Figure 1:16. The RF generator is generally operated between 1100-1500 W and provides RF power to the coil, this results in an oscillating current within the coil, which in turn

produces an electromagnetic field. A high voltage spark is then applied to the argon flowing through the torch to ionise the gas. This releases electrons which are then accelerated in the magnetic field and cause further ionisation of the gas by colliding with argon atoms. This results in a chain reaction, which effectively sustains the plasma and is known as the plasma discharge.<sup>27, 37</sup> The argon plasma is maintained at atmospheric pressure, but temperatures within the plasma range from 6000-10 000 K. At these temperatures almost everything is ionised, making ICP-MS a versatile analytical tool capable of detecting most elements in the periodic table.

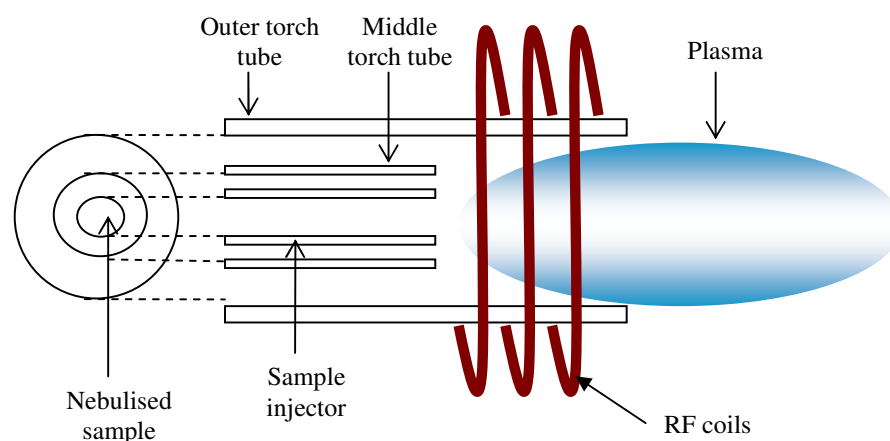


**Figure 1:16: RF coil and torch arrangement.**

### 1.3.1.3 The Interface Region

It was mentioned in the above section that the plasma is formed and maintained at atmospheric pressure. But, the mass analyser and detector are operated in a vacuum at approximate pressures of  $10^{-6}$  mbar. For this reason, the pressure has to be reduced so the analyte ions can be analysed in vacuum. The role of the interface is to sample ions from the atmospheric pressure plasma and step down the pressure, so ions can be extracted through to the analyser region.

Two water cooled metal cones (usually made from nickel or platinum) make up the interface region. The first larger cone is called the sampler cone and has an orifice of approximately 0.8-1.2 mm in the centre and is positioned at the end of the plasma. Behind

the sampler cone sits the skimmer cone, which has a slightly smaller orifice diameter of  $\sim 0.6$  mm.<sup>38</sup> The region between the two cones is called the expansion region and is evacuated to pressures of approximately 2-3 mbar, which is effectively an intermediate pressure between the atmospheric plasma and the vacuum of the analyser region. As the atmospheric pressure plasma ions are transported through the sampler cone, the plasma expands and the ions exceed the speed of sound. This results in a shock wave forming behind the sampler cone, within which is the zone of silence. Figure 1:17 illustrates the interface region along with the positions of the shock wave and zone of silence. The skimmer cone effectively sits within the zone of silence and samples ions from this region.<sup>27</sup>

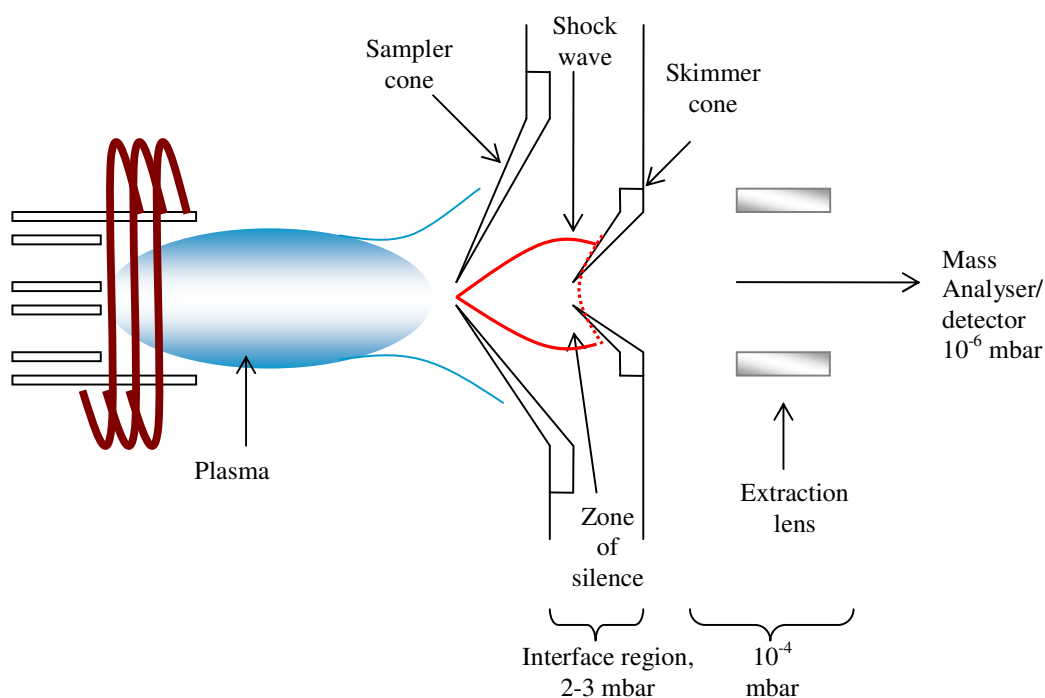


**Figure 1:17: The interface region.**

### 1.3.1.4 Mass Analyser and Detectors

The role of the mass analyser is to separate the ions that were generated in the plasma, according to their mass-to-charge ratio ( $m/z$ ). Once extracted through the interface region, the ion beam is directed towards the mass analyser by a series of lenses. These lenses are



essentially metal components that have voltages applied to them, and enable the ion beam to be electro-statically directed to the analyser.

There are many types of mass analyser available. These include; quadrupole, collision/reaction cell, time-of-flight (TOF), electrostatic and magnetic analysers. The quadrupole analysers are the most common, mainly due to their stability and relatively low cost. The theory and principles behind the operation of the collision/reaction cells and electrostatic and magnetic analysers will be discussed in sections 1.3.2.2 and 1.3.2.3 respectively. The theory of the remaining mass analysers is beyond the scope of this introduction, but such literature is available elsewhere.<sup>27</sup>

Once the plasma ions have been separated according to their  $m/z$  they are directed to a detection system. The most common detectors are those based on the electron multiplier and Faraday cup. The latter of these is normally employed for extending the dynamic range of the instrument and will be mentioned in more detail in section 1.3.2.3.<sup>27</sup>

### **1.3.2 Application of ICP-MS to Genomics Research**

There has been increasing interest over the past two decades concerning the analysis and detection of DNA. The inspiration for this interest has come from the ability to identify individual gene sequences and effectively decode the genome. There are many methods available for the detection and quantitative determination of DNA, each has their merits and drawbacks. The traditional method of detecting DNA is to covalently attach fluorescent labels to the molecule.<sup>39, 40</sup> The DNA-fluorophore conjugates are stable and can withstand the conditions used during polymerase chain reaction (PCR) procedures, but the fluorescent labels and instrumentation are costly.<sup>39</sup> Radioisotope labelling is another popular method of detecting and quantifying DNA,<sup>41</sup> as in the Post Labelling Assay (PLA), which employs <sup>32</sup>P.<sup>42</sup> Even though this technique is sensitive, there are concerns about safety, cost and time taken to carry out the analysis.

Surface Enhanced Resonance Raman Scattering (SERRS) has been recently employed for detecting and quantifying nucleotides. Raman signals of Raman active molecules are

enhanced by employing roughened metal surfaces and metal particles. Raman scattering can be dramatically enhanced by Ag and Au. Hence, nucleic acids and other biomolecules labelled with these metals can be detected at low levels.<sup>39, 43, 44</sup> Further Raman signal enhancement can be obtained by depositing Ag metal onto Au particles.<sup>39</sup> It has been reported that SERRS can exhibit limits of detection three orders of magnitudes lower than those obtained with fluorescent analysis methods.<sup>40</sup>

There have been numerous other methods of quantifying DNA, some of these methods based on optical,<sup>39</sup> electrical<sup>45</sup> and colorimetric methods.<sup>46</sup>

It has already been discussed that ICP-MS can be employed for the detection of biologically important molecules if these molecules contain ICP detectable elements. Table 1:4 summarises the metals associated with some commonly known metalloproteins. Conversely, if the biomolecule does not contain an element which is easily detected by ICP-MS, or lower limits of detection are required, the analyte can be labelled with an elemental tag.<sup>6, 13, 15-17, 47-49</sup>

**Table 1:4: Elements contained in typical metalloproteins.<sup>50</sup>**

Element	Metalloenzyme/ Metalloprotein
Fe	Transferrin, Ferritin, Catarase, Nitrogenase, Chitochrome.
Mo	Nitrogenase
Zn	Carbonic anhydrase, Carboxypeptidase, Alcohol dehydrogenase, Alkaline phosphatase, DNA polymerase and RNA polymerase.
Cu	Plastocyanine
Se	Gluthathion peroxidase
Ni	Urease

Phosphorus is contained in DNA and phosphorylated proteins, likewise S is contained in the amino acids methionine and cysteine, thus nucleic acids and proteins can be detected by ICP-MS.<sup>2</sup> However, the analysis of these two biologically important elements is fairly problematic due to the high ionisation potential of P and S and the abundance of polyatomic interferences at the low  $m/z$  ratios. These interferences originate from the

sample solvent and atmospheric gases. Table 1:5 summarises the ionisation potentials and common interferences associated with these two elements.

**Table 1:5: Ionisation potential and common interferences for P and S.**

Element	First Ionisation Potential (eV)	Common Interferences	Limit of Detection
P	10.5	$^{14}\text{N}^{16}\text{O}^1\text{H}^+$ , $^{15}\text{N}^{15}\text{N}^1\text{H}^+$ , $^{15}\text{N}^{16}\text{O}^+$	1 ng ml <sup>-1</sup> (quadrupole)
		$^{14}\text{N}^{17}\text{O}^+$ , $^{13}\text{C}^{18}\text{O}^+$ , $^{12}\text{C}^{18}\text{O}^1\text{H}^+$	<50 pg ml <sup>-1</sup> (high res)
S	10.4	$^{16}\text{O}_2^+$ , $^{14}\text{N}^{18}\text{O}^+$ , $^{14}\text{N}^{18}\text{O}^1\text{H}^+$ , $^{15}\text{N}^{17}\text{O}^+$ ,	20 ng ml <sup>-1</sup> (quadrupole)
		$^{15}\text{N}^{16}\text{O}^1\text{H}^+$	<50 pg ml <sup>-1</sup> (high res)

The introduction of collision/reaction cell technology and high resolution instruments has overcome the problems associated with P and S analysis. Both methods minimise interferences associated with these elements.<sup>2, 10</sup> However, the sensitivity of these two elements is still inferior compared to metal ions. The principles of collision cells and high resolution instruments will be discussed in subsequent sections, along with the recent applications of ICP-MS to biological analysis.

### 1.3.2.1 Cool Plasma

ICP-MS instruments are generally operated with a forward power of between 1100-1500 W, however, by decreasing the forward power to approximately 800 W, plasma temperature is lowered and a cool plasma is produced. Operating a cool plasma has the advantages of reducing many argon based polyatomic interferences that occur during normal operation. This is one method of minimising the formation of problematic interferences. However, the cool plasma approach is susceptible to matrix effects. For example, HPLC eluents containing organic solvents or buffers may cause severe matrix effects such as signal suppression.<sup>51</sup>

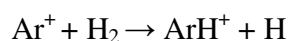
### 1.3.2.2 Collision/Reaction Cells

An alternative method of removing interferences is to move the analyte away from the problematic mass-to-charge ratio. This can be achieved by reacting the analyte ion with a

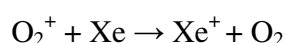
reactive gas to form an ion of higher  $m/z$ , which can then be measured. Alternatively, the interfering species can be converted to a different mass or to a neutral species, so the analyte ion can be measured free from interferences. Either method results in the removal of the interfering species. However, such reactions may also create increased interferences in other parts of the spectrum.<sup>51</sup> The removal of interferences takes place in a collision/reaction cell, which is a multipole consisting of either; a quadrupole, hexapole or octapole. The cell rods have RF (and DC in the case of quadrupole cells) applied to them. Collision/reaction cells therefore act as an ion focussing guide and not a mass separation device due to the RF only field.<sup>51</sup> Quadrupole cells however can be employed in the RF only or RF/DC mode, allowing mass separation in the latter case.<sup>52</sup> Once inside the cell, ions collide with a collision gas, which is present at low pressure and typically bled into the multipole at a rate of 0.5-10 ml min<sup>-1</sup>. The collision cell is generally operated in conjunction with a RF/DC quadrupole mass filter and is positioned between the interface and the mass analyser. Hence, the incoming ion beam enters the collision/reaction cell and undergoes the appropriate reactions before entering the quadrupole mass filter.

There are six main reactions which can take place within collision/reaction cells, these are summarised below along with examples of each reaction:

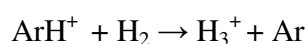
- i. Hydrogen atom transfer<sup>53</sup>



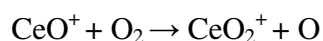
- ii. Charge transfer<sup>54</sup>



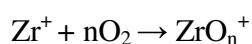
- iii. Proton transfer<sup>53</sup>



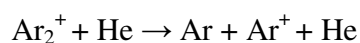
- iv. Condensation<sup>55</sup>



- v. Association<sup>55</sup>



- vi. Collisional dissociation



The charge transfer reaction between  $O_2^+$  and Xe was successfully used to reduce the  $^{32}O_2$  interference enabling  $^{32}S$  determination.<sup>54</sup>

Collision/reaction cells were originally developed for organic MS to generate daughter fragments/product ions from parent species. The chances of identifying the structure of the parent molecule increased with increasing collision induced fragmentation steps. However, in elemental MS polyatomic interferences had to be minimised, so secondary reactions were a disadvantage.<sup>51</sup> There are several types of collision/reaction cell for ICP-MS which are commercially available. Table 1:6 summarises a few of the commercially available collision/reaction cell ICP-MS instruments, along with the type of multipole employed.

**Table 1:6: Commercially available collision/reaction cells.**<sup>52</sup>

<b>Instrument</b>	<b>Manufacturer</b>	<b>Multipole</b>	<b>RF or DC potentials</b>
PQ ExCell	Thermo Elemental	Hexapole	RF only
7500c	Agilent	Octapole	RF only
Sciex Elan DRC	Perkin Elmer-Sciex	Quadrupole	RF only or RF and DC

The extent of cell reactions can be controlled by manipulating ion energy input. By making the collision/reaction cell potential more positive with respect to the plasma potential, or by using high reaction gas pressures, the ion kinetic energy can be retarded upon entering the cell. Slower ions tend to have larger reaction cross sections, therefore increasing cell reactions, this effect is known as the ion kinetic energy effect (IKEE).<sup>56, 57</sup> Dexter *et al.*, demonstrated that cell reactivity is significantly effected by IKEE for both exothermic and endothermic reactions, where exothermic reaction rates are increased by implementing IKEE and endothermic reaction rates are decreased.<sup>56</sup>

Unwanted secondary reactions can take place in the cell, resulting in unwanted product ions that need to be removed. These unwanted products from the collision cell are prevented from entering the quadrupole by discrimination by kinetic energy or mass.<sup>51</sup> By adjusting the collision cell bias in relation to the quadrupole, the unwanted products of the reaction can be prevented from entering the mass analyser. For example, by making the collision cell slightly less positive than the quadrupole, analyte ions which have more energy than the collision cell bias are transmitted to the quadrupole and the unwanted species which

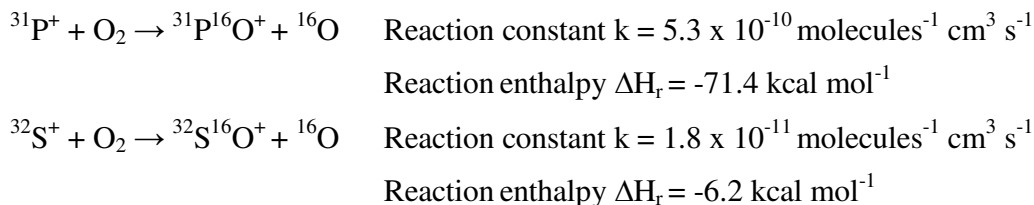
have the same energy as the cell bias are rejected.<sup>51</sup> This is commonly known as kinetic energy discrimination (KED).<sup>51, 58</sup> An energy barrier is effectively created between the collision cell and quadrupole. Only the analyte ions which have the required energy are able to cross this barrier and enter the quadrupole. Hence, collision/reaction cell rates can be increased and unwanted product ions from the cell removed by implementing IKEE and KED respectively.<sup>56</sup> KED can only be employed if there is a significant energy difference between the analyte and unwanted product ions.<sup>52, 57</sup> All three of the instruments detailed in Table 1:6 can employ KED.

Mass discrimination is another way of rejecting the unwanted collision cell products. The diffuse stability boundaries of higher order multipoles, makes them unable to discriminate by mass.<sup>51</sup> However, quadrupoles are mass discriminatory, since they operate in DC and RF modes and the stability boundaries are well defined. Since these cells can discriminate against mass, unwanted product ions are easily removed. Reactive gases such as ammonia and methane are commonly used, which are more effective at reducing interferences than the inert gases such as helium.<sup>51</sup> It should also be noted that the quadrupole cell can also discriminate using KED.<sup>52</sup>

The presence of a collision/reaction gas in the multipole results in decreased transmission of lighter ions due to scattering. This effect is more pronounced for heavier collision gases (e.g. O<sub>2</sub>) compared to lighter gases (e.g. He). Transmission of heavier ions can be enhanced by the presence of a collision gas,<sup>32</sup> since the lighter gas molecules prevent the heavier analyte ions diffusing out of the cell. This is referred to as collisional focussing and is relevant to both elemental and molecular mass spectrometry.<sup>27, 54</sup>

Collision/reaction cells have been used extensively for the detection of <sup>31</sup>P and <sup>32</sup>S.<sup>9-11, 32, 54, 59-61</sup> The common interferences for these elements are summarised in Table 1:5. One method of minimising interferences at *m/z* 31 and 32 is to employ oxygen collision gas to form the oxide of P or S. The corresponding oxide ion is then measured at *m/z* 47 and 48 for <sup>31</sup>P<sup>16</sup>O and <sup>32</sup>S<sup>16</sup>O respectively.<sup>9, 11, 59</sup> Thus, the *m/z* of P and S is

increased by 16, which moves the analytes away from the polyatomic interferences at  $m/z$  31 and 32.



The above data (obtained from reference 9) shows that the reactions of S and P with oxygen are kinetically and thermodynamically favourable. However, the reaction of oxygen with the major interferences;  $\text{O}_2^+$ ,  $\text{NO}^+$  and  $\text{NOH}^+$  do not occur due to the reactions being kinetically and thermodynamically unfavourable in the cell conditions.<sup>9</sup> Bandura *et al.*, also noted that  ${}^{47,48}\text{Ti}$  could interfere with  ${}^{31}\text{P}^{16}\text{O}$  and  ${}^{32}\text{S}^{16}\text{O}$ , however, Ti readily reacts with oxygen at a rate comparable to P and S reaction rates ( $k = 5.0 \times 10^{-10}$ ).<sup>9</sup> Thus, any  ${}^{47,48}\text{Ti}$  in a sample would be oxidised to  $\text{TiO}^+$  and thus be removed from  $m/z$  47 and 48.

An alternative collision cell reaction for the direct determination of  ${}^{31}\text{P}$  employs He collision gas in conjunction with a collision/reaction cell.<sup>1, 60-62</sup> The interfering polyatomic ions (predominantly  ${}^{14}\text{N}^{16}\text{O}^1\text{H}$  and  ${}^{15}\text{N}^{16}\text{O}$ ) collide with the He gas to a greater extent than the elemental  ${}^{31}\text{P}$  analyte, due to their greater cross sectional area. As a result, the polyatomic ions decelerate and lose energy rapidly due to the collisions. Then by applying KED, an energy barrier is essentially created that allows the higher energy  ${}^{31}\text{P}$  ions through to the mass analyser, but prevents the lower energy polyatomic ions being transmitted.<sup>60</sup> In addition to employing He for reducing polyatomic interferences, Mason *et al.*, reduced interfering polyatomic ions at  $m/z$  32 by employing a hexapole collision cell with mixtures of He, Xe and  $\text{H}_2$  gases.<sup>54</sup>

### 1.3.2.3 High Resolution ICP-MS

Resolution is defined from the following equation;  $R = m/\Delta m$ , where  $m$  is the analyte mass and  $\Delta m$  is the peak width at 5% peak height. Quadrupole based instruments have typical mass resolution capabilities of 300, yet resolutions of 10 000 are possible with high resolution instruments.<sup>27, 63</sup> The improved resolving power of high resolution instruments

enables P/S to be separated from their corresponding polyatomic interferences, and thus enables P and S to be determined directly and avoids using collision/reaction cells. Table 1:7 shows the resolution required to separate P and S from some common interferences, such resolutions cannot be achieved with a standard quadrupole based instrument.

**Table 1:7: Resolution required to separate P and S from their common interferences.**<sup>27, 64</sup>

Isotope	Interference	Resolution
<sup>31</sup> P	<sup>14</sup> N <sup>16</sup> O <sup>1</sup> H	970
	<sup>16</sup> O <sub>2</sub>	1800
<sup>32</sup> S	<sup>14</sup> N <sup>18</sup> O	1061
	<sup>15</sup> N <sup>16</sup> O <sup>1</sup> H	1040
	<sup>14</sup> N <sup>16</sup> O <sup>1</sup> H <sup>1</sup> H	770

High resolution instruments employ two types of analyser; electrostatic and magnetic mass analysers. The magnetic analyser can be placed before the electrostatic analyser (ESA), in what is known as the reversed Nier-Johnson geometry, whereas the alternative arrangement is referred to as the forward Nier-Johnson geometry.<sup>27</sup> The reversed Nier-Johnson geometry is employed in the Element 2 sector field instrument; the reasons for this will be explained later in this section; whilst the forward geometry is employed in the Thermo-Finnigan Neptune and Nu Plasma multi-collector instruments. Figure 1:18 shows a schematic of a typical reversed Nier-Johnson magnetic sector instrument.



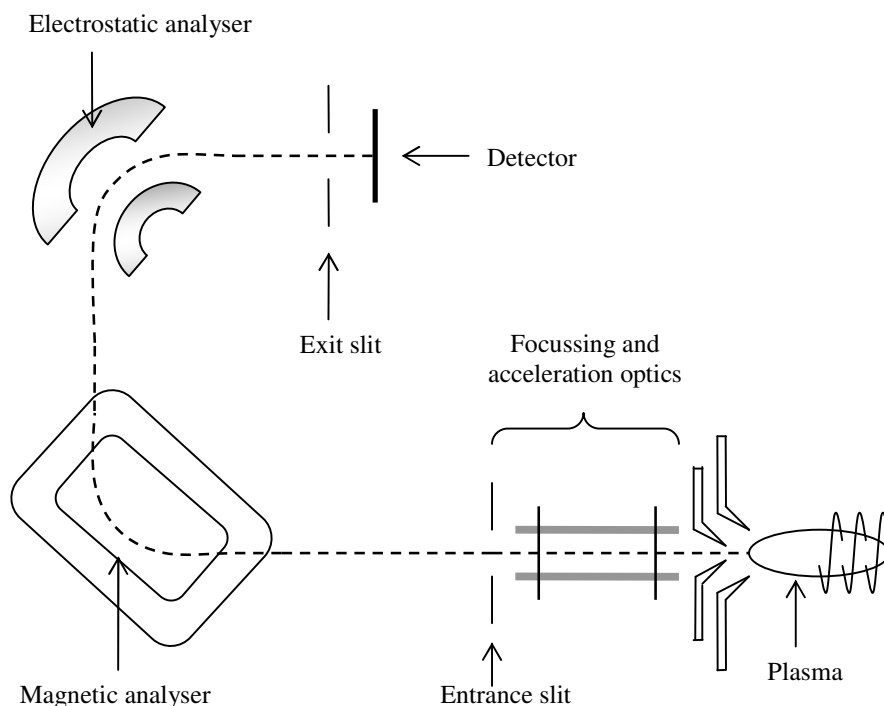


**Figure 1:18: Schematic of a reverse Nier-Johnson magnetic sector instrument.**

Ions formed in the plasma are accelerated along a curved flight path at approximately 8 kV where they pass through an ion lens system before reaching the magnetic analyser, which is water cooled to provide good mass stability.<sup>65</sup> The magnetic field is perpendicular to the flight path and is both mass and energy discriminatory. Ions are separated according to mass due to the fact that ions are deflected in the magnetic field according to their mass-to-charge ratio.<sup>27, 66</sup>

A limitation on resolution in ICP-MS is the wide ion energy spread. The ESA is therefore energy focussing and helps improve resolution.<sup>12</sup> By having an ESA after the magnet, the energies of the ions are focussed before reaching the detector,<sup>66</sup> which in turn lowers the overall energy spread of the ions. A 2 eV kinetic energy spread has been reported for ions entering the Element 2 (Thermo Finnigan, Bremen, Germany) mass spectrometer.<sup>67</sup> This has the effect of improving abundance sensitivity and hence resolution; which is an obvious advantage in ICP-MS.<sup>27</sup> An ESA typically consist of two curved plates with DC voltage applied to them, the inner plate is usually negatively charged and the outer plate positively

charged. Hence, the inner plate attracts ions and the outer plate repels them, thus ions are focussed and deflected as they pass through the two plates.<sup>27,65</sup>

Ions are separated according to  $m/z$  only when these two mass analysers are used in conjunction, since the magnetic analyser is mass and energy discriminatory and the ESA is energy only.<sup>27</sup> Both analysers provide angular focussing, that is the ion beam is focussed as it exits the analyser. For this reason, such instruments are referred to as double focussing.<sup>12,27</sup>

Electron multiplier detectors are commonly employed in ICP-MS instruments. The detection system used in the Element 2 (Thermo Finnigan, Bremen, Germany) is a dual mode secondary electron multiplier (SEM). After passing through the magnetic and electrostatic analyser, the ion beam hits a conversion dynode where electrons are produced. These electrons are then directed to the SEM where secondary electrons are formed upon impact with the multiplier surface. The secondary electrons impact again on the electron multiplier surface forming more and more electrons, which results in a cascade effect. The current from the released electrons can then be converted to a signal. Counting and analogue SEM detection modes are available in the Element 2. Analogue detection mode allows elements of approximately  $1 \text{ mg l}^{-1}$  concentration to be measured. A Faraday detector can be employed for extending the linear range further, with concentrations of approximately  $1000 \text{ mg l}^{-1}$  potentially measured. A Faraday cup is essentially a hollow device which the ion beam enters. The charge (positively charged ion beam) is collected on a capacitor which is then discharged, the ion detection system then processes the number of discharges.<sup>65</sup> The approximate intensity (counts per second) that each detector operates along with the approximate concentrations measurable with each detector is shown in Figure 1:19 (data taken from reference 68).

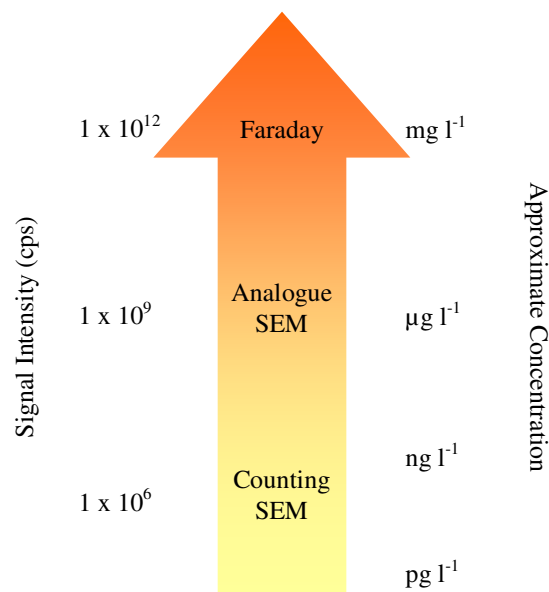


**Figure 1:19: Approximate signal intensity and concentration range of each detector for the Element 2XR.** <sup>68</sup>

The resolution of most commercial instruments can be adjusted. For example, the Element 2 is a second generation high resolution instrument and has three fixed resolution settings; low (resolution  $\sim 300$ ), medium (resolution  $\sim 4000$ ) and high (resolution  $\sim 10\,000$ ). The resolution is set by adjusting the widths of slits which are positioned at the entrance and exit of the mass spectrometer, these slits are known as the entrance and exit slits.<sup>12</sup> Low resolution is achieved by using wide slits, as the slit width decreases the resolution increases. Thus, high resolution has the disadvantage of degrading sensitivity due to the narrow slit widths. At a resolution setting of 1460 which is needed to resolve  $^{31}\text{P}$  from  $^{15}\text{N}^{16}\text{O}$ , ion transmission is only 53%.<sup>63</sup> Only 1-2% ion transmission is obtained in high resolution setting compared to low resolution. This can be a problem if low limits of detection are needed.

Flat topped peaks are obtained when operating in low resolution mode, which are useful for obtaining precise measurements, since the signal intensity should be the same wherever the peak is sampled due to the flat top.<sup>12</sup> The peak shape becomes progressively more triangular as the resolution is increased. This causes measurements to become less precise,

since signal intensity will vary considerably depending on where the peak is sampled.<sup>27</sup> In high resolution mass spectrometry, peak widths become progressively narrower at the low mass end of the spectrum and as resolution increases. This is because peak width is a function of both mass and resolution, as defined by the equation  $R = m/\Delta m$ .<sup>67</sup> Despite the reduction in sensitivity upon increasing resolving power, these instruments by character have good sensitivity and low background levels in low resolution mode. As a result, heavier mass elements such as Au and Pt which only require low resolution can exhibit extremely low limits of detection.<sup>12, 27, 63</sup>

Two modes of scanning are available for high resolution instruments; magnetic scanning and voltage scanning. A Hall probe controls the magnetic field in the magnetic analyser, and is located within the magnet gap.<sup>27</sup> Magnetic scanning has the disadvantage of being very slow due to the time required for the magnet to move between masses and settle.<sup>27, 63, 67</sup> An additional disadvantage of magnetic analysers is a phenomenon known as magnet hysteresis.<sup>69</sup> If a magnetic field is applied to a material, the material will experience a change due to the applied magnetic field, but it will not return back to its original state when the applied magnetic field is removed. Another field of opposite direction is required to return the material back to its original state, which ultimately increases the time of a magnet scan in mass spectrometry. Voltage scanning has the advantage of being much faster.<sup>64</sup> In this mode of measurement, the magnetic field is held constant whilst the voltage is varied to transmit the analyte ions. Voltage scanning can measure a peak up to 30% above the mass where the magnet is settled, hence the magnet does not necessarily have to be moved when voltage scanning is employed.<sup>67</sup>

Along with a choice of voltage or magnet scanning, the Element 2 has two scanning modes; mass accuracy and speed. The choice of scan is dependent upon the application. For standard quantitative analysis of solutions, mass accuracy should be implemented. This scanning mode is set by default in the instrument software and is used when mass accuracy is important and not scanning speed. Conversely, for applications requiring faster magnet scanning, such as chromatographic and laser ablation applications, speed scanning should be selected.<sup>70</sup>

There are three fixed magnet positions on the Element 2; zero mass ( $m/z$  0), rest mass ( $m/z$  ~100) and high mass ( $m/z$ ~ 254). The two different scanning modes refer to the way the magnet jumps between these masses during the scanning cycle. Each method will be discussed in turn.<sup>70</sup>

### **Mass Accuracy**

The magnet jump cycle during a mass accuracy scan is summarised in Figure 1:20. Before the measurement of the analytes begins, the magnet goes through an initial scanning cycle, where the magnet jumps from the rest mass to the high mass and then to the zero mass point.<sup>70</sup> The final step in the initial magnet cycle is for the magnet to jump from the zero mass point to the first analyte isotope.<sup>70</sup> Only after the initial scan are the isotopes of interest scanned and measured. However, before returning to the first analyte isotope for a repeat scan, the magnet again jumps to the high mass then the zero mass point. After the required number of scans has been carried out, the magnet returns to the rest mass. The continual jumping of the magnet between the fixed reference points during a scan inevitably increases analysis time, especially when multiple isotopes are to be determined.<sup>70</sup>

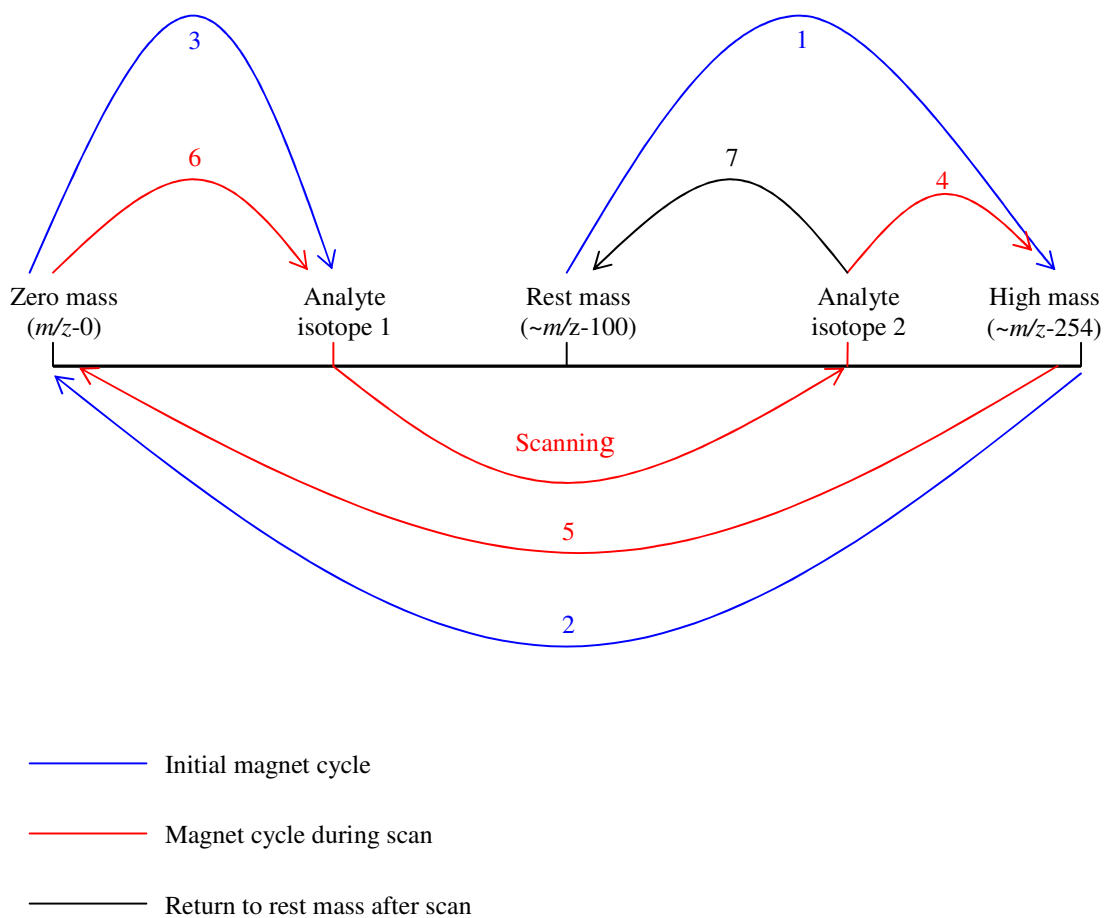


**Figure 1:20: Magnet cycle during mass accuracy scan.**

### Speed Scanning

This scanning mode has a much shorter scanning cycle, thus less time is spent moving and settling between masses, which has the effect of decreasing analysis times. This is particularly important where fast transient peaks are to be measured and as many data points as possible are required. The schematic in Figure 1:21 summarises the magnet movement during a speed scan. It is important to note that an initial magnet cycle is not conducted during a speed scan. Also, the magnet does not jump to the high mass, followed by the zero mass point during the scan cycle as observed with mass accuracy scanning. Ultimately, speed scanning involves the magnet repeatedly jumping to and from the selected isotopes only.<sup>70</sup> Again once scanning is complete, the magnet returns to the rest

mass. Settling time refers to the time taken for the magnet to move and settle between the selected isotopes during a scan. The default settling times given in a method can be amended to decrease analysis time further, but caution should be taken when reducing settling times too much, since this will have the effect of decreased signal intensity for the selected analyte.

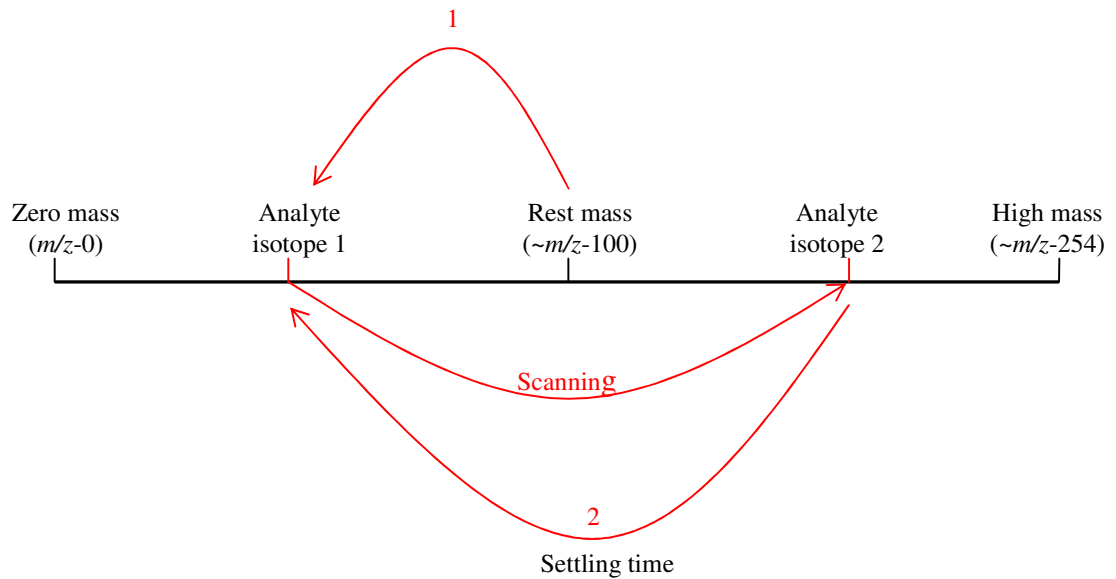


**Figure 1:21: Magnet cycle during speed scanning.**

## 1.4 Linear Ion Trap Mass Spectrometry

Since all structural information is lost during ICP analysis, complementary analytical techniques are advantageous for providing such information. Organic mass spectrometry allows for structural analysis and can be used as a complementary technique to ICP-MS as opposed to a competing technique.<sup>1, 2, 4, 5, 49</sup> Both elemental and structural information can be obtained when using the two mass spectrometry methods in parallel, which may be useful in the fields of genomics and proteomics.<sup>49</sup>

Linear ion trap instruments have found a niche within genomic and proteomic research, predominantly for the determination of nucleic acid and peptide sequences.<sup>71-74</sup> Figure 1:22 shows a schematic of a typical ion trap instrument. There are parallels between the instrumentation found in organic and inorganic mass spectrometers. The ion trap employs an atmospheric pressure ionisation source, ion optics/ion guides, mass analyser to isolate ions of interest and finally a detection system. This is similar to elemental mass spectrometry; however, the principles of operation of some aspects do vary between the two mass spectrometry techniques as will be discussed.

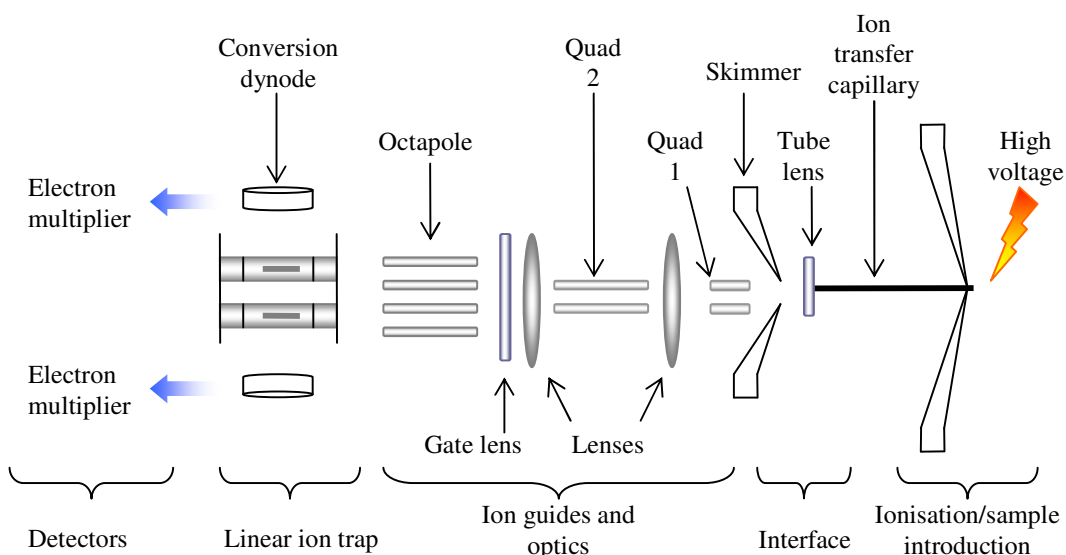


**Figure 1:22: Schematic showing the linear ion trap instrumentation of a Thermo Finnigan LTQ.**



## 1.4.1 Instrumentation

### 1.4.1.1 Ionisation

There are many techniques available for analyte ionisation, these include; electrospray ionisation (ESI), atmospheric pressure chemical ionisation (APCI) and atmospheric pressure photoionisation (APPI) amongst others. The choice of ionisation technique depends on the nature of the sample and the application. Only electrospray ionisation (ESI) will be discussed here due to its relevance in this project. Information regarding the other ionisation techniques is available elsewhere.<sup>75-77</sup>

ESI can be applied to any compound that forms an ion in solution, making it especially good for biological molecules that often are highly charged and polar. For example, nucleic acids contain nitrogen containing nucleobases, which can become protonated and thus carry a positive charge in solution. Therefore, high molecular weight molecules such as nucleic acids and proteins can be analysed when using ESI due to multiple charging of the analyte ions, which creates a range of mass-to-charge ratios that most mass spectrometers can comfortably analyse.<sup>78</sup> The process of ESI is illustrated in Figure 1:23. A solution containing the analyte flows through a fused silica capillary towards the ESI needle, which has a high voltage applied to it, typically in the region of 3-6 kV.<sup>76, 79</sup> The liquid surface is disrupted by the applied electric field, which results in a fine mist containing small charged droplets being formed. This is known as an electrospray, although nebulisation can also be assisted with a nebuliser gas.<sup>79, 80</sup> There are two accepted mechanisms of ion formation; charge residue model (CRM) and ion evaporation model (IEM).<sup>81</sup> In both cases the sample solvent evaporates from the droplets, which results in increased charge density on the droplets, due to their decreasing size. According to the charge residue model, the electrostatic repulsion within the droplet will eventually exceed the surface tension of the sample solvent. At this point, which is known as the Rayleigh stability limit or coulomb explosion,<sup>76, 82</sup> the droplets divide into even smaller droplets. The process of dividing droplets is repeated until all the solvent is removed, at which point the analyte/parent ions are converted to a free ion in the gas phase.<sup>78</sup> In the case of the ion evaporation model, ions

are evaporated from the droplet at a certain droplet size due to coulombic repulsion.<sup>81</sup> The entire electrospray process occurs at atmospheric pressure.

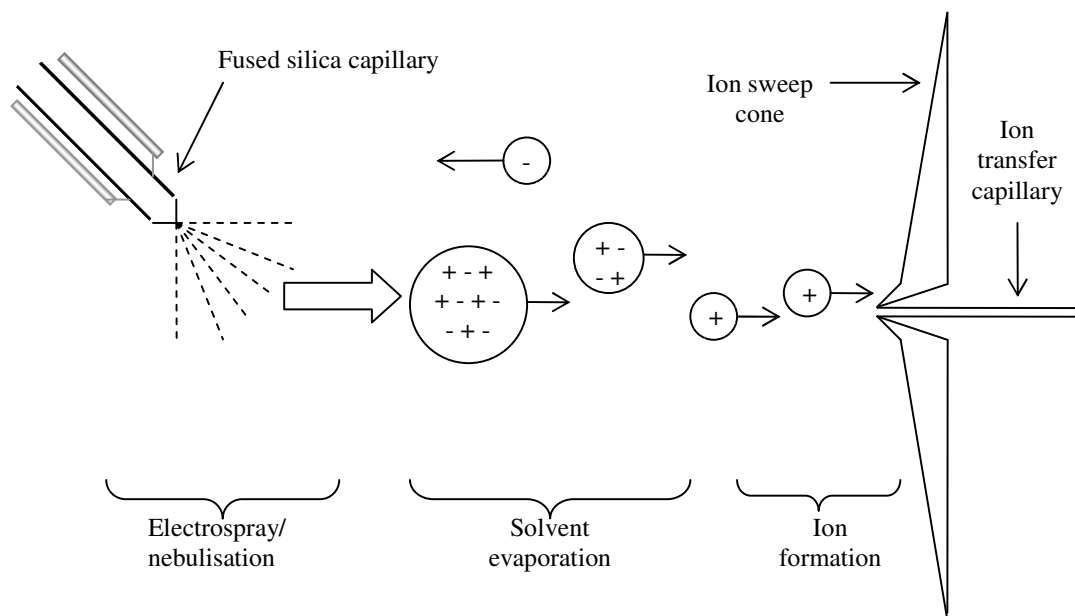


**Figure 1:23: ESI process in positive ion mode.**

The efficiency of ESI depends on the applied voltage, droplet size, volatility and surface tension of the sample solvent. A compound with high charge will have improved ionisation compared to a lower charged compound.<sup>78</sup> Likewise, a higher voltage is required for producing a stable electrospray for high surface tension solvents.<sup>79</sup>

Positive or negative ions can be generated at the source depending on the application. If positive ions are to be analysed the ESI needle is positively charged, so positive ions are repelled from the needle and ejected into the transfer capillary. Likewise, the needle is negatively charged for the analysis of negative ions. When sample quantity is restricted and only small sample volumes are available, nanospray ionisation (NSI) is possible. The ionisation process is identical to ESI, but ionisation and mass spectrometry analysis is possible with sample volumes as low as 1  $\mu$ l.

Matrix-assisted laser desorption ionisation (MALDI) is also widely used for the analysis of large biomolecules such as DNA and proteins.<sup>75, 83, 84</sup> As its name suggests, the ionisation

process involves the use of a laser (ultraviolet or infrared) to ionise the analyte with the aid of a matrix. The matrix contains small organic molecules that strongly absorb the laser incident light.<sup>75</sup> Singly charged ions are predominantly formed by MALDI as opposed to multiply charged species observed with ESI, and Time-of-flight (TOF) mass analysers are typically employed. In addition, MALDI is more tolerant to salts, buffers and solvents, although the removal of such contaminants improves the quality of the mass spectra. Conversely, the presence of buffers in ESI can contaminate the source and create very complicated spectra due to the formation of adducts. Therefore, volatile buffers at low concentration are preferred for ESI.<sup>75</sup>

#### **1.4.1.2 Interface**

The ions formed in the ionisation source are transferred to the mass analyser *via* the transfer capillary, which is heated to approximately 270 °C for ESI. Upon exiting the transfer capillary, the ions travel through the tube lens where the ions are focussed for transmission through the skimmer. As in ICP, the skimmer acts to step down the pressure between the interface (~1.3 mbar) and the mass analyser region (~0.067 mbar).<sup>78</sup>

#### **1.4.1.3 Ion Guides and Optics**

Once the ions are transmitted through the skimmer, they travel through a series of ion guides and lens. Two quadrupoles and an octapole help guide the ions to the mass analyser. Quadrupole 1 and 2 consists of four square profile rods, which have RF and DC voltages applied to them. The ions initially enter quadrupole 1; those ions with a stable path through the quadrupole are transmitted. Subsequently, the ions are guided by a lens to quadrupole 2. Finally, the ions are guided through the gate lens followed by the octapole and then the mass analyser. The injection of ions into the mass analyser is controlled by the gate lens (see Figure 1:22).<sup>78</sup>

#### 1.4.1.4 Quadrupole Linear Ion Trap Mass Analyser

Like a conventional quadrupole, the quadrupole linear ion trap consists of the four parallel rods, but the rods of a linear ion trap are cut into three separate sections; two end sections and a centre section. The centre rod is 37 mm in length and the two end sections are 12 mm in length. Two of the central rods have a 30 x 0.25 mm slit cut into them to allow ions to be ejected from the analyser, these rods are therefore known as the exit rods.<sup>78, 85</sup>

A DC voltage is applied to each of the quadrupole rod sections, the central section having a lower potential than the two end sections, which has the effect of trapping the incoming ions in the axial direction.<sup>78, 85</sup> Table 1:8 shows the potentials applied to each rod section during positive ion storage and analysis. A large potential well is created in the centre quadrupole section during mass analysis, due to the increased potential of +20 V on the two end sections. The potentials are reversed for negative ion storage and analysis.<sup>78</sup>

**Table 1:8: DC potentials of the linear ion trap during positive ion storage and transmission.<sup>78</sup>**

Rod Section	Ion Storage Potential (V)	Mass Analysis Potential (V)
Front	-9	+20
Centre	-14	-14
Back	-12	+20

Storage in the radial direction is achieved by applying AC voltages to the quadrupole rods. The frequency of the AC voltage is constant and in the radio frequency range, but the amplitude varies, this voltage is referred to as the main RF voltage.<sup>78</sup> During ion storage the main RF voltage is low; so ions are stable within the quadrupole; this is called the RF storage voltage. During analysis, the RF potential is ramped at a constant rate which has the effect of causing ions of increasing mass-to-charge ratio to become unstable and oscillate in the radial direction. Eventually, the ions become so unstable that they are ejected through the exit rods. The resonance voltage is the voltage at which the ion of defined  $m/z$  is ejected from the quadrupole ion trap. The ejected ions impinge on the conversion dynodes to produce ions which are consequently directed to electron multiplier detectors.<sup>78</sup>

The ion storage, isolation, fragmentation and scan out events that take place in the trap are summarised below and are illustrated in Figure 1:24-Figure 1:27, which only show the central quadrupole sections for diagram simplicity.

i. Ion Storage

- DC voltages applied to the three quadrupole rod sections, the central sections having a lower voltage to create a potential well and trap ions in the axial (z) direction.
- Main RF voltage amplitude is low, so ions are stable in the radial (x,y) direction and therefore confined in the mass analyser. This is known as the storage voltage.<sup>78</sup>

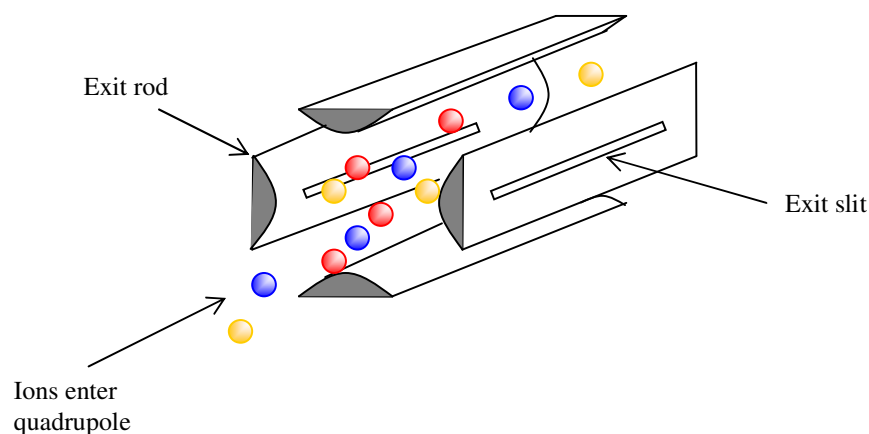


**Figure 1:24: Ion Storage.**

ii. Ion Isolation

- Applicable to single ion monitoring (SIM), selected reaction monitoring (SRM), consecutive reaction monitoring (CRM) and general tandem MS ( $MS^n$ ).
- AC voltage is applied to the exit rods in what is called the ion isolation waveform voltage.<sup>78</sup>
- An ion of specified  $m/z$  is trapped by the main RF and ion isolation waveform, whilst all other ions are ejected from the ion trap.

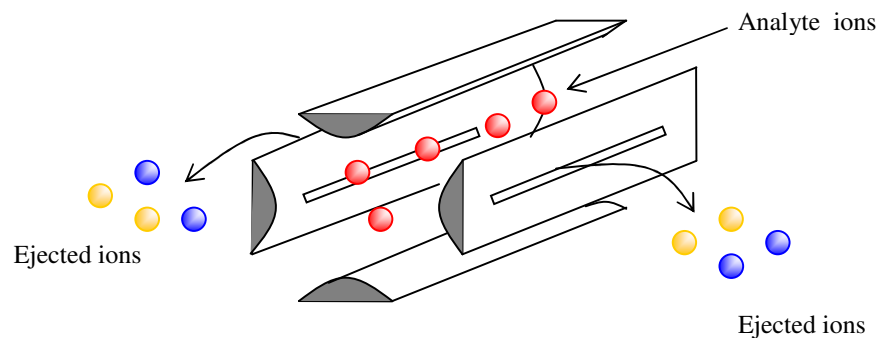


**Figure 1:25: Ion isolation.**

iii. Collision/Fragmentation

- Applicable to SRM, CRM and MS<sup>n</sup>.
- Ion movement in the radial direction is stimulated by voltages, which are applied to the exit rods and is known as the resonance excitation voltage.<sup>78</sup>
- This voltage is not sufficient to eject the ions, but causes the ions to collide with He.<sup>78</sup>
- Eventually the parent ion will fragment due to successive collisions with He, to form product ions.

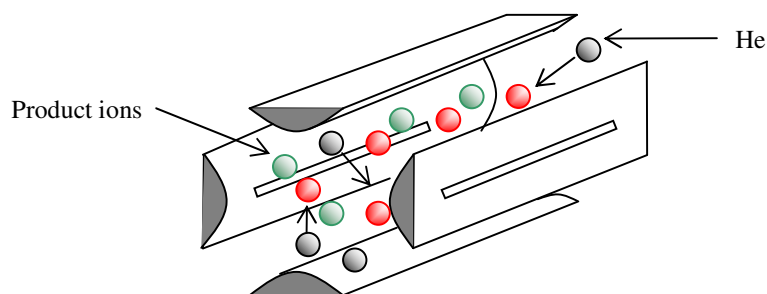


**Figure 1:26 Parent ion fragmentation.**

iv. Ion Scan Out

- Ion ejection is facilitated by the resonance ejection RF voltage that is applied to the exit rods.<sup>78</sup>
- The amplitude of the resonance ejection RF voltage is ramped to resonate the ions.<sup>78</sup>

- During resonance the ion moves further away from the centre of the trap. Space charge effects are smaller and the main RF voltage is stronger the further away from the trap centre, which has the effect of ejecting the ion.<sup>78</sup>

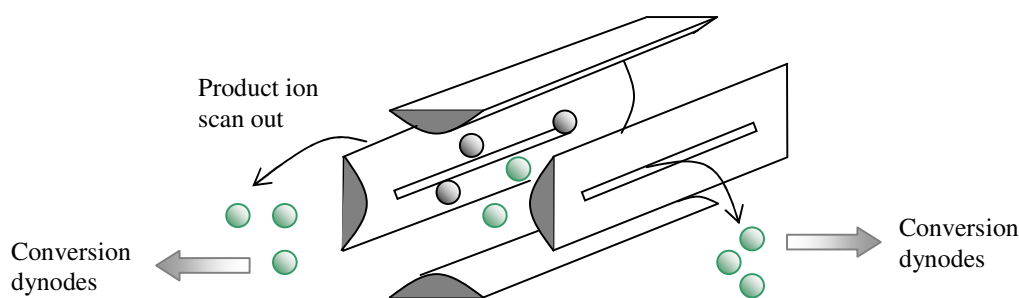


**Figure 1:27: Product ion scan out from the linear ion trap.**

Linear ion traps have numerous advantages over the traditional three dimensional ion traps. Firstly, linear ion traps exhibit enhanced trapping efficiencies due to the reduced axial motion induced by collisions with the He dampening gas.<sup>86</sup> Space charge effects are defined as the repulsion of ions of like charge which inevitably occurs in mass spectrometry.<sup>87</sup> This effect is detrimental to mass spectrometer performance, since it results in broad peaks, loss of resolution and reduced sensitivity.<sup>86, 88</sup> Since linear ion traps are larger than their three dimensional counterparts, they are capable of storing more ions before space charge effects become apparent.<sup>85, 86</sup> In addition, ions are focussed along the axial direction, in a line along the centre of the linear ion trap, compared to point focussing with three dimensional traps. It has been reported that line focussing may be beneficial in minimising space charge effects.<sup>86</sup>

The ion trap allows the analyte ion with defined  $m/z$  to be stored, fragmented and then transmitted to the detector. Unlike ICP-MS where fragmentation and secondary reactions are to be avoided within collision/reaction cells, molecular mass spectrometry utilises such reactions for structure elucidation.<sup>75</sup> As discussed above, the mass analyser is filled with He gas which can be used to induce fragmentation of the parent ions through collisions. The resulting fragment ions are called product ions, which can be analysed. This type of mass analysis can be repeated many times depending on how much structural information is

required for a compound, since each fragmentation step reveals more information on structure. An MS/MS experiment employs two stages of ion selection and fragmentation, followed by analysis of the product ions. However,  $MS^n$  can be used, where  $n$  is the number of stages in the mass analysis.

As well as inducing fragmentation, He gas also acts as a buffering gas and induces collisional focusing. The kinetic energy of the injected ions is reduced in the ion trap by collisions with He which ultimately prevents ions diffusing out of the quadrupole, but keeps them near the centre of the analyser. This has the effect of increasing sensitivity.<sup>75, 78, 85</sup>

#### **1.4.1.5 Detector**

Noise is minimised in the linear ion trap by orientating the two electron multiplier detectors off-axis (Figure 1:22). As ions are ejected from the linear ion trap *via* the exit rod slits, they impinge on a conversion dynode where secondary particles are produced upon impact. If the instrument is operated in negative ion mode, the conversion dynode will release positively charged particles, conversely, negative particles are released from the conversion dynode when in positive ion mode.<sup>78</sup> The secondary charged particles are then directed towards the off-axis secondary electron multiplier which works in a similar manner to those described in section 1.3.2.3.

#### **1.4.2 Scanning Modes**

It has been discussed that the linear ion trap is capable of trapping a parent ion and either analysing this ion directly in a single MS experiment, or fragmenting the ion once or multiple times with He to produce parent ions. In addition, there are several types of scan available for obtaining information on a particular ion, namely; full scan, selected ion monitoring (SIM), selected reaction monitoring (SRM), consecutive reaction monitoring (CRM) and zoom scan. Figure 1:28 shows the scanning modes available.



#### 1.4.2.1 Full Scan

The full scan mode allows all the ions associated with the sample to be detected, since all the parent ions are sequentially scanned out of the ion trap. Full scanning lacks sensitivity, but it does provide a lot of information. Full scanning is also very slow, since all the ions in a given mass range specified by the operator are scanned out of the ion trap and detected.<sup>78</sup>

#### 1.4.2.2 Selected Ion Monitoring (SIM)

In SIM target ions of specified  $m/z$  are only monitored, thus this scan mode is more sensitive and faster than the full scan, since more time is spent monitoring the ions of interest and ejecting the unwanted ions. The parent ions are stored in the ion trap and all the ions apart from those of interest are scanned out of the mass analyser. Then a selected ion mass spectrum is created by scanning out of the parent ions of interest. However, if another compound other than the analyte forms parent ions at the same  $m/z$  as the ions of interest, they will also be detected as the target ion, therefore, SIM gives low specificity.<sup>78</sup>

#### 1.4.2.3 Selected Reaction Monitoring (SRM)

SRM is similar to SIM, but it is a two stage MS scan that is more specific. The parent ions are stored in the ion trap and all the ions except those of interest (which have been specified) are scanned out of the trap. The parent ions of interest are then fragmented with He to form product ions. The product ions of interest which have also been specified are selected whilst all the other ions are ejected from the mass analyser. A SRM mass spectrum is then obtained by scanning out the product ions of interest.<sup>78</sup> SRM is more specific than SIM, since both the parent and corresponding product ions are monitored. Hence, it is unlikely that an interfering compound will form a parent ion and product ion of the same  $m/z$  as the analyte.<sup>75, 78</sup>

#### 1.4.2.4 Consecutive Reaction Monitoring (CRM)

CRM is similar to SIM and SRM, but involves more MS steps, where  $MS^n$  can be achieved. As with SIM and SRM, the parent ions are stored in the ion trap and all ions except those of specified  $m/z$  are ejected. Fragmentation of the selected parent ion is then achieved with the

The collision gas and the product ion of interest is selected, whilst all the other product ions are ejected. The selected product ion effectively becomes the new parent ion, which is fragmented further to yield new product ions. The process is repeated where the entire product ions except the one specified is ejected out of the mass analyser, whilst the selected product ion then becomes the new parent ion for further fragmentation. This process is repeated up to MS<sup>10</sup> and has the advantage of increasing specificity. A CRM mass spectrum is achieved after the final mass analysis step, where the selected product ions are then scanned out of the mass analyser.<sup>78</sup>

#### 1.4.2.5 Zoom Scan

This high resolution scan allows the molecular weight and charge state of an ion to be determined, by evaluating <sup>12</sup>C/<sup>13</sup>C isotopic separation. Hence, this function is useful if the molecular weight of an unknown compound is to be calculated. Further details of this function can be found elsewhere.<sup>78</sup>



**Figure 1:28: Scanning modes available for the linear ion trap.**

### 1.4.3 Experiment Modes

There are several types of experiment available with this type of instrumentation. The type of experiment selected depends on the information required, the sample type (e.g. analyte is only present at trace levels or present amongst a complex mixture) and how much is known about the parent ions and their corresponding product ions. The types of experiment that will be discussed in this section are as follows; general MS and MS<sup>n</sup>, data dependent, ion mapping and ion tree.

#### 1.4.3.1 MS and MS<sup>n</sup>

For general MS experiments, the masses of the parent ions need to be known and in the case of MS<sup>n</sup> experiment; the masses of both the parent and product ions need to be known. The more steps involved in the MS<sup>n</sup> experiment, the more detailed information regarding the compound obtained.<sup>78</sup>

#### 1.4.3.2 Data Dependent Experiments

Very little user input is required for data dependent experiments, yet detailed structural information can be obtained. If very little information is known about the sample, a data dependent experiment can be created where the ion trap can select the most predominant parent ions, trap them whilst ejecting minor parent ions. The selected parent ions can then be fragmented and the most predominant product ions within a given mass range can then be isolated and fragmented further. This type of experiment gives detailed information on the parent ions in the sample.<sup>78</sup> Figure 1:29 summarises the steps involved during a MS/MS data dependent experiment, although MS<sup>n</sup> is possible.

Alternatively, if information about the parent ions is known, their masses can be specified and the ions selected and fragmented to give product ion spectra. A list of parent ions that should be ignored can also be created to prevent MS<sup>n</sup> of unwanted parent ions. This type of experiment collects detailed MS information on each stage of the mass analysis.<sup>78</sup>

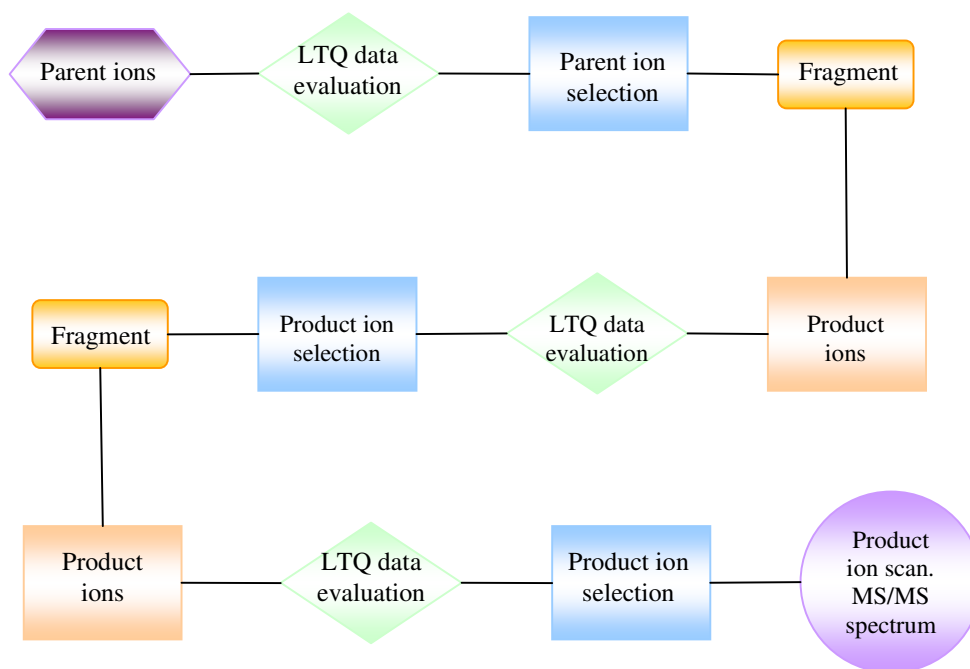


**Figure 1:29:** A summary of the processes occurring within the linear ion trap during a data dependant experiment.

### 1.4.3.3 Other Experiment Types

Ion tree and ion mapping are further types of experiment which are possible with the linear ion trap. Ion tree experiments can be data dependent where the instrument decides the next stage of the experiment by collecting and evaluating the data, or the parent ion can be specified for  $MS^n$ . There are two ways of prioritising LTQ data collection: depth focus or breadth focus, in either case, the instrument will select the most intense parent ion (unless specified by the user).<sup>78</sup> In the case of depth focus, the instrument will perform the specified number of MS experiments (e.g.  $MS^4$ ) before moving to the next most intense parent ion and performing the specified number of  $MS^n$  experiments on that ion. Breadth focus will perform MS on all the parent ions (whether chosen by the instrument or specified by the user) and then move onto the next  $MS^n$  level and analyse the product ions. The number of MS experiments is specified by the user.<sup>78</sup>

Ion mapping experiments allow unknown compounds in a mixture to be analysed and characterised in detail. There are three main types of ion mapping experiment, namely; total

ion map, parent ion map and neutral loss.<sup>75, 78</sup> Product ions scans from parent ions are obtained in a total ion map experiment. Thus, the user can establish which parent ions fragmented to yield specific product ions. Likewise a parent ion mapping experiment identifies the parent ions that formed specific product ions. Evidence of neutral fragment loss can be obtained with a neutral loss ion map. The details of ion tree and ion map experiments are beyond the scope of this introduction, but further information is available elsewhere.<sup>75, 78</sup>

## 2 Elemental Labelling

### 2.1 Introduction

The previous chapter outlined the various problems associated with P and S measurement by ICP-MS and briefly highlighted the potential of metal nano-particle labelling. This chapter will concentrate on the notion of nano-particle labelling of nucleic acids by detailing two methods of incorporating Au nano-particles into oligonucleotides. The advantages and limitations associated with each method will be highlighted. Although the emphasis is on nucleic acids, the methods can potentially be applied to proteins and related molecules.

The signal intensity given by ICP-MS is proportional to the number of similar metal atoms present in the sample. Hence, if nano-particle labelling of biomolecules is to be used quantitatively, it is vital to know how many nano-particles and therefore metal atoms have been incorporated into the biomolecule. This can be achieved if the labelling reaction is site specific, which is viable if the biomolecule and nano-particle both contain reactive groups.<sup>7</sup> Site specific labelling has been achieved by employing Au labelled antibodies to bind and therefore label specific antigens.<sup>13, 48, 89</sup> The interaction between biotin and avidin proteins is the strongest non-covalent interaction known with association constants in the region of  $10^{15} \text{ M}^{-1}$ ,<sup>90</sup> thus nano-particle labelling using these two molecules has also been used.<sup>39, 45, 46, 91</sup> In addition, DNA sequences can be modified to contain thiol groups which then have strong affinity for Au surfaces.<sup>39, 41, 91-94</sup> This approach has been used in DNA micro-arrays.<sup>39, 41, 93</sup> Biomolecules can even be labelled using electrostatic interactions, due to the array of charges present on many biopolymers.<sup>95</sup> The alternative method of achieving site specific labelling is to modify the biomolecule so it contains a reactive group such as a primary amine or sulfhydryl group. The derivatised biomolecule can then be reacted with a nano-particle also containing a reactive organic ligand such as maleimide or sulfo-*N*-hydroxy-succinimide to achieve stoichiometric labelling.<sup>95</sup>

Biomolecule conjugation to metal surfaces also has the advantage that the biological activity of the biomolecule can be maintained.<sup>94</sup> This advantage is exploited in the case of

Au labelled antibodies and proteins, which maintain their native structure and recognise their corresponding antigens to enable Au labelling. The conjugation of biomolecules to metal surfaces has been employed extensively in micro-arrays and electron microscopy. The majority of biomolecule-nano-particle conjugation reactions have employed Au nano-particles. Gold has been favoured because it is electron dense and therefore highly visible in electron microscopy.<sup>96</sup> However, research has been carried out with respect to bonding DNA to other metals such as; Ag, Cu, Pd and Pt.<sup>22, 39, 97-100</sup> Lanthanide labels have also been successfully used to label antibodies for immunoassay reactions.<sup>16, 25, 89</sup>

Silver and Au enhancement are employed in electron microscopy and involve applying Ag or Au solutions to the Au labelled molecules. The Au nano-particles have autocatalytic properties that cause the reduction of Ag/Au ions on the Au surface. The deposited metal has its own catalytic properties, causing more Ag/Au to be deposited onto the label's surface. The accumulation of metal creates larger metal clusters with diameters much larger than the original label. These grains allow easier observation on immunoblots, polyacrylamide and other gels.<sup>95</sup> Enhancement may also be beneficial in ICP-MS as the number of metal atoms increases, resulting in increased sensitivity.<sup>46, 95, 16</sup> Although further signal enhancement will be achieved, quantitative analysis would be very difficult since the number of metal atoms per biomolecule would be unknown.

Colloidal Au particles are easy to synthesis and commercially available, making them popular in many applications employing biomolecule-metal conjugation. However, there are numerous disadvantages of colloidal Au that could cause problems in atomic spectrometric applications. Firstly colloidal Au particles carry a negative charge, which could result in non-specific binding on the biomolecule, adversely effecting quantification.<sup>101</sup> In addition, colloidal Au particles are known to become unstable and dissociate in solution.<sup>101</sup> The size of the particles should also be considered, since research in the field of laser ablation (LA) has shown that particles below 90 nm in diameter are completely atomised and vaporised in the plasma,<sup>102</sup> thus the particle size must be controlled. Although there are no commercially available nano-particles which display all the desired characteristics for atomic spectrometry, there are probes which can be

successfully employed for quantitative analysis. These commercially available Au nanoparticles contain approximately 80 Au atoms and have many advantages over their colloidal Au counterparts.<sup>91, 98, 101</sup> Firstly, these nanogold particles are neutral and are stabilised by phosphine groups,<sup>96, 103, 104</sup> minimising any non-specific binding.<sup>101</sup> Nanogold particles are also stable in solution<sup>96, 103</sup> and over a wide range of ionic concentrations.<sup>101</sup> The vaporisation and atomisation of the Au nano-particles should not be problematic, since the nano-particles have a uniform Au core diameter of 1.4 nm,<sup>95, 96, 103</sup> although the presence of the stabilising organic ligands increases the total diameter to 2.7 nm.<sup>101</sup> Most importantly, these probes are functionalised with a range of ligands and biological recognition sites to provide near stoichiometric, site specific labelling.<sup>95</sup> Well characterised, commercially available probes of this type were chosen for use in this study. Two Au probes were investigated: Monomaleimido Nanogold (MMN) and Streptavidin FluoroNanogold (SFNG), both probes were obtained from Nanoprobes (Stonybrook, New York, USA) and contained an Au core consisting of ~80 Au atoms.

This chapter concentrates on the Au nano-particle labelling of short chain, single stranded DNA fragments known as oligonucleotides. The ICP-MS analysis of Au labelled DNA has been reported elsewhere,<sup>48</sup> however, the method employed DNA hybridised with a peptide sequence. Gold labelled secondary antibodies were used to label a monoclonal antibody, which was located at the peptide site on the hybrid biomolecule.<sup>48</sup> Such labelling is therefore dependent upon incorporating peptide sequences into the nucleic acid. In addition to Au labelling of DNA, DNA can be detected and potentially quantified using a metallo-intercalator as described by Tanner *et al.*<sup>105</sup> This method is applicable to double stranded DNA where the metal complex intercalates between nucleotide pairs. Cellular DNA was identified using a Rh metallo-intercalator.<sup>105</sup> The two methods detailed in this chapter differ to the reported procedures in that they are site specific (see below) but are not base sequence specific or dependent upon peptide sequences. These methods are therefore generic and can be applied to any nucleic acid that contains sulfhydryl or biotin functionality.



Gold does have some disadvantages when used as a biomolecule label in ICP-MS analysis. Firstly, the element is mono-isotopic and has high affinity for the surfaces of sample introduction systems.<sup>25</sup> This results in inefficient wash-out from the sample introduction system, leading to carry over between samples. Bovine serum albumin (BSA) and hydrochloric acid solutions have been used to minimise this effect.<sup>25</sup> BSA complexes to the Au, facilitating its removal from the sample introduction system. Other sulfur containing molecules such as the amino acid cysteine have been used as a wash solution to minimise Au memory effects.<sup>106</sup> *Aqua regia* and hydrochloric acid solutions are also useful for removing residual Au, since Au is very soluble in these acids. These issues will be discussed in subsequent sections.

## 2.2 Instruments and Reagents

A PQ ExCell ICP-MS instrument with collision cell technology (CCT) was provided by Thermo Electron (Winsford, Cheshire, UK). The Element 2XR high resolution ICP-MS instrument was obtained from Thermo-Finnigan (Bremen, Germany). The basic operating parameters for the PQ ExCell and Element 2XR are shown in Table 2:1 and Table 2:2 respectively. Both instruments were tuned daily with 1 ng ml<sup>-1</sup> <sup>115</sup>In to obtain maximum signal intensity and stability. Tuning of the high resolution lenses on the Element 2XR was achieved with a tune solution containing 1 ng ml<sup>-1</sup> <sup>56</sup>Fe. The lenses were tuned to obtain maximum resolution between the <sup>56</sup>Fe and <sup>40</sup>Ar<sup>16</sup>O peaks. In addition, the <sup>140</sup>Ce<sup>16</sup>O/<sup>140</sup>Ce ratio was monitored daily on both instruments to ensure the oxide level was below 5%.

**Table 2:1: PQ ExCell operating parameters.**

Parameter	Setting
Gas flows	Cool = 12.8 l min <sup>-1</sup> Auxiliary = 0.80 l min <sup>-1</sup> Nebuliser = 1.0-1.2 l min <sup>-1</sup>
Quadrupole bias	+ 1V
Hexapole bias *	~+ 6 V for <sup>48</sup> SO ~+ 7.5-8 V for <sup>47</sup> PO
Forward power	1350 W
CCT O <sub>2</sub> flow *	0.4 ml min <sup>-1</sup>
Nebuliser	100 µl min <sup>-1</sup> or 1 ml min <sup>-1</sup> glass Conikal (Glass Expansions, Melbourne, Australia)
Spray chamber	Impact bead

\* These parameters were only relevant when the collision cell was in operation for the determinations of P and S.

**Table 2:2: Element 2XR operating parameters.**

Parameter	Setting
Gas flows	Cool = 15.5 l min <sup>-1</sup> Auxiliary = 0.82 l min <sup>-1</sup> Nebuliser = 1.0-1.2 l min <sup>-1</sup>
Scan type	E-Scan
Scanning mode	Mass accuracy (solution analysis) or speed (chromatography mode)
Detection mode	Triple
Resolution	Low (Au and Pt) or medium (P)
Forward power	1300 W
Spray chamber	Cyclonic or double pass (Glass Expansions, Melbourne, Australia)
Nebuliser	PFA-ST type (Elemental Scientific, Omaha, USA) or 1ml min <sup>-1</sup> Conikal (Glass Expansions, Melbourne, Australia)

Mass accuracy scanning mode was employed when the Element 2XR was operated in standard solution mode. Conversely, the speed scanning mode was implemented when the instrument was being employed as a selective detector when coupled to HPLC. Triple detection mode, which is noted in Table 2:2, refers to the automatic selection of either the counting secondary electron multiplier (SEM), analogue SEM or faraday cup by the

Element 2XR. Further details on the Element scanning and detection modes are given in Chapter 1.

A HP 1090 Series 2 HPLC system, complete with a diode array detector from Agilent Technologies (Waldronn, Germany) was used for HPLC-ICP-MS experiments. A LDC Spectromonitor 3200 variable wavelength UV detector (VG data systems, Manchester, UK) and HP3396A integrator (Hewlett Packard) and was used for obtaining UV data during gel filtration. In addition, a Shimadzu UV-1650 UV/vis spectrometer (Milton Keynes, UK) was employed for UV/vis analysis of collected fractions obtained during gel filtration chromatography.

A TSKgel-DNA-NPR analytical and guard column was obtained from Tosoh Bioscience (Stuttgart, Germany). Both columns were 4.6 mm in diameter and had a particle size of 2.5  $\mu\text{m}$ . The analytical column was 7.5 cm in length and the guard column was 0.5 cm in length. The properties of the column are detailed in Appendix 1 (Chapter 8). Ni-NTA-Agarose beads were from Qiagen (Crawley, West Sussex, UK). These agarose beads were functionalised with nitrolotriactic acid (NTA), which consequently enabled immobilisation of metal ions for immobilised metal affinity chromatography (IMAC). Synthetic oligonucleotides labelled at the 5' end with a disulfide group and 25 base length (25 mer) oligonucleotides modified with a sulfhydryl group were obtained from Alpha DNA (Montreal, Quebec, Canada), as were other synthetic oligonucleotide 10 mers containing a 5' phosphate group. Unmodified oligonucleotide 25 mers were obtained from Invitrogen (Paisley, Renfrewshire, UK). Oligonucleotides biotinylated at the 5' end were obtained from Biotex (Berlin, Germany). The sequences of all synthetic nucleic acids used in this report are shown in Table 2:3. Note that the term 'mer' refers to the number of nucleobases in the oligonucleotide chain.

**Table 2:3: Oligonucleotide sequences.**

Oligonucleotide	Sequence (5'→3')	Backbone Molecular Weight
5' thiolated di-nucleotide	GG	597
5' thiolated 25 mer	TGA AGA AAT TCA GTT CAT AGC TTG G	7721
5' phosphorylated 10 mer	TGC ATT TCG A	3019
Unmodified 25 mer	TGA AGA AAT TCA GTT CAT AGC TTG G	7721
5' biotinylated 18 mer	TAT CTG TTC ACC CGA AAG	6145
5' biotinylated 24 mer	TAT CTG TTC ACC GCA AAT CTG TGG	8000

Deionised water (18  $\Omega$ M) was obtained from either an Elga purified water system (High Wycombe, Buckinghamshire, UK) or an Elix high purity water system from Millipore (Watford, Hertfordshire, UK). Tetramethylammonium hydroxide (TMAH) was from Apollo Scientific (Stockport, Cheshire, UK). Tetramethylammonium chloride (TMACl) was prepared by adding hydrochloric acid to TMAH until the required pH was obtained. Super pure hydrochloric and nitric acid were obtained from Romil (Cambridge, Cambridgeshire, UK). Trisodium citrate, sodium chloride, acetic acid, HPLC grade methanol, acetonitrile, dithiothreitol (DTT) and ammonium sulfate were obtained from Fisher Scientific (Loughborough, Leicestershire, UK). TWEEN-20, citric acid (free acid), tris base, N-ethyl-N'-(3-dimethylaminopropyl)carbodiimide (EDC), 5,5'-dithio-bis-(2-nitrobenzoic acid) and phosphorus buffered saline pouches were obtained from Sigma Aldrich (Steinheim, Germany). Ammonium chloride, sodium phosphate monobasic (Biochimika), cysteine hydrochloride and EDTA (free acid) was obtained from Fluka (Buchs, Switerland). Imidazole was supplied by Alfa Aesar (Karlsruhe, Germany). Superdex-75 preparative grade was purchased from Amersham Pharmacia (Uppsala, Sweden).

Numerous solid phase extraction (SPE) products were used throughout the investigation. C18 SPE and divinylbenzene (DVB) columns were supplied by Alltech (Carnforth, Lancashire, UK). Varian (Oxford, Oxfordshire, UK) kindly supplied Bond Elut Jr. PSA anion exchange cartridges.

## 2.3 Monomaleimido Nanogold Labelling of Sulfhydryl Modified DNA

### 2.3.1 Introduction to Monomaleimido Nanogold labelling

Monomaleimido nanogold (MMN) has a molecular weight of approximately 15 KDa and contains a single maleimide ligand, which is covalently attached to an Au core containing ~80 Au atoms. Only one maleimide functionality is present on the MMN conjugate, which reacts specifically with one sulfhydryl group on the biomolecule to provide stoichiometric labelling.<sup>95</sup> The structure of the probe can be seen in Figure 2:1; details of its synthesis have been reported by Jahn<sup>96</sup> and Hainfeld *et al.*,<sup>101</sup> The maleimide functionality may react with amines above pH 7; therefore, all reactions were carried out at pH < 7 to ensure specific sulfhydryl labelling occurred. Since the maleimide functionality hydrolyses in solution, MMN was used immediately once dissolved.<sup>95</sup>

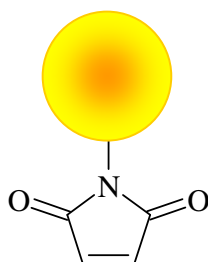


**Figure 2:1: Monomaleimido Nanogold.**

The reaction of MMN with sulfhydryl modified DNA is shown in the schematic in Figure 2:2. Although the emphasis is on sulfhydryl labelled nucleic acids, sulfhydryl containing amino acids on peptides can also be labelled with MMN.

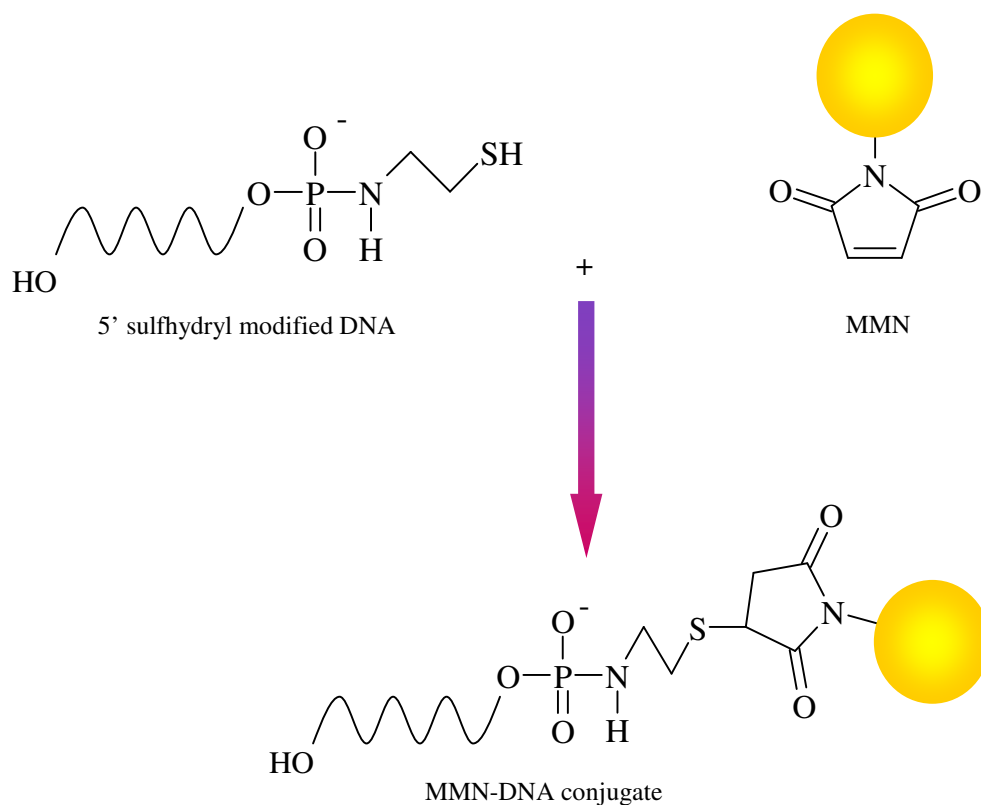


**Figure 2:2: Reaction between sulfhydryl modified DNA and MMN.**

The reaction takes place in mild reaction conditions, typically below room temperature within 24 hours at pH ~6.5.

### 2.3.2 Sulfhydryl Derivatisation of DNA

Although sulfhydryl modified oligonucleotides are commercially available, it will be necessary to incorporate the reactive group in-house if the technique is to have an application in bioanalysis. An article by Ghosh et al.,<sup>107</sup> detailed a procedure for modifying the 5' terminal phosphate of nucleic acids to a sulfhydryl group. The reaction steps are summarised below in Figure 2:3 and Figure 2:4.<sup>107</sup> The actual nucleic acid modification was achieved using the method reported by Ghosh, however, two methods of separating the stage 1 and stage 2 products were investigated. The first method employed gel filtration and the second method used anion exchange SPE. The latter separation method also employed

tris(carboxyethyl)phosphine (TCEP) as an alternative reducing agent to dithiolthreitol (DDT). Both methods will be discussed.

Stage 1 of the derivatisation required 0.1 M imidazole, 0.15 M EDC and 0.25 M cystamine at pH 6.5. EDC and imidazole help form a reactive ester, which then facilitates the formation of a covalent bond between the terminal phosphate of the nucleic acid and the primary amine of cystamine. The reaction was allowed to proceed at 23 °C for 16 hours.

### Stage 1

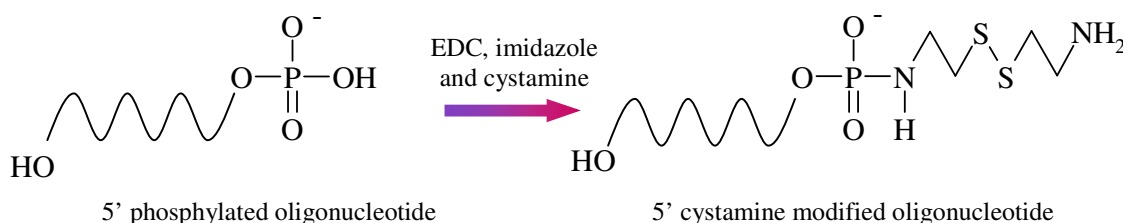


**Figure 2:3: Stage 1 of the sulfhydryl derivatisation reaction.**

Stage 2 of the reaction involved cleaving the disulfide on the cystamine residue to yield a reactive sulfhydryl group. Reduction was carried out with either DDT or TCEP. Both reagents resulted in cleavage of the disulfide bonds within 60 minutes, although it will be discussed later that TCEP was the preferred reducing agent.

### Stage 2

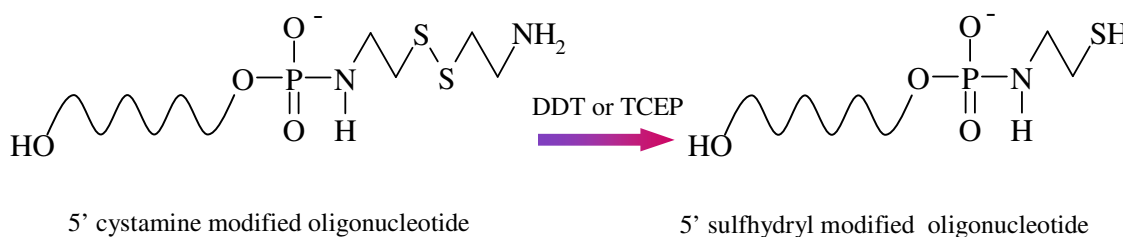


**Figure 2:4: Stage 2 of the sulfhydryl derivatisation reaction.**

Thus, 16 nmoles of 5'-phosphorylated 10 mer were added to 0.6 ml of a solution containing; 0.25 M cystamine, 0.15 M EDC and 0.1 M imidazole. The reaction mixture was incubated at 23 °C for 16 hours in a heated water bath. The resulting stage 1 product

(oligonucleotide-cystamine derivative) was then purified on a Sephadex G-10 column to remove excess reagent from the product. The eluent used for purification consisted of 0.15 M ammonium chloride and 1 mM EDTA, pH 6.3. The gel filtration purification was not used by Ghosh *et al.*,<sup>107</sup> but developed here to purify the stage 1 and stage 2 products. The gel filtration media and column was prepared by suspending 2 g of Sephadex G-10 media in ~10 ml of deionised water. The suspension was allowed to stand for at least 3 hours at room temperature, after which time the suspension was poured in one slow motion into a plastic column (1 cm diameter x 7 cm). Deionised water was passed through the column until the column bed level settled. Equilibration of the column with 5-10 column volumes of buffer (0.15 M ammonium chloride and 1 mM EDTA, ~pH 6.3) was then carried out prior to sample purification. Sephadex G-10 has a molecular weight cut-off below 700 Da, resulting in the oligonucleotide (MW ~3019) eluting first near the void volume and the reactants being retained on the column. The stage 1 product was collected as it eluted from the column and was mixed with a reducing agent containing 0.1 M DTT, 0.15 M ammonium chloride and 1 mM EDTA, pH 8.3. The reduction was carried out at 23 °C for 1 hour. DTT cleaves the disulfide bond present in the stage 1 product (oligonucleotide-cystamine derivative) to produce the stage 2 product, namely the 5'-sulfhydryl modified 10 mer. The stage 2 product (sulfhydryl modified oligonucleotide) was then separated on a Sephadex G-10 column as discussed above.

During the gel filtration purification steps carried out on the stage 1 and 2 products, the column outlet was connected to the inlet of a variable wavelength UV detector. The UV detector outlet was then connected to the back of the ICP nebuliser, so both UV and MS data were collected during the purification of both steps. This was carried out to confirm the elution of the oligonucleotides. A schematic of the instrumentation set up is illustrated in Figure 2:5. The PQ ExCell ICP-MS instrument was employed during the gel filtration purification; refer to Table 2:1 for instrument parameters. The collision cell was employed with oxygen collision gas, so the oxides of P and S at  $m/z$  47 and 48 respectively were detected. The P signal was monitored to confirm the elution of the oligonucleotide species and the S signal confirmed the elution of the stage 1 product (oligonucleotide-cystamine species) and excess unreacted cystamine and DTT in the reaction mixture.



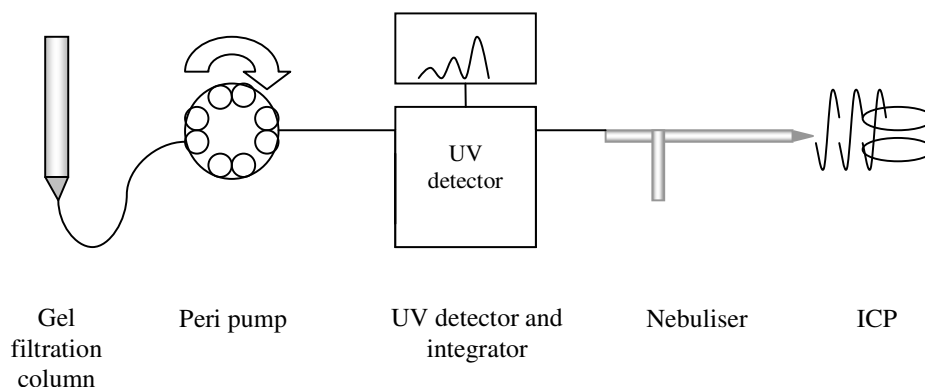


**Figure 2:5: Instrument set up.**

It was established that gel filtration was slow, time consuming and an inefficient method of sample purification. There was evidence that the excess cystamine was not being resolved from the DNA, this will be explained in more detail in the results section. As a result of these limitations, alternative separation procedures were investigated and anion exchange SPE was chosen for separation of the stage 1 and stage 2 product. An alternative reducing agent was also investigated.

### **Anion Exchange Separation and TCEP Reduction.**

Anion exchange SPE was thought to be a good method of separation, since the modified oligonucleotide would be retained on the phase, whilst the excess reagents would be eluted with very little retention. This method of separation was less time consuming since the phase was pre-prepared and did not require extensive equilibration prior to use like gel filtration. Varian PSA Bond Elute Jr. phases were employed for the separation steps, the method is summarised in Figure 2:6. The Varian PSA phase was chosen because it consisted of ethylenediamine-N-propyl anion exchange resin, which contained two amine groups: primary amine (pKa 10.1) and a secondary amine (pKa 10.9), thus providing higher capacity.<sup>108</sup> Highly polar compounds were not retained strongly on the phase due to its high carbon content, which provided good recovery for oligonucleotides.<sup>108</sup>

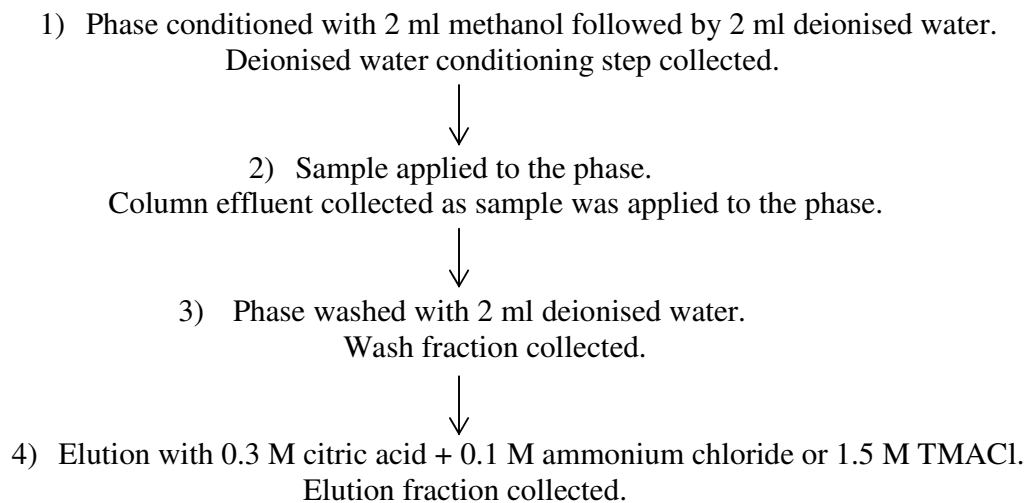
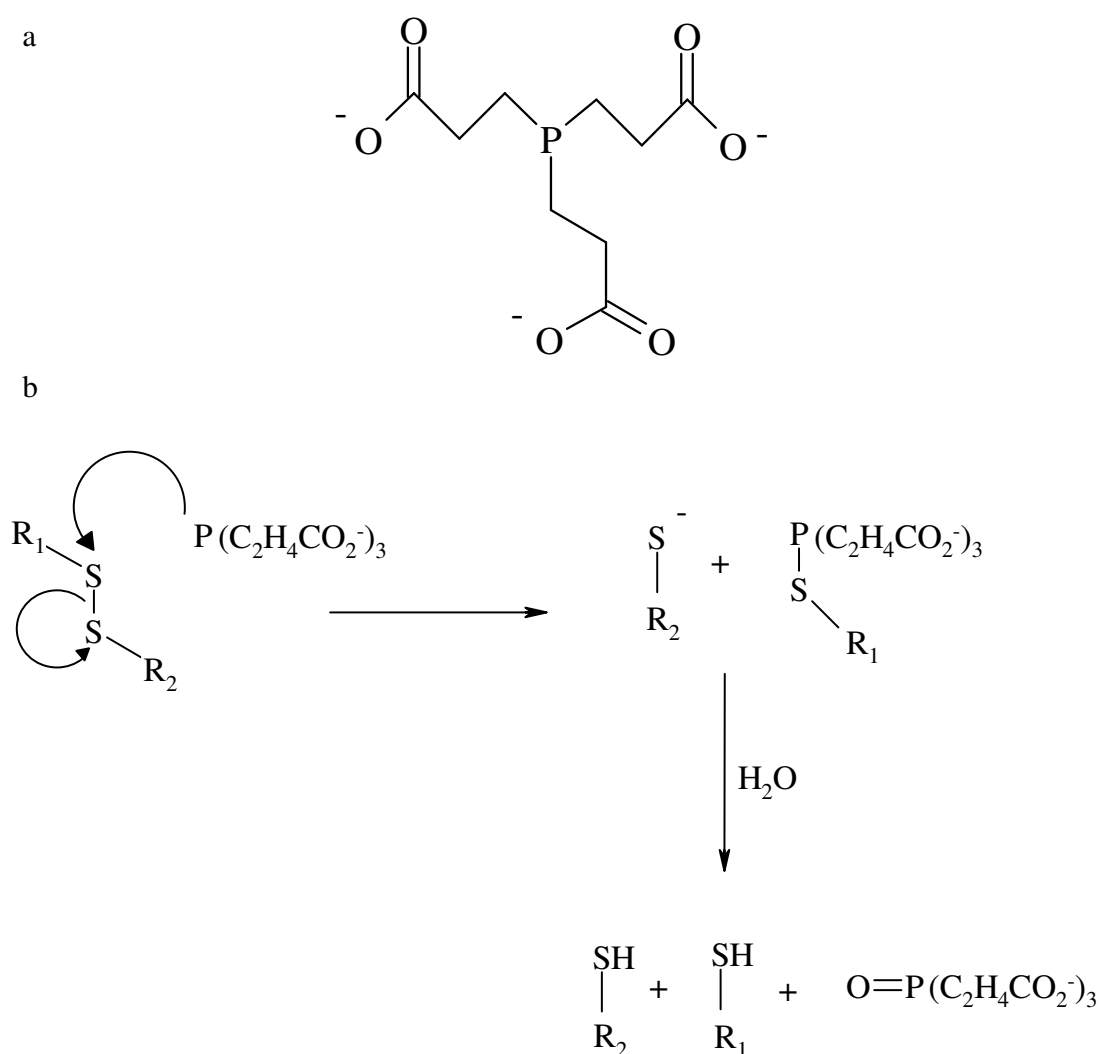


**Figure 2:6: Anion exchange SPE separation method for modified oligonucleotides.**

The column eluents resulting from steps 1-4 of the separation were all collected and analysed by UV/vis to confirm the presence of the oligonucleotide. The deionised water phase conditioning step (step 1) was analysed to ensure the phase was not contaminated with any absorbing species that may have interfered with DNA detection. A UV spectrum of the sample application fraction (step 2) confirmed that the analyte was not eluting immediately upon application to the phase. The eluent resulting from the water wash stage (step 3) confirmed that the oligonucleotides were retained and finally the eluent from step 4 confirmed the elution of the nucleic acids from the phase. The above separation method was employed for both the separation of the stage 1 (oligonucleotide-cystamine species) and the stage 2 (sulfhydryl modified oligonucleotide) product. Eluents containing 1.5 M TMACl or 0.3 M citric acid and 0.1 M ammonium chloride were chosen, since both solutions had high ionic strength that was thought to be relatively ICP-MS compatible and sodium salts were avoided.

DTT is commonly used for cleaving disulfide bonds to form the reactive sulfhydryl group. However, this reagent contains thiol groups, which would have competed with the thiolated DNA for maleimide, if not completely removed from the sample prior to labelling. As a result, TCEP was used in the second stage of the reaction. TCEP is an effective reducing reagent, resulting in cleavage of disulfide bonds and avoids the problems associated with

DTT. The structure of TCEP and its mechanism of action is shown in Figure 2:7. TCEP immobilised on agarose beads is more effective than DTT and it is not mandatory to remove the reducing agent before adding the MMN since it does not contain thiol groups. However, some studies have reported that the presence of TCEP does reduce the efficiency of maleimide-sulphydryl cross-linking reactions to a certain degree.<sup>109</sup> TCEP is also effective at a wider range of pH values, whereas DTT should only be used at pH >8.<sup>109</sup> By employing TCEP immobilised on agarose beads, the oligonucleotides were reduced in one step and then easily removed from the immobilised reducing agent by centrifugation. Slow inefficient gel filtration methods were therefore avoided.



The stage 1 product (oligonucleotide-cystamine species) was prepared in the same way as discussed above (0.1 M imidazole, 0.25 M cystamine and 0.15 M EDC, 23 °C for 16 hours). After the 16 hour reaction period, a 0.5 ml aliquot of the stage 1 product was separated on the SPE phase using the method outlined in Figure 2:6. Following separation, a 0.5 ml aliquot of the separated stage 1 product was then added to 0.5 ml immobilised TCEP gel and allowed to stand at room temperature for 10 minutes. The suspension was then centrifuged at 1000 rpm for 1 minute and the supernatant containing the reduced oligonucleotide was removed and applied to a conditioned PSA anion exchange cartridge. Separation and elution of the stage 2 product (sulfhydryl modified oligonucleotide) was then carried out according to the procedure outlined in Figure 2:6.

Since the reducing agent was immobilised on agarose beads, it was easily removed from the analyte and there was no chance of the MMN reaction being hindered by other thiols, as in the case of DTT. For each mole of disulfide bond broken, two moles of reactive sulfhydryl are produced (Figure 2:7). As a result, the anion exchange separation step was required to isolate the sulfhydryl modified oligonucleotide and remove the other half of the disulfide which also contained a sulfhydryl group. One potential limitation with this separation method is that the unreduced oligonucleotides may not be resolved from their sulfhydryl modified counterparts. Therefore, UV spectroscopy could not be used to calculate reaction efficiency.

Ellman's assay was employed in an attempt to confirm that sulfhydryl modified oligonucleotides were produced during the second stage of the reaction. This is a well documented assay that allows the concentration of sulfhydryl groups to be determined. The procedure used is outlined below and is a slight modification from the procedure suggested by Pierce Biotechnology.<sup>111</sup> The S containing amino acid cysteine was used as a standard in the determination of free sulfhydryl groups present in the reduced oligonucleotide samples. By preparing a range of cysteine standards at a known concentration, a calibration curve was prepared and the concentration of sulfhydryl groups present in the second reaction was therefore determined. Cysteine hydrochloride standards were prepared in a 0.1 M sodium phosphate buffer containing 1 mM EDTA, pH 8. The standards were prepared in the

concentration range 1-20  $\mu\text{M}$ . Ellman's reagent (5,5'-dithiolbis(2-nitrobenzoic acid) or DTNB) was prepared at a concentration of 4 mg ml<sup>-1</sup> in the sodium phosphate buffer.

The mechanism of the assay is illustrated in Figure 2:8. DTNB (Ellman's reagent) reacts with free sulfhydryl groups in solution to form a mixed disulfide by-product and thio-bis-(2-nitrobenzoic acid) (TNB). The TNB product is yellow in colour and absorbs at 412 nm. Thus, by measuring the absorbance of the standard cysteine solutions containing DTNB at 412 nm, calibrations were carried out.

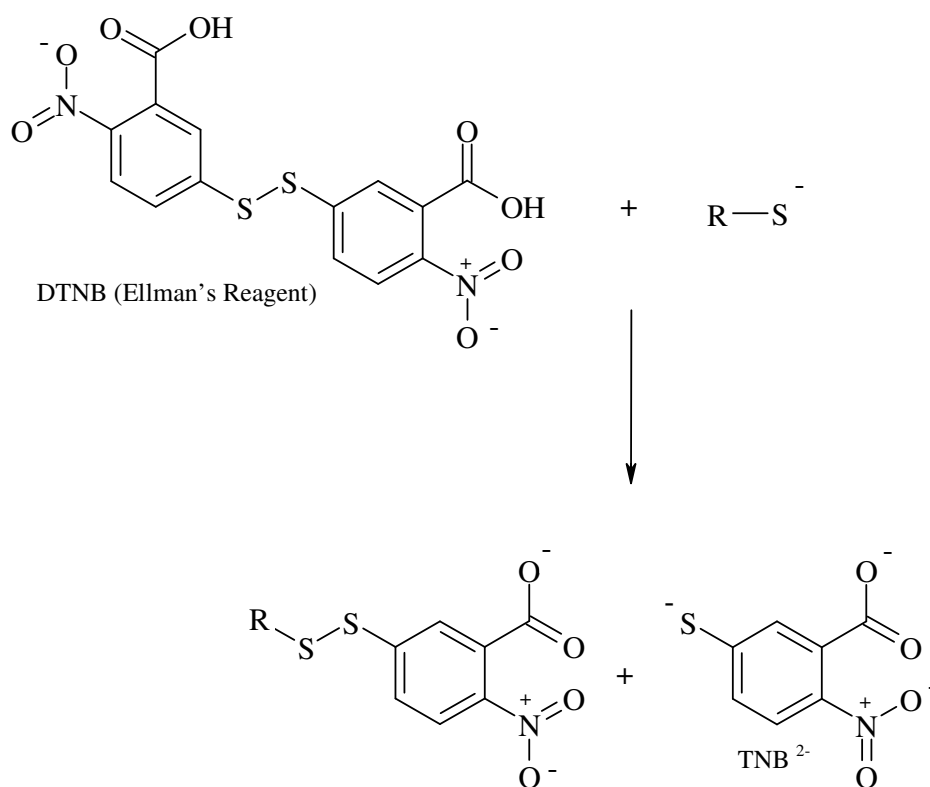


**Figure 2:8: Mechanism of Ellman's assay.<sup>111</sup>**

The standard solutions were prepared by mixing 0.5 ml sodium phosphate buffer with 250  $\mu\text{l}$  cysteine standard solution and 50  $\mu\text{l}$  DTNB. The solutions were mixed and allowed to stand for 15 minutes at room temperature, before the absorbances of the resulting standard solutions were measured at 412 nm. A calibration curve was then plotted.

The unknown solutions were also prepared by mixing 0.5 ml sodium phosphate buffer with 250  $\mu\text{l}$  sample and 50  $\mu\text{l}$  DTNB. Incubation for 15 minutes at room temperature was also carried out for the samples to be determined. By calculating the concentration of sulphhydryl groups expected, the efficiency of the reaction could be determined.

### **2.3.3 Method of Labelling**

#### **2.3.3.1 Labelling of Di-nucleotides**

Di-nucleotides have a very important role in cancer research studies, which will be discussed in detail in Chapter 3. As a result, the MMN labelling method commenced with 5' thiolated di-nucleotides. Although di-nucleotides containing 5' thiol functionality were commercially available, they were provided in the disulfide form. As a result, the disulfide bond required cleaving with the aid of a reducing agent to obtain the reactive sulphhydryl group. Thus, a 100  $\mu\text{l}$  aliquot of 5' disulfide di-nucleotide (100  $\mu\text{M}$ ) was added to 100  $\mu\text{l}$  of reducing agent which contained: 0.1 M DTT + 1 mM EDTA + 0.15 M ammonium chloride, pH 8.3. The mixture was allowed to stand for one hour at room temperature before an aliquot of the reduced di-nucleotide was purified by gel filtration. A Sephadex G-10 gel filtration column (7 cm x 1 cm) was used to remove excess DTT. As stated previously, removal of excess DTT is necessary to avoid the reagent competing with the functionalised oligonucleotide for maleimide sites and adversely effecting the MMN labelling reaction.

The gel filtration media and column used for DTT removal was prepared as discussed previously in section 2.3.2. The column outlet was connected to a variable wavelength UV detector with peristaltic pump tubing. A peristaltic pump operating at approximately 200  $\mu\text{l min}^{-1}$  pumped eluent from the column into the UV detector. The detector outlet was connected directly to the back of the ICP-MS nebuliser (see experimental set-up in Figure 2:5). The column was equilibrated with 0.15 M ammonium chloride + 1 mM EDTA, pH 6.3. After an adequate equilibration time, a 100  $\mu\text{l}$  aliquot of the di-nucleotide (50  $\mu\text{M}$ ) + DTT mixture (0.1 M DTT + 0.15 M ammonium chloride + 1 mM EDTA, pH 8.3) was injected on the top of the column. The UV detector was set to 260 nm, whilst the PQ

ExCell ICP-MS measured  $m/z$  47 and 48 (see Table 2:1 for operating conditions). Table 2:4 summarises the gel filtration operating conditions.

**Table 2:4: Instrument operating conditions for di-nucleotide desalting.**

Parameter	Setting
Column flow rate	200 $\mu\text{l min}^{-1}$
Eluent	0.15 M ammonium chloride + 1 mM EDTA, pH 6.3
UV detector wavelength	260 nm

Once it was confirmed by ICP-MS that the di-nucleotide and DTT were resolved on the gel filtration column, the purified di-nucleotide was collected from the column outlet as it eluted, and added to MMN. The MMN was supplied lyophilised and was dissolved in 200  $\mu\text{l}$  deionised water to yield 6 nmoles of MMN in phosphate buffered saline (PBS-20 mM phosphate, 150 mM NaCl), pH 6.5. The MMN contained phosphate buffer, which may interfere with the di-nucleotide phosphate signal, so the chromatographic method used for the MMN-DNA conjugate purification had to resolve the phosphate buffer from the di-nucleotide. A 100  $\mu\text{l}$  aliquot of the separated di-nucleotide fraction was added to 150  $\mu\text{l}$  MMN and stored at 4 °C for approximately 20 hours. These reaction conditions were recommended by the manufacturer of the MMN<sup>95</sup> and similar conditions were employed by other research groups.<sup>92</sup> Before the di-nucleotide was added to the MMN solution, a 50  $\mu\text{l}$  aliquot of MMN was taken and diluted 100 fold with deionised water and used as a retention time marker for HPLC-ICP-MS. In addition, a sample containing the di-nucleotide only at a concentration of 10  $\mu\text{M}$  was also prepared and used as a retention time marker. The HPLC operating conditions used for the separation of the conjugates are shown in Table 2:5; any amendments to the conditions shown will be stated were appropriate.

**Table 2:5: HPLC conditions used in the purification of di-nucleotide-Au conjugates.**

Stationary phase	TSKgel-DNA-NPR, 4.6 mm x 7.5 cm, 2.5 $\mu$ M	
Mobile phase	A: 5 mM or 20 mM Tris-HCl, pH 9 B: 5 mM or 20 mM Tris + 0.1 M ammonium chloride, pH 9	
Gradient	Time (mins)	%B
	0	0
	3	0
	15	100
Flow rate	0.5-0.7 ml min <sup>-1</sup>	
Injection volume	10 $\mu$ l	
Stop time	15 minutes	
Post time	4 minutes	
Wavelength	260 nm	

### 2.3.3.2 Labelling of 25 mer Oligonucleotides

Thiol modified di-nucleotides were initially chosen in this investigation due to their relevance in cancer research studies (see Chapter 3). However, these short chain oligonucleotides were commercially supplied in the disulfide form, so a reduction step was necessary to yield the reactive sulfhydryl group. These sample preparation procedures, which were described above were long and tedious, so longer chain 25 mers were also investigated. The longer oligonucleotides were supplied as the reactive sulfhydryl form and were received in an inert Ar environment, to prevent re-oxidation of the sulfhydryl groups to the disulfide. Thus the DTT reduction step was not required. Using the pre-functionalised oligonucleotides helped confirm that the labelling method was viable.

The labelling procedure involved re-suspending the dried 5' sulfhydryl modified oligonucleotide in deionised water to a concentration of 10  $\mu$ M. The stock oligonucleotide solutions were stored in the freezer, whilst the 10  $\mu$ M working solutions were stored in the refrigerator to avoid repetitive freeze-thawing and accelerated degradation of the nucleic acids. The refrigerated oligonucleotide solutions were used within one week of preparation due to long term instability once in solution.<sup>112</sup> An 80  $\mu$ l aliquot of 5'-thiol modified 25 mer (10  $\mu$ M) was mixed with 150  $\mu$ l MMN (30  $\mu$ M). The reaction mixture therefore contained 0.8 nmoles DNA (3.5  $\mu$ M) and 4.5 nmoles MMN (19.6  $\mu$ M), resulting in a 5.6



fold molar excess of MMN. The mixture was allowed to react for approximately 20 hours at 4 °C.

The separation and analysis of the MMN-oligonucleotide conjugates was initially carried out using on-line anion exchange HPLC, but here the peaks containing the unbound and bound MMN were fraction collected off-line and then analysed by ICP-MS. There are several reasons for avoiding on-line separations with ICP-MS; the main reason being that the mobile phases used for anion exchange chromatography are not always compatible with ICP-MS due to the high salt content. High salt levels may cause the nebuliser to become blocked, as well as coating the multipoles and ion optics within the instrument. The basic HPLC conditions used for the separation of MMN-25 mer conjugates was identical to that outlined in Table 2:5. However, the mobile phases used were of higher ionic strength and the gradient was modified as shown in Table 2:6.

**Table 2:6: MMN-25 mer conjugate separation method.**

Stationary phase	TSKgel-DNA-NPR Guard column 4.6 mm x 0.5 cm, 2.5 µM	
Mobile phase	A:20 mM Tris-HCl, pH 8	
	B:20 mM Tris + 0.1 M ammonium chloride + 0.3 M citrate pH 8	
Gradient	Time (mins)	%B
	0	10
	10	90
	12	90
Flow rate	1 ml min <sup>-1</sup>	
Stop time	12 minutes	
Post time	4 minutes	
Injection volume	5 µl	
Column temperature	Room temperature	
Wavelength	260 nm	

A TSKgel-DNA-NPR guard column with a 0.5 cm length phase was used for the separation of the conjugates. The short length phase resulted in speedier run times, and elution of the oligonucleotides occurred at lower salt concentrations than those used with the longer analytical column.

### **Optimisation of Reaction Conditions**

Once MMN tagging was achieved, it was necessary to establish the optimum reaction conditions. The reaction conditions outlined above were recommended by the manufacturer<sup>95</sup> and were utilised by other researchers,<sup>92</sup> but it was unknown whether the reaction proceeded better at slightly higher temperatures (without compromising the stability of the probe). The optimum reaction time was another factor that needed to be established. As a result, reaction optimisation experiments were carried out, which involved preparing two reactions, both containing 6 nmoles MMN (200  $\mu$ l) and 1 nmole 5' sulfhydryl 25 mer (10  $\mu$ l). The final concentration of MMN and 25 mer in the reaction mixtures was 28.6  $\mu$ M and 4.8  $\mu$ M respectively. One of the reactions was stored at 4 °C and the other reaction was kept at room temperature. At time intervals of 1, 5, 10, 24, and 48 hours after the reaction mixtures were prepared, a 30  $\mu$ l aliquot was taken from the reaction vial and diluted to 300  $\mu$ l with 20 mM tris-HCl, pH 8. The diluted aliquots were then separated by HPLC using the conditions outlined in Table 2:6 to resolve the bound and unbound MMN. Two further reactions were also prepared, both contained 2.25 nmoles MMN and 0.5 moles of DNA, resulting in a 4.5 fold molar excess of MMN. Again one reaction was stored at 4 °C and the other at room temperature. These two reactions were allowed to proceed for 65 hours before being diluted (50  $\mu$ l reaction mixture to 500  $\mu$ l tris-HCl buffer), separated and fraction collected. During the separation step, the column effluent was collected between 0-0.5 minutes (fraction 1) and 7-7.5 minutes (fraction 2). These two fractions contained unbound MMN and DNA bound MMN respectively. The collected fractions were then diluted further before the Au was determined by ICP-MS. The PQ ExCell instrument was used for all Au determinations in the MMN labelling experiments.

## 2.4 Results of Monomaleimido Nanogold Labelling

### 2.4.1 Sulfhydryl Derivatisation

As stated in Section 2.3.2, both UV and ICP-MS data were obtained during the gel filtration purification of the stage 1 (oligonucleotide-cystamine species) and stage 2 (sulfhydryl modified oligonucleotide) products of the sulfhydryl modification. The  $^{31}\text{P}^{16}\text{O}$  signal obtained from the ICP-MS confirmed the elution of the unmodified oligonucleotide and the oligonucleotide derivatives. Likewise, the elution of the oligonucleotide-cystamine species (stage 1 product) could be further confirmed by the  $^{32}\text{S}^{16}\text{O}$  signal, since the stage 1 product contained both P and S. The elution of cystamine was also detected by the ICP-MS at  $m/z$  48. Figure 2:9 shows the  $^{31}\text{P}^{16}\text{O}$  and  $^{32}\text{S}^{16}\text{O}$  ICP-MS data obtained during a stage 1 purification step. The stage 1 reaction mixture was diluted 50 fold prior to injection on the column. It should also be noted that the two sets of data shown in Figure 2:9 were from the same sample; both the  $^{31}\text{P}^{16}\text{O}$  and  $^{32}\text{S}^{16}\text{O}$  signals were measured simultaneously during separation.

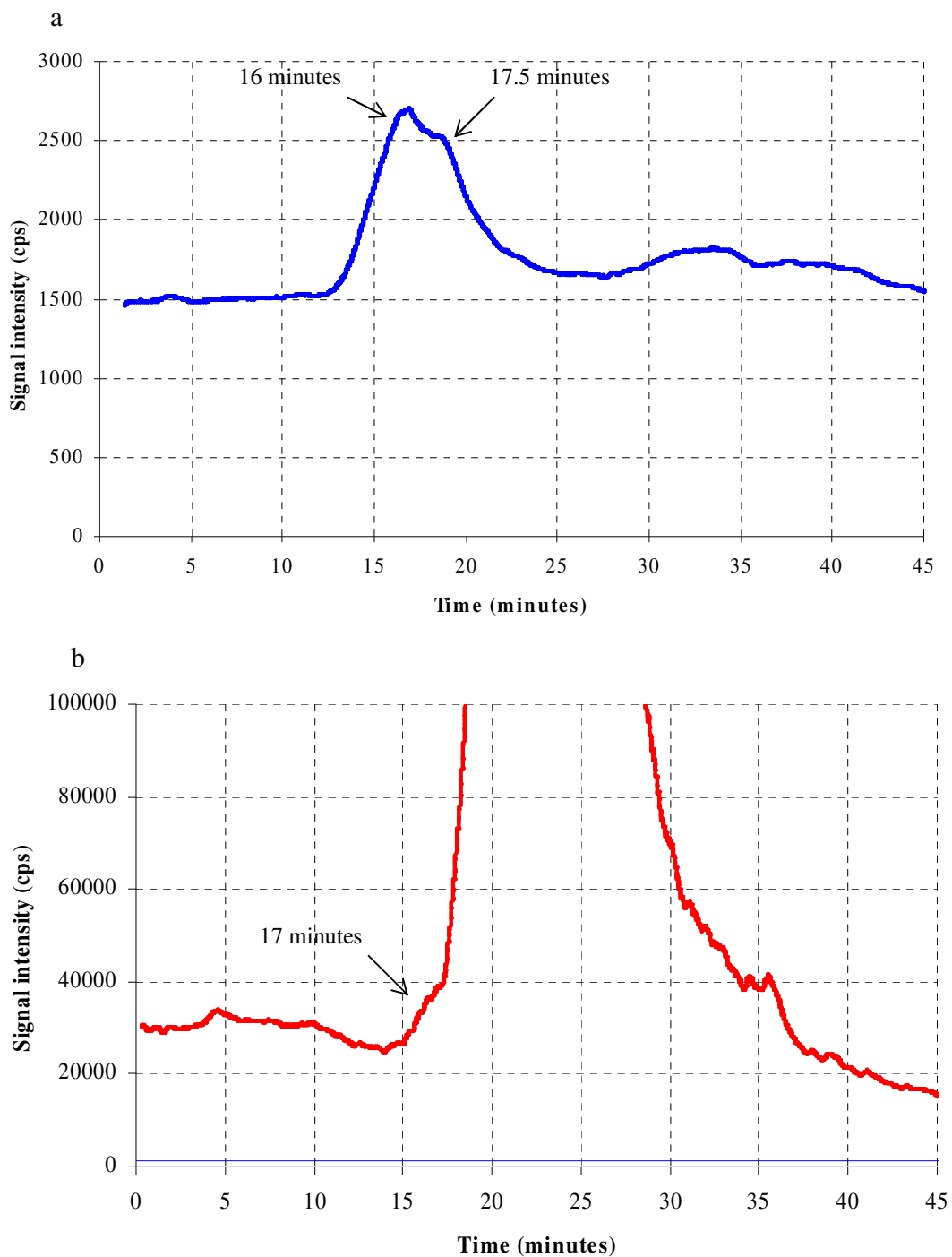


**Figure 2:9: a)  $^{31}\text{P}^{16}\text{O}$  signal intensity and b)  $^{32}\text{S}^{16}\text{O}$  signal intensity during the stage 1 (oligonucleotide-cystamine species) gel filtration purification step. Eluted with 0.15 M ammonium chloride and 1 mM EDTA, pH ~6.3, 200  $\mu\text{l}$  injection volume.**

The  $^{31}\text{P}^{16}\text{O}$  signal (Figure 2:9a) exhibited a peak between ~12-23 minutes which corresponded to the eluting 10 mer oligonucleotide. However, this peak actually appeared

to be two peaks co-eluting, the first peak at ~16 minutes and a second at ~17.5 minutes. The first peak at 16 minutes was likely to be the Stage 1 product (oligonucleotide-cystamine species), since it had a larger molecular weight than the unmodified 10 mer. The second peak at 17.5 minutes was probably unmodified 10 mer, since this was the lighter oligonucleotide species. The  $^{32}\text{S}^{16}\text{O}$  signal (Figure 2:9b) showed a small increase in response between 15-17.5 minutes and then a huge response between 17.5-30 minutes. The small rise in  $^{32}\text{S}^{16}\text{O}$  signal intensity observed between 15-17.5 minutes corresponded to the first  $^{31}\text{P}^{16}\text{O}$  peak at 16 minutes, which was thought to be the oligonucleotide-cystamine species. These two sets of data suggested that the stage 1 product was eluting between 15-17 minutes, since the oligonucleotide-cystamine species contained both P and S. The excess S containing reagents eluted from approximately 18 minutes onwards. Note how the signal intensities of the two sets of data vary. The  $^{31}\text{P}^{16}\text{O}$  counts were quite low compared to the huge  $^{32}\text{S}^{16}\text{O}$  response, in which an excess of 500 000 counts per second (cps) was observed. This was due to the large excess of cystamine (9000 fold excess of cystamine) that was used in the reaction. The UV data supported the  $^{31}\text{P}^{16}\text{O}$  data and is shown in Figure 2:10.

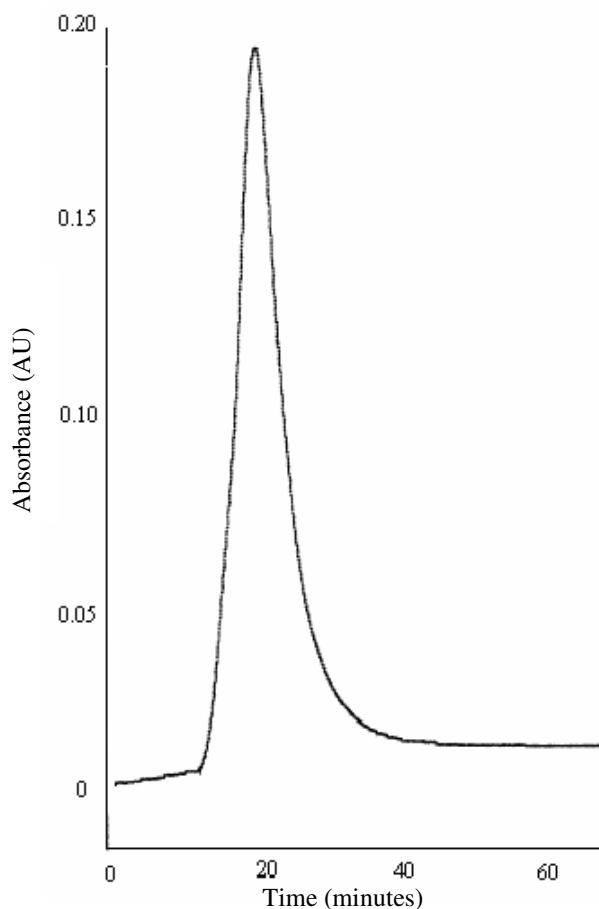


**Figure 2:10: UV chromatogram during the stage 1 (oligonucleotide-cystamine species) gel filtration purification step. Eluted with 0.15 M ammonium chloride and 1 mM EDTA, pH ~6.3, 50  $\mu$ l injection volume, 25 pmoles of oligonucleotide.**

Only one peak was observed in the UV chromatogram of the stage 1 purification step (Figure 2:10). However, the ICP-MS data suggested that more than one oligonucleotide species eluted from the column, with the stage 1 product eluting at approximately 16 minutes. All three sets of data show that the modified oligonucleotide was not totally resolved from the excess cystamine in the reaction mixture. The lack of resolution was most obvious in Figure 2:10, where only one peak was observed at 260 nm.

The stage 1 reaction was repeated but in the absence of EDC, the aim was to see what effect the reagent had on the first reaction step. Figure 2:11 shows the UV chromatogram of the stage 1 reaction mixture at 260 nm during separation of a Sephadex G-10 gel filtration column.

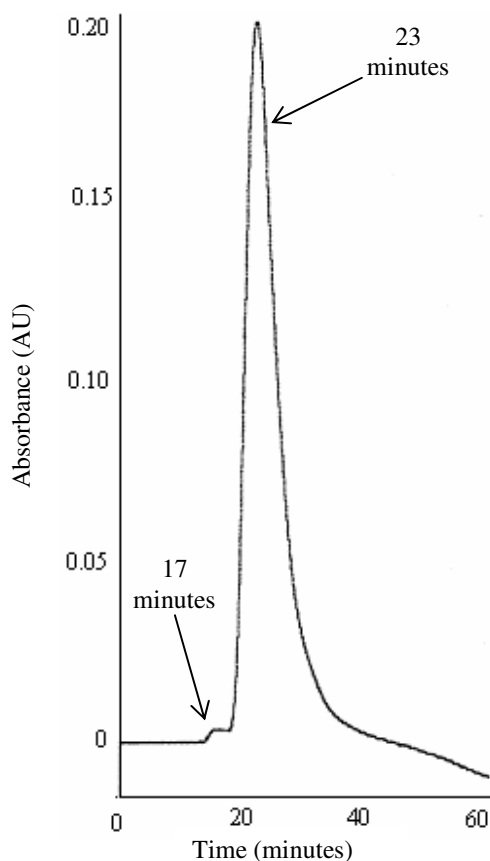


**Figure 2:11: Chromatogram at 260 nm of the stage 1 product (oligonucleotide-cystamine species) in absence of EDC during gel filtration separation. Eluted with 0.15 M ammonium chloride and 1 mM EDTA, pH ~6.3, 50  $\mu$ l injection volume, 25 pmoles oligonucleotide.**

Note how two peaks are present in the chromatogram shown in Figure 2:11. The first peak at 17 minutes was extremely small and corresponded to the retention time of the stage 1 product (oligonucleotide-cystamine species), as shown by the  $^{31}\text{P}^{16}\text{O}$  and  $^{32}\text{S}^{16}\text{O}$  data in Figure 2:9. The second peak at 23 minutes corresponded to the excess reagents. Hence, it can be confirmed from this data that EDC is essential for the formation of the stage 1 product.

Figure 2:12 shows the ICP-MS data obtained for  $^{31}\text{P}^{16}\text{O}$  and  $^{32}\text{S}^{16}\text{O}$  during the gel filtration of the stage 2 product (sulfhydryl modified oligonucleotide). The  $^{31}\text{P}^{16}\text{O}$  signal (Figure 2:12a) revealed oligonucleotide elution between 13 and 25 minutes. However, like with the first stage product, the second stage product appeared to have more than one peak present, suggesting more than one type of oligonucleotide was eluting. The first peak at 16 minutes

was thought to be the stage 1 product (oligonucleotide-cystamine species), which had not been reduced by DTT, whilst the second co-eluting  $^{31}\text{P}^{16}\text{O}$  peak at 21 minutes was thought to be the sulfhydryl modified 10 mer (stage 2 product). Therefore, the second  $^{31}\text{P}^{16}\text{O}$  peak was required for the subsequent MMN labelling reaction.



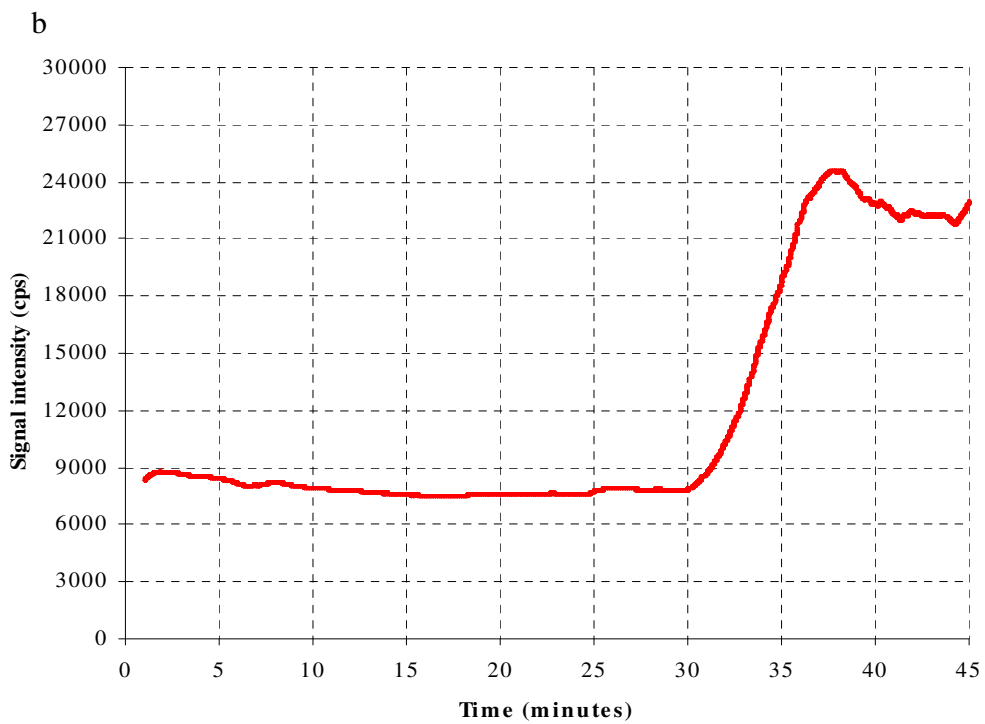
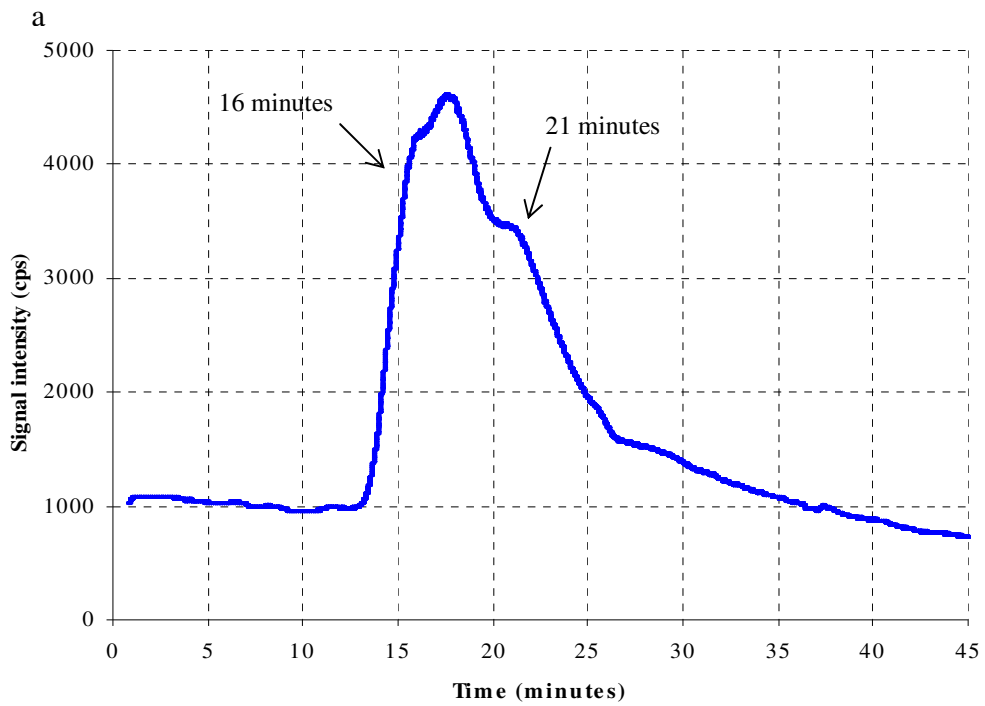


**Figure 2:12: a)  $^{31}\text{P}^{16}\text{O}$  Signal intensity and b)  $^{32}\text{S}^{16}\text{O}$  signal intensity during the gel filtration purification of the stage 2 product (sulfhydryl modified oligonucleotide). Eluted with 0.15 M ammonium chloride and 1 mM EDTA, pH ~6.3.**

The  $^{32}\text{S}^{16}\text{O}$  MS data (Figure 2:12b) revealed that the elution of excess DTT occurred at approximately 30 minutes, suggesting the oligonucleotide and excess DTT were well resolved. As a result, DTT should not interfere with the MMN labelling reaction. Two other  $^{32}\text{S}^{16}\text{O}$  peaks were expected at approximately 16 and 21 minutes, corresponding to the stage 1 and stage 2 modified oligonucleotides. Both these oligonucleotide species would have contained S, but no signal was observed in the  $^{32}\text{S}^{16}\text{O}$  chromatogram. One explanation for this is that the S concentration would have been too low for detection.

The UV chromatogram corresponding to the stage 2 (sulfhydryl modified oligonucleotide) purification is shown in Figure 2:13. The first peak at ~15 minutes coincided with the first  $^{31}\text{P}^{16}\text{O}$  peak observed in the MS data, which was thought to be the unreduced oligonucleotide-cystamine derivative (stage 1 product). The second UV peak at ~20 minutes coincided with the remaining  $^{31}\text{P}^{16}\text{O}$  signal, which probably corresponded to the stage 2 product (sulfhydryl modified oligonucleotide). The third peak in the UV chromatogram at 28 minutes onwards corresponded to the excess DTT. Again this was in good agreement with the ICP data, which showed a very high signal for  $^{32}\text{S}^{16}\text{O}$  eluting from the column from approximately 30 minutes onwards.

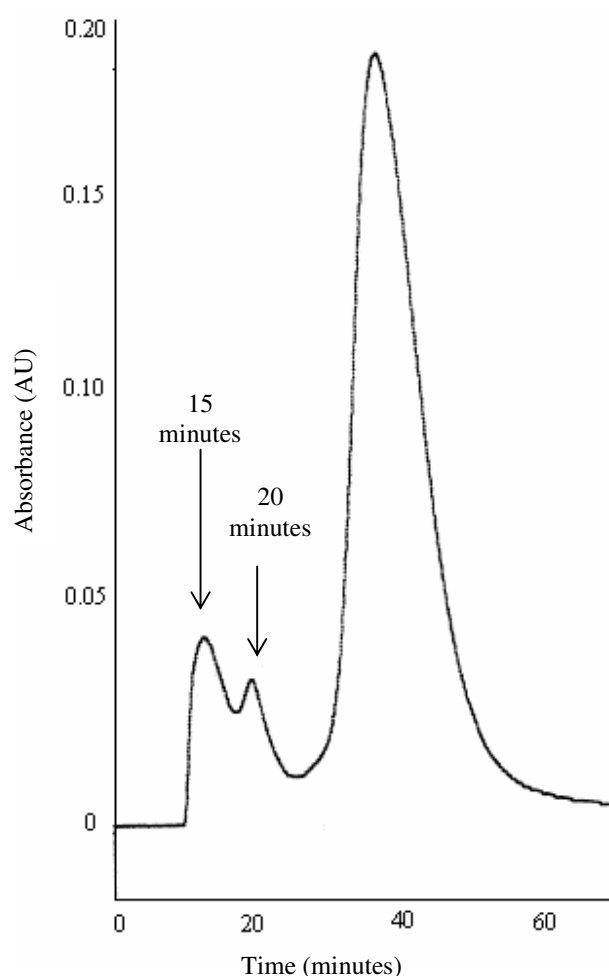


**Figure 2:13: UV chromatogram at 260 nm of stage 2 (sulfhydryl modified oligonucleotide) gel filtration purification. 0.15 M ammonium chloride and 1 mM EDTA, pH ~ 6.3.**

Figure 2:12 and Figure 2:13 both show that more than one oligonucleotide species eluted from the phase. It has been established that the stage 1 product (unreduced oligonucleotide-cystamine species) eluted at approximately 15 minutes and the stage 2 product (sulfhydryl modified oligonucleotide) eluted at ~21 minutes. However, the stage 1 oligonucleotide peak at 15 minutes was larger than the stage 2 oligonucleotide peak, suggesting that not all the stage 1 product was being reduced by DTT. The reason for this was attributed to the pH of the reducing DTT mixture. It has been documented that DTT is more effective at pH >8.<sup>109, 110</sup> However, in the above experiments, the first stage reaction mixture was being eluted from the gel filtration column with a buffer at pH 6.3. The collected stage 1 species was then used directly in the reduction step. Although the DTT mixture was adjusted to pH 8.5, the addition of the stage 1 species at pH 6.3 may have decreased the pH below 8. Thus,

the effectiveness of the DTT was compromised. To overcome this problem, the stage 1 product (oligonucleotide-cystamine species) was eluted from the gel filtration column with a buffer at pH 8.3. The modified oligonucleotide fraction was then collected from the column and added to the DTT reducing solution, which was also at pH 8.3. Upon separating the stage 2 product, the second peak (sulfhydryl modified oligonucleotide) was larger than the first. The UV chromatogram for this separation is shown in Figure 2:14 and suggests that the pH of the reducing agent was critical, for maximum disulfide reduction, a pH >8 was required.

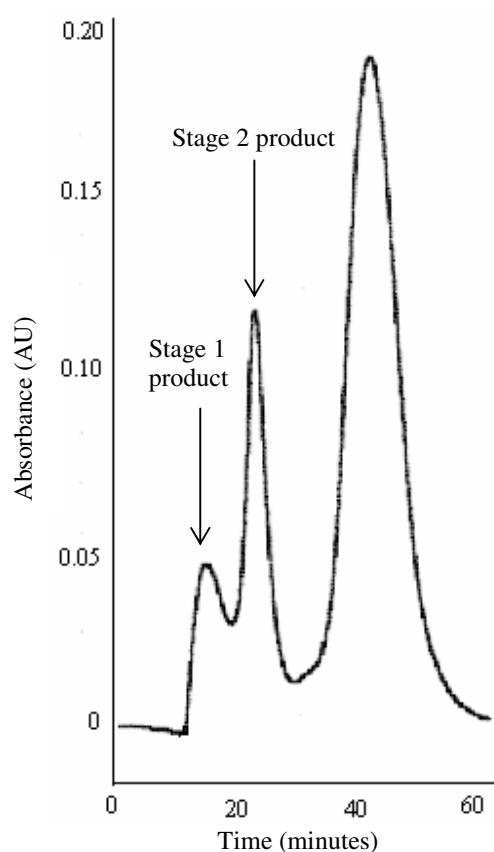


**Figure 2:14:** UV chromatogram at 260 nm of the stage 2 (sulfhydryl modified oligonucleotide) reaction mixture after reduction with DTT at pH 8.

### **Anion Exchange Separation of Modified Oligonucleotides**

Before the SPE separation method was applied to the sulfhydryl derivatised oligonucleotides, the retention and elution of unmodified oligonucleotides was assessed on the Varian PSA phase. Briefly, a solution containing 5  $\mu$ M of unmodified 25 mer

oligonucleotide was prepared in deionised water, and the UV spectrum of the sample was taken between 200-400 nm. A 1 ml aliquot of the sample was then applied to a conditioned SPE phase, which was subsequently washed with 1 ml deionised water. Elution of the oligonucleotide was then achieved with 2 ml TMACl (1.5 M). Figure 2:15 shows the overlaid UV spectra corresponding to the column eluent resulting from the phase conditioning step, sample application step, deionised water wash and TMACl elution.

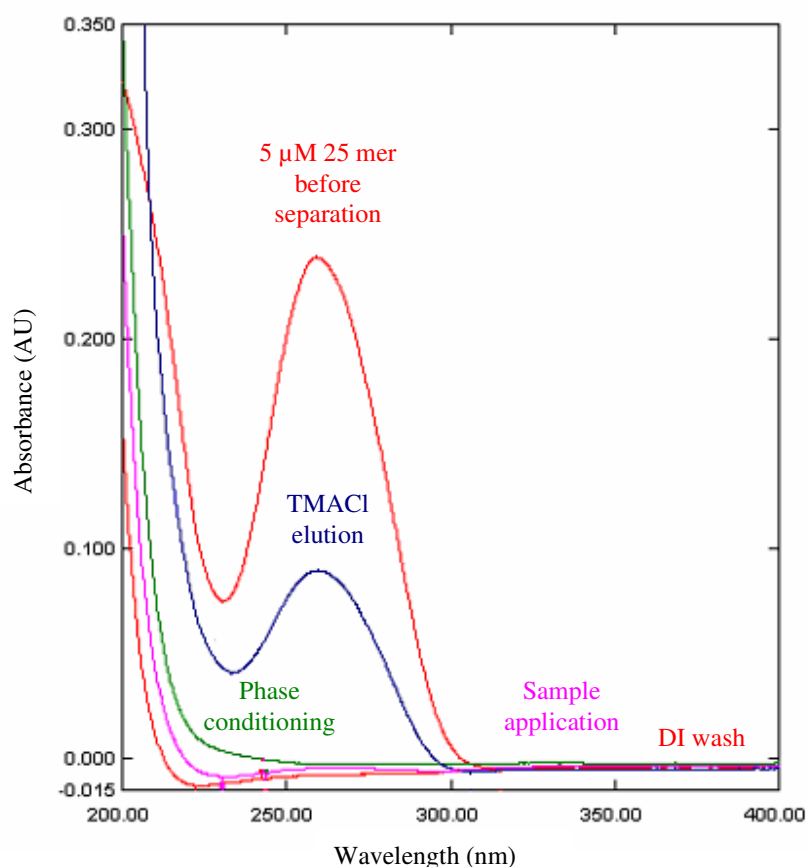


**Figure 2:15: Overlaid UV spectra of column eluents during various stages of a 25 mer oligonucleotide anion exchange SPE separation.**

From the UV data in Figure 2:15, it was calculated that 94% of the oligonucleotide was recovered from the phase during TMACl elution, confirming that the oligonucleotide was retained on the anion exchange phase, but more importantly the oligonucleotide was easily eluted with a high ionic strength mobile phase with good levels of recovery. Once it was confirmed that the phase was adequate at retaining oligonucleotides, and that the nucleic

acids could be eluted with relative ease, the separation method was applied to the sulfhydryl derivatised oligonucleotides.

The stage 1 reaction mixture (oligonucleotide-cystamine species before reduction, 0.5 ml) was injected onto a conditioned SPE cartridge and the phase was washed with 2 ml deionised water to remove the excess un-reacted reagents. Elution of the modified oligonucleotide was then achieved using 1.5 ml buffer containing 0.1 M ammonium chloride and 0.3 M citric acid, pH 7. The eluent was originally 1.5 M TMACl (Figure 2:15), but high background absorbance's were encountered which was attributed to the reagent being contaminated. Therefore, the eluent was changed to 0.3 M citric acid and 0.1 M ammonium chloride, pH 7. The wash step and oligonucleotide elution fractions were collected and analysed by UV/vis spectroscopy to confirm the elution of the reagents. Figure 2:16 shows the overlaid UV/vis spectra of the: phase conditioning step (step 1), sample application (step 2), deionised water wash step (step 3) and the oligonucleotide elution step (step 4). The spectrum from the phase conditioning step revealed that there was no absorbing species from the phase that may have interfered with the DNA detection. The spectrum corresponding to the sample application step (eluent collected during sample application) revealed that no analyte was eluted immediately upon application to the phase. The deionised water wash eluent had a very high absorbance below 300 nm, which was a consequence of the EDC and imidazole. Distinctive maxima at 257 nm can be seen in the citric acid, ammonium chloride elution step which corresponded to the oligonucleotide.

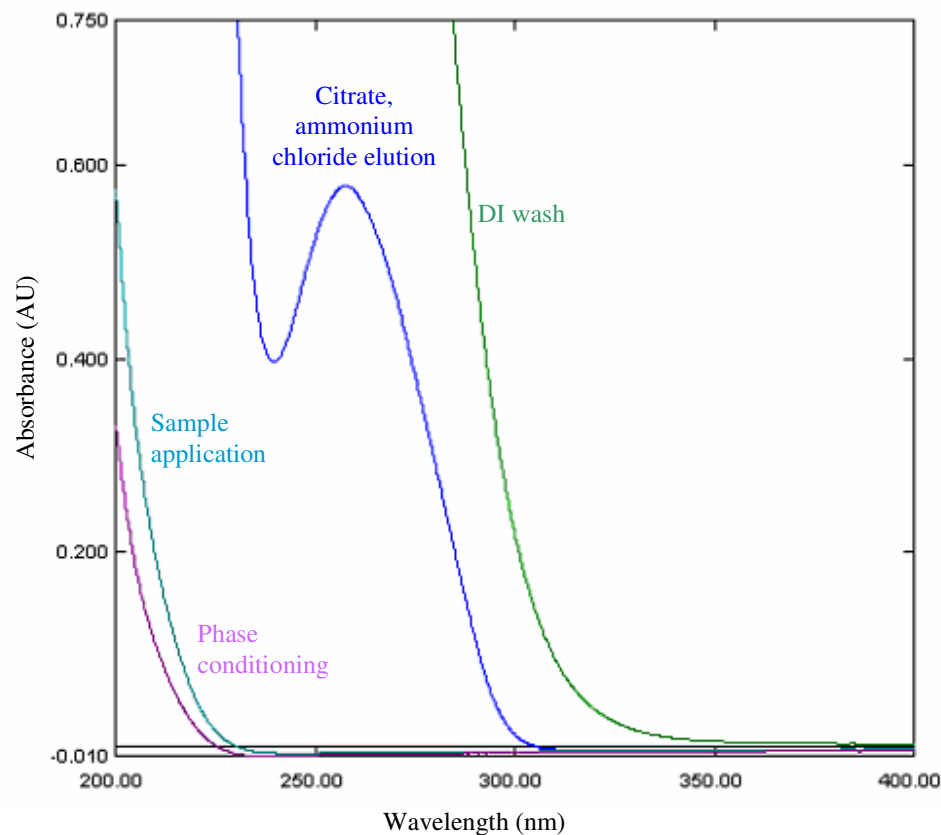


**Figure 2:16: Overlaid UV spectra of column eluents during various stages of anion exchange SPE of the stage 1 product (oligonucleotide-cystamine species), DNA concentration  $\sim 9 \mu\text{M}$ .**

The separated oligonucleotide from the stage 1 reaction was collected and reduced with the TCEP reducing beads to form the reactive sulfhydryl oligonucleotides. The reduced oligonucleotides were then separated on the anion exchange SPE cartridges as discussed above. The overlaid UV spectra in Figure 2:17 shows the phase conditioning step, sample application, deionised water wash step and the citrate, ammonium chloride elution step which resulted in elution of the modified DNA. Anion exchange separation of the oligonucleotides appeared to be successful, however, from these spectra it could not be confirmed whether the phosphate groups were actually converted to the sulfhydryl form.

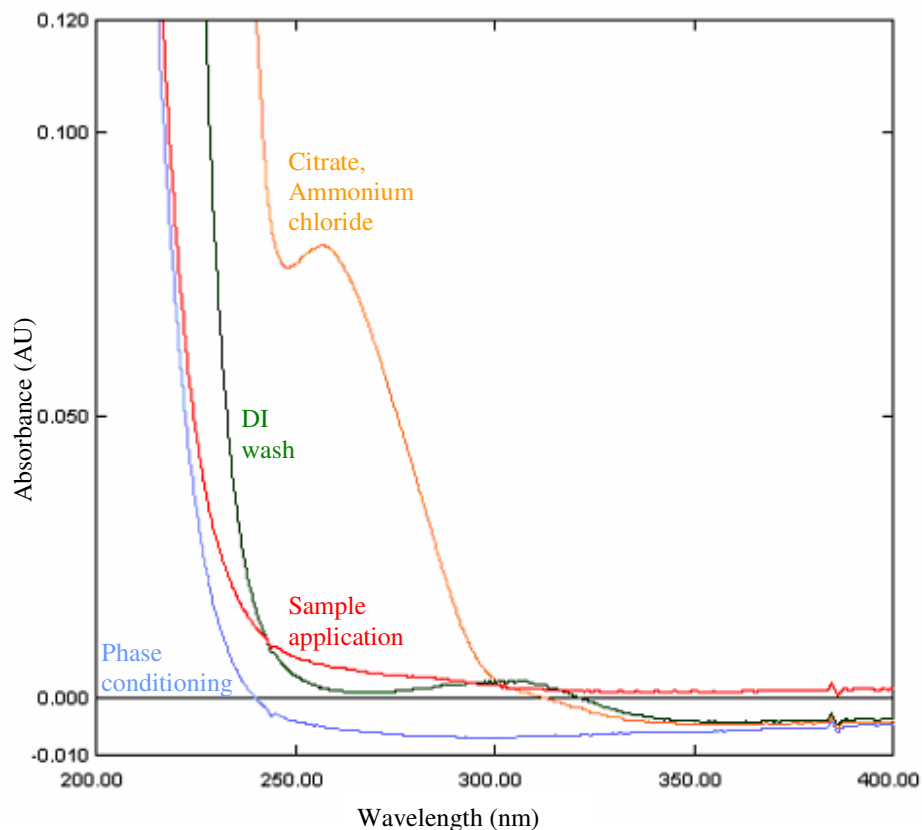


**Figure 2:17: Overlaid UV spectra of column eluents during various stages of anion exchange SPE of the stage 2 product, DNA concentration  $\sim 2 \mu\text{M}$ .**

Figure 2:17 clearly shows that DNA was eluted in the citrate, ammonium chloride elution steps. The recovery of the oligonucleotide from the phase was calculated to be 100% and 86% for the stage 1 and stage 2 separations respectively. This suggested that very little oligonucleotide was lost during the separations. However, the reaction efficiency for both stages was not calculated.

Ellman's assay was assessed for its suitability in confirming the presence of sulfhydryl groups in the sulfhydryl modified oligonucleotide sample. The concentration of sulfhydryl groups could then be calculated, allowing the reaction efficiency to be determined. The linearity of the cysteine calibration curves were quite poor, which was attributed to the very low absorbance readings obtained from the low concentration cysteine standards (typical absorbance readings ranged from 0.018-0.044 AU for a 1-20  $\mu\text{M}$  cysteine calibration). In



all cases, the calculated concentration of sulfhydryl groups in the samples was much higher than expected. The procedure that was followed recommended preparing calibration curves in the concentration range 0.1-10 mM cysteine.<sup>111</sup> Since the concentration of sulfhydryl groups in this particular investigation was anticipated to be much lower than 0.1-10 mM, the calibration was prepared in the range 1-20  $\mu$ M cysteine. Therefore, it was decided that Ellman's assay was not suitable for the determination of very low levels ( $\mu$ M range) of sulfhydryl groups used here, and that 1-20  $\mu$ M was probably below the assay limit of detection, hence spurious results were obtained.<sup>111</sup>

## **2.4.2 Labelling Results**

### **2.4.2.1 Labelling of Di-nucleotides**

As discussed in section 2.3.3.1, the disulfide modified di-nucleotides were reduced with DTT; the reduced oligonucleotides were then separated from excess DTT by gel filtration before being added to MMN. The separation of unbound MMN and MMN labelled di-nucleotides in the resulting reaction mixture was carried out with the TSKgel-DNA-NPR analytical column (7.5 cm x 4.6 mm), which was coupled directly to an ICP-MS instrument. Prior to injection, a 100  $\mu$ l aliquot of the di-nucleotide-MMN tagging mixture was diluted with the same volume of deionised water in a micro HPLC vial. The diluted reaction mixture was then injected directly onto the anion exchange column. Figure 2:18 shows the HPLC-ICP-MS data, corresponding to  $^{31}\text{P}^{16}\text{O}$  and  $^{197}\text{Au}$  signals observed during the separation of the MMN-di-nucleotide tagging reaction mixture.

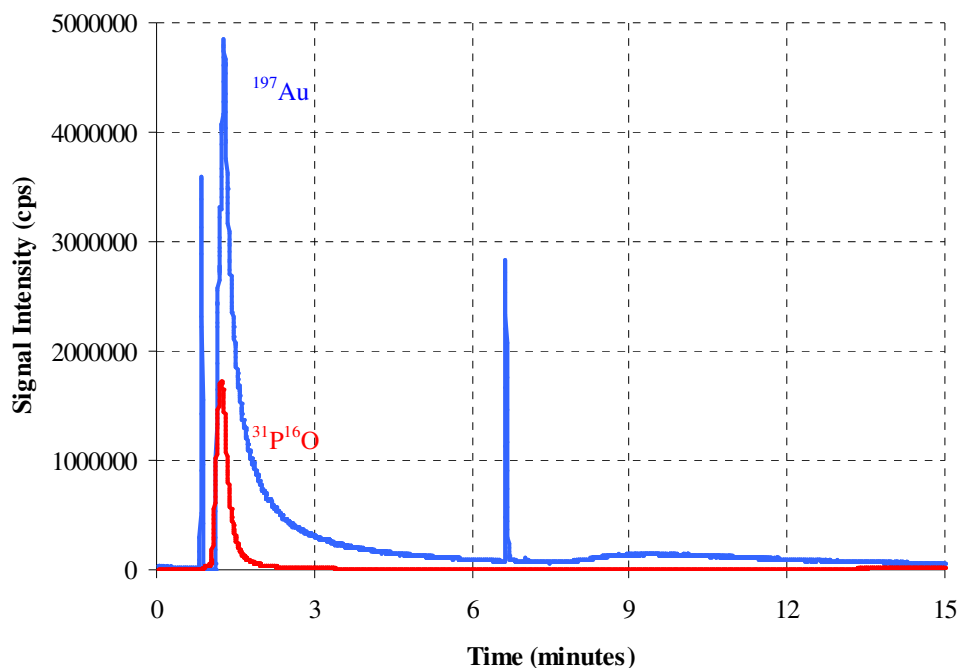


**Figure 2:18:**  $^{197}\text{Au}$  and  $^{31}\text{P}^{16}\text{O}$  signal intensity during separation of the MMN-di-nucleotide tagging reaction mixture. TSKgel-DNA-NPR 7.5 cm x 4.6 mm column, mobile phase A = 20 mM tris-HCl, pH 9, B = 20 mM tris + 0.3 M citrate and 0.1 ammonium chloride, pH 9. 0 mins = 0% B, 2 min = 0% B, 15 min = 100% B, 17 min = 100% B. Flow rate =  $0.7 \text{ ml min}^{-1}$ , 10  $\mu\text{l}$  injection volume.

From Figure 2:18, it appears that there were three Au peaks at 0.87, 1.27 and 6.67 minutes. However, it was realised that in fact there were only two Au peaks, the first two Au signals at 0.87 and 1.37 minutes were actually part of the same peak. The sample was not diluted enough before injection, hence the Au signal intensity exceeded the detector threshold ( $>5\,000\,000$  cps), at the peak apex, which resulted in a signal intensity of zero being recorded around the peak apex, thus giving the appearance of two peaks. Therefore, the first Au peak (0.87 and 1.37 minutes peaks combined) was very broad with the width at the base  $\sim 5$  minutes. The Au signal did not return to baseline level and even increased further at  $\sim 9$  minutes. The erratic, elevated baseline and broad Au peak may have resulted from overloading the column with MMN. The Au peak at 6.67 minutes was not reproducible and could not be explained; suggesting that this signal was an artefact. At 1.25 minutes, a  $^{31}\text{P}^{16}\text{O}$  peak was observed. At this stage it was unknown whether the  $^{31}\text{P}^{16}\text{O}$  peak was due to the di-nucleotide or the phosphate buffer that was present in the MMN. UV data was also

collected during the separation, however, only the first Au peak at 0.87 minutes was detected by the UV detector.

A lot of unanswered questions were raised from the experiment, namely, why was the Au baseline erratic, what was the identity of the  $^{31}\text{P}^{16}\text{O}$  peak and the cause of the spurious Au peak at 6.67 minutes. As a result, the procedure was repeated again, but some amendments to the separation and detection method were made. The disulfide modified di-nucleotide was reduced and purified by gel filtration as discussed previously. But, to ensure the correct fraction was collected from the column during the separation of the di-nucleotide and DTT, the gel filtration column was connected to both a UV detector and ICP-MS. Thus, the UV, P and S signals were monitored simultaneously during purification to ensure that the correct oligonucleotide fraction was being used for MMN labelling. Figure 2:19 shows the elemental ( $^{31}\text{P}^{16}\text{O}$  and  $^{32}\text{S}^{16}\text{O}$ ) chromatograms, during the gel filtration separation of the sulfhydryl modified di-nucleotide and DTT.

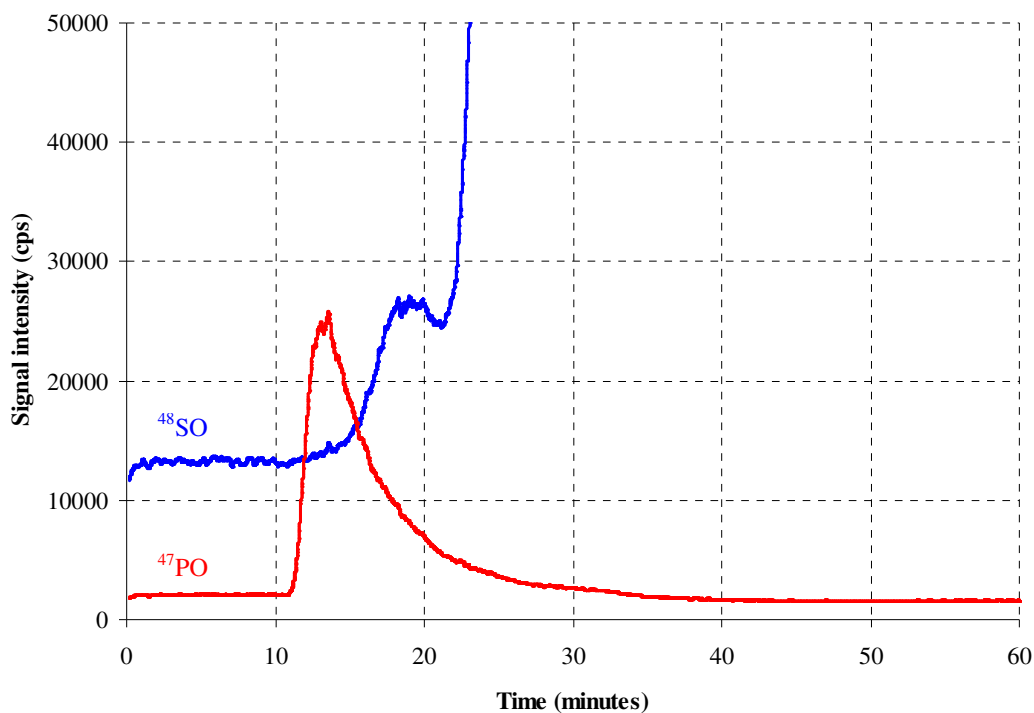


**Figure 2:19:**  $^{31}\text{P}^{16}\text{O}$  and  $^{32}\text{S}^{16}\text{O}$  signal intensity during the gel filtration separation of sulfhydryl modified di-nucleotide and DTT.

The sulfhydryl modified oligonucleotide contained both P and S, Figure 2:19 confirmed that both P and S were present at approximately 16 minutes, suggesting that the oligonucleotide eluted at this retention time. However, the S signal dramatically increased from 20 minutes onwards due to the excess DTT in the reaction mixture. As a result, great care was needed to ensure that the sulfhydryl modified di-nucleotide was collected but not the DTT. For this reason, the oligonucleotide fraction eluting between 11-16 minutes was collected for MMN labelling. A 100  $\mu$ l aliquot of the reduced di-nucleotide was then added to 150  $\mu$ l MMN. The reaction was allowed to proceed at 4 °C for approximately 24 hours.

Before, the reaction mixture was separated and detected by HPLC-ICP-MS, it was diluted 50 fold in 5 mM tris-HCl and the separation parameters were modified. The ionic strength of the HPLC mobile phase was reduced (mobile phase A = 5 mM tris-HCl, pH 9, mobile phase B = 5 mM tris + 0.1 M ammonium chloride, pH 9) to ensure that the di-nucleotide was retained on the anion exchange resin. The previous experiment resulted in a  $^{31}\text{P}^{16}\text{O}$  peak at 1.25 minutes (Figure 2:18). If this peak was due to the di-nucleotide, then it eluted very quickly, but more importantly, it eluted at the same time as the MMN resulting in no separation. Reducing the mobile phase ionic strength should ensure that the oligonucleotide was retained for longer and thus resolved from the unbound MMN.

The  $^{197}\text{Au}$  and  $^{31}\text{P}^{16}\text{O}$  chromatograms from the repeated tagging experiment are shown in Figure 2:20. A large  $^{197}\text{Au}$  peak was observed at approximately 1.3 minutes, which corresponded to the free unbound MMN. As expected, the MMN had no retention on the anion exchange phase, since the neutral nano-particle had no interaction with the positively charged amine groups on the non-porous resin. After elution of the unbound MMN, the Au signal returned to baseline, but rose again after ~9 minutes and continued rising throughout the separation. At 11.8 minutes a small Au peak was observed, which was initially thought to correspond to the MMN-di-nucleotide conjugate. However, it was discovered that the unlabelled di-nucleotide eluted at 12.8 minutes, suggesting the Au peak at 11.8 minutes was not due to the bound di-nucleotide. In addition, a similar Au peak was also observed in the blank injection at the same retention time, further confirming that the Au peak at 11.8 minutes was not due to the labelled oligonucleotide. The large  $^{31}\text{P}^{16}\text{O}$  peak at

approximately 13 minutes was due to a contaminant, either on the column or in the injection system. This large signal was observed at exactly the same time in every injection and co-eluted with the di-nucleotide. This definitively confirmed the Au peak at 11.8 minutes was not attributed to the MMN labelled di-nucleotides.

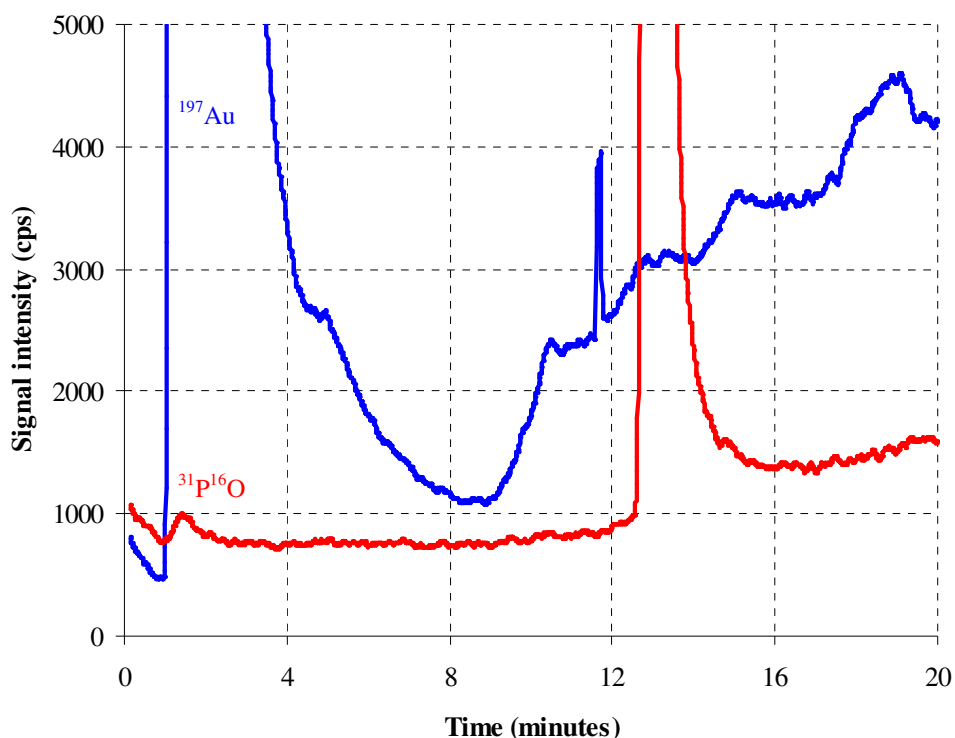


**Figure 2:20:** ICP-MS data for the MMN-di-nucleotide tagging reaction mixture. TSKgel-DNA-NPR 7.5 cm x 4.6 mm column. Mobile phase A = 5 mM tris-HCl, pH 9 B = 5 mM tris + 0.1 M ammonium chloride, pH 9. 0 min = 0% B, 3 min = 0% B, 15 min = 100% B. Flow rate = 0.5 ml min<sup>-1</sup>. 10  $\mu$ l injection volume.

Although the above tagging reaction mixture was diluted 50 fold prior to HPLC-ICP-MS analysis, a response exceeding 200 000 counts per second was still obtained for the Au peak at 1.3 minutes. Therefore, the rising baseline from 9 minutes onwards could have resulted from column overloading. The column was cleaned and repeatedly flushed with both high ionic strength eluents, and eluents containing 20% organic solvent in an attempt to remove any retained material from the phase. The experiment was then repeated with more diluted reaction mixtures in an attempt to avoid overloading the column and elevating the baseline.

The tris-HCl mobile phase was also reconsidered, since it is known that the maleimide ligand can become reactive towards primary amines above pH 7. Tris-HCl base (tris(hydroxymethyl)aminomethane) contains a primary amine and was used as the HPLC eluent at pH 9 throughout the study. The possibility of the tris-HCl buffer reacting with the unbound MMN was considered, alternatively, the high pH could have degraded the probe. The manufacturer of the probe confirmed that MMN was stable in the presence of amines at high pH values once MMN was bound to sulfhydryl groups, hence this should not have been an issue. In addition, the maleimide ligand on any unbound MMN would have hydrolysed, hence not reacting with the tris base. Despite the manufacturer's reassurance that tris-HCl was suitable for conjugate separation, the separation was repeated using bicine buffer (5 mM bicine, pH 9) in place of tris-HCl. Bicine contains a tertiary amine so should not have any reactivity towards MMN. In addition, the pKa value and buffering range of bicine is similar to tris-HCl. Despite these amendments to the procedure, a small rise in Au background throughout the separation was still observed, although not as pronounced as when tris-HCl was used in the eluent. A key finding was that the small Au peak that was previously observed at 11.8 minutes, and was initially thought to be the MMN-di-nucleotide conjugate, was observed during the separation of the MMN retention time marker (no oligonucleotide present). The chromatograms of the MMN retention time marker and MMN-di-nucleotide reaction mixture, using the bicine mobile phase are shown Figure 2:21.

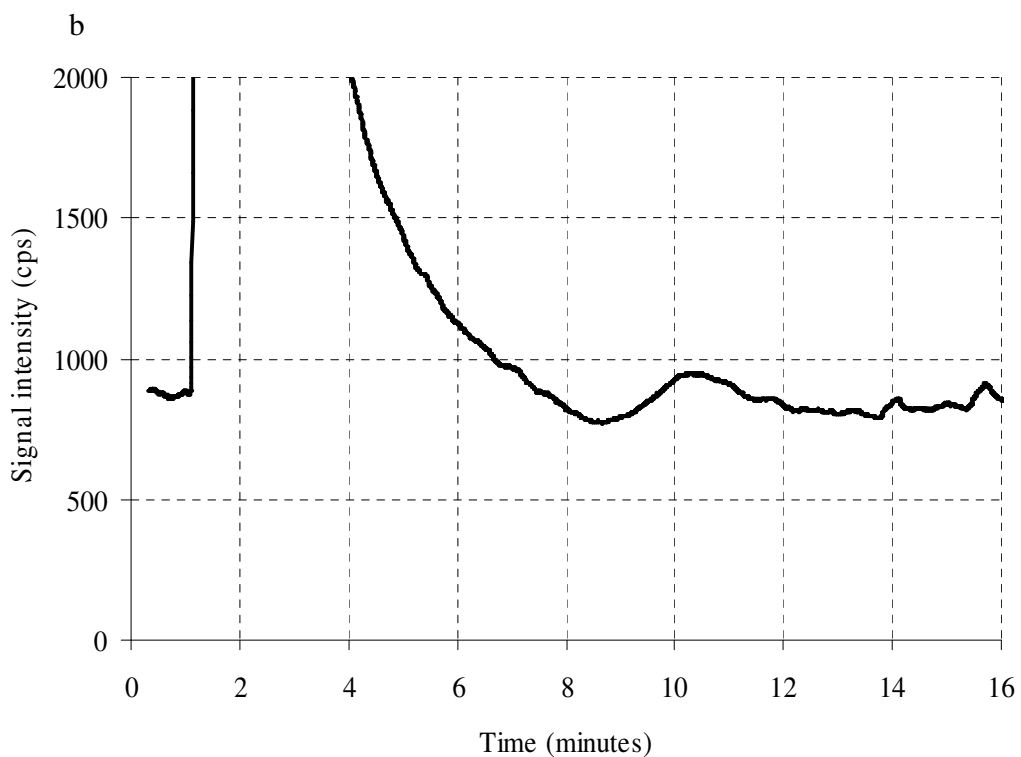
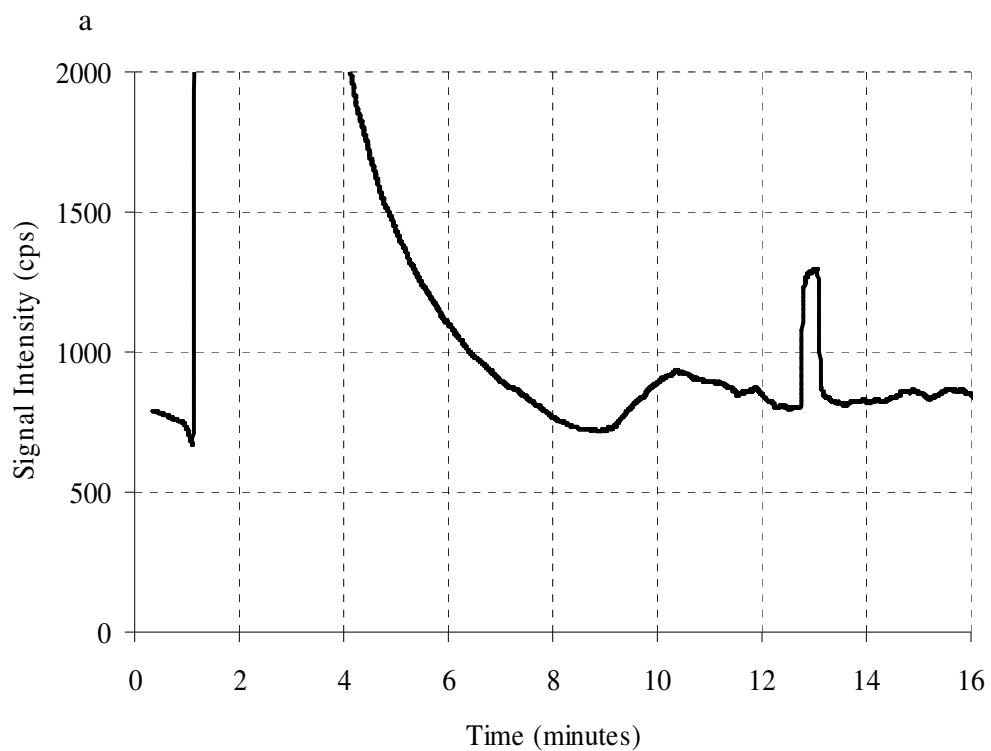


**Figure 2:21: a) Au signal during the injection of the MMN retention time marker. b) Au signal intensity during separation of the MMN-di-nucleotide tagging reaction mixture. Bicine was employed as an eluent for both injections.**

Despite attempts to ensure the sample preparation procedure was adequate for Au labelling, the MMN-di-nucleotide tagging experiments were unsuccessful. The limiting factor to success was thought to be the sample preparation procedure, which involved several steps; reduction of the disulfide bond with DTT, followed by removal of DTT by gel filtration. ICP-MS was used in conjunction with UV detection to ensure the correct oligonucleotide fraction was being used for MMN labelling. However, gel filtration is a relatively inefficient method of sample purification; even trace quantities of DTT in the collected di-nucleotide fraction may have adversely affected the maleimide-sulfhydryl coupling. Thus, the gel filtration separation may not have been sufficient for DTT removal. Reoxidation of the sulfhydryl group to yield the disulfide may be another factor that was resulting in poor tagging results. Reformation of the disulfide bond can occur by exposing the oligonucleotide to the atmosphere. Trace metal ions can also aid reformation of the disulfide, although 1 mM EDTA was added to the gel filtration eluent and reaction buffer to complex any divalent metal ions that could have potentially reoxidised the oligonucleotide. The oligonucleotides had an approximate retention time of 20 minutes. The formation of disulfide bonds between oligonucleotides to produce di-nucleotides bridged by a disulfide bond would have rendered the di-nucleotides un-reactive upon elution.

#### **2.4.2.2 Labelling of 25 mer Oligonucleotides**

The 25 mer labelling reactions were more successful than those for the di-nucleotides. The 25 mer oligonucleotides used in this particular stage of the investigation were supplied in the reactive sulfhydryl form, instead of the disulfide form as in the case of the di-nucleotides. As a result, the 25 mers did not require additional sample preparation. Initially, a sample of unmodified 25 mer (containing no MMN) containing the same base sequence as the sulfhydryl modified 25 mer was injected onto the TSKgel-DNA-NPR guard column, to establish the retention time. In addition, a MMN retention time marker was injected to establish the retention time of the unbound MMN. The retention times of unbound MMN and 25 mer were 0.10 and 6.98 minutes respectively. The UV chromatograms of both reagents can be seen in Figure 2:22. Citric acid has a residual absorbance at 260 nm, consequently the UV baseline increased during gradient elution due to the increasing proportion of citric acid.



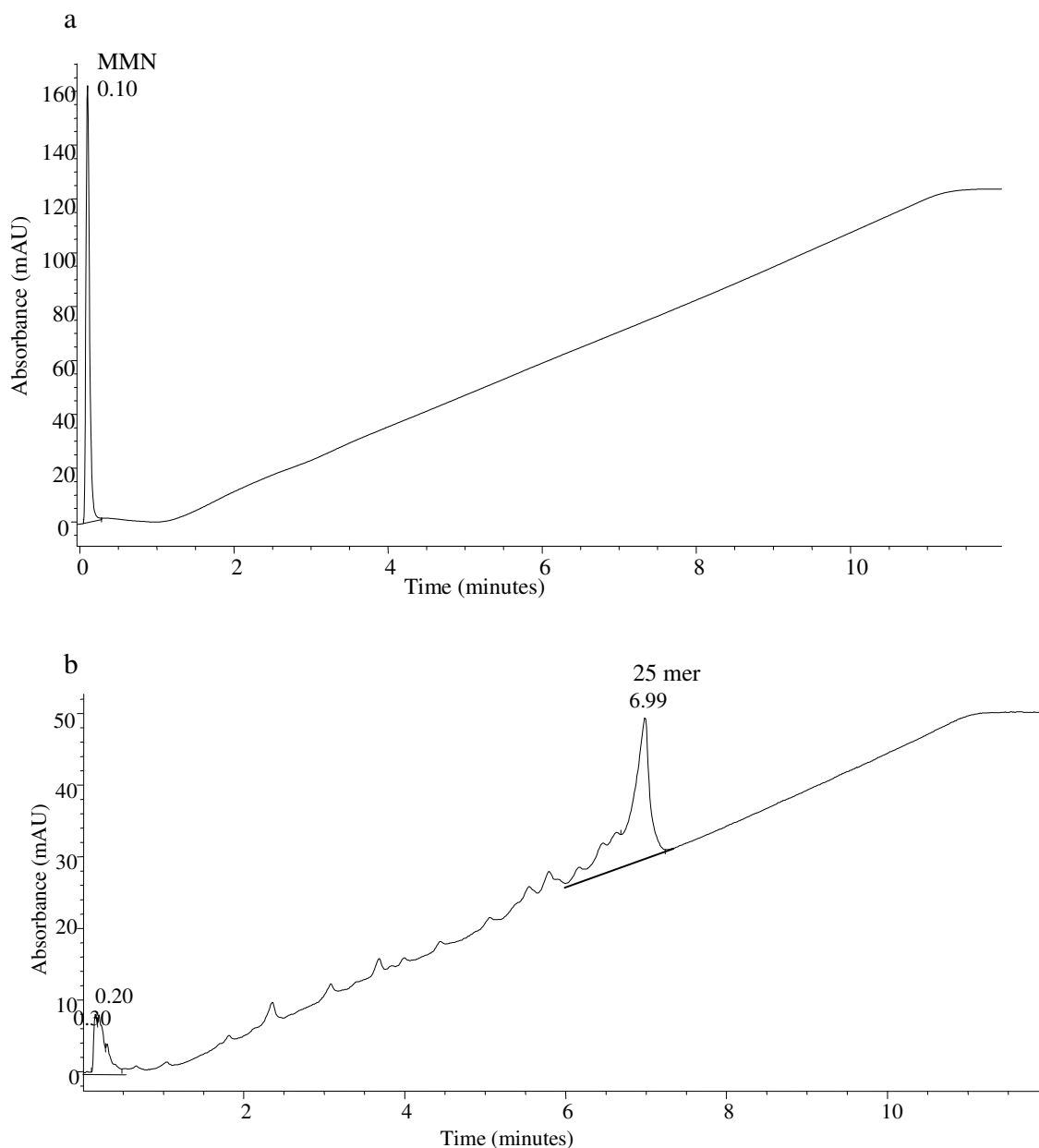


**Figure 2:22: a) Unbound MMN (3  $\mu$ M). b) Unlabelled and unmodified 25 mer oligonucleotide (10  $\mu$ M). Both samples eluted from a TSKgel-DNA-NPR guard column with 20 mM tris-HCl, pH 9 (A) and 20 mM tris + 0.3 M citrate and 0.1 M ammonium chloride, pH 9 (B). Gradient = 10% B at 0 min, 90% B at 10 min and 90% B at 12 min. Flow rate = 1 ml min<sup>-1</sup>. Wavelength = 260 nm.**

The UV chromatogram of the tagging mixture is shown in Figure 2:23. Note that the peak corresponding to unbound MMN appeared at 0.13 minutes as expected, but an additional small broad peak was observed at 7.06 minutes, which was thought to correspond to the MMN-25 mer conjugate. This retention time was slightly later than the unbound 25 mer

(6.99 minutes), but if the oligonucleotide was covalently bound to a 15 KDa probe, then it is not unrealistic to expect a slight shift in retention time.

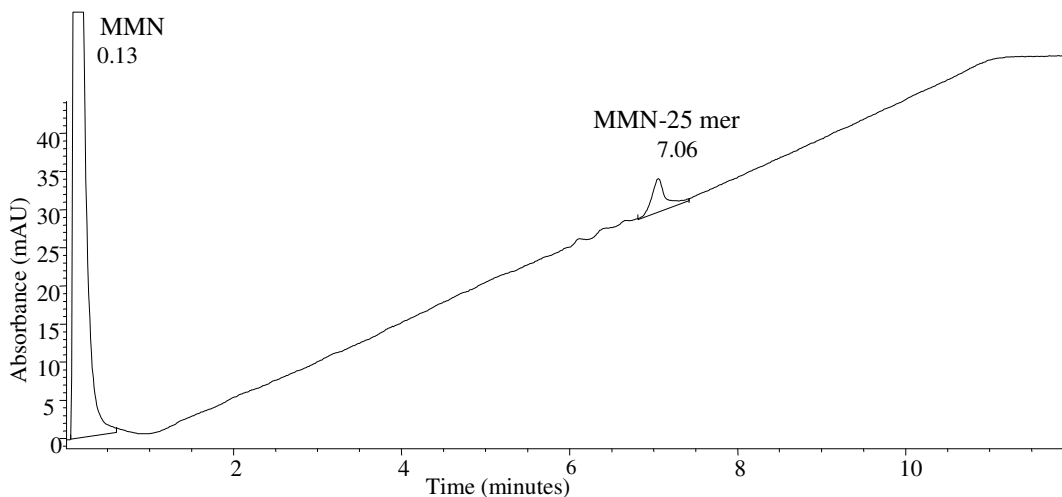


**Figure 2:23:** Chromatogram of the MMN-25 mer tagging reaction mixture eluted from a TSKgel-DNA-NPR guard column with 20 mM tris-HCl, pH 9 (A) and 20 mM tris + 0.3 M citrate and 0.1 M ammonium chloride, pH 9 (B). Gradient = 10% B at 0 min, 90% B at 10 min and 90% B at 12 min. Flow rate = 1 ml min<sup>-1</sup>. Wavelength = 260 nm.

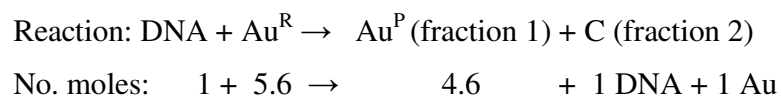
The MMN-25 mer reaction mixture was injected onto the column again, but the following fractions were collected from the column outlet during elution: 0-3 minutes (fraction 1) and 7-9 minutes (fraction 2). These fractions were collected during the following injections and separations; blank, unmodified 25 mer, MMN only and tagging reaction mixture separation. Fractions were collected between 0-3 minutes and 7-9 minutes because these time frames correspond to the elution of the unbound MMN and MMN-25 mer conjugate respectively. The fractions were diluted accordingly and analysed by ICP-MS. The summarised data is shown in Table 2:7, which shows that significant Au counts were observed in the tagging sample fractions; ~100 000 and 3300 cps were obtained for fractions 1 and 2 respectively. The Au signal in each of the tagging sample fractions was significantly higher than the signal observed in the blank injection fractions.

**Table 2:7: Summarised ICP-MS data for HPLC fractions collected during elution of the MMN-25 mer samples.**

Sample	Fraction 1: 0-3 min	Fraction 2: 7-9 min
	Au (cps)	Au (cps)
Blank	300	204
MMN retention time marker	52492	
25 mer retention time marker		96
Reaction mixture	96172	3349

The chromatogram corresponding to the MMN-25 mer mixture, shown in Figure 2:23 revealed that the majority of the MMN was unbound, hence it eluted in the void volume at 0.13 minutes. ICP-MS data confirmed that the peak at 7.06 minutes contained significant Au counts and therefore corresponded to the MMN-25 mer conjugate. Unfortunately, data was not collected for fraction 2 of the MMN retention time marker and fraction 1 of the 25 mer retention time marker.

Once nano-particle labelling of the DNA was indicated, it was necessary to calculate the efficiency of reaction. It is important to obtain maximum labelling efficiency to enable maximum signal enhancement and therefore sensitivity. In the above experiment, the MMN was in a 5.6 fold molar excess of DNA, and only one MMN probe will bind to a DNA molecule giving a 1:1 labelling ratio:



Where:

DNA = sulfhydryl modified DNA added to the reaction.

Au = free MMN. Superscript R refers to the reactant MMN and P refers to the MMN upon completion of the reaction.

C = MMN-DNA conjugate formed during the reaction.

The ratios of Au signal intensities for the two collected fractions were compared in order to calculate the labelling efficiency. If the reaction was 100% efficient, then the mole ratio of Au<sup>P</sup> to C would be 4.6. e.g.

$$\text{Au Mole Ratio} = \frac{\text{Au}^{\text{P}}}{\text{C}} = \frac{4.6}{1} = 4.6$$

Therefore, 4.6 times as many Au counts should have been observed in fraction 1 (Au<sup>P</sup>) compared to fraction 2 (C). In the above case, 96 172 cps and 3 349 cps of Au were observed in the first and second fractions of the reaction mixture respectively. Fraction 1 and 2 consisted of 3 ml and 2 ml respectively, therefore, if the appropriate dilution factors are applied, 43.08 times as many Au counts were observed in fraction 1 (Au<sup>P</sup>), so the observed Au ratio becomes:

$$\text{Observed Au Mole Ratio} = \frac{\text{Au}^{\text{P}}}{\text{C}} = \frac{96172}{2232.67} = 43.08$$

Once the Au ratios corresponding to 100% labelling and observed labelling are calculated, the labelling efficiency can be established by comparing the two ratios;

$$\% \text{ Labelling Efficiency} = \frac{4.6}{43.08} \times 100 = 10.68 \%$$

Therefore ~1/10<sup>th</sup>, or 10.7% of the DNA was successfully labelled in the above example.

The relative responses of Au and P by ICP-MS also have to be considered, and the enhancement in signal has to be calculated to demonstrate that elemental labelling does improve biomolecule detection by ICP-MS. Since DNA contains phosphate groups, detection is possible through P measurement, but as already discussed, P measurement by ICP-MS does have its limitations. In the above experiment, the oligonucleotide contained 25 P atoms. If each labelled oligonucleotide contained 80 Au atoms, a P:Au ratio of 24:80 or 1:3.3 was achieved. Therefore, 3.3 times as many Au atoms were present on each labelled oligonucleotide compared to P. However, the relative sensitivities of P and Au

have to be considered, which was determined by ICP-MS. Briefly, two calibration curves were prepared, one for Au and the other for P. The gradients of the Au and P calibration curves were 12 421 and 101 respectively (x axis expressed as ng ml<sup>-1</sup>). Thus, the Au gradient was 123 times greater than that of P, or it can be said that Au gave 123 times greater signal than P, proving that Au has a greater sensitivity than P when measured by ICP-MS. But, each labelled oligonucleotide contained 3.3 times more Au atoms than P. As a result, the 123 Au enhancement factor can be multiplied by 3.3 to give 406, demonstrating that 406 times greater sensitivity was obtained when measuring Au labelled 25 mer oligonucleotides compared to measuring P alone. If the 406 enhancement factor is multiplied by the 10.7% labelling efficiency (calculated above), a 43 fold greater signal was obtained when measuring MMN labelled 25 mers compared to P. This calculation demonstrates that even low labelling efficiencies can result in significant signal enhancement and could be used to obtain lower limits of detection.

The above calculated signal enhancement factor was applicable to 25 mers, but it should be considerably greater for smaller nucleic acids such as the di-nucleotides. Di-nucleotides contain two P atoms, thus if these short chain nucleic acids were labelled with 80 Au atoms, then there would be 40 times as many Au atoms compared to P. If the 123 Au enhancement factor is then multiplied by the factor of 40, potentially 4920 times greater response would be obtained when detecting Au labelled di-nucleotides by ICP-MS compared to measuring P alone. In the case of di-nucleotides which only contain two P atoms, the limits of detection when measuring P alone would be quite poor due to the low number of P atoms per nucleic acid, so the signal enhancement achieved by Au labelling would be more beneficial to short chain nucleic acids.

### **Optimisation of Reaction Conditions**

The MMN labelling samples were stored for various periods of time, at either room temperature or 4 °C, and then separated by HPLC and the fractions were collected from the column outlet at, 0-0.5 minutes (fraction 1) and 7-7.5 minutes (fraction 2) during elution. Fractions 1 and 2 corresponded to the unbound MMN and MMN-DNA conjugates respectively. A blank injection consisting of 20 mM tris-HCl sample solvent was also

fraction collected at 0-0.5 minutes and 7-7.5 minutes, to establish the background Au counts on the column. The Au signal intensities for the blank, reaction samples and retention time markers are summarised in Table 2:8. The unbound MMN eluted within fraction 1 and any MMN labelled 25 mer should have eluted in fraction 2. Hence, the Au signal intensity in each fraction was determined to establish the MMN labelling efficiency.

**Table 2:8: <sup>197</sup>Au signal intensity for the MMN optimisation reactions.**

<b>Sample</b>	<b>Fraction 1 Au signal (cps)</b>	<b>Fraction 2 Au signal (cps)</b>
Blank	195.34	227.00
25 mer only	95.67	139.33
Nanogold only	4484.70	211.34
<b>4 °C reactions</b>		
1 hour	38616.81	452.34
5 hour	57660.14	749.02
10 hour	77733.93	619.35
24 hour	83788.01	674.35
48 hour	71604.05	730.35
65 hour	29888.58	480.01
<b>Room temperature reactions</b>		
1 hour	47996.83	423.01
5 hour	36819.07	842.03
10 hour	61581.46	784.36
24 hour	72449.58	1121.38
48 hour	81653.37	1023.04
65 hour	19100.43	455.01

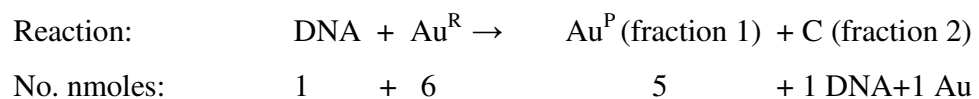
All of the above samples contained Au in fraction 2 (DNA-MMN conjugate fraction) that were above the background Au signal. The room temperature reactions generally gave higher Au counts than the lower temperature reactions, with the exception of the 1 and 65 hour samples. The Au counts presented in Table 2:8 were relatively low. A 2% *aqua regia* solution was aspirated between samples to aid Au wash out from the sample introduction system. *Aqua regia* was chosen because Au is very soluble in this acid; hence it should be effective at minimising carry over between samples. However, it was noted that the Au signal intensity increased during the *aqua regia* wash, suggesting that some Au was adhering to the walls of the sample introduction system and not being measured, resulting

in relatively low signal intensities for the labelled conjugates, as shown in Table 2:8. Thus, when *aqua regia* was aspirated, the deposited Au was being removed from the sample introduction system. As a result, the above Au signal intensities for the two sets of fractions may not be accurate thus effecting the reaction efficiency calculations.

The very high Au backgrounds that were observed during the acid wash did not decrease over time as expected. This suggested that the Au contamination was due to the sample bottles or reagents rather than the sample introduction system. The polypropylene sample bottles were therefore soaked in 5-10% *aqua regia* before use. This had the desired effect of removing residual Au from the bottles prior to analysis and reduced the background Au signal upon acid aspiration. It has also been reported that the S containing amino acid, cysteine is effective at complexing residual Au on the surfaces of sample introduction systems, and improving Au wash out between samples.<sup>106</sup> Gold has high affinity for S since Au is a soft Lewis acid and S a soft Lewis base. A 10 mM cysteine solution was prepared and aspirated, which resulted in the Au signal increasing. This was again due to the cysteine complexing to Au in the sample introduction system and aiding wash out. Various wash out procedures containing *aqua regia* and cysteine were investigated; the most effective procedure involved aspirating both 5% *aqua regia* followed by 10 mM cysteine between samples. In addition, spiking Au solutions with *aqua regia* (2-5% acid) improved Au signal intensity. This was presumably because the acid stabilised the analyte in solution.

The above analysis was repeated, but the collected fractions were diluted 20 fold with 5% *aqua regia* prior to ICP-MS determination. Gold standards were also prepared at a concentration range of 1-3 ng ml<sup>-1</sup> in a 5% *aqua regia* matrix to allow quantification of Au in each fraction. The Au signal intensities for each fraction are shown in Table 2:9 and were used to calculate the labelling efficiency of each reaction. The labelling efficiency was calculated in the same way to that detailed above (Chapter 2.4.2.2), namely, the observed and 100% labelling Au ratio were calculated and used to calculate overall labelling efficiency. The dilution factors were considered; hence the appropriate dilution factors were applied to the Au counts, to ensure the ratios were calculated using equivalent signal intensities. The reaction stoichiometry then had to be considered. The majority of

optimisation samples contained 6 nmoles of MMN and 1 nmole of DNA, therefore this stoichiometry will be used as an example:



Since, 1 nmole of DNA was present in the reaction; the maximum number of moles of MMN in the conjugate fraction was 1 nmole, since MMN binds to thiol containing compounds in a 1:1 stoichiometry. The data for each sample is shown in Table 2:9.



**Table 2:9: Reaction optimisation results and corresponding reaction efficiencies.**

Sample	Overall dilution factor	Au counts (cps)	nMoles of Au in Reaction	Expected Au <sup>P</sup> /C Ratio	Observed Au <sup>P</sup> /C Au Ratio	Labelling Efficiency (%)
Blank Fraction 1	200	471.71			3.1566	
Blank Fraction 2	201	149.43				
25 mer only Fraction 1	202	118.97			0.9638	
25 mer only Fraction 2	200	123.43				
Nanogold Only Fraction 1	201	12905.20			40.9036	
Nanogold Only Fraction 2	202	315.50				
1hr 4 degrees Fraction 1	844	39693.58	6	5	156.1425	<b>3.20</b>
1hr 4 degrees Fraction 2	200	1072.27				
1hr RT Fraction 1	847	40935.72	6	5	143.7576	<b>3.48</b>
1hr RT Fraction 2	200	1205.08				
5hr 4 degrees Fraction 1	816	52646.08	6	5	185.0718	<b>2.70</b>
5hr 4 degrees Fraction 2	202	1148.81				
5hr RT Fraction 1	820	41294.20	6	5	97.7066	<b>5.12</b>
5hr RT Fraction 2	201	1721.17				
10hr 4 degrees Fraction 1	809	35638.86	6	5	120.3896	<b>4.15</b>
10 hr 4 degrees Fraction 2	200	1198.05				
10 hr RT Fraction 1	818	38290.48	6	5	142.6340	<b>3.51</b>
10hr RT Fraction 2	201	1094.34				
24hr 4 degrees Fraction 1	821	24523.80	6	5	123.0922	<b>4.06</b>
24 hr 4 degrees Fraction 2	200	817.89				
24 hr RT Fraction 1	867	22545.08	6	5	75.9091	<b>6.59</b>
24 hr RT Fraction 2	200	1289.86				
48 hr 4 degrees Fraction 1	828	22807.83	6	5	161.4230	<b>3.10</b>
48 hr 4 degrees Fraction 2	200	585.55				
48 hr RT Fraction 1	808	26078.04	6	5	152.8676	<b>3.27</b>
48 hr RT Fraction 2	202	683.55				
65 hr 4 degrees Fraction 1	811	12726.30	2.25	3.5	290.0989	<b>1.21</b>
65 hr 4 degrees Fraction 2	201	176.83				
65 hr RT Fraction 1	801	13106.98	2.25	3.5	272.2664	<b>1.29</b>
65 hr RT Fraction 2	200	192.80				

Very low Au counts were observed in the blank and retention time markers. This was true for both fractions, again suggesting that the observed Au in fraction 2 of the optimisation

samples was due to the MMN-DNA conjugate. The calculated labelling efficiencies ranged from 1.21-6.59%, with the highest labelling efficiency corresponding to the 24 hour room temperature reaction. Generally, the room temperature reactions gave higher labelling efficiencies compared to those reactions stored at 4 °C. This observation was expected, since ambient room temperature would not have compromised the stability of the MMN probe and higher temperatures generally favour faster reaction times. The 10 hour reactions were the only exception to this rule, where the lower temperature reaction gave a slightly higher labelling efficiency.

The data presented in Table 2:9 does not display any trends. It was expected that the labelling efficiency would gradually increase with increasing reaction time, until a plateau was reached and the efficiency would remain fairly constant. Instead of the expected trend, the labelling efficiencies were quite variable as illustrated in Figure 2:24, which shows graphically the variation in labelling efficiencies with reaction time. The efficiency of the room temperature reactions initially increased with reaction time, but then decreased at 10 hours, followed by a large increase in efficiency at 24 hours, where the maximum labelling efficiency was observed.

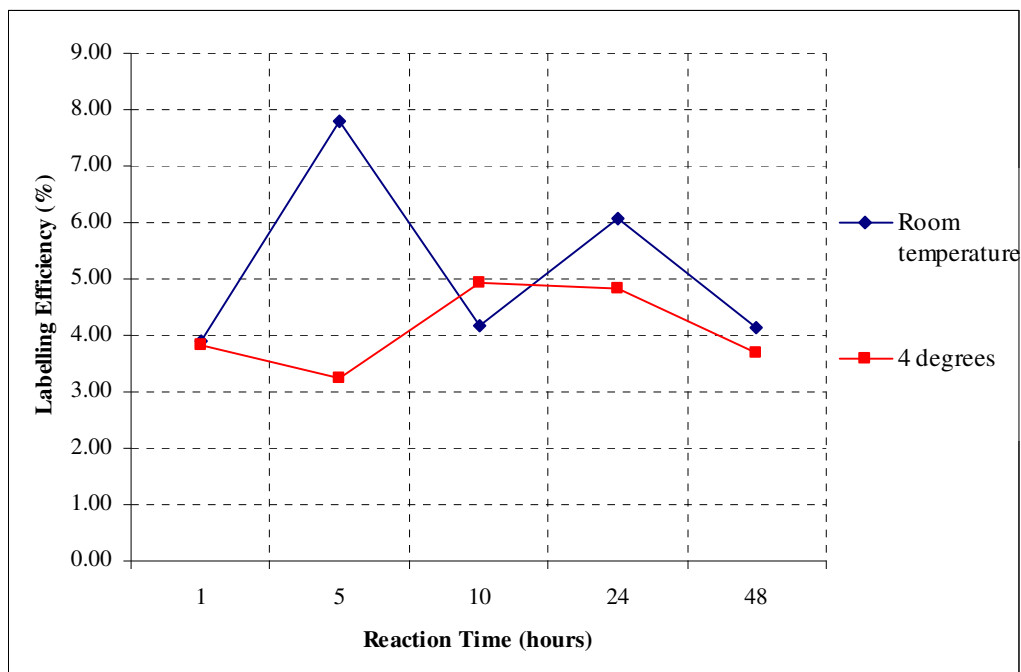


Figure 2:24: MMN labelling efficiency with time.

The highest labelling efficiency for the 4 °C reactions was observed at 10 hours with 4.15% labelling achieved. The 65 hour reactions gave much lower labelling efficiency values (1.21-1.29%). These two samples were taken from different reactions which only contained a 4.5 fold excess of MMN (6 fold excess of MMN was used in 1-48 hour reaction mixtures), hence these reactions were not included in Figure 2:24. It is possible that the lower molar excess of MMN resulted in lower labelling efficiencies. Alternatively, these two reactions may have been compromised upon preparation resulting in poor reaction yields.

Despite investigating reaction time and temperature, poor labelling yields were still observed. The labelling efficiency values in Table 2:9 are much lower than those seen in the calculation on page 121, where 10.7% MMN labelling was achieved. In summary, the reaction does not appear to be controlled as illustrated in Figure 2:24, indicating that unknown factors are effecting the reaction. Further investigation into this reaction is required to obtain reproducible yields. These experiments were carried out with sulfhydryl modified 25 mers which did not require lengthy sample preparation prior to labelling. Although some success had been obtained in the initial experiments, poor yields prompted the decision to seek alternative methods of elemental labelling.

Although calibration standards were prepared in order to quantify the Au contained in each fraction, this information was not employed in the calculation of labelling efficiencies. However, the standards were employed to check the response of the instrument to Au and also to check the instrument for signal drift during the analyses.

One potential limitation of the anion exchange separation method is that the unbound MMN species eluted first in the void volume, followed by the MMN-DNA conjugate. It is possible that the Au response observed in the second fractions (MMN-DNA conjugate fraction), contained residual Au from the unbound MMN. This is plausible especially since the main limitation of Au is its 'sticky' nature, which results in carry over between samples. Although the blank, 25 mer oligonucleotide and MMN retention time markers exhibited low Au levels in the second fractions (Table 2:9), indicating that this was not the case, it

may be worth investigating this aspect of the separation to ensure any Au present in the second fraction is due to MMN-DNA and not residual Au remaining in the column from the unbound MMN species. Since cysteine and acid solutions were shown to improve Au wash out and reduce memory effects, it may be beneficial to add these to the mobile phase to aid Au wash out from the stationary phase. Conversely, a reversed phase separation should result in the MMN-DNA conjugate eluting first (highly charged species), followed by the less charged unbound MMN. This order of elution would prevent residual Au from unbound MMN being mistaken for Au corresponding to MMN-DNA, since the MMN-DNA species is eluted first.

### **2.4.3 Monomaleimido Nanogold Labelling Summary**

Preliminary results indicated that thiol modification did take place on 5' phosphorylated oligonucleotides that were treated in-house with EDC, imidazole and cystamine. However, more analysis is required to confirm that efficient sulfhydryl modification was achieved. The presence of the reactive group could be confirmed with organic mass spectrometry, since structural information can be easily obtained, although this was not attempted here it should be considered for future development.

The labelling of the sulfhydryl modified di-nucleotides with MMN proved to be difficult and very little success was achieved. The problems were attributed to the lengthy and difficult sample preparation procedures which involved cleaving the disulfide modification with DTT and separating the reactive di-nucleotide from excess DTT by means of gel filtration. As a result of these difficulties alternative reducing agents and separation methods were investigated.

More success was achieved with the labelling of sulfhydryl modified 25 mers, these longer oligonucleotides were provided in the reactive sulfhydryl form. Although the results suggested that these nucleic acids were labelled with MMN, the labelling efficiency was very low. Investigations aimed at establishing the optimum reaction time and temperature for labelling were carried out. Unfortunately, poor labelling efficiencies were again calculated for the MMN reactions and the reaction yields were highly variable. The anion

exchange separation of bound and unbound MMN also needs to be investigated further to ensure all the Au is eluted from the anion exchange phase.

The 'sticky' nature of Au meant that appropriate wash solutions were required to minimise carry over between samples. A combination of *aqua regia* and cysteine proved to be effective at removing Au from the surfaces of the sample introduction system. It may be beneficial to employ this combination of wash solutions in conjunction with the anion exchange column to prevent Au build up on the phase.



between biotinylated DNA and SFNG is summarised in Figure 2:26. This reaction is straightforward, with SFNG-DNA conjugates forming below room temperature within 24 hours.

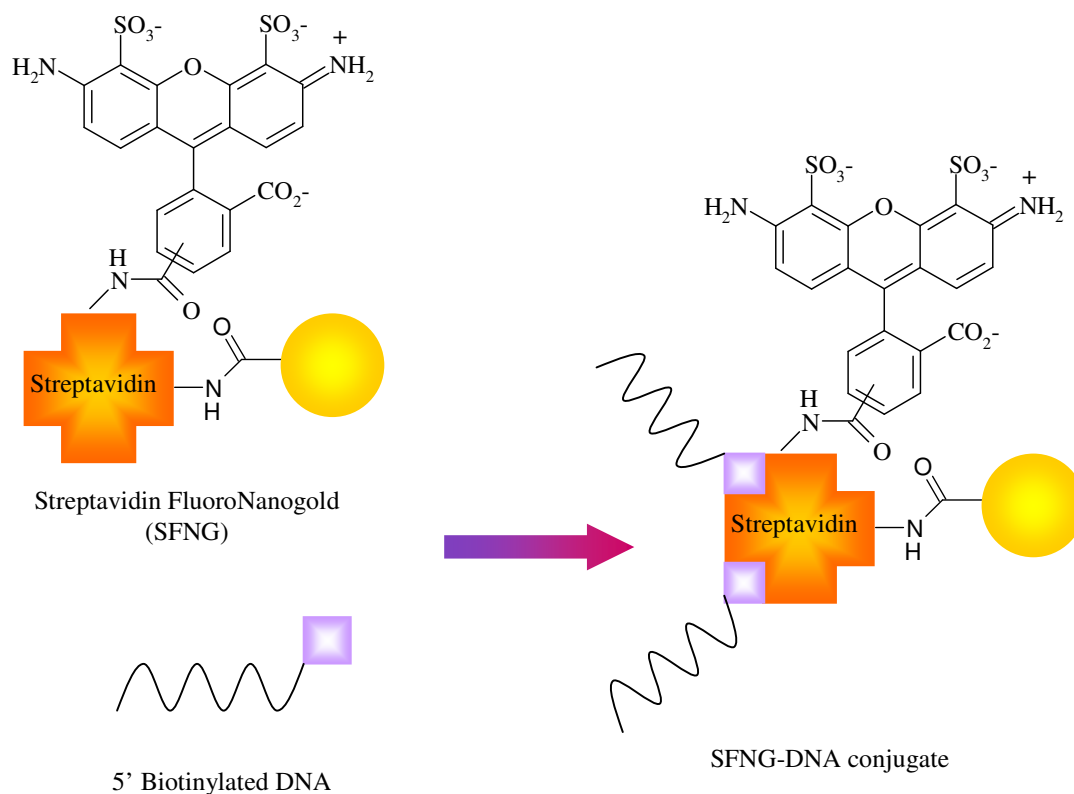


**Figure 2:26: Streptavidin FluoroNanogold labelling of biotinylated DNA.**

## 2.5.2 Biotinylation of DNA

The work in this section focuses on the labelling of biotinylated DNA with a SFNG probe. As in the case of sulfhydryl modified oligonucleotides, biotinylated oligonucleotides are commercially available, but for there to be a viable labelling method with an ultimate application, the DNA has to be modified to incorporate the reactive biotin group. This section outlines a potential method for the biotinylation of 5' phosphate groups on nucleic acids. The modification procedure was obtained from Pierce Biotechnology,<sup>116</sup> but similar biotinylation methods have been reported elsewhere.<sup>117</sup> The DNA biotinylation route is shown in Figure 2:27.

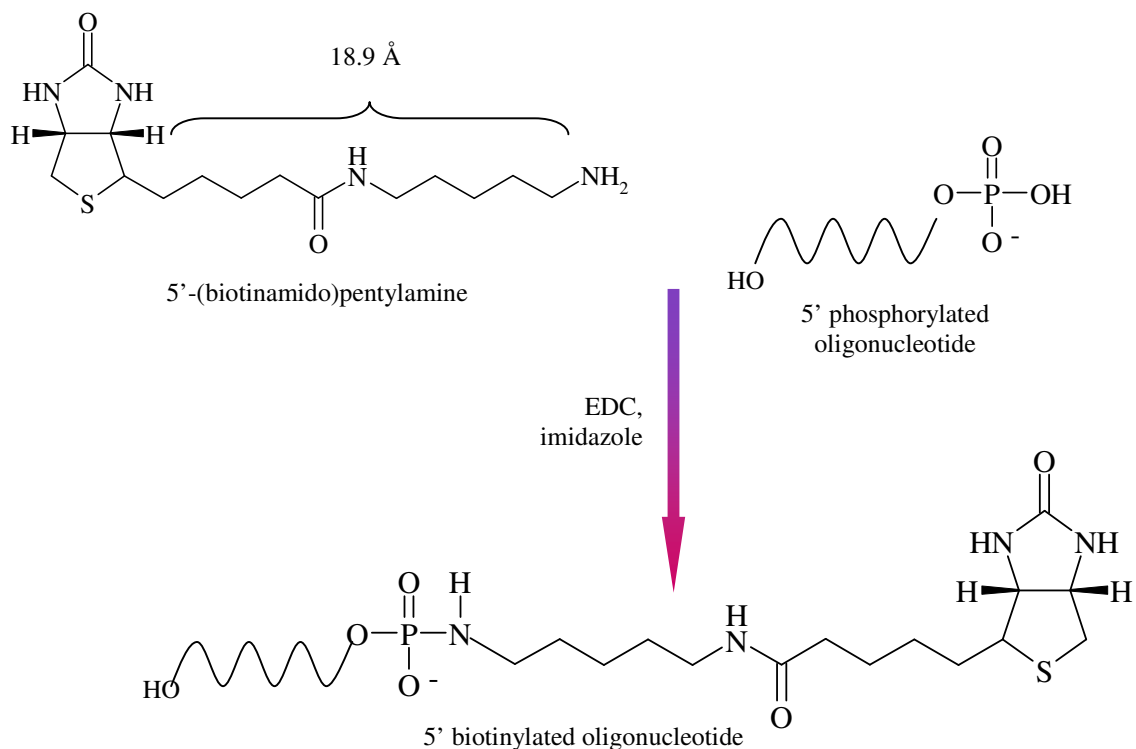


**Figure 2:27: Biotinylation of DNA 5' phosphate.**

Following modification, the biotinylated DNA needs to be separated from excess reagent. This could potentially be achieved using anion exchange SPE, since the DNA will be retained on the charged phase and the excess reagent eluted. However, the SPE method would not necessarily separate the biotinylated DNA from the unmodified DNA.

Upon biotinylation, the distance between the biotin moiety and the terminal 5' phosphate group would be 18.9 Å.<sup>118</sup> This spacer arm is intended to minimise any steric effects that may occur during the labelling reaction. If more than one biotinylated DNA molecule binds to one streptavidin protein, it is possible that steric restraints may effect the labelling reaction. However, any steric effects should be minimised by having an 18.9 Å spacer between the biotin and DNA.



### **2.5.3 Method of Labelling**

Since the affinity between biotin and streptavidin is very strong, the labelling method was straight forward and did not involve complicated and lengthy sample preparation procedures. In addition, both the SFNG and biotinylated DNA were stable in solution, which made sample handling easier. SFNG labelling of biotinylated DNA was achieved by adding the DNA to an excess of SFNG. The reaction mixture was then left for approximately 24 hours at 4 °C to allow the reaction to proceed.

### **2.5.4 Methods of Separation**

Once the labelling reaction was complete, a separation procedure was necessary to resolve the SFNG-DNA conjugate from the unbound SFNG. Numerous modes of separation were investigated for this labelling strategy. Each one will be discussed along with the advantages and disadvantages of each.

#### **2.5.4.1 Gel Filtration**

Gel filtration is a liquid phase separation operating at low pressures. Gel filtration separates species according to size, thus the technique works by size exclusion. The stationary phase consists of a porous carbohydrate-polymer matrix. Larger molecules cannot fit within the stationary phase pores and are therefore excluded and eluted from the phase. Conversely, small molecules infuse within the pores and are retained on the phase. This results in a sieving effect, where larger molecules are eluted first followed by small molecules.<sup>119, 120</sup> The phases used in gel filtration are relatively stable at a range of pH values.

There are many types of phase available each having different selectivity's (different molecular weight ranges) and molecular weight cut-off points. The media used to separate SFNG-oligonucleotide conjugates from unbound material was Superdex-75. This media is composed of cross-linked dextran and agarose and has an average particle size of 34 µm, and an optimum molecular weight separation range of 3000-70 000 Da. Species falling within this molecular weight range will be successfully separated; however, molecules with

a molecular weight exceeding 100 000 Da will not be retained in the pores and therefore eluted in the void volume. Thus, the exclusion limit of Superdex-75 is 100 000 Da.

Superdex-75 was chosen because the oligonucleotide molecular weight was towards the bottom end of the media's optimum molecular weight range and the molecular weight of the bound SFNG-DNA conjugates was towards the top end of the optimum separation range. As a result, the free and bound oligonucleotides should separate. The molecular weights of the species involved in the tagging experiment are summarised in Table 2:10.

**Table 2:10: Molecular weight of SFNG, biotinylated oligonucleotides and SFNG conjugates.**

<b>Species</b>	<b>Molecular weight</b>
SFNG	~75 500
18 mer biotinylated oligonucleotide	6145
18 mer oligo-SFNG conjugate	~81 600-87 790*
24 mer biotinylated oligonucleotide	8000
24 mer oligo-SFNG conjugate	~83 500-91 500*

\*The molecular weight of the SFNG- oligonucleotide conjugates depends on the number of oligonucleotides bound to the streptavidin protein. Only one or two biotinylated oligonucleotides will bind to SFNG due to steric restraints.

Superdex-75 was supplied as a suspension in a 20% ethanol solution. The media was already pre-swollen and was prepared as follows:

- The required amount of Superdex suspension was filtered using a glass filter to remove the ethanol.
- 5-10 column volumes of deionised water were used to wash the media.
- The media was then re-suspended in deionised water. The resulting suspension contained approximately 50% settled media and 50% water.
- 200 µl of TWEEN-20 was added to the Superdex suspension.
- The suspension was mixed gently by swirling the beaker.
- The suspension was poured into a packing reservoir, which was attached to a 30 cm x 1 cm column. The suspension was poured in one slow, smooth motion.

- A peristaltic pump (Minipuls 2, Gilson) was connected to the column outlet and set to pump at  $\sim 0.20 \text{ ml min}^{-1}$ .
- The column was left to pack at this flow rate for 2-3 hours or until the column bed had settled. The column was topped up with deionised water at regular intervals to ensure the media did not run dry.
- Deionised water was then pumped through the column for a further 3 hours at  $0.20 \text{ ml min}^{-1}$ .

Once the column bed had settled, the column was ready for equilibration with the elution buffer, followed by sample separation.

#### **2.5.4.2 Anion Exchange HPLC**

This mode of separation operates on charge interaction. A positively charged stationary phase was employed, which resulted in retention of the negatively charged phosphate groups on DNA. Likewise the SFNG was also retained due to the carboxylic and sulfonic acid groups on the fluorophore. It also was expected that streptavidin contributed to the retention of SFNG due to the carboxylic acid groups on the amino acids. However, it was hoped that a method could be developed to resolve the unbound SFNG from the SFNG-DNA conjugate. The TSKgel-DNA-NPR analytical column was used for anion exchange separation (see Appendix 1 for details). The anion exchange stationary phase consisted of a non-porous resin, which was chosen since it does not possess intra-particle voids that would cause the high molecular weight molecules to be excluded. As a result, non-porous resins enable relatively quick, high resolution separations of high molecular weight molecules. This phase had a relatively low capacity due to the lack of intra-particle voids; therefore, small injection volumes were used to prevent overloading the column. This phase was used for all anion exchange separations, but numerous mobile phases were investigated.

There were two criteria for the choice of mobile phase; firstly it was important that the mobile phase eluted both the DNA and SFNG. Secondly, the mobile phase had to be

compatible with ICP-MS. The basic HPLC parameters are outlined in Table 2:11. Any amendments to the chromatography conditions will be stated where appropriate.

The HPLC separation optimisation was carried out off-line to the ICP-MS, as a result UV data was initially obtained and not ICP-MS data. The Alexa Fluor-488 dye and nanogold both have very high absorption coefficients, for example, at 280 nm the nanogold particle has an absorption coefficient of approximately  $3 \times 10^5 \text{ dm}^3 \text{ mol}^{-1} \text{ cm}^{-1}$ . As a result, the probe should be easily detected by the UV detector allowing off-line chromatography optimisation prior to elemental analysis.

**Table 2:11: HPLC parameters employed for the anion exchange separation of the SFNG and SFNG-DNA conjugates.**

Parameter	Setting
Stationary phase	TSKgel-DNA-NPR, 7.5 cm x 4.6 mm, 2.5 $\mu\text{m}$ .
Mobile phase	Variable
Flow rate	0.7 ml min <sup>-1</sup>
Detection wavelength	257 nm
Gradient	Variable
Stop time	Variable
Post time	Variable
Injection volume	5 $\mu\text{l}$
Column temperature	Room temperature

Solutions containing unbound SFNG were initially injected onto the HPLC phase to establish the retention time of the probe. The mobile phases investigated were as follows:

- 20 mM Tris-HCl, pH 9 with a gradient of 20 mM Tris-HCl + 50 mM trisodium citrate + 0.5 M TMACl, pH 9
- Phosphorus buffered saline (20 mM sodium phosphate, 150 mM sodium chloride), pH 7.2
- pH gradient (25 mM Tris-HCl, pH 9 and 25 mM sodium phosphate + 25 mM trisodium citrate, pH 3)
- 20% DMSO in 25 mM trisodium citrate, pH 9 isocratic
- 50 mM ammonium sulfate, pH 3 isocratic
- 20% acetonitrile in 100 mM triethylammonium acetate, pH 7 isocratic.

### 2.5.4.3 Immobilised Metal Affinity Chromatography

Another mode of chromatography investigated in this particular project was immobilised metal affinity chromatography (IMAC). In this mode of affinity chromatography, the metal (usually a divalent or trivalent transition metal) is immobilised on agarose beads. The biomolecule, which may be DNA or proteins interacts with the immobilised metal and is therefore retained on the phase. The retained biomolecule can be eluted with a competing compound or by adjusting the pH of the elution buffer. There have been many reports in the literature regarding the use of IMAC for biomolecule separations.<sup>121-125</sup>

The choice of metal determines the selectivity of the phase, which depends on the part of the analyte that is to be retained on the column. Iron(III) and Ga(III) are hard Lewis acids and therefore interact with hard Lewis bases, such as phosphate groups on the biomolecule. However, Ni(II), Cu(II) and Zn(II) are softer Lewis acids and interact with the nitrogen bases on the imidazole rings of purine nucleobases. Iron(III) was chosen in this investigation, so the DNA was retained due to the presence of the phosphate backbone. The stationary phase was prepared as described below and was a slight modification of the procedure reported by Hart *et al.*<sup>126</sup> It was hoped that the oligonucleotides would be retained due to the phosphate groups, but the SFNG would have little retention resulting in an easy separation method.

#### Fe(III)-NTA-Agarose Phase Preparation

- Ni(II)-NTA-Agarose (750 µl) was placed into a micro centrifuge tube. To this, the same volume of deionised water was added. The suspension was shaken manually and then centrifuged at 6000 rpm for 5 minutes.
- The supernatant was discarded and then the above step was repeated twice more to wash the agarose.
- The agarose beads were then washed three times with 750 µl of 0.1 M EDTA in 1 M sodium hydroxide. During these wash steps the EDTA complexed to the NTA-agarose bound Ni, thus removing the metal from the agarose beads.
- A 750 µl volume of deionised water was used to wash the stripped beads followed by a 750 µl aliquot of 0.1 M acetic acid. The supernatant was again discarded.

- The Fe(III) was then introduced to the phase by adding 750  $\mu$ l of a solution containing 0.1 M iron(III) chloride in 0.1 M acetic acid. The mixture was again shaken, centrifuged and the supernatant discarded.
- An acetic acid wash was carried out after the modification, followed by three further deionised water wash steps.
- The Fe(III)-NTA-agarose beads were re-suspended in 750  $\mu$ l deionised water and split into three equal fractions each containing approximately 0.5 ml of suspension. One fraction was used as a blank/control sample (control sample consisted of deionised water only), the second for an oligonucleotide sample and the third for a SFNG sample.
- The excess water was removed from the beads and 0.4-0.5 ml of sample was applied to the Fe(III)-NTA-agarose phase.
- The loaded beads were shaken and allowed to stand for two hours at 4 °C, with shaking every 30 minutes.

After the two hour incubation time, the suspension containing the IMAC phase and sample were poured into a small gel filtration column. The column was connected to a vacuum manifold. The excess liquid in the column was allowed to drain away. The column eluent was collected and kept for UV/vis analysis. The phase was then washed with three 0.5 ml aliquots of deionised water followed by three 0.5 ml aliquots of 0.1 M sodium hydroxide. The column eluent was collected during each wash and elution step and UV/vis was used to determine where the two species of interest eluted.

#### **2.5.4.4 Reversed Phase HPLC**

Reversed phase HPLC (RP-HPLC) employs a non-polar stationary phase and polar mobile phases containing various proportions of organic solvent. The mode of separation is based on hydrophobic interaction. Non-polar molecules have more interaction with the non-polar phase and are therefore retained on the column and exhibit longer retention times. In contrast, polar species have less affinity with the stationary phase and more interaction with the polar mobile phase and are eluted first. The strength of the mobile phase is increased by adding greater amounts of organic modifier, which has the effect of eluting the non-polar

species from the stationary phase. Consequently, the elution strength of the mobile phase is increased by raising the proportion of organic solvent in the eluent. Reverse phase separations can be coupled to ICP-MS more easily than most other modes of chromatography, there are several reasons for this. Firstly, the mobile phase consists of aqueous solvents which are ICP-MS compatible. Although organic modifiers are used in reversed phase chromatography, they can be used in conjunction with ICP-MS providing the content is kept relatively low (<15%). Alternatively, the organic solvent can be easily removed by evaporation prior to ICP-MS analysis. In addition, HPLC flow rates are typically 0.5-1 ml min<sup>-1</sup>, which is compatible with nebuliser flow rates.

A C18 column was used for all SFNG reversed phase separations. Mobile phases containing various proportions of methanol and acetonitrile in deionised water were assessed for their suitability in eluting the SFNG species from the phase. In addition to RP-HPLC being compatible with ICP-MS, the charged SFNG probe should have very little interaction with the non-polar stationary phase, thus providing easier separation with good levels of recovery. This is a contrast to anion exchange chromatography where SFNG appeared to be retained quite irreversibly on the charged anion exchange phase (see results, section 2.6.1.2).

A HP 1090 Series 2 HPLC instrument with diode array UV detection, operating off-line to ICP-MS was initially employed to establish the retention times of the unlabelled oligonucleotides and SFNG. Once it was established that the two species had different retention times, the separation was carried out on-line with ICP-MS. The Element 2XR ICP-MS instrument was employed for the determination of Au in the SFNG/DNA samples. The basic HPLC parameters are outlined in Table 2:12, whilst Table 2:2 summarises the ICP-MS operating conditions.

**Table 2:12: Basic HPLC operating parameters for the C18 separation of SFNG and SFNG-DNA conjugates.**

<b>Parameter</b>	<b>Setting</b>
Stationary phase	Hypersil C18, 250 mm x 4.6 mm (120 Å) or Waters $\mu$ Bondapak C18 300 mm x 3.9 mm, 10 $\mu$ m (125 Å).
Mobile phase	Acetonitrile/water or methanol/water of varying proportions
Flow rate	0.6 - 1 ml min <sup>-1</sup>
Detection wavelength	280 nm
Gradient	Variable
Stop time	Variable
Post time	Variable
Injection volume	10 $\mu$ l
Column temperature	Room temperature

The Element 2XR instrument was operated in speed scanning mode for all chromatographic data acquisitions. The resulting Au chromatograms were exported as an Xcalibur file and then opened with the Xcalibur program (Version 2.0, Thermo Finnigan, San Jose, California, US), which was employed to process ESI-MS data on the LTQ linear ion trap mass spectrometer. This allowed the Au chromatograms, which were obtained on the Element to be integrated, thus peak areas and retention times were accurately obtained for each Au chromatogram. In addition, the chromatographic data was also exported as a text file and subsequently opened in Microsoft Office Excel, which simply allowed the chromatographic data to be viewed without the need for the Xcalibur viewing software.



## 2.6 Results of Streptavidin FluoroNanogold Labelling

### 2.6.1 Methods of Separation

#### 2.6.1.1 Gel Filtration

Unfortunately, gel filtration was found to be unsuitable for the separation of SFNG from SFNG-DNA conjugates due to the poor resolving power of the technique. The longest oligonucleotides (24 mer) had a molecular weight of ~8 000 Da, therefore, if two 24 mers bound to each streptavidin protein; the corresponding conjugate would have a MW ~91 500 Da and the unbound SFNG MW ~75 500 Da. This small molecular weight difference (1.2 fold difference in MW) resulted in partial resolution, which would have resulted in difficult quantification. Ultimately, baseline resolution of the two species was required for quantitative analysis. This implies that for gel filtration to be successful in purifying these conjugates, an excess of biotinylated oligonucleotide was required in the tagging reaction mixture, so when the reaction has gone to completion, there should be no free SFNG, but an excess of unbound oligonucleotide. It should be reasonably straight forward to separate the excess free oligonucleotide (MW~6 000-8 000 Da) from the much heavier SFNG-DNA conjugates (MW ~81 600-91 500 Da). Even though the use of gel filtration is possible, the species to be labelled has to be in excess and not the probe which negates quantification.

In addition, problems were encountered when packing the media into columns. It was difficult to obtain an even column bed. The performance of the column was tested with both blue dextran and acetone. Blue dextran was used to establish the void volume of the column. The average molecular weight of the dextran was  $\sim 2 \times 10^6$ , thus it was totally excluded from the phase. Acetone was used to establish the efficiency of the column, which was achieved following the procedure outlined by the manufacturer.<sup>120</sup> Briefly, the column outlet was connected to a UV detector and integrator as described previously. The acetone peak was then used to calculate the column efficiency using the equation below.<sup>120</sup>

$$N/m = 5.54(V_e/W_{1/2})^2 1000/L$$

Where:

$N/m$  = Number of theoretical plates per meter.

$V_e$  = Elution volume (ml)

$W_{1/2}$  = Peak width at half height (ml)

$L$  = Height of Superdex bed (mm)

For Superdex media, efficiency values of approximately 10 000  $N/m$  should be obtained.<sup>120</sup> However, the best value achieved was 382  $N/m$ . As a result of these problems and other limitations it was decided to look for alternative methods for separation.

#### **2.6.1.2 Anion Exchange HPLC**

Several mobile phases were assessed for their suitability for SFNG elution from the anion exchange phase. The basic chromatographic conditions used were kept constant throughout this part of the investigation and are shown in Table 2:11 in the method section. The first phase to be investigated was:

A: 20 mM Tris-HCl, pH 9

B: 20 mM Tris-HCl + 0.5M TMACl + 50 mM trisodium citrate, pH 9

Gradient elution was employed with mobile phase B gradually increasing throughout the separation. The buffers used in this mobile phase should be compatible with ICP-MS. The ionic strength of the eluent was very high, owing to the presence of citrate, which has a triple negative charge. It was hoped that the high ionic strength eluent would be sufficient to elute the highly charged SFNG from the anion exchange phase. However, SFNG failed to elute with this mobile phase. As a result, the retention mechanism was thought to have some hydrophobic character rather than just ionic, thus 10% acetonitrile was added to mobile phase B. The high ionic strength phase containing organic solvent also failed to elute SFNG.

Phosphorus buffered saline (PBS) was the next mobile phase to be investigated. SFNG was supplied in a solution containing 20 mM phosphate buffer and 150 mM sodium chloride at

pH 7.4. The probe was soluble and stable in this buffer, so mobile phases containing the following were prepared:

A: 20 mM sodium dihydrogen phosphate, pH 7.2

B: 20 mM sodium dihydrogen phosphate, 0.5 M sodium chloride, 5.4 mM potassium chloride, pH 7.2

Gradient elution was again carried out with a gradual increase of mobile phase B. SFNG did not appear to elute using the mobile phases outlined above. However, when the column was removed from the instrument and reconnected in the reverse flow direction, a huge absorbance was observed. Upon further inspection, it appeared that the signal slowly decreased over a period of ~12 minutes, suggesting that the signal was not due to the SFNG, but probably due to deposited material and contaminants on the top of the column.

All previous anion exchange chromatography had been conducted with an escalating gradient of salt, thus increasing ionic strength in an attempt to elute the analyte. However, pH gradients had not yet been investigated. Anion exchange separation of proteins can be carried out using pH gradients as reported elsewhere,<sup>127, 128</sup> and it was used in this study for the elution of SFNG. This method of elution involved using an initial mobile phase with a higher pH, and then gradually decreasing the mobile phase pH to the same pH as the protein isoelectric point (pI). At this stage, the positive and negative charges on the protein are balanced, so the protein net charge is zero and SFNG should elute. The buffers used to create a pH gradient were as follows:

A: 25 mM Tris-HCl, pH 9

B: 25 mM sodium dihydrogen phosphate, 25 mM trisodium citrate, pH 3

The above buffers produced a gradient starting from pH 9 and decreasing to pH 3. The pKa values and buffering ranges of all three buffers overlapped, and therefore created a decreasing pH gradient throughout the elution. At pH 9, all the streptavidin carboxylic acid groups would have been ionised and therefore interacted with the anion exchanger. When the mobile phase composition gets to ~pH 5.5, the protein will have a net charge of zero, since this is the streptavidin isoelectric potential (pI). However, the mobile phase was taken

down to pH 3, which is two pH units below the protein pI. At pH 3 all the amine and acid groups on the protein were protonated, resulting in a net positive charge, which should result in SFNG elution. Despite efforts to elute the probe with pH gradients, no signal was observed.

The manufacturer of SFNG was contacted and their advice was requested with respect to the chromatographic separation of the conjugate.<sup>95</sup> After obtaining advice, a mobile phase containing 20% DMSO in 25 mM trisodium citrate, pH 9 was tested. DMSO solubilises the Alexa Fluor-488 fluorophore, so it was thought that DMSO was a good solvent to use in conjunction with the probe. No peaks were observed when the SFNG was injected into the column, however, the mobile phase was diluted two fold and the SFNG was re-injected. The aim of this was to weaken the mobile phase eluent strength and confirm that the probe was not eluting in the void volume and being masked by noise at the start of the injection. However, this was not the case and yet again, nothing was observed.

Since none of the above mobile phases had successfully eluted the SFNG, degradation of the probe in solution was a consideration. However, even if the SFNG had dissociated in solution, the fluorophore and aromatic amino acids would have still been present resulting in some UV response. This suggested that the SFNG was being retained almost irreversibly on the phase.

One anion that had not been investigated was sulfate. The sulfate anion is a very strong eluent in anion exchange chromatography; therefore, a buffer containing 50 mM ammonium sulfate at pH 3 was prepared. The mobile phase had a very high ionic strength and the pH was below the pI point of streptavidin, so the protein part of the probe should not have had any interaction with the phase using this eluent. The first blank injection carried out with this eluent resulted in a large peak with a retention time of 9 minutes. This huge absorbance was probably due to built up contamination on the column which was eluted with the strong eluent. A further blank injection did not give the same result. The SFNG injection exhibited a flat baseline, although a small peak in the baseline was observed at 10.4 minutes. Further SFNG injections gave a small peak at 10.4 minutes,

however, if this was due to the SFNG, the signal was very weak and the possibility of a contaminant in the sample was considered.

Ion-pair HPLC was then investigated. The same chromatographic conditions detailed in Table 2:11 were employed, but the mobile phase consisted of 100 mM triethylammonium acetate in 20% acetonitrile, pH 7 (isocratic). A response was observed at ~0.5 minutes, although the signal was weak and no better than that observed with the ammonium sulfate mobile phase.

Although a lot of work was conducted with SFNG and anion exchange separations, no real success was obtained. It was concluded that the sulfonic acid groups on the Alexa Fluor-488 dye were retained irreversibly on the anion exchange resin. Although a very small amount of SFNG may be eluted with a high ionic strength mobile phase, the recoveries would have been very small. Hence, alternative methods of separation were again investigated.

### **2.6.1.3 Immobilised Metal Affinity Chromatography**

The column eluents collected from the phase during the separation procedure were scanned with a UV spectrometer between 200-400 nm for oligonucleotide detection, and 200-600 nm for SFNG detection. Figure 2:28 shows the spectra of both the oligonucleotide and SFNG before they were applied to the phase. The oligonucleotide yielded a maximum at 256.40 nm, whilst SFNG gave an absorbance at 493.20 nm, which corresponded to the Alexa Fluor 488 absorbance ( $\epsilon_{490\text{ nm}} = 71\,000\text{ cm}^{-1}\text{ M}^{-1}$ ).<sup>129</sup> However, a stronger absorbance was observed at approximately 260-280 nm for SFNG, corresponding to the nanogold particle, which as stated previously has an absorption coefficient of  $\sim 3 \times 10^5$  at 280 nm.

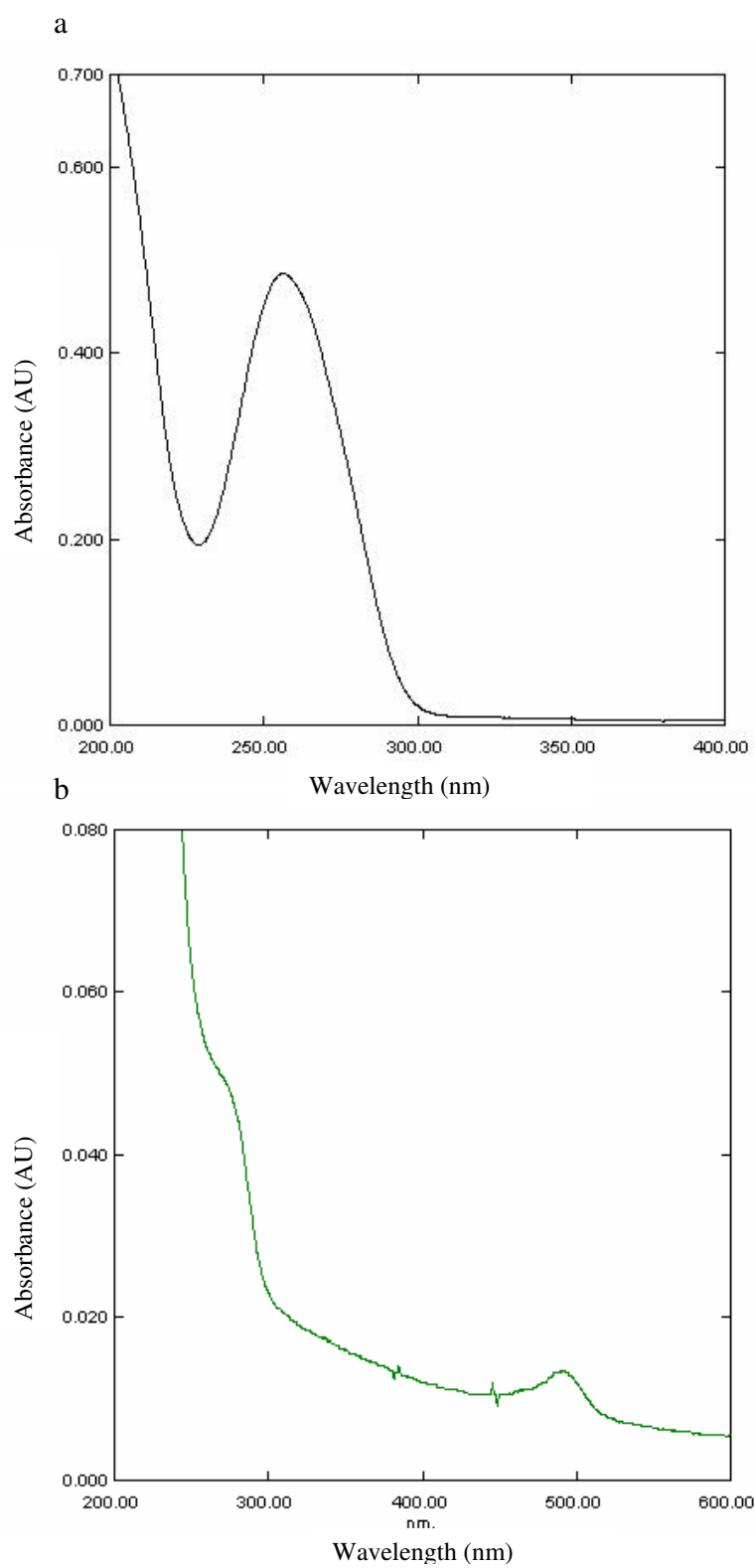


**Figure 2:28: a) 10  $\mu\text{M}$  25 mer oligonucleotide spectrum before IMAC separation. b) SFNG spectrum before IMAC separation (0.18  $\mu\text{M}$  nanogold and  $\sim$  0.85  $\mu\text{M}$  Alexa fluor-488).**

One set of IMAC beads was used as a control in which deionised water was added to the phase. The aim of the control was to ensure no background absorbance from the phase was effecting the UV/vis detection of DNA or SFNG. The UV data from the control column fractions did not reveal any significant absorbance that would potentially interfere with the DNA or SFNG detection.

The deionised water column eluents from the oligonucleotide and SFNG loaded IMAC phases did not reveal any absorbance, thus confirming that both the oligonucleotides and SFNG were retained on the IMAC phase. The three sodium hydroxide elution steps did result in oligonucleotide elution, which was shown by absorbance maxima at 256 nm. The overlaid spectra in Figure 2:29 show the first, second and third sodium hydroxide elution steps of the oligonucleotide from the IMAC phase. Recovery calculations revealed that approximately 90% of the oligonucleotide was recovered from the phase with sodium hydroxide elution. Recoveries of 55.3%, 27% and 9.3% were obtained in the first, second and third sodium hydroxide wash steps respectively.

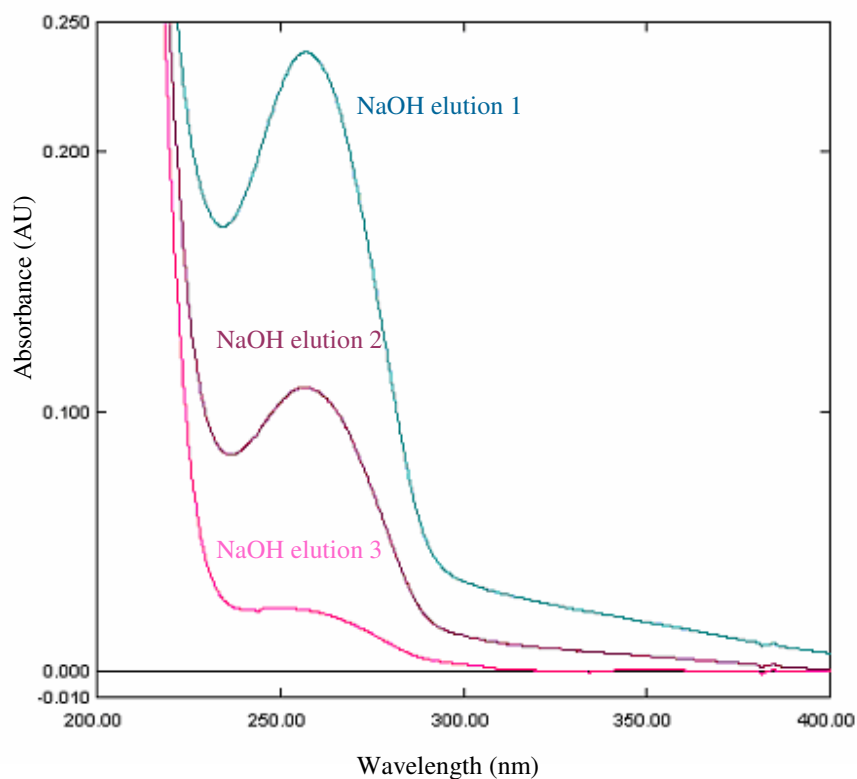


**Figure 2:29: Overlaid spectra of the three sodium hydroxide elution steps for DNA elution from the IMAC phase.**

Figure 2:30 shows the overlaid spectra corresponding to the three sodium hydroxide elution steps of SFNG from the IMAC phase. The spectra exhibit absorbance at 494 nm corresponding to the fluorophore, although the absorbance was very weak. The nanogold absorbance at 280 nm gave a better indication of elution than the Alexa Fluor 488 dye. Further sodium hydroxide elution fractions did not show any sign of the probe. It should be noted that the Alexa Fluor dye was only present at a concentration of  $\sim 0.85 \mu\text{M}$  in the original sample. Hence after sodium hydroxide elution, the fluorophore concentration and absorbance would have been very weak.

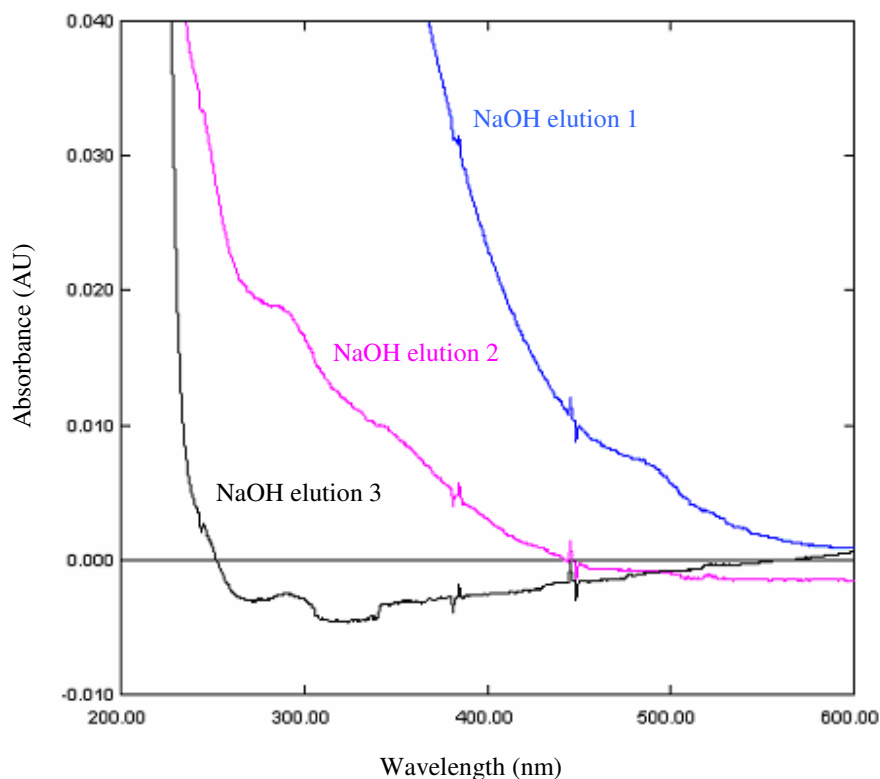


**Figure 2:30: Overlaid spectra for the three sodium hydroxide elution steps of SFNG from IMAC phase.**

It can be concluded from these experiments that both the oligonucleotides and SFNG were retained on the Fe(III)-NTA-agarose phase, but co-eluted with base under the conditions used. However, it may be the case that the two species had different affinities to the phase, if so, different concentrations of base may successfully resolve the two species, resulting in separation of bound and unbound SFNG. The IMAC phase contained Fe(III), which has affinity for hard bases such as phosphate groups. If the streptavidin protein contained



phosphorylated amino acids, then these would also be retained on the IMAC phase. However, if the specificity of the phase is altered by changing the immobilised metal to Ni(II), then the streptavidin may not be retained, but DNA should still display retention due to the imidazole groups on the purine rings interacting with Ni(II). This aspect has yet to be investigated.

A further consideration is that the eluent has to be compatible with ICP-MS; hence alternative bases to sodium hydroxide will have to be found. Tetramethylammonium hydroxide (TMAH) or tetramethylammonium chloride (TMACl) may be suitable for the elution of the oligonucleotide conjugates from the IMAC phase. Due to lack of time IMAC separation was not pursued any further.

#### **2.6.1.4 Reversed Phase HPLC**

Mobile phases consisting of methanol-water and acetonitrile-water mixtures were used in an attempt to elute SFNG from a C18 phase. SFNG should have very little, if any retention on a non-polar C18 reverse phase column. As a result, the probe should be successfully eluted with high levels of recovery using mild conditions. Although organic solvents were used, they can be easily removed prior to ICP analysis, or the HPLC flow can be split post column to minimise the solvent flow to the plasma. Initially solutions containing SFNG or oligonucleotide only were injected onto the C18 column to establish the retention times of the two species.

Initial tests employed an isocratic acetonitrile-water (50:50) mixture to elute SFNG from a C18 guard column. A UV response was obtained which was attributed to the elution of SFNG. As a result, the same sample was injected onto a C18 analytical column (Hypersil C18 column 250 mm x 4.6 mm) and additional peaks were observed in the SFNG chromatogram when compared to the blank injection, which were again attributed to SFNG eluting from the phase. Additional peaks at 1.27 and 1.82 minutes were observed in the SFNG chromatogram. However, these peaks eluted very quickly suggesting that there was very little interaction between the probe and stationary phase. As a result, the eluent strength was decreased by employing an isocratic methanol-water mixture (50:50). Upon

eluting the SFNG with the weaker solvent, a peak was observed at 1.94 minutes. The methanol content was reduced further so the mobile phase contained 35% methanol, which resulted in the SFNG eluting at 2.39 minutes. A sample containing 5' biotinylated 24 mer was also injected on the column and eluted using the isocratic 35% methanol mobile phase, and a retention time of 1.45 minutes was observed. The chromatograms of the biotinylated 24 mer and SFNG, eluted with 35% methanol are shown in Figure 2:31.

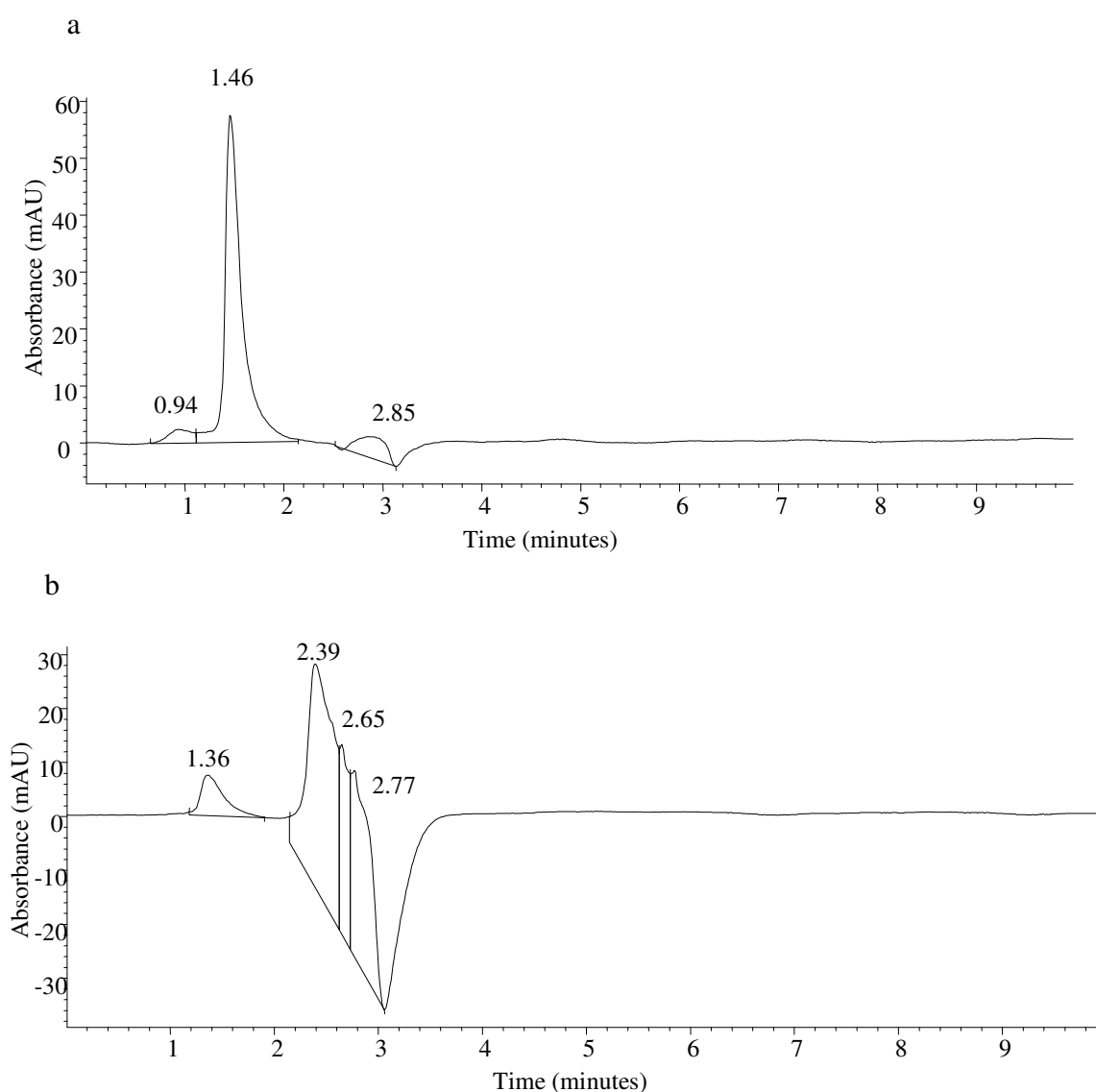


**Figure 2:31: a) 5' biotinylated 24 mer retention time marker. b) SFNG retention time marker. Both species eluted from a Hypersil C18 column (250 mm x 4.6 mm) with 35% methanol isocratic elution. Flow rate = 0.6 ml min<sup>-1</sup>, 10 µl injection volume. 260 nm detection wavelength.**

The peak at 1.36 minutes displayed in Figure 2:31b was also observed in the blank injection and therefore not attributed to SFNG. The baseline in Figure 2:31b exhibited a negative absorbance at 3 minutes. This suggests that there was a positive absorbance from the mobile phase, which was removed upon eluting the SFNG, no explanation could be given since the mobile phase only consisted of methanol and water. Once it was established that the SFNG and unbound oligonucleotide had different retention times, a SFNG-DNA reaction mixture was prepared. Briefly, 125  $\mu$ l SFNG (1.33  $\mu$ M streptavidin) was added to 68  $\mu$ l biotinylated 24 mer oligonucleotide (5  $\mu$ M). Hence the reaction mixture contained; 0.34 nmoles biotinylated 24 mer and 0.17 nmoles streptavidin, which equated to 0.67 nmoles of biotin binding sites (total of four biotin binding sites per streptavidin). A two fold excess of biotin binding sites was present in the reaction mixture. The tagging reaction mixture was placed in the refrigerator for 24 hours at 4 °C.<sup>95</sup> After 24 hours, a 100  $\mu$ l aliquot was taken and 55  $\mu$ l of methanol was added to the aliquot. This was done to ensure the sample solvent and mobile phase compositions were matched in terms of organic solvent content. The sample was then injected and the isocratic mobile phase consisting of 35% methanol in water was used to separate the mixture. Figure 2:32 shows the tagging reaction mixture chromatogram, where three main peaks were observed at; 1.42, 2.55 and 3.04 minutes. The peaks at 1.42 and 2.55 minutes were thought to be the biotinylated 24 mer and the unbound SFNG respectively, since these retention times were consistent with those seen for the retention time markers (see Figure 2:31). The additional peak at 3.04 minutes was thought to be the SFNG-DNA conjugate. Three peaks were expected, however, the identity of the two remaining smaller peaks at 1.81 and 2.34 minutes were unknown.

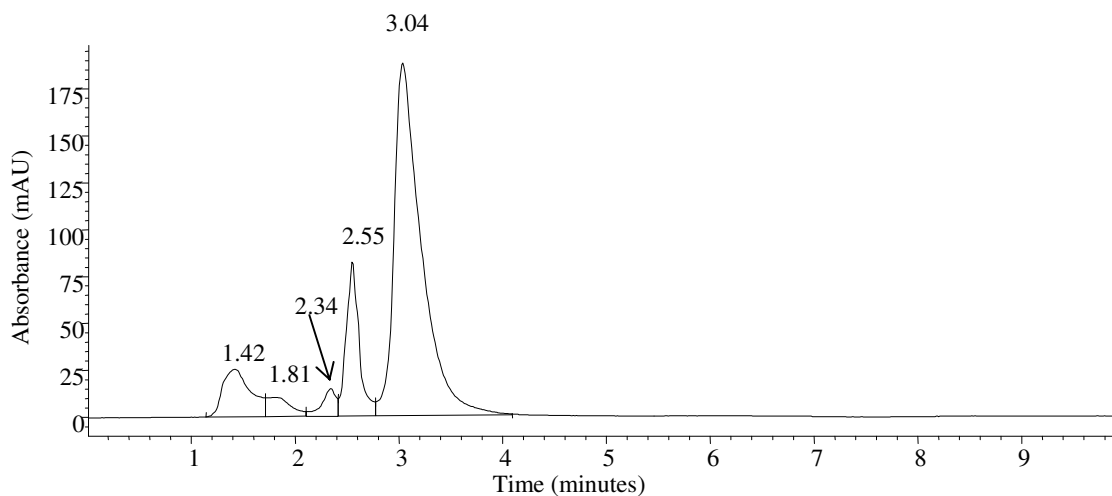


**Figure 2:32: Chromatogram of the SFNG-biotinylated DNA reaction mixture, eluted from a Hypersil C18 column (250 mm x 4.6 mm) with 35 % methanol, isocratic elution, 0.6 ml min<sup>-1</sup> flow rate, 10 µl injection volume. 260 nm detection wavelength.**

Once it was established that the SFNG-DNA labelling mixture gave additional peaks to those seen in the SFNG and 24 mer retention time marker chromatograms, the sample was injected again, but fractions were collected from the column outlet at the following time periods throughout the separation; 1.2-1.7 minutes, 2.3-2.8 minutes and 3-3.5 minutes. These three fractions were denoted fractions 1, 2 and 3 respectively. The same fractions were also collected during injection and elution of the retention time markers and the sample blank (35% methanol). Each of the collected fractions consisted of 300 µl (0.6 ml min<sup>-1</sup> flow rate which was collected for a total of 0.5 minutes in each fraction), but contained approximately 35% methanol. Once all the fractions had been collected, the methanol was allowed to evaporate. This was achieved by placing the samples in a heated (50 °C) water bath with a gentle stream of argon flowing over the collected fractions. The removal of methanol was necessary to ensure the samples were ICP-MS compatible. Also, by removing the organic solvent, the standards did not have to be matrix matched with the samples in terms of solvent content.

Once the samples had been evaporated down to near dryness, they were reconstituted with water to a volume of 0.5 ml. Further dilutions were carried out on the re-suspended samples with 2% hydrochloric acid prior to ICP-MS analysis. Gold calibration standards (10 pg ml<sup>-1</sup>–1000 pg ml<sup>-1</sup>) were also prepared in 2% hydrochloric acid. These samples were

analysed on the Element 2 XR ICP-MS and the Au in each fraction was quantified. Table 2:13 summarises the data and shows the Au concentration in each of the collected fractions.

**Table 2:13: Au concentrations in separated fractions.**

Sample	Au conc. (ng ml <sup>-1</sup> )
Blank fraction 1	0.22
Blank fraction 2	0.08
Blank fraction 3	0.10
24 mer only fraction 1	0.12
24 mer only fraction 2	0.13
25 mer only fraction 3	0.16
SFNG only fraction 1	0.67
SFNG only fraction 2	1.08
SFNG only fraction 3	0.52
SFNG-DNA fraction 1	5.67
SFNG-DNA fraction 2	2.28
SFNG-DNA fraction 3	1.39

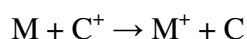
The Au concentrations were relatively low in the blank and 24 mer oligonucleotide (retention time marker) fractions as expected. However, the second fraction of the SFNG retention time marker had elevated Au levels which confirmed that the unbound SFNG eluted between 2.3-2.8 minutes, which was consistent with the UV data (Figure 2:31b). The third peak at 3 minutes in the SFNG-DNA labelling mixture (Figure 2:32) was thought to be the conjugate. However, this fraction proved to contain the least amount of Au of all the tagging fractions. The first fraction contained the most Au, suggesting that the SFNG-DNA conjugate eluted between 1.2-1.7 minutes. One explanation is that the SFNG-DNA conjugate was so large (up to 91 500 Da) that it was totally excluded from the porous C18 phase, thus eluting very quickly. The conjugate would also be highly charged due to the presence of the additional DNA molecules, also explaining why the conjugate would have very little retention on the C18 phase. It should also be noted that more than one biotin binding site on the streptavidin molecule may be available for binding, thus more than one conjugate species may be formed during the reaction. The SFNG probe could have one or

two biotinylated DNA molecules bound to the streptavidin protein, resulting in two potential conjugate species, each having different molecular weights and charges. Hence, the two additional peaks (1.81 and 2.34 minutes) observed in the tagging chromatogram (Figure 2:32) could also be conjugates.

The next step was to carry out the separation on-line with ICP-MS. However, the methanol content in the mobile phase had to be reduced from 35% to less than 10%. There were two reasons for reducing the amount of organic modifier in the mobile phase. Firstly, 35% organic solvent could potentially make the plasma unstable and the high organic matrix may have suppressed Au ionisation. In addition, carbon deposition around the sampler cone will be more pronounced with higher organic solvent content resulting in signal drift and reduced sensitivity. The separation method was therefore modified so the mobile phase contained 5% methanol. The low level of organic solvent did not adversely affect the plasma and carbon deposition was minimal. Isocratic elution is preferred when using HPLC-ICP-MS, since the mobile phase composition remains constant resulting in constant plasma conditions. In contrast, gradient elution involves changing the mobile phase composition. Thus, the plasma conditions are also constantly changing with the changing matrix, which can result in varying signal intensities due to suppressed or enhanced analyte ionisation during the separation.

Before the separation was carried out on-line, the effect of 5% methanol on Au signal intensity was established. Initially two solutions containing  $1 \text{ ng ml}^{-1}$   $^{115}\text{In}$  were prepared; one solution was prepared in 2% hydrochloric acid and the other was prepared in 5% methanol. The resulting signal intensity for In was  $2.5 \times 10^6$  cps and 750 000 cps in the hydrochloric acid matrix and 5% methanol matrix respectively. Hence, a 33% reduction in  $^{115}\text{In}$  signal was observed in the methanol matrix. Initially this was attributed to the increased matrix levels in the plasma having a cooling effect and thus reducing In ionisation. Two further solutions both containing Au at a concentration of  $0.50 \text{ ng ml}^{-1}$  were also prepared. Again one solution was prepared in 2% hydrochloric acid and the other was prepared in 5% methanol. Unlike the In signal, signal intensities of 97 692 cps and 116 111 cps were observed for the Au solutions in the hydrochloric acid and methanol

matrix respectively, resulting in a 19% increase in Au sensitivity in the presence of methanol. This was quite unexpected, since it was initially thought that the organic matrix would suppress Au ionisation resulting in reduced sensitivity. However, there have been numerous reports of carbon enhancing the signal intensity of elements having high first ionisation potentials (generally those elements with first ionisation potentials between 9-11 eV).<sup>130-134</sup> Such reports have concentrated on the signal enhancement for Se and As. It is now common practise to introduce carbon (either as a gas or organic solvent) to the sample introduction system when analysing Se or As to enhance sensitivity.<sup>130, 135, 136</sup> Rodushkin *et al.*,<sup>137</sup> and Allain *et al.*,<sup>133</sup> reported that Au signal intensity (amongst other elements) was enhanced in the presence of carbon.<sup>137</sup> Carbon induced enhancement has been explained by charge transfer reactions in the plasma, where carbon ions transfer charge to analyte ions which have a lower ionisation potential than carbon itself (11.3 eV).<sup>131</sup> The proposed charge transfer mechanism was described by Hu *et al.*,<sup>132</sup> and is summarised below.



Enhancement in signal has also been attributed to reduced surface tension due to the presence of organic solvent, which improves sample uptake and nebulisation efficiency.<sup>130</sup> Since the In signal intensity dramatically decreased in the presence of 5% methanol and the Au signal increased, it was unlikely that reduced surface tension was responsible for increasing Au signal in the above case, but rather attributed to the charge transfer mechanism.<sup>131, 132</sup> In addition, volatile solvents are known to expand in the plasma and thus widen the central channel. Liu *et al.*,<sup>131</sup> suggested that lighter elements diffuse more rapidly through the already expanded central channel than heavier analyte ions, thus a decreasing signal intensity is observed for lighter ions compared to heavier species.<sup>131</sup> This argument would explain why the <sup>115</sup>In signal decreased in 5% methanol, but the heavier <sup>197</sup>Au signal intensity did not. In any case, the enhancement in analyte signal by the HPLC mobile phase was an advantage.

The coupling of the HPLC and ICP-MS involved inserting a T-piece between the column exit and nebuliser. This enabled the eluent flow to be split, so only 200-300  $\mu\text{l min}^{-1}$  of solvent entered the nebuliser. Figure 2:33 shows a schematic of the LC coupling and

illustrates how the mobile phase flow can be split with the aid of a T-piece. The aim was to limit the amount of organic solvent entering the plasma. The lengths of Teflon tubing used to connect the column to the nebuliser are shown in Figure 2:33; the internal diameter of the tubing was 150  $\mu\text{m}$ . Both the lengths and diameters of tubing determine the proportion of flow splitting, a small internal diameter was required to minimise band broadening and ultimately retain resolution. A Waters  $\mu\text{Bondapak C18}$  column (300 mm x 3.9 mm) was employed for the HPLC-ICP-MS analysis of the SFNG-DNA reactions.

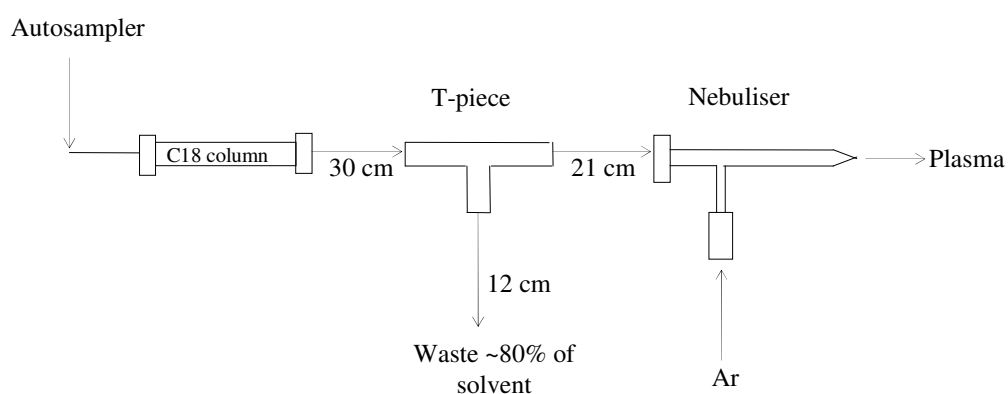


**Figure 2:33:** Schematic showing the coupling of a HPLC column to a nebuliser with the aid of a flow splitter.

The chromatograms in Figure 2:34 show the Au signals during elution of unbound SFNG (SFNG standard containing 21.12  $\text{ng ml}^{-1}$  Au) and SFNG-DNA (24 mer biotinylated oligonucleotide) tagging mixture. The unbound SFNG eluted at 1.72 minutes as signified by the single Au peak in Figure 2:34a. Two Au peaks were observed in Figure 2:34b, the first peak at 1.06 minutes corresponding to the SFNG-DNA conjugate and the second peak at 1.80 minutes relating to the unbound SFNG, which had a retention time consistent with the unbound SFNG shown in Figure 2:34a.



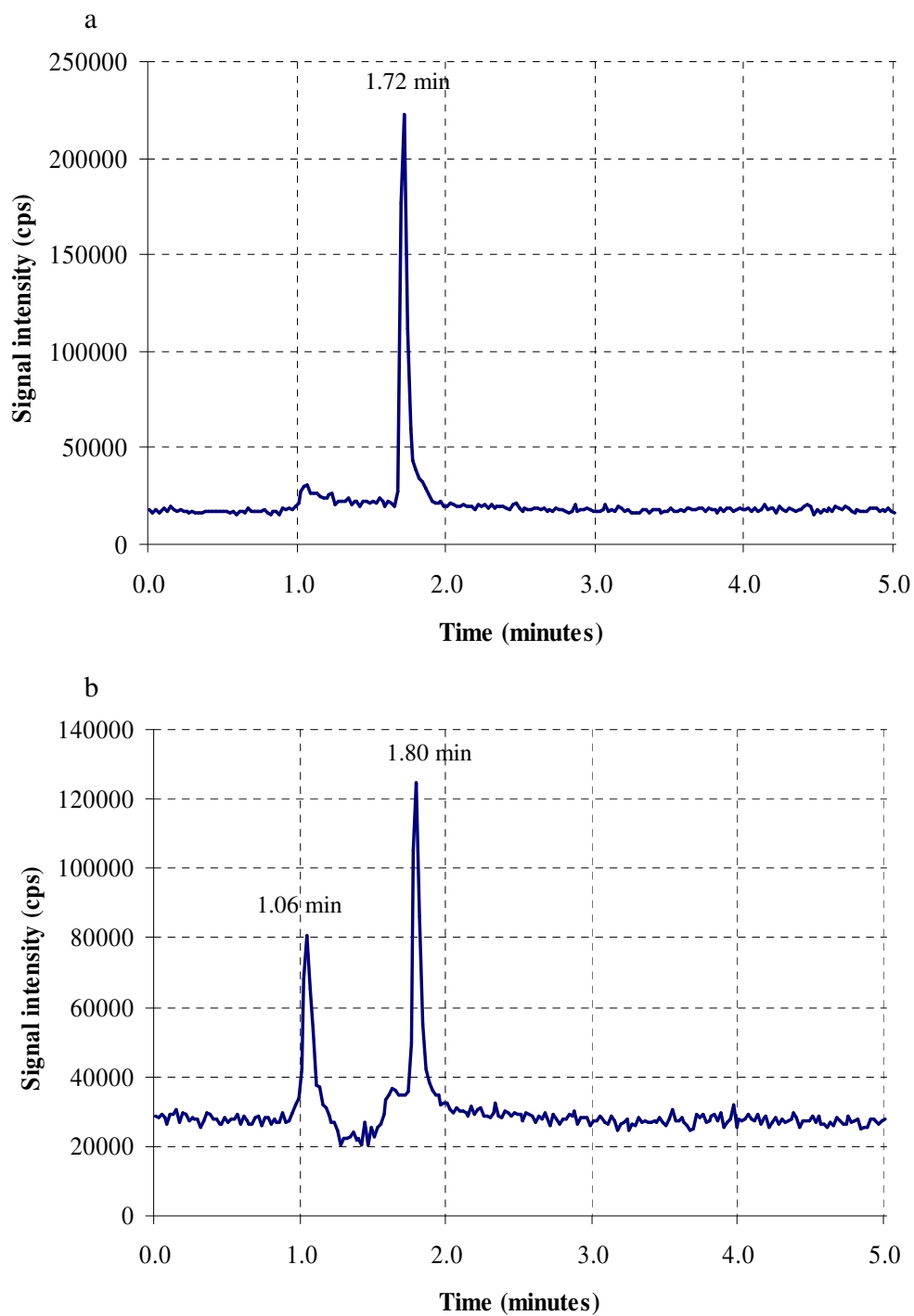
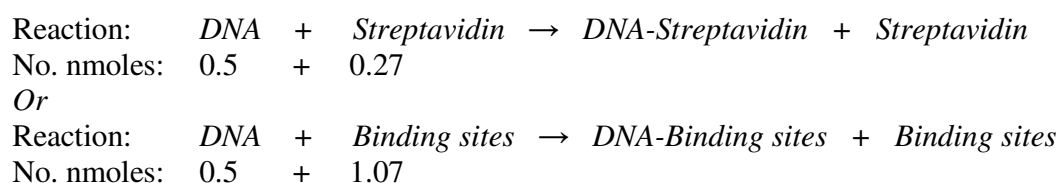


Figure 2:34: a)  $^{197}\text{Au}$  chromatogram of unbound SFNG containing  $21.12 \text{ ng ml}^{-1} \text{ Au}$ . b)  $^{197}\text{Au}$  chromatogram of SFNG-DNA reaction mixture containing  $14.8 \text{ ng ml}^{-1} \text{ Au}$ . Both samples were eluted from a Waters  $\mu\text{Bondapak C18}$  column (300 mm x 3.9 mm, 10  $\mu\text{m}$ ) with 5% methanol isocratic mobile phase. 10  $\mu\text{l}$  injection volume.

The retention times of the unbound SFNG and SFNG-DNA conjugate shown in Figure 2:34 were quite different to those observed in Table 2:13 in which the eluting species were fraction collected and then analysed by ICP-MS. The reason for this was attributed to the change in stationary phase; the fraction collected samples were separated on a Hypersil C18 column, but the on-line separation was achieved with a Waters C18 column. Although both columns contained a C18 phase, they originated from different manufacturers' and had different dimensions, which may have effected the retention times. In addition, ionic strength was thought to have influenced the retention time; this aspect will be discussed later in this section.

The SFNG-DNA conjugate was the first species to elute because of its large size and therefore, it was likely to be largely excluded from the C18 phase. More importantly, the bound SFNG carried a highly charged oligonucleotide, resulting in less hydrophobic interaction with the surface of the non-polar stationary phase. The void volume of the Waters  $\mu$ Bondapak column was determined with a 100  $\mu$ M solution of uracil, which eluted after 3.87 minutes. Therefore, both SFNG species eluted within the void volume, suggesting that they were totally excluded from the pore space in the column and were retained due to surface interactions.

The SFNG-DNA reaction mixture shown in Figure 2:34 contained 0.5 nmoles biotinylated 24 mer oligonucleotide and 0.27 nmoles of streptavidin or 1.07 nmoles of biotin binding sites (four binding sites per streptavidin). Therefore, the above reaction mixture contained a 2.14 molar excess of biotin binding sites compared to biotinylated DNA. The reaction can therefore be written in two different ways by considering either the number of moles of streptavidin or biotin binding sites in relation to the DNA.



Due to steric restraints only ~two biotin binding sites per streptavidin will be accessible to biotin, resulting in 0.54 nmoles of available biotin binding sites, or effectively an equal number of moles of biotin and binding sites. If all the biotinylated DNA molecules are labelled it would result in two DNA molecules per streptavidin protein. More importantly, this scenario would result in all the SFNG being bound, thus only one Au peak corresponding to SFNG-DNA conjugate would be observed in Figure 2:34. Since this is not the case, the peaks in Figure 2:34 were integrated giving areas of; 50 130 and 57 399 for the 1.06 and 1.80 minute peak respectively. Thus 46.6% of SFNG in the sample was bound, or considering 0.27 nmoles of streptavidin was present, 0.124 nmoles of streptavidin was bound to DNA. Considering this information, a maximum of 50% DNA labelling (0.25 nmoles DNA labelled) can be achieved and only if two DNA molecules bind per SFNG. The DNA labelling efficiency decreases to 25% (0.124 nmoles DNA labelled) if only one DNA binds per SFNG. These scenarios are summarised below.

1:1 Reaction: DNA + Streptavidin → 1DNA-Streptavidin + Streptavidin

No. nmoles: 0.5 + 0.27 → 0.124-0.124 + 0.146

Or, if two DNA molecules bind to SFNG:

2: 1 Reaction: DNA + Streptavidin → 2 DNA-Streptavidin + Streptavidin

No. nmoles: 0.5 + 0.27 → 0.25-0.124 + 0.146

Although the amount of bound SFNG can be established, the above calculation does not identify the number of occupied biotin binding sites per streptavidin molecule because the experiment tracks gold not DNA, or effectively the labelling stoichiometry. The preferred labelling ratio is 1 DNA:1 SFNG since it results in each DNA molecule being labelled with ~ 80 Au atoms. If two DNA molecules bound to one SFNG in a 2:1 ratio, then the number of Au atoms per DNA decreases to 40. As explained in the above case, the ratio of unbound SFNG/SFNG-DNA peak areas would be the same irrespective of one or two DNA molecules binding per streptavidin. This aspect of SFNG labelling will be discussed again in subsequent sections.

In addition to labelling efficiency, the enhancement in signal due to SFNG labelling has to be calculated, which was achieved by preparing an Au and P calibration curve and comparing the gradients. The Au calibration standards were prepared in the concentration range 0.20 – 1.5 ng ml<sup>-1</sup> and the P calibration standards ranged from 10-200 ng ml<sup>-1</sup>. The Element 2 XR ICP-MS was used in the low and medium resolution mode for Au and P respectively. Gradients of 265 765 and 1082 were obtained for Au and P calibrations respectively, thus, a 246 times greater response was obtained for Au compared to P. Of course the gradient for P is reduced by working at medium resolution, but that is a necessary setting for the measurement. The biotinylated oligonucleotides used in the above example were 24 nucleobases in length, thus each oligonucleotide possessed 24 P atoms. Considering each oligonucleotide was labelled with 80 Au atoms, there were 3.3 times as many Au atoms compared to P. Thus, the 246 Au enhancement factor can be multiplied by 3.3 to give a total signal enhancement of 812 for Au labelled oligonucleotides, assuming there were 80 Au atoms per nano-particle. SFNG was assayed in a subsequent experiment (Section 2.6.1.4, Quantification) and the actual number of Au atoms per nano-particle determined.

It should be noted at this point that the 246 fold enhancement in signal obtained by Au, which resulted in a 812 total signal enhancement for SFNG labelled oligonucleotides was much greater than the signal enhancement calculated for MMN labelled oligonucleotides on page 122 (section 2.4.2.2). In the case of MMN, Au gave a 123 times greater response than P, resulting in a 406 fold signal enhancement (working on assumption of 80 Au atoms) when the MMN were attached to the oligonucleotide. The same type of Au nano-particle is incorporated on both SFNG and MMN, consisting of approximately 80 Au atoms. However, the MMN experiments were carried out on the PQ ExCell quadrupole instrument, whilst the Element 2XR was used for the SFNG experiments described above. It can only be assumed that the sensitive detection of heavier elements in low resolution operation of the double focussing instrument was responsible for the greater Au response, which in turn resulted in greater Au enhancement factors for the SFNG labelling experiments.

The SFNG-DNA reaction mixture which was shown in Figure 2:34 was injected again, but at a concentration 10 times greater than that of Figure 2:34. The retention time of the unbound SFNG was 2.41 minutes, which was considerably later than that previously observed (Figure 2:34). However, the SFNG-DNA conjugate still had a retention time of 1.06 minutes. SFNG was supplied in a solution containing 20 mM phosphate buffer and 0.150 M sodium chloride. The more concentrated SFNG solution therefore contained more salt and hence had a higher ionic strength. Therefore, a plausible explanation is that the ionic strength had an effect on the streptavidin configuration in solution, which in turn may have effected the retention time of the unbound SFNG. However, the exact effect of ionic strength on the protein structural configuration was unknown. The retention time of the SFNG-DNA conjugate did not change, presumably due to the highly charged oligonucleotide molecules having very little affinity for the non-polar phase, thus the conjugate eluted at the same retention time as seen previously. Since the unbound SFNG retention time was dependent upon concentration, it was deemed necessary to inject retention time markers in every experiment to confirm the retention time of the unbound SFNG species and ensure the correct Au species was being employed for quantification.

A control sample was also prepared, which involved adding non-biotinylated oligonucleotide (unmodified 25 mer) to a 3.6 fold molar excess of biotin binding sites. The reaction conditions were similar to those described above and the chromatogram is shown in Figure 2:35. A single Au peak was observed in Figure 2:35, with the retention time consistent with unbound SFNG. The absence of a SFNG-DNA peak (expected at ~1.0 minutes), implies that the reaction was dependent on the biotin functionality on the oligonucleotide and was therefore site specific.

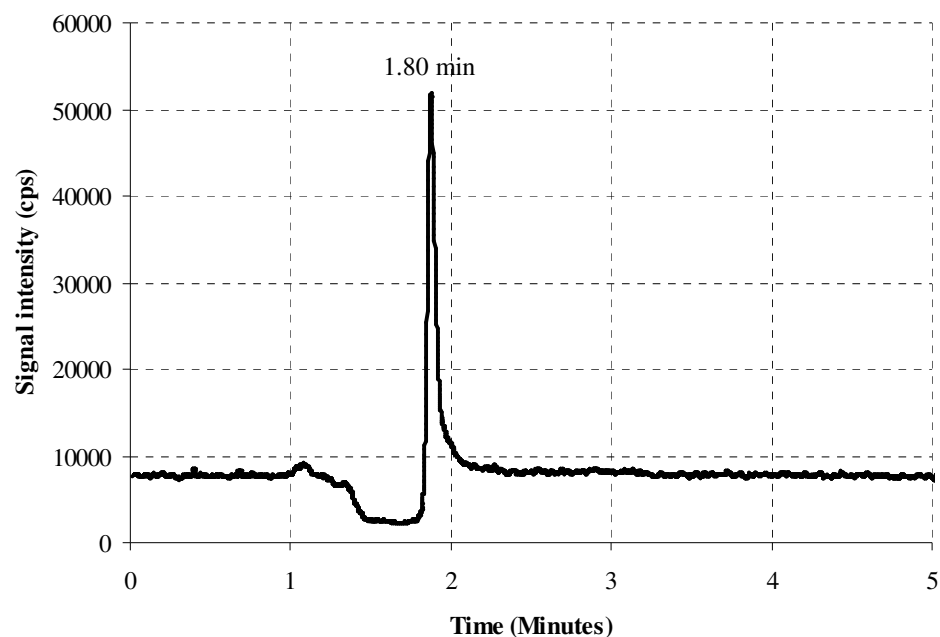


**Figure 2:35:**  $^{197}\text{Au}$  chromatogram of SFNG control reaction containing 3.6 fold molar excess of binding sites and unmodified 25 mer. Eluted from a Waters  $\mu\text{Bondapak C18}$  column (300 mm x 3.9 mm, 10  $\mu\text{m}$ ) with 5% methanol isocratic mobile phase. 10  $\mu\text{l}$  injection volume.

It has been shown that the SFNG labelling route is viable, but in order to validate the method used above, several factors need to be investigated:

1. Instrument configuration: Need to ensure the coupling of the HPLC to the ICP-MS is suitable in terms of stability and sensitivity.
2. Quantification: The response of nanogold needs to be compared against atomic spectrometry Au standard, since the nanogold clusters may behave different in the plasma to aqueous ionic Au.
3. Mass balance: Is the amount of Au injected equal to the amount recovered post separation? A discrepancy in injected and recovered Au could indicate that the nanogold is adsorbing onto the stationary phase walls, or that the mobile phase is not strong enough to elute the nanogold.
4. Labelling efficiency and labelling ratio: The percentage of SFNG labelled DNA needs to be calculated. In addition, the number of DNA molecules bound to each SFNG needs to be established in each reaction.

Each of the above aspects will be considered in turn.

## 1. Instrument Configuration

Several SFNG-biotinylated DNA reactions were prepared, each contained different molar excesses of biotin binding sites in relation to biotinylated DNA. Reactions containing an equal number of moles of biotinylated DNA and binding sites, two fold excess, four fold excess and ten fold excess of biotin binding sites compared to DNA were prepared and were denoted 1:1, 1:2, 1:4 and 1:10 respectively. Each sample was incubated at 4 °C for approximately 24 hours before being diluted and injected onto a C18 HPLC column; the resulting Au signal was then detected by ICP-MS. The HPLC-ICP-MS parameters were similar to those used previously. Again, the eluent flow to the plasma was restricted to  $\sim 200 \mu\text{l min}^{-1}$ , by employing a flow splitter. The samples were diluted in deionised water prior to analysis, hence a blank sample consisting of deionised water was injected at regular intervals to assess the Au baseline and carry over. Figure 2:36 shows the chromatogram corresponding to the first blank injection, which was carried out before the samples were injected.

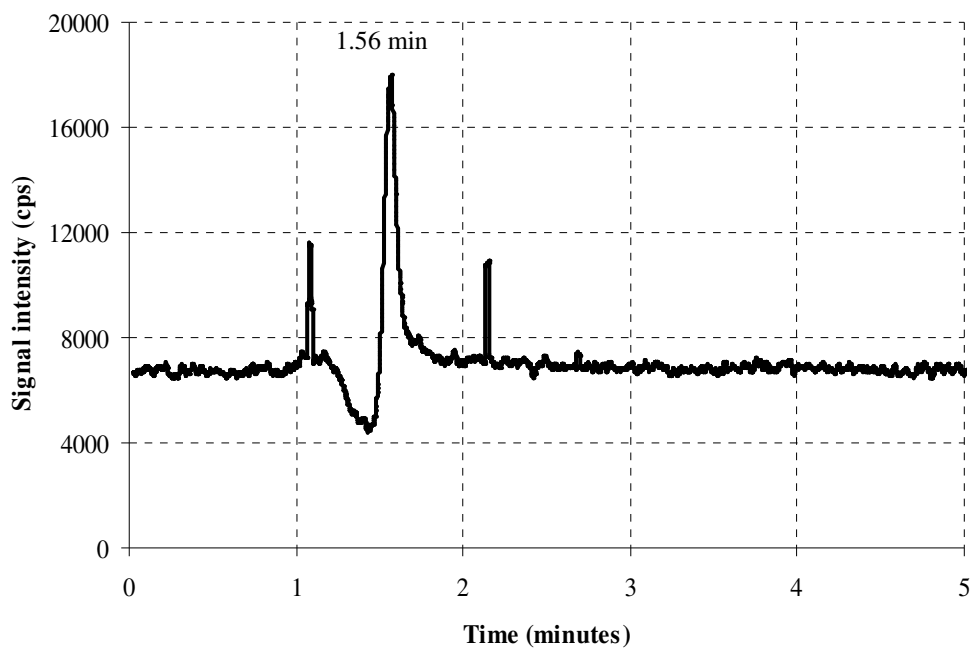


Figure 2:36: <sup>197</sup>Au signal intensity during injection of a deionised water blank. Eluted from a Waters  $\mu$ Bondapak C18 column (300 mm x 3.9 mm) with 5% methanol isocratic elution at  $1 \text{ ml min}^{-1}$ ,  $10 \mu\text{l}$  injection volume.

A peak at 1.56 minutes was clearly evident in Figure 2:36. This retention time was quite similar to the retention time of the unbound SFNG, thus the peak in the blank chromatogram was thought to be carry over of Au, presumably due to contamination in the injector system. As discussed previously Au has the disadvantage of being 'sticky' in nature, resulting in carry over. Further blank injections did not remove the peak, therefore, it was decided to integrate the peak in the blank and subtract the area from the samples during any quantification calculations. The chromatogram in Figure 2:36 also exhibits a couple of spikes, which were quite erratic and not reproducible and therefore thought to be artefacts. The chromatograms corresponding to the 1:1 and 1:2 DNA:binding site reaction mixtures are shown in Figure 2:37. These chromatograms demonstrate that the SFNG labelling reaction and separation were reproducible, with the bound and unbound SFNG species clearly resolved and detected.



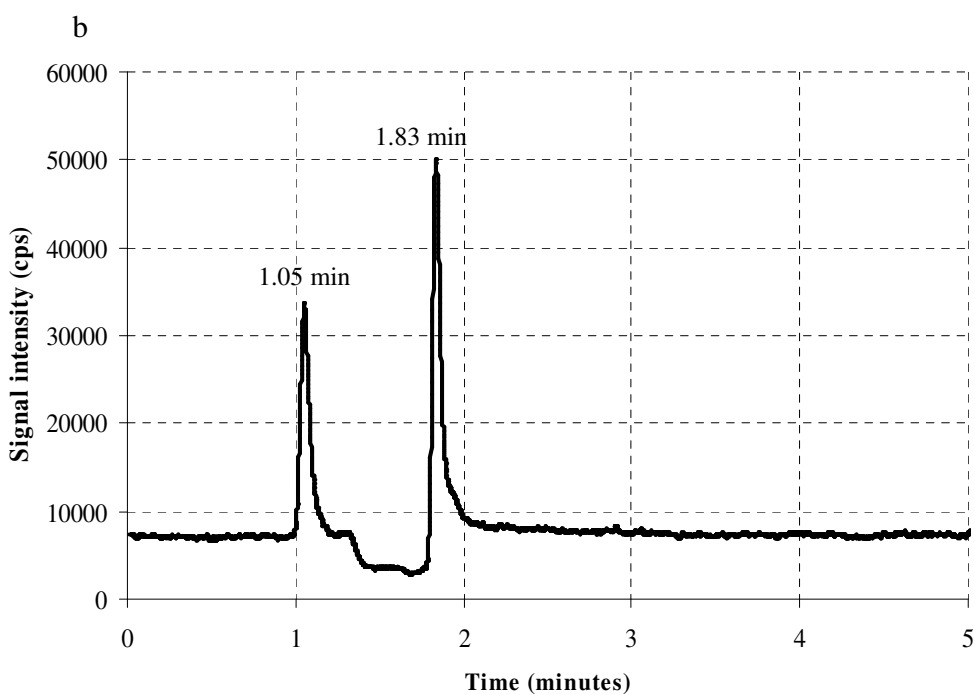
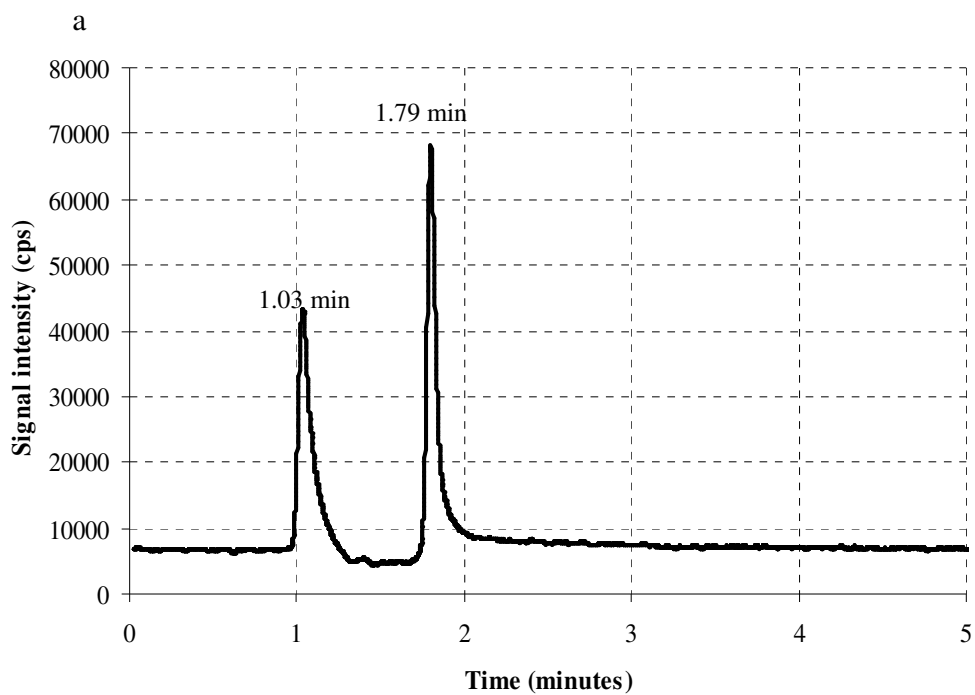
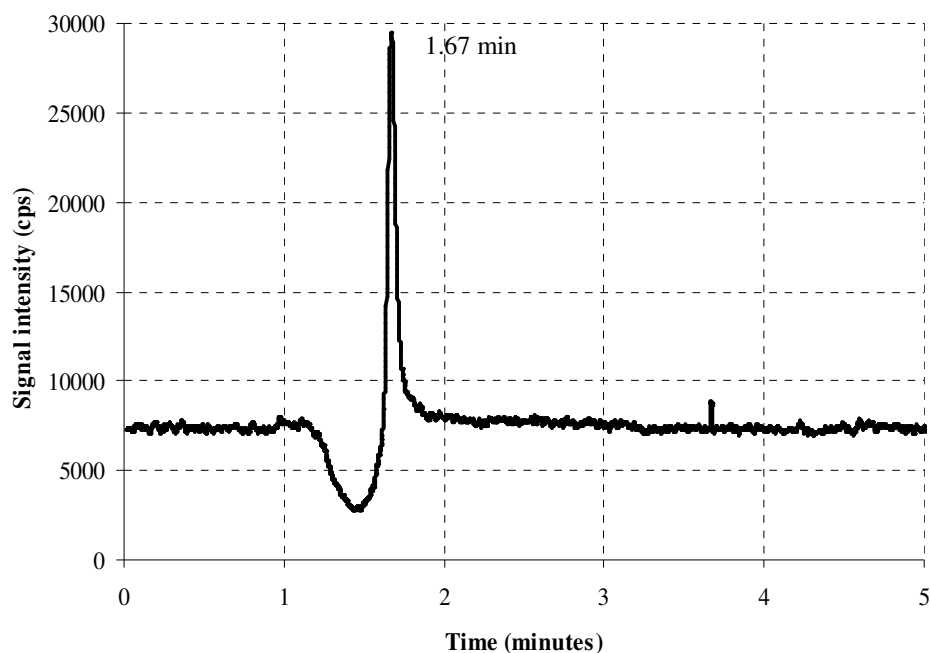


Figure 2:37: a)  $^{197}\text{Au}$  signal intensity during injection of 1:1 DNA:biotin binding site reaction. b)  $^{197}\text{Au}$  signal intensity during injection of the 1:2 DNA:biotin binding site reaction. Both samples eluted from a Waters Bondapak C18 column (300 mm x 3.9 mm) with 5% methanol isocratic elution at  $1\text{ ml min}^{-1}$ , 10  $\mu\text{l}$  injection volume.

The 1:4 and 1:10 DNA:biotin binding site reactions did not exhibit the SFNG-DNA conjugate peak which was expected around 1 minute. Hence the chromatograms corresponding to these two failed reactions are not shown. Figure 2:38 shows an Au chromatogram of a deionised water blank injection which was injected after the above labelling mixtures.



**Figure 2:38:**  $^{197}\text{Au}$  signal intensity during injection of deionised water blank. Eluted from a Waters Bondapak C18 column (300 mm x 3.9 mm) with 5% methanol isocratic elution at  $1 \text{ ml min}^{-1}$ ,  $10 \mu\text{l}$  injection volume.

Figure 2:38 shows that the peak at 1.67 minutes is larger than that seen in the first blank injection in Figure 2:36. The increase in Au signal in the blank injections was thought to be due to the HPLC configuration. In normal operation of the HP 1090 LC system, the eluent flows through the column and then back into the instrument through the injector system. This has an effect of flushing the injector system. However, to minimise band broadening and to maintain resolution, the tubing connecting the column outlet and nebuliser was kept at a minimum length. As a result, the HPLC mobile phase was split post column, so ~20% of the flow went to the nebuliser and ~80% went directly to waste. The injector system flush was therefore by-passed, which may have resulted in the accumulation of SFNG in

the injection system, thus causing carry over and producing small peaks in the blank injections. As a result, the coupling of the HPLC to the ICP-MS was modified. Briefly, the diode array UV detector that was integrated into the HP1090 was bypassed completely. The SFNG-DNA labelling reactions were diluted between 600-3500 fold with deionised water (depending on the Au concentration in the reaction mixtures) prior to ICP-MS analysis. These extremely low concentrations of SFNG and DNA were below the UV detector's limit of detection. Hence, it was not deemed necessary to include the detector in the coupling. The flow splitter was employed again to achieve a 20:80 split in mobile phase post column, 20% was directed to the nebuliser as described previously, but the remaining 80% was directed back into the HPLC, to flush the injector system. Although this did not completely eliminate carry over, it was reduced considerably. Complete removal of Au carry over between injections would require optimisation of the separation method. *Aqua regia* and hydrochloric acid have already been mentioned with regard to improving Au wash out time. However, these strong acids can not be used in conjunction with a silica stationary phase due the pH limitations of such phases (limited to pH 4-9). The addition of cysteine or another S containing species may be required in the mobile phase to complex Au and prevent adsorption onto the injector system, chromatographic phase and connection tubing between the column and nebuliser. However, S containing mobile phase additives was not investigated here.

## 2. Quantification

The SFNG was assayed to determine the number of Au atoms per nanogold particle. Two Au calibration curves were prepared, one for SFNG and one for an elemental Au standard. The slopes of the calibration curves were 4 510 624 (x axis expressed as nM streptavidin) and 265 217 (x axis expressed as ng ml<sup>-1</sup>) for SFNG and elemental Au respectively. From the data it was calculated that there were 86 Au atoms per nanogold particle. This figure is slightly higher than that given by the manufacturer, who state ~80 Au atoms per nanogold particle.<sup>95</sup> However, the manufacturer states that there is an average of one nanogold particle to each streptavidin molecule,<sup>95</sup> more than one nanogold particle per protein would increase the average number of Au atoms per particle and there may also be a small fraction of nanogold not bound to streptavidin. If either of these species were present they should be

resolved from the SFNG-DNA conjugate during HPLC separation. No evidence of additional peaks was observed in any of the chromatograms. The figure of 86 Au atoms per nanogold particle was used for further calculations, although this assay was only applied to one batch of SFNG, it is unknown whether the figure varies between batches.

The enhancement in signal due to SFNG labelling assumes that the nanogold particles are completely ionised in the plasma and thus behave as Au atoms. Once the average number of Au atoms per nanogold particle was established, Au calibration curves for SFNG and elemental Au standards were compared for consistency. The gradients for the two sets of calibration data were 266 226 and 265 217 (x axis expressed as  $\mu\text{g l}^{-1}$  in both cases) for SFNG and elemental Au respectively. The two gradients were virtually identical, confirming that SFNG gave a similar response to the atomic Au solutions and is therefore ionised efficiently in the plasma. However, it should be noted that ICP-MS was employed to assay the SFNG to obtain the figure of 86 Au atoms per nano-particle. This figure was then used to prepare SFNG standard solutions and the slopes of SFNG and elemental Au calibration curves were compared, to check the assay data was correct. It does not however provide definitive proof that the nano-particles were completely processed within the plasma. This would require the figure of 86 Au atoms per nano-particle to come from an independent method. Recent work has suggested that for the plasma to process particles in a truly composition independent fashion requires them to be less than 90 nm in size (based upon the analysis of glass).<sup>102</sup> Considering the nanogold particles were only 1.4 nm in diameter, it can be concluded that the particles were completely ionised. The presence of the fluorophore and streptavidin protein are not likely to have adversely effected the ionisation of the nanogold particle, since these are organic molecules, which as already discussed, may have beneficial effects due to their carbon content.

The above analysis revealed that 86 Au atoms were present per nano-particle, considering these nano-particles are fully ionised in the plasma, a more accurate enhancement calculation can be conducted. In previous experiments biotinylated 24 mer oligonucleotides have been labelled with 86 Au atoms (as calculated above), resulting in 3.58 times more Au atoms compared to P atoms. Multiplying this figure by the Au enhancement factor of 246,

results in an 882 fold increase in signal for 24 mers labelled with SFNG, providing one DNA molecule binds to one SFNG.

Although Au quantification can be achieved with SFNG solutions containing known concentrations of Au, an alternative method of quantifying Au signals was employed by Baranov *et al.*,<sup>10, 16</sup> in which Ir was used as an internal standard. In addition, an acidic solution containing a known concentration of Tl was introduced post column *via* a T-piece just before the ICP sample introduction system. The ratio of Ir/Tl signals was employed to establish the stability of the system, whilst the Au signal was quantified using the Ir signal, which was expected to have a similar response to Au due to the similar first ionisation potentials and masses of Au and Ir.<sup>10, 16</sup>

### **3. Mass Balance**

The 1:1 DNA:biotin binding site reaction that was observed above in Figure 2:37 was injected using the modified instrument configuration discussed above. A solution of unbound SFNG containing  $9.34 \text{ ng ml}^{-1}$  Au was also injected; this solution was used for quantifying Au in the separated peaks of the reaction mixture. The chromatogram of the standard and the re-injected 1:1 DNA:biotin binding site reaction can be seen in Figure 2:39.

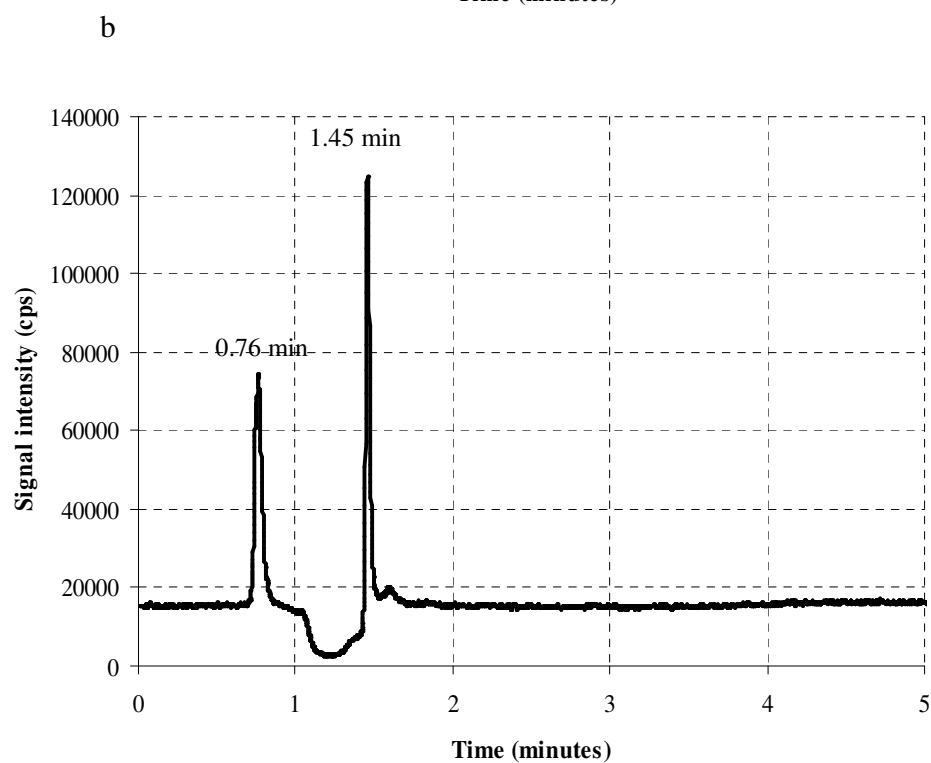
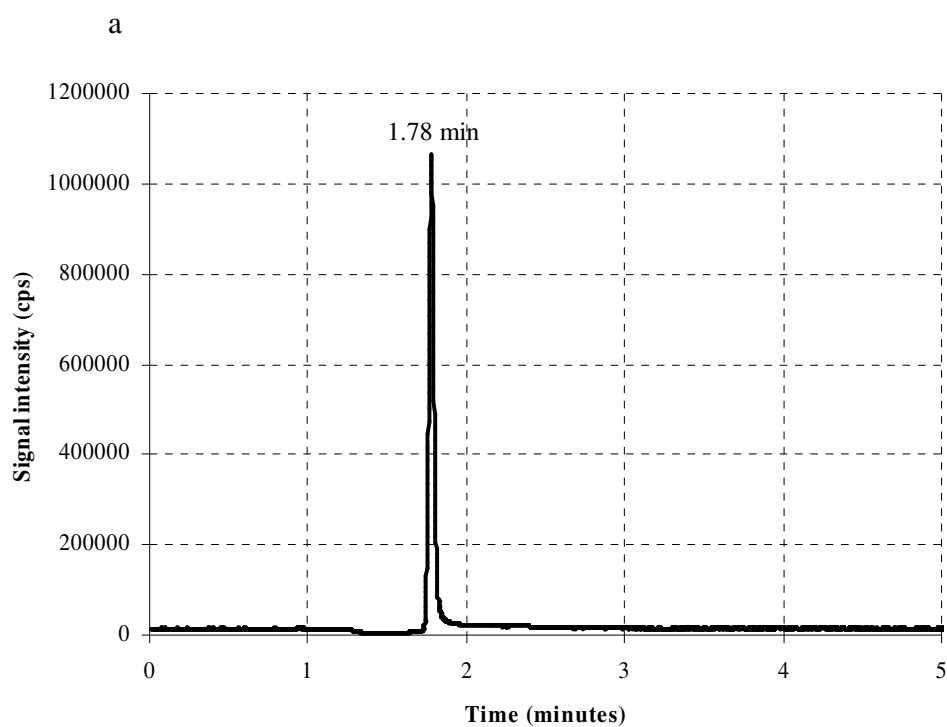


**Figure 2:39: a)  $^{197}\text{Au}$  signal intensity during injection of a SFNG standard containing  $9.34 \text{ ng ml}^{-1} \text{ Au}$ . b)  $^{197}\text{Au}$  signal intensity during injection the equal molar biotin binding site reaction. Both samples eluted from a Waters  $\mu\text{Bondapak C18}$  column (300 mm x 3.9 mm) with 5% methanol isocratic elution at  $1 \text{ ml min}^{-1}$ ,  $10 \mu\text{l}$  injection volume.**

The Au concentration in each of the peaks shown in Figure 2:39b was quantified using the SFNG standard peak area (Figure 2:39a). Briefly, the total peak area of the SFNG standard was divided by the Au concentration in the SFNG standard to give the unit area per  $\text{ng ml}^{-1}$  of Au. From Figure 2:39b it was calculated that peak 1 at 0.76 minutes contained  $0.75 \text{ ng ml}^{-1}$  Au, and peak 2 at 1.45 minutes contained  $0.34 \text{ ng ml}^{-1}$  Au, hence, the total Au recovered equated to  $1.09 \text{ ng ml}^{-1}$ . However, the Au concentration of the injected reaction mixture was  $11.3 \text{ ng ml}^{-1}$ , suggesting that only  $\sim 10\%$  of the injected Au was recovered (note the injection volumes were the same so that concentration is mass equivalent). The same calculation was carried out on the 1:2 DNA:biotin binding site reaction (Figure 2:37) and a recovery of  $10.6\%$  was achieved. The discrepancy in the mass balance calculations was initially thought to be one of two factors:

- SFNG and DNA were absorbing onto the walls of the polypropylene reaction vessels.
- SFNG was being trapped on the column instead of being completely eluted.

The Waters C18 column was cleaned in an attempt to remove residual Au and hence improve the baseline. The column was connected to the HPLC in the reversed flow direction (but not connected to the detector) and flushed with  $5\%$  methanol. It was hoped that any nanogold that had adsorbed at the head of the column would be removed by the continuous reversed flushing. The wash eluents were collected for subsequent ICP-MS analysis. Gold counts of  $\sim 1.4 \times 10^6$  cps were observed for the first column backflush, equating to  $\sim 2 \text{ ng ml}^{-1}$  Au, which had collected at the head of the column. The Au signal intensity gradually decreased for subsequent reverse flush eluents, suggesting that SFNG had accumulated at the head of the column as expected.

After thorough cleaning of the column, two fresh SFNG tagging samples were prepared. The first reaction contained  $0.107$  nmoles of biotin binding sites and  $0.115$  nmoles of  $5'$  biotinylated 24 mer oligonucleotide ( $2.24 \mu\text{M}$ ), resulting in a  $0.93$  fold excess of binding sites (i.e. DNA slightly exceeded probe in terms of moles). This sample will be referred to as the 1:1 DNA:biotin binding site reaction. The second sample, which will be referred to as the 1:7.5 DNA: biotin binding site reaction, contained  $0.44$  nmoles biotin binding sites

and 58.7 pmoles of biotinylated DNA (2.24  $\mu\text{M}$ ), resulting in a 7.5 fold excess of binding sites. The two reactions mixtures were diluted so they contained an Au concentration of 5.66  $\text{ng ml}^{-1}$  and 5.55  $\text{ng ml}^{-1}$  for the 1:1 and 1:7.5 DNA:biotin binding sites respectively. A SFNG standard containing 3.66  $\text{ng ml}^{-1}$  Au was also prepared and used to quantify the Au contained in each of the peaks. After each injection, the column was disconnected from the nebuliser and reconnected to the HPLC system in the reverse flow direction. The column was then flushed in the reverse direction for approximately 2 minutes. During this time, the column eluent was collected and analysed. The aim was to establish whether any nanogold was accumulating at the head of the column during injection. It was hoped that this would help establish an accurate mass balance. The chromatograms corresponding to the 1:1 and 1:7.5 DNA:biotin binding site reactions are shown in Figure 2:40.



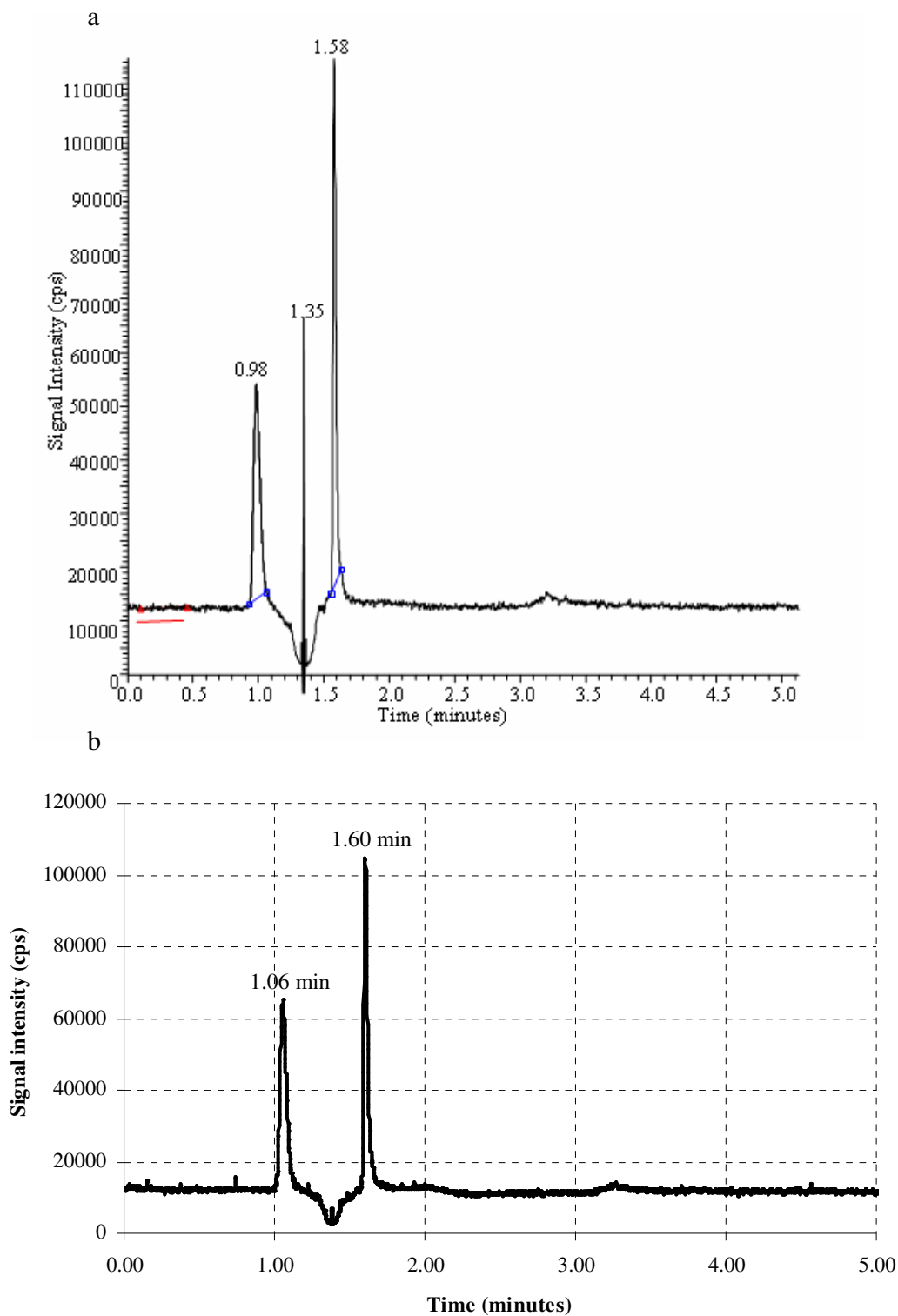


Figure 2:40: a)  $^{197}\text{Au}$  signal intensity during injection of the 1:1 DNA:biotin binding site reaction mixture. b)  $^{197}\text{Au}$  signal intensity during injection of the 1:7.5 DNA:biotin binding site reaction mixture. Both samples eluted from a Waters  $\mu\text{Bondapak C18}$  column (300 mm x 3.9 mm) with 5% methanol isocratic elution at  $1\text{ ml min}^{-1}$ ,  $10\ \mu\text{l}$  injection volume.

Duplicate injections of the SFNG standard gave an average peak area of 181 887 (RSD = 0.75%), which was divided by the Au concentration of 3.66 ng ml<sup>-1</sup> to give 49 695.90 unit area/ng ml<sup>-1</sup> Au. The chromatogram corresponding to the 1:1 DNA:biotin binding site reaction (Figure 2:40a) revealed that 2.70 ng ml<sup>-1</sup> and 3.07 ng ml<sup>-1</sup> Au was present in the SFNG-DNA peak (0.98 minutes) and unbound SFNG peak (1.58 minutes) respectively, thus a total of 5.77 ng ml<sup>-1</sup> Au was recovered. Considering 5.66 ng ml<sup>-1</sup> Au was injected on the column, the resulting recovery was calculated to be 102%. The same calculation was performed on the 1:7.5 DNA:biotin binding site chromatogram in which 2.98 ng ml<sup>-1</sup> and 3.11 ng ml<sup>-1</sup> Au was calculated for the 1.06 and 1.60 minute peak respectively. Therefore, a total of 6.09 ng ml<sup>-1</sup> Au was recovered, resulting in a 109% recovery (5.55 ng ml<sup>-1</sup> Au was injected on the column).

The chromatograms in Figure 2:40 had an Au baseline of ~12 000 cps, which equated to approximately 70 pg ml<sup>-1</sup> Au. This baseline level did not decrease, but remained constant. This continuous flux of Au was thought to be hydrophobically bound SNFG from previous injections slowly eluting from the column. Repeated injections of nanogold produced an accumulation of Au at the head of the column that could be reduced, but not totally removed by back flushing. The observed background Au signal may also have been enhanced due to the presence of 5% methanol in the mobile phase which was shown to increase Au signals by ~19%. The column eluents resulting from the reversed column flush post injection also revealed that ~70 pg ml<sup>-1</sup> Au was present for both samples. This value of 70 pg ml<sup>-1</sup> was constant for all column backflushes, suggesting that no nanogold was depositing on the column head during the above experiment, and that all the Au was being eluted and thus detected.

This data suggested that 100% recovery of the Au was possible if the column was cleaned before each injection of SFNG. These calculations ensure that all the Au is being detected, thus providing accurate quantification. The slightly elevated recoveries (>100%) were thought to be due to errors in background correction. It is hoped that this can be remedied by further improving the separation method.

The above chromatograms exhibited a dip in the baseline at approximately 1.4 minutes. This reduction in signal was consistent and observed in all chromatograms, suggesting it was an injection related event. The mobile phase consisted of 5% methanol, but the samples were diluted in deionised water. From the order of elution in Figure 2:40, it can be established that the SFNG-DNA conjugate eluted first, followed by the sample solvent, which contained a higher proportion of water compared to the mobile phase, and finally the unbound SFNG eluted. If the background Au was hydrophobically bound then the elution of the water sample solvent (weaker eluent than methanol) would transiently reduce the Au flux from the column. Further, reduced carbon load and higher surface tension of the water would reduce the Au signal, causing a temporary reduction in the baseline signal. In addition, a spike was observed in the 1:1 DNA:biotin binding site reaction at 1.35 minutes. This peak was found to be inconsistent and not reproducible, suggesting it was an artefact and not a true Au species.

#### **4. Labelling Efficiency and Labelling Ratio**

From the chromatogram in Figure 2:40b (1:7.5 DNA:binding site reaction), it can be concluded that 53.5% of the nanogold (compared to the amount injected) and hence streptavidin was bound to DNA. Considering 0.11 nmoles of streptavidin (0.44 nmoles binding sites) was present in the reaction, the number of moles of bound streptavidin was 58.9 pmoles. If one biotinylated DNA molecule bound to one streptavidin protein, then 58.9 pmoles of DNA also bound. Considering 58.7 pmoles of DNA was in the reaction mixture, 100.3% of the DNA was labelled with SFNG. This data suggests that with a 7.5 molar excess of potential binding sites, or a 7.5/4 ~2 fold molar excess of nanogold probe, only one binding site per protein molecule was occupied.

The labelling efficiency of the 1:1 DNA:biotin binding site reaction was also calculated as described above, but the labelling stoichiometry was not as straight forward to calculate. A total of 47.7% or 12.85 pmoles of SFNG was bound to DNA, if one DNA molecule bound to one streptavidin protein, then 12.85 pmoles of DNA would also be labelled. But considering 115 pmoles of biotinylated DNA was used in the reaction, this only equates to an 11.2% labelling efficiency. Conversely, two DNA molecules bound to one streptavidin

protein would result in 25.7 pmoles of labelled DNA and thus a 22.3% labelling efficiency. In this particular case there is more than one outcome; either one or two DNA molecules bound to one streptavidin.

In an attempt to resolve this uncertainty, the retention time of the bound and unbound SFNG species were considered; if two DNA molecules bind to SFNG (2:1), the retention time of the species should be less than that of the 1:1 species which is known to elute at ~1.06 minutes (Figure 2:40b), since the 2:1 species would be much larger and the separation has a significant size exclusion character. The retention time of the SFNG-DNA species for the equal molar reaction was 0.98 minutes (Figure 2:40a), which was shorter than the retention time of the 1:7.5 DNA:SFNG species (Figure 2:40b). However, the 8 second difference in retention time between the two SFNG-DNA species was not considered significant enough to suggest that the SFNG species in Figure 2:40 were bound to different numbers of DNA molecules. A more accurate method of determining labelling stoichiometry has to be developed.

It is accepted in ligand chemistry that as more ligands bind to a substrate such as a metal ion, the stepwise formation constants ( $K_n$ ) generally decreases in the order  $K_1 > K_2 > K_3$ , where the subscript numbers represent the increasing ligand number.<sup>138</sup> Thus, the addition of subsequent ligands onto a substrate becomes more difficult. There are several reasons for this effect, namely: steric restraints and reduction in binding sites and ligand molecules upon successive binding and reduction in charge on the metal ion. It was expected that this would be the case for biotin binding to streptavidin, especially considering the oligonucleotide may contribute greater steric effects, and thus the preferred binding ratio was expected to be 1 DNA:1 SFNG. However a report by Williams *et. al.*,<sup>139</sup> suggested otherwise. The binding of biotin to streptavidin is said to be positively cooperative, that is the binding of the first biotin moiety stabilises the streptavidin structure and actually promotes further biotin binding. Thus successive biotin binding occurs with increasing affinities.<sup>139</sup> Although only 1-2 biotin binding sites are accessible on SFNG, it may be that two biotinylated oligonucleotides per streptavidin are actually favoured. However, it is unknown what effect the Alexa Fluor-488 molecules and Au nano-particle have on the

protein structure and if positively cooperative binding is still valid in these circumstances. The presence of these additional molecules may create larger steric effects, thus the 1:1 DNA:SFNG binding ratio may actually be favoured.

The SFNG-DNA reaction mixtures appeared to degrade over a period of a few weeks. When the samples were injected within two weeks of preparation, only one Au peak at ~1.60 minutes was observed. This was attributed to the DNA degrading over time. It is possible that the DNA degraded in solution over time or even absorbed onto the walls of the sample vials. Such degradation would have ultimately resulted in the bound and unbound SFNG having similar molecular weights and charges and ultimately the same retention time. However, reproducible results were generally obtained when the SFNG-DNA reactions were separated and detected within a few days of preparation.

### **2.6.2 Summary**

The relative success of the SFNG labelling route was thought to be due to two factors. Firstly, both the SFNG and biotinylated DNA were stable in solution and at room temperature, resulting in easier sample handling. Specialised reaction conditions and extensive sample preparation procedures were not necessary. In addition, the labelling reaction was very easy and straight forward, which was attributed to the strong interaction between biotin and streptavidin.

Several modes of separation were investigated in order to separate the bound and unbound SFNG. Numerous problems were encountered; gel filtration did not give adequate resolution and irreversible adsorption of the SFNG probe was observed on the anion exchange resin. IMAC did show some promise, although reversed phase HPLC was proven to be the most successful separation method. It was demonstrated that RP-HPLC gave good recoveries of SFNG. Also, the mobile phase was compatible with ICP-MS and the Au signal was enhanced in the methanol matrix, which was a further advantage. More importantly, the RP-HPLC method gave excellent resolution, with the bound and unbound SFNG being resolved within 3 minutes. There is however room for improvement with

respect to the reverse phase separation method, especially concerning carry-over. The addition of cysteine or another S containing molecule to the mobile phase may be necessary to prevent carry over between injections. The use of a non-porous resin or monolith column may also be beneficial, since these phases are more suited to macromolecule separations. In addition, polymeric monolithic phases such polystyrene divinylbenzene (PS-DVB) are more tolerant to extreme pH, thus acid solutions could be employed to remove residual Au.

The improved SFNG-DNA binding efficiency compared to that of the MMN-thiol labelling route (~10% and 100% DNA labelling efficiencies achieved for the MMN and SFNG methods respectively) provided a much greater enhancement and detection power. The DNA signal could be enhanced by 882 fold when one DNA molecule bound to one SFNG in a 1:1 binding stoichiometry. When a 7.5 fold excess of SFNG was employed, a 1:1 SFNG:DNA stoichiometry was observed, as demonstrated by the recovered DNA and Au. However, the stoichiometry was uncertain when a much smaller excess of SFNG was employed in the reaction. As a result, accurate methods of determining SFNG-DNA labelling stoichiometry need to be investigated further and this is currently one limitation of the method.

Ultimately, two routes of nucleic acid labelling were identified using either MMN or SFNG. Both methods are capable of enhancing biomolecule signal and thus detection limits by ICP-MS, although there are numerous advantages and disadvantages associated with both methods. The preliminary results associated with the SFNG-biotinylated DNA labelling route have been published,<sup>17</sup> although there is still room for improvement in this area of biomolecule signal enhancement.

The vast majority of the time and effort put into developing the MMN and SFNG labelling procedures has concerned researching appropriate separation techniques to resolve the bound and unbound nanogold. The actual ICP-MS analysis has been the least time consuming and complicated. The following characterises the factors that are important in the separation and indicates how each of the methods investigated performed:

1. Good resolution of the bound and unbound nanogold species
  - Low and inadequate resolution obtained by gel filtration
  - Good resolution achieved with anion exchange and RP-HPLC
2. Reasonably short separation times
  - Long separation times observed with gel filtration (~20-60 minutes)
  - RP-HPLC baseline resolution within 3 minutes
3. Mobile phase compatibility with ICP-MS
  - High salt levels in anion exchange HPLC are problematic
  - Methanol used in RP-HPLC was not troublesome with flow splitting
4. On-line coupling capability with ICP-MS (also dependent upon point 3)
  - RP-HPLC coupling was fairly straight forward due to mobile phase and flow rate compatibility
  - IMAC coupling may be more technically demanding since eluent and sample introduction system may need modifying
5. Good recoveries of nanogold species.
  - Poor SFNG recovery observed with anion exchange due to irreversible adsorption of SFNG onto phase.
  - Excellent recoveries (~100%) for RP-HPLC, since charged bio-molecules have very little interaction with C18 phase

## 3 Platinum Metallodrugs

### 3.1 Introduction

The treatment and diagnostic-imaging of disease is confined not only to organic compounds, but also employs inorganic metal complexes. Such inorganic compounds containing a metallic element to treat or diagnose disease are known as metallodrugs. There are a wide range of metals that are known to have therapeutic or diagnostic properties. These include some Pt complexes, which are known to have anti-tumour properties, likewise, Au<sup>36, 140</sup>, Tc<sup>36</sup> and V<sup>140</sup> amongst others have a niche in medicine. Table 3:1 summarises some metallodrugs and their function in medicine and Figure 3:1 shows the structures of some common drug complexes.

**Table 3:1: Therapeutic functions of some metal complexes.**

<b>Metal</b>	<b>Function</b>
Platinum	Anti-tumour agent <sup>141</sup>
Ruthenium	Anti-tumour agent <sup>141</sup>
Rhodium	Anti-tumour agent <sup>141</sup>
Gold	Treatment of arthritis and potential anti-tumour agent <sup>140</sup>
Vanadium	Anti-diabetic agent <sup>140</sup>
Bismuth	Anti-ulcer agent <sup>140</sup>
Technicium	Tissue imaging <sup>36</sup>

It is important to understand a drug's mechanism of action and potential side effects in order to develop future generations of drug with superior properties. More so, it is essential to ensure that the patient is receiving safe levels of the drug that are not posing a health risk greater than that of the disease itself. The metabolites of the metallodrug and its hydrolysis products also need to be assessed for their toxicity or potential biological activity.<sup>66</sup> In addition, the transportation efficiency of the drug to reach the target site is important and may be dependent upon metallodrug-protein binding and releasing efficiency.<sup>142</sup>



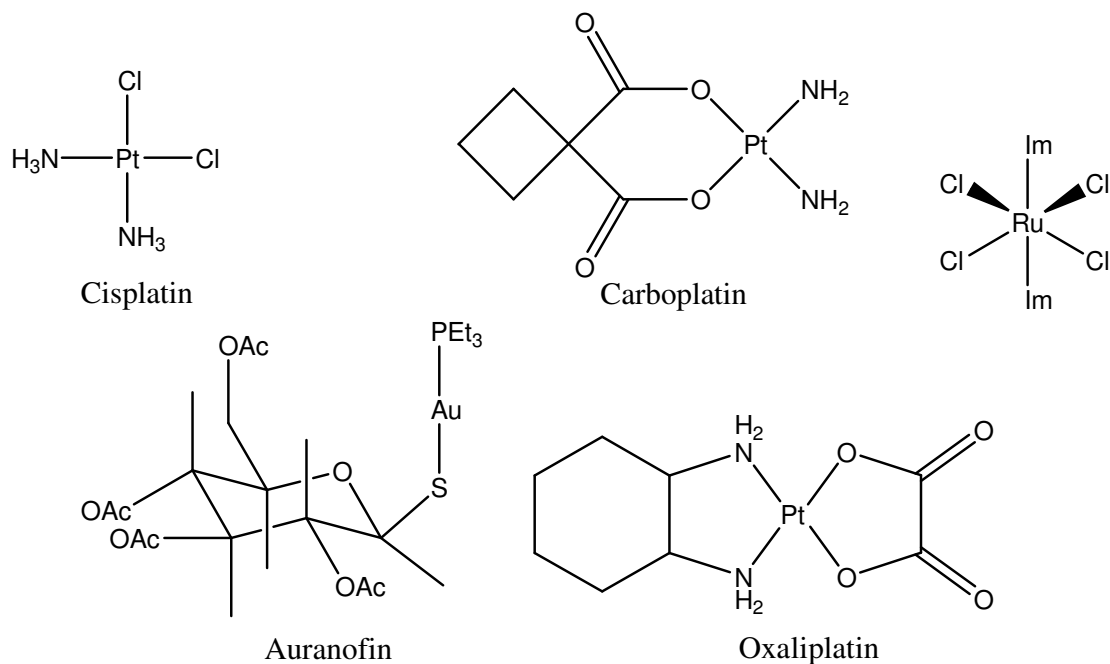


**Figure 3:1: Examples of common therapeutic metallodrugs.**

The interactions of the drug with non-target species such as proteins may also be of importance. For example, cisplatin (cis-diamminedichloroplatinum(II)) is a cytotoxic compound, but when complexed to proteins, the drug exhibits no anti-tumour properties.<sup>141, 142</sup> Conversely, ruthenium based anti-tumour drugs have been reported to maintain their activity upon binding to certain proteins.<sup>142</sup> It has been known for some time that DNA is the target for Pt based metallodrugs. Extensive research has been carried out to establish how Pt based drugs interact with DNA and other non-target species.<sup>141-146</sup>

### 3.1.1 Cisplatin

Patients suffering with cancers of the head, neck, ovaries, testes or colon are treated with Pt based metallodrugs.<sup>36, 141, 144, 145, 147, 148</sup> The most prominent Pt based metallodrug is cisplatin, which has demonstrated a huge success in treating certain tumours, but it has harsh side effects that include severe kidney complications<sup>145</sup> and neurotoxicity.<sup>149</sup> As a result, second and third generations of Pt drugs have been synthesised and investigated.

The Pt-based anti-cancer drugs such as cisplatin and oxaliplatin are known to interact with DNA *in-vivo* (and *in-vitro*) to form Pt-DNA adducts. DNA replication and transcription processes are thought to be inhibited by adduct formation.<sup>147-149</sup> The hydrophobic cisplatin complex is capable of passing through cell membranes, but once in the low chloride medium of the cell cytoplasm, the Pt complex loses its chloride ligands and undergoes ligand exchange reactions with water molecules. This results in a reactive (hydrated) species that interacts with DNA nucleobases.<sup>147, 150</sup> Numerous studies have shown that both cisplatin and oxaliplatin preferentially form adducts with guanine (G) nucleobases, followed by adenine (A) bases on DNA (see also Chapter 4).<sup>141, 148, 151</sup> The vast majority (~60-65%) of adducts formed are intra-stranded cross-links between two neighbouring guanine bases (GG).<sup>144, 148, 149</sup> Intra-stranded cross-links between neighbouring AG adducts are the next dominant species formed, accounting for approximately 25-30% of adducts.<sup>144, 149</sup> Other minor adducts include: intra-stranded GNG (cross-links between non-adjacent guanines), inter-stranded and monofunctional cross-links, which make up the remaining percentage of species produced.<sup>152</sup> Figure 3:2 summarises the ligand exchange reactions and DNA binding observed with cisplatin.

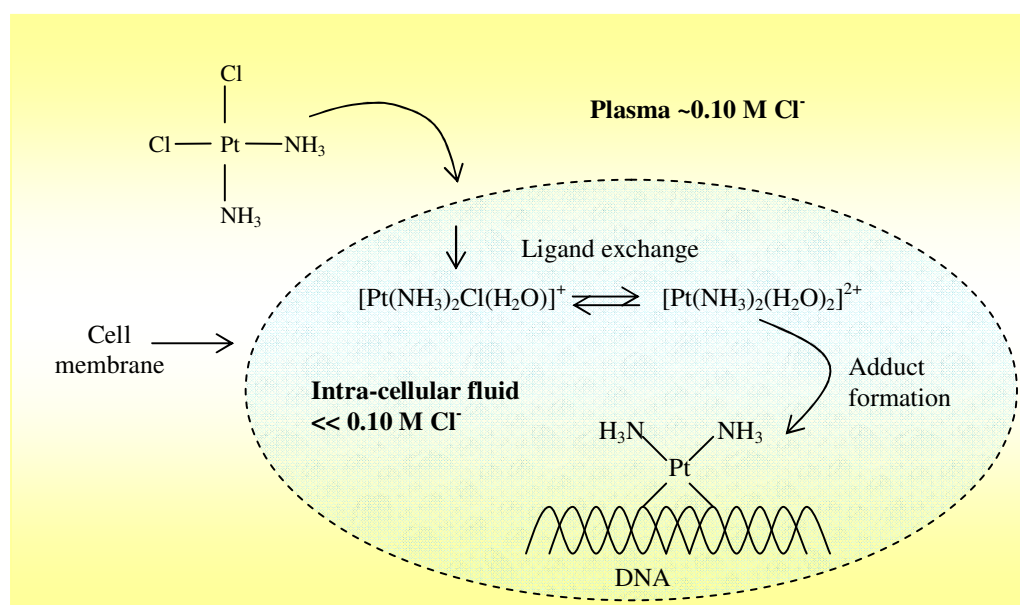


**Figure 3:2: Cisplatin ligand exchange and DNA adduct formation.**

Although Pt-AG adducts account for approximately 25-30% of adducts formed, Pt-GA adducts do not form with DNA. The reasons for this were explained by Mantri *et. al.*,<sup>153</sup> who reported that the intermediate formed prior to Pt-AG di-adduct formation was stabilised by a phosphate group on the DNA backbone. However, the same was not true for the formation of the Pt-GA di-adduct. Thus the formation of Pt-AG was kinetically more favourable compared to Pt-GA.<sup>153, 154</sup> The types of Pt adducts formed with DNA are illustrated in Figure 3:3.

### 3.1.2 Oxaliplatin

Oxaliplatin is a third generation anti-tumour agent that is used for treating colorectal cancer.<sup>149, 155, 156</sup> Although oxaliplatin has many side effects, these are less severe compared to cisplatin. In addition, oxaliplatin has been successful in treating cisplatin resistant cell lines and tumours.<sup>144, 155, 156</sup>

Oxaliplatin undergoes ligand exchange in physiological conditions, where the oxalate ligand is replaced by two chloride ligands to form  $[\text{Pt}(\text{dach})(\text{Cl})_2]$ .<sup>157</sup> Once within the cell, the complex becomes hydrated,<sup>155</sup> and forms adducts with DNA nucleobases, preferentially binding to guanine as in the case of cisplatin (Figure 3:3).<sup>149, 156</sup> Oxaliplatin reacts with plasma proteins and like cisplatin becomes un-reactive when bound to proteins such as glutathione.<sup>155</sup> Despite the similarities between cisplatin and oxaliplatin, numerous differences in their mechanisms have been reported. Firstly, oxaliplatin forms fewer cross-links with DNA compared to cisplatin, yet it exhibits comparable cytotoxic activity.<sup>149, 155-158</sup> Arnould *et. al.*, reported that five times fewer oxaliplatin adducts were formed on colon cancer cell lines compared to cisplatin, for the same cytotoxic effect.<sup>155</sup> The DNA adducts formed by oxaliplatin are more hydrophobic than their cisplatin counterparts, due to the presence of the diaminocyclohexane (dach) ligand, and are thought to interact with hydrophobic regions of proteins.<sup>149</sup> Also, the presence of the dach non-leaving group results in oxaliplatin forming bulky adducts, which may disrupt DNA structure more than cisplatin.<sup>149, 155</sup> Disruption to the conformation of DNA may have dramatic consequences on replication and transcription.

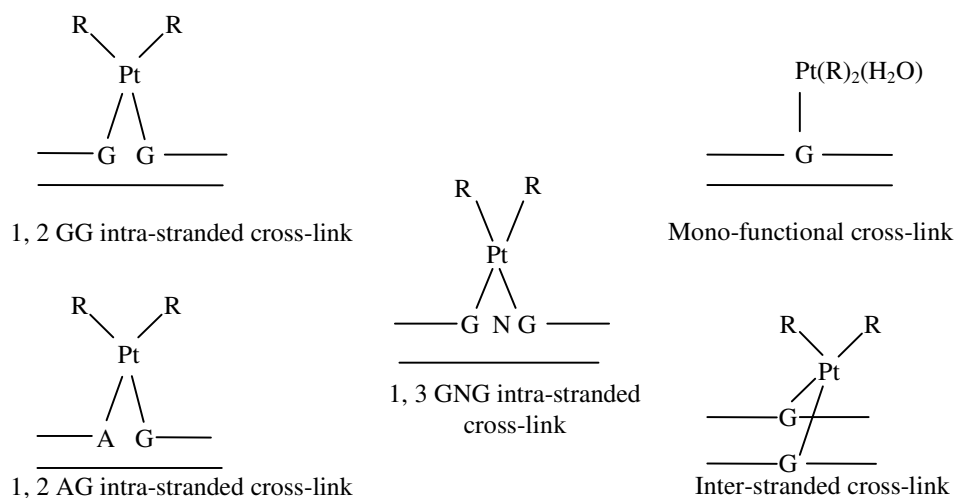


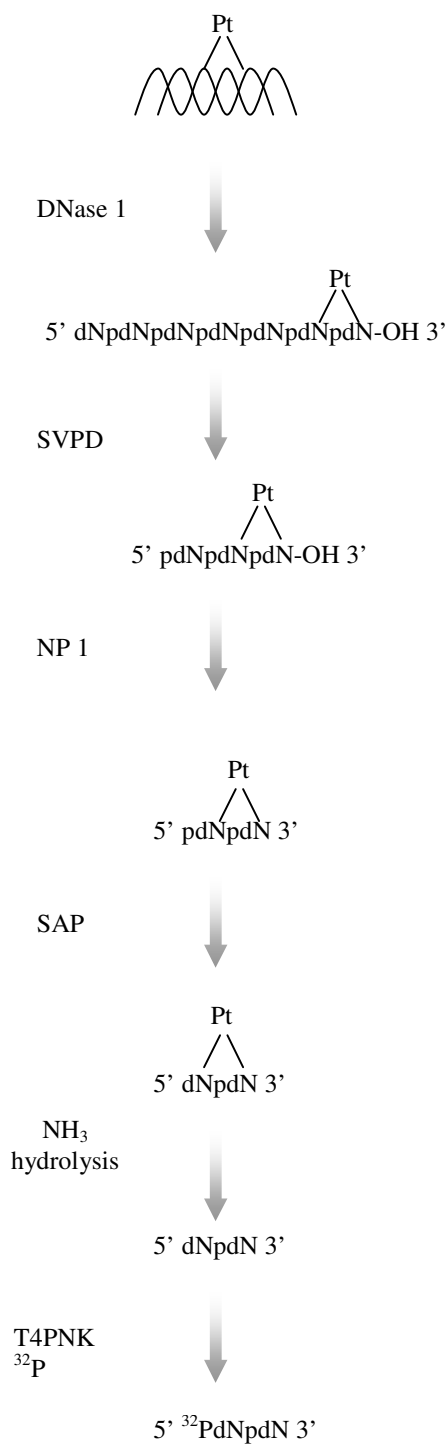
**Figure 3:3: Intra-stranded and inter-stranded Pt-adducts formed with DNA. Note, ligand R refers to the non-leaving group, which is diaminocyclohexane in the case of oxaliplatin and ammonia in the case of cisplatin.**

### 3.1.3 Metallodrug Detection

There are numerous biological assays designed for detecting Pt-DNA adducts, namely, the comet assay<sup>156, 159, 160</sup> and post labelling assay (PLA).<sup>42, 161, 162</sup> Both of these assays provide a way of detecting DNA damage by Pt drugs. The comet assay is a qualitative method of detecting DNA damage. Cells treated with Pt drugs are embedded in agarose and then irradiated with x-ray radiation, which induces DNA strand breaks and thus causes the DNA to relax. The DNA then electrophoretically migrates through the gel to form a comet like tail from the cell body. The presence of Pt cross-links retards DNA migration, therefore reducing tail movement which indicates the presence of cross-links.<sup>156, 159</sup> The protocols, advantages and potential applications of this assay were discussed by Tice *et. al.*<sup>160</sup>

The PLA provides a way of quantifying Pt-DNA adducts by employing a <sup>32</sup>P label as illustrated in Figure 3:4. The assay involves treating the platinated DNA to an enzymatic digest prior to <sup>32</sup>P labelling. Within the enzymatic mixture there are several enzymes, namely: DNase 1, snake venom phosphodiesterase (SVPD), nuclease P1 (NP1), shrimp alkaline phosphatase (SAP) and T4 polynucleotide kinase (T4PNK).<sup>42, 161</sup> Following

incubation with cisplatin and the subsequent enzymatic digestion, the adducted sites are labelled with  $^{32}\text{P}$ . The reaction mixture is then separated by polyacrylamide gel electrophoresis (PAGE), and the separated radio-labelled di-nucleotides that represent adduct sites can then be detected.<sup>161</sup> It has been reported that one adduct in  $10^9$ - $10^{10}$  nucleotides can be detected with the PLA.<sup>151, 162, 163</sup> It should be noted that the PLA is capable of detecting intra-stranded AG and GG cross-links, but not inter-stranded or mono-functional cross-links. However, as already stated the inter-stranded GG and AG cross-links account for ~90-95% of all adducts formed.



DNase 1 cuts the genomic DNA into smaller fragments.

SVPD then cleaves phosphodiester bonds along the DNA strand, working from 3'→5'. Nuclease P1 has a similar role, but works from the opposite direction *i.e.* 5'→3'. These enzymes create mono-nucleotides.

However, when the enzymes reach a platinated site, where a Pt atom bridges two neighbouring nucleotides, the phosphodiester bond between these bridged nucleotides can not be cleaved due to the presence of the Pt. As a result, di-nucleotides are formed where Pt lesions are present. Therefore, amongst the mixture of mono-nucleotides, Pt-di-nucleotides will also be present.

The terminal 5' phosphate is then cleaved from the mono-nucleotides and di-nucleotides in the digested mixture by SAP.

At this point, the Pt atom is cleaved from the di-nucleotides by NH<sub>3</sub> hydrolysis. This is carried out so the next enzyme, T4PNK can phosphorylate the di-nucleotides. It is crucial to note here that only the di-nucleotides are re-phosphorylated, since T4PNK is a kinase enzyme that only uses polynucleotides as a substrate and not the mono-nucleotides. Therefore, only the di-nucleotides that represent previously platinated sites are phosphorylated with <sup>32</sup>P.

**Figure 3:4: The post labelling assay.**

The interactions of metallodrugs with biological molecules other than DNA are also of interest.<sup>141</sup> For example, albumin accounts for ~52% of plasma proteins and contains many disulfide bonds, from cysteine and tryptophan residues, making it susceptible to cisplatin adduct formation.<sup>141</sup> Methods such as; NMR, circular dichroism (CD) and fluorescence spectroscopy have been employed to study metallodrug-protein interactions.<sup>141</sup> Chromatographic techniques coupled with molecular mass spectrometry have also been employed for the structural characterisation of Pt species.<sup>151, 164-167</sup> Molecular mass spectrometry can be employed to establish the targets of metallodrug binding. It will be described later how ESI-MS was employed to study the interaction of oxaliplatin with DNA nucleobases.

ICP-MS is also suited to the study of metallodrug interactions, mainly due to the presence of the metal ion allowing for quantitative determination at very low levels in complex matrices.<sup>66, 168</sup> The main disadvantage of ICP-MS is that the technique cannot distinguish between various adduct types (refer to Figure 3:3) since all structural information is lost in the plasma ionisation source, thus only total Pt is measured.<sup>169</sup> This problem can be overcome by coupling chromatographic separation techniques to ICP-MS, which allows for the separation of different metallodrug species prior to ICP-MS analysis. This is important since biological systems are complex and many species of metallodrug adducts may form both *in-vitro* and *in-vivo*. HPLC with ICP-MS detection appears to be the method of choice for metallodrug studies.<sup>66, 142, 147, 151, 170-173</sup> Szpunar amongst others have detailed the hyphenation of liquid chromatography with ICP-MS and has highlighted the advantages and limitations.<sup>66, 174</sup> There have been several reports on the use of capillary electrophoresis coupled to ICP-MS for metallodrug research.<sup>175, 176</sup>

Meczes *et al.*, detailed the immunoreactivity of an antibody specific to cisplatin and carboplatin DNA adducts.<sup>152</sup> It was established that the antibody recognises 1, 2 intra-stranded GG and AG cisplatin adducts (Pt-GG and Pt-AG) with high sensitivity. However, factors such as the surrounding DNA sequence also appeared to effect antibody recognition.<sup>152</sup> An earlier publication by Tilby *et al.*,<sup>177</sup> also employed monoclonal antibodies to detect and quantify cisplatin and carboplatin adducts.<sup>177</sup> The antibody

detection of cisplatin adducts was taken a step further by Liedert *et al.*,<sup>169</sup> who employed two monoclonal antibodies specific to Pt-GG and Pt-AG adducts to quantify adducts in cells at clinically relevant levels.<sup>169</sup>

Such reports demonstrate the array of instrumental and biological methods available for metallodrug research. This chapter will concentrate on developing an assay based on ICP-MS for detecting and quantifying Pt-DNA adducts at the clinically important level, whilst the challenges associated with analysing biological samples by ICP-MS will be highlighted.

## **3.2 Quantifying Pt adduct Formation by ICP-MS**

### **3.2.1 Introduction**

The aim of this research was to develop an ICP-MS method for determining Pt-DNA adducts in DNA samples after treatment with either cisplatin or oxaliplatin. Ultimately, the aim was to develop a clinical test suitable for determining Pt-DNA adducts in the DNA obtained from patients undergoing chemotherapy. An assay capable of determining Pt-DNA adducts formed *in-vivo* should help identify patients who are responding effectively to the selected cancer drug. More importantly, it will potentially identify those patients who are not responding to the treatment, thus the treatment could be stopped and the unpleasant side effects minimised or avoided. This work was carried out in collaboration with Dr Rachel LePla, Dr Chris Harrington and Dr Don Jones from the Cancer Prevention and Biomarkers Research Group at Leicester University. The treatment of DNA with cisplatin and oxaliplatin, along with the PLA to confirm Pt binding, was carried out at Leicester University by Dr Rachel LePla.

Although biological assays such as the PLA, comet assay and antibody detection methods are well established for detecting adduct formation at very low levels (refer to section 3.1.3), they have their drawbacks. Firstly, the comet assay only provides qualitative information. The PLA is time consuming and expensive due to the range of enzymes employed to digest the DNA. In addition, the PLA utilises a radioisotope for adduct detection and quantification, which introduces additional hazards. Antibody methods of



detecting cisplatin-DNA adducts again may involve extensive sample preparation and there can be complications in adduct recognition, as detailed by Meczes.<sup>152</sup> In comparison, an assay based on ICP-MS, which is capable of detecting trace levels of Pt, should allow adduct quantification with ease. Further, the method should be much less time consuming due to reduced sample preparation and rapid data acquisition.

The challenge with this assay is that the Pt levels in DNA are likely to be very low. It has been reported by Welters *et al.*,<sup>178</sup> that 93 Pt-GG adducts and 30 Pt-AG adducts formed per  $10^7$  nucleobases in a tumour biopsy.<sup>178</sup> A review by Jamieson and Lippard<sup>145</sup> also reported that as little as 9 Pt atoms are present per DNA molecule.<sup>145</sup> However, the number of Pt adducts formed with genomic DNA varies between cell types due to numerous pharmacokinetic factors which were briefly discussed elsewhere.<sup>169</sup> A quantitative method applicable to clinical samples (DNA obtained from chemotherapy patients) must be capable of detecting very low dose rates and thus ultra trace Pt levels. The amount of blood and hence DNA obtainable from a patient is limited, typically 10 ml blood can be taken from a patient. However, the number of white blood cells within the blood sample will vary depending on the health of the patient, thus the quantity of extractable DNA may vary significantly between patients. As a result of these factors, the ICP-MS method must be capable of not only detecting trace levels of Pt, but also trace levels of the adducts in very small quantities of DNA.

Dr. Peter Winship was the first researcher within the Atomic Spectroscopy Group at Loughborough University to work on this area of research.<sup>179</sup> Initial studies were conducted with the PQ ExCell quadrupole ICP-MS instrument, details of the initial experiments and results are reported elsewhere.<sup>179</sup> Cisplatin and oxaliplatin adducts were successfully detected in calf thymus DNA (ctDNA) samples that were treated with drug doses ranging from 1 Pt per 100 nucleotides (1:100) to 1 Pt per 100 000 nucleotides (1:100K). However, the analysis was carried out on approximately 1 mg ctDNA.<sup>179</sup> The work carried out by Winship was advanced in this chapter with the aid of a high resolution ICP-MS instrument and a different approach to sample preparation. The double focussing instrument enabled both trace levels of Pt and high levels of P associated with DNA backbone to be determined

simultaneously. In addition, due to the high sensitivity and low background levels associated with high resolution instruments, lower drug doses and thus lower levels of adducts could be detected, which were of more relevance to clinical studies.

The research presented in this chapter was conducted on cisplatin and oxaliplatin treated ctDNA. These initial experiments employed ctDNA to establish the viability of the method before it was carried out on human cell lines or patient samples. Using ctDNA meant that larger quantities of DNA and thus Pt drug could be used to ensure the methods were viable, before progressing to the measurement of trace levels of adducts formed *in-vivo* in humans.

### 3.2.2 Instrument Parameters

An Element 2XR high resolution ICP-MS instrument (Thermo Finnigan, Bremen, Germany) was employed for all Pt and P determinations. The instrument was operated in standard solution mode with the basic parameters shown in Table 3:2. Any deviations or additional instrument parameters will be stated where appropriate.

**Table 3:2: Element 2XR instrument parameters.**

Cones	Ni sampler and skimmer
Nebuliser	200 $\mu\text{l min}^{-1}$ Micromist (Glass Expansions, Victoria, Australia), or 100 $\mu\text{l min}^{-1}$ PFA-ST (Elemental Scientific, Omaha, USA)
Spray chamber	Double pass or cyclonic (Glass Expansions, Victoria, Australia)
Analytes	$^{31}\text{P}$ and $^{195}\text{Pt}$
Magnet mass	30.968 (P) and 194.899 (Pt)
Resolution	Low (Pt) and medium (P)
Mass range	30.968-30.978 (P) and 194.899-195.029 (Pt)
Scan type	E-scan
Detection mode	Triple
Gas flows	Cool = 15.5 $\text{l min}^{-1}$ Auxiliary = 0.82 $\text{l min}^{-1}$ Nebuliser = 1-1.13 $\text{l min}^{-1}$
Forward power	1240-1300 W

The analogue secondary electron multiplier (SEM) and Faraday cup allowed the high P signal to be measured. Nickel cones were used in all analysis since the platinum cones

resulted in very high Pt background signals, which made the trace cisplatin and oxaliplatin determinations impossible. Normally platinum cones are preferred for samples containing high levels of carbon, and enable the use of oxygen addition to prevent carbon build up. This is not possible for Pt determinations and this in part led to the use of a digestion procedure to remove carbon as described later.

### **3.2.2.1 Analysis of Whole ctDNA**

The treatment of the ctDNA was carried out at Leicester University by Dr. Rachel LePla of the Biomarkers and Cancer Prevention Research Group. Briefly, 1 mg of ctDNA was treated with cisplatin or oxaliplatin solution. The concentration and volume of Pt drug added to each ctDNA solution was dependent upon the required dose. For both drugs, doses of between 1 Pt per 100 nucleotides (1:100) to 1 Pt per 1 500 000 (1:1 500K) nucleotides were provided. After 24 hour incubation period at 37 °C with cisplatin or oxaliplatin, the ctDNA was precipitated with isopropanol and 3 M sodium acetate. The precipitate was then removed and washed three times with 70% ethanol solution to remove any unbound drug. All traces of organic solvent were then removed by vacuum centrifugation and the resulting ctDNA pellet was re-suspended in deionised water and supplied for analysis. The concentration of recovered DNA was calculated by Dr. LePla with UV/Vis spectroscopy. Both the cisplatin and oxaliplatin treated ctDNA samples described above were initially analysed by ICP-MS without any further sample preparation to establish total Pt content. Platinum binding was confirmed by performing the PLA, this was also carried out by Dr. LePla and is summarised in Figure 3:4.

Solutions containing high concentrations of whole undigested ctDNA were delivered to a Micromist nebuliser with the aid of a peristaltic pump at a flow rate of  $\sim 200 \mu\text{l min}^{-1}$ . A peristaltic pump was required for sample delivery due to the poor uptake and nebulisation of the viscous DNA solutions.

### 3.2.2.2 Analysis of Digested DNA

In addition to the wide range of drug doses described above, a further set of cisplatin and oxaliplatin treated ctDNA was provided by Dr. LePla. These samples again contained ctDNA at a concentration of approximately  $1.3 \text{ mg ml}^{-1}$ , but the ctDNA was treated with much lower doses of drug, namely: 1:100K, 1:300K, 1:500K, 1:1000K and 1:1500K of cisplatin or oxaliplatin. The sample preparation procedure was similar to that described above in section 3.2.2.1. These samples were subjected to a chemical digest to remove the organic matrix and improve the Pt signal of the lower dose samples.

The obvious way to remove the ctDNA matrix was to perform an acid digest on the Pt treated DNA. The Biomarkers and Cancer Research Group at Leicester University use an ammonia hydrolysis method to cleave the Pt drug from the DNA. The method was detailed by Winship.<sup>179</sup> Briefly, 0.5 ml cisplatin or oxaliplatin treated ctDNA solution was added to 0.5 ml of 25% ammonia solution and incubated at  $70 \text{ }^{\circ}\text{C}$  for 48 hours to cleave the drug from the DNA. The cleaved drug was then separated from the ctDNA by molecular weight centrifuge filters. These filters have a molecular weight cut-off of 10 000 Da, hence, the low molecular weight species such as unbound drug is filtered and collects towards the bottom of the centrifuge tube. Conversely, the high molecular weight ctDNA should not pass through, but becomes trapped on the filters resulting in separation of the cleaved drug and DNA for ICP-MS analysis. This method was used and investigated by Winship.<sup>179</sup> However, it was established that significant amounts of the drug was retained on the filter and thus not recovered at the base of the centrifuge tube. This was attributed to the ammonia hydrolysis method not efficiently cleaving the Pt drug; therefore, some Pt was still associated with the high molecular weight ctDNA and retained on the filter. In addition, a lot of P was detected at the base of the centrifuge tube, suggesting that some DNA was not being retained, but passing through the filter. This may have been due to the ammonia hydrolysis method partially digesting the DNA and the smaller fragments passing through the filter along with the Pt.<sup>179</sup> Further, the efficiency of the filters may not have been 100% resulting in some Pt drug being retained and likewise some DNA passing through the filter.<sup>179</sup> Since the ammonia hydrolysis and molecular weight filter method showed limitations, other methods of ctDNA removal were investigated.

A method detailed by Yamada *et al.*,<sup>180</sup> digested Pt treated ctDNA in the presence of nitric acid and hydrogen peroxide at 65 °C. The resulting digest solution could then be analysed directly by ICP-MS and was used to establish the involvement of certain proteins in adduct removal.<sup>180</sup> A similar digest method employing nitric acid was also reported by Ghezzi *et al.*,<sup>168</sup> The method reported by Yamada was successfully used to detect adducts in DNA quantities of ~10 µg.<sup>180</sup> This method was employed in this study but modified slightly. Thus, 80 µl of nitric acid (~68%) was added to 100 µl treated ctDNA in a polypropylene tube. The acidified mixture was incubated at 65 °C for one hour. After the initial one hour period, 80 µl of hydrogen peroxide (30%) was added to the digest mixture and allowed to stand at 65 °C for a further four hours.<sup>180</sup> The caps of the vials containing the digested mixture were then removed and a stream of argon gas was allowed to flow over the vials to aid evaporation. The samples were evaporated to dryness and then re-suspended in 2% hydrochloric acid prior to ICP-MS analysis. The additional step of evaporating the digest mixtures to dryness (thereby removing nitric acid and hydrogen peroxide), followed by re-suspension with hydrochloric acid, was beneficial because it allows a pre-concentration step if required. In addition, hydrochloric acid is the preferred medium for Pt. The resulting digested ctDNA samples were delivered to the PFA-ST nebuliser by self aspiration.

### 3.2.3 Results

#### 3.2.3.1 Analysis of Whole ctDNA

Since ctDNA contains ~10% P, solutions containing known concentrations of ctDNA were used to prepare a calibration curve to enable P quantification. Initially, solutions containing between 1-3 mg ml<sup>-1</sup> ctDNA were prepared for calibration. However, above 2 mg ml<sup>-1</sup> the solutions gave non-linear responses, presumably due to poor sample transport and reduced nebulisation efficiency due to the viscosity of the solutions. As a result, the ctDNA solutions were diluted to concentrations ranging from 0.1-1 mg ml<sup>-1</sup>, the resulting calibration curve can be seen in Figure 3:5.

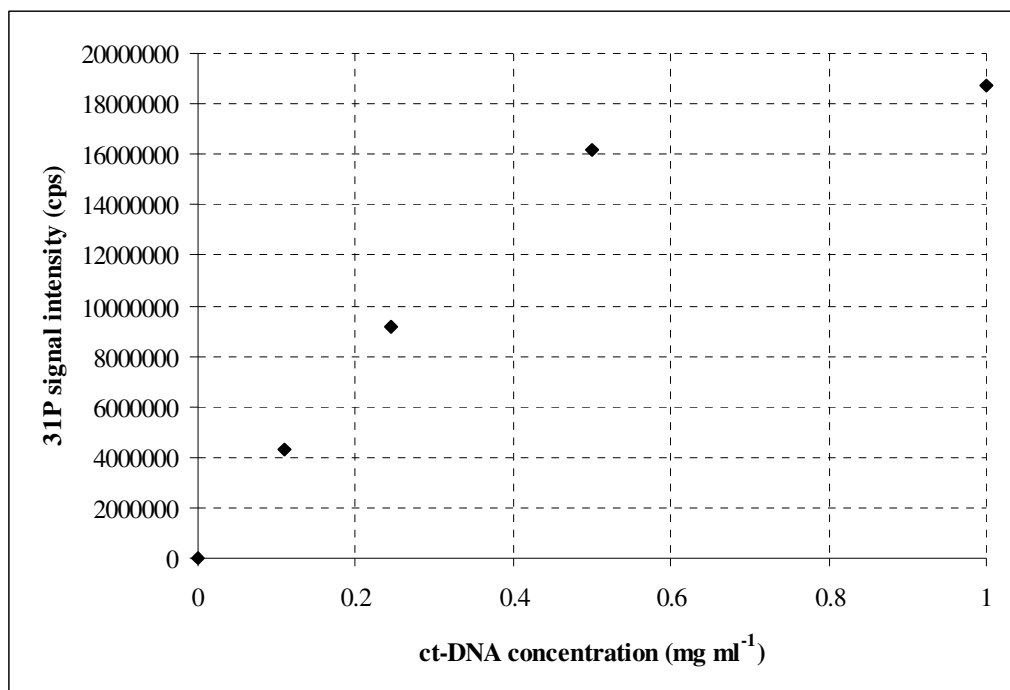


**Figure 3:5:** <sup>31</sup>P signal intensity against ctDNA concentration.

Figure 3:5 clearly shows that there is a deviation from linearity above 0.5 mg ml<sup>-1</sup> ctDNA. This deviation was again likely to be due the viscosity of the solution at higher DNA concentrations, or possibly due to a matrix effect from carbon. Carbon has been recognised as being able to enhance the signal for some high ionisation potential elements such as Se,<sup>136</sup> but here curvature towards the concentration axis occurred so it was assumed that viscosity was the major influence. Alternatively carbon deposition on the cones may have been occurring, but as indicated above (section 3.2.2), oxygen addition was not recommended because of the need to use Ni cones.<sup>181</sup> The linearity of the above calibration curve improved upon omitting the 1 mg ml<sup>-1</sup> ctDNA standard, as shown in Figure 3:6.

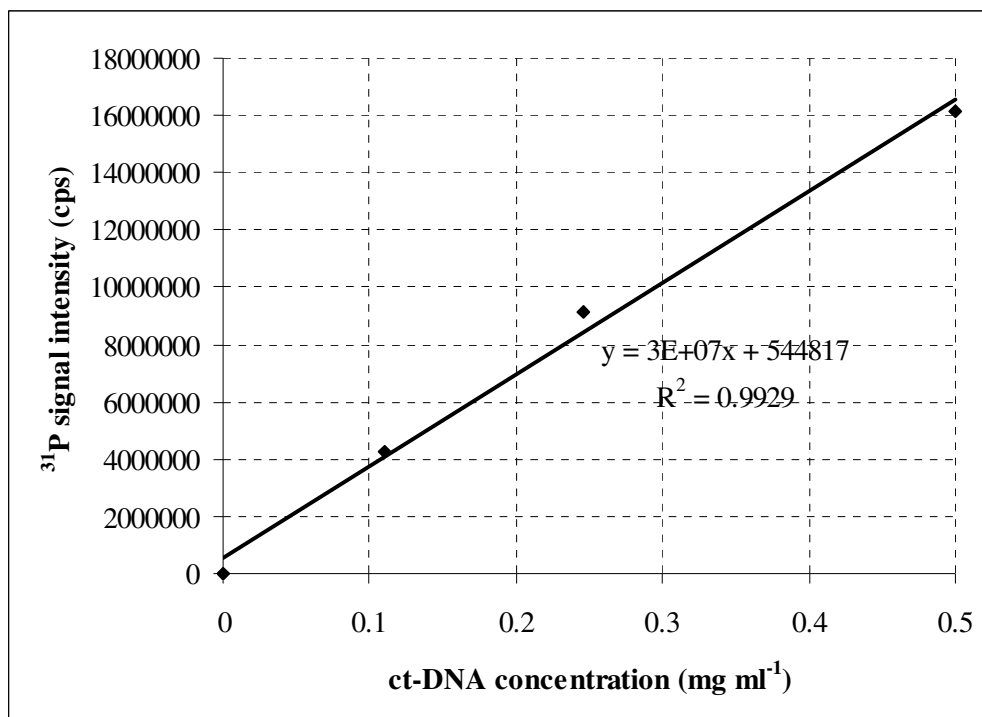


Figure 3:6: <sup>31</sup>P signal intensity against ctDNA concentration (0.1-0.5 mg ml<sup>-1</sup> ctDNA).

Figure 3:5 and Figure 3:6 suggest that for efficient transport and nebulisation, the platinated ctDNA samples containing whole ctDNA should be diluted. Hence, oxaliplatin treated ctDNA samples were diluted two fold so they contained 0.5 mg ml<sup>-1</sup> ctDNA. This was achieved by taking a ~250  $\mu$ l aliquot of the stock ctDNA sample (1 mg ml<sup>-1</sup>) and diluting it with the same volume of deionised water to yield ctDNA samples containing ~0.50 mg ml<sup>-1</sup> ctDNA, which equated to each sample containing ~0.25 mg ctDNA. Those samples containing higher Pt doses were diluted further with a 0.5 mg ml<sup>-1</sup> ctDNA sample solvent to ensure the matrix was constant for all samples.

A ctDNA calibration curve was prepared by measuring the <sup>31</sup>P signal of ctDNA solutions containing 0.1-0.75 mg ml<sup>-1</sup> ctDNA. Platinum standard solutions (0.022-1.85 ng ml<sup>-1</sup>) were prepared to allow for quantification and were spiked with 0.5 mg ml<sup>-1</sup> ctDNA to ensure approximate matrix matching. This was particularly important since at this stage it was unknown whether the ctDNA matrix would cause matrix effects, resulting in Pt signal suppression or enhancement. Unfortunately, acid wash solutions could not be used between

samples to minimise carry over and memory effects, due to the DNA precipitating in the presence of nitric and hydrochloric acid. In an effort to minimise carry over, deionised water was aspirated between each sample and a blank was also placed between samples to assess carry over.

Even at 0.75 mg ml<sup>-1</sup> ctDNA, a small degree of non-linear behaviour was displayed in the ctDNA calibration; however, the ctDNA calibration data was employed to establish the ctDNA concentration in each sample. From the determined ctDNA concentrations, the P concentration in each sample could be calculated since P makes up 10.069% of the mass of DNA (the average molecular weight of a nucleotide is 307.61 Da and the accurate mass of P is 30.9738). The Pt calibration was linear and Pt data were successfully obtained for oxaliplatin treated ctDNA. In addition to calculating the total Pt concentration associated with each sample, additional information could also be obtained. Since the concentration of ctDNA was known, the number of nucleotides per litre could be calculated along with number of Pt atoms exposed per litre. Such information was used to calculate the number of Pt-DNA adducts formed. These calculations were originally employed and detailed by Winship,<sup>179</sup> but are briefly described below in Equation 1.1-3. Table 3:3 summarises the data collected for oxaliplatin treated ctDNA.

**Equation 1.1: Number of nucleotides per litre**

$$\text{No. Nucleotides per Litre} = \left( \frac{([\text{DNA}] \times 0.001)}{307.61} \right) \times \text{Avagadro's Constant}$$

Where [DNA] is the concentration of DNA in mg l<sup>-1</sup>.

**Equation 1.2: Number of Pt atoms exposed per litre**

$$\text{No. of Pt atoms exposed/litre} = \text{No. Nucleotides/litre} \times \text{No. drug molecules/nucleotide}$$

**Equation 1.3: The number of Pt-DNA adducts formed**

$$\text{No. Pt-nucleotide adducts per litre} = \left[ \frac{([\text{Pt}] \times 0.001)}{195.078} \right] \times \text{Avagadro's Constant}$$

Where [Pt] is the concentration of Pt in mg l<sup>-1</sup>.



Note:

307.61 = the average molecular weight of a polymerised (DNA incorporated) nucleotide. The average molecular weight of a free nucleotide is 325.61, but since polymerised nucleotides form through reaction with the 5' phosphate of a free nucleotide and 3' hydroxyl of the growing DNA chain, water is lost, hence a mass of 18 was subtracted from the average free nucleotide molecular weight of 325.61 to obtain 307.61.

195.078 = the accurate relative atomic mass of Pt.

**Table 3:3: Oxaliplatin data from treated ctDNA (0.5 mg ml<sup>-1</sup> ctDNA matrix).**

Sample	Dilution factor	<sup>195</sup> Pt counts (cps)	Pt conc (ng ml <sup>-1</sup> )	Final Pt conc (ng ml <sup>-1</sup> )	Final Pt conc (mg l <sup>-1</sup> )	No. OxPt per nucleotide	DNA conc (mg ml <sup>-1</sup> ) UV data	No. Nucleotides Per litre	No. Pt atoms exposed per litre	No. adducts per litre	<sup>31</sup> P Counts (cps)	DNA Conc (mg ml <sup>-1</sup> ) ICP data	<sup>31</sup> P Conc (mg l <sup>-1</sup> )	Pt/P Ratio
Control	1.93	316.70	-0.01	-0.02	0.0000	0.000000	1.17	2.29E+21	0.00E+00	0.00E+00	10210778.4	0.60	60.66	-3.84E-07
1:500K	1.98	5604.40	0.27	0.54	0.0005	0.000002	1.01	1.98E+21	3.96E+15	1.65E+15	8839840.6	0.51	51.27	1.04E-05
1:250K	2.00	9381.40	0.47	0.95	0.0009	0.000004	1.09	2.13E+21	8.50E+15	2.92E+15	8157923.7	0.46	46.60	2.03E-05
1:100K	5.53	9524.20	0.48	2.66	0.0027	0.000010	1.03	2.01E+21	2.01E+16	8.20E+15	6953792.4	0.38	38.36	6.92E-05
1:10K	18.99	22222.00	1.16	22.01	0.0220	0.000100	1.03	2.01E+21	2.01E+17	6.80E+16	6382520.1	0.34	34.45	6.39E-04
1:5K	51.48	23149.70	1.21	62.22	0.0622	0.000200	1.12	2.19E+21	4.38E+17	1.92E+17	6664844.1	0.36	36.38	1.71E-03
1:1000	279.37	24871.20	1.30	363.34	0.3633	0.001000	1.09	2.13E+21	2.13E+18	1.12E+18	6713488.9	0.36	36.72	9.90E-03
1:500	760.48	9978.80	0.50	383.63	0.3836	0.002000	1.03	2.02E+21	4.05E+18	1.18E+18	6089746.8	0.32	32.45	1.18E-02
1:300	717.56	26519.30	1.39	996.47	0.9965	0.003333	1.03	2.02E+21	6.72E+18	3.08E+18	6377861.4	0.34	34.42	2.90E-02
1:200	1473.53	18143.40	0.94	1386.48	1.3865	0.005000	1.04	2.04E+21	1.02E+19	4.28E+18	6470596.6	0.35	35.05	3.96E-02
1:150	1953.21	17222.80	0.89	1741.69	1.7417	0.006667	1.10	2.15E+21	1.43E+19	5.38E+18	6597623.3	0.36	35.92	4.85E-02
1:100	3867.81	8872.10	0.45	1722.29	1.7223	0.010000	1.03	2.01E+21	2.01E+19	5.32E+18	7035644.9	0.39	38.92	4.42E-02

The ctDNA concentration associated with each sample was calculated by Dr. Rachel LePla to be  $\sim 1 \text{ mg ml}^{-1}$  (determined with UV/vis spectroscopy), refer to column 8 of Table 3:3. However, each sample was diluted two fold prior to ICP-MS analysis to reduce the sample viscosity, resulting in each sample containing  $\sim 0.5 \text{ mg ml}^{-1}$  ctDNA. In addition, any further sample dilutions were carried out with a  $0.5 \text{ mg ml}^{-1}$  ctDNA solution, so ultimately each sample should have contained  $\sim 0.5 \text{ mg ml}^{-1}$  ctDNA. The ICP-MS determined ctDNA concentrations are shown in column 13 of Table 3:3, and should be half the value of the UV determined concentrations, i.e.  $\sim 0.5 \text{ mg ml}^{-1}$ . The ctDNA concentration in the control sample, which was the first ctDNA sample to be analysed, was calculated to be  $0.60 \text{ mg ml}^{-1}$  by ICP-MS. If this value is multiplied by 1.93 to incorporate the dilution factor, a concentration of  $1.16 \text{ mg ml}^{-1}$  ctDNA is obtained, which is consistent with the UV data provided by Dr. LePla. However, the ICP-MS determined ctDNA concentrations gradually decreased as successive samples were aspirated, as signified by the decreasing P signal intensity. The P signal intensity and therefore ctDNA concentration for remaining samples was significantly lower than expected, indicating that unknown factors were effecting the analysis. Sample viscosity and high carbon content were initially thought to be responsible for the variation in ctDNA concentration. Considering these observations, the UV determined ctDNA concentrations were used for subsequent calculations, whilst the ICP-MS determined ctDNA concentrations were deemed unreliable.

The data shown in Table 3:3 indicates that between  $\sim 40\text{-}50\%$  of the drug formed adducts. This can be seen by comparing the values in the two columns labelled; number of Pt atoms exposed per litre and number of adducts per litre. Taking the 1:1000 sample as an example,  $2.13 \times 10^{18}$  Pt atoms were exposed per litre and  $1.12 \times 10^{18}$  adducts per litre formed, thus 51% of the drug formed adducts with ctDNA. These values were much larger than expected, but it should be noted that these samples were prepared *in-vitro* with ctDNA, hence the DNA was acting as a bare ligand with no protection from the cell membrane or proteins as in the case of *in-vivo* preparations. Although the percentage of drug binding did vary slightly ( $\sim 40\text{-}50\%$ ) between samples, the lowest percentage was observed for the 1:100 sample where only 26% of the drug formed adducts. Presumably, this was due to the

larger dose of drug saturating the A and G bases, thus some of the drug was unable to form adducts.

Considering that approximately 50% of Pt atoms formed adducts, the actual detection limit was not the lowest dose of 1:500 000, but in fact half of this value. Briefly, the lowest drug application or dose was 1 Pt per 500 000 nucleotides, which equates to  $2 \times 10^{-6}$  Pt atoms per nucleotide. If 50% of Pt atoms formed adducts, the adduct limit of detection in the above analysis was actually  $1 \times 10^{-6}$  Pt atoms per nucleotide (or 1 Pt per  $1 \times 10^6$  nucleotides) in 250  $\mu\text{g}$  DNA.

From the data in Table 3:3, it was also possible to establish a relationship between the number of adducts formed per litre and the number of oxaliplatin molecules per nucleotide. Figure 3:7 illustrates this relationship, whilst Figure 3:8 shows the linear relationship between the Pt/P concentration ratio (concentration in units of  $\text{mg l}^{-1}$  for both elements) and number of nucleotides per drug molecule. Note that the x axis in Figure 3:7 and Figure 3:8 was derived from the data provided by Dr. LePla.

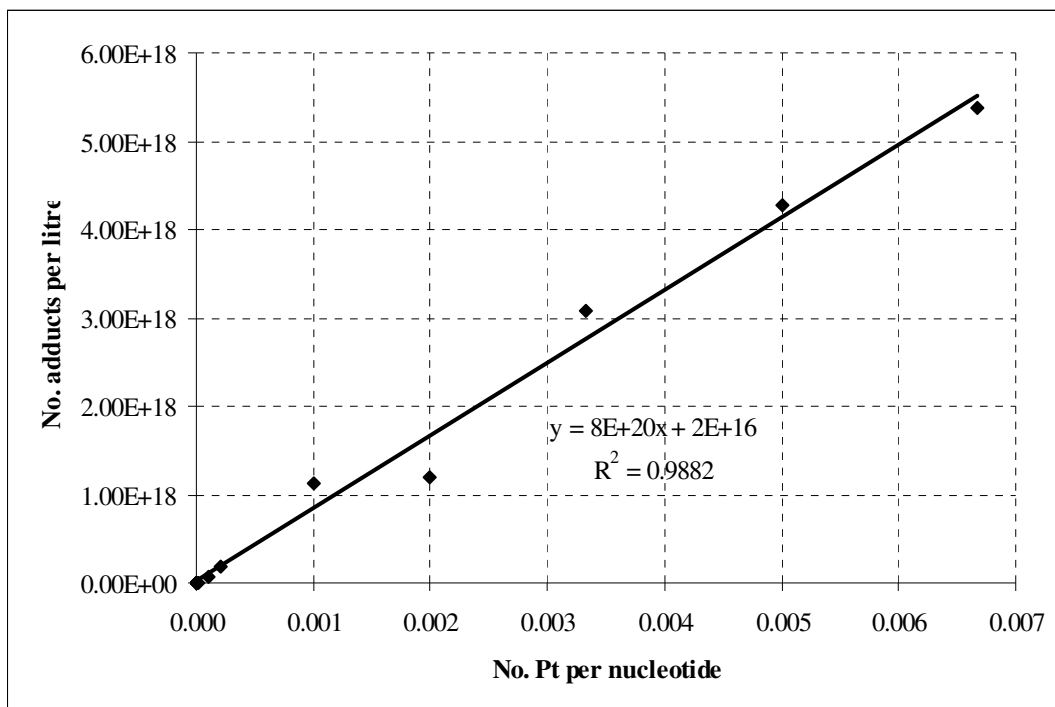
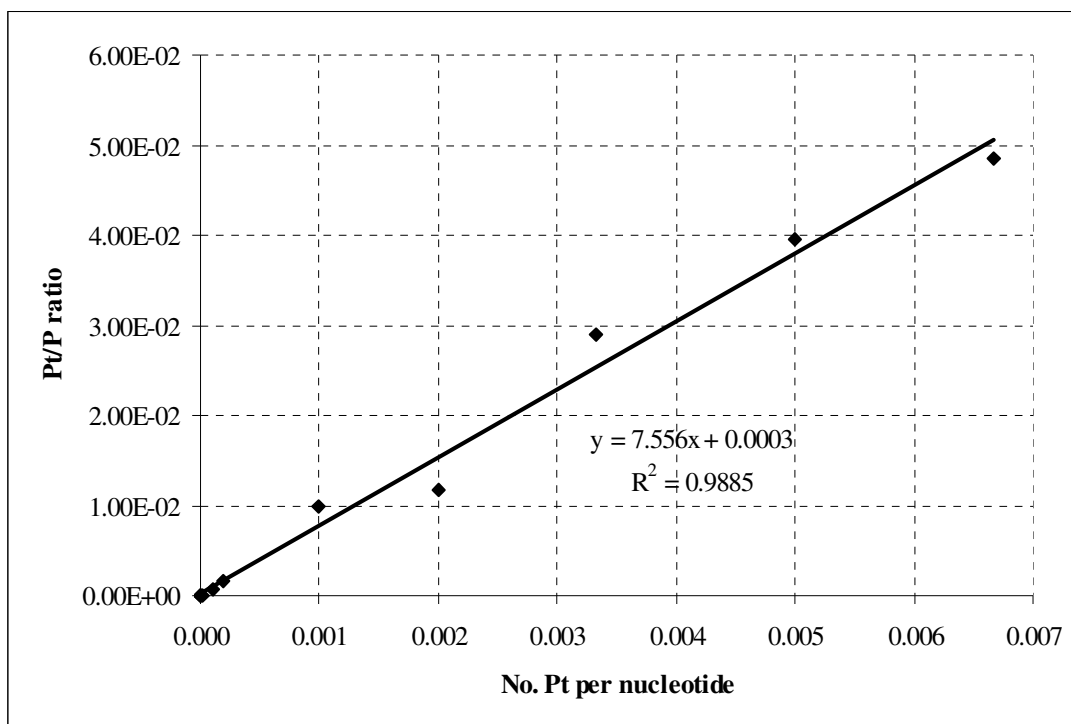


Figure 3:7: Number of oxaliplatin adducts per litre against number of oxaliplatin per nucleotide (0.25 mg ctDNA).



**Figure 3:8: Pt/P concentration ratio against number of nucleotides per oxaliplatin molecule (0.25 mg ctDNA).**

A linear relationship can be observed in Figure 3:7, demonstrating that the number of Pt-DNA adducts formed per litre was directly proportional to the number of drug molecules per nucleotide. Therefore, as the number of drug molecules increased (increased dose rate), the number of adducts formed also increased in a linear relationship. In addition, the ratio of Pt/P concentration was also proportional to the number of drug molecules per nucleotide. Significant carbon deposition was observed around the orifice of the sampler cone upon completing the experiment. As a result, it was decided that the analysis should be repeated but the platinated ctDNA samples should be diluted further to reduce the carbon loading.

In the repeated analysis, cisplatin and oxaliplatin treated ctDNA samples were diluted to 0.25 mg ml<sup>-1</sup> ctDNA. *i.e.* a four fold dilution on the original samples. This was achieved by taking ~250 µl aliquot of the stock ctDNA sample (containing ~1 mg ml<sup>-1</sup> ctDNA) and adding ~750 µl deionised water to yield ctDNA samples containing 0.25 mg ml<sup>-1</sup> ctDNA, which equated to ~ 0.25 mg ctDNA being analysed. Any further dilutions were carried out with a 0.25 mg ml<sup>-1</sup> ctDNA sample solvent to keep the ctDNA concentration and matrix

constant. This resulted in the viscosity and carbon content being reduced even further. Pt standards ranging from 0.052-16.1 ng ml<sup>-1</sup> in 0.25 mg ml<sup>-1</sup> ctDNA were prepared. The results for oxaliplatin and cisplatin treated ctDNA can be observed in Table 3:4 and Table 3:5 respectively. Equation 1.1-3 were used for the calculations.

**Table 3:4: Oxaliplatin data from treated ctDNA (0.25 mg ml<sup>-1</sup> ctDNA matrix).**

Sample	Dilution factor	<sup>195</sup> Pt counts (cps)	Pt conc (ng ml <sup>-1</sup> )	Pt conc (mg l <sup>-1</sup> )	No. oxPt per nucleotide	DNA conc (mg ml <sup>-1</sup> ) UV data	No. nucleotides per litre	No. Pt atoms exposed per litre	No. adducts per litre	<sup>31</sup> P Counts (cps)	DNA conc (mg ml <sup>-1</sup> ) ICP data	<sup>31</sup> P conc (mg l <sup>-1</sup> )	Pt/P ratio
Control	4.01	571.5	-0.2	-0.0002	0	1.17	2.29E+21	0.00E+00	0.00E+00	37021629.5	0.28	28.05	-0.000006
1:500K	3.97	12899.1	0.3	0.0003	0.000002	1.01	1.98E+21	3.96E+15	8.16E+14	26562478.9	0.20	19.88	0.000013
1:250K	6.60	16446.2	0.6	0.0006	0.000004	1.09	2.13E+21	8.50E+15	1.97E+15	16198761.5	0.12	11.78	0.000054
1:100K	3.89	66544.1	2.0	0.0020	0.00001	1.03	2.01E+21	2.01E+16	6.30E+15	22938755.2	0.17	17.05	0.000120
1:10K	3.81	565868.5	18.2	0.0182	0.0001	1.03	2.01E+21	2.01E+17	5.63E+16	25101105.1	0.19	18.74	0.000974
1:5K	8.47	513739.2	36.8	0.0368	0.0002	1.12	2.19E+21	4.38E+17	1.14E+17	25505974.8	0.19	19.05	0.001931
1:1000	32.79	650859.7	180.8	0.1808	0.001	1.09	2.13E+21	2.13E+18	5.58E+17	19145013.9	0.14	14.08	0.012840
1:500	40.68	806645.9	278.4	0.2784	0.002	1.03	2.02E+21	4.05E+18	8.60E+17	13746893.5	0.10	9.86	0.028227
1:300	100.82	514098.4	438.2	0.4382	0.003	1.03	2.02E+21	6.72E+18	1.35E+18	14497623.3	0.10	10.45	0.041930
1:200	117.87	509984.8	508.1	0.5081	0.005	1.04	2.04E+21	1.02E+19	1.57E+18	13062797.4	0.09	9.33	0.054469
1:150	166.20	549061.3	772.0	0.7720	0.007	1.10	2.15E+21	1.43E+19	2.38E+18	12658600.6	0.09	9.01	0.085646
1:100	233.46	516125.6	1018.7	1.0187	0.01	1.03	2.01E+21	2.01E+19	3.15E+18	9619933.2	0.07	6.64	0.153444

**Table 3:5: Cisplatin data from treated ctDNA (0.25 mg ml<sup>-1</sup> ctDNA matrix).**

Sample	Dilution factor	<sup>195</sup> Pt counts (cps)	Pt conc (ng ml <sup>-1</sup> )	Pt conc (mg l <sup>-1</sup> )	No. cisPt per nucleotide	DNA conc (mg ml <sup>-1</sup> ) UV data	No. nucleotides per litre	No. Pt atoms exposed litre	No. adducts per litre	<sup>31</sup> P Counts (cps)	DNA conc (mg ml <sup>-1</sup> )	<sup>31</sup> P conc (mg l <sup>-1</sup> )	Pt/P ratio
Control	4.16	358.4	-0.2	-0.0002	0	1.03	2.01E+21	0.00E+00	0.00E+00	10825518.8	0.08	7.58	-0.000022
1:500K	3.96	21885.9	0.6	0.0006	0.000002	1.12	2.20E+21	4.40E+15	1.75E+15	13122696.1	0.09	9.38	0.000061
1:250K	4.00	36541.6	1.1	0.0011	0.000004	1.08	2.12E+21	8.47E+15	3.32E+15	9455398.3	0.06	6.51	0.000165
1:100K	4.00	102866.9	3.3	0.0033	0.00001	1.15	2.25E+21	2.25E+16	1.03E+16	9980338.4	0.07	6.92	0.000482
1:10K	20.53	118841.7	19.9	0.0199	0.0001	1.06	2.07E+21	2.07E+17	6.16E+16	6729739.1	0.04	4.38	0.004551
1:5K	13.33	398607.7	44.8	0.0448	0.0002	1.15	2.26E+21	4.52E+17	1.38E+17	6148964.7	0.04	3.93	0.011406
1:1000	8.42	2751573.3	197.5	0.1975	0.001	1.02	2.00E+21	2.00E+18	6.10E+17	5712337.7	0.04	3.59	0.055071
1:500	194.97	310924	509.1	0.5091	0.002	1.13	2.22E+21	4.43E+18	1.57E+18	5205336.9	0.03	3.19	0.159630
1:300	278.78	245536.7	572.3	0.5723	0.003	1.12	2.20E+21	7.32E+18	1.77E+18	5007022.8	0.03	3.03	0.188610
1:200	474.53	249184.4	989.0	0.9890	0.005	1.17	2.28E+21	1.14E+19	3.05E+18	4861418.6	0.03	2.92	0.338613
1:150	566.79	249283.2	1181.8	1.1818	0.007	1.08	2.12E+21	1.41E+19	3.65E+18	4857053.0	0.03	2.92	0.405084
1:100	651.65	389693.1	2140.0	2.1400	0.01	1.10	2.15E+21	2.15E+19	6.61E+18	5101874.6	0.03	3.11	0.688403

The P signal intensities and therefore calculated ctDNA concentrations (columns 11 and 12 respectively) in Table 3:4 and Table 3:5 were highly variable, even though all the samples contained  $0.25 \text{ mg ml}^{-1}$  ctDNA. In the above case, the oxaliplatin samples were analysed first followed by cisplatin. The ICP-MS determined ctDNA concentration of the oxaliplatin control sample was  $0.28 \text{ mg ml}^{-1}$ , if the dilution factor of 4.01 is considered, a ctDNA concentration of  $1.12 \text{ mg ml}^{-1}$  is obtained, which is consistent with the UV determined concentration of  $1.17 \text{ mg ml}^{-1}$ . The P signal intensities and therefore ICP determined ctDNA concentrations decreased steadily throughout the analysis, with  $\sim 7$  fold decrease in signal observed during analysis of the oxaliplatin and cisplatin samples. The correlation between ICP-MS and UV determined ctDNA concentrations were expected to be closer in the more dilute ctDNA samples, due to the reduced matrix. However, this was not the case, the ICP-MS determined ctDNA concentrations in Table 3:3, which contained  $\sim 0.5 \text{ mg ml}^{-1}$  ctDNA were closer to the concentrations calculated by UV, whilst the more dilute ctDNA solutions (Table 3:4 and Table 3:5) gave the largest deviations. The sample introduction system was inspected post analysis for signs of blockages, but the nebuliser, torch and sample cones appeared to be free from such obstructions. Again, these spurious P counts were attributed to matrix effects, namely high carbon content and sample viscosity. Considering these observations, the ICP-MS determined ctDNA concentrations were considered to be unreliable, thus the UV determined ctDNA concentrations were used for further data analysis (e.g. to calculate the number of nucleotides per litre and the number of Pt atoms per nucleotide etc.).

The total Pt concentrations for oxaliplatin (Table 3:4) were lower than those seen previously in Table 3:3. For example, the 1:100 oxaliplatin sample gave a total Pt concentration of  $1.72 \text{ mg l}^{-1}$  in the first experiment (Table 3:3) and  $1.02 \text{ mg l}^{-1}$  in the second experiment (Table 3:4), again pointing to the fact that matrix effects may be responsible. The long term continual aspiration of viscous, high carbon material may have caused the unstable and decreasing signals. This would also explain why the P signal intensities gradually decreased with the lowest P signals observed in the cisplatin samples.



The data in Table 3:4 and Table 3:5 shows that between 15-30% of oxaliplatin and 25-40% of cisplatin formed adducts. For both drugs, the highest percentage of Pt adduct formation is generally found at the lower drug doses (e.g. between 1:500K-1:1000). At doses greater than 1:1000 the percentage of Pt forming adducts generally decreased, with the lowest percentages generally found at the very highest dose rates of between 1:300-1:100. This suggests that a saturation point is reached and all available adduct sites on the DNA are occupied at the very high Pt doses. The percentage of oxaliplatin adducts was lower in the above experiment compared to the first analysis seen previously in Table 3:3. The reason for this can only be attributed to matrix effects, since both sets of data were obtained from the same set of samples. Figure 3:9 shows the relationship between the numbers of adducts per litre and number of drug molecules per nucleotide for oxaliplatin and cisplatin. Note that the values on the x axis (number of Pt atoms per litre) were calculated from the data given by Dr LePla.

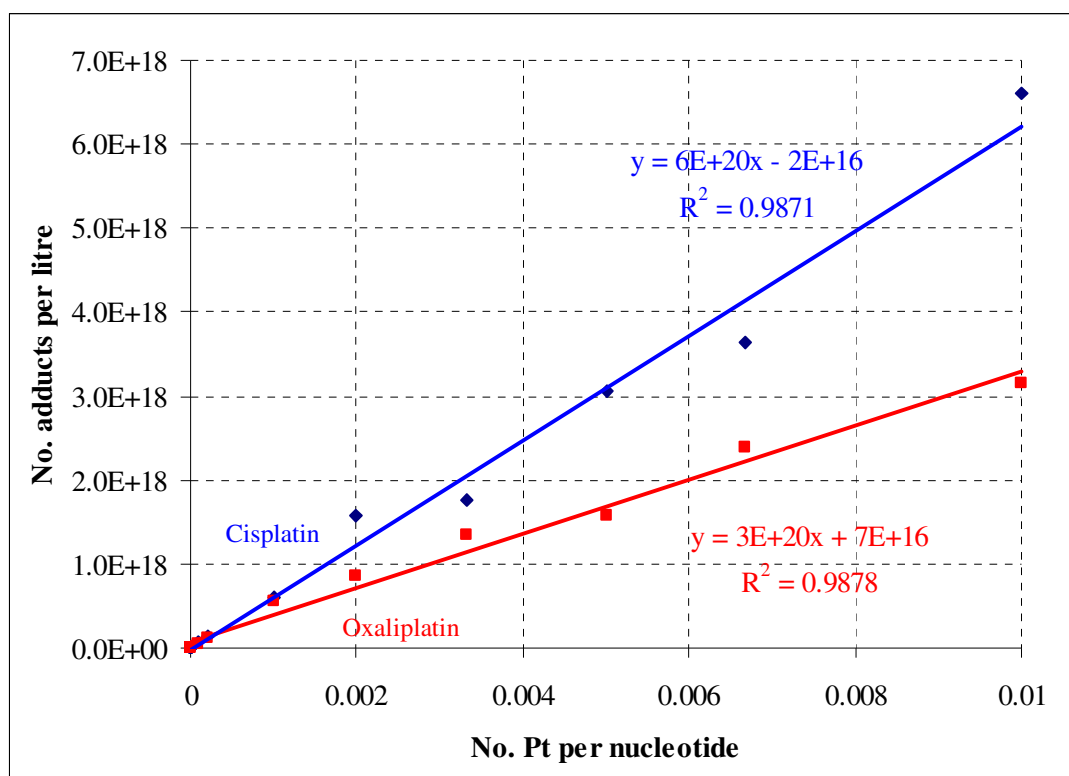
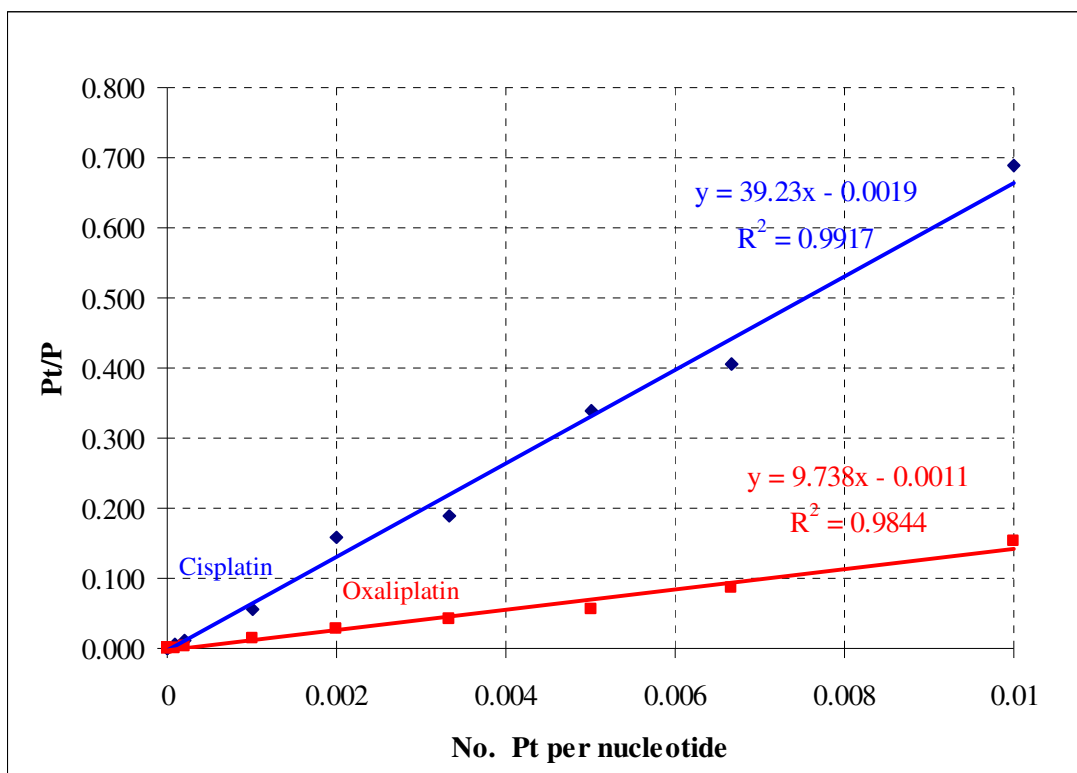


Figure 3:9: Number of cisplatin and oxaliplatin adducts per litre formed against number Pt molecules per nucleotide (0.25 mg ctDNA).

A linear relationship was again observed between the number of adducts formed and the number of drug molecules per nucleobase. This relationship was displayed by both drugs. However, from Figure 3:9 the gradient for the cisplatin data was twice as high as that for oxaliplatin ( $6 \times 10^{20}$  and  $3 \times 10^{20}$  for cisplatin and oxaliplatin respectively), indicating that cisplatin formed more Pt-DNA adducts per litre compared to oxaliplatin. This observation is consistent with the reported literature, which states that cisplatin forms more adducts than oxaliplatin (see 3.1.2 above). Figure 3:10 shows the relationship between Pt/P ratio and the number of nucleotides per Pt for both cisplatin and oxaliplatin.



**Figure 3:10: Pt/P ratio against the number of drug molecules per nucleotide (0.25 mg ctDNA).**

From Figure 3:10 it can be established that as the number of Pt molecules increased (increased dose rate), the ratio of Pt concentration/P concentration also increased in a linear fashion. The above data therefore supports the data shown in Figure 3:9, as dose rate increases, the number of adducts formed increases and thus the concentration of total bound Pt increases as expected.

It has been shown in the data presented so far in this chapter that the presence of the ctDNA matrix was problematic in terms of viscosity and carbon content. Carbon deposition on the sampler cone was significant and sample uptake was only possible with the aid of a peristaltic pump. The Element 2XR instrument gave a signal intensity of  $\sim 1.6 \times 10^6$  cps for  $1 \text{ ng ml}^{-1}$   $^{115}\text{In}$  upon tuning prior to the above analysis ( $1 \times 10^6$  cps/ppb  $^{115}\text{In}$  is the quoted sensitivity by Thermo-Finnigan).<sup>65</sup> Considering  $^{195}\text{Pt}$  is only 33% abundant and the first ionisation potential of Pt is approximately double that of In, a signal intensity of  $\sim 256\,000$  cps was expected for  $1 \text{ ng ml}^{-1}$   $^{195}\text{Pt}$ , which equates to approximately  $4 \times 10^6$  cps for a solution containing  $16 \text{ ng ml}^{-1}$  Pt. However, the highest Pt calibration standard of  $16 \text{ ng ml}^{-1}$  only gave a signal intensity of  $\sim 1.9 \times 10^6$  cps, which was a 53% reduction of the expected Pt signal. These observations suggested that matrix effects were causing a large reduction in sensitivity. If the high carbon matrix is removed prior to analysis, better sensitivity should be obtained. To confirm that the ctDNA matrix was suppressing the Pt signal, two calibration curves were prepared; one set of calibration standards contained Pt in a 2% hydrochloric acid matrix, whilst the second set of standards contained Pt in a  $0.25 \text{ mg ml}^{-1}$  ctDNA matrix. Both sets of standards ranged from  $0.50\text{--}2 \text{ ng ml}^{-1}$  Pt and the calibration curves can be seen in Figure 3:11.

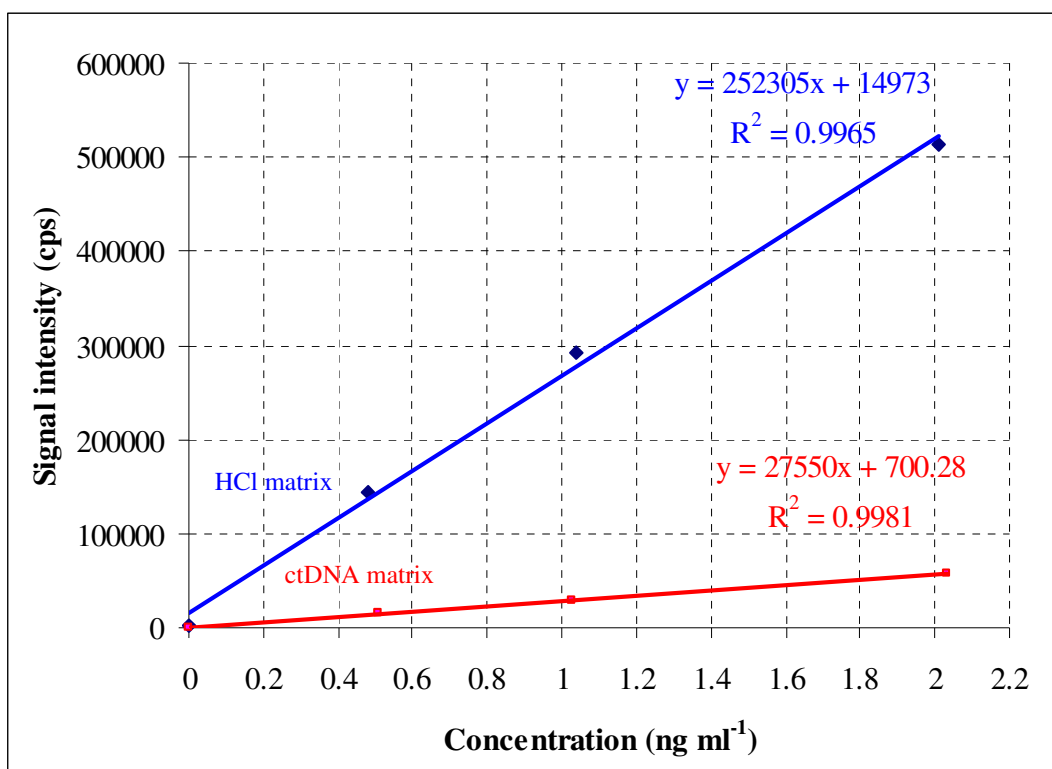


Figure 3:11: Pt calibration curves in a 2% hydrochloric acid and 0.25 mg ml<sup>-1</sup> ctDNA matrix.

The data presented in Figure 3:11 shows that the gradients for the two calibrations were 252 305 and 27 550 counts per ng ml<sup>-1</sup> for the hydrochloric acid and ctDNA matrix respectively. Thus, by comparing the gradients of the two calibration curves, it was established that the 0.25 mg ml<sup>-1</sup> ctDNA matrix suppressed Pt signal by 89%. In addition, the Pt limit of detection (LOD) was determined for both sets of calibration data using the formula shown in Equation 2.

**Equation 2: Limit of detection.**

$$\text{Limit of detection} = \frac{(3 \times SD_{\text{blank}})}{m}$$

Where:

$SD_{\text{blank}}$  = standard deviation of the blank.

$m$  = the gradient of the calibration slope.

The LOD formula shown above is dependent upon the instrument blank and sensitivity, the LOD for Pt was calculated to be  $0.99 \text{ pg ml}^{-1}$  and  $6.38 \text{ pg ml}^{-1}$  in the hydrochloric acid matrix and ctDNA matrix respectively.

These results confirm that the ctDNA matrix was problematic and needed to be removed prior to ICP-MS analysis. By removing the high carbon matrix, the Pt response should be higher (~90% improvement in signal) and lower drug doses should be detected and quantified. Table 3:4 and Table 3:5 show that even when the lowest drug dose of 1:500 000 was diluted four fold to contain  $0.25 \text{ mg ml}^{-1}$  ctDNA, the Pt counts were 12 514 cps and 21 537 cps for oxaliplatin and cisplatin respectively. These signal intensities equated to 0.3 and  $0.6 \text{ ng ml}^{-1}$  Pt. Hence, if the ctDNA matrix is removed the expected signal intensity for these low dose samples should be much higher than those observed in the above data tables.

### **3.2.3.2 Analysis of Digested DNA**

Trial experiments were performed before the nitric acid/hydrogen peroxide digest procedure was carried out on the cisplatin and oxaliplatin treated ctDNA supplied by Dr. LePla. The trial experiments consisted of spiking a  $1 \text{ mg ml}^{-1}$  ctDNA solution with a Pt standard of known concentration ( $21 \text{ ng ml}^{-1}$ ). A 100 mg aliquot of the Pt spiked ctDNA solution was then digested (in duplicate) as described in section 3.2.2.2. Upon completing the digest, the sample was evaporated to dryness and re-suspended in 1.5 ml hydrochloric acid (2% w/w). The resulting digest solutions contained 1.39 (digest A) and  $1.45 \text{ ng ml}^{-1}$  (digest B) Pt in 2% hydrochloric acid. A Pt standard solution containing  $1.37 \text{ ng ml}^{-1}$  Pt in 2% hydrochloric acid was prepared along with  $1.4 \text{ ng ml}^{-1}$  Pt standard solution in  $0.25 \text{ mg ml}^{-1}$  ctDNA matrix. The signal intensities of all the Pt solutions were compared to establish whether the nitric acid/hydrogen peroxide digest was effective at digesting the ctDNA and therefore removing the non-spectroscopic interferences. The data is summarised in Figure 3:12. A control sample consisting of digested ctDNA in the absence of Pt standard was also prepared.

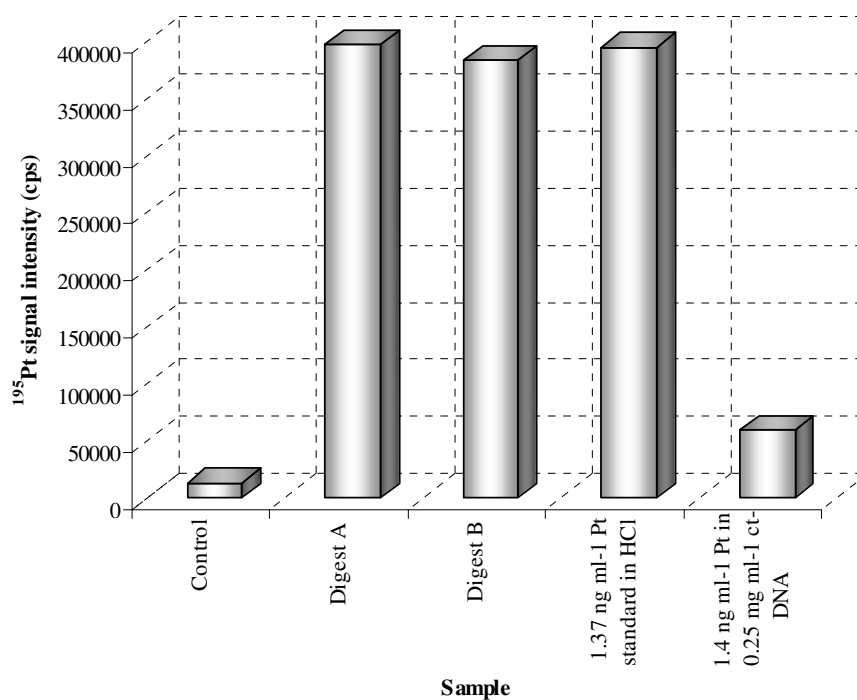


**Figure 3:12: Pt signal intensity for digested DNA samples and Pt standards in hydrochloric acid and DNA matrix.**

The re-suspended digest samples gave very similar counts to the 1.37 ng ml<sup>-1</sup> Pt standard in hydrochloric acid, whilst the solution containing Pt at a concentration of 1.4 ng ml<sup>-1</sup> in 0.25 mg ml<sup>-1</sup> ctDNA resulted in very low counts as expected. An approximate eight fold difference in Pt signal intensity was observed between the ctDNA and aqueous acid matrix. From Figure 3:12 it can be concluded that the nitric acid/hydrogen peroxide digest was effective at digesting the organic matter, which resulted in reducing non-spectroscopic interferences. No matrix effects were observed in the digested DNA samples, this was confirmed by the equivalent Pt signal intensities in the digest samples and the 1.37 ng ml<sup>-1</sup> Pt standard in hydrochloric acid. In addition, the viscosity of the DNA solutions decreased after digestion, so self aspirating nebulisers could be employed, which had the advantage of improved signal stability and reduced sample consumption compared to pumped nebulisers.

Once it was confirmed that the nitric acid/hydrogen peroxide procedure was successful in digesting the DNA and removing the matrix interferences, it was applied to ctDNA samples that had been treated with cisplatin or oxaliplatin. These samples were again prepared by

Dr. LePla at Leicester University. The following dose rates were supplied for both drugs: 1:100K, 1:300K, 1:500K, 1:1000K and 1:1500K. Each sample stock solution contained approximately 1.3 mg ml<sup>-1</sup> ctDNA and a 100 mg aliquot of each sample was initially taken and digested as described above, hence the actual mass of DNA digested was approximately 130 µg. After digestion, the samples were reduced to dryness and re-suspended in 2% hydrochloric acid (0.5 ml), which was accurately weighed to establish the dilution factor for each sample. The results for the cisplatin and oxaliplatin samples are summarised in Table 3:6 and Table 3:7 respectively, where the mass of ctDNA digested is clearly shown. The Pt concentrations look reasonable, with the Pt concentration gradually increasing with increasing dose rate as expected for both drugs. The lowest cisplatin dose rate of 1:1500K gave a higher Pt signal than expected, as did the oxaliplatin 1:1000K sample. The reason for this could only be explained by potential contamination during the sample preparation procedure.

**Table 3:6: Pt signal intensity and concentration in digested cisplatin treated samples.**

<b>Cisplatin sample</b>	<b>Pt per nucleotide</b>	<b><sup>195</sup>Pt counts (cps)</b>	<b>Dilution factor</b>	<b>Pt conc (ng ml<sup>-1</sup>)</b>	<b>Mass of DNA digested (µg)</b>
Control	0.0000000	1201.1	4.17	0.13	115.18
1:100K	0.0000100	241356.1	5.10	4.53	125.13
1:300K	0.0000033	78917.3	5.18	1.60	138.42
1:500K	0.0000020	58375.9	4.65	1.09	127.63
1:1000K	0.0000010	35809.1	4.75	0.73	131.34
1:1500K	0.0000007	76633.9	5.15	1.55	134.88

**Table 3:7: Pt signal intensity and concentration in digested oxaliplatin treated samples.**

<b>OxPt sample</b>	<b>Pt per nucleotide</b>	<b><sup>195</sup>Pt counts (cps)</b>	<b>Dilution factor</b>	<b>Pt conc (ng ml<sup>-1</sup>)</b>	<b>Mass of DNA digested (µg)</b>
Control	0.0000000	1425.0	2.05	0.003	130.00
1:100K	0.0000100	78945.3	2.53	1.02	131.92
1:300K	0.0000033	25969.6	2.51	0.32	132.73
1:500K	0.0000020	21549.3	1.99	0.21	136.76
1:1000K	0.0000010	24557.8	2.00	0.24	136.35
1:1500K	0.0000007	11165.5	2.03	0.11	135.85

Figure 3:13 shows the above data graphically, where the number of adducts formed was calculated as described previously and then plotted against the number of Pt atoms per nucleotide. It should be noted that the x axis (number of Pt atoms per nucleotide) was

calculated from the information given by Dr. Rachel Le Pla. A linear relationship between Pt signal and drug dose rate was observed as expected. The cisplatin 1:1500K and oxaliplatin 1:1000K results, which gave slightly higher Pt signals than expected, were included in Figure 3:13. Before these two data points were included in the graphs, regression analysis was carried out on the respective data sets where the standard error (95% confidence level) of the data was established, along with the predicted y values (No. Pt-DNA adducts formed per litre). It was shown in the suspect cisplatin and oxaliplatin samples that the number of Pt-DNA adducts formed per litre (determined by ICP-MS) was outside of the predicted y value  $\pm 1$  standard error (SE), but within  $\pm 2$  SE. Since 2 SE give the greatest confidence, it was decided not to omit the suspect data points but to include them in the graphs shown below.

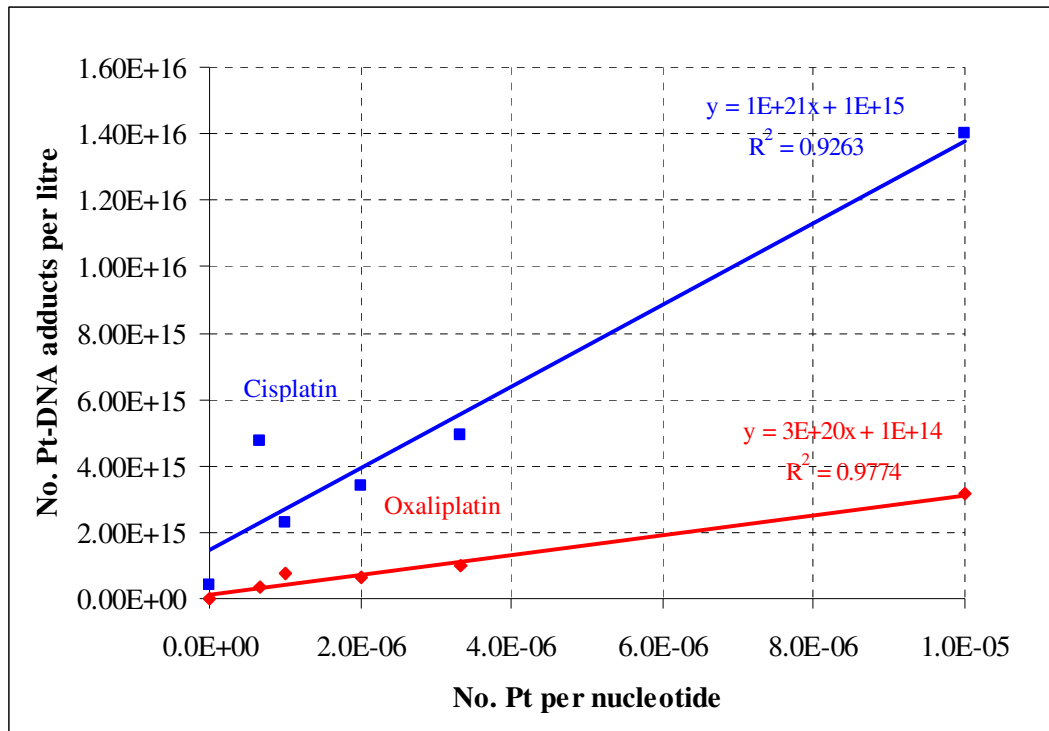


**Figure 3:13: Relationship between Pt signal and the number of Pt atoms per nucleotide for both cisplatin and oxaliplatin following digestion with nitric acid and hydrogen peroxide.**

The above sets of data illustrate that the nitric acid/hydrogen peroxide was effective at digesting the organic matrix and removing matrix effects. More importantly, the digest was applied to relatively small quantities of DNA (~130  $\mu$ g) and still allowed for the very low



doses of Pt drug to be determined and quantified. The linearity of the data in Figure 3:13 was poor compared to that seen in Figure 3:9, where whole ctDNA was analysed. This can be attributed to the lower quantities of DNA under analysis and the much lower drug application rates.

Figure 3:12 illustrates that the Pt standard containing ctDNA matrix gave signal intensity eight times lower than the digested ctDNA containing Pt. Thus, the Pt signal intensities in Table 3:7 (acid digested ctDNA) were expected to be eight times greater than those in Table 3:4, which showed data for samples containing whole ctDNA at  $0.25 \text{ mg ml}^{-1}$ . When the Pt counts were compared for equivalent amounts of ctDNA,  $\sim 1.5$  times greater Pt signal intensity was obtained in the digested ctDNA samples (Table 3:7) compared to the whole ctDNA (Table 3:4). Although a much larger increase in Pt signal intensity was expected, it should be noted that the two sets of data originated from different sets of samples, which could explain why the two sets of data do not completely correspond.

The nitric acid/hydrogen peroxide digest was repeated on the Pt treated ctDNA samples, but a much lower quantity of sample and therefore DNA was digested. As stated previously, if the method is to be applied to patient samples, only small quantities of DNA may be obtained, so the method has to be suitable for use on approximately  $10 \mu\text{g}$  of DNA. This quantity of DNA could realistically be obtained from patients, but  $100 \mu\text{g}$  DNA or greater may not be feasible. The cisplatin treated ctDNA stock samples which were digested previously (see above experiments) were used in this analysis. Briefly, an aliquot of the cisplatin stock solution ( $\sim 12 \text{ mg}$ ) was added to a polypropylene microcentrifuge vial, accurately weighed and then digested as described previously. Figure 3:14 shows the relationship between the number of Pt-DNA adducts formed against the number of Pt atoms per nucleotide for cisplatin treated ctDNA. The mass of ctDNA digested in this experiment ranged from  $13\text{-}18 \mu\text{g}$ . Although, the data shows a general increase in Pt concentration with increasing dose rate, the 1:1000K sample from this batch exhibited very high Pt counts ( $\sim 31527 \text{ cps}$ ). Again, regression analysis was carried out on the data, which showed that the 1:1000K data point was within the predicted  $y$  value  $\pm 2 \text{ SE}$  (95% confidence level) and included in Figure 3:14.

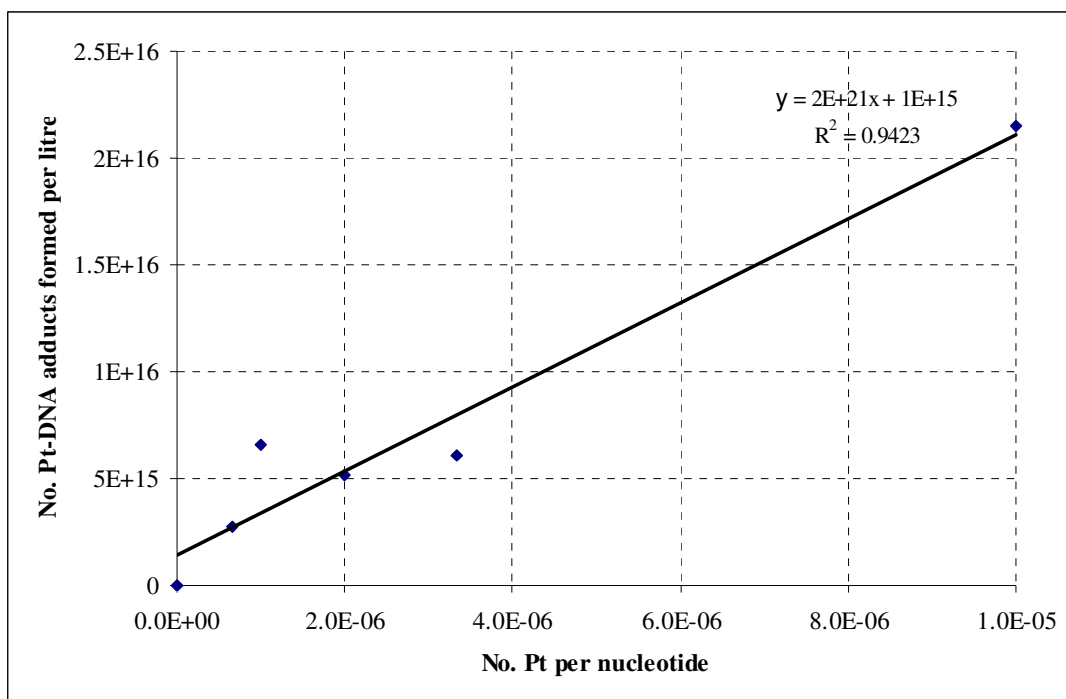


**Figure 3:14: Relationship between the number of adducts formed and the number of drug molecules per nucleotide for cisplatin treated ctDNA digested with nitric acid and hydrogen peroxide.**

The next step involved digesting the oxaliplatin treated ctDNA samples along with a repeated attempt at digesting the cisplatin treated ctDNA. For both sets of samples approximately 12  $\mu\text{g}$  ctDNA was digested. Both the  $^{195}\text{Pt}$  and  $^{31}\text{P}$  signals were measured for these two sets of samples, Figure 3:15 and Figure 3:16 show the data for these two digests. The cisplatin data was slightly better than that obtained for oxaliplatin. The oxaliplatin control and 1:300K samples gave very high Pt signals that were not consistent with the remaining samples. Regression analysis showed that the control was within  $\pm 2$  SE of the predicted values, but the 1:300K sample was outside the predicted values. For this reason, the 1:300K sample was omitted from Figure 3:15 and Figure 3:16. Figure 3:15 illustrates the linear relationship between the number of Pt-DNA adducts formed and the number of drug molecules per nucleotide. It should be noted that the cisplatin samples again displayed greater Pt concentrations and therefore greater numbers of adducts than oxaliplatin as expected. Figure 3:16 shows the linear relationship between Pt/P ratios and the number of drug molecules per nucleotide, as expected the ratio increased with increased dose of drug. However, the linearity of these two sets of data was inferior to those seen in Figure 3:9.

This was again attributed to error associated with the low Pt signal intensities resulting from the small quantities of DNA analysed and the low dose rates.

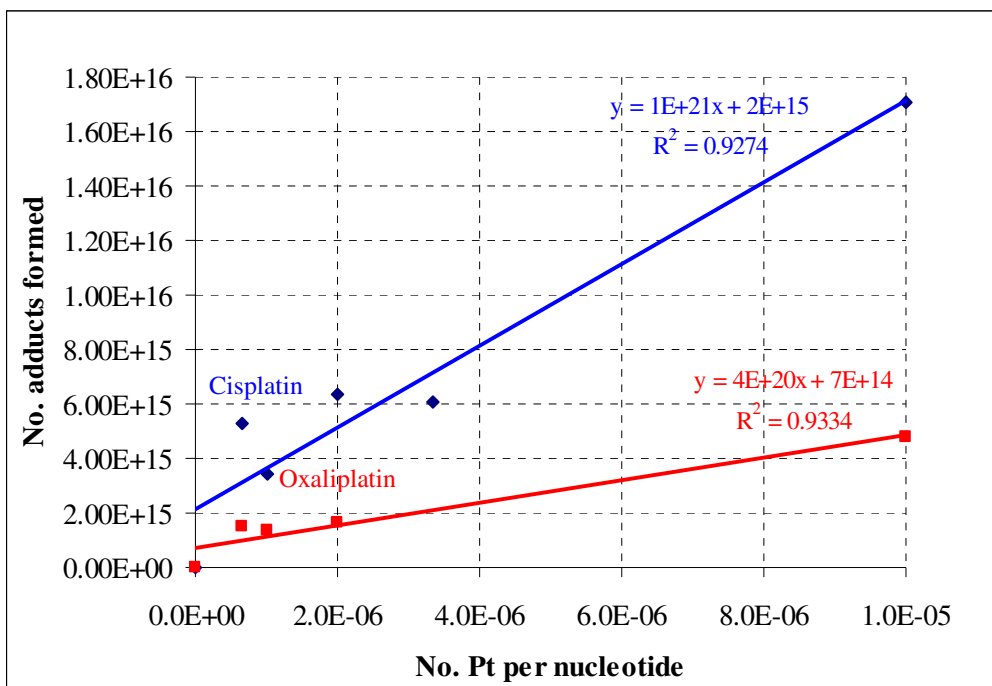


Figure 3:15: The relationship between number of Pt-DNA adducts formed and the number of drug molecules per nucleotide, for both cisplatin and oxaliplatin treated ctDNA digested with nitric acid/hydrogen peroxide. Approximately 12  $\mu$ g of ctDNA digested.

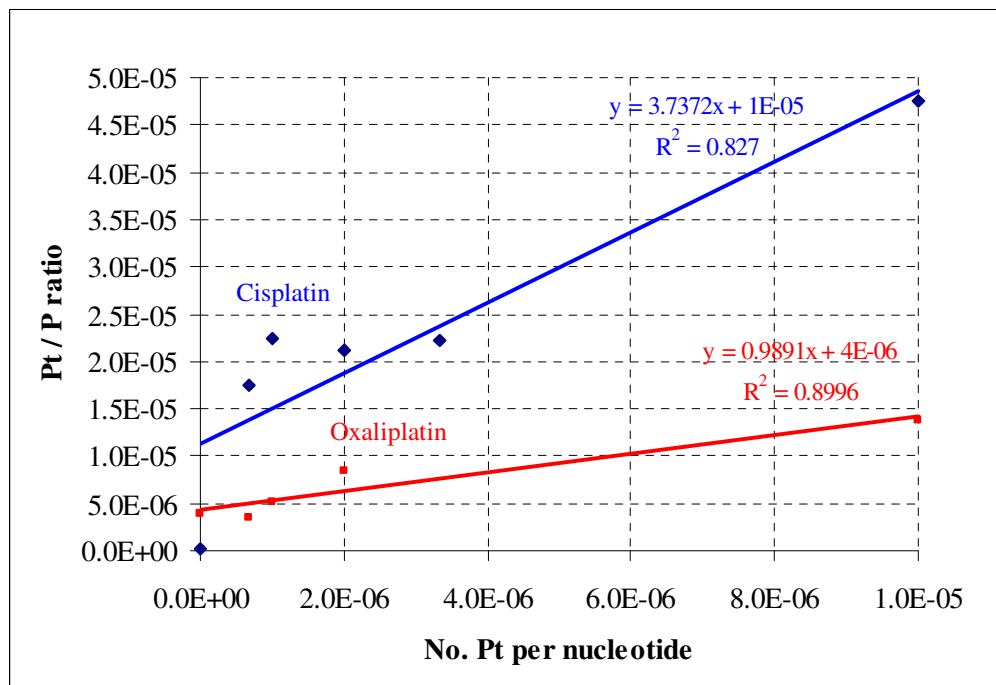


Figure 3:16: Pt/P ratio against the number of drug molecules per nucleotide for both cisplatin and oxaliplatin treated ctDNA digested with nitric acid/hydrogen peroxide. Approximately 12  $\mu$ g of ctDNA digested.

### 3.2.4 Summary

The application of ICP-MS to the detection and quantification of Pt-DNA adducts, formed after incubation with either cisplatin or oxaliplatin anti-cancer drugs has been demonstrated. It has been established that HR-ICP-MS can be employed for detecting the high levels of P associated with the DNA backbone and trace levels of Pt associated with Pt-DNA adducts. The DNA solutions could be analysed whole without additional sample preparation, and the Pt measured with doses as low as 1:500 000 nucleobases being detected. However, severe matrix effects were observed which resulted in a suppression of the Pt signal. These matrix effects were a consequence of the high carbon matrix which is associated with biological materials such as DNA. Carbon deposition on or around the orifice of the sampler cone was problematic and resulted in signal drift. In addition, the viscosity of the whole DNA solutions compromised sample uptake and nebulisation efficiency. These problems were overcome and lower drug dose rates were successfully detected by digesting the DNA in a mixture of nitric acid and hydrogen peroxide. Drug doses as low as 1:1 500 000 nucleobases could then be detected.

In addition to drug doses of 1:1 500 000 being detected, such levels were successfully quantified in samples containing ~12 µg ctDNA when digested with nitric acid and hydrogen peroxide. This is particularly important if the method is to be applied to clinical samples, where DNA has to be extracted from blood samples obtained from chemotherapy patients and the quantity of DNA is restricted. However, ~12 µg DNA would be possible to obtain from patient blood samples.

The research detailed in this chapter has illustrated the potential of ICP-MS in detecting and quantifying low doses of Pt in microgram quantities of DNA. The digest and analysis method detailed here was successfully employed during an MSc. Project carried out by Albano Fialho at Loughborough University.<sup>182</sup> In this project, two lung cancer cell lines (A549 and H23) were treated with cisplatin or oxaliplatin. The digest method was then applied to 40 µg of extracted DNA, with the associated Pt successfully detected and quantified.<sup>182</sup> The next step would be to extract blood from patients undergoing treatment with these drugs, extract and then analyse the DNA. If the extent of Pt-DNA adduct

formation can be detected in clinical samples, it could help identify those patients who are responding to treatment and those who are not responding as well. More importantly, if those patients who are not responding, are identified early in the treatment phase, the treatment could be stopped and the severe side effects associated with these drugs could be minimised. Levels of adduct formation will be much lower *in-vivo*, since the cell is exposed to the drug and not the DNA directly. However, clinical adduct levels may be higher than 1:1500K measured here.

A recent publication detailed very similar work to that discussed in this chapter.<sup>183</sup> The authors described a method based on capillary LC-ICP-MS, which was used to separate and detect Pt-GG adducts, which were produced *in-vivo* upon treating *D. Melanogaster* with cisplatin.<sup>183</sup> The authors studied the correlation between cisplatin adduct levels (determined by LC-ICP-MS) and genotoxicity (determined by the comet assay), however, the author did not study oxaliplatin.<sup>183</sup> The reported detection limit for the capillary LC-ICP-MS method was 1 adduct per  $10^6$  nucleotides,<sup>183</sup> which is similar to the doses detected in this chapter, although the author did not specify the total mass of DNA required to detect 1 Pt adduct per  $10^6$  nucleotides.

## 4 Investigation of Oxaliplatin Interactions with DNA Nucleobases by means of Organic Mass Spectrometry

### 4.1 Introduction

There have been numerous investigations into the interactions of oxaliplatin with proteins<sup>141, 173</sup> and the effect of DNA binding in the presence of specific proteins, particularly those rich in sulfur containing amino acids.<sup>141, 184, 185</sup> Extensive studies investigating the interaction of oxaliplatin with DNA nucleobases have also been conducted. However, the techniques used to study oxaliplatin-DNA interactions have been predominantly x-ray crystallography,<sup>186</sup> NMR<sup>144, 187</sup> and biological assays such as the Comet assay.<sup>156</sup> These techniques have their disadvantages, namely; crystals of a suitable quality are required for crystallography and relatively large quantities of high purity sample are required for NMR.<sup>188, 189</sup> Mass spectrometry has been used to study and characterise cisplatin-DNA adducts,<sup>151, 164, 190</sup> but to our knowledge, the same has not been true for the study of oxaliplatin-DNA adducts. ESI-MS has been employed to investigate the structure of oxaliplatin adducts with methionine and guanine monophosphate (GMP).<sup>184</sup> A LC-ESI-MS/MS method has been developed previously to measure GG and AG intra-stranded cross-links in oxaliplatin treated DNA, where limits of detection for the two cross-links were determined.<sup>167</sup> These authors reported proposed structures for the two major oxaliplatin adducts and their corresponding fragments, however, the source was operated in negative ion mode, not positive as used here, and detailed fragmentation pathways for the remaining oxaliplatin-DNA adducts were not investigated. Here the focus is on the interactions of oxaliplatin with the nucleobases adenine, guanine, cytosine and thymine, where the drug was combined with free nucleobases as opposed to oligonucleotides or intact DNA. This fundamental investigation provides the initial step towards a more complete understanding of the drug's interaction and binding mode with intact DNA where other factors such as steric strain and binding site geometry might impact upon binding location and stability of the drug complex.

A linear ion trap mass spectrometer employing ESI was employed here to study the binding of oxaliplatin to DNA nucleobases. Oxaliplatin was combined with each DNA nucleobase and the identities of all the resulting complexes were investigated using ESI-MS. The preferential binding of oxaliplatin to guanine and adenine in the presence of all four nucleobases will be discussed. It will also be demonstrated that ESI-MS<sup>n</sup> is an ideal technique for the study of oxaliplatin-nucleobase interactions since structural information can be obtained in relatively short periods of time and the disadvantages of NMR and x-ray crystallography are avoided.<sup>190</sup>

In addition to demonstrating the potential of linear ion trap mass spectrometry in metallodrug studies, this chapter will also highlight the complementary nature of organic and inorganic mass spectrometry; namely, inorganic mass spectrometry was employed in the previous chapter to detect and quantify trace amounts of Pt drug bound to DNA. Conversely the following chapter details structural information and fragmentation pathways of oxaliplatin-nucleobase adducts.

The work detailed in this chapter was conducted in the Atomic Spectrometry Research Group, under the supervision of Dr Barry Sharp and in collaboration with Dr Tamer Shoeib, who was a visiting academic from the British University in Egypt.

## **4.2 Instrumentation and Reagents**

A Thermo Finnigan LTQ linear ion trap mass spectrometer (Thermo Finnigan, San Jose, California) was used for all mass spectrometric determinations. Version 2.0 of the Xcalibur software (Thermo Finnigan, San Jose, California) was employed for all data processing. The instrument was calibrated with a mixture of ultra mark and caffeine in accordance with the manufacturer's recommendations. Resolution was calculated according to  $R=m/\Delta m$ . Resolving powers achieved were in the order of 1200 for higher mass di-adducts, although lower mass species exhibited resolving powers of approximately 800-1000. The LTQ Ion Max auto-tune routine was used to obtain settings for lens, quadrupole and octapole voltages for maximum transmission of the ions of interest. Helium gas admitted into the ion trap at a maintained pressure of approximately  $10^{-3}$  Torr was used as the buffer gas to



improve the trapping efficiency and as the collision gas for collision induced dissociation (CID) experiments. Experiments designed to elucidate ion structures or fragmentation pathways were performed as follows: the ion of interest was selected with an isolation width set to 1  $m/z$  units (unless stated otherwise), collisional activation was introduced by setting the activation amplitude (which defined the amplitude of the radio frequency (RF) voltage applied) at 25–35% of the maximum voltage available (determined empirically), and the activation Q setting (used to adjust the frequency of the RF-excitation voltage) was set at 0.25 unit. Sample solutions were continuously infused at a flow rate of 5  $\mu\text{l min}^{-1}$  into the pneumatically assisted electrospray probe using dry nitrogen as the nebulising gas. The basic instrument operating conditions are summarised in Table 4:1. The instrument ion optics and gas flows were tuned daily with the analyte of interest to obtain maximum signal intensity and stability.

**Table 4:1: ESI-MS operating conditions.**

Scan type	Positive ion
Nebulising gas	$\text{N}_2$
Flow rate	5 $\mu\text{l min}^{-1}$
Spray voltage	5-5.5 kV
Sheath gas flow (arbitrary units)	tuned daily (typically ~0-10)
Auxiliary gas flow (arbitrary units)	tuned daily (typically ~0-10)

The nucleobases, adenine (A), guanine (G), cytosine (C) and thymine (T) were obtained from Fisher Scientific (Loughborough, UK), as was HPLC grade methanol. Oxaliplatin was kindly supplied by Dr. LePla, but the drug originated from Sanofi-Synthelab (Surrey, UK). The drug was in powder form and was dissolved in deionised water to a concentration of 2.6  $\text{mg ml}^{-1}$  (6.6 mM oxaliplatin) to form the stock solution, which was used to prepare further drug-nucleobase solutions. All solutions were prepared in 50% methanol in deionised water.

Initial experiments concentrated on identifying the oxaliplatin parent ion and fragmentation products in the absence of nucleobase. Since oxaliplatin would be present in all solutions, it was considered important to become familiar with its fragmentation pathway before progressing to more complex mixtures containing nucleobases. As a result, a solution

containing oxaliplatin at a concentration of 3.3 mM in 50% methanol was prepared and infused into the mass spectrometer before the drug-nucleobase interactions were investigated.

Initially four solutions containing oxaliplatin were prepared; each oxaliplatin solution contained a different base, so the drug was present in a mono-base solution. Two solutions containing the drug with all four nucleobases were prepared, one of these solutions contained oxaliplatin at an equi-molar concentration to each of the bases. The second mixed solution contained an excess of oxaliplatin in the presence of the four bases. A final solution containing oxaliplatin with adenine and guanine at near equal molar concentrations was also prepared. The concentration of drug and base in each solution is shown in Table 4:2.

**Table 4:2: Concentration of oxaliplatin and nucleobase in individual and mixed base solutions.**

Solution	Reagent Concentration
1	3.3 mM oxaliplatin + 9.4 mM adenine
2	1.6 mM oxaliplatin + 5.8 mM cytosine
3	1.6 mM oxaliplatin + 1.6 mM guanine
4	1.6 mM oxaliplatin + 8.3 mM thymine
5	1.7 mM oxaliplatin + 1.6 mM A, C, G and T
6	3.0 mM oxaliplatin + 0.46 mM A, C, G and T
7	2.2 mM oxaliplatin + 1.5 mM adenine + 1.7 mM guanine

The drug to nucleobase molar concentrations were adjusted to obtain clear spectra, consequently these ratios corresponded to the order of formation constants as indicated by the analysis of the mass spectra, which will be discussed in subsequent sections. Each solution was allowed to sit at room temperature overnight before being analysed. Solutions 1-4 each contained oxaliplatin and a single nucleobase and were employed to confirm the formation of oxaliplatin adducts in each case. Solutions 5 and 6 were used to study the formation of oxaliplatin adducts in the presence of all four nucleobases. Further, solution 7 was employed to study the preferential binding of oxaliplatin to adenine and guanine.

## 4.3 Results

### 4.3.1 Oxaliplatin Analysis

A 3.3 mM oxaliplatin solution absent of nucleobase was infused into the mass spectrometer and analysed using the instrument conditions summarised in Table 4:1. Prior to nucleobase binding oxaliplatin loses the oxalate ligand, which acts as a leaving group enabling adduct formation, whilst the diaminocyclohexane (dach) ligand remains attached to the Pt centre. The full scan mass spectrum of the oxaliplatin sample exhibited a cluster of ions around  $m/z$  398 and 307, corresponding to the whole oxaliplatin complex and the oxaliplatin without the oxalate leaving group (Pt-dach) respectively. A full scan spectrum of the drug is shown in Figure 4:1.

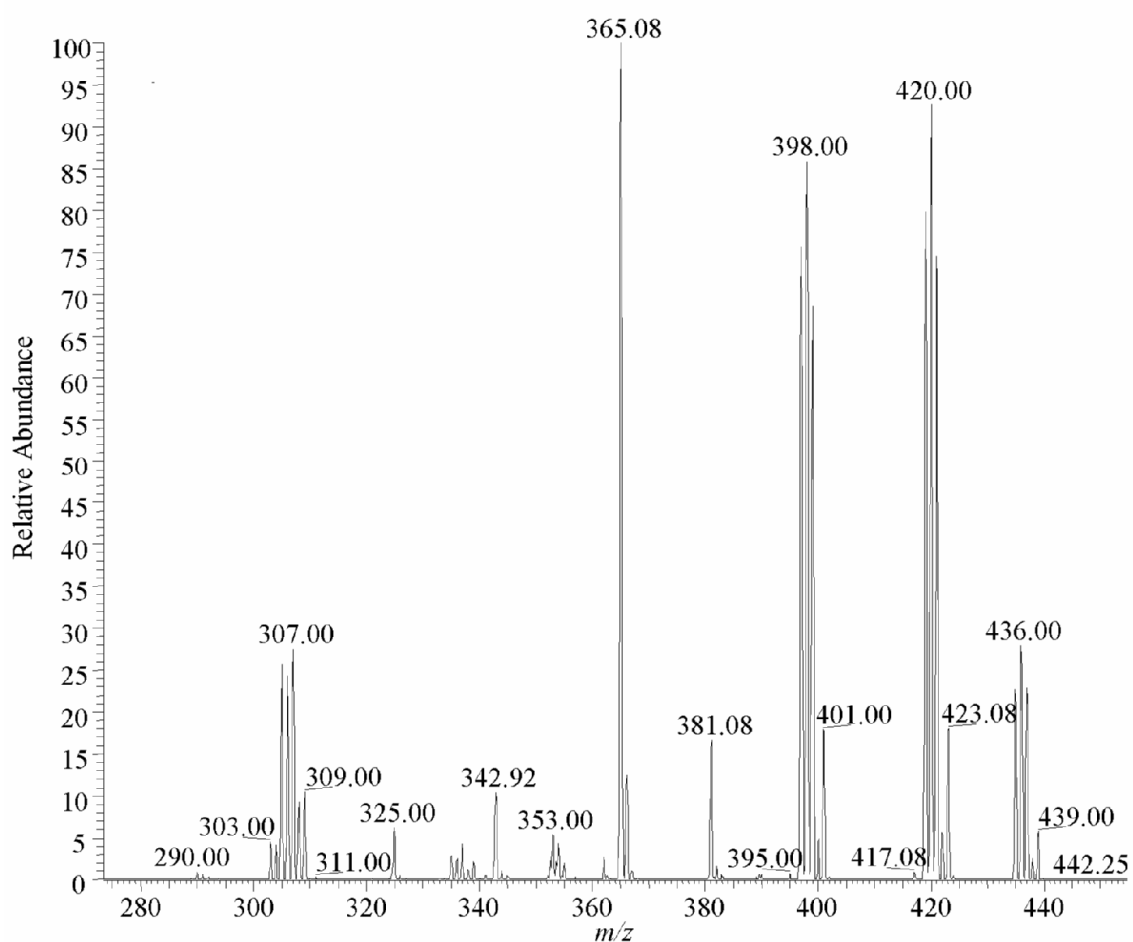
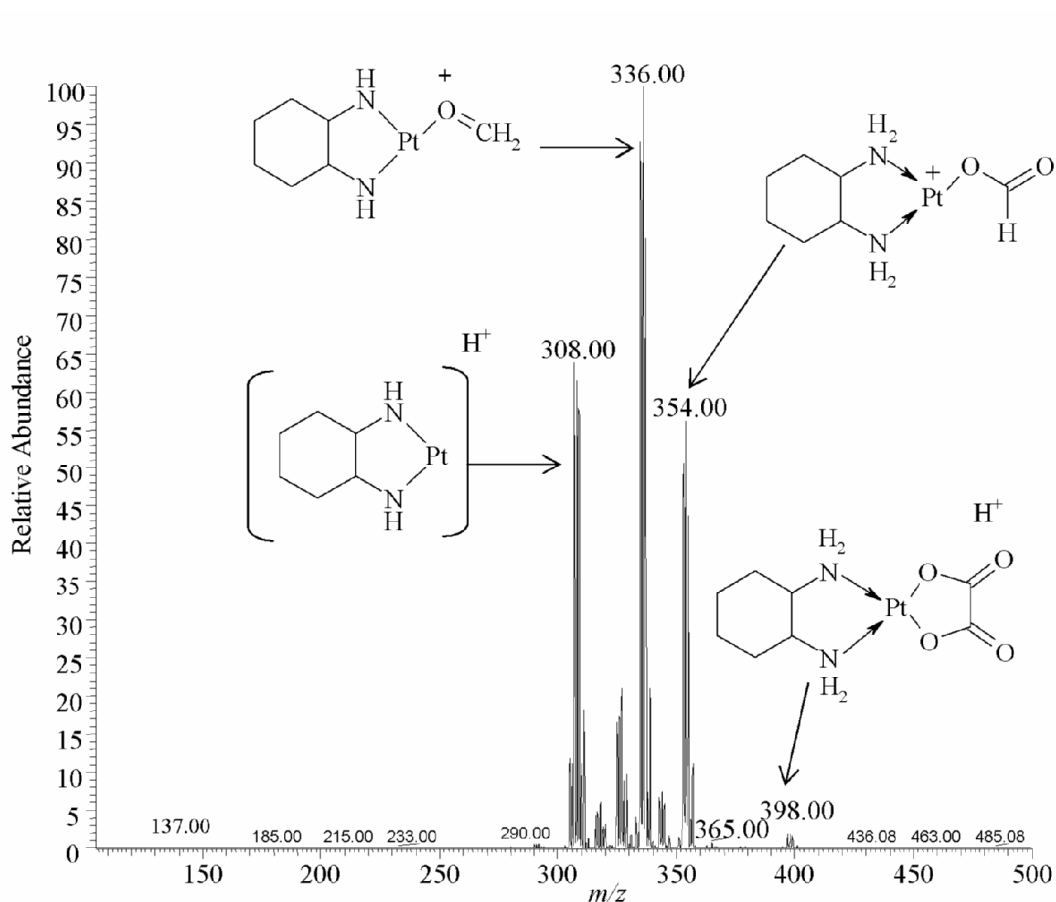


Figure 4:1: Full scan mass spectrum of 3.3 mM oxaliplatin.

Figure 4:1 shows that the dominant Pt containing species present in the mass spectrum were at  $m/z$  307, 398 and 420. The Pt isotopic pattern corresponding to  $^{194}\text{Pt}$  (32.8%),  $^{195}\text{Pt}$  (33.8%),  $^{196}\text{Pt}$  (25.3%) and  $^{198}\text{Pt}$  (7.2%) was clearly observed for each of these dominant species, with the heights of the Pt peaks clearly represented the isotopic abundances which are shown in brackets above. The peak at  $m/z$  365 was present in the majority of mass spectra, but could not be assigned and did not exhibit the characteristic Pt isotopic pattern, indicating that it did not correspond to a Pt containing species. Since the peak was present in mass spectra containing oxaliplatin only, it was attributed to an impurity or ingredient present in the drug. The Pt species at  $m/z$  420 was thought to be a Na adduct of the oxaliplatin drug, whilst the remaining two species were initially thought to be the parent oxaliplatin ion ( $^{195}\text{Pt}$   $m/z$  398) and the diaminocyclohexane platinum complex ( $^{195}\text{Pt}$   $m/z$  308). To confirm the two latter assumptions, the identity of the peaks at  $m/z$  398 and  $m/z$  308 were confirmed using MS/MS. The principles of tandem and multiple mass spectrometry were detailed in Chapter 1. Briefly, the ions of interest were selected and thus ‘trapped’ within the quadrupole, whilst all other ions were ejected from the ion trap. Fragmentation was then induced by bombarding the selected parent ions with He collision gas. The resulting product ions were then scanned out of the quadrupole ion trap and detected to produce a MS/MS spectrum, which helped reveal the identity of the adducts. A further mass spectrometry experiment was sometimes possible ( $\text{MS}^3$ ) providing the ion signal was of sufficient intensity, which helped further confirm the identity of the species.

The MS/MS spectrum of the parent ion ( $m/z$  398) is shown in Figure 4:2. Note that the spectrum in Figure 4:2 was obtained using a peak isolation width of 10 Da; hence all the peaks  $\pm 5$  mass units from  $m/z$  398 were selected and fragmented to give numerous product ions. As a result, the Pt isotopic pattern was observed for all product ions.



**Figure 4:2:** MS/MS spectrum of product ions obtained by CID of the oxaliplatin parent ion at  $m/z$  398, collision energy = 20 eV, isolation width =10 Da.

Figure 4:2 shows three main fragmentation product ions at  $m/z$  308, 336 and 354. Unfortunately, since the ion signal was quite weak, further MS experiments could not be carried out on these product ions. However, an attempt was made at identifying the molecular structure of the dominant product ions, as seen in Figure 4:2. It was thought that the isotopic peaks around  $m/z$  354 corresponded to the parent ion minus a mass of 44, which equated to a loss of  $\text{CO}_2$  from the oxalate ligand. A mass loss of 62 was also observed to give product ions at  $m/z$  336, which were attributed to the loss of  $\text{CO}_2 + \text{H}_2\text{O}$ , again from the oxalate ligand. The final product ions around  $m/z$  308 corresponded to the diaminocyclohexane platinum (Pt-dach) complex, which is effectively oxaliplatin minus the oxalate leaving group. The structures shown in Figure 4:2 are thought to be the most rational, but were not definitively proven.

The three main isotopes of the oxaliplatin parent ion at  $m/z$  397, 398 and 399 were then fragmented with a peak isolation width of 1 Da (peaks within  $\pm 0.5$  mass units of the ion of interest were selected and fragmented), the ion tree in Figure 4:3 summarises the product ions formed upon fragmenting each of the isotopic parent ions. The mass spectra from these experiments can be seen in Figure 9:1-Figure 9:3 in Appendix 2.1 (Section 9.1).

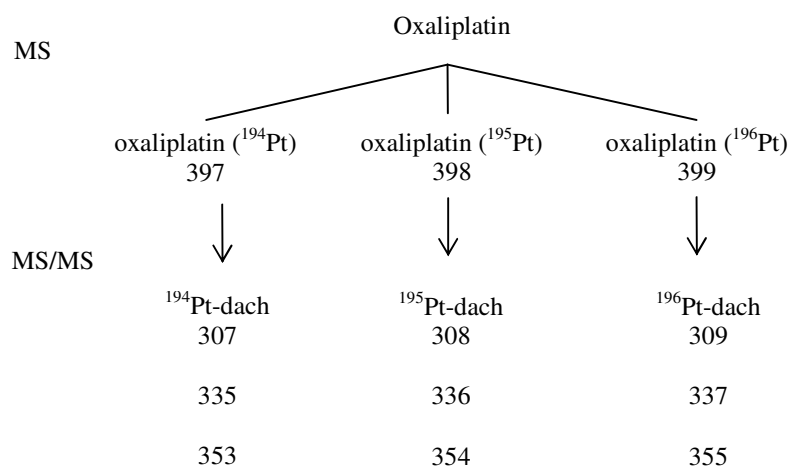


**Figure 4:3: Oxaliplatin fragmentation ion tree.**

As stated previously, oxaliplatin loses the oxalate ligand prior to nucleobase binding to form the Pt-dach species at  $m/z$  308 ( $^{195}\text{Pt}$ ). Therefore, it was expected that the peaks corresponding to the Pt-dach species ( $m/z$  308) and oxaliplatin parent ion ( $m/z$  398) would be observed in all further mass spectra containing the drug.

### 4.3.2 Evidence of Adduct Formation

Upon infusing the oxaliplatin solutions containing individual nucleobase (oxaliplatin solutions 1-4, refer to Table 4:2), it was established that the drug formed both mono-adducts (oxaliplatin bound to one nucleobase) and di-adducts (oxaliplatin bound to two nucleobases) with all four nucleobases, when present individually in solution. In all four mono-base solutions the complexes were formed at the expected mass-to-charge ratios and the identity of each species was further confirmed by performing multiple MS experiments on the ions of interest.

The mass spectra of each sample exhibited a cluster of ions around  $m/z$  398 and 308; as discussed above, these isotopic peaks corresponded to the whole oxaliplatin complex and the Pt-dach species respectively. Table 4:3 summarises the mass-to-charge ratios of the  $^{194}\text{Pt}$  containing ions observed in each of the oxaliplatin solutions. Although the masses in Table 4:3 refer to the  $^{194}\text{Pt}$  isotopic species, the Pt isotopic pattern was clearly observed for all adducts, further confirming the binding of the drug to the individual bases. For clarification the fragmentation of the  $^{194}\text{Pt}$  adducts will be discussed, although the same principles apply to the 195 and 196 Pt complexes.

**Table 4:3: Oxaliplatin adducts formed with individual DNA nucleobases.**

<b>Ion</b>	<b><math>m/z</math></b>
<b>Adenine-oxaliplatin solution</b>	
[adenine-H] <sup>+</sup>	136
$^{194}\text{Pt}(\text{adenine})^+$	442
$^{194}\text{Pt}(\text{adenine})_2^+$	577
<b>Cytosine-oxaliplatin solution</b>	
[cytosine-H] <sup>+</sup>	112
$^{194}\text{Pt}(\text{cytosine})^+$	418
$^{194}\text{Pt}(\text{cytosine})_2^+$	529
<b>Guanine-oxaliplatin solution</b>	
[guanine-H] <sup>+</sup>	152
$^{194}\text{Pt}(\text{guanine})^+$	458
$^{194}\text{Pt}(\text{guanine})_2^+$	609
<b>Thymine-oxaliplatin solution</b>	
[thymine-H] <sup>+</sup>	127
$^{194}\text{Pt}(\text{thymine})^+$	433
$^{194}\text{Pt}(\text{thymine})_2^+$	559

Each oxaliplatin-nucleobase di-adduct lost a neutral nucleobase upon CID, resulting in the formation of mono-adducts at the expected  $m/z$ . Fragmentation of the mono-adducts resulted in the loss of  $\text{H}_2$  and ammonia. The de-protonated ions were signified by product ions with  $m/z$  two and four mass units lower than the parent ion, suggesting successive losses of  $\text{H}_2$  from the complex. Such losses of neutral  $\text{H}_2$  molecules during CID has been reported elsewhere,<sup>191, 192</sup> although the reported fragmentation occurred on Ag complexes as opposed to Pt complexes. The de-protonated mono-adducts further fragmented to lose a neutral base, thus numerous species around  $m/z$  307 were observed. In addition, product ions having a mass difference of 17 were observed, which is consistent with ammonia removal. The fragmented  $\text{H}_2$  and ammonia could have originated from either the dach ligand or the nucleobases. The exact origin of these fragmented species cannot be definitively established. Finally, the neutral base was also removed from the mono-adducts

during CID to produce the free Pt-dach complex at  $m/z$  307, as shown in Figure 4:4. The mass spectra, suggested structures and fragmentation pathways for each oxaliplatin-nucleobase adduct are shown in Figure 4:4-Figure 4:11, where the species derived from  $^{194}\text{Pt}$  are shown. The fragmentation pathways and structures shown are thought to be the most rational, but are not definitive.

#### 4.3.2.1 Oxaliplatin-Adenine Adduct Fragmentation

Figure 4:4 shows the MS/MS spectra of both the mono and di- adducts of adenine, where the main peaks have been labelled with the proposed species. Figure 4:4 was derived from the  $^{194}\text{Pt}$  parent species only, thus the Pt isotopic pattern was not observed for the parent ion. In addition, because only one isotope was selected for CID, only one product ion isotope was observed and not the whole suite of Pt isotopes.

Adenine base was lost from the di-adduct at  $m/z$  577 upon CID to yield the mono-adduct at  $m/z$  442 (see Figure 4:4a). The  $^{194}\text{Pt}$ -A adduct at  $m/z$  442 fragmented further to give a dominant product ion at  $m/z$  440, indicating the loss of  $\text{H}_2$  (see Figure 4:4b). The ions at  $m/z$  423 and 305 (Figure 4:4b) were thought to coincide with the loss of ammonia and adenine from the dominant product ion at  $m/z$  440 respectively. The fragmentation pathway of oxaliplatin-adenine adducts is summarised in Figure 4:5; very similar schemes were observed for the remaining three oxaliplatin-nucleobase adducts. The structures in Figure 4:5 show the Pt atom interacting with the N7 position of the adenine base (refer to Chapter 1 for purine and pyrimidine ring numbering system), which is the most likely position due to its high nucleophilicity.<sup>151, 164, 183</sup> However, the exact position of oxaliplatin-adenine interaction was not confirmed here and the structures shown are thought to be the most rational. The full scan mass spectrum of the oxaliplatin-adenine mono-base solution is shown in Figure 9:4 (Appendix 2.2). The mass spectra showing the fragmentation of the 195 and 196 Pt-AA and Pt-A species are shown in Figure 9:5-Figure 9:8 in Appendix 2.2. In addition, the MS<sup>3</sup> spectrum of the  $^{195}\text{Pt}$ -AA adduct is illustrated in Figure 9:9. These spectra were used to establish the fragmentation pathways illustrated in Figure 4:5.



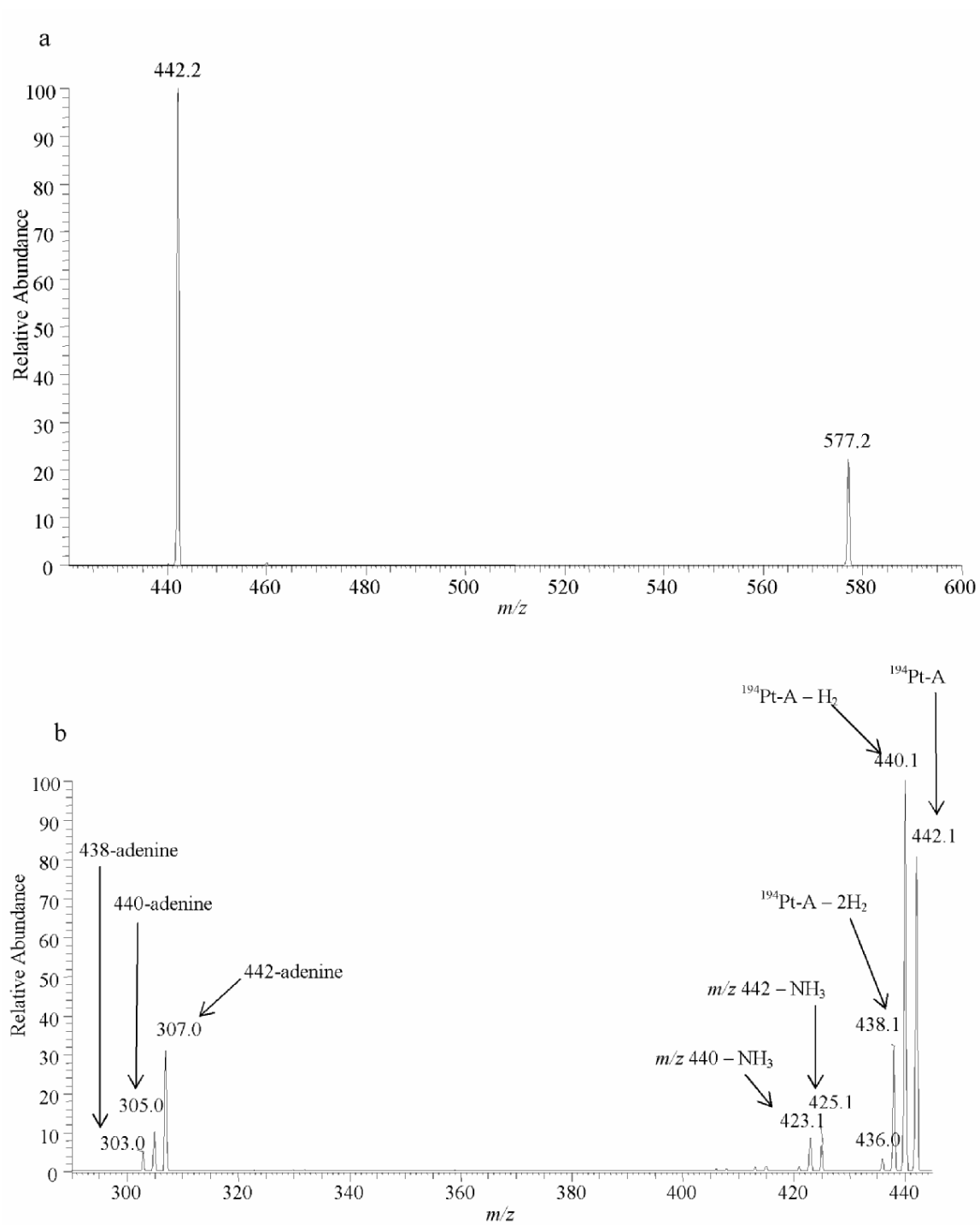


**Figure 4: MS/MS spectrum of product ions obtained by CID of: a)  $^{194}\text{Pt-AA}$  adduct at  $m/z\ 577$ , collision energy = 20 eV, isolation width = 1 Da. b)  $^{194}\text{Pt-A}$  adduct at  $m/z\ 442$ , collision energy = 20 eV, isolation width = 1 Da.**

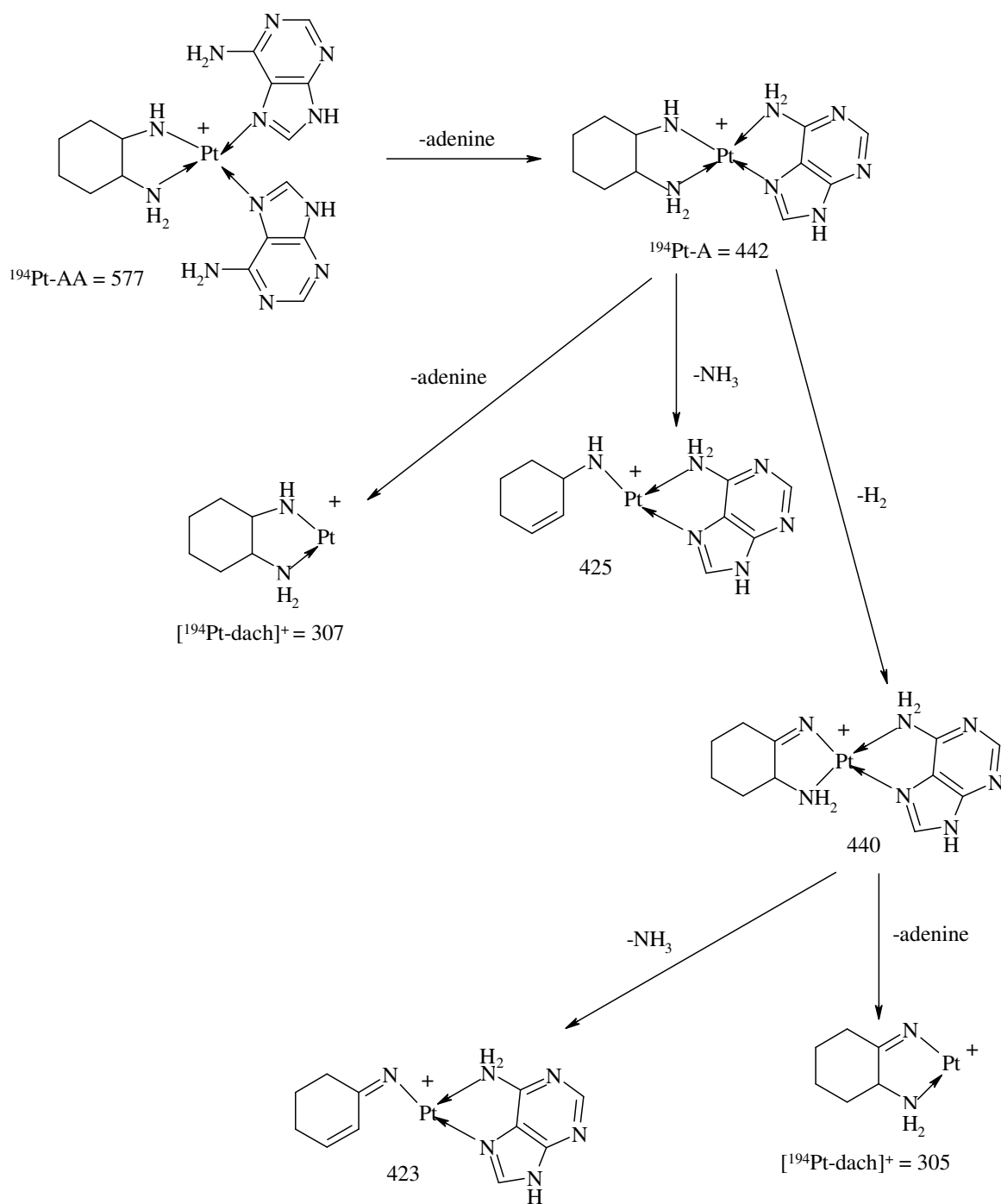
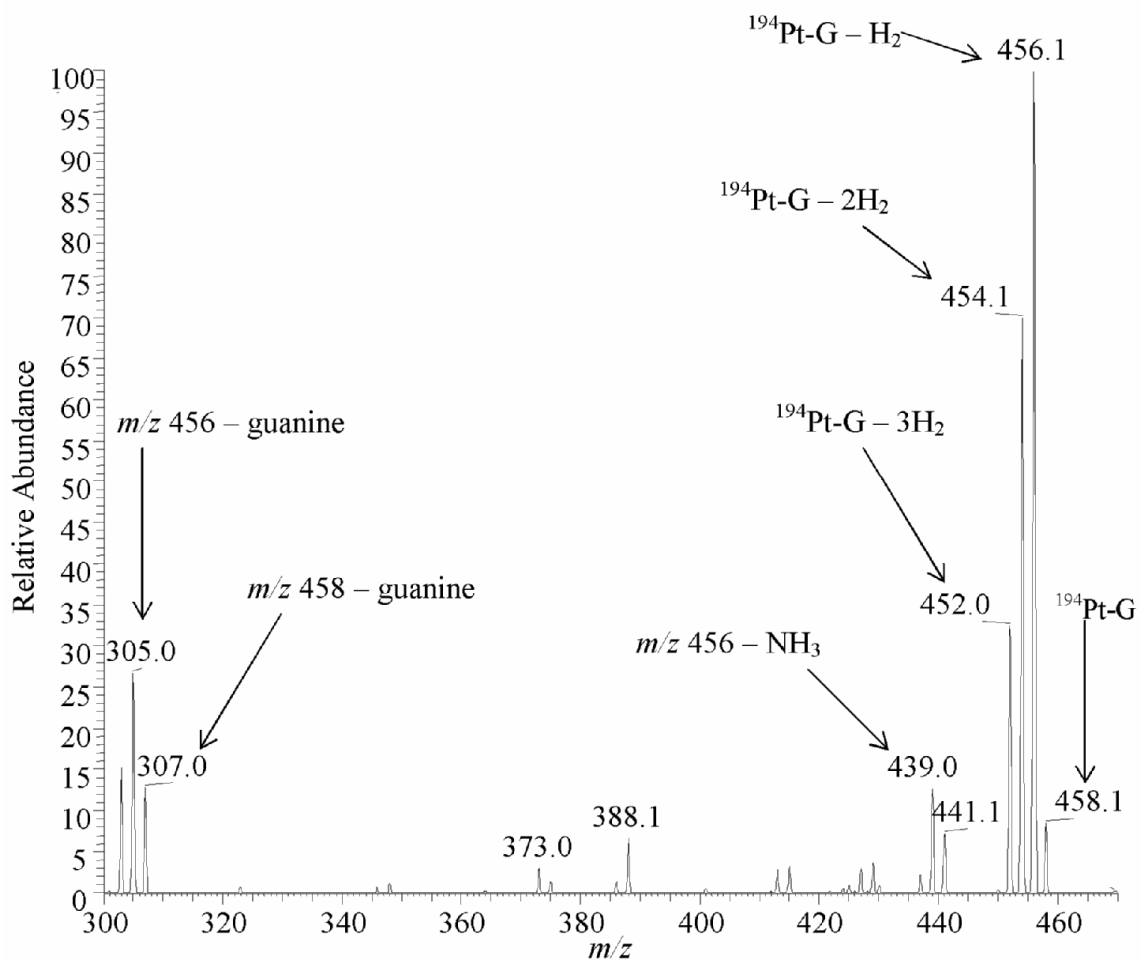


Figure 4:5: Proposed fragmentation pathway for  $^{194}\text{Pt}$ -adenine adducts.

#### 4.3.2.2 Oxaliplatin-Guanine Adduct Fragmentation

The  $^{194}\text{Pt-GG}$  ion at  $m/z$  609 was selected and fragmented to give the  $^{194}\text{Pt-G}$  product ion at  $m/z$  458, indicating the loss of guanine. Further fragmentation of the  $m/z$  458 ion resulted in product ions, which are shown in the  $\text{MS}^3$  spectrum in Figure 4:6. It should again be noted that the guanine mono-adduct fragmented to produce many product ions, but the most dominant was that at  $m/z$  456, resulting from the mono-adduct losing  $\text{H}_2$ . The summarised fragmentation pathway and suggested product ion structures are shown in Figure 4:7. Figure 9:11-Figure 9:17 in Appendix 2.2 show the spectra corresponding to the full scan mass spectrum of the guanine mono-base solution, the  $\text{MS/MS}$  and  $\text{MS}^3$  spectra corresponding to the 195 and 196 Pt-GG and Pt-G adducts.

As in the case of adenine, Figure 4:7 shows oxaliplatin forming adducts with the N7 position of guanine, which is thought to be the most likely site of drug interaction.<sup>151, 164</sup> In addition, the guanine oxygen atom is also shown to be interacting with the Pt centre *via* a dative bond. It has been reported that  $\text{cis-}[\text{Pt}(\text{NH}_3)_2]^{2+}$  complexes such as cisplatin interact with both the N7 and oxygen atom on guanine, which subsequently disrupts GC base pairing in double stranded DNA.<sup>193</sup> Considering both cisplatin and oxaliplatin behave similarly with DNA and proteins, it is not unrealistic to suspect that oxaliplatin also forms a dative bond with the oxygen atom on guanine as shown in Figure 4:7.



**Figure 4:6:** MS<sup>3</sup> spectrum of product ions obtained by CID of the  $^{194}\text{Pt-G}$  adduct at  $m/z$  458, which was obtained through CID of the  $^{194}\text{Pt-GG}$  ion at  $m/z$  609. Collision energy = 15 eV, isolation width = 1 Da.

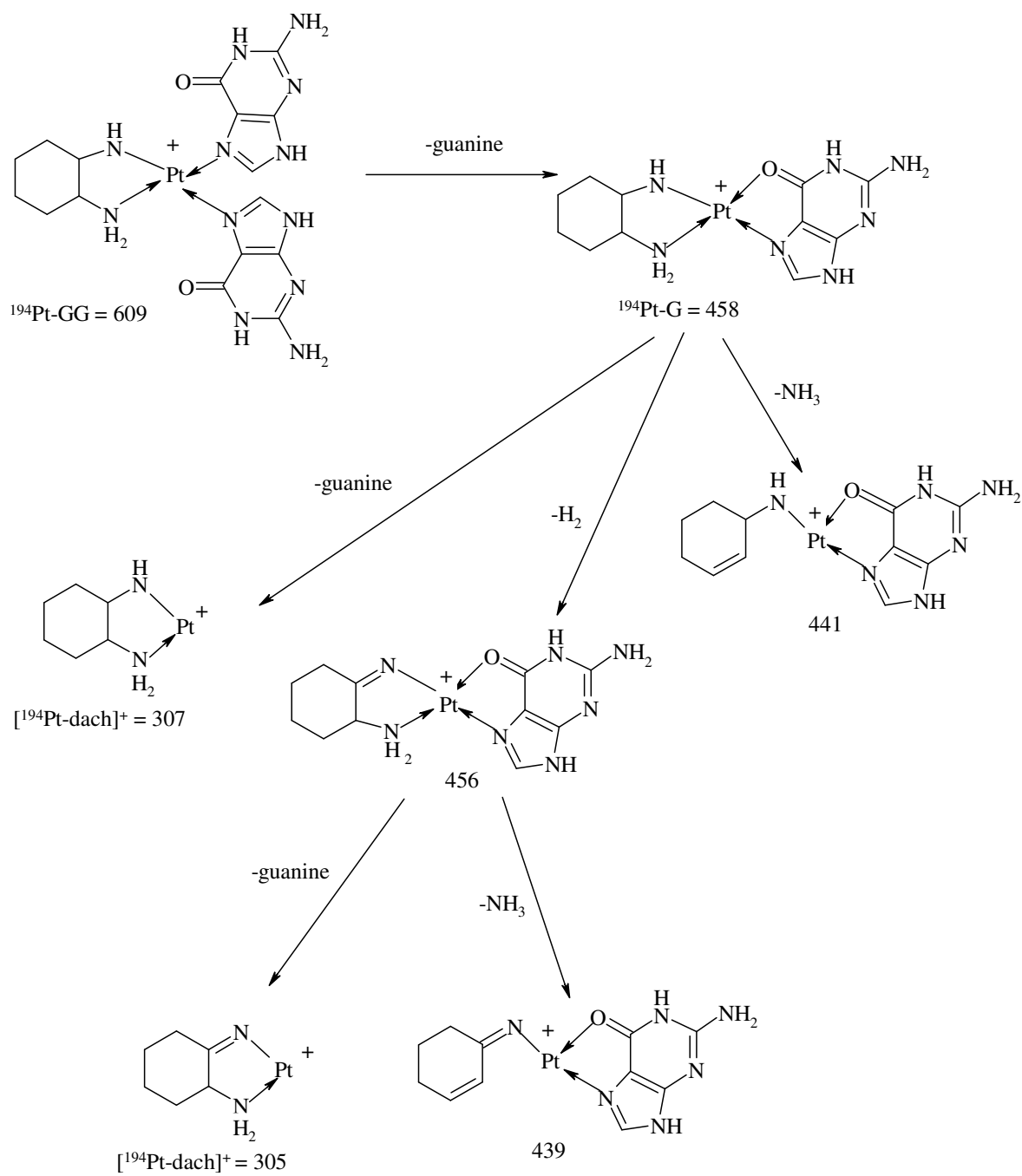


**Figure 4:7: Fragmentation pathway of oxaliplatin-guanine adducts.**

#### 4.3.2.3 Oxaliplatin-Thymine Adduct Fragmentation

Fragmentation data was obtained only for the thymine mono-adduct, since the di-adduct ( $m/z$  560) was present at very low levels and the signal for this ion was not sufficient to perform MS<sup>n</sup> experiments. It has already been suggested that oxaliplatin preferentially interacts with purine bases and this data suggests that the drug has a particularly low affinity for thymine, resulting in the very low abundance of the di-adduct. Figure 4:8 shows that the <sup>194</sup>Pt-T ion at  $m/z$  433 fragmented to give a dominant product ion at  $m/z$  429, which is consistent with the removal of 2H<sub>2</sub> from the mono-adduct. This is in contrast to the other three nucleobase adducts, which fragmented to form a dominant product ion with two less protons.

Figure 4:9 shows the proposed structures and fragmentation pathway, whilst the spectra corresponding to full scan mass spectrum of the oxaliplatin-thymine solution and CID of the 195 and <sup>196</sup>Pt-T adducts are in Appendix 2.2, Figure 9:18-Figure 9:20. There was very little reported in the literature regarding the co-ordination site of Pt drugs with thymine, presumably because these drugs do not readily interact with the pyrimidine bases. The Pt co-ordination site shown in Figure 4:9 is donated the N1 position. If the thymine was in the form of a nucleotide (i.e. bound to deoxyribose sugar), it would bind to the sugar through the N1 nitrogen atom (see Chapter 1 for nucleotide structures). However, since thymine is present without the sugar, the N1 position is the most nucleophilic, hence the most likely place for Pt co-ordination. Conversely, the other nitrogen atom in the thymine ring (N3) is adjacent to two carbonyl groups, which are highly electronegative and may result in the lone pair electrons on the N3 nitrogen atom being less available than those at the N1 position.

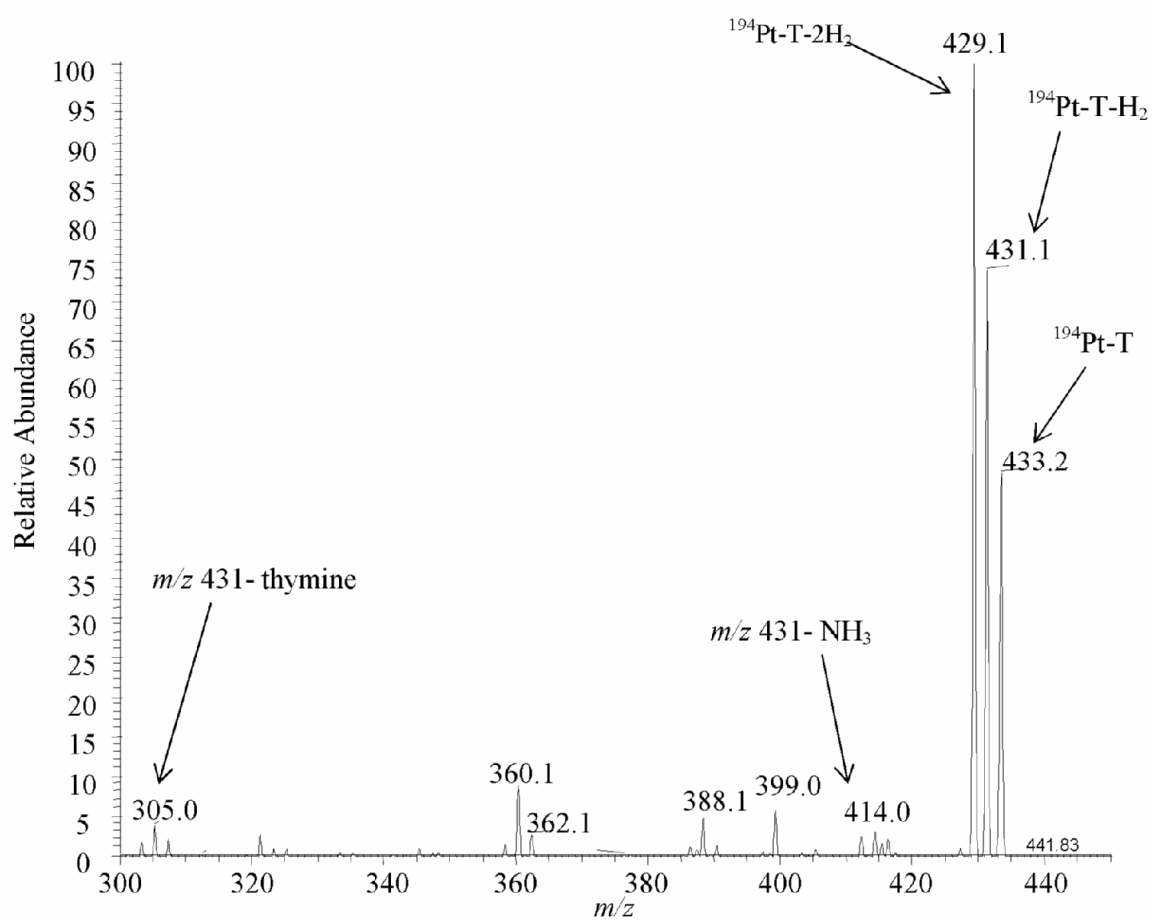
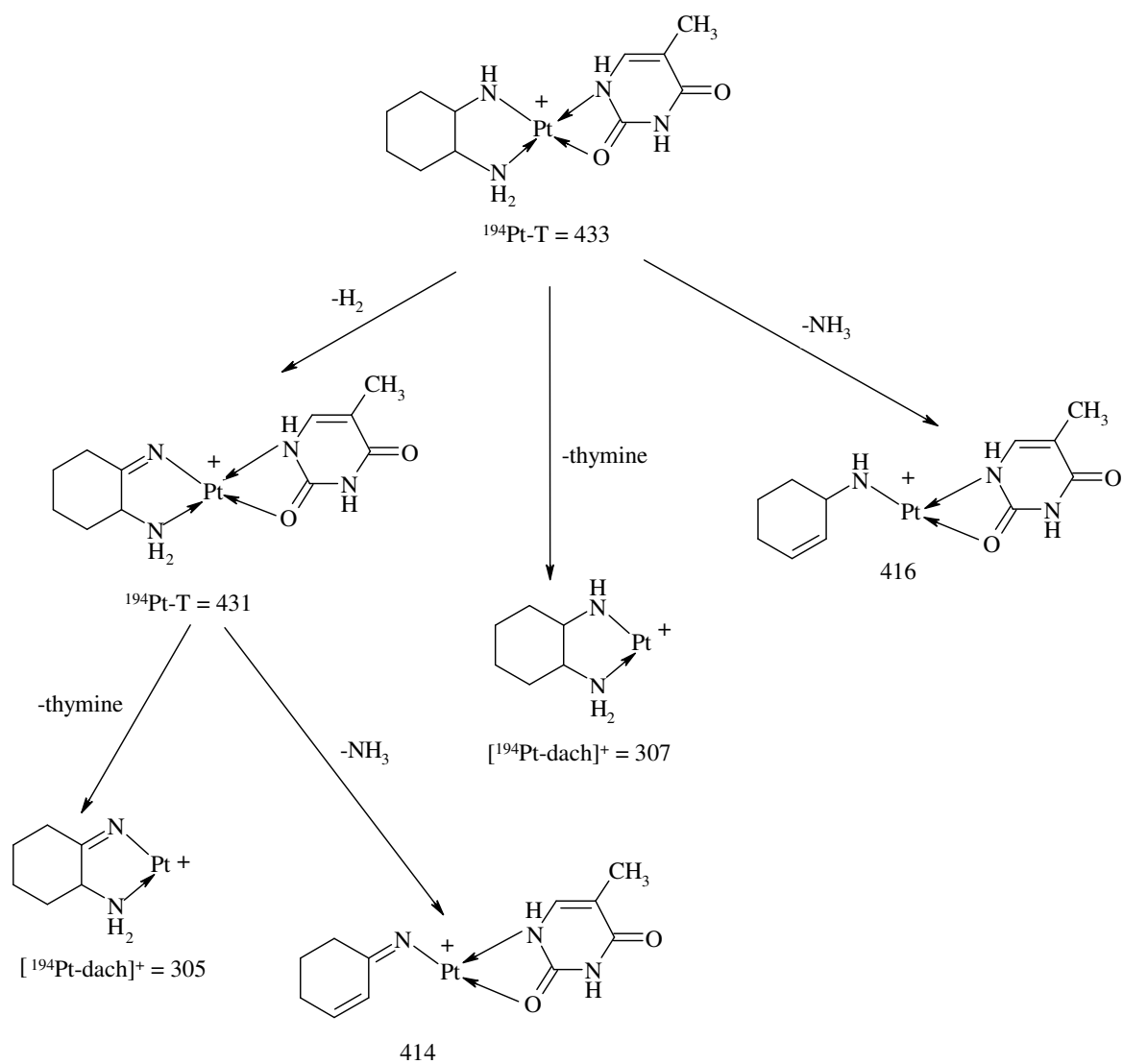


Figure 4:8: MS/MS spectrum of product ions obtained from CID of the  $^{194}\text{Pt-T}$  adduct at  $m/z$  433, collision energy = 20 eV, isolation width =1 Da.



**Figure 4:9: Fragmentation pathway for oxaliplatin-thymine adducts.**



#### 4.3.2.4 Oxaliplatin-Cytosine Adduct Fragmentation

Up until now discussions on adduct fragmentation have concentrated on the  $^{194}\text{Pt}$  species, however, the  $^{195}\text{Pt}$  species will be employed for the cytosine discussions to illustrate how all the Pt isotopic species behaved the same during CID. The MS/MS spectra for the mono and di-adduct are shown in Figure 4:10. Note, the spectrum in Figure 4:10a was obtained with an isolation width of 10 Da, thus all the parent ions  $\pm 5$  mass units of  $m/z$  530 would have been selected for MS/MS analysis, hence the presence of the ion at  $m/z$  531. The cluster of ions around  $m/z$  525 is most likely a result of proton removal from the various cytosine di-adducts during CID, with  $m/z$  525 being the most abundant. The summarised fragmentation pathway and suggested structures are shown in Figure 4:11. The spectra corresponding to the full scan and tandem MS of the  $^{196}\text{Pt-C}$  and  $^{195}\text{Pt-CC}$  species are shown in Appendix 2.2, Figure 9:21-Figure 9:23. The structures shown in Figure 4:11 show the oxaliplatin co-ordinating to cytosine through the N3 position in addition to the oxygen atom. The N3 position is nucleophilic making it a likely co-ordination site for Pt. In addition, it has been reported that trans-Pt species can co-ordinate to cytosine through the N3 atom,<sup>194</sup> as can cisplatin.<sup>183</sup>

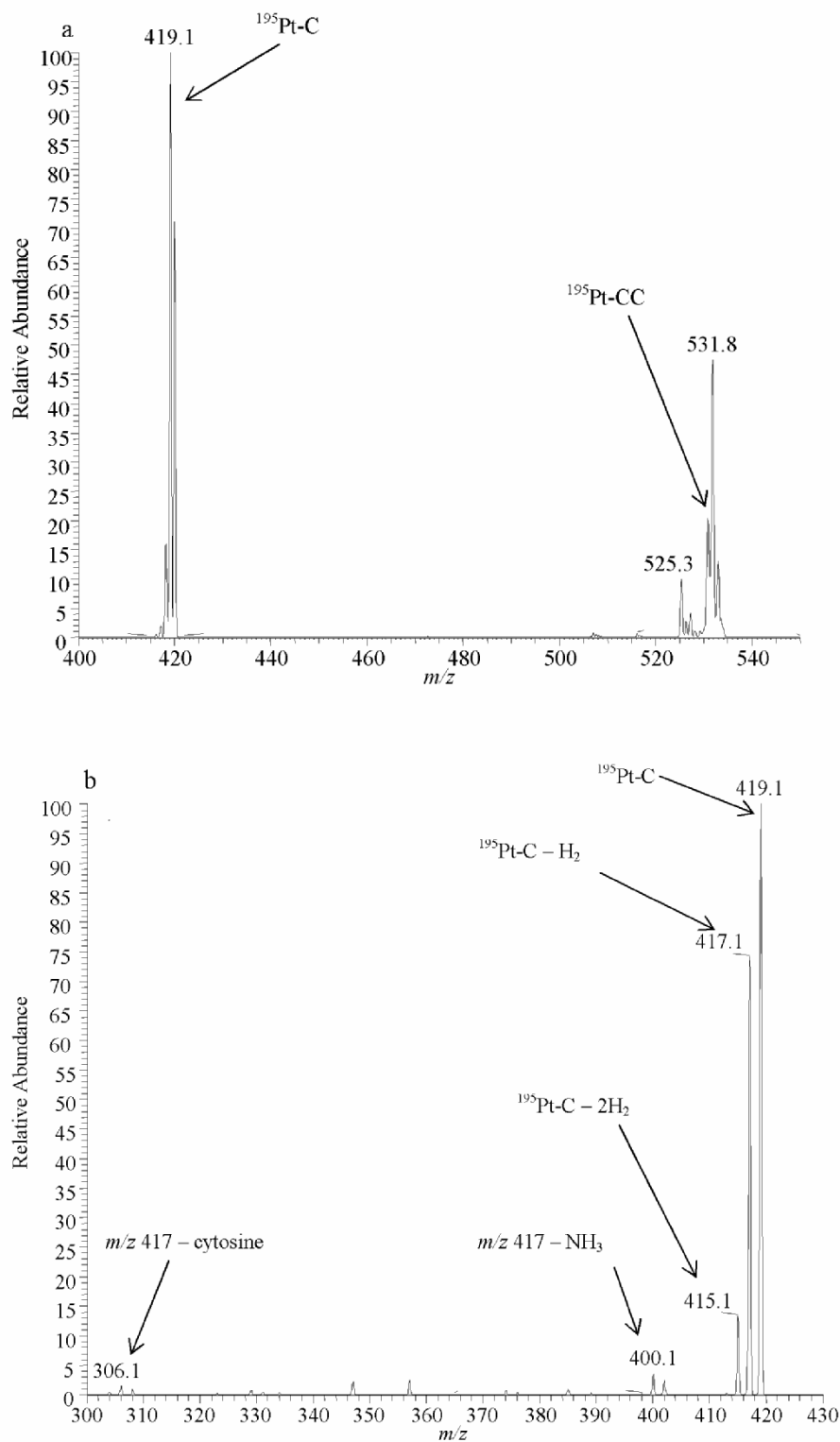


**Figure 4:10: MS/MS spectrum of product ions obtained by CID of: a)  $^{195}\text{Pt-CC}$  adduct at  $m/z$  530, collision energy = 10 eV, isolation width = 10 Da. b)  $^{195}\text{Pt-C}$  ion at  $m/z$  419, collision energy = 20 eV, isolation width = 1 Da.**

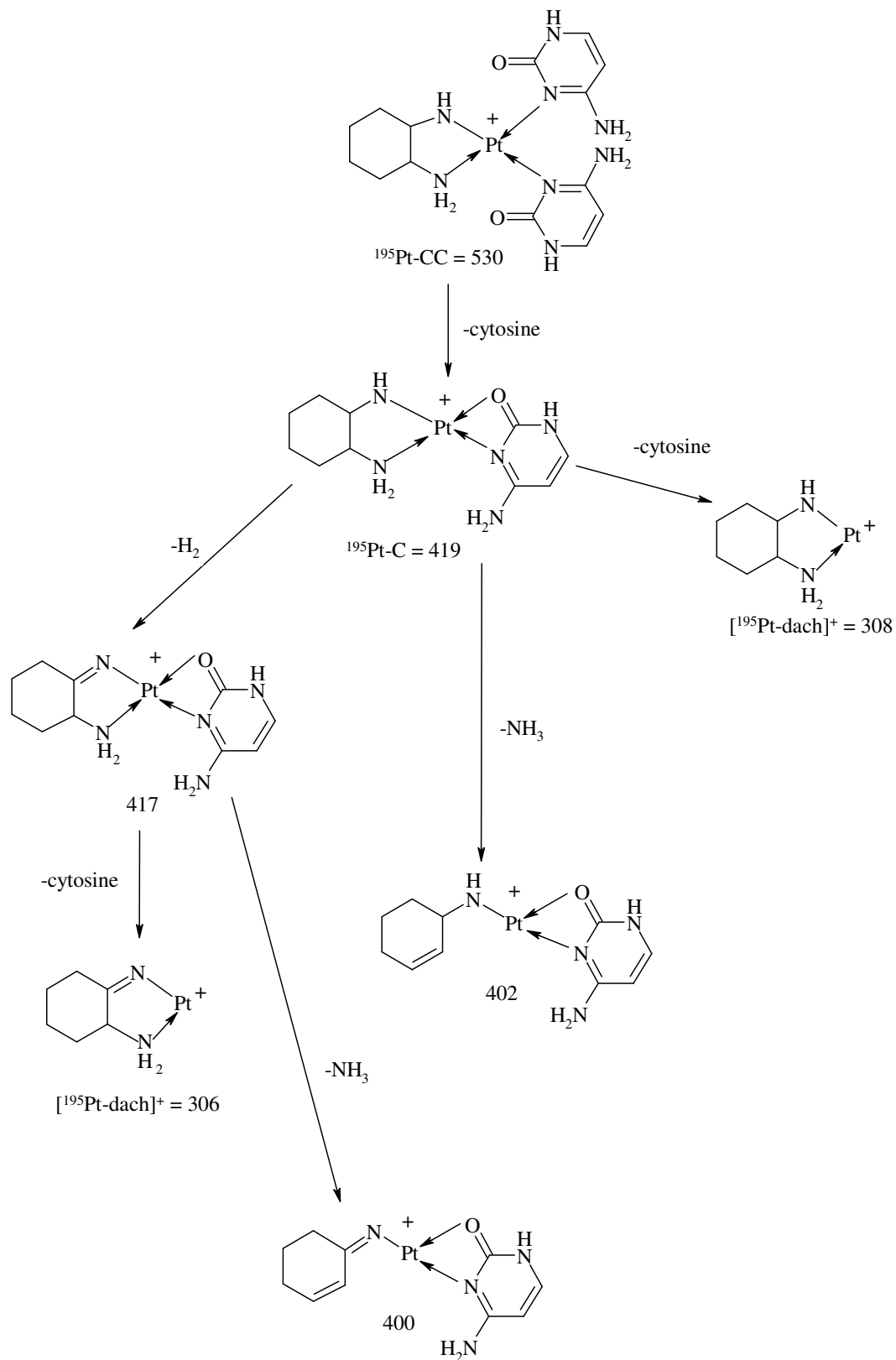


**Figure 4:11: Fragmentation pathway of the oxaliplatin-cytosine adducts.**

#### 4.3.2.5 Branching Diagrams

The successive loss of H<sub>2</sub>, ammonia and neutral nucleobases from the oxaliplatin adducts has been illustrated in Figure 4:4-Figure 4:11. Only small abundances of the protonated nucleobases were observed in the mass spectra upon CID, which was attributed to the nucleobases fragmenting to preferentially form neutral species. More importantly, this behaviour was consistent for all four nucleobase adducts. In addition to the product ions discussed above, numerous hydrated complexes of adenine and guanine were observed. It is known that Pt(II) complexes are more stable when co-ordinated to four ligands to produce square planar geometries. The reasons for this are well known and are discussed elsewhere.<sup>138</sup> Thus, the formation of the mono-adducts gives the Pt atom a co-ordination of three, prompting the addition of a fourth ligand such as water to the Pt centre, creating a stable square planar complex. Since guanine preferentially binds to the drug, followed by adenine the complexes, [Pt(dach)G(H<sub>2</sub>O)]<sup>+</sup> and [Pt(dach)A(H<sub>2</sub>O)]<sup>+</sup> were evident in the spectra, whilst the hydrated complexes of cytosine and thymine were less evident due to the much lower affinities of these nucleobases to oxaliplatin.

The branching diagrams in Figure 4:12 summarise the main adduct fragmentation, where the hydrated adenine and guanine fragments are included. The spectra showing the fragmentation of the three dominant Pt-G(H<sub>2</sub>O) species are shown in Appendix 2.2, Figure 9:24-Figure 9:26. In each case the hydrated adduct was selected with isolation width of 1 Da and fragmented to produce the corresponding Pt-G ion, which was selected and fragmented further in a MS<sup>3</sup> experiment to produce many product ions characteristic of the Pt-G species that were discussed above for the guanine mono-base solution. Unfortunately, tandem MS was not conducted on the Pt-A(H<sub>2</sub>O) species at *m/z* 460, thus the identity of this species could not be definitively proven and no product ions are indicated. Note that the three dominant Pt isotopic species are included in Figure 4:12 to further show how all three isotopic complexes behaved similarly.

It should be noted that Figure 4:12 shows a range of Pt-dach species, covering a mass range of approximately 4 Da that were formed upon fragmenting the mono-adducts. The range of Pt-dach masses were a consequence of proton loss from the mono-adducts. Each mono-

adduct lost between two and six protons upon CID to form various deprotonated mono-base adducts. These deprotonated mono-adducts then fragmented further, losing the nucleobase to produce several deprotonated Pt-dach species. This effect was illustrated in the fragmentation pathways in Figure 4:5, Figure 4:7, Figure 4:9 and Figure 4:11 above.

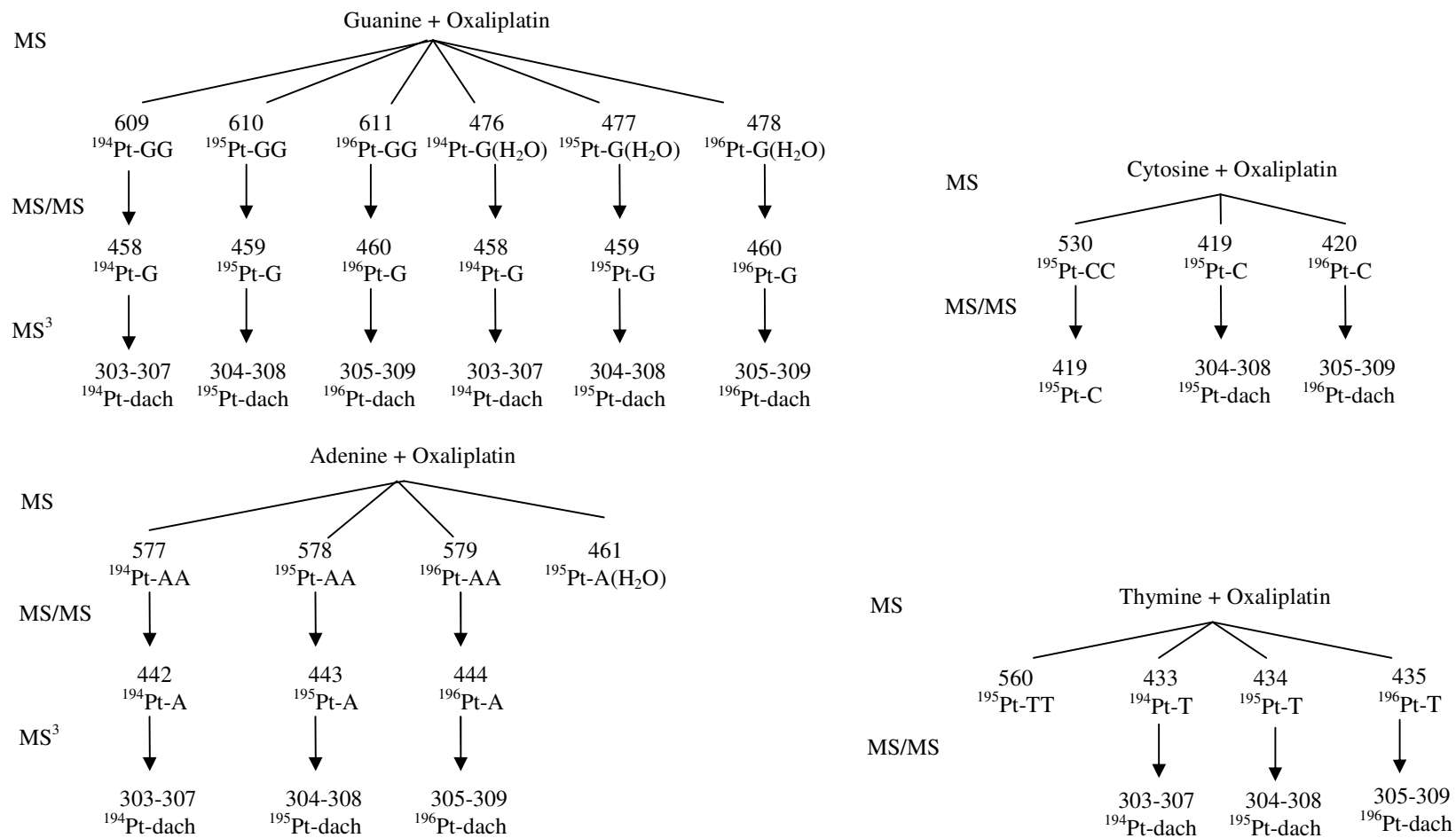


**Figure 4:12: Branching diagrams summarising the fragmentation of oxaliplatin nucleobase adducts.**

### 4.3.3 Isobaric Interferences

Until now  $^{194}\text{Pt}$  species have been primarily used as examples when discussing fragmentation pathways, the reason being to simplify the discussions by concentrating on one isotope. In addition these species were mainly free from isobaric interferences, which are inevitable in these situations where complex spectra with multiple isotopes are being analysed. However, serious isobaric overlaps did occur between some species and are discussed here. Such interferences could have resulted in misinterpretation of mass spectra and therefore incorrect fragmentation pathways being constructed.

The first such interference occurred between the  $^{194}\text{Pt-A(H}_2\text{O)}$  and  $^{196}\text{Pt-G}$  complexes, which both have the same nominal mass of 460. Evidence of the  $^{194}\text{Pt-A(H}_2\text{O)}$  species interfering with the  $^{196}\text{Pt-G}$  complex during single stage mass spectrometry can be seen in Figure 4:13, which shows a mass spectrum of the solution containing all four bases in the presence of excess drug. Figure 4:13 clearly shows the isotopes of the Pt-G species around  $m/z$  459. The dominant guanine mono-adduct contained  $^{195}\text{Pt}$ , suggesting that  $^{195}\text{Pt-G}$  at  $m/z$  459 should be most abundant of all the Pt-G ions. However, from Figure 4:13 the dominant ion was  $m/z$  460, which corresponds to  $^{196}\text{Pt-G}$ . This can be explained since the  $^{194}\text{Pt-A(H}_2\text{O)}$  ion, which also occurs at  $m/z$  460 was contributing to the  $^{196}\text{Pt-G}$  signal, causing this peak to be larger than expected. This isobaric interference was observed in Figure 4:13 since the sample contained all four bases. In the absence of adenine, three main peaks at  $m/z$  458, 459 and 460 were observed, corresponding to  $^{194}\text{Pt-G}$ ,  $^{195}\text{Pt-G}$  and  $^{196}\text{Pt-G}$  respectively. See Figure 4:14, which shows that the relative abundance of the 458 and 460 peaks were roughly equal, whilst the 459 peak was dominant as expected. Likewise, in the absence of guanine, the oxaliplatin-adenine solution displayed isotopic peaks around  $m/z$  461, again with the most abundant peak at  $m/z$  461 due to the presence of the dominant  $^{195}\text{Pt}$  isotope. Refer to Figure 9:4 in Appendix 2.2 for the full scan mass spectrum of the oxaliplatin-adenine mono-base solution. As already stated, tandem MS was not carried out on the Pt-A(H<sub>2</sub>O) complexes, thus the observed species in Figure 4:13 were not investigated further.

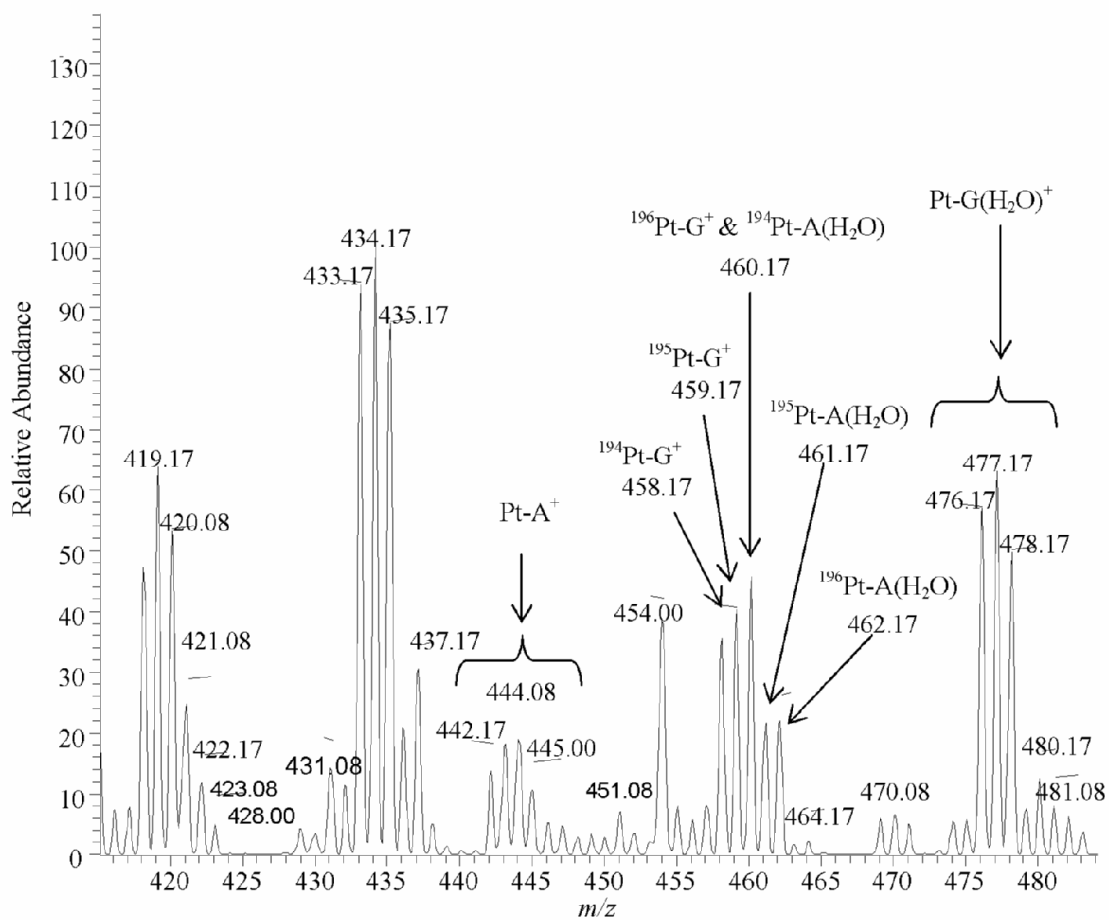


**Figure 4:13: Mass spectrum of product ions from the oxaliplatin solution containing all four nucleobases and an excess of drug, with the Pt-G and Pt-A(H<sub>2</sub>O) isotopes labelled.**



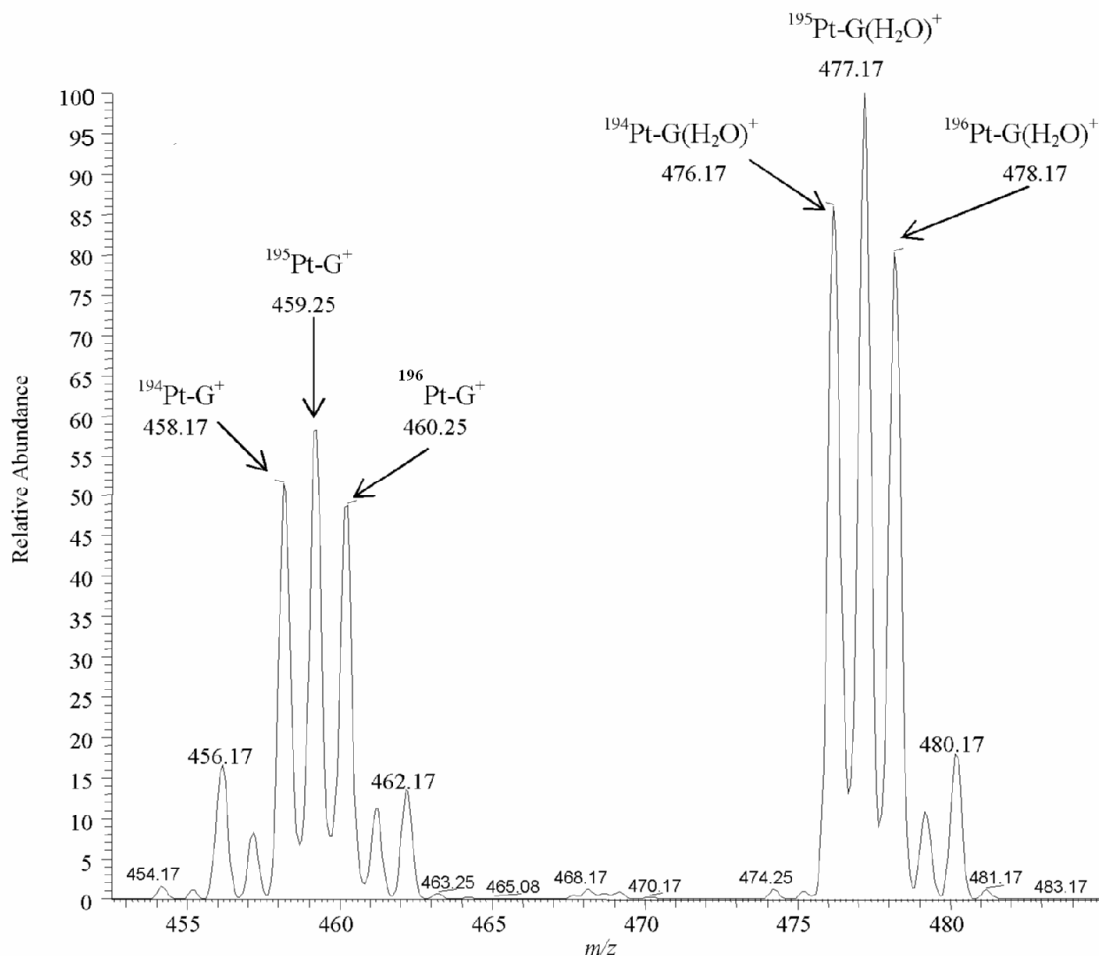


**Figure 4:14: Mass spectrum (expanded scale) of product ions obtained from the oxaliplatin-guanine mono-base solution, showing the Pt-G and Pt-G(H<sub>2</sub>O) isotopes.**

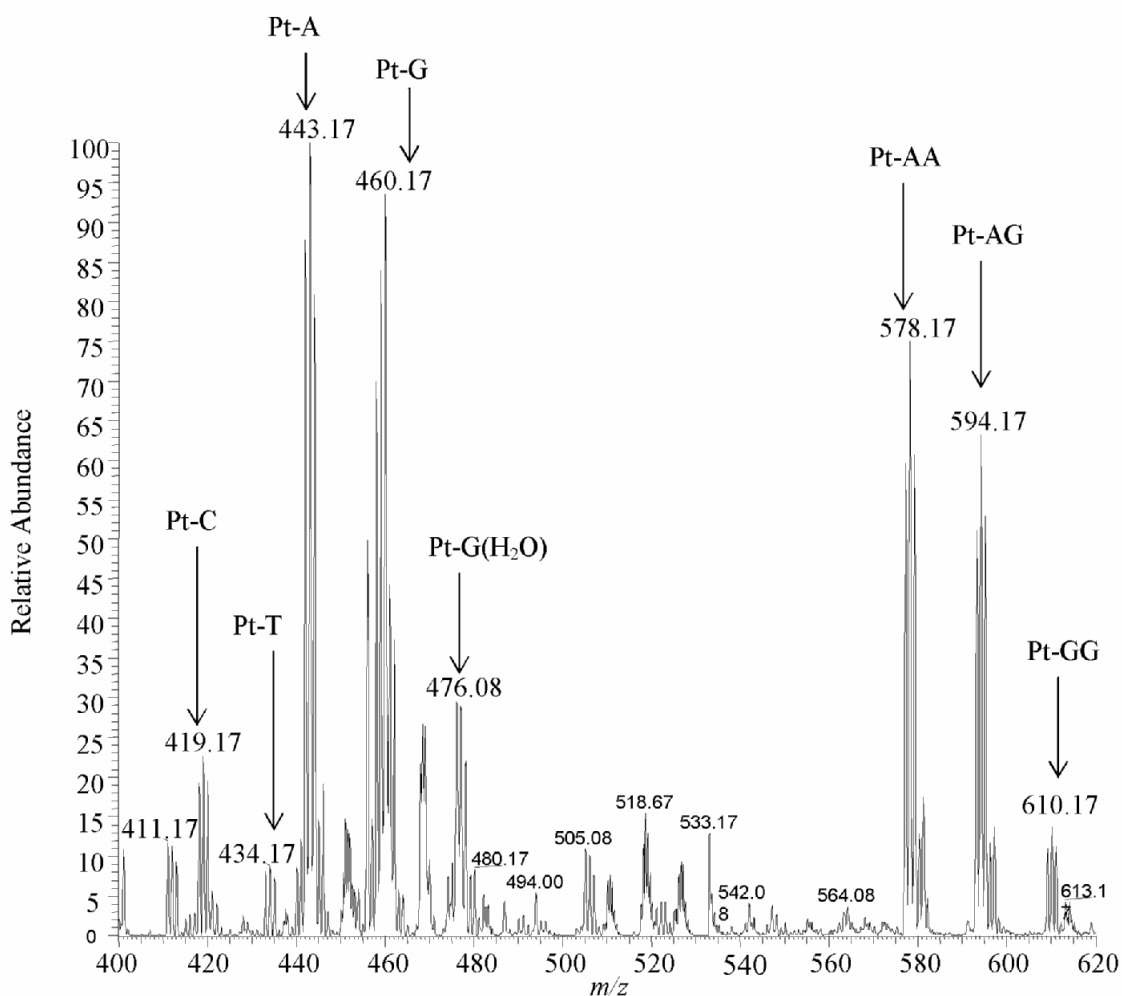
Such interferences were also possible with the  $^{196}\text{Pt-C}$  and  $[\text{}^{194}\text{Pt}(\text{dach})(\text{C}_2\text{O}_4)]\text{Na}^+$  drug adduct, both of which occur at the nominal mass of 420. The full scan mass spectrum of oxaliplatin in the absence of nucleobase is shown in Figure 4:1, where isotopic peaks around  $m/z$  420 are clearly visible and were thought to correspond to the oxaliplatin- $\text{Na}^+$  adduct. However, these species were not investigated further by tandem mass spectrometry.

Figure 9:22 in Appendix 2.2 shows the mass spectrum resulting from MS/MS of the  $^{196}\text{Pt-C}$  adduct. The mass spectrum clearly shows the mono-adduct losing  $\text{H}_2$  (product ions at  $m/z$  416 and 418) and cytosine base (product ions at  $m/z$  305, 307 and 309). These observations are consistent with the fragmentation pathways shown in Figure 4:11 and Figure 4:12, and suggest that although the  $^{196}\text{Pt-C}$  and  $[\text{}^{194}\text{Pt}(\text{dach})(\text{C}_2\text{O}_4)]\text{Na}^+$

species have the same nominal mass, the spectrum and fragmentation pathway of the  $^{196}\text{Pt-C}$  adduct can still be studied without interference from the oxaliplatin- $\text{Na}^+$  adduct.

#### 4.3.4 Oxaliplatin Binding in the Presence of all Four Nucleobases

Once it was confirmed that each base formed adducts with the drug, the solutions containing oxaliplatin together with all four bases were analysed. The full positive ion scan of the solution containing adenine, cytosine, guanine, thymine and oxaliplatin all at near equal molar concentrations is shown in Figure 4:15. The adducts corresponding to mono-adenine oxaliplatin ( $^{194}\text{Pt-A}$   $m/z$  442), mono-guanine oxaliplatin ( $^{194}\text{Pt-G}$   $m/z$  458) and the mono cytosine adduct ( $^{194}\text{Pt-C}$   $m/z$  418) were all observed in the mass spectrum shown in Figure 4:15. Initially the mono-adduct of thymine was thought to be absent from the spectrum, so tandem MS was not carried out on this species. However, later expansion of the full scan mass spectrum showed that the mono thymine adduct ( $^{194}\text{Pt-T}$   $m/z$  434) was present, but only at very low levels. It should therefore be noted that Appendix 2.3 does not include tandem MS data for the Pt-T species. The di-adducts of adenine ( $^{194}\text{Pt-AA}$ ) and guanine ( $^{194}\text{Pt-GG}$ ) were also observed at  $m/z$  577 and 609 respectively. In addition, the di-adduct containing both adenine and guanine ( $^{194}\text{Pt-AG}$   $m/z$  593) was also present. The identity of each adduct was again confirmed using multiple stage MS, refer to Figure 9:27-Figure 9:41 in Appendix 2.3 for all spectra corresponding to the fragmentation of the species observed in Figure 4:15. Various other peaks corresponding to unbound adenine, cytosine, guanine and thymine at  $m/z$  136, 112, 152, 127 respectively were also observed. Peaks corresponding to  $^{194}\text{Pt-dach}$  ( $m/z$  307), mono-solvated Pt-dach ( $[\text{}^{194}\text{Pt dach}(\text{H}_2\text{O})]^+$   $m/z$  324) and oxaliplatin ( $m/z$  398) were also present in solution as expected.



**Figure 4:15: Full scan mass spectrum of the oxaliplatin solution containing A, C, G and T. The oxaliplatin was present in a near equal molar concentration to each of the bases.**

Despite the abundance of adducts formed in the above solution, there were many adducts that were absent in the mixed nucleobase solution, but present in the individual nucleobase solutions. The absent adducts included the di-adducts of cytosine (Pt-CC  $m/z$  529) and thymine (Pt-TT  $m/z$  560). In addition, adducts corresponding to the mixed cytosine and thymine di-adducts were also absent. In summary, these results show when all four nucleobases were present in solution at near equi-molar concentration to the drug, oxaliplatin preferentially bound to guanine and adenine, as reported in the literature, cytosine formed adducts with oxaliplatin to a lesser extent, whilst the yield of thymine adducts was minimal.

Cytosine and thymine oxaliplatin adducts were clearly observed from mixed base solutions, but only when the drug was present in a large molar excess in relation to the

nucleobases. Figure 4:16 shows the full scan mass spectrum of the drug solution which contained all four nucleobases in the presence of excess drug.

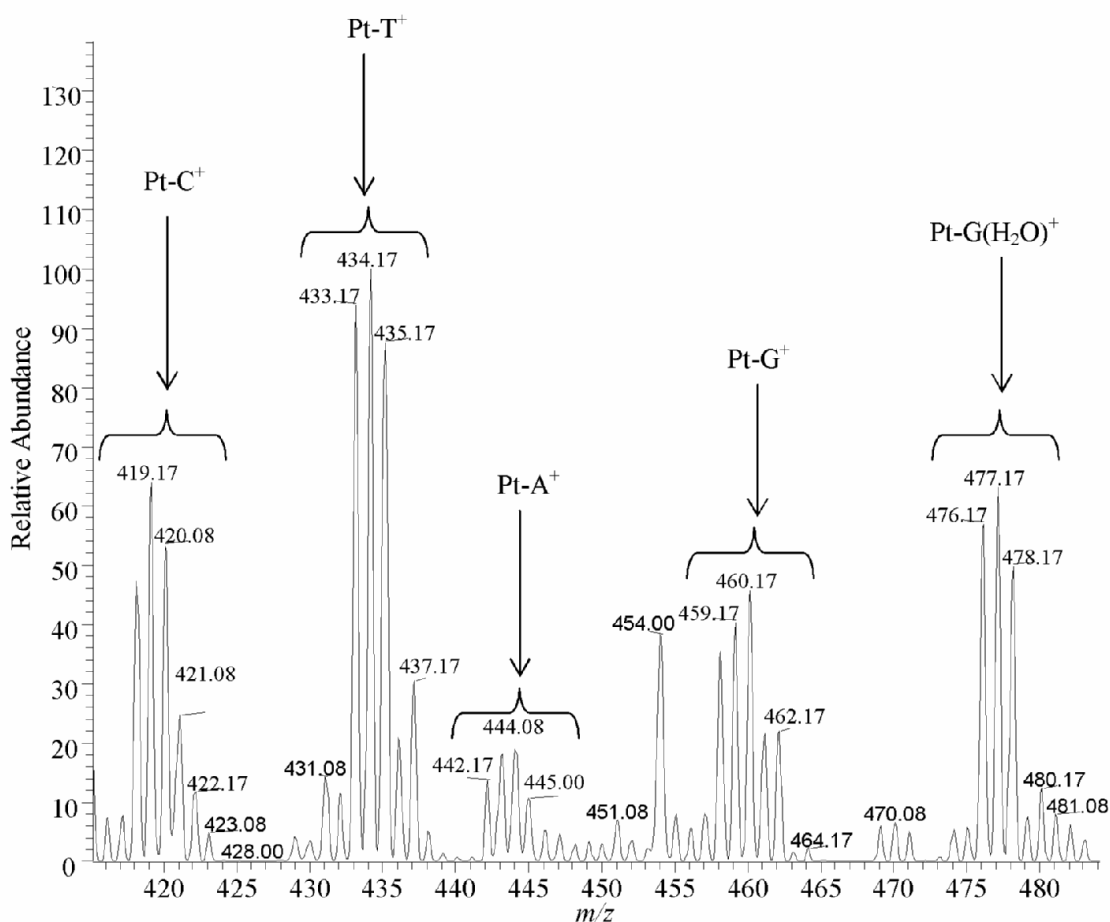


**Figure 4:16: Full scan mass spectrum of oxaliplatin solution containing excess drug with all four nucleobases.**

Numerous species were again present in the mass spectrum. Peaks at  $m/z$  112 and 127 corresponding to unbound cytosine and thymine respectively were again observed. Unbound adenine and guanine were also present at  $m/z$  136 and 152 respectively, but the signals for these two species were very much weaker. The weaker adenine and guanine signals may be another indicator of the stronger binding of these bases to the drug. Alternatively, the degree of ionisation of adenine and guanine may have been lower than that of thymine and cytosine, resulting in a weaker signal for these two bases (although there was no evidence to support this in the other spectra).

Mono-adducts corresponding to Pt-A ( $m/z$  442), Pt-C ( $m/z$  419), Pt-G ( $m/z$  458) and Pt-T ( $m/z$  433) were observed, as shown in Figure 4:16, but in contrast to equi-molar drug conditions, no di-adducts were evident. It has already been discussed that the

stepwise formation constants ( $K_n$ ) generally decreases in the order  $K_1 > K_2 > K_3 > \dots > K_n$  (where the subscript numbers represent the increasing ligand number) with successive ligand binding to a given metal.<sup>138</sup> Thus, the addition of subsequent ligands onto a metal becomes less favourable; there are several reasons for this effect. Firstly, steric hindrance may make it difficult for more than one ligand to bind to the metal. Secondly, as more ligands bind to a metal centre, the charge density of the metal decreases, hence, subsequent ligands have reduced affinity. Finally, both the number of available coordination sites (balanced by metals exhibiting a preferred coordination number) and free ligand concentration are reduced with each successive binding.<sup>138</sup> There are exceptions to these rules where structural changes to the co-ordination complex may increase subsequent formation constants.<sup>138</sup> The data presented in Figure 4:16 confirmed the general rules, when oxaliplatin was present in excess of the nucleobases, the drug preferentially bound to the minimum number of bases, which was one per drug molecule. The identity of the mono-adducts observed in Figure 4:16 was again confirmed with tandem mass spectrometry; the corresponding spectra are shown in Figure 9:42-Figure 9:47 in Appendix 2.4 and show how each of the mono-adduct species fragmented to produce the free drug along with numerous products consistent with the loss of protons and ammonia. The fragmentation pathways were similar to those outlined in Figure 4:12.

### 4.3.5 Preferential Binding Studies

The preferential binding of oxaliplatin with adenine and guanine was further investigated. The solution containing oxaliplatin with adenine and guanine only was infused into the mass spectrometer. The full scan MS of this sample is shown in Figure 4:17. The di-adduct containing both adenine and guanine (Pt-AG) was selected and fragmented with increasing collision energies. The relative intensities of the parent ion (Pt-AG) and product ions (Pt-G and Pt-A) were recorded with every 1 eV increase in collision energy between 0-30 eV. The branching diagram of the oxaliplatin solution containing adenine and guanine is illustrated in Figure 4:18, where the <sup>194</sup>Pt isotopic species was used to illustrate the fragmentation of the mixed di-adduct. The mass spectra showing the tandem MS of the mixed base di-adduct are shown in Figure 9:48-Figure 9:52 in Appendix 2.4. Further, Figure 9:48-Figure 9:52 show how the mixed

base di-adduct fragmented to produce two distinct product ions, further MS<sup>3</sup> experiments on the product ions to confirm the presence of adenine and guanine.

The <sup>195</sup>Pt species was used during the experiment, since it was the most abundant and gave the largest signal intensity. Thus the <sup>195</sup>Pt-AG (*m/z* 594), <sup>195</sup>Pt-G (*m/z* 459) and <sup>195</sup>Pt-A (*m/z* 443) species were monitored when applying the increasing collision energies. The aim of this experiment was to establish the preferential binding and affinity of adenine and guanine to the drug.

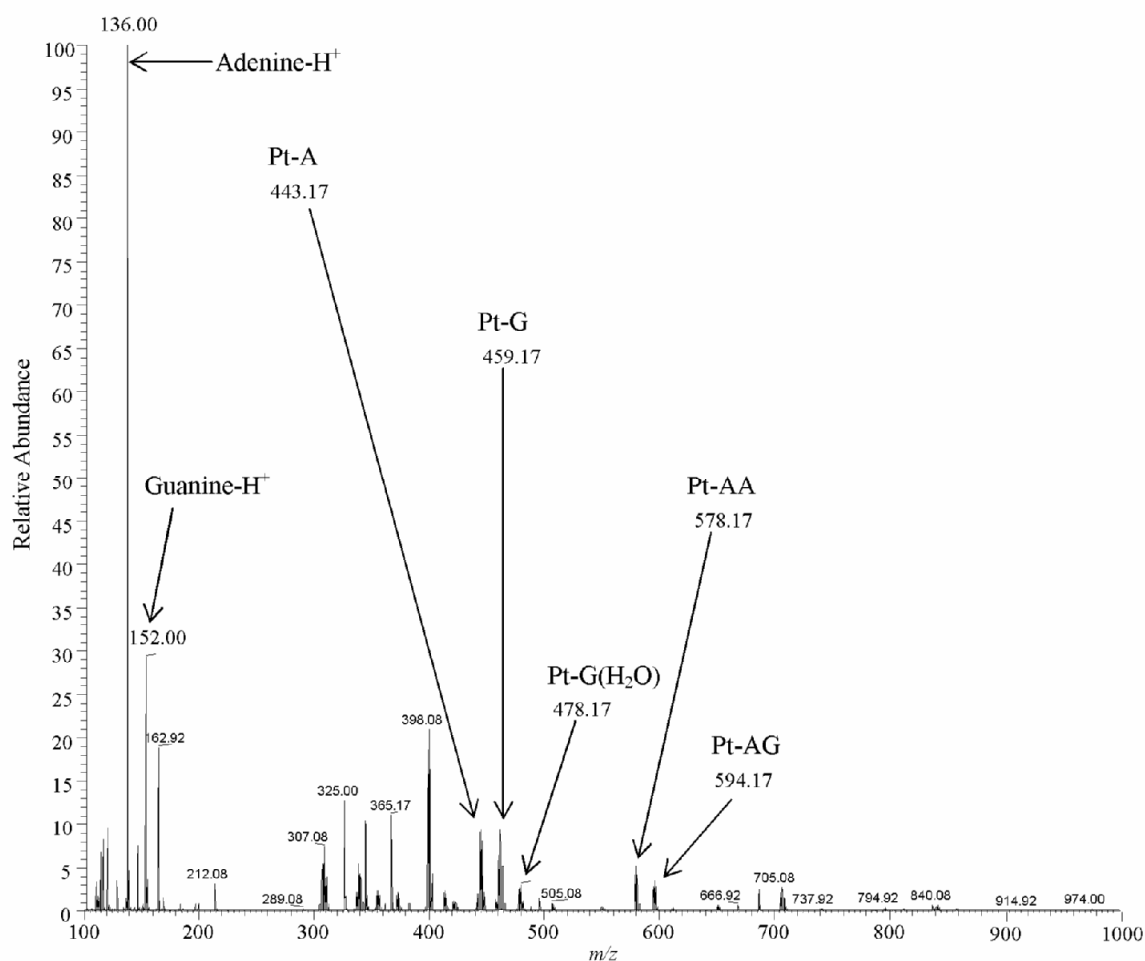


**Figure 4:17: Full positive ion scan of the adenine, guanine and oxaliplatin solution.**

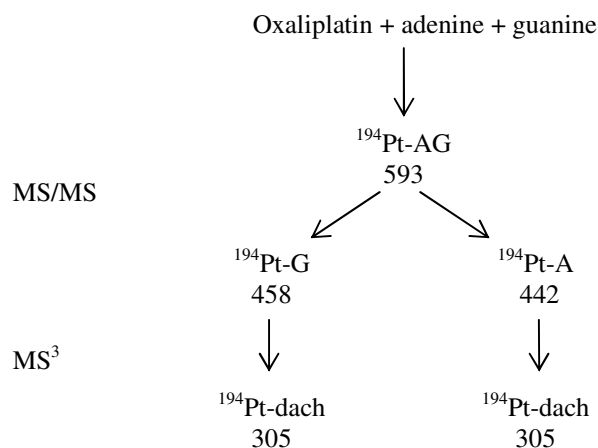


**Figure 4:18: Branching diagram summarising the fragmentation of the Pt-AG adduct.**

Upon increasing collision energy, the relative intensities of the product ions at  $m/z$  459 and 443 increased, whilst the parent ion ( $m/z$  594) intensity decreased as expected. However, the relative intensities of the two product ions were not equal; the Pt-G product ( $m/z$  459) was more abundant than the Pt-A ( $m/z$  443) ion. Thus, guanine appeared to bind more strongly to the drug, whilst the adenine base was more likely to fragment. Figure 4:19 shows the relative intensities of all three ions during each 1 eV increase in collision energy. Note that the parent ion was the most abundant ion up until ~20 eV, thus the x axis on Figure 4:19 only starts from 15 eV.

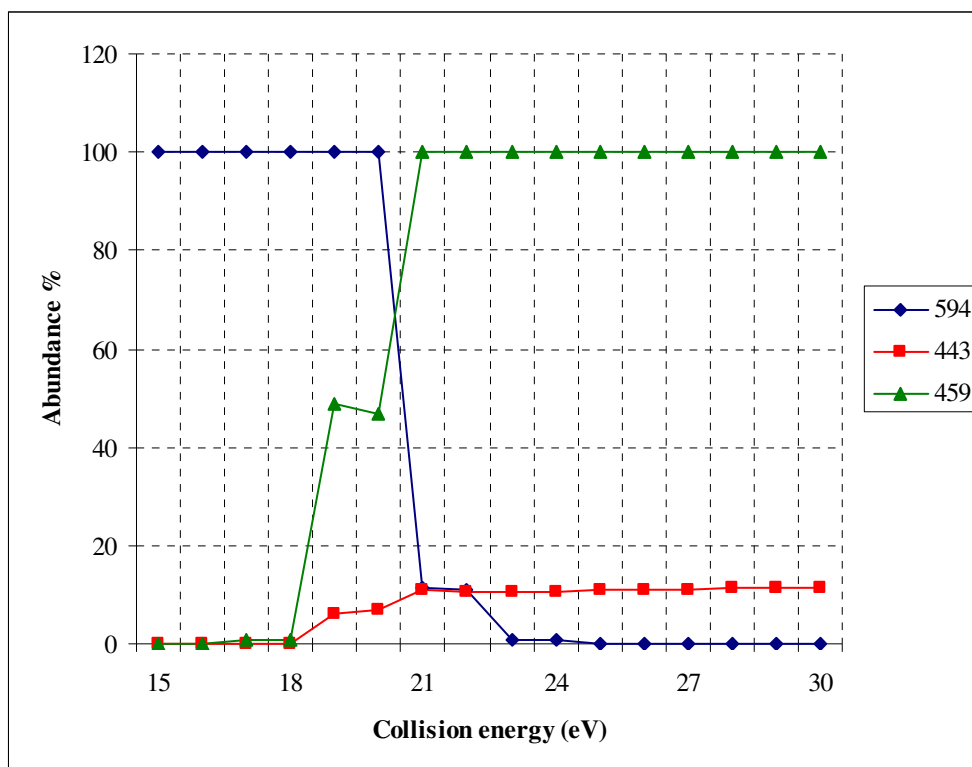


**Figure 4:19: Relative signal intensities of the Pt-AG adduct ( $m/z$  594) and the product ions, Pt-G ( $m/z$  459) and Pt-A ( $m/z$  443) during increasing collision energies.**

Figure 4:19 clearly illustrates that at lower collision energies (<20 eV), the Pt-AG adduct ( $m/z$  594) was the dominant species, but above this collision energy, the di-adduct parent ion fragmented to form two mono-adduct product ions (Pt-G and Pt-A).

Following the fragmentation of the Pt-AG adduct to form the Pt-A and Pt-G adducts, MS<sup>3</sup> experiments were conducted, where the <sup>195</sup>Pt-G ion was selected and fragmented with increasing increments of collision energy (1 eV increments) and the formation of the free drug (Pt-dach) and guanine base were monitored. The same was carried out on the <sup>195</sup>Pt-A product ion. From these two sets of data (not shown), adenine fragmented from the drug at ~13 eV and guanine at 15 eV, again confirming that guanine had greater affinity for oxaliplatin compared to adenine. Virtually no peaks corresponding to unbound adenine and guanine bases were observed during the above mass spectrometry analyses, again suggesting that the unbound bases fragmented as neutral species.

The experiment discussed above was only applied to the Pt-AG adduct and its corresponding product ions. A further area of research would be to conduct similar



studies on the other oxaliplatin adducts and compare the various nucleobase binding energies.

## 4.4 Summary

Oxaliplatin-nucleobase interactions have been studied using ESI-MS<sup>n</sup>. It was shown that oxaliplatin formed adducts with all four nucleobases when present individually in solution. Multiple stage ESI-MS data revealed successive losses of H<sub>2</sub>, ammonia and nucleobase from each of the adducts. The MS<sup>n</sup> data enabled detailed fragmentation pathways to be established for each oxaliplatin-nucleobase species and proposed structures for each product ion were presented, demonstrating the ease and versatility of ESI-MS for the study of drug-DNA interactions.

The preferential binding of oxaliplatin to adenine and guanine was also verified by the small proportion of cytosine and thymine adducts formed in the mixed base solution. However, mono-adducts of all four bases were clearly observed when the drug was present in excess of all four bases. This follows the expected pattern of mono-substitution being favoured over di-substitution and a reduction in successive formation constants. Further evidence of preferential adenine and guanine binding was shown when fragmenting the Pt-AG adduct. Two product ions corresponding to Pt-A and Pt-G were produced, however, the product corresponding to Pt-G was always dominant compared to Pt-A, suggesting that guanine remains attached to the metal, whilst adenine preferentially fragments, thus demonstrating that guanine has a greater affinity for the drug.

It has been illustrated that linear ion trap ESI-MS can be employed for investigating oxaliplatin-DNA interactions. However, it should be noted that this study was conducted on free nucleobases as oppose to oligonucleotides or intact genomic DNA. Factors such as steric restraints may well effect oxaliplatin interactions with nucleobases incorporated in the DNA molecule. The next step would be to conduct these experiments on oxaliplatin treated oligonucleotides or genomic DNA and establish whether drug-base affinity is the same as discussed above. Detailed structural information can be revealed in relatively short periods of time, although confirmation of

structure still requires use of other techniques such NMR, crystallography or computational methods.

## 5 Anion Exchange HPLC-ICP-MS of Single Nucleotide Polymorphisms (SNPs)

### 5.1 Introduction

Previous chapters have demonstrated how the ICP-MS signal of DNA can be enhanced by means of metal nano-particle labelling, or by Pt adducts in the case of cisplatin and oxaliplatin treated DNA. This chapter illustrates how ICP-MS can be used to detect DNA by measuring the P associated with the sugar-phosphate backbone. A HPLC separation method was developed for separating nucleic acids which differ only by one nucleobase. The HPLC was then coupled to an ICP-MS to allow for on-line separation and element specific detection. The HPLC separation method was used in conjunction with P ICP-MS detection methods, developed by Peter Winship in the Analytical Atomic Spectroscopy Research Group as part of his PhD thesis.<sup>179</sup> This chapter demonstrates the ease of coupling chromatographic systems to ICP-MS instruments and also the limitations of P detection by quadrupole ICP-MS.

Single nucleotide polymorphisms (SNPs) are defined as a single incorrect nucleobase insertion into a gene sequence. Such errors are usually harmless and can occur in coding and non-coding regions of the genome. SNPs are the most common genetic variation and are utilised in evolution studies and population genetics.<sup>195</sup> However, certain polymorphisms can cause serious genetic diseases.<sup>196</sup> In addition, the way individuals react towards pharmaceuticals is sometimes determined by a certain SNP. As a result, the study of SNPs is of great interest to medicine and pharmaceutical research.<sup>195-197</sup> The ability to identify SNPs and use them as a diagnostic tool for disease, tailoring drugs to suit people with a certain polymorphisms and to predict how people with certain SNP will react to a drug is a desirable goal.<sup>195-197</sup>

Two different 25 base length oligonucleotides (25 mers) were employed in this study. The oligonucleotides differed in base sequence by a single base thus mimicking a SNP. A method of separating the oligonucleotides by anion exchange HPLC coupled to ICP-MS is detailed, although numerous publications have reported on similar hyphenated techniques.<sup>1, 32, 60, 198, 199</sup> The HPLC system used in this study was complete with UV

absorption detection, thus the eluting oligonucleotides were detected due to the chromophores associated with the bases. In addition the ICP-MS detected the eluting nucleic acids by P which is contained in the sugar phosphate back bone. Two methods of P measurement were investigated; collision cell technology (CCT) with oxygen reaction gas and a cool plasma method. Collision/reaction cell methods of P measurement have been extensively studied using either O<sub>2</sub><sup>9, 10, 52, 59</sup> or He<sup>1, 61, 62</sup> reaction gases, these methods were discussed in detail in Chapter 1. To our knowledge this is the first time the cool plasma method has been employed for P determinations in conjunction with nucleic acids. Both UV absorption and elemental mass spectrometry data were obtained during the chromatographic separations. Both sets of data confirmed that the oligonucleotides could be resolved on an anion exchange column.

## 5.2 Instrumentation and Reagents

The oligonucleotide 25 mers used in this part of the investigation were obtained from Invitrogen (Paisley, UK), the sequences are shown in Table 5:1 and are denoted unmodified 25 mers 1 and 2. The oligonucleotides were not modified with any additional functional groups and were diluted in 20 mM Tris-HCl buffer at pH 9 to a concentration of 10 µM.

**Table 5:1: Oligonucleotide Base Sequences.**

Oligonucleotide	Sequence (5'→3')	Backbone Molecular Weight
Unmodified 25 mer 1	TGA AGA AAT TCA GTT CAT AGC TTG T	7696
Unmodified 25 mer 2	TGA AGA AAT TCA GTT CAT AGC TTG G	7721

The stationary phase was a TSKgel-DNA-NPR analytical column (7.5 cm x 4.6 mm) and was obtained from Tosoh Bioscience (Stuttgart, Germany). Tetramethylammonium hydroxide (TMAH) was from Apollo Scientific (Stockport, Cheshire). Citric acid (free acid) and tris base was obtained from Sigma Aldrich. Ammonium chloride was obtained from Fluka (Buchs, Switserland). Hydrochloric acid (super pure acid grade) was from Romil (Cambridge, UK). Oxygen gas (99.999% purity) was obtained from BOC (Sussex, UK).

A PQ ExCell ICP-MS instrument (Thermo Electron Corporation, Winsford, Cheshire) complete with a quadrupole mass filter and collision cell technology (CCT) was used

for the chromatographic detection of SNPs. The torch position and ion optics were tuned daily with  $^{115}\text{In}$  to obtain maximum sensitivity and stability. Both methods of P detection resulted in the formation of  $^{31}\text{P}^{16}\text{O}^+$  at  $m/z$  47 as discussed in Chapter 1.

An Agilent HP 1090 series 2 HPLC system (Agilent Technologies, Waldbronn, Germany) was employed for all separations. The instrument was equipped with a variable wavelength UV detector (Applied Biosystems) and HP3396A integrator (Hewlett Packard), which was employed for the acquisition of UV data. The same mobile phases and chromatographic conditions were used for both methods of P detection and are summarised in Table 5:2.

**Table 5:2: HPLC parameters for the separation of SNPs.**

Parameter	Setting	
Stationary Phase	TSKgel-DNA-NPR, 7.5 cm x 4.6 mm, 2.5 $\mu\text{m}$ particle size	
Mobile phase	A= 20 mM Tris-HCl, pH 9 B= 20 mM Tris + 0.3 M Citrate + 0.1 M $\text{NH}_4\text{Cl}$ , pH 9	
Flow rate	0.7 ml $\text{min}^{-1}$	
Injection Volume	5 $\mu\text{l}$	
Wavelength	257 nm	
Gradient	Time (min)	% B
	0	40
	15	100
	20	100
Stop time	20 minutes	
Post time	4 minutes	

The UV detector outlet was connected directly to the back of a 1 ml  $\text{min}^{-1}$  Conikal nebuliser (Glass Expansions, Australia), using PEEK tubing. The HPLC eluent was not split post column as detailed in Chapter 2, but the entire column eluent entered the nebuliser. An impact bead spray chamber was also employed; the schematic in Figure 5:1 illustrates the instrumental set-up. Any amendments to the chromatographic conditions will be stated where appropriate. The ICP-MS was operated in transient time resolved analysis (TRA) mode.

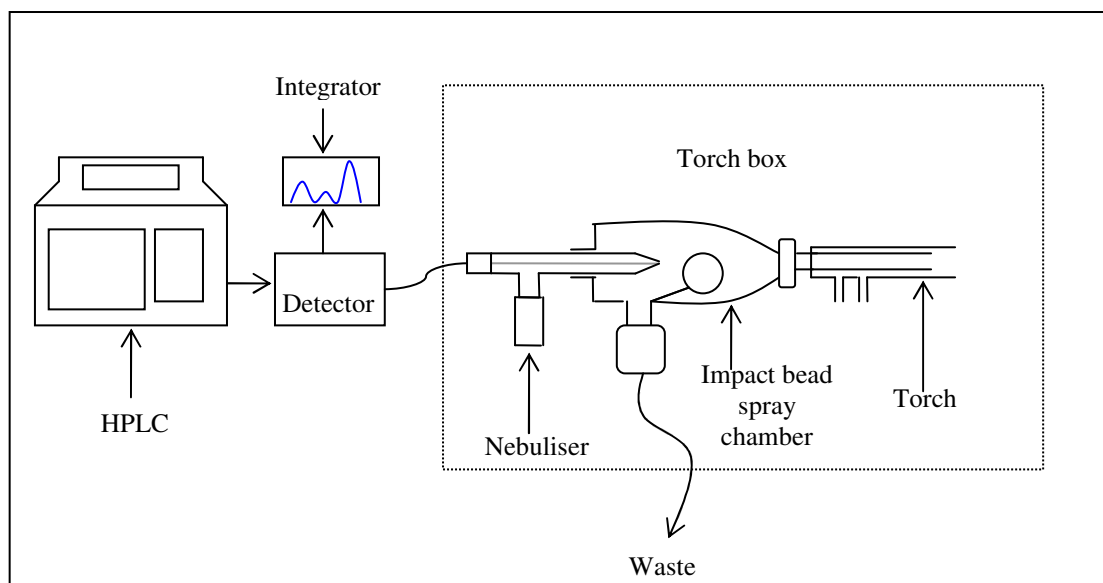


**Figure 5:1: Schematic showing the HPLC and ICP-MS coupling.**

### 5.2.1 Collision Cell

The first method investigated was that employing the CCT with O<sub>2</sub> as the reaction gas, the ICP-MS operating conditions are summarised in Table 5:3. Note that the forward power was maintained at 1350 W, but O<sub>2</sub> was bled into the collision cell to facilitate <sup>31</sup>P<sup>16</sup>O<sup>+</sup> formation.

**Table 5:3: ICP-MS operating parameters for the collision cell method.**

Parameter	Setting
Gas Flows	Cool = 12.8 l min <sup>-1</sup> Auxiliary = 0.80 l min <sup>-1</sup> Nebuliser = 1.0-1.2 l min <sup>-1</sup>
Quadrupole bias	+ 1V
Hexapole Bias	~+ 7.5-8 V
Forward Power	1350 W
CCT O <sub>2</sub> Flow	0.4 ml min <sup>-1</sup>
Nebuliser	1 ml min <sup>-1</sup> glass conikal
Spray Chamber	Impact bead

The formation of <sup>31</sup>P<sup>16</sup>O<sup>+</sup> and the removal of polyatomic interferences were discussed extensively in Chapter 1. It was noted that <sup>47</sup>Ti could potentially interfere with the <sup>31</sup>P<sup>16</sup>O<sup>+</sup> signal; however, it is unlikely that <sup>47</sup>Ti would be present in the biological samples and Ti readily reacts with oxygen to form an oxide at a higher *m/z* ratio.<sup>9</sup>

The Ion kinetic energy effect (IKEE) was implemented by adjusting the hexapole bias to 7.5-8 V. By applying a positive potential to the collision cell, the kinetic energy of the incoming plasma ions would be retarded, thus facilitating the reaction between  $^{31}\text{P}^+$  and  $\text{O}_2$  collision cell gas. The main P interferences at  $m/z$  31 are  $^1\text{H}^{14}\text{N}^{16}\text{O}$  and  $^{15}\text{N}^{16}\text{O}$  (refer to Table 1:5). It was discussed in section 1.3.2.2 that these polyatomic species do not react with  $\text{O}_2$  due to such reactions being thermodynamically and/or kinetically unfavourable, thus these polyatomic species would not interfere with  $^{31}\text{P}^{16}\text{O}^+$ .<sup>9</sup> For these reasons, kinetic energy discrimination (KED) was not implemented and the quadrupole was maintained at a lower potential to the collision cell (1 V).

### **5.2.2 Cool Plasma**

The second method employed a 'cool plasma' for measuring P, which used a forward power of 800 W compared with 1350 W used in standard and collision cell mode. At this lower forward power the formation of  $^{31}\text{P}^{16}\text{O}^+$  occurs in the plasma which can then be directly measured. The operating parameters for the cool plasma method were identical to those above (Table 5:3); however, the collision cell and  $\text{O}_2$  reaction gas was not used, and the forward power was decreased to 800 W. Since the collision cell was not in operation, the hexapole bias was at the default setting (-1.93V).

## **5.3 Results**

### **5.3.1 Collision Cell**

Retention time markers containing either 25 mer 1 or and 25 mer 2 were injected first using the chromatographic conditions outlined in Table 5:2. The UV chromatogram corresponding to 25 mer 1 is shown in Figure 5:2, in which a retention time of 15.24 minutes was observed.

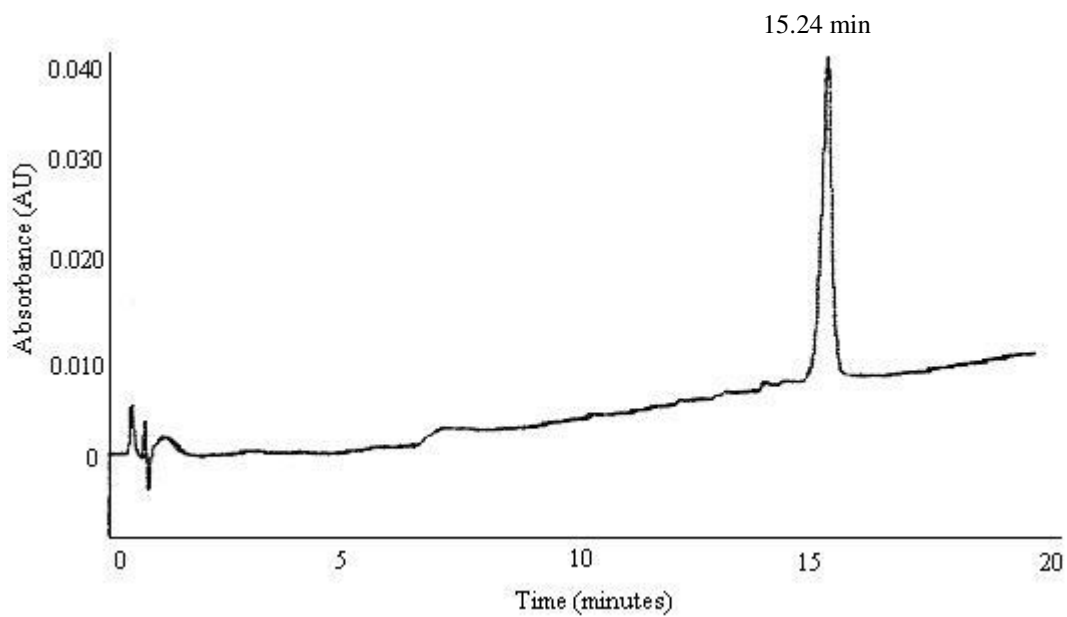


**Figure 5:2: UV chromatogram of 25 mer 1 (10  $\mu$ M) eluted from a TSKgel-DNA-NPR column (7.5 cm x 4.6 mm), 40% B at 0 mins, 100% B at 15 mins and 100% B at 20 mins, 0.7 ml min<sup>-1</sup>, 5  $\mu$ l injection volume, 260 nm detection wavelength.**

Figure 5:3 shows both the UV and mass spectrometry data during the elution of 25 mer 2. It should be noted that both sets of data were obtained during a single injection of the oligonucleotide. A retention time of 16.01 minutes was obtained for 25 mer 2.



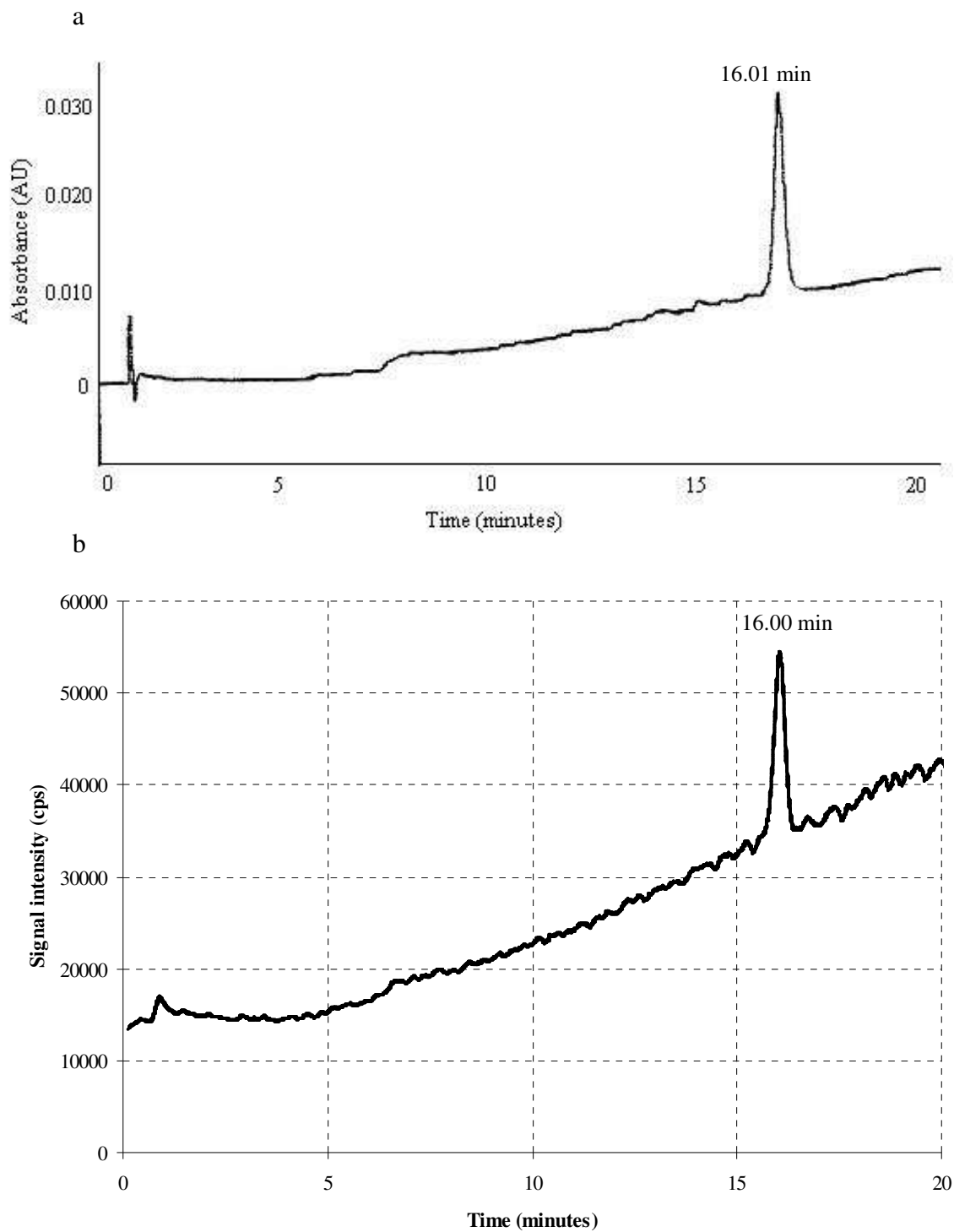
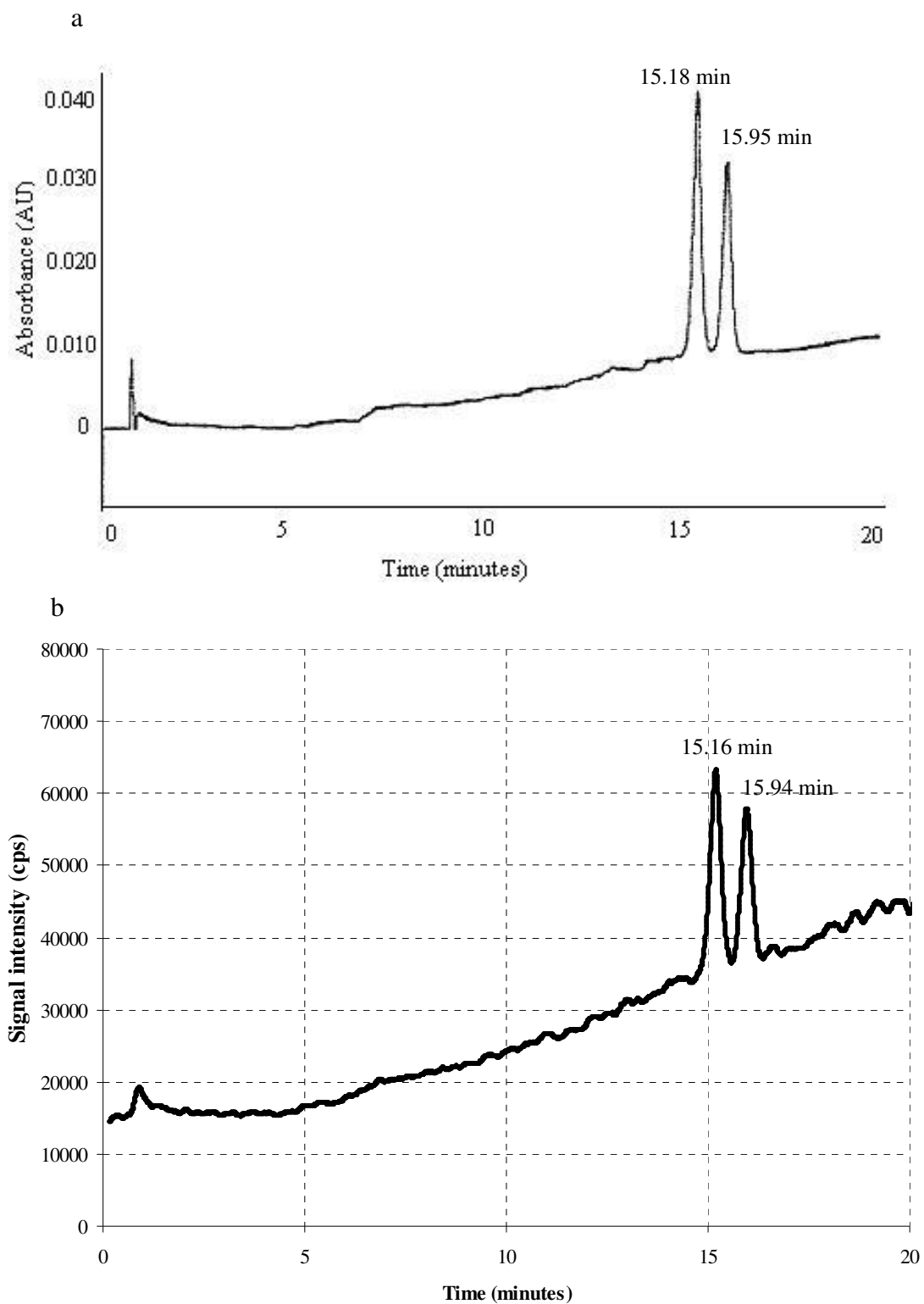


Figure 5:3: a) UV Chromatogram corresponding to 25 mer 2 (10  $\mu\text{M}$ ), 260 nm detection wavelength. b) ICP-MS  $^{47}\text{PO}$  signal intensity during elution of 25 mer 2. Oligonucleotide eluted from a TSKgel-DNA-NPR column (7.5 cm x 4.6 mm), 40%B at 0 mins, 100%B at 15 mins and 100% B at 20 mins, 0.7 ml  $\text{min}^{-1}$ , 5  $\mu\text{l}$  injection volume.

Once it was confirmed that the two 25 mer oligonucleotides had different retention times, a mixture containing the two 25 mers at equal concentrations (10  $\mu$ M) was injected and eluted using the same gradient. Refer to Figure 5:4 for the UV and mass spectrometry data for the 25 mer mixture, which shows how the two oligonucleotides were successfully resolved by the separation method. Again the two sets of data shown in Figure 5:4 were obtained simultaneously during a single injection of the oligonucleotide mixture.



**Figure 5:4:** a) UV Chromatogram corresponding the oligonucleotide mixture containing 25 mer 1 and 2, each at a concentration of 10  $\mu\text{M}$ , 260 nm detection wavelength. b) ICP-MS  $^{47}\text{PO}$  signal intensity during elution of the oligonucleotide mixture, eluted from a TSKgel-DNA-NPR column (7.5 cm x 4.6 mm), 40%B at 0 mins, 100%B at 15 mins and 100% B at 20 mins, 0.7 ml  $\text{min}^{-1}$ , 5  $\mu\text{l}$  injection volume.

Note that the retention times of the oligonucleotides in the  $^{31}\text{P}^{16}\text{O}$  chromatograms shown in Figure 5:3b and Figure 5:4b are slightly earlier than the retention times observed in the UV chromatograms, even though the UV detector was positioned before the ICP-MS. Since there was no communication between the HPLC and ICP-MS, the ICP-MS data acquisition was started manually upon injection of the samples, thus the retention times observed with ICP-MS may not be as accurate as the UV retention times.

The resolution between the two oligonucleotide peaks was calculated for both sets of data shown in Figure 5:4 and compared. Equation 3 was used for calculating resolution:

**Equation 3: Peak resolution**       $\text{Rs} = 2(\text{tr}_b - \text{tr}_a) / (\text{W}_a + \text{W}_b)$

Where:

tr = retention time of oligonucleotide

W = peak width

Subscript a and b refers to the first and second eluted oligonucleotide respectively.

Peak resolution using UV data:

$$\begin{aligned} \text{Rs} &= 2(15.95 - 15.18) / (0.4 + 0.4) \\ &= 1.93 \end{aligned}$$

Peak resolution using MS data:

$$\begin{aligned} \text{Rs} &= 2(15.94 - 15.16) / (0.44 + 0.44) \\ &= 1.77 \end{aligned}$$

The resolution values obtained for both sets of data were above 1.50, which suggests that the oligonucleotides were baseline resolved. Although the resolution for the ICP-MS data was slightly lower than that of the UV data, the loss in resolution was not significant and baseline resolution was still observed in the  $^{31}\text{P}^{16}\text{O}$  chromatogram.

The UV and ICP chromatograms exhibited a rising baseline. In the UV chromatograms this was attributed to the residual absorbance of citrate increasing as the citrate concentration increased during the gradient elution. Since ICP-MS is an elemental detector, the rising baseline in the  $^{31}\text{P}^{16}\text{O}$  chromatograms was thought to be caused by interferences at  $m/z$  47. The cause of interferences at this  $m/z$  was likely to be due to nitrogen and carbon based polyatomic species such as;  $^1\text{H}^{14}\text{N}^{16}\text{O}^{16}\text{O}$ ,  $^{15}\text{N}^{16}\text{O}^{16}\text{O}$ ,

$^{13}\text{C}^{18}\text{O}^{16}\text{O}$ ,  $^{12}\text{C}^{18}\text{O}^{16}\text{O}^1\text{H}$  and  $^{15}\text{N}^{14}\text{N}^{18}\text{O}$  resulting from the mobile phase.<sup>134</sup> Mobile phase B contained Tris base, ammonium chloride and citrate, so by increasing the proportion of mobile phase B during the gradient elution, the amount of nitrogen and carbon was also increasing. As a result, carbon and nitrogen based polyatomic interferences at  $m/z$  47 would have increased resulting in the rising baseline. Since KED was not implemented, both the  $^{31}\text{P}^{16}\text{O}^+$  analyte and the interfering polyatomic species from the plasma would have been transmitted through to the quadrupole and thus detected. In an attempt to reduce this rising baseline, the gradient was modified (Table 5:4) to use a lower percentage of mobile phase B, but the run time was extended to 30 minutes to compensate for the weaker gradient.

**Table 5:4: Shallow gradient used for the HPLC-ICP-MS of SNPs, in an attempt to reduce the rising baseline.**

Time (min)	% B
0	50
30	80

Figure 5:5 shows the UV chromatogram and  $^{31}\text{P}^{16}\text{O}^+$  signal intensity during elution of the oligonucleotide mixture using the above shallow gradient. Retention times of 22 and 24.40 minutes were observed in the UV data for 25 mers 1 and 2 respectively. The peaks were broad, but well resolved with a 2.4 minute time gap between them; this is a consequence of the longer retention time. The ICP-MS data shows retention times of 22.16 and 24.71 minutes which coincides with the UV chromatogram. However, the peaks were less well defined above the baseline. Although, a 2.4 minute peak separation is observed in the UV chromatogram, the peaks were broader and the calculated resolution (calculated using equation 3) was 1.78 and 1.96 for the UV and ICP data respectively, which was comparable to that obtained with the 20 minute gradient observed in Figure 5:4. In addition, although a lower background was achieved with the shallow gradient, more pronounced peaks were observed with the original 20 minute gradient (see Table 5:2). After considering the above factors it was decided that there was no analytical benefit of using the shallow gradient.

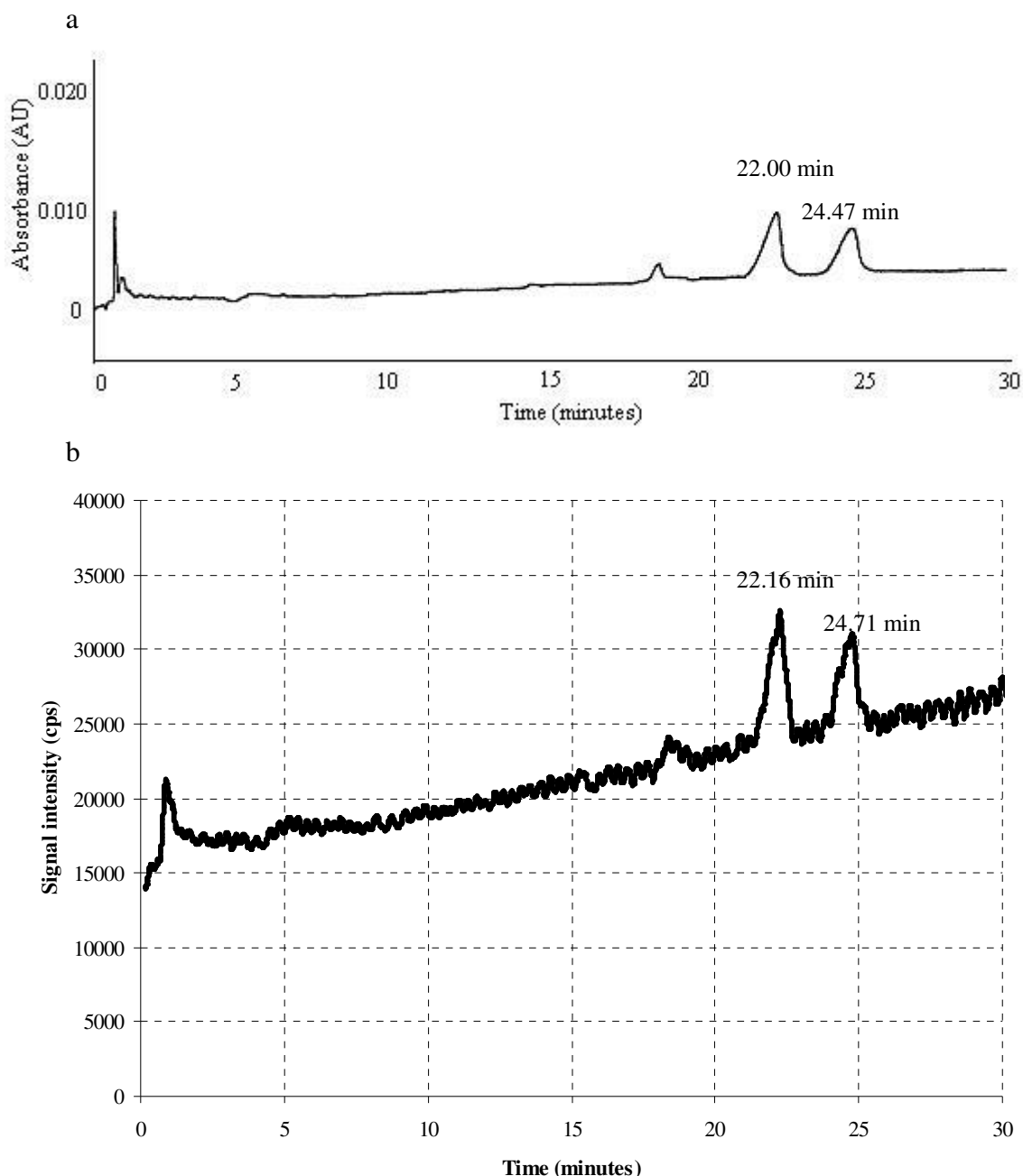


**Figure 5:5:** a) UV Chromatogram corresponding to 25 mer 1 and 2 each at a concentration of 10  $\mu\text{M}$ , 260 nm detection wavelength. b) ICP-MS  $^{47}\text{PO}$  signal intensity during elution of 25 mer 1 and 2 mixture. Oligonucleotide eluted from a TSKgel-DNA-NPR column (7.5 cm x 4.6 mm), 50%B at 0 min, 80%B at 30 min,  $0.7 \text{ ml min}^{-1}$ , 5  $\mu\text{l}$  injection volume.

The choice of mobile phase was an important consideration when coupling HPLC to ICP-MS, since the ICP is not tolerant to organic solvents and high concentration buffers.<sup>62</sup> This was a particularly important consideration when employing anion exchange chromatography, as this mode of separation employs an increasing gradient of salt to increase the ionic strength of the mobile phase and elute the analyte.<sup>36</sup> Sodium chloride, typically up to 1 M is traditionally used for increasing the eluent ionic

strength. However, ICP-MS is not compatible with high concentrations of Na since it has a low first ionisation potential and is preferentially ionised over other elements including the analyte in the plasma. As a result, the plasma equilibrium is disrupted and analyte ionisation is suppressed, this is known as a non-spectral interference.<sup>27, 200</sup> Alternative salts therefore have to be considered. In this method, the gradient consisted of a mixture of citrate and ammonium chloride. At pH 9, citrate carries a triple negative charge, making it a very strong anion. However, for reasons not fully understood, citrate alone would not elute the 25 mer oligonucleotides, so ammonium chloride was also added to the eluent. Such a mixture of salts appeared to be ICP-MS compatible.

Other mobile phases were investigated prior to the Tris, citrate and ammonium chloride gradient. One of the phases investigated was tetramethylammonium chloride (TMACl). This mobile phase appeared to be suitable for ICP-MS analysis but it resulted in severe suppression of the  $m/z$  47 signal, thus the oligonucleotides were not being detected by ICP-MS, even though UV data clearly showed the oligonucleotides eluting.

### **5.3.2 Cool Plasma**

The cool plasma method of  $^{31}\text{P}^{16}\text{O}^+$  detection was also applied to the detection of SNPs. This involved reducing the plasma forward power to 800 W. The 25 mer mixture was injected and eluted using the 20 minute gradient outlined in Table 5:2, refer to Figure 5:6 for the  $^{31}\text{P}^{16}\text{O}^+$  chromatogram. The UV chromatogram is not shown, since it is identical to that seen in Figure 5:4a above.

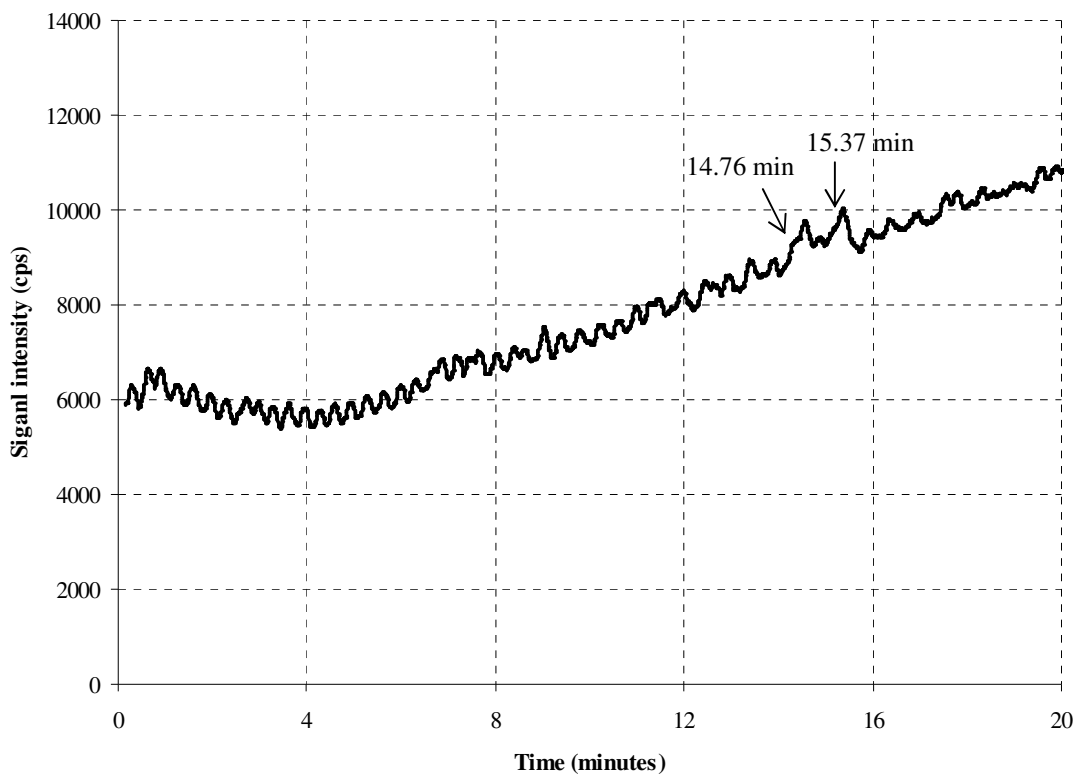


**Figure 5:6:** ICP-MS  $^{31}\text{P}^{16}\text{O}$  signal intensity during elution of 25 mer 1 and 2 mixture ( $10\ \mu\text{M}$ ). Oligonucleotide eluted from a TSKgel-DNA-NPR column ( $7.5\ \text{cm} \times 4.6\ \text{mm}$ ), 40%B at 0 mins, 100%B at 15 mins and 100% B at 20 mins,  $0.7\ \text{ml}\ \text{min}^{-1}$ ,  $5\ \mu\text{l}$  injection volume.

The oligonucleotides eluted around 15 minutes as shown in the UV chromatogram in Figure 5:4a, but Figure 5:6 only shows two very weak  $^{31}\text{P}^{16}\text{O}^+$  peaks at 14.76 and 15.37 minutes. The shallow gradient which was outlined in Table 5:4 was also applied to the cool plasma method and retention times of approximately 22 and 24 minutes were observed in the UV data, but no  $^{31}\text{P}^{16}\text{O}^+$  peaks were observed when this gradient was used in conjunction with cool plasma method. The UV data confirmed that the oligonucleotides were eluting, but the ICP-MS data did not exhibit any  $^{31}\text{P}^{16}\text{O}^+$  peaks at the corresponding retention times. One possible explanation is that at a low forward power, the plasma was unable to cope with the high matrix which consisted of high concentration salts from the mobile phase. The formation of  $^{31}\text{P}^{16}\text{O}^+$  may have been suppressed in the plasma under such conditions, resulting in the absence of  $^{31}\text{P}^{16}\text{O}^+$  peaks as the oligonucleotides eluted.



#### 5.4 Summary for Anion Exchange HPLC-ICP-MS of SNP's

A method of separating and detecting DNA SNPs by HPLC-ICP-MS has been demonstrated. Anion exchange chromatography was successful in resolving oligonucleotides that differed in sequence by one base. In addition, ICP-MS with CCT was successful in detecting the P signal associated with DNA. Both UV and ICP-MS data was acquired simultaneously during the separation of the oligonucleotides, which enabled the retention times to be verified. Both sets of data corresponded well in terms of retention time.

Two methods of P determination were discussed. The first method employed CCT and O<sub>2</sub> reaction gas to convert P into <sup>31</sup>P<sup>16</sup>O<sup>+</sup>. This method was successful in detecting the eluted oligonucleotides, with both species baseline resolved. More importantly, resolution was not lost upon the coupling of the HPLC to the ICP-MS. The cool plasma method of P detection was not successful. Even though the UV data confirmed that the oligonucleotides were eluting, the P signal in the ICP-MS data was very weak. As discussed above, the likely explanation for this is that the reduced plasma power and high matrix levels suppressed PO formation.

A rising baseline was observed in the ICP data throughout the separation step, which was attributed to nitrogen and carbon based polyatomic interferences at *m/z* 47. The increasing gradient of tris-HCl, citrate and ammonium chloride was thought to be the cause of these increasing interferences. By employing KED the polyatomic interferences may have been prevented from entering the quadrupole, thus minimising the rising baseline at *m/z* 47 during the gradient elution. The application of KED is an aspect that should be investigated in the future.

It has been demonstrated that the HPLC-ICP-MS method using CCT is suitable for detecting P containing species such as DNA. The HPLC-ICP-MS method developed in this chapter can be employed qualitatively, but quantitative analysis will be limited due to the gradient elution employed. It was briefly discussed in Chapter 2 that isocratic elution is preferred when coupling HPLC systems to ICP-MS, since the mobile phase composition is constant throughout the separation. Conversely, gradient elution results in a changing mobile phase composition which ultimately results in the plasma

conditions constantly changing throughout the separation step. This was evident in the rising baseline which was attributed to increasing mobile phase B as the elution progressed. Thus, it would be difficult to quantify separated analytes, since the degree of analyte ionisation may vary at different stages of the separation.<sup>201</sup> An internal standard could be added to the mobile phase to assess the degree of signal suppression during the elution and should be considered for quantitative analysis.

## 6 Conclusions

The application of elemental mass spectrometry in genomics and related research has been demonstrated in this thesis. It has been shown that nucleic acids can be detected by ICP-MS due to the high P content in the nucleic acid sugar phosphate backbone. However, there are numerous problems associated with P detection, particularly concerning its poor detection limit. This problem can be alleviated if the nucleic acid analyte is labelled with Au nano-particles. Gold has a lower ionisation potential than P and does not suffer the same polyatomic interferences owing to its higher mass. As a result, enhancements in nucleic acid detection by ICP-MS were observed for Au labelled oligonucleotides. Of the two labelling methods investigated, that employing biotin derivatised oligonucleotides and streptavidin functionalised Au particles (SFNG) was the most successful. The SFNG-DNA conjugates were successfully separated from un-reacted SFNG with HPLC-ICP-MS. Labelling efficiencies of 100% were observed, which resulted in an 882 fold enhancement in signal for 25 mer oligonucleotides. More importantly, all the Au was recovered from the HPLC column. Much lower labelling efficiencies and hence signal enhancements were observed when labelling sulfhydryl derivatised oligonucleotides with maleimide functionalised Au nano-particles (MMN). This was attributed to the lengthy and difficult sample preparation required to initiate labelling. Further, both the sulfhydryl derivatised oligonucleotides and MMN were reactive once in solution or when exposed to air, adding to the difficulties.

The labelling methods developed here have advantages over those already published. Firstly, both the SFNG and MMN methods are site specific and stoichiometry can be established.<sup>17</sup> Secondly, these methods are not dependent on nucleic acid base sequence or peptide sequences,<sup>48</sup> hence they can be applied to any bio-molecule possessing a biotin or sulfhydryl functionality. Further, the signal enhancement obtained with SFNG and MMN is only dependent on the efficiency of one conjugation step. This is in contrast to the peptide labelling method reported by Patel *et al.*, which was dependent on the protein-cDPTA derivatisation efficiency followed by the efficiency of Eu binding to the chelating agent.<sup>49</sup>

ICP-MS can be applied to clinical samples; this concept was demonstrated in Chapter 3, where ctDNA was treated with either cisplatin or oxaliplatin anti-cancer drugs. Although the treated ctDNA could be analysed by ICP-MS without any additional sample preparation, severe matrix effects resulted in Pt signal suppression. Consequently, digestion of the ctDNA resulted in decreased matrix effects and allowed Pt dose rates of 1Pt atom per 1 500 000 nucleotides to be detected in approximately 12 µg DNA. Such a sensitive mass spectrometric method may have important implications in clinical research, where trace levels of metallodrug need to be detected and quantified in a limited amount of patient sample. Consequently, this approach was proven by an MSc. student who successfully applied the procedure to two cancer cell lines which were treated with cisplatin or oxaliplatin.

Finally, the complementary nature of elemental and molecular mass spectrometry was highlighted in Chapter 4. Here, ESI linear ion trap mass spectrometry was employed to study the binding and subsequent fragmentation pathways of oxaliplatin with DNA nucleobases. Detailed fragmentation pathways could be established and proposed structures were presented.

## **6.1 Further Research**

### **6.1.1 Improving Existing Methodologies**

The first aspect to consider is improving the methodologies developed in this thesis. It was established in Chapter 2 that RP-HPLC-ICP-MS could be used to separate SFNG-DNA conjugates with the mass balance reaching 100%, suggesting that all the Au was recovered from the column. However, to ensure this was the case, the column had to be disconnected from the nebuliser and reverse flushed after each injection to ensure Au was not accumulating at the head of the column. This may be avoided if an S containing compound such as cysteine is added to the mobile phase to aid Au removal from the chromatographic phase and ICP sample introduction system. Gold has high affinity for S, so its addition to the mobile phase may ensure that all the injected Au is detected by the ICP-MS.

Another approach in improving the HPLC separation is to use polymeric chromatography phases such as PS-DVB instead of silica phases. Polymeric phases are generally more tolerant to extremes in pH compared to their silica counterparts. As a result, low concentrations of *aqua regia* or HCl may be added to the mobile phase to aid Au removal from the column. As discussed previously, Au is relatively soluble and stable in HCl, which may also result in its efficient removal. Monolithic polymeric phases are also more suited to the separation of large molecules such as DNA and proteins, owing to rapid diffusion and lack of intra-particle voids which hamper macromolecule separations.

Another potential area for improvement is in the chromatography described in Chapter 5. The baseline of the  $^{31}\text{P}^{16}\text{O}$  chromatograms in this Chapter appeared to increase during gradient elution. The rising baseline was attributed to the increased formation of carbon and nitrogen containing polyatomic interferences at  $m/z$  47, caused by the increasing amounts of citrate and ammonia chloride mobile phase. Although IKEE was implemented by applying a positive potential to the collision cell, KED was not implemented and the quadrupole bias was maintained at 1V. However, by increasing the positive potential on the quadrupole, it may be possible to discriminate between the  $^{31}\text{P}^{16}\text{O}$  analyte and polyatomic interferences, thus minimising the rising baseline during gradient elution. Such experiments were not conducted here, but may improve the  $^{31}\text{P}^{16}\text{O}$  chromatograms.

### **6.1.2 Combining Elemental Labelling with Pt-DNA Adduct Detection**

The concept of signal enhancement by means of metal or nano-particle labelling has been demonstrated, as has the application of ICP-MS in the analysis of clinical samples. The next step in this research would be to combine these two aspects, namely to label Pt-DNA adducts with Au nano-particles to further increase the detection of Pt-DNA adducts by ICP-MS. This final section looks at two methods which could be employed to further enhance the detection of Pt-DNA adducts. Both methods utilise established biological techniques in conjunction with metal nano-particle labelling and elemental mass spectrometry. Although neither of these methods has been investigated, it is hoped that they will pave the way for future developments in both cancer research studies and elemental mass spectrometry.

### 6.1.2.1 Elemental Labelling with the Post Labelling Assay

The nanogold labelling procedures observed in Chapter 2 could potentially be used to label Pt-DNA adducts formed after treatment with Pt drugs. SFNG was assayed in Chapter 2 and a figure of 86 Au atoms per nano-particle was calculated. The incorporation of 86 Au atoms onto the platinated sites would result in a significant enhancement in signal by ICP-MS, resulting in the detection of ultra trace levels of Pt-DNA adducts.

Platinum and Au have similar masses ( $m/z$  195 and 197 respectively) and similar first ionisation potentials (Pt = 9 eV and Au = 9.2 eV), thus the two elements would be expected to give similar signals by ICP-MS. However, unlike Au which is monoisotopic, Pt has six isotopes with the most abundant at  $m/z$  195 (33.8% abundant). Therefore, the  $^{195}\text{Pt}$  signal intensity would be expected to be 33% lower than the signal given by  $^{197}\text{Au}$  at the same concentration. Given that each nano-particle contains 86 Au atoms and Au gives three times greater signal than the most abundant Pt isotope, a total enhancement factor of 258 should be possible for nanogold labelled di-nucleotides compared to measuring Pt alone.

The site specific labelling of Pt-DNA adducts with nanogold could be achieved if used in conjunction with the post labelling assay. Figure 3:4 illustrates the assay and shows how the adduct sites are converted to di-nucleotides upon enzymatic digestion. The final step in the assay requires the di-nucleotides to be phosphorylated at the 5' end by the enzyme T4PNK, which only phosphorylates the di-nucleotides and hence the previously platinated sites. In the conventional PLA,  $^{32}\text{P}$  is used for phosphorylation. The digest mixture containing the radio-labelled di-nucleotides and mono-nucleotides can then be separated by gel electrophoresis and the  $^{32}\text{P}$  detected. However, in the case of elemental labelling, cold phosphorus can be used for phosphorylating the di-nucleotides and then the 5' phosphate can be derivatised to incorporate either biotin or a sulfhydryl group. The newly incorporated reactive group can then be labelled with SFNG or MMN depending on the reactive group employed. The modified PLA is summarised in Figure 6:1 and illustrates how the di-nucleotides, which represent previously platinated sites are specifically labelled with ~86 Au atoms, whilst the mono-nucleotides that correspond to the non-adducted sites are not labelled and thus not detected by ICP-MS.

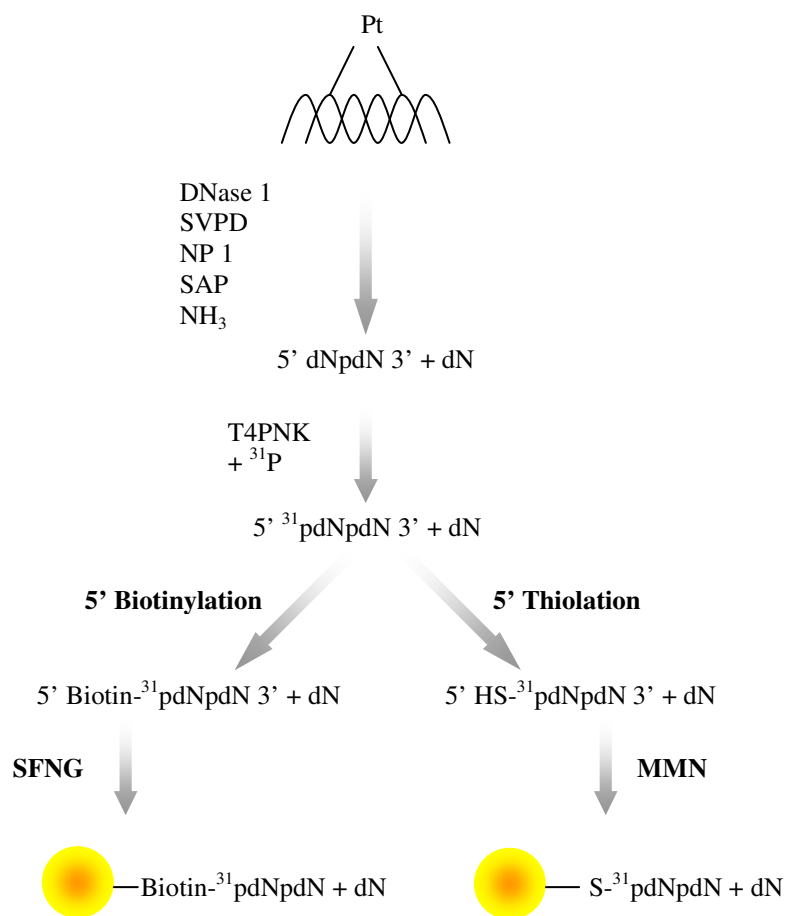


**Figure 6:1: Site specific nanogold labelling of Pt adducts using the PLA.**

Considering the same type of nanogold particle is present in both SFNG and MMN,<sup>95</sup> both nanogold labelling routes incorporate approximately 86 gold atoms onto the dinucleotides. This method could potentially allow for the ultra trace detection of Pt-DNA adducts by ICP-MS.

### 6.1.2.2 Elemental Labelling of Adduct Recognition Antibodies

Antibodies specific to cisplatin intra-stranded GG and AG cross-links have been identified and used in the analysis of Pt-DNA adducts and provide yet another alternative method of ultra sensitive adduct detection.<sup>152, 169, 177</sup> Such antibodies could be used in a sandwich type immunoassay, where cisplatin treated DNA is incubated with adduct recognition antibodies. In a second step, a secondary antibody can then be employed to bind to the adduct recognition antibody. If the secondary antibody carries an Au or rare earth nano-particle, the ICP-MS detection of Pt adducts can be dramatically improved. Figure 6:2 shows the schematic of the potential method.

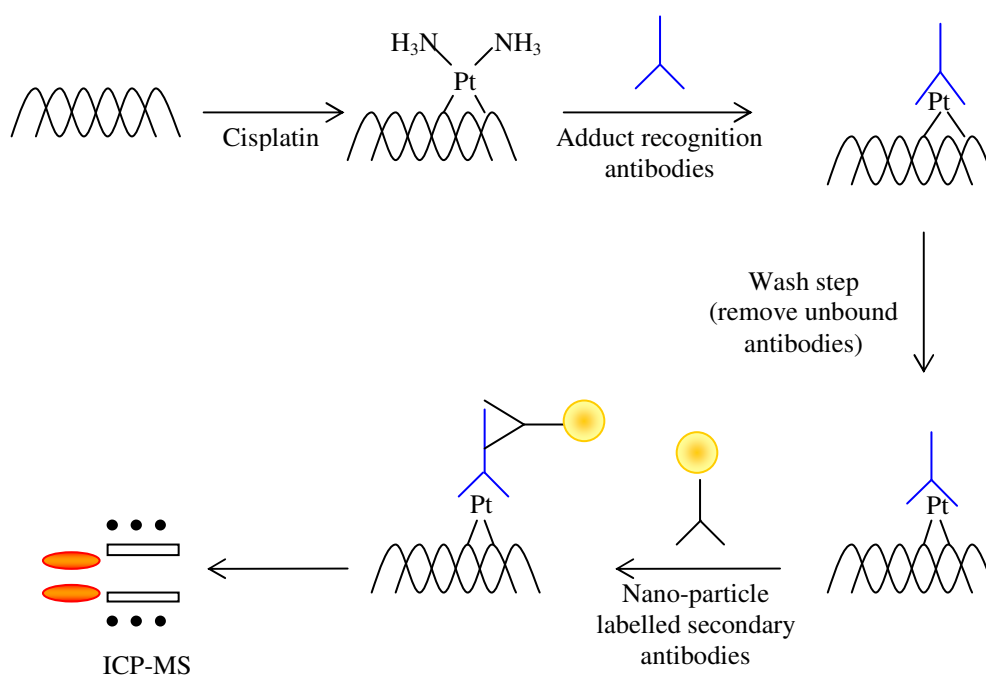


**Figure 6:2: Potential metal nano-particle immunological assay combined with ICP-MS for cisplatin-DNA adduct detection.**

The actual enhancement in signal due to nano-particle labelled antibodies will inevitably be dependent upon the metal employed and the number of metal atoms present on the secondary antibody. In addition, the affinity of the selected secondary antibody to the primary antibody will effect the overall signal enhancement. The nano-particle based immunological method should be capable of detecting between ~90-95% of all Pt species formed, since the antibodies recognise GG and AG intra-stranded cross-links.<sup>152, 169</sup> However, the above method is only viable if a secondary antibody specific to the adduct recognition antibodies can be identified. In addition, the secondary antibody will have to be labelled with metal nano-particles, unless such metal containing antibodies are commercially available.



## 7 References

- 1 D. Pröfrock, P. Leonhard and A. Prange, *J. Anal. At. Spectrom.*, 2003, **18**, 708-713.
- 2 M. Wind and W. D. Lehmann, *J. Anal. At. Spectrom.*, 2004, **19**, 20-25.
- 3 W. Brüchert and J. Bettmer, *J. Anal. At. Spectrom.*, 2006, **21**, 1271-1276.
- 4 N. Jakubowski, R. Lobinski and L. Moens, *J. Anal. At. Spectrom.*, 2004, **19**, 1-4.
- 5 R. Lobinski, D. Schaumlöffel and J. Szpunar, *Mass Spectrom. Rev.*, 2006, **25**, 255-289.
- 6 A. Sanz-Medel, *Anal. Bioanal. Chem.*, 2008, **390**, 1-2.
- 7 A. Sanz-Medel, M. Montes-Bayón, M. Del Rosario Fernández de laCampe, J. Ruiz Encinar and J. Bettmer, *Anal. Bioanal. Chem.*, 2008, **390**, 3-16.
- 8 D. Pröfrock, P. Leonhard, S. Wilbur and A. Prange, *J. Anal. At. Spectrom.*, 2004, **19**, 623-631.
- 9 D. R. Bandura, V. I. Baranov and S. D. Tanner, *Anal. Chem.*, 2002, **74**, 1497-1502.
- 10 V. I. Baranov, Z. A. Quinn, D. R. Bandura and S. D. Tanner, *J. Anal. At. Spectrom.*, 2002, **17**, 1148-1152.
- 11 S. Hann, G. Koellensperger, C. Obinger, P. G. Furtmüller and G. Stringeder, *J. Anal. At. Spectrom.*, 2004, **19**, 74-79.
- 12 J. M. Marchante-Gayón, *Anal. Bioanal. Chem.*, 2004, **379**, 335-337.
- 13 O. Ornatsky, V. I. Baranov, D. R. Bandura, S. D. Tanner and J. Dick, *J. Immunological Methods*, 2006, **308**, 68-76.
- 14 S. Hu, S. Zhang, Z. Hu, Z. Xing and X. Zhang, *Anal. Chem.*, 2007, **79**, 923-929.
- 15 S. D. Müller, R. A. Diaz-Bone, J. Felix and W. Goedecke, *J. Anal. At. Spectrom.*, 2005, **20**, 907-911.
- 16 V. I. Baranov, Z. A. Quinn, D. R. Bandura and S. D. Tanner, *Anal. Chem.*, 2002, **74**, 1629-1636.
- 17 S. L. Kerr and B. L. Sharp, *Chem. Comm.*, 2007, 4537-4539.
- 18 P. D. Winship, *PhD. Doctoral Thesis*, Loughborough University, Department of Chemistry, 2007.
- 19 Y. Petty, *DNA Structure, Replication, Transcription and Protein Synthesis*, 29/09/04, <http://www.ncc.gmu.edu/dna>
- 20 M. K. Campbell, *Biochemistry*, 2nd Ed., Saunders, 1995

- 21 D. Donohue, *PNAS*, 1956, **42**, 60-65.
- 22 D. Cui, C. S. Ozkan, S. Ravindran, Y. Kong and H. Gao, *MBC*, 2004, **1**, 113-121.
- 23 Kimball, *Kimballs Biology Pages*, 22/11/04,  
<http://users.rcn.com/jkimball.ma.ultranet/BiologyPages/D/DNAReplication.html>
- 24 G. Karp, *Cell and Molecular Biology*, 3rd Ed., Wiley & Sons, New York, 2001.
- 25 V. I. Baranov, Z. A. Quinn, D. R. Bandura and S. D. Tanner, 9th International conference on plasma source mass spectrometry, Durham University, 2004.
- 26 C. Fosset, B. A. McGaw, M. D. Reid and H. J. McArdle, *J. Inorg. Biochem.*, 2005, **99**, 1018-1022.
- 27 A. Montaser, *Inductively coupled plasma mass spectrometry*, Ed., Wiley VCH, Washington D.C, 1998
- 28 G. Álvarez-Llamas, M. R. Fernández de la Campa and A. Sanz-Medel, *Trends in Anal. Chem.*, 2005, **24**, 28-36.
- 29 J. L. Neilsen, A. Abildtrup, J. Christensen, P. Watson, A. Cox and C. W. McLeod, *Spectrochim. Acta B*, 1998, **53**, 339-345.
- 30 I. Feldmann, C. U. Koehler, P. H. Roos and N. Jakubowski, *J. Anal. At. Spectrom.*, 2006, **21**, 1006-1015.
- 31 J. L. Gómez-Ariza, T. Garcia-Barrera, F. Lorenzo, V. Bernal, M. J. Villegas and V. Oliveira, *Anal. Chimica Acta*, 2004, **524**, 15-22.
- 32 M. Montes-Bayón, D. Pröfrock, A. Sanz-Medel and A. Prange, *J. Chromatogr. A*, 2006, **1114**, 138-144.
- 33 B. Bouyssié, J. Szpunar and R. Lobinski, *Spectrochim. Acta B*, 2002, **57**, 805-827.
- 34 A. Sanz-Medel, M. Montes-Bayón and M. L. Fernández Sánchez, *Anal. Bioanal. Chem.*, 2003, **377**, 236-247.
- 35 J. Szpunar, *Anal. Bioanal. Chem.*, 2004, **378**, 54-56.
- 36 J. Szpunar and R. Lobinski, *Pure & Appl. Chem.*, 1999, **71**, 899-918.
- 37 R. Thomas, *Spectroscopy*, 2001, **16**, 26-30.
- 38 R. Thomas, *Spectroscopy*, 2001, **16**, 26-28.
- 39 W. Fritzsche and T. A. Taton, *Nanotechnology*, 2003, **14**, R63-R73.
- 40 K. Faulds, R. P. Barbagallo, J. T. Keer, E. Smith and D. Graham, *Analyst*, 2004, **129**, 567-568.

- 41 R. Csáki, R. Möller, W. Straube, J. M. Köhler and W. Fritzsche, *Nuc. Acids Res.*, 2001, **29**, e81.
- 42 D. Pluim, M. Maliepaard, R. C. A. M. Van Waardenburg, J. H. Beijnen and J. H. M. Schellens, *Anal. Biochem.*, 1999, **275**, 30-38.
- 43 Y. C. Cao, R. Jin, J. Nam, C. S. Thaxton and C. A. Mirkin, *J. Am. Chem. Soc.*, 2003, **125**, 14676-14677.
- 44 O. V. Salata, *J. Nanobiotechnology*, 2004, **2**,
- 45 J. Wang, D. Xu, A. N. Kawde and R. Polsky, *Anal. Chem.*, 2001, **73**, 5576-5581.
- 46 I. Alexandre, S. Hamels, S. Dufour, J. Collet, N. Zammattéo, F. De Longueville, J. L. Gala and J. Remacle, *Anal. Biochem.*, 2001, **295**, 1-8.
- 47 J. J. M. Llano, E. J. Andreu and E. Knecht, *Anal. Biochem.*, 1996, **243**, 210-217.
- 48 A. Merkoci, M. Aldavert, G. Tarrasón, R. Eritja and S. Alegret, *Anal. Chem.*, 2005, **77**, 6500-6503.
- 49 P. Patel, P. FJons, R. Handy, C. F. Harrington, P. Marshall and H. Evans, *Anal. Bioanal. Chem.*, 2008, **390**, 61-65.
- 50 H. Haraguchi, *J. Anal. At. Spectrom.*, 2004, **19**, 5-14.
- 51 R. Thomas, *Spectroscopy*, 2001, **17**, 42-48.
- 52 S. D. Tanner, V. I. Baranov and D. R. Bandura, *Spectrochim. Acta B*, 2002, **57**, 1361-1452.
- 53 G. C. Eiden, C. J. Barinaga and D. W. Koppenaal, *Rapid Commun. Mass Spectrom.*, 1997, **11**, 37-42.
- 54 P. R. D. Mason, K. Kaspers and M. J. Van Bergen, *J. Anal. At. Spectrom.*, 1999, **14**, 1067-1074.
- 55 L. A. Simpson, M. Thomsen, B. J. Alloway and A. Parker, *J. Anal. At. Spectrom.*, 2001, **16**, 1375-1380.
- 56 M. A. Dexter, H. R. Reid and B. L. Sharp, *J. Anal. At. Spectrom.*, 2002, **17**, 676-681.
- 57 V. Chrastný, M. Komàrek, M. Mihaljevic and J. Štichová, *Anal. Bioanal. Chem.*, 2006, **385**, 962-970.
- 58 N. Yamada, J. Takahashi and K. Sakata, *J. Anal. At. Spectrom.*, 2002, **17**, 1213-1222.
- 59 C.-H. Yang and S.-J. Jiang, *Spectrochim. Acta B*, 2004, **59**, 1389-1394.
- 60 D. Pröfrock, P. Leonhard, W. Ruck and A. Prange, *Anal. Bioanal. Chem.*, 2005, **381**, 194-204.

- 61 D. D. Richardson, B. M. Sadi and J. A. Caruso, *J. Anal. At. Spectrom.*, 2006, **21**, 396-403.
- 62 M. Kovacevic, R. Leber, S. D. Kohlwein and W. Goessler, *J. Anal. At. Spectrom.*, 2004, **19**, 80-84.
- 63 R. Thomas, *Spectroscopy*, 2001, **16**, 22-27.
- 64 T. Prohaska, C. Latkoczy and G. Stingeder, *J. Anal. At. Spectrom.*, 1999, **14**, 1501-1504.
- 65 Thermo-Finnigan, *Element 2XR Hardware Manual*, Revision A 119 1410,
- 66 E. M. Brouwers, M. Tibben, H. Rosing, J. H. M. Schellens and J. H. Beijnen, *Mass Spectrom. Rev.*, 2008, **27**, 67-100.
- 67 M. Hamester, D. Wiederin, J. Wills, W. Kerl and C. B. Douthitt, *Fresenius' J. Anal. Chem.*, 1999, **364**, 495-497.
- 68 Thermo, *Element XR detector*, 13/01/2007,  
[www.thermo.com/com/cda/product/detail/1.,10121169,00.html](http://www.thermo.com/com/cda/product/detail/1.,10121169,00.html)
- 69 B. K. Chakrabarti and M. Acharyya, *Rev. Modern Phys.*, 1999, **71**, 847-859.
- 70 Thermo-Finnigan, 15/10/07, <http://www.thermo.com>
- 71 J. C. Smith and D. Figeys, *Molecular Biosystems*, 2006, **2**, 364-370.
- 72 H. W. Xie and T. J. Griffin, *J. Proteome Res.*, 2006, **5**, 1003-1009.
- 73 P. Waridel, A. Frank, H. Thomas, V. Surendranath, S. Sunyaev, P. Pevzner and A. Shevchenko, *Proteomics*, 2007, **7**, 2318-2329.
- 74 F. L. Brancia, *Expert Rev. Proteomics*, 2006, **3**, 143-151.
- 75 E. Hoffmann and V. Stroobant, *Mass spectrometry - principles and applications*, 2nd Ed., Wiley, Chichester, 2002.
- 76 M. Herderich, E. Richling, R. Roscher, C. Schneider, W. Schwab, H.-U. Humpf and P. Schreier, *Chromatographia*, 1997, **45**,
- 77 A. J. Taylor, R. S. T. Linforth, B. A. Harvey and A. Blake, *Food Chemistry*, 2000, **71**, 327-338.
- 78 Thermo-Finnigan, *Finnigan LTQ hardware manual*, 97055-97013 Revision A,
- 79 R. D. Smith, J. A. Loo, C. G. Edmonds, C. J. Barinaga and H. R. Udseth, *Anal. Chem.*, 1990, **62**, 882-899.
- 80 M. G. Ikonomou, A. T. Blades and P. Kebarle, *Anal. Chem.*, 1991, **63**, 1989-1998.
- 81 M. Gamero-Castano and J. Fernandez de la Mora, *Anal. Chimica Acta*, 2000, **406**, 67-91.

- 82 J. B. Fenn, M. M. Mann, C. K. Meng, S. F. Wong and C. M. Whitehouse, *Science*, 1989, **246**, 64-71.
- 83 S. Sauer, *Clinical Chimica Acta*, 2006, **363**, 95-105.
- 84 Z. Zhang, L. Zhou, S. Zhao and H. Deng, *J. Am. Soc. Mass Spectrom.*, 2006, **17**, 1665-1668.
- 85 R. E. March and J. F. J. Todd, *Quadrupole ion trap mass spectrometry*, 2nd Ed., Wiley, New York, 2005.
- 86 J. W. Hager, *Rapid Commun. Mass Spectrom.*, 2002, **16**, 512-526.
- 87 K. Busch, *Spectroscopy*, 2004, **19**, 35-38.
- 88 N. Praphairaksit and R. S. Houk, *Anal. Chem.*, 2000, **72**, 2356-2361.
- 89 Z. A. Quinn, V. I. Baranov, S. D. Tanner and J. L. Wrana, *J. Anal. At. Spectrom.*, 2002, **17**, 892-896.
- 90 E. Morag, E. A. Bayer and M. Wilchek, *J. Biochem.*, 1996, **316**, 193-199.
- 91 R. D. Powell, C. M. R. Halsey, D. L. Spector, S. L. Kaurin, J. McCann and J. F. Hainfield, *J. Histochem. Cytochem*, 1997, **45**, 947-956.
- 92 A. P. Alivisatos, K. P. Johnson, X. Peng, T. E. Wilson, C. J. Loweth, M. P. Bruchez and P. G. Schultz, *Nature*, 1996, **382**, 609-611.
- 93 C. M. Niemeyer, B. Ceyhan, S. Gao, L. Chi, S. Peschel and U. Simon, *Colloid Polymer Science*, 2001, **279**, 68-72.
- 94 M. Campàs and I. Katakis, *Anal. Chimica Acta*, 2006, **556**, 306-312.
- 95 Nanoprobes, *Nanoprobes Incorporated*, 08/10/04, <http://www.nanoprobes.com>
- 96 W. Jahn, *J. Struct. Biol.*, 1999, **127**, 106-112.
- 97 Y. C. Cao, R. Jin and C. A. Mirkin, *J. Am. Chem. Soc.*, 2001, **123**, 7961-7962.
- 98 R. D. Powell, C. M. Halsey, W. Liu, V. N. Joshi and J. F. Hainfeld, *J. Struct. Biol.*, 1999, **127**, 177-184.
- 99 M. Mertig, L. C. Ciacchi, R. Seidel, W. Pompe and A. De Vita, *Nano letters*, 2002, **2**, 841-844.
- 100 J. F. Hainfeld, C. J. Foley, L. E. Maelia and J. J. Lipka, *J. Histochem. Cytochem.*, 1990, **38**, 1787-1793.
- 101 J. F. Hainfeld and F. R. Furuya, *J. Histochem. Cytochem.*, 1992, **40**, 177-184.
- 102 H. R. Kuhn, M. Guillong and D. Günther, *Anal. Bioanal. Chem.*, 2004, **378**, 1069-1074.
- 103 J. Werner, *J. Struct. Biol.*, 1999, **127**, 106-112.

- 104 C. J. McNeal, R. E. P. Winpenny, J. M. Hughes, R. D. Macfarlane, L. H. Pignolet, L. T. J. Nelson, T. G. Gardner, L. H. Irgens, G. Vigh and J. P. Fackler, *Inorg. Chem.*, 1993, **32**, 5582-5590.
- 105 S. D. Tanner, O. Ornatsky, D. R. Bandura and V. I. Baranov, *Spectrochim. Acta B*, 2007, **62**, 188-195.
- 106 W. Chen, P. Wee and I. D. Brindle, *J. Anal. At. Spectrom.*, 2000, **15**, 409-413.
- 107 S. S. Ghosh, P. M. Kao, A. W. McCue and H. L. Chappelle, *Bioconjug. Chem.*, 1990, **1**, 71-76.
- 108 Varian, *PSA anion exchanger*, 06/07/07, [www.varianinc.com](http://www.varianinc.com)
- 109 E. Burmeister Getz, M. Xiao, T. Chakrabarty, R. Cooke and P. R. Selvin, *Anal. Biochem.*, 1999, **273**, 73-80.
- 110 D. J. Cline, S. E. Redding, S. G. Brohawn, J. N. Psathas, J. P. Schneider and C. Thorp, *Biochemistry*, 2004, **43**, 15195-15203.
- 111 Pierce, *Pierce Biotechnology, Document No. 0311 Ellman's Reagent*, 06/07/07,
- 112 S. Aldrich, *Oligonucleotide storage conditions*, 02/02/08, <http://www.sigmaaldrich.com>
- 113 A. Loos, U. Edy, J. Gradinaru, K. Bernauer, C. W. Schlaepfer, M. Meyer, S. Mazurek, M. Novic and T. R. Ward, *Inorg. Chem.*, 2006, **45**, 660-668.
- 114 M. González, L. A. Bagatelli, I. Echabe, J. L. R. Arrondo, C. E. Argaraña, C. R. Cantor and G. D. Fidelio, *J. Biological Chem.*, 1997, **272**, 11288-11294.
- 115 A. Torreggiani and G. Fini, *J. Raman Spectrosc.*, 1998, **29**, 229-236.
- 116 *Modify and label oligonucleotide 5' phosphate groups (TR0030.1)*, June 2006, [www.piercenet.com](http://www.piercenet.com)
- 117 S. Orrù, I. Caputo, A. D'Amato, M. Rouoppolo and C. Esposito, *J. Biological Chem.*, 2003, **278**, 31766-31773.
- 118 *EZ-Link Pentylamine-biotin (0379.3)*, June 2006, [www.piercenet.com](http://www.piercenet.com)
- 119 D. Redbard and A. Chrambach, *PNAS*, 1970, **65**, 970-977.
- 120 *Gel filtration: principles and methods*, 14/08/07, <http://www1.gelifesciences.com>
- 121 C. Min and G. L. Verdine, *Nuc. Acids Res.*, 1996, **24**, 3806-3810.
- 122 J. C. Murphy, D. L. Jewell, K. I. White, G. E. Fox and R. C. Willson, *Biotechnol. Prog.*, 2003, **19**, 982-986.
- 123 R. Gutierrez, E. M. M. dei Valle and M. A. Galan, *Separation Purification Rev.*, 2007, **36**, 71-111.

- 124 P. R. Jalili, D. Sharma and H. L. Ball, *J. Am. Soc. Mass Spectrom.*, 2007, **18**, 1007-1017.
- 125 S. R. Schmidt, F. Schwelkart and M. E. Andersson, *J. Chromatogr. B*, 2007, **849**, 154-162.
- 126 S. R. Hart, M. D. Waterfield, A. L. Burlingame and R. Cramer, *J. Am. Soc. Mass Spectrom.*, 2002, **13**, 1042-1051.
- 127 T. Andersen, M. Pepaj, R. Trones, E. Lundanes and T. Greibrokk, *J. Chromatogr. A*, 2004, **1025**, 217-226.
- 128 K. Zhu, J. Zhao, D. Lubman, F. R. Miller and T. J. Barder, *Anal. Chem.*, 2005, **77**, 2745-2755.
- 129 Invitrogen, 29/06/07, [www.invitrogen.com](http://www.invitrogen.com)
- 130 E. H. Larson, *J. Anal. At. Spectrom.*, 1994, **9**, 1099-1105.
- 131 S. Liu and D. Beauchemin, *Spectrochim. Acta B*, 2006, **61**, 319-325.
- 132 Z. Hu, S. Hu, S. Gao, Y. Liu and S. C. Lin, *Spectrochim. Acta B*, 2004, **59**, 1463-1470.
- 133 P. Allain, J. M. Mermet and T. Delaporte, *Anal. Chem.*, 1991, **63**, 1497-1498.
- 134 M. Kovacevic, W. Goessler, N. Mikac and M. Veber, *Anal. Bioanal. Chem.*, 2005, **383**, 145-151.
- 135 R. Munoz Olivas, C. R. Quetel and O. F. X. Donard, *J. Anal. At. Spectrom.*, 1995, **10**, 865-870.
- 136 M. Kovacevic and W. Goessler, *Spectrochim. Acta B*, 2005, **60**, 1357-1362.
- 137 I. Rodushkin, P. Nordlund, E. Engström and D. C. Baxter, *J. Anal. At. Spectrom.*, 2005, **20**, 1250-1255.
- 138 D. F. Shriver, P. W. Atkins and C. H. Langford, *Inorganic Chemistry*, 2nd Ed., Oxford University Press, Oxford, 1994
- 139 D. H. Williams, E. Stephens and M. Zhou, *J. Mol. Biol.*, 2003, **329**, 389-399.
- 140 S. Ahmad, A. A. Isab, S. Ali and A. Al-Arfaj, *Polyhedron*, 2006, **25**, 1633-1645.
- 141 A. R. Timerbaev, C. G. Hartinger, S. S. Aleksenko and B. K. Keppler, *Chem. Rev.*, 2006, **106**, 2224-2248.
- 142 J. Szpunar, A. Makarov, T. Pieper, B. K. Keppler and R. Lobinski, *Anal. Chimica Acta*, 1999, **387**, 135-144.
- 143 B. P. Esposito and R. Najjar, *Co-ordination Chemistry Reviews*, 2002, **232**, 137-149.

- 144 S. G. Chaney, S. L. Campbell, B. Temple, E. Bassett, Y. Wu and M. Faldu, *J. Inorganic Biochem.*, 2004, **98**, 1551-1559.
- 145 E. R. Jamieson and S. J. Lippard, *Chem. Rev.*, 1999, **99**, 2467-2498.
- 146 H. T. Chifotides, K. M. Koshlap, L. M. Pérez and K. R. Dunbar, *J. Am. Chem. Soc.*, 2003, **125**, 10714-10724.
- 147 D. N. Bell, J. J. Liu, M. D. Tingle and M. J. McKeage, *J. Chromatogr. B*, 2006, **837**, 29-34.
- 148 A. Rodger, K. K. Patel, K. J. Sanders, M. Datt, C. Sacht and M. J. Hannon, *J. Chem. Soc., Dalton Trans.*, 2002, 3656-3663.
- 149 L. E. Ta, L. Espeset, J. Podratz and A. J. Windebank, *NeuroToxicology*, 2006, **27**, 992-1002.
- 150 J. Reedijk, *PNAS*, 2003, **100**, 3611-3616.
- 151 D. Garcia Sar, M. Montes-Bayón, E. Blanco Gonzalez and A. Sanz-Medel, *J. Anal. At. Spectrom.*, 2006, **21**, 861-868.
- 152 E. L. Meczes, A. Azim-Araghi, C. J. Ottley, D. G. Pearson and M. J. Tilby, *Biochem. Pharmacol.*, 2005, **70**, 1717-1725.
- 153 Y. Mantri, S. J. Lippard and M. H. Baik, *J. Am. Chem. Soc.*, 2007, **129**, 5023-5030.
- 154 M. S. Davies, S. Berners-Price and T. W. Hambley, *J. Inorg. Biochem.*, 2000, **79**, 167-172.
- 155 S. Arnould, I. Hennebelle, P. Canal, R. Bugat and S. Guichard, *Eur. J. Cancer*, 2003, **39**, 112-119.
- 156 G. M. Almeida, T. L. Duarte, W. P. Steward and G. D. D. Jones, *DNA Repair*, 2006, **5**, 219-225.
- 157 J. M. Woynarowski, W. G. Chapman, C. Napier, M. C. S. Herzig and P. Juniewicz, *Molecular Pharmacol.*, 1998, **54**, 770-777.
- 158 E. Raymond, S. Faivre, S. G. Chaney, J. Woynarowski and E. Cvitkovic, *Mol. Cancer Therapeutics*, 2002, **1**, 227-235.
- 159 P. L. Olive and D. P. Banath, *Experimental Cell Res.*, 1995, **221**, 19-26.
- 160 R. R. Tice, E. Agurell, D. Anderson, B. Burlinson, A. Hartmann, H. Kobayashi, Y. Miyamae, E. Rojas, J. C. Ryu and Y. F. Sasaki, *Environ. Molecular Mutagenesis*, 2000, **35**, 206-221.
- 161 G. D. D. Jones, L. Dickinson, J. Lunec and M. N. Routledge, *Carcinogenesis*, 1999, **20**, 503-507.



- 162 M. V. Reddy and K. Randerath, *Environ. Health Perspectives*, 1987, **76**, 41-47.
- 163 B. M. Elliott, *Mutagenesis*, 1990, **5**, 615-616.
- 164 H. Iijima, H. B. Patrzyc, J. B. Dawidzik, E. E. Budzinski, H.-C. Cheng, H. G. Freund and H. C. Box, *Anal. Biochem.*, 2004, **333**, 65-71.
- 165 A. Springer, C. Burgel, V. Böhrsch, R. Mitric, V. Bonacic-Koutecky and M. W. Linscheid, *ChemPhysChem*, 2006, **7**, 1779-1785.
- 166 R. Mandal and X.-F. Li, *Rapid Commun. Mass Spectrom.*, 2006, **20**, 48-52.
- 167 R. C. Le Pla, K. J. Ritchie, C. J. Henderson, C. R. Wolf, C. F. Harrington and P. B. Farmer, *Chem. Res. Toxicol.*, 2007, **20**, 1177-1182.
- 168 A. Ghezzi, M. Aceto, C. Cassino, E. Gabano and D. Osella, *J. Inorg. Biochem.*, 2004, **98**, 73-78.
- 169 B. Liedert, D. Pluim, J. H. M. Schellens and J. Thomale, *Nucleic Acid Res.*, 2006, **34**, e47.
- 170 S. Hann, Z. Stefánka, K. Lenz and G. Stingeder, *Anal. Bioanal. Chem.*, 2005, **381**, 405-412.
- 171 S. Hann, G. Kollensperger, Z. Stefanke, G. Stingeder, M. Furhacker, W. Buchberger and R. M. Mader, *J. Anal. At. Spectrom.*, 2003, **18**, 1391-1395.
- 172 V. Vacchina, L. Torti, C. Allievi and R. Lobinski, *J. Anal. At. Spectrom.*, 2003, **18**, 884-890.
- 173 R. Mandal, M. B. Sawyer and X.-F. Li, *Rapid Commun. Mass Spectrom.*, 2006, **20**, 2533-2538.
- 174 J. Szpunar, *Trends in Anal. Chem.*, 2000, **19**, 127-137.
- 175 Z. Huang, A. R. Timerbaev, B. K. Keppler and T. Hirokawa, *J. Chromatogr. A*, 2006, **1106**, 75-79.
- 176 A. R. Timerbaev, S. S. Aleksenko, K. Polec-Pawlak, R. Ruzik, O. Sernenova, C. G. Hartinger, S. Oszwaldowski, M. Galanski, M. Jarosz and B. K. Keppler, *Electrophoresis*, 2004, **25**, 1988-1995.
- 177 M. J. Tilby, C. Johnson, R. J. Knox, J. Cordell, J. J. Roberts and C. J. Dean, *Cancer Res.*, 1991, **51**, 123-129.
- 178 M. J. P. Welters, M. Maliepaard, A. J. Jacobs-Bergmans, R. A. Baan, J. H. M. Schellens, J. Ma, W. J. F. Van der Vijhg, J. M. Braakhuis and A. M. J. Fichtinger-Schepman, *Carcinogenesis*, 1997, **18**, 1767-1774.
- 179 P. D. Winship, *PhD. Doctoral thesis*, Loughborough University, Department of Chemistry, 2006

- 180 K. Yamada, N. Kato, A. Takagi, M. Koi and H. Hemmi, *Anal. Bioanal. Chem.*, 2005, **382**, 1702-1707.
- 181 B. Gammelgaard and B. P. Jensen, *J. Anal. At. Spectrom.*, 2007, **22**, 235-249.
- 182 A. Fialho, *MSc. Project*, 2007.,
- 183 D. Garcia Sar, M. Montes-Bayón, L. Aguado Ortiz, E. Blanco Gonzalez, L. M. Sierra and A. Sanz-Medel, *Anal. Bioanal. Chem.*, 2008, **390**, 37-44.
- 184 A. Küng, D. B. Strickmann, M. Galanski and B. K. Keppler, *J. Inorg. Biochem.*, 2001, **86**, 691-698.
- 185 F. R. Luo, T.-Y. Yen, S. D. Wyrick and S. G. Chaney, *J. Chromatogr. B*, 1999, **724B**, 345-356.
- 186 B. Spingler, D. A. Whittington and S. J. Lippard, *Inorg. Chem.*, 2001, **40**, 5596-5602.
- 187 Y. B. Wu, P. Pradhan, J. Havener, S. Cambell and S. G. Chaney, *Abstract of papers of the American Chemical Society*, 2004, **228**, U178.
- 188 X. Yan, J. Watson, P. Shing Ho and M. L. Deinzer, *MCP*, 2004, **3**, 10-23.
- 189 M. A. Raji, P. Frycak, M. Beall, M. Sakrout, J.-M. Ahn, Y. P. Bao, D. W. Armstrong and K. A. Schug, *Int. J. Mass Spectrom.*, 2007, **262**, 232-240.
- 190 P. Iannitti-Tito, A. Weimann, G. Wickham and M. M. Sheil, *Analyst*, 2000, **125**, 627-634.
- 191 T. Shi, J. Zhao, T. Shoeib, K. W. Micheal Sui and A. C. Hopkinson, *Eur. J. Mass Spectrom.*, 2004, **10**, 931-940.
- 192 T. Shoeib, A. C. Hopkinson and K. W. Micheal Sui, *J. Phys. Chem. B*, 2001, **105**, 12399-12409.
- 193 A. Pelmeshnikov, I. Zilberberg, J. Leszezynski, A. Famulari, M. Sironi and M. Raimondi, *Chem. Phys. Letters*, 1999, **314**, 496-500.
- 194 F. Huq, J. Q. Yu, H. Daghri and P. Beale, *J. Inorg. Biochem.*, 2004, **98**, 1261-1270.
- 195 S. T. Sherry, M. H. Ward, M. Kholodov, J. baker, L. Phan, E. M. Smigielski and K. Sirotkin, *Nuc. Acids Res.*, 2001, **29**, 308-311.
- 196 T. A. Sivakumaran, K. Kucheria and P. J. Oefner, *Current Science*, 2003, **84**, 291-296.
- 197 Y. P. Bao, M. Huber, T.-F. Wei, S. S. Marla, J. J. Storhoff and U. R. Muller, *Nuc. Acids Res.*, 2005, **33**, e15.
- 198 K. Inagaki, T. Umemura, H. Matsuura and H. Haraguchi, 2000, **16**, 787-788.

- 199 D. G. Sar, M. Montes-Bayón, E. Blanco and A. Sanz-Medel, *J. Anal. At. Spectrom.*, 2006, **21**, 861-868.
- 200 I. Rodushkin, T. Ruth and D. Klockare, *J. Anal. At. Spectrom.*, 1998, **13**, 159-166.
- 201 L. Bendahl and B. Gammelgaard, *J. Anal. At. Spectrom.*, 2005, **20**, 410-416.

## 8 Appendix 1: TSKgel-DNA-NPR Phase

The anion exchange stationary phase chosen for the separation of nucleic acids and nucleic acid-Au conjugates was a non-porous resin functionalised with diethylaminoethane (DEAE) anion exchanger. The structure of DEAE is illustrated in Figure 8:1. The phase has a pKa of approximately 11.2, so the tertiary amine functional group carries a positive charge at or below pH 9. Therefore, compounds carrying a negative charge are retained on the phase and positive or neutral species repel the phase and are eluted. However, a mixture of negatively charged compounds may be separated from one another if the species have different charge densities and /or hydrophobicities, since they will have different degrees of interaction with the phase.

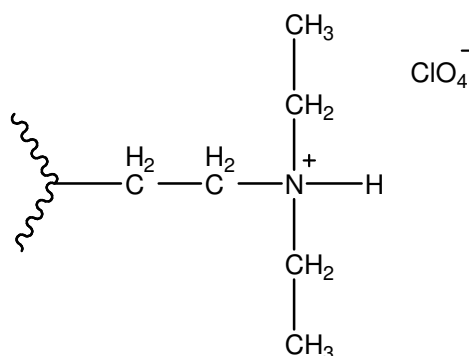


**Figure 8:1: Structure of the DEAE phase.**

The stationary phase is commercially known as; TSKgel-DEAE-NPR. A non-porous resin was chosen for the separation of large biomolecules, since the phase is free from intraparticulate pores and voids. This has the advantage of preventing the large molecules becoming irreversibly trapped within the intraparticulate pores. Also, the mass transfer of the molecules is increased, which is advantageous due to the naturally low diffusivity observed with large biomolecules. Table 8:1 summarises the properties of the stationary phase.

**Table 8:1: properties of the TSKgel-DEAE-NPR Stationary Phase.**

Property	TSKgel-DNA-NPR
Dimensions	4.6 mm x 750 mm, 2.5 $\mu$ m
Pore size	Non porous media
pH stability	2-12
Max salt conc	$\leq$ 1 M
Max organic solvent	$\leq$ 20%

## 9 Appendix 2: LTQ Data from oxaliplatin-DNA adducts

### 9.1 Appendix 2.1: Oxaliplatin Mass Spectrometry Data (in the absence of nucleobase)

The following spectra were obtained from a 3.3 mM oxaliplatin solution in the absence of nucleobase.

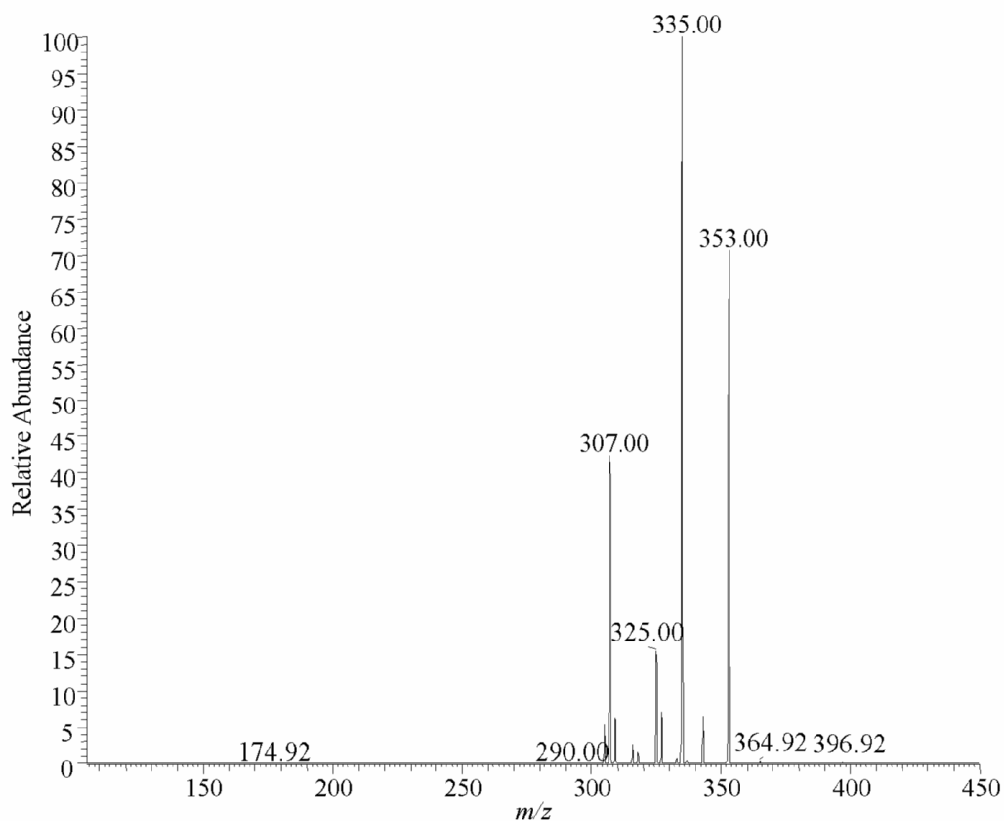


**Figure 9:1: MS/MS spectrum of product ions obtained by CID of oxaliplatin parent ion at  $m/z$  397, collision energy = 20 eV and isolation width = 1 Da.**

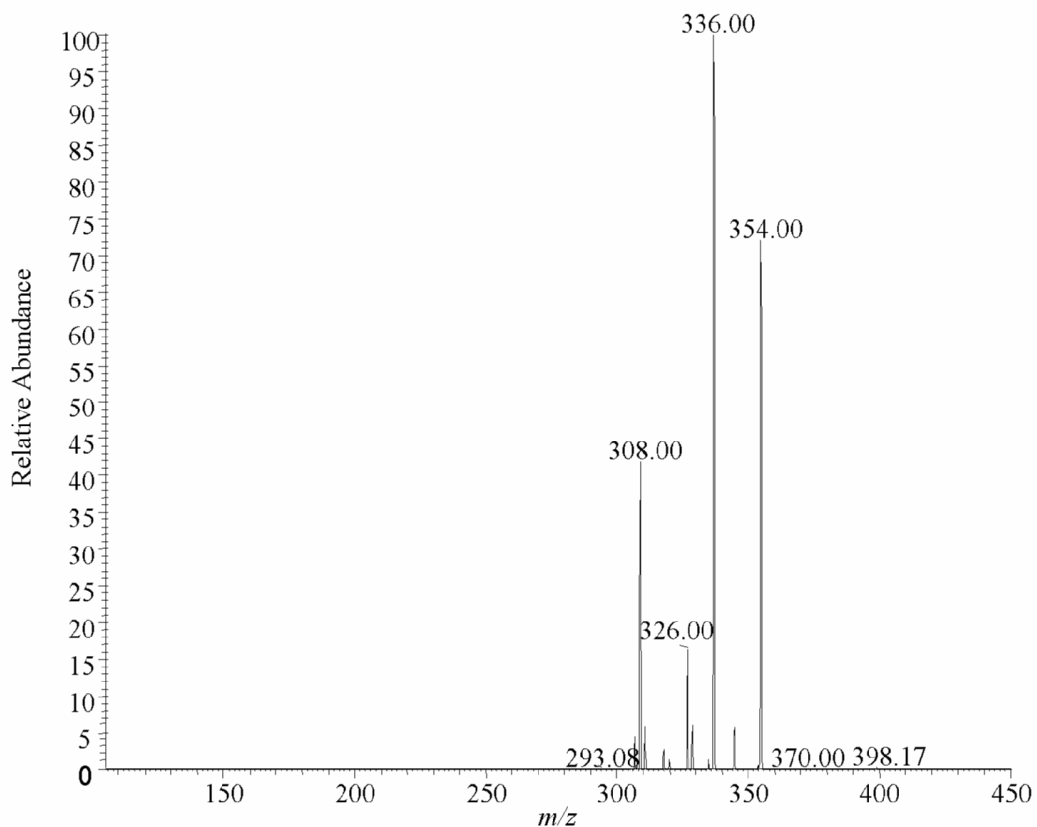


**Figure 9:2: MS/MS spectrum of product ions obtained by CID of oxaliplatin parent ion at  $m/z$  398, collision energy = 20 eV and isolation width = 1 Da.**

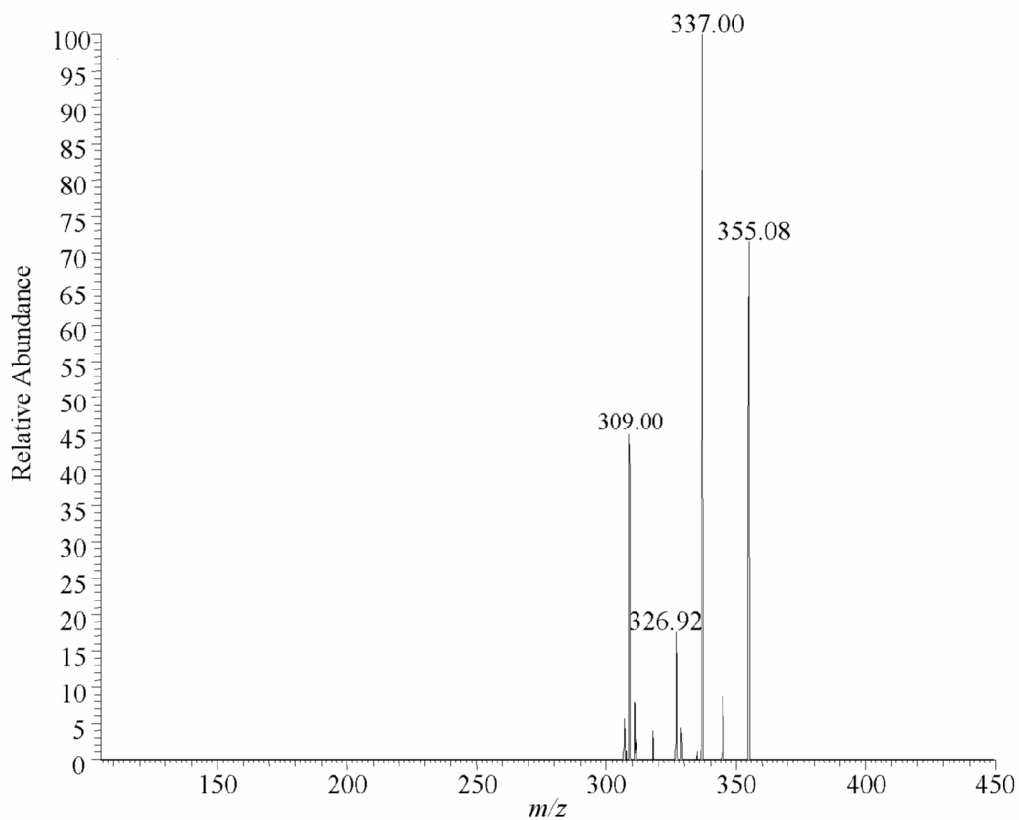


**Figure 9:3: MS/MS spectrum of product ions obtained by CID of oxaliplatin parent ion at  $m/z$  399, collision energy = 20 eV and isolation width = 1 Da.**

## 9.2 Appendix 2.2: Mass Spectrometry Data from Oxaliplatin Mono-Nucleobase Solutions

### Oxaliplatin-Adenine Mass Spectra

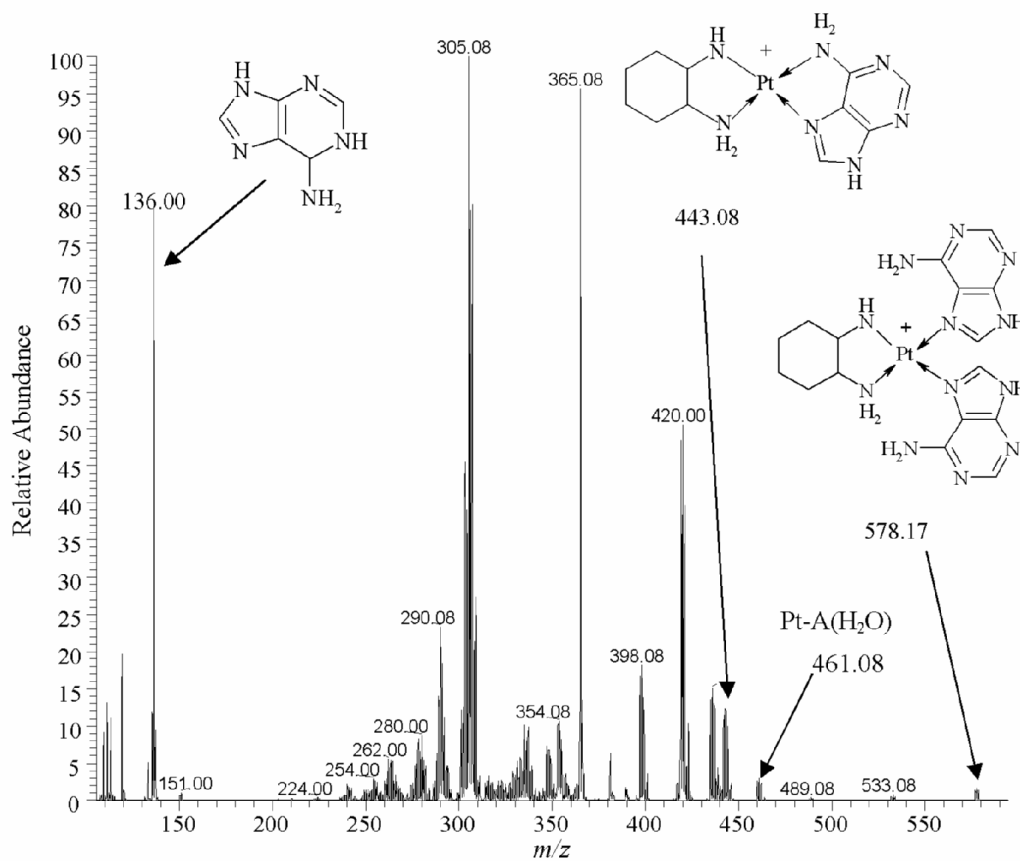
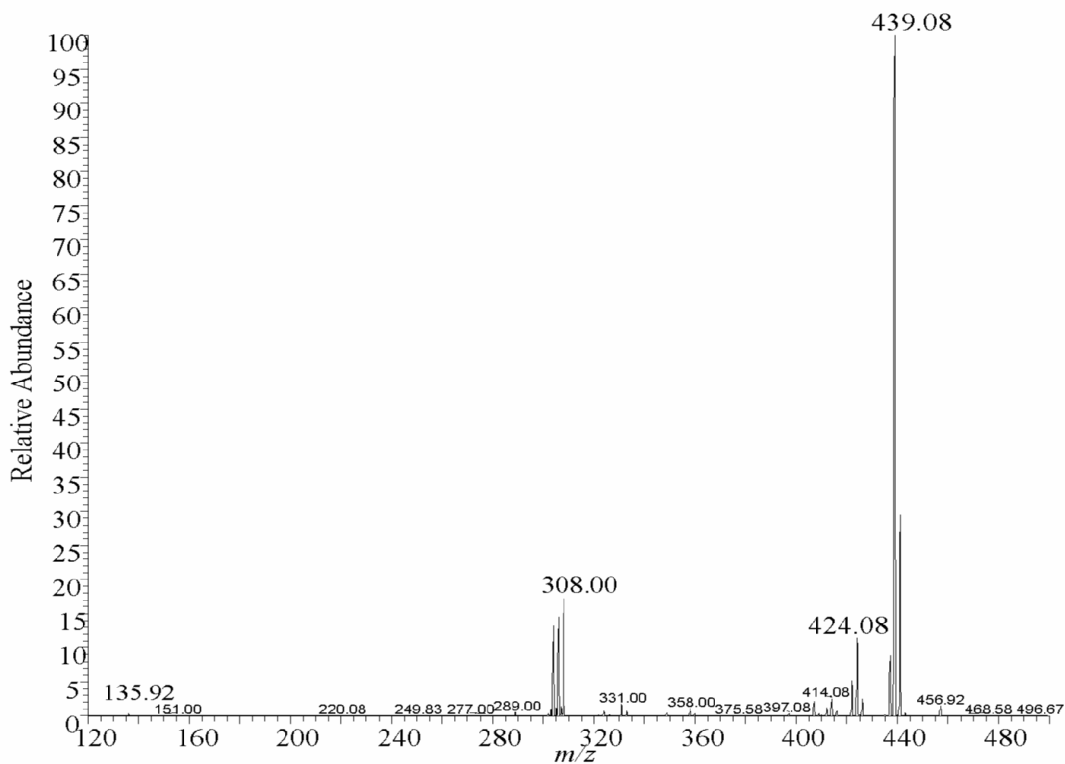
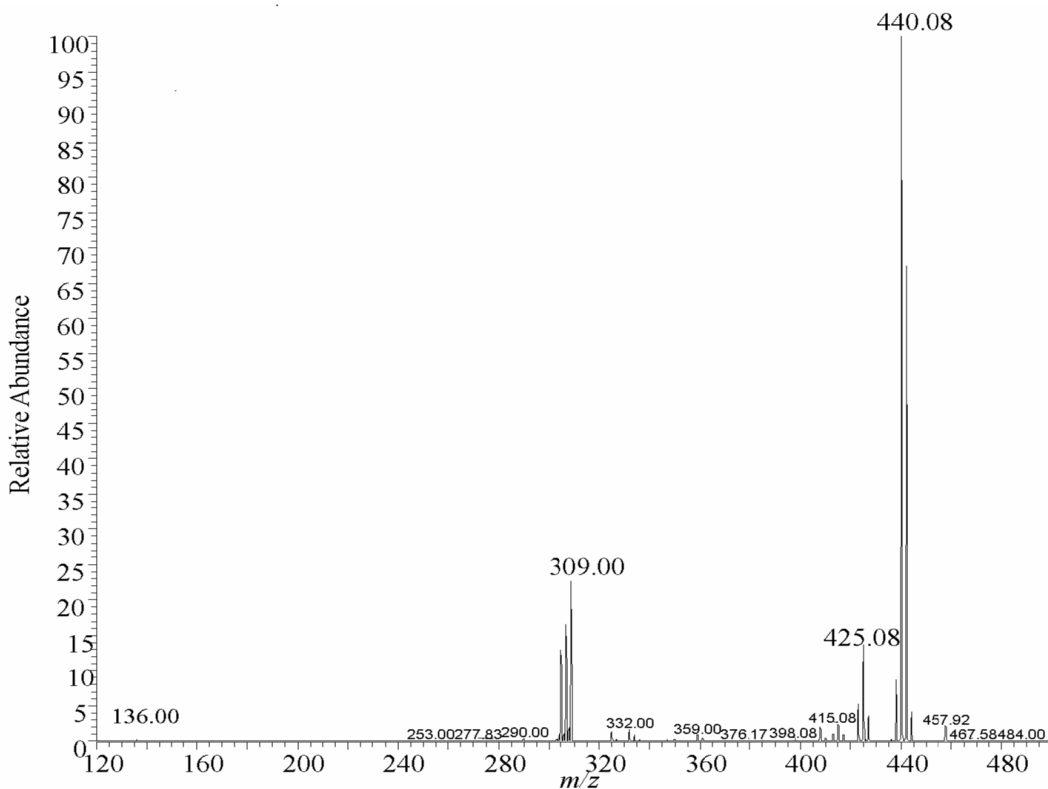


Figure 9:4: Full scan mass spectrum of oxaliplatin-adenine mono-base solution.



**Figure 9:5: MS/MS of product ions obtained by CID of the  $^{195}\text{Pt}$ -A adduct at  $m/z$  443 to yield the free Pt drug at  $m/z$  304-308 and free adenine base at  $m/z$  136. Collision energy = 20 eV and isolation width = 1 Da.**



**Figure 9:6: MS/MS of product ions obtained by CID of the  $^{196}\text{Pt}$ -A adduct at  $m/z$  444 to yield the free Pt drug at  $m/z$  309 and free adenine base at  $m/z$  136. Collision energy = 15 eV and isolation width = 1 Da.**



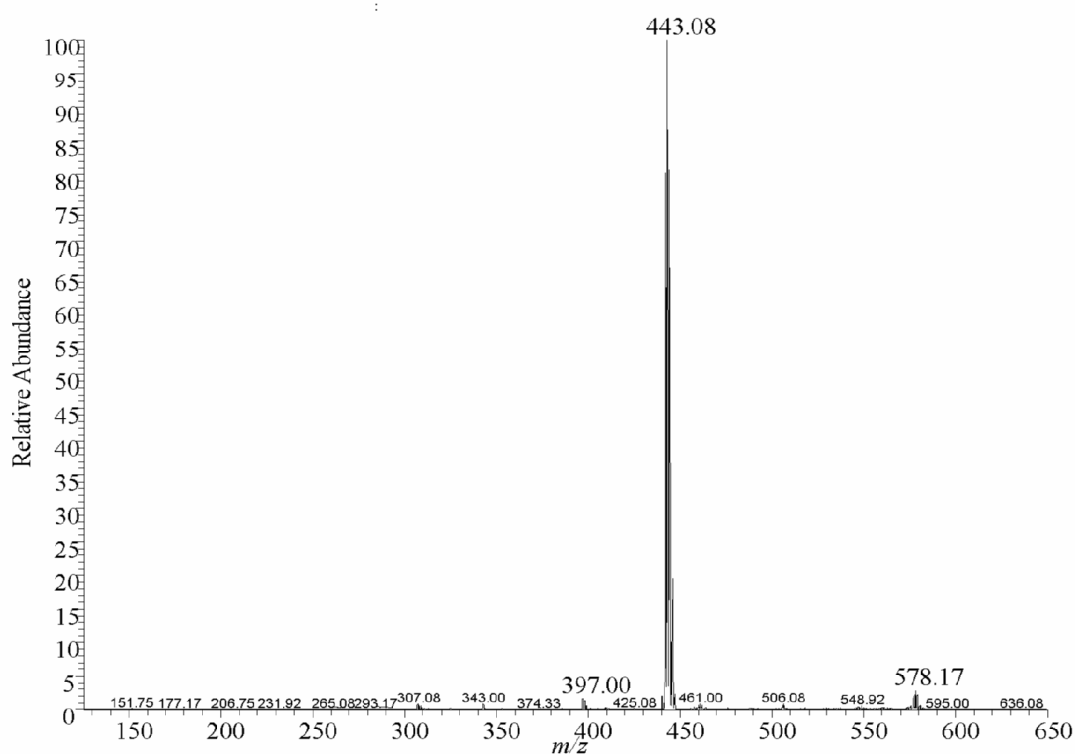


**Figure 9:7:** MS/MS spectrum of product ions obtained by CID of the  $^{195}\text{Pt}$ -AA adduct at  $m/z$  578 to yield the  $^{195}\text{Pt}$ -A adduct at  $m/z$  443. Collision energy = 20 eV and isolation width = 10 Da.

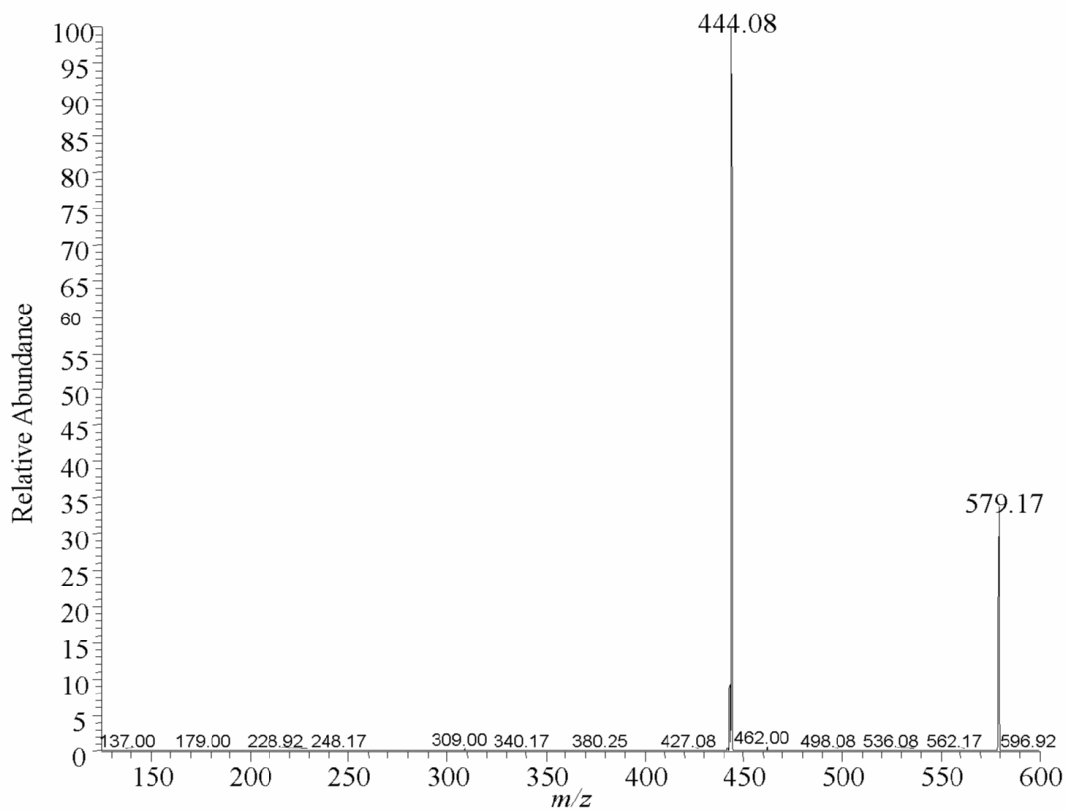


**Figure 9:8:** MS/MS spectrum of product ions obtained by CID of the  $^{196}\text{Pt}$ -AA adduct at  $m/z$  579 to yield the Pt-A adduct at  $m/z$  444. Collision energy = 20 eV and isolation width = 1 Da.

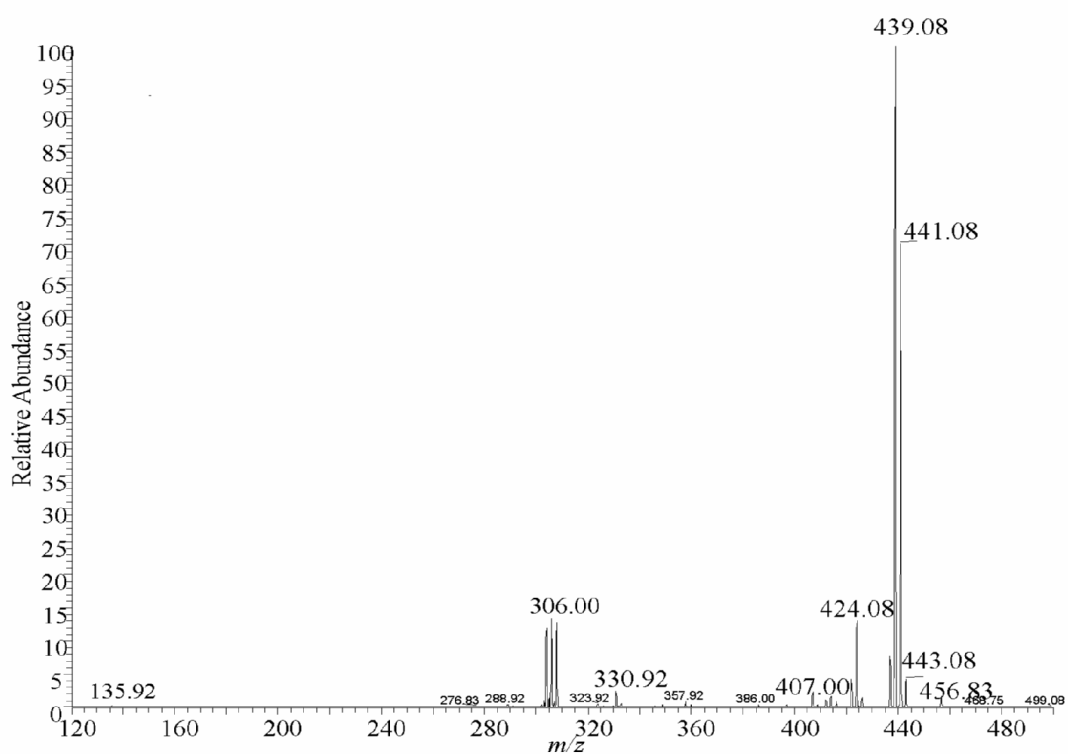


**Figure 9:9:** MS<sup>3</sup> spectrum of product ions obtained by CID of the <sup>195</sup>Pt-A adduct at *m/z* 443 (collision energy = 15 eV), which was obtained by CID of the <sup>195</sup>Pt-AA adduct at *m/z* 578 using collision energy of 20 eV.

## Oxaliplatin-Guanine Mass Spectra

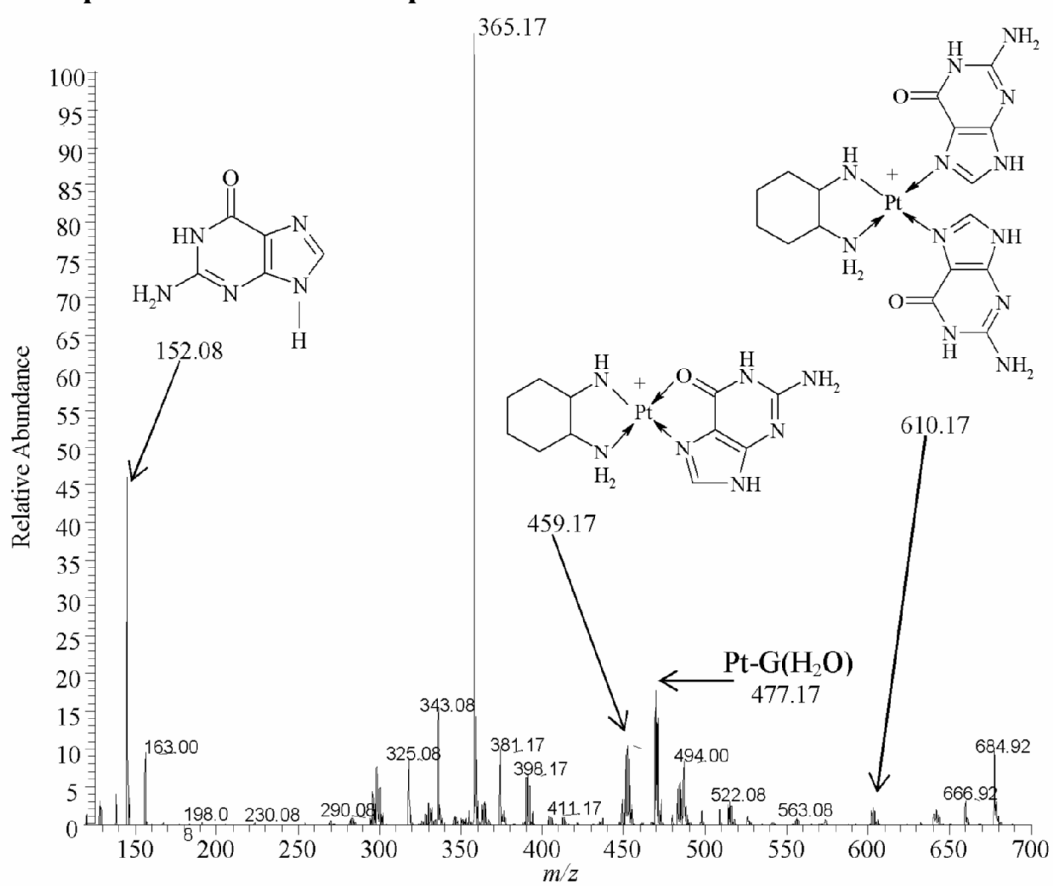
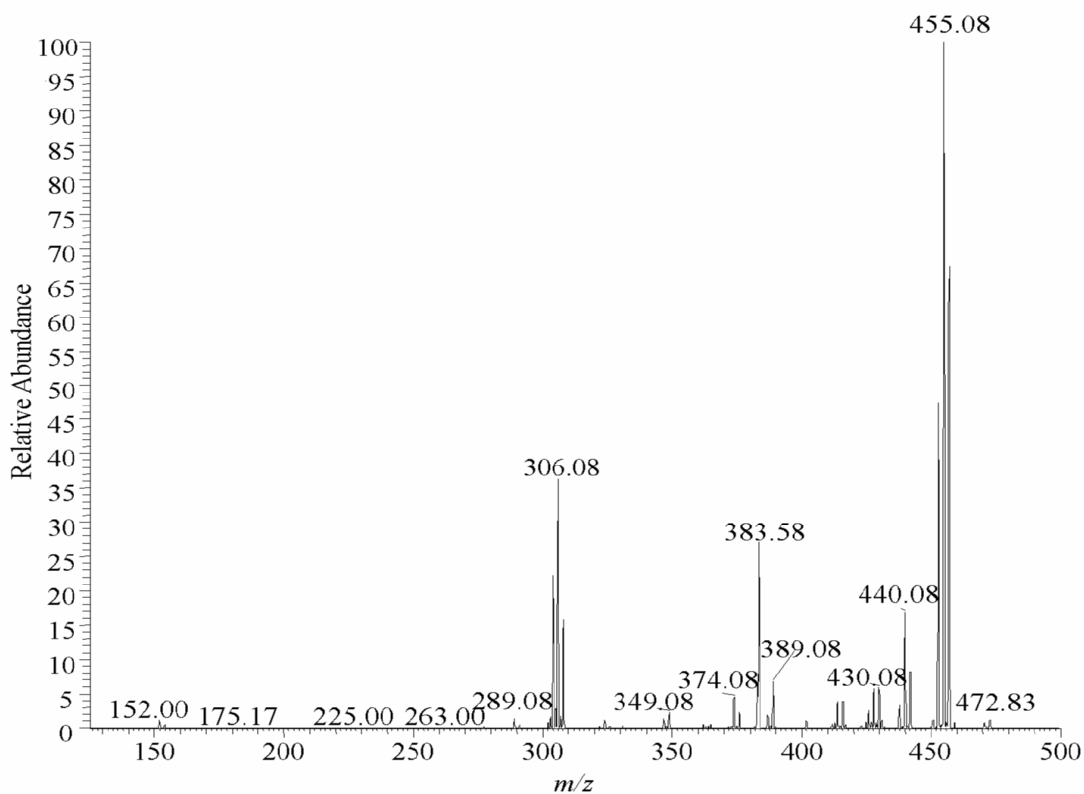
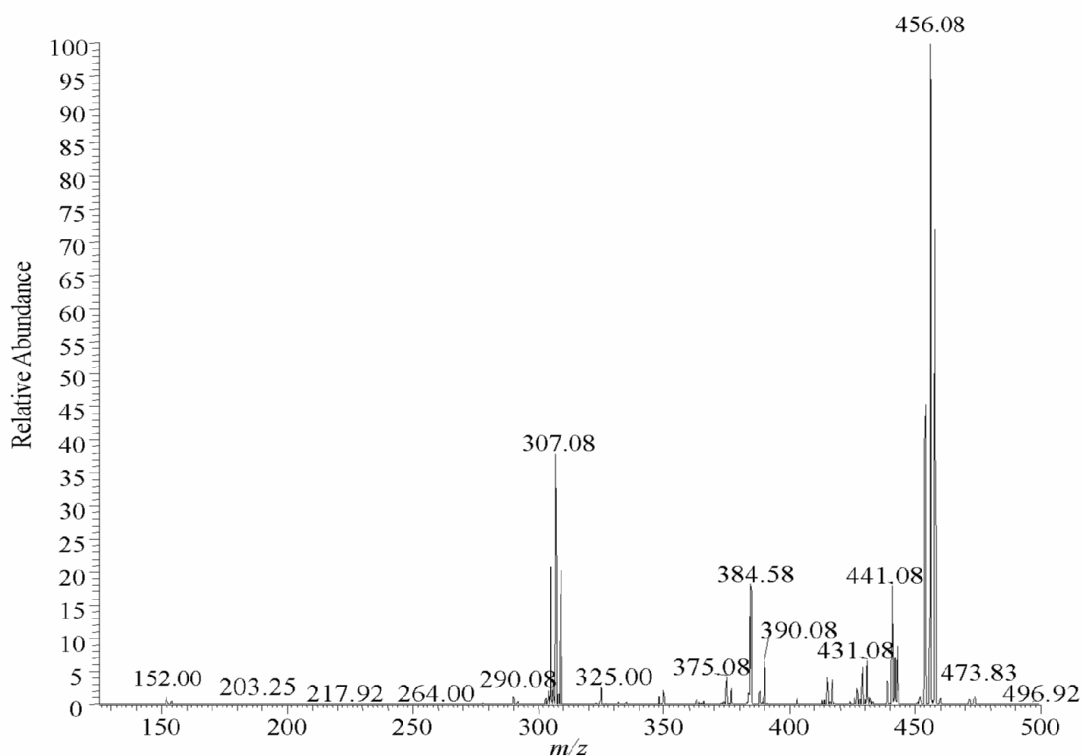


Figure 9:10: Full scan mass spectrum of the oxaliplatin-guanine mono-base solution.



**Figure 9:11:** MS/MS spectrum of product ions obtained by CID of the  $^{195}\text{Pt-G}$  adduct at  $m/z$  459 to yield the free Pt drug at  $m/z$  306 and free guanine base at  $m/z$  152. Collision energy = 20 eV and isolation width = 1 Da.



**Figure 9:12:** MS/MS spectrum of product ions obtained by CID of the  $^{196}\text{Pt-G}$  at  $m/z$  460 to yield the free Pt drug at  $m/z$  307 and free guanine base at  $m/z$  152. Collision energy = 20 eV and isolation width = 1 Da.

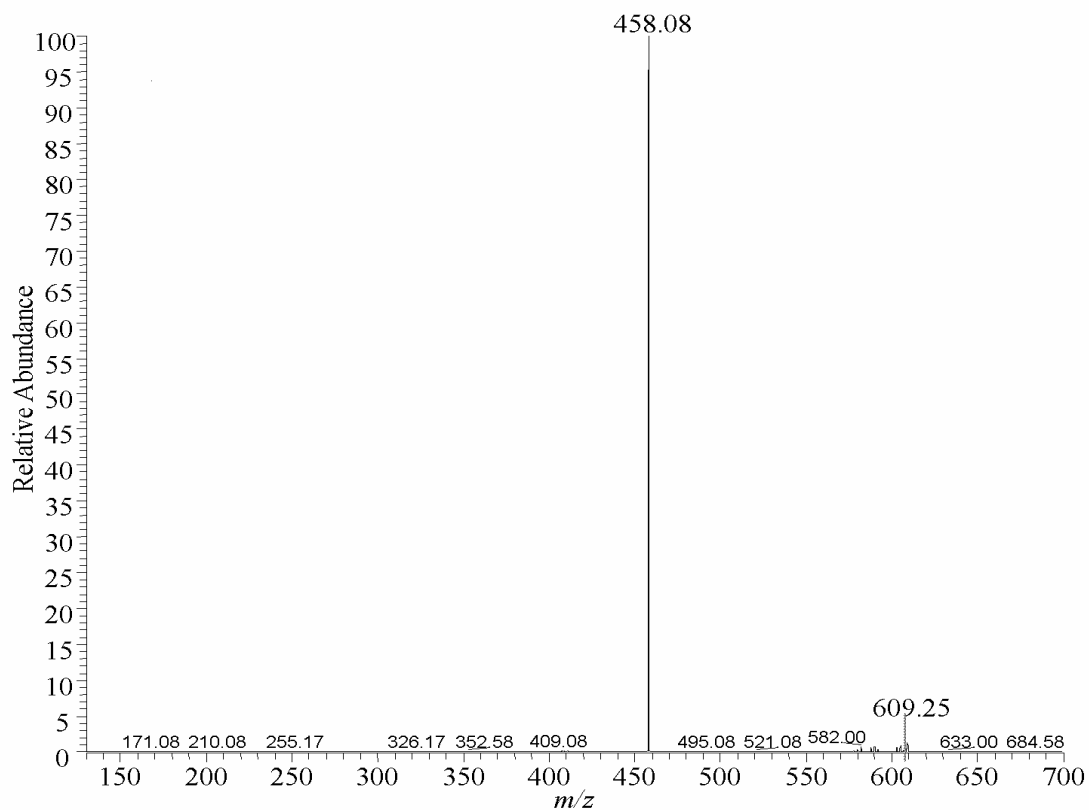


**Figure 9:13:** MS/MS spectrum of product ions obtained by CID of the  $^{194}\text{Pt}$ -GG adduct at  $m/z$  609 to yield the Pt-G adduct at  $m/z$  458. Collision energy = 20 eV and isolation width = 1 Da.

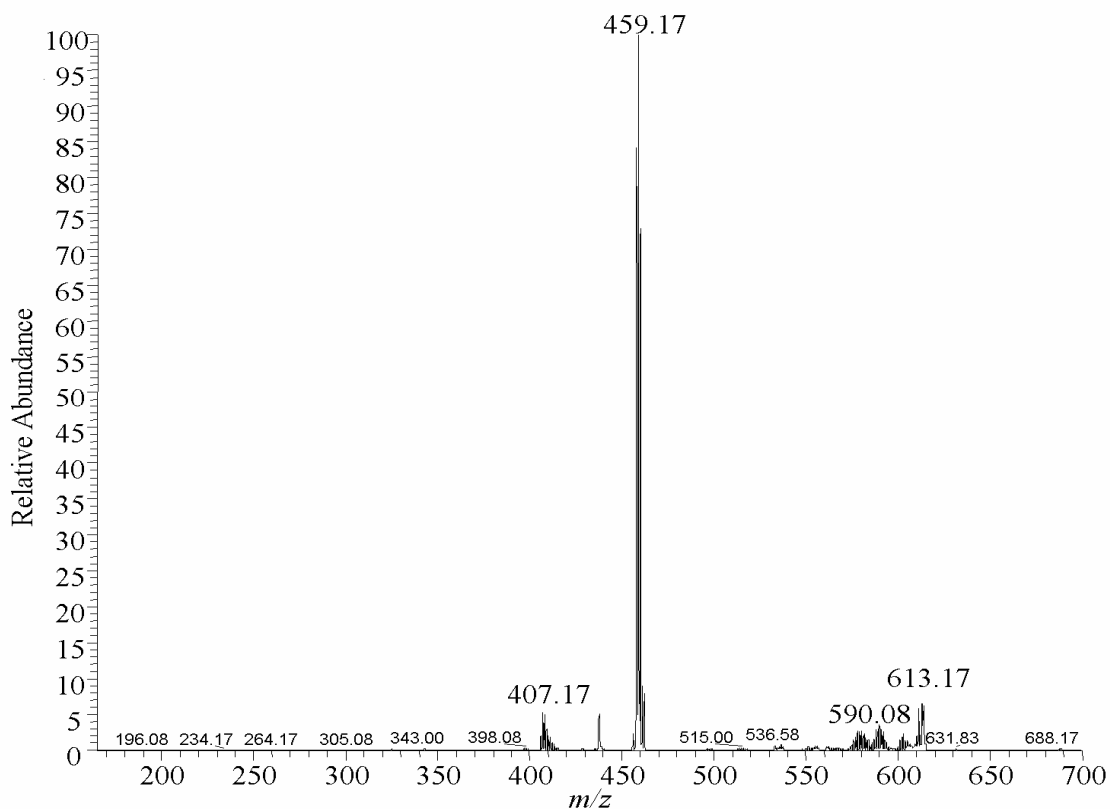


**Figure 9:14:** MS/MS spectrum of product ions obtained by CID of the  $^{195}\text{Pt}$ -GG adduct at  $m/z$  610 to yield the  $^{195}\text{Pt}$ -G adduct at  $m/z$  459. Collision energy = 15 eV and isolation width = 10 Da.

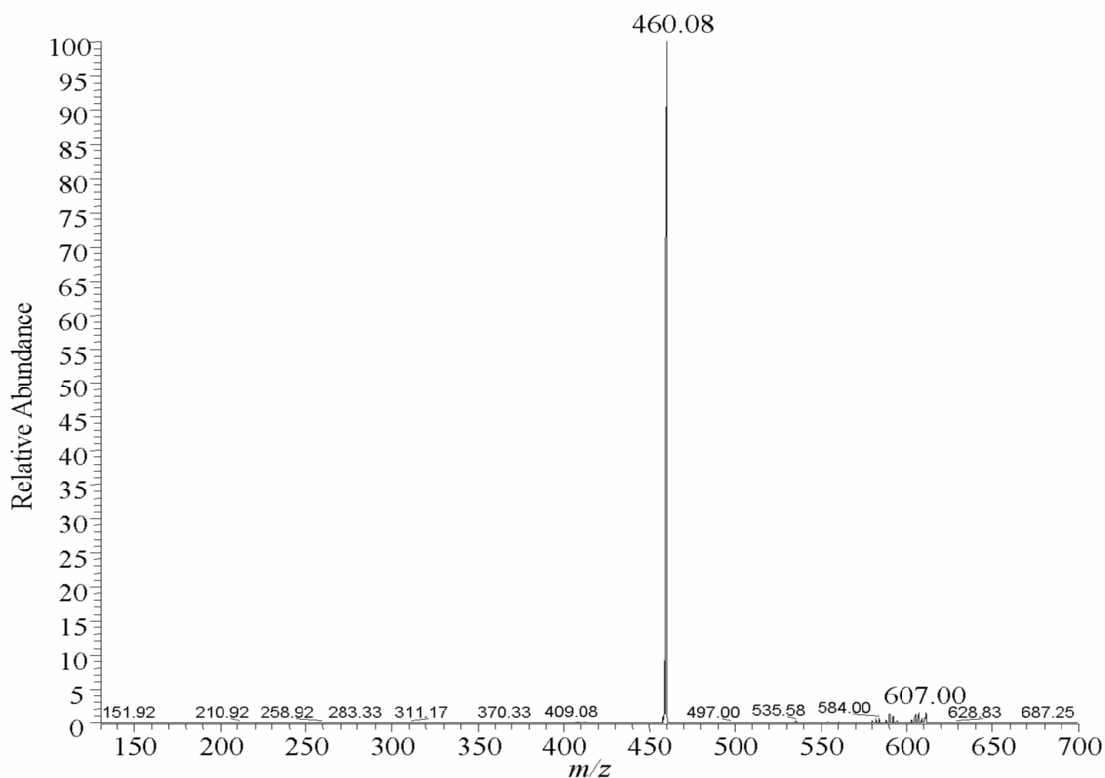


**Figure 9:15:** MS/MS spectrum of product ions obtained by CID of the  $^{196}\text{Pt}$ -GG adduct at  $m/z$  611 to yield the  $^{196}\text{Pt}$ -G adduct at  $m/z$  460. Collision energy = 20 eV and isolation width = 1 Da.

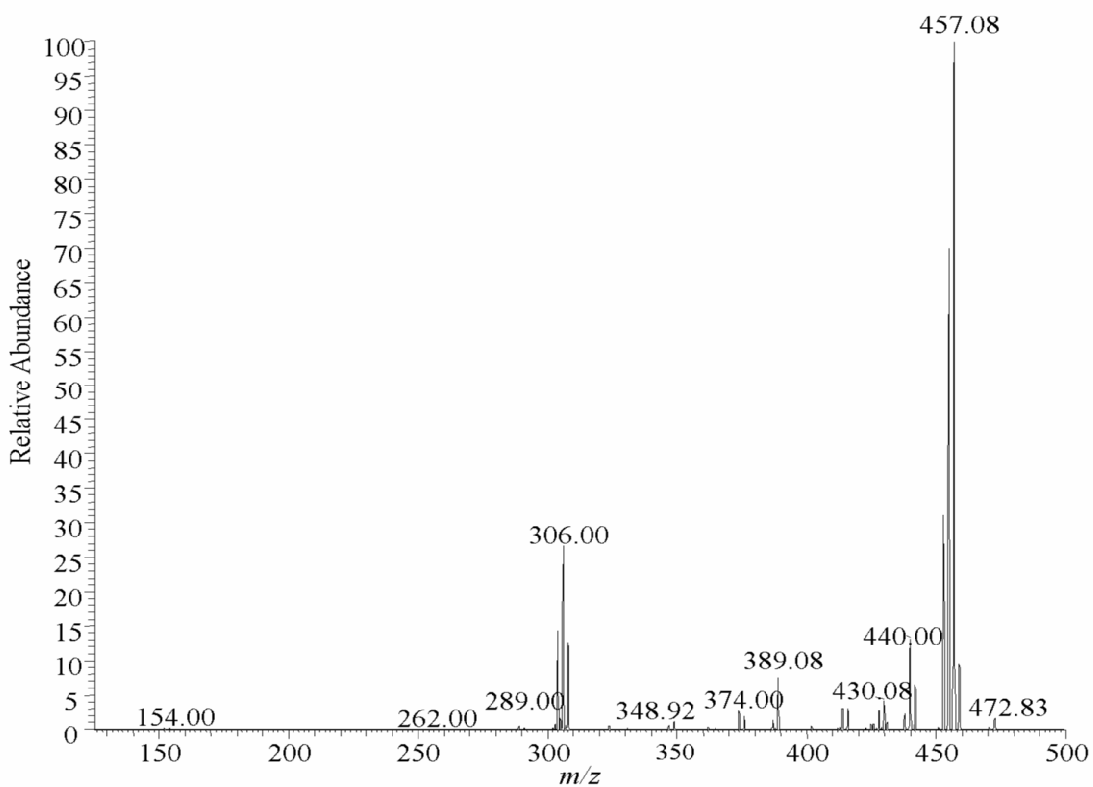


**Figure 9:16:** MS<sup>3</sup> spectrum of product ions obtained by CID of the  $^{195}\text{Pt}$ -G adduct at  $m/z$  459 (collision energy = 15 eV), which was obtained by CID of the  $^{195}\text{Pt}$ -GG adduct at  $m/z$  610 (collision energy = 20 eV).

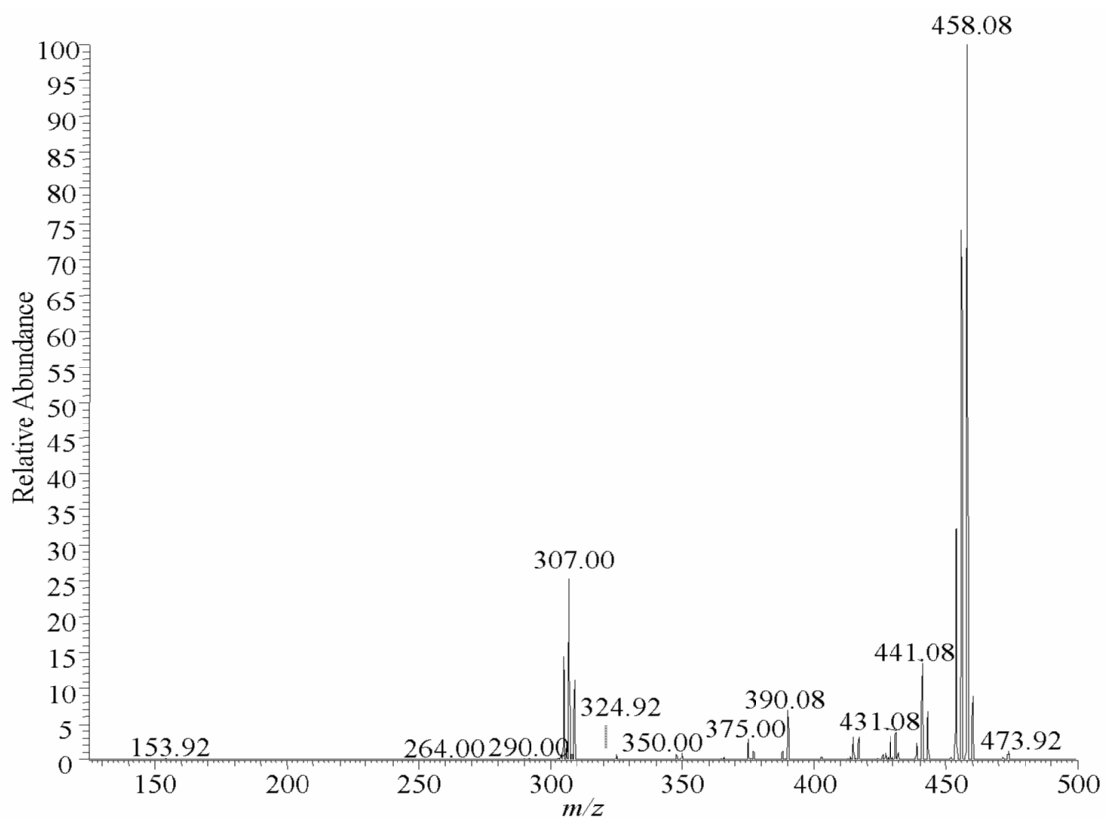


**Figure 9:17: MS<sup>3</sup> spectrum of product ions obtained by CID of the <sup>196</sup>Pt-G adduct at *m/z* 460 (collision energy =15 eV), which was obtained by CID of the <sup>196</sup>Pt-GG adduct at *m/z* 611 (collision energy = 20 eV).**

## Oxaliplatin-Thymine Mass Spectra

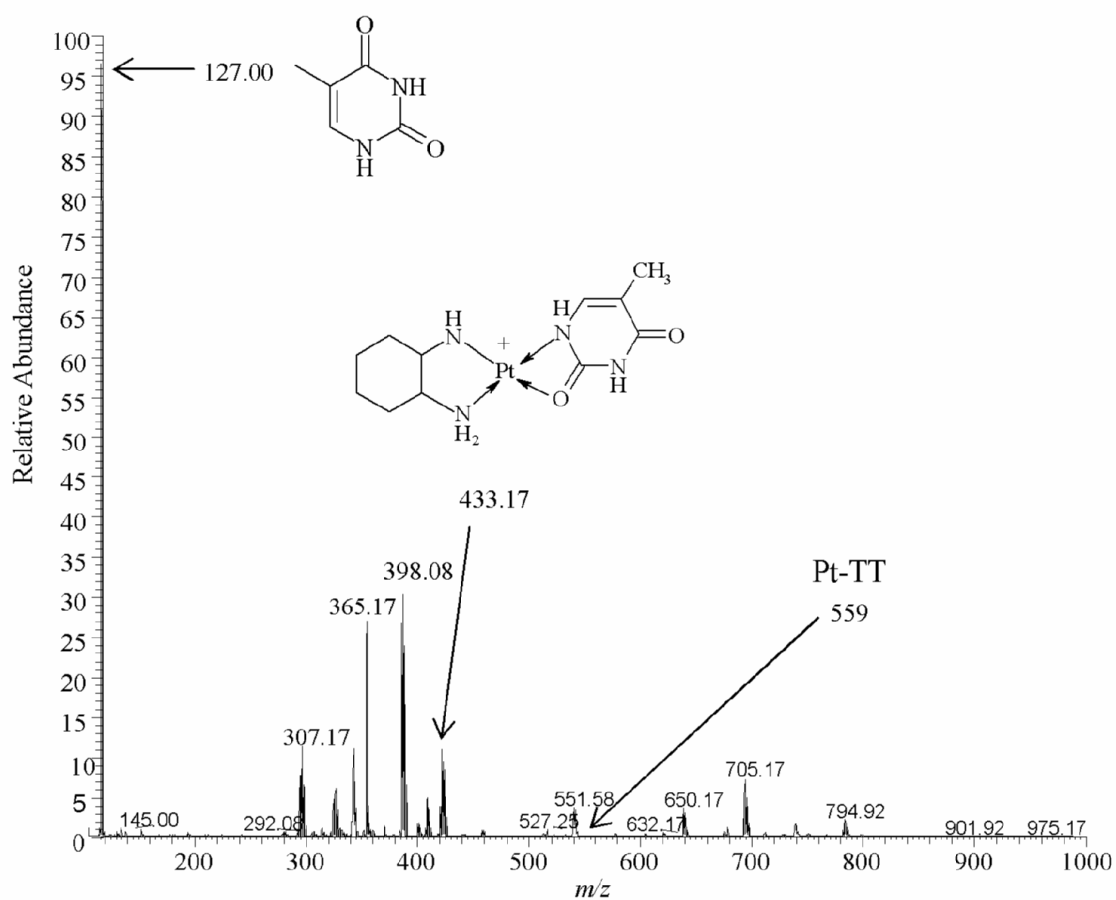
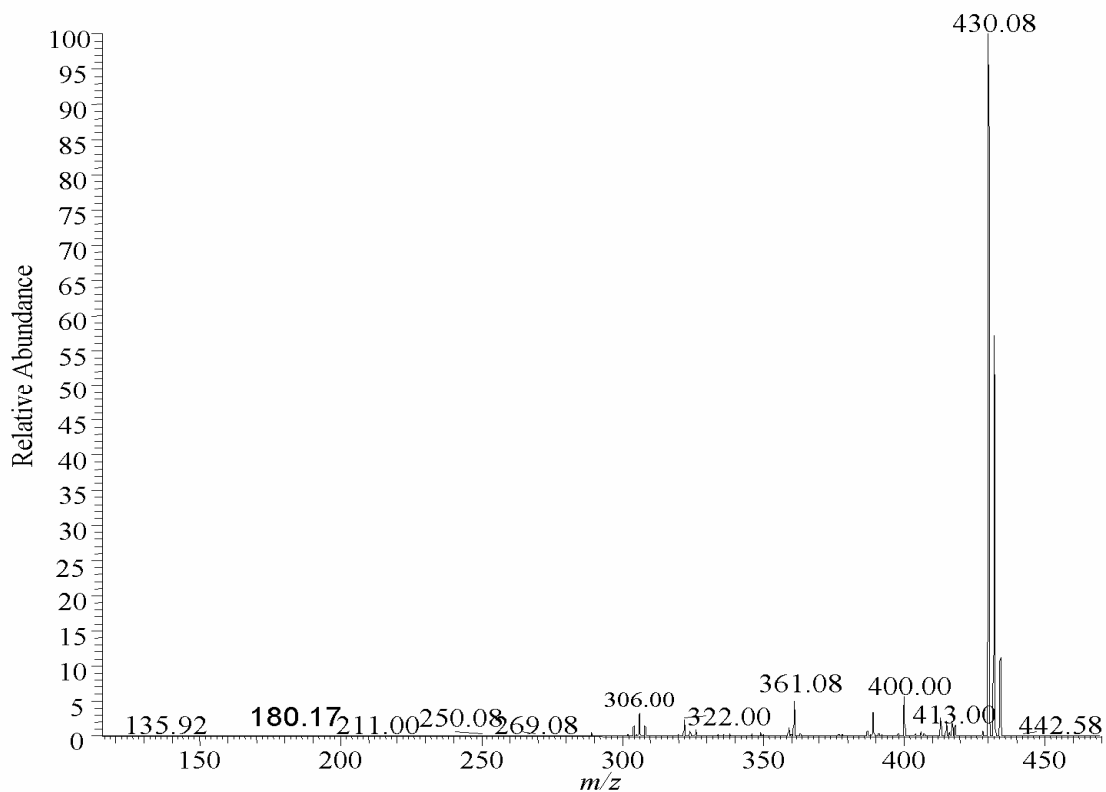
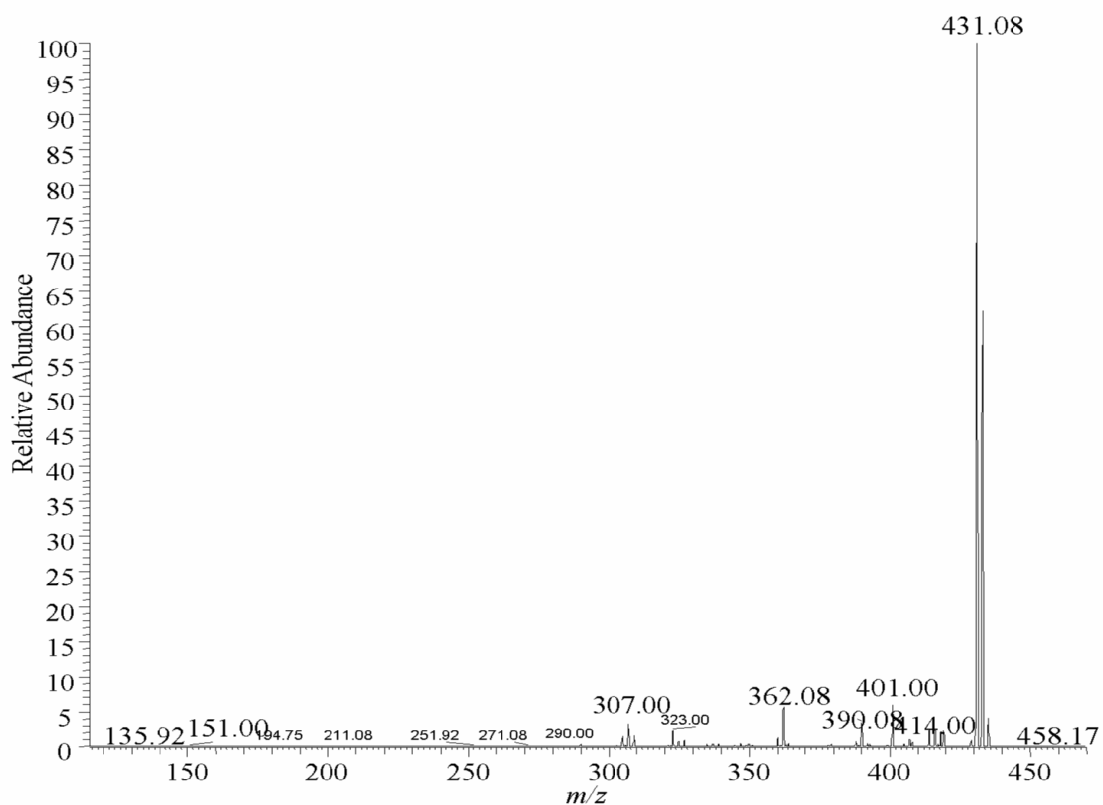


Figure 9:18: Full scan mass spectrum of oxaliplatin-thymine mono-base solution.





**Figure 9:19:** MS/MS spectrum of product ions obtained by CID of the  $^{195}\text{Pt}$ -T adduct at  $m/z$  434 to yield the free drug at  $m/z$  306. Collision energy = 20 eV and isolation width = 1 Da.



**Figure 9:20:** MS/MS spectrum of product ions obtained by CID of the  $^{196}\text{Pt}$ -T adduct at  $m/z$  435 to yield the free drug at  $m/z$  307. Collision energy = 20 eV and isolation width = 1 Da.

## Oxaliplatin-Cytosine Mass Spectrometry Data

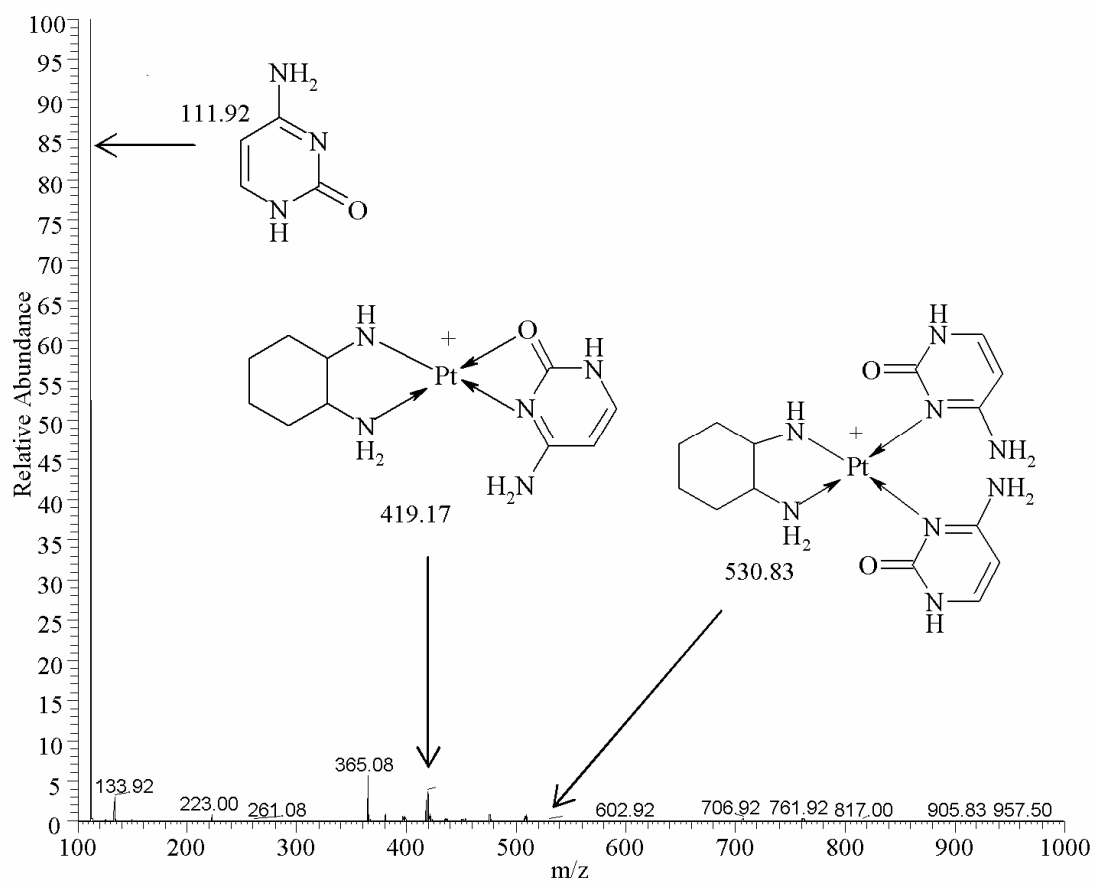
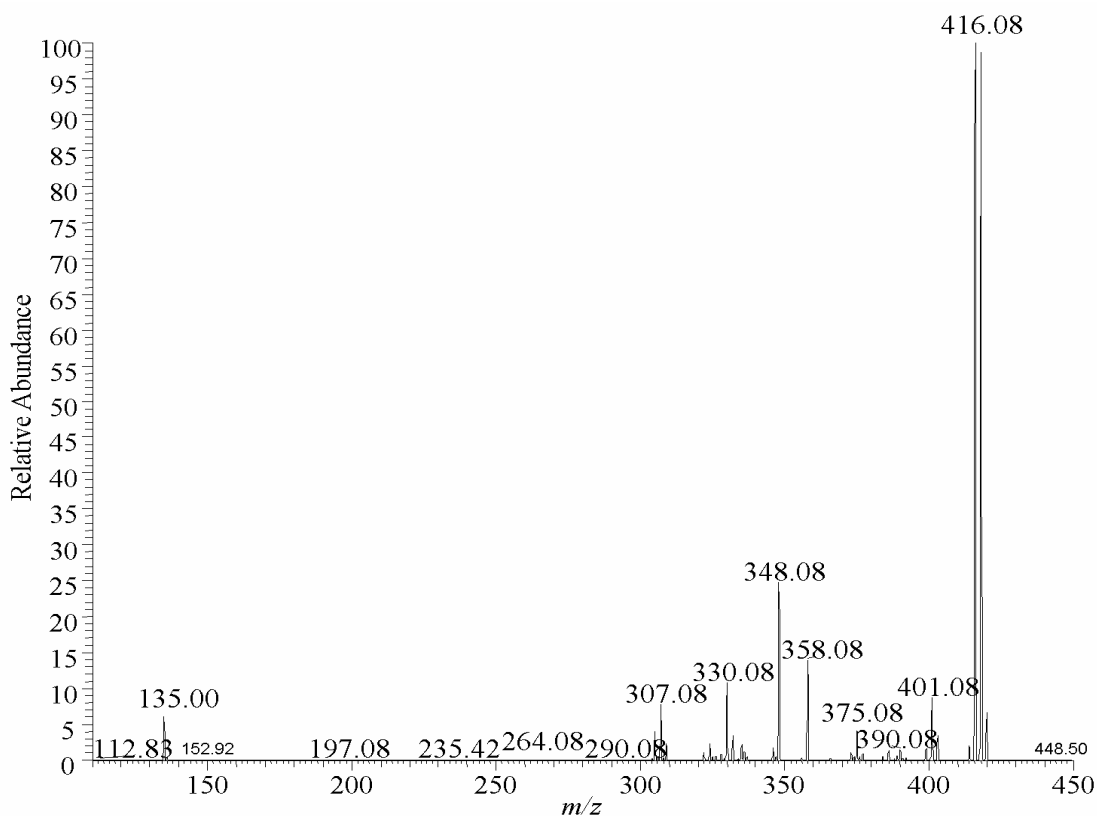
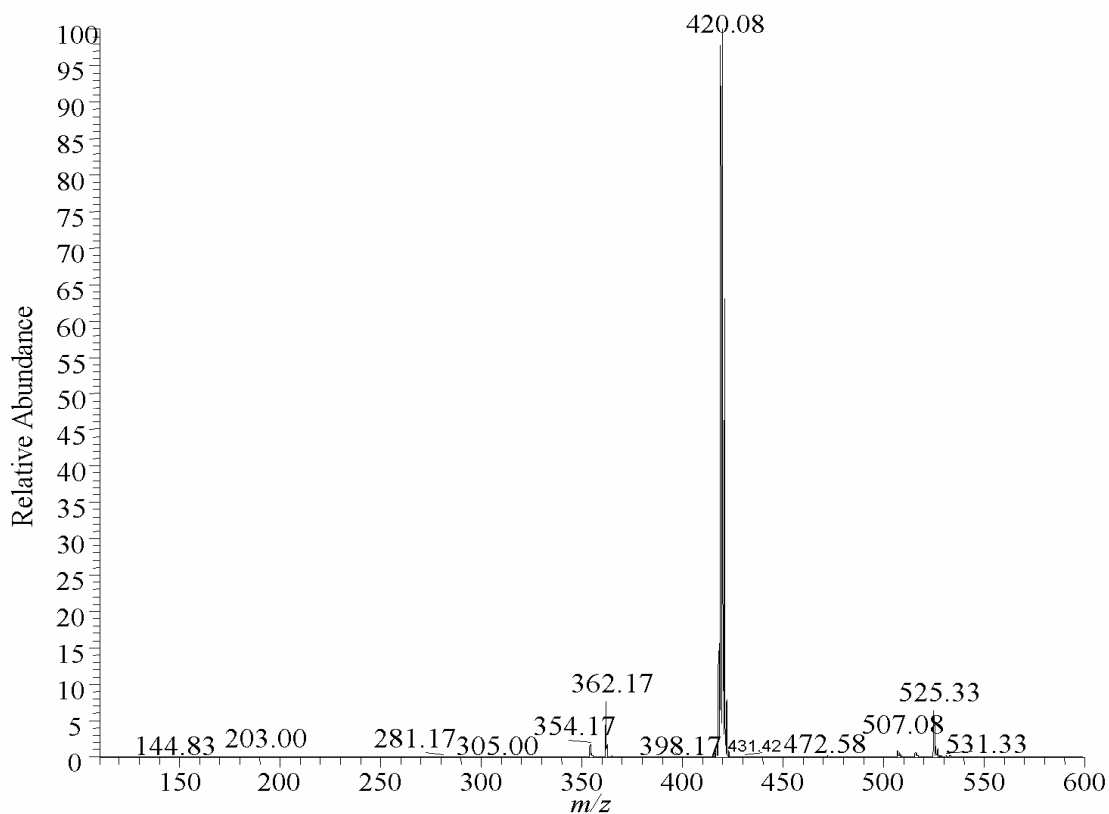


Figure 9:21: Full scan mass spectrum of the oxaliplatin-cytosine mono-base solution.



**Figure 9:22:** MS/MS spectrum of product ions obtained by CID of the  $^{196}\text{Pt-C}$  adduct at  $m/z$  420 to yield the free drug at  $m/z$  307. Collision energy = 20 eV and isolation width = 1 Da.



**Figure 9:23:** MS/MS spectrum of product ions obtained by CID of the  $^{195}\text{Pt-CC}$  adduct at  $m/z$  530 to yield the mono-adduct, collision energy = 20 eV and isolation width = 10 Da.

## Hydrated Complexes of Guanine

These spectra were obtained from the oxaliplatin-guanine mono-base solution and show how the hydrated guanine complex fragmented to form the Pt-G mono-adduct. Further CID was conducted on the Pt-G product ion to yield many product ions, which were characteristic to Pt-G fragmentation.

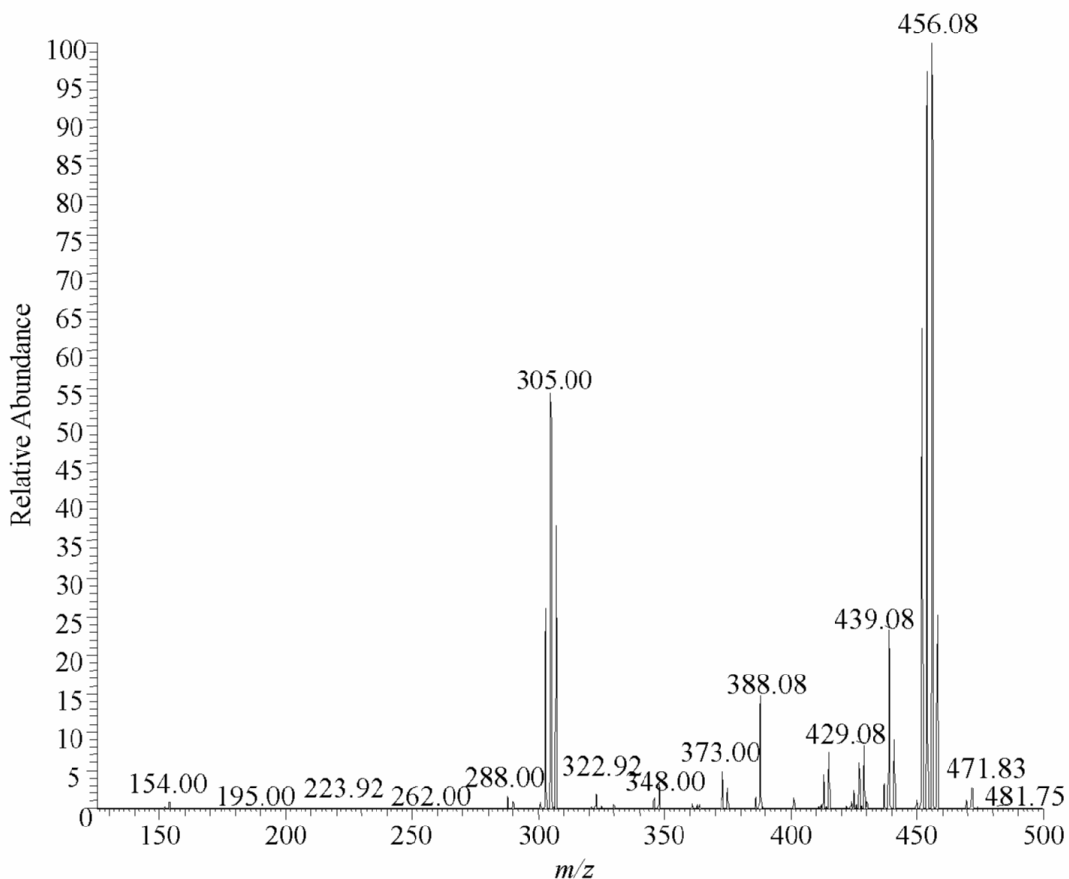


**Figure 9:24:** MS<sup>3</sup> spectrum of product ions obtained by CID of the <sup>194</sup>Pt-G adduct at *m/z* 458, (collision energy = 20 eV) which was obtained by CID of the <sup>194</sup>Pt-G(H<sub>2</sub>O) adduct at *m/z* 476. Collision energy of 15 eV

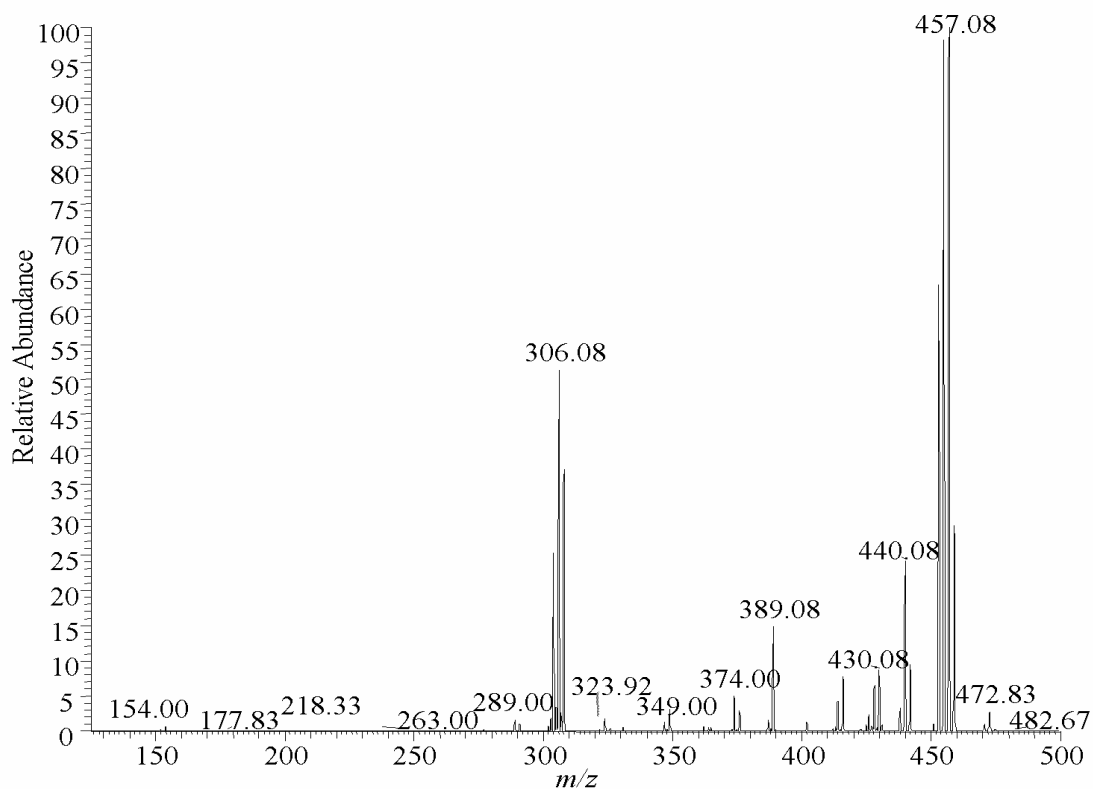


**Figure 9:25:** MS<sup>3</sup> spectrum of product ions obtained by CID of the <sup>195</sup>Pt-G adduct at *m/z* 459, (collision energy = 15 eV) which was obtained by CID of the <sup>195</sup>Pt-G(H<sub>2</sub>O) adduct at *m/z* 477. Collision energy of 20 eV.

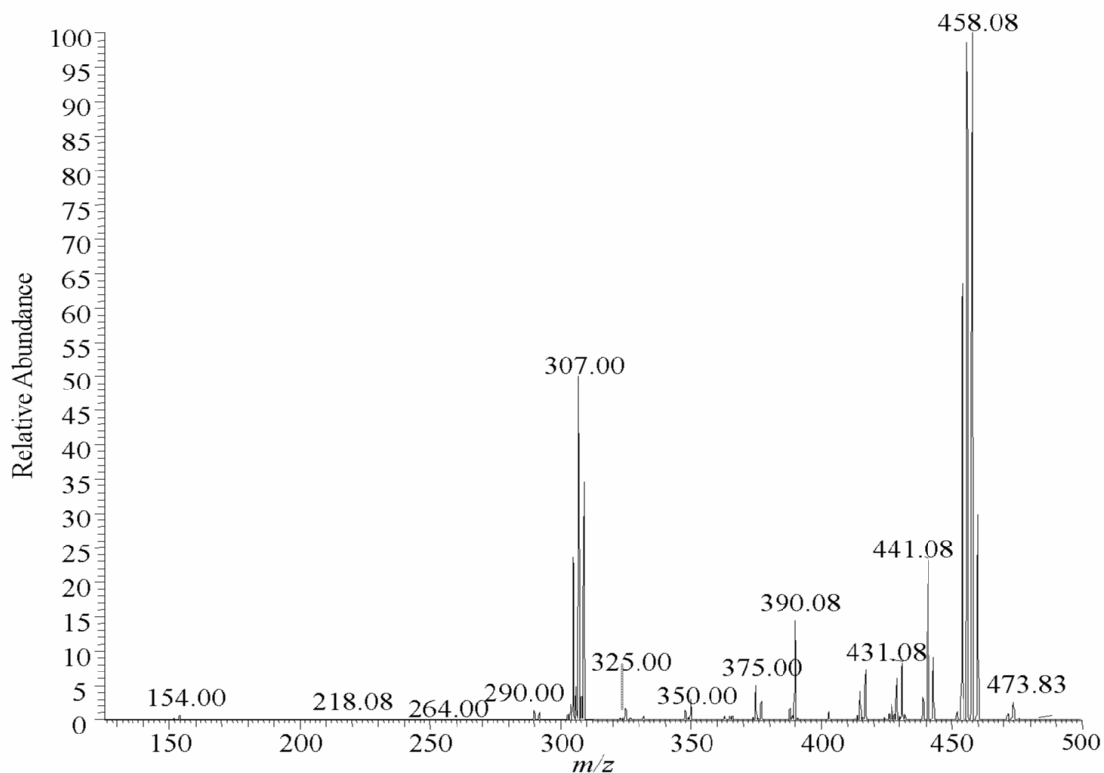


**Figure 9:26:** MS<sup>3</sup> spectrum of product ions obtained by CID of the <sup>196</sup>Pt-G adduct at *m/z* 460, (collision energy = 20 eV) which was obtained by CID of the <sup>196</sup>Pt-G(H<sub>2</sub>O) adduct at *m/z* 478, collision energy = 15 eV.

### 9.3 Appendix 2.3: Oxaliplatin mixture containing A, C, G and T in equal-molar proportions

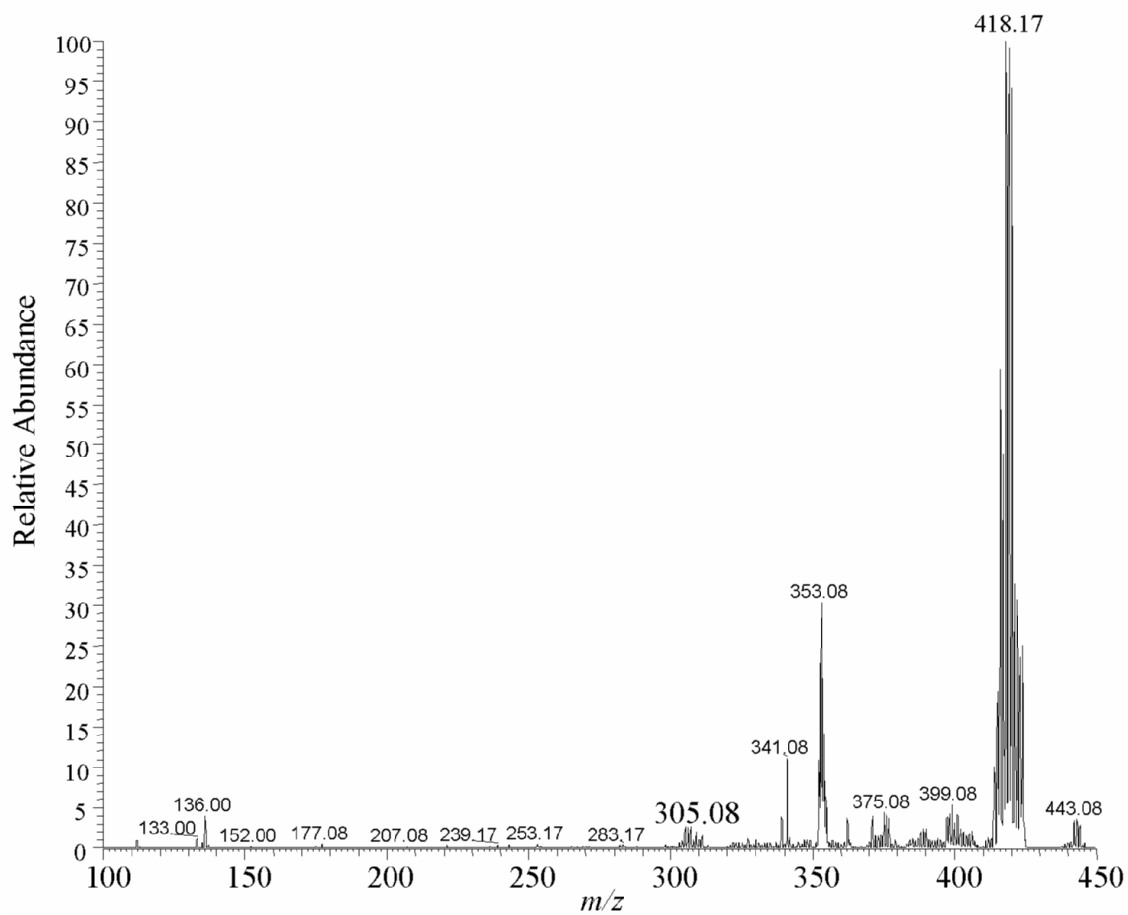


**Figure 9:27:** MS/MS spectrum of product ions obtained by CID of the  $^{196}\text{Pt}$ -C adduct at  $m/z$  420 to yield the free drug at  $m/z$  305. Collision energy = 15 eV and isolation width = 10 Da.

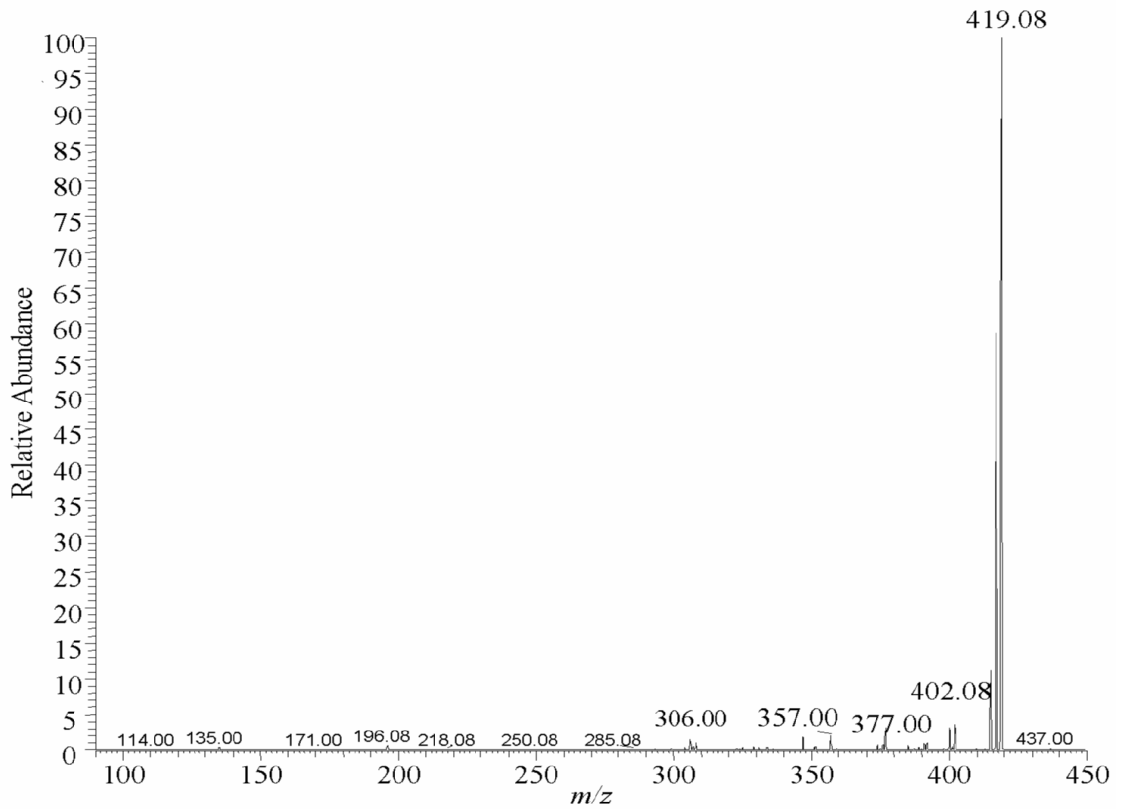


**Figure 9:28:** MS/MS spectrum of product ions obtained by CID of the  $^{196}\text{Pt-C}$  adduct at  $m/z$  420 to yield the free drug at  $m/z$  306. Collision energy = 20 eV and isolation width = 1 Da.

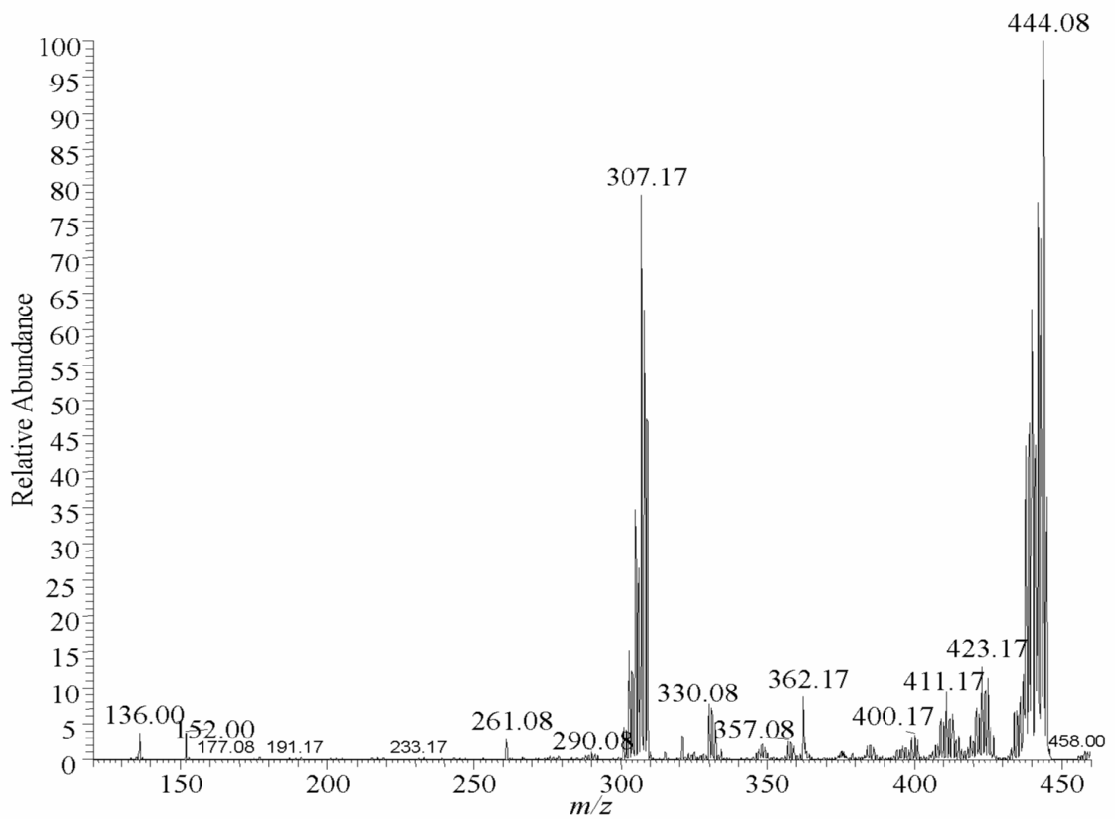


**Figure 9:29:** MS/MS of spectrum of product ions obtained by CID of the Pt-A adduct at  $m/z$  441 to yield the free drug at  $m/z$  307. Collision energy = 15 eV and isolation width = 10 Da.

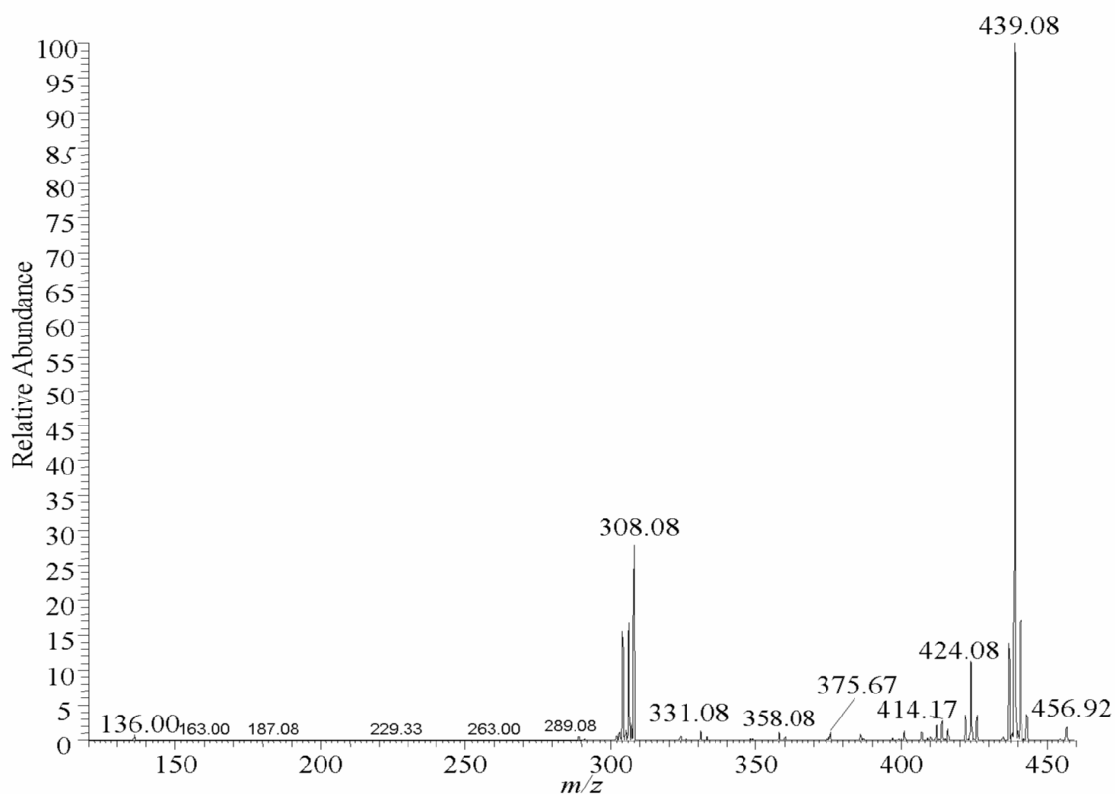


**Figure 9:30:** MS/MS spectrum of product ions obtained by CID of the  $^{195}\text{Pt-A}$  adduct at  $m/z$  443 to yield the free Pt drug at  $m/z$  308 and free adenine base at  $m/z$  136. Collision energy = 20 eV and isolation width = 1 Da.

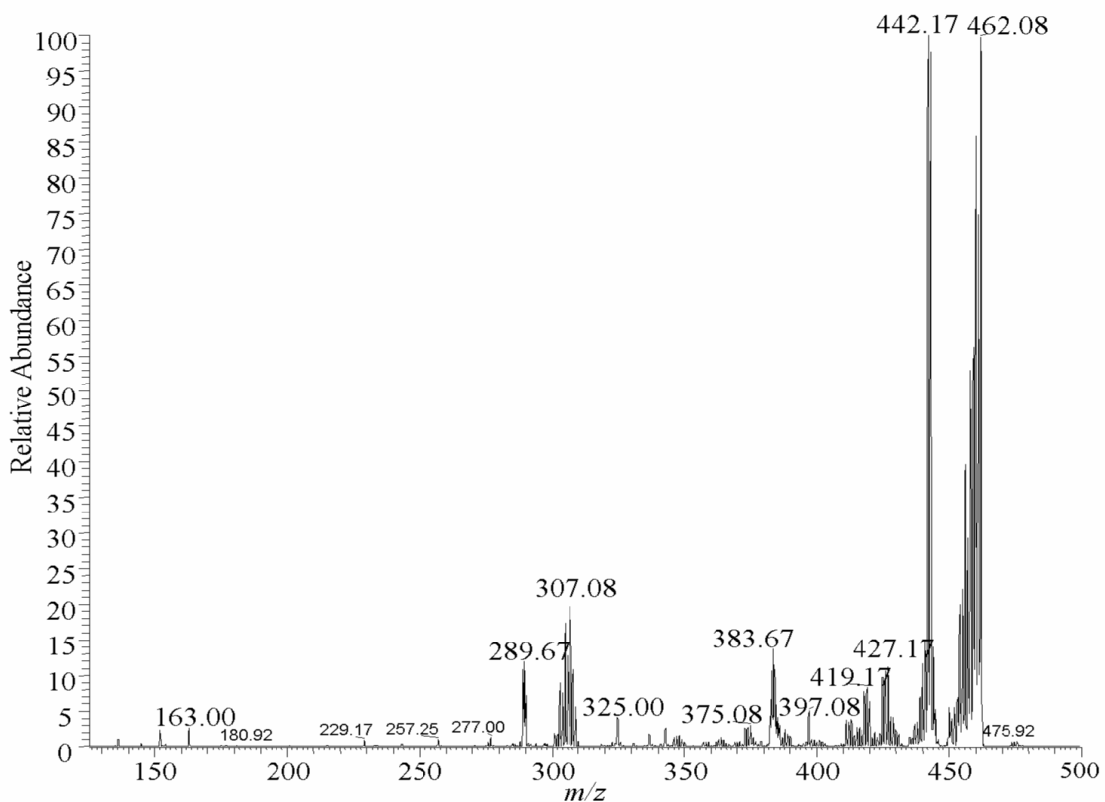


**Figure 9:31:** MS/MS spectrum of product ions obtained by CID of the  $^{194}\text{Pt-G}$  adduct at  $m/z$  458 to yield the free Pt drug at  $m/z$  307. Collision energy = 15 eV and isolation width = 10 Da.



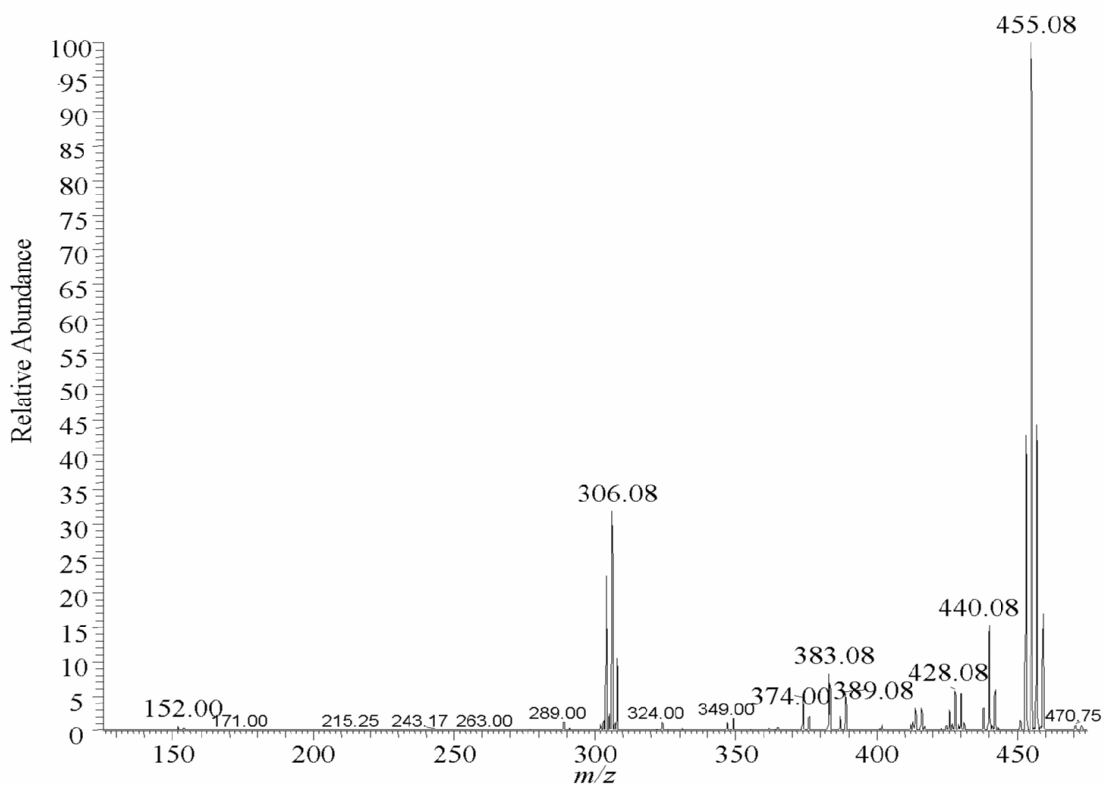


**Figure 9:32:** MS/MS spectrum of product ions obtained by CID of the  $^{195}\text{Pt-G}$  adduct at  $m/z$  459 to yield the free Pt drug at  $m/z$  306 and free guanine base at  $m/z$  152. Collision energy = 20 eV and isolation width = 1 Da.

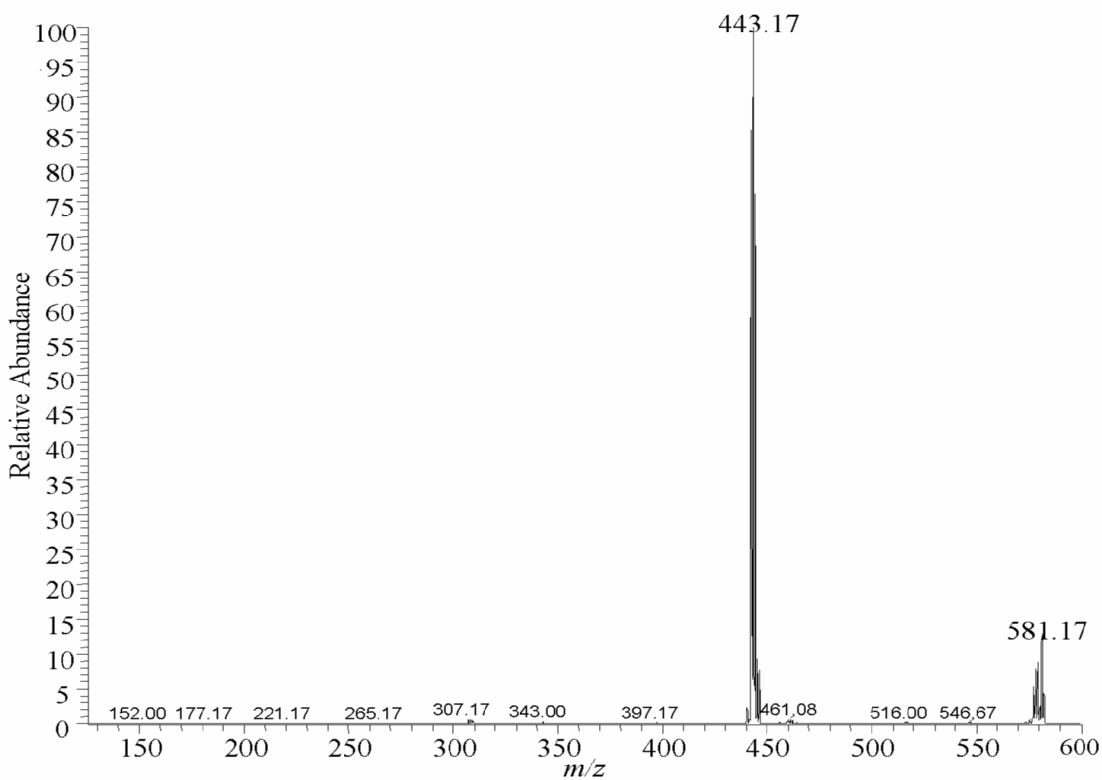


**Figure 9:33:** MS/MS spectrum of product ions obtained by CID of the  $^{195}\text{Pt-AA}$  adduct at  $m/z$  578 to yield the Pt-A adduct at  $m/z$  443. Collision energy = 15 eV and isolation width = 10 Da.

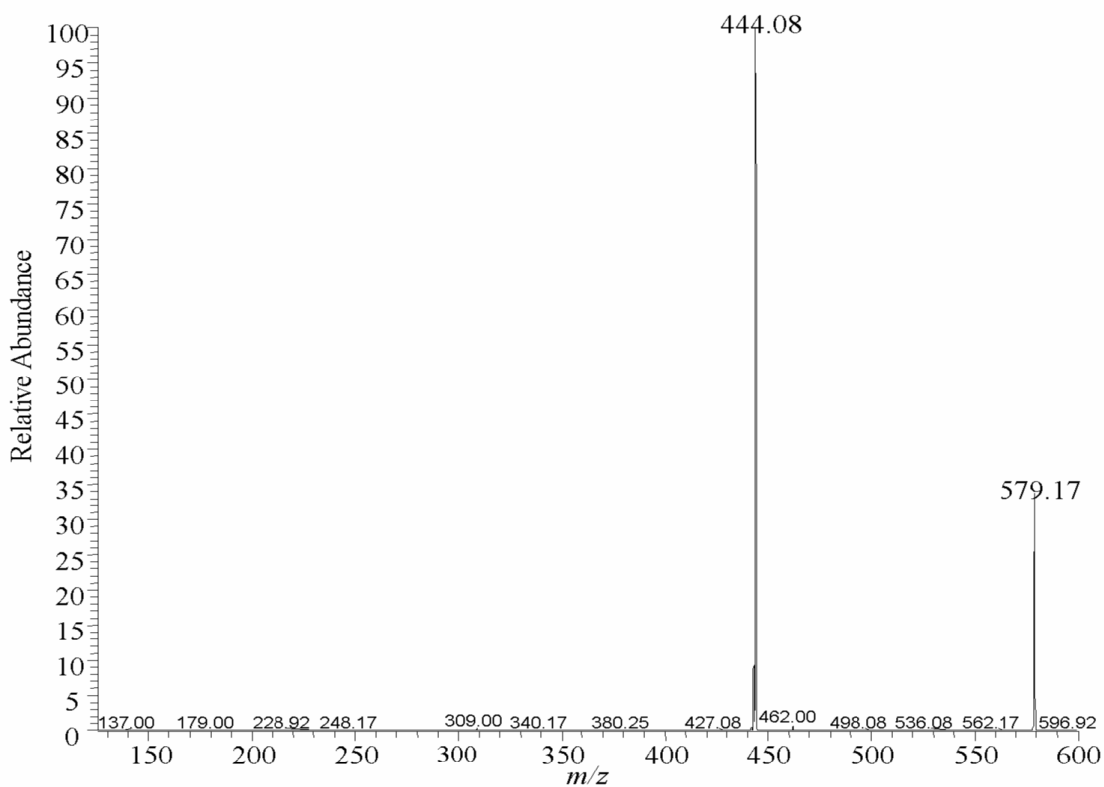


**Figure 9:34:** MS/MS spectrum of product ions obtained by CID of the  $^{196}\text{Pt-AA}$  adduct at  $m/z$  579 to yield the  $^{196}\text{Pt-A}$  adduct at  $m/z$  444. Collision energy = 20 eV and isolation width = 1 Da.

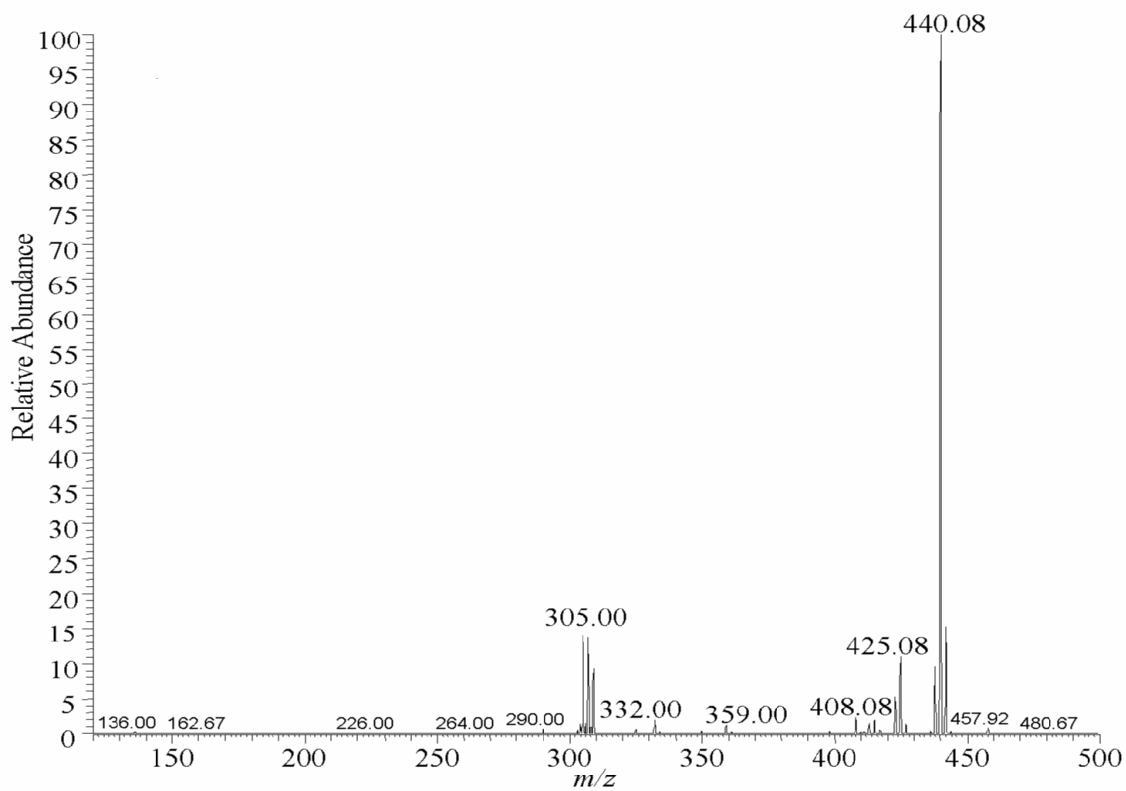


**Figure 9:35:** MS<sup>3</sup> spectrum of product ions obtained by CID of the  $^{196}\text{Pt-A}$  adduct at  $m/z$  444 (collision energy = 20 eV and isolation width = 1 Da), which were obtained through CID of  $^{196}\text{Pt-AA}$  adduct at  $m/z$  579 (collision energy = 20 eV and isolation width = 1).

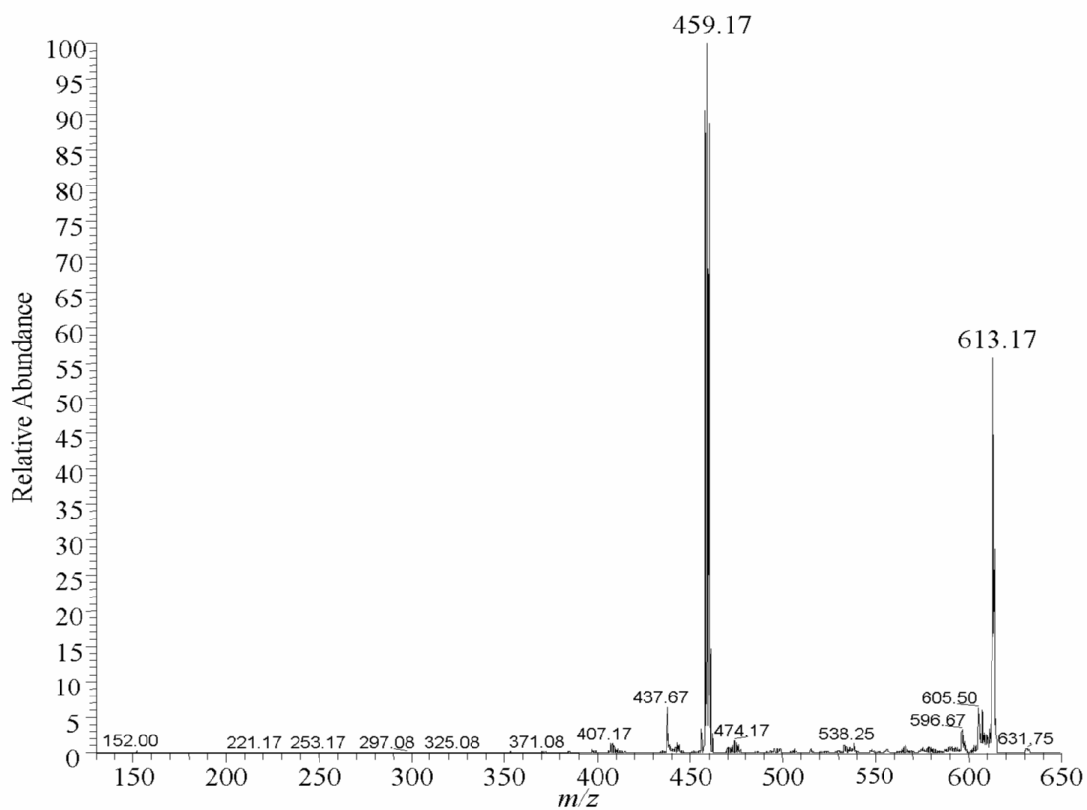


**Figure 9:36:** MS/MS spectrum of product ions obtained by CID of the  $^{195}\text{Pt}$ -GG adduct at  $m/z$  610 to yield the Pt-G adduct at  $m/z$  459. Collision energy = 15 eV and isolation width = 10 Da.

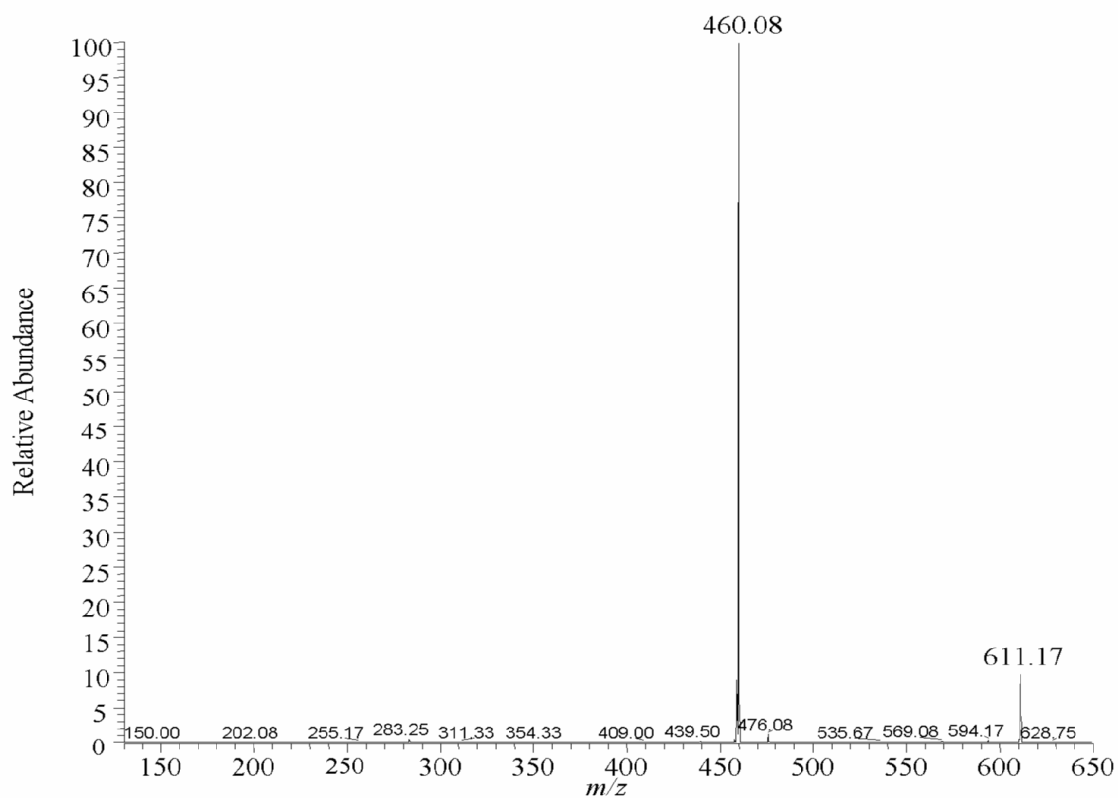


**Figure 9:37:** MS/MS spectrum of product ions obtained by CID of the  $^{196}\text{Pt}$ -GG adduct at  $m/z$  611 to yield the  $^{196}\text{Pt}$ -G adduct at  $m/z$  460. Collision energy = 20 eV and isolation width = 1 Da.

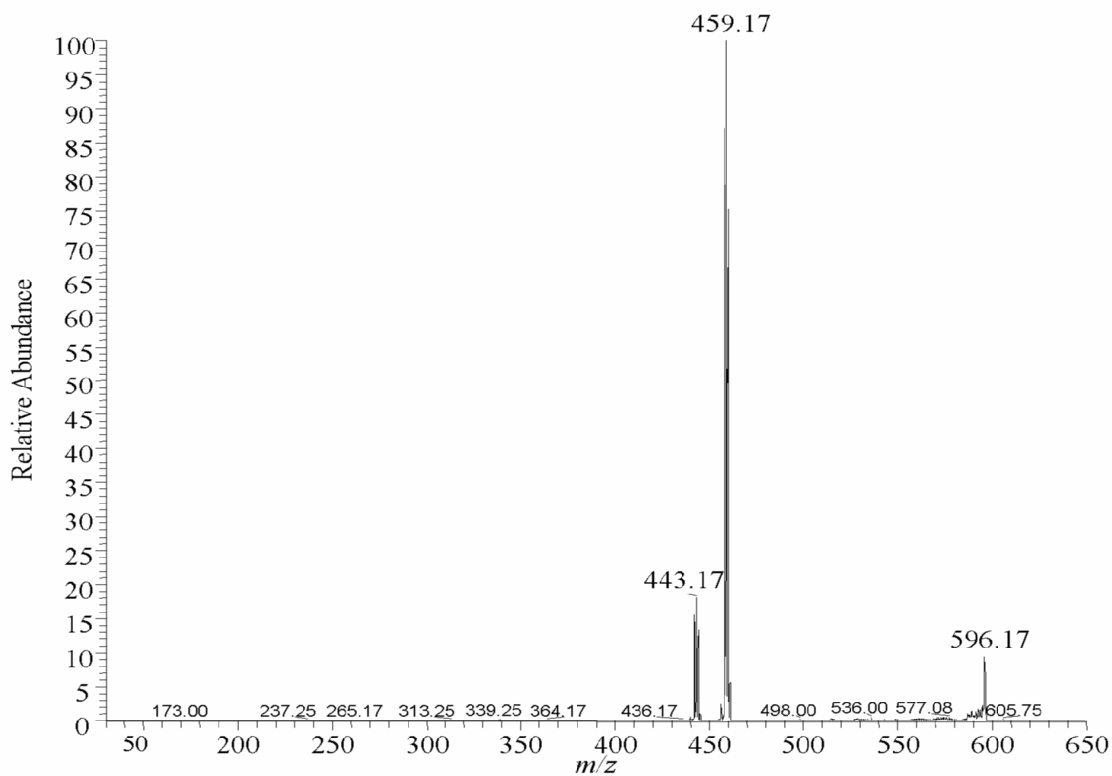


**Figure 9:38:** MS/MS spectrum of product ions obtained by CID of the Pt-AG adduct at  $m/z$  592 to yield the Pt-G and Pt-A adduct at  $m/z$  459 and 443 respectively. Collision energy = 20 eV and isolation width = 10 Da.

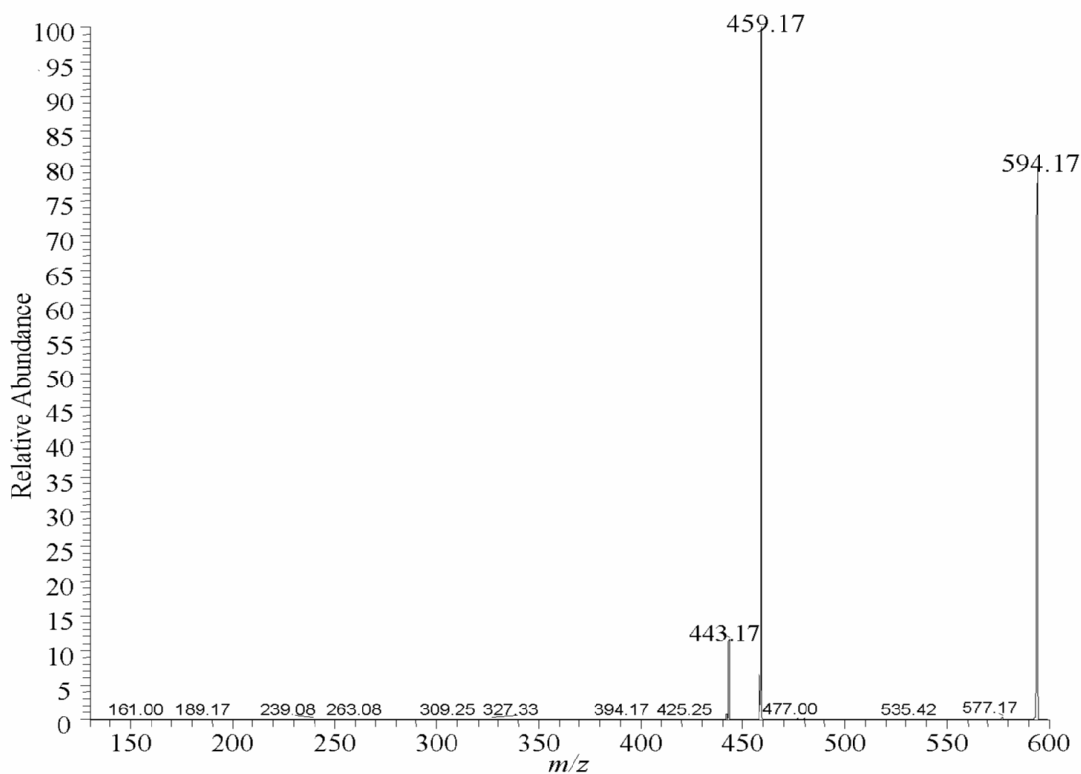


**Figure 9:39:** MS/MS spectrum of product ions obtained by CID of the  $^{195}\text{Pt}$ -AG adduct at  $m/z$  594 to yield the  $^{195}\text{Pt}$ -A and  $^{195}\text{Pt}$ -G adducts at  $m/z$  443 and 459 respectively. Collision energy = 20 eV and isolation width = 1 Da.

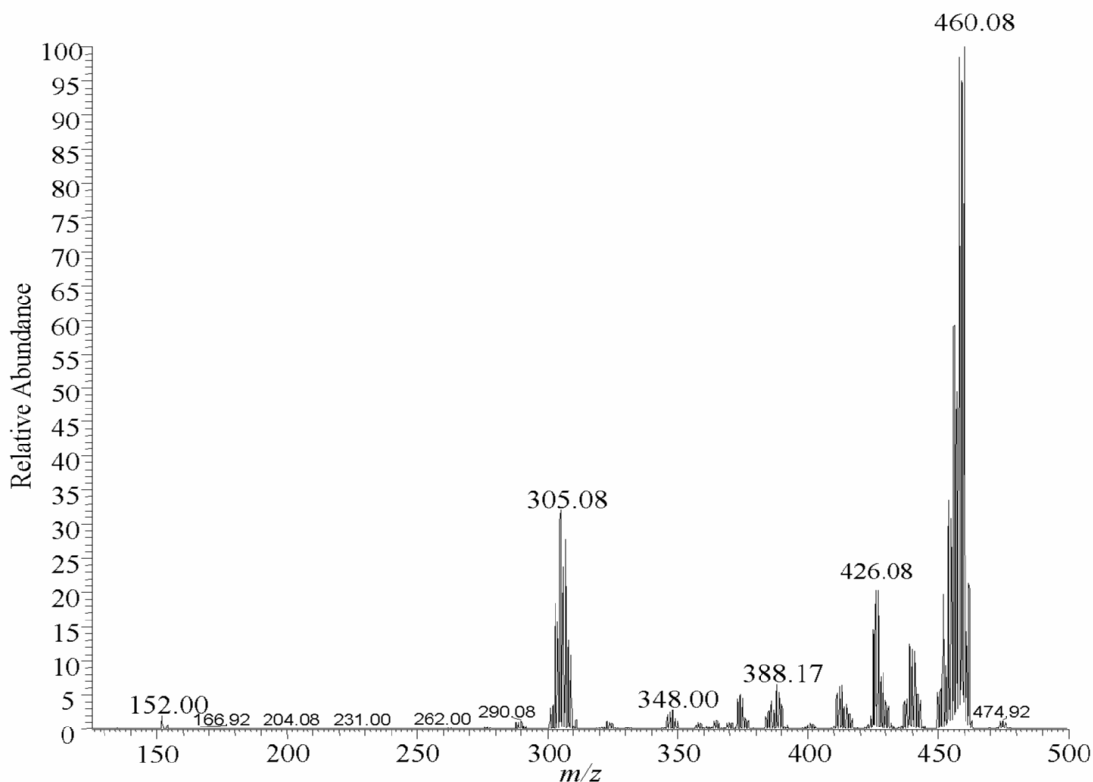


**Figure 9:40:** MS<sup>3</sup> spectrum of product ions obtained by CID of the Pt-G adduct at  $m/z$  459 (collision energy = 20 eV and isolation width = 10), which was obtained by CID of the Pt-AG adduct at  $m/z$  594 (collision energy = 15 eV and isolation width = 10 Da).

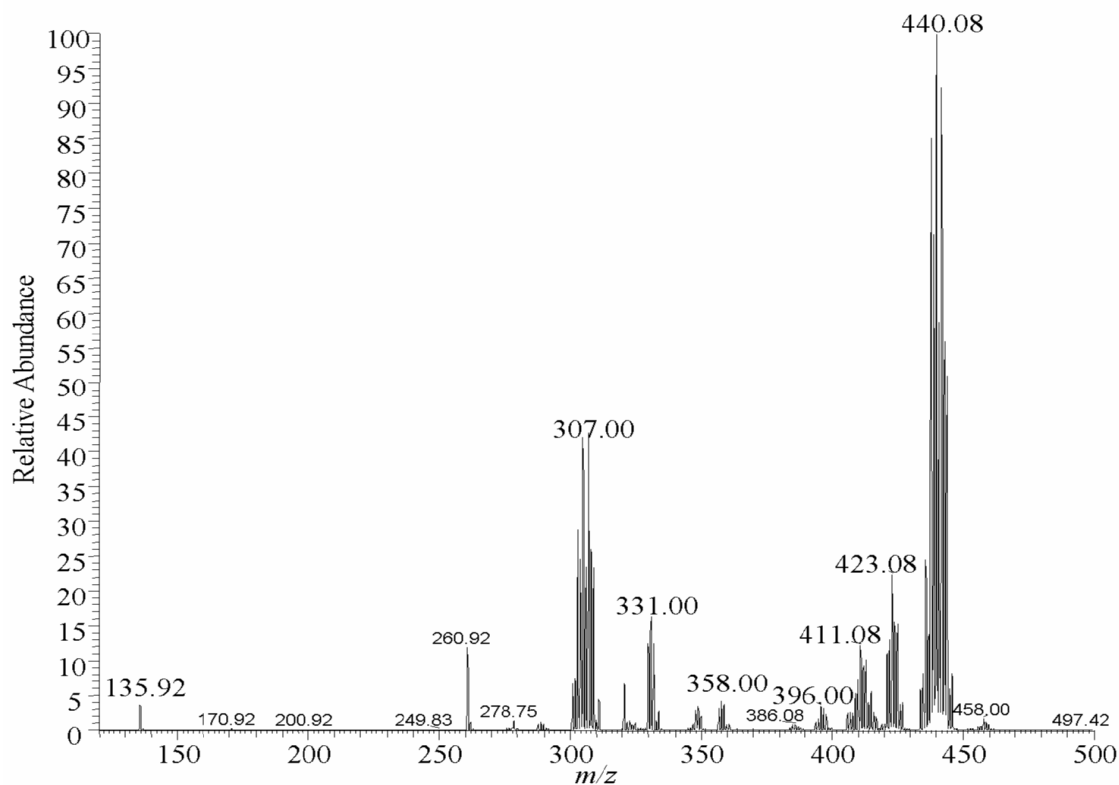


**Figure 9:41:** MS<sup>3</sup> spectrum of product ions obtained by CID of the Pt-A adduct at  $m/z$  443 (collision energy = 15 eV), which was obtained by CID of the Pt-AG adduct at  $m/z$  594 (collision energy = 20 eV and isolation width = 10 Da).

## 9.4 Appendix 2.4: Oxaliplatin mixture containing A, C, G and T with an excess of oxaliplatin

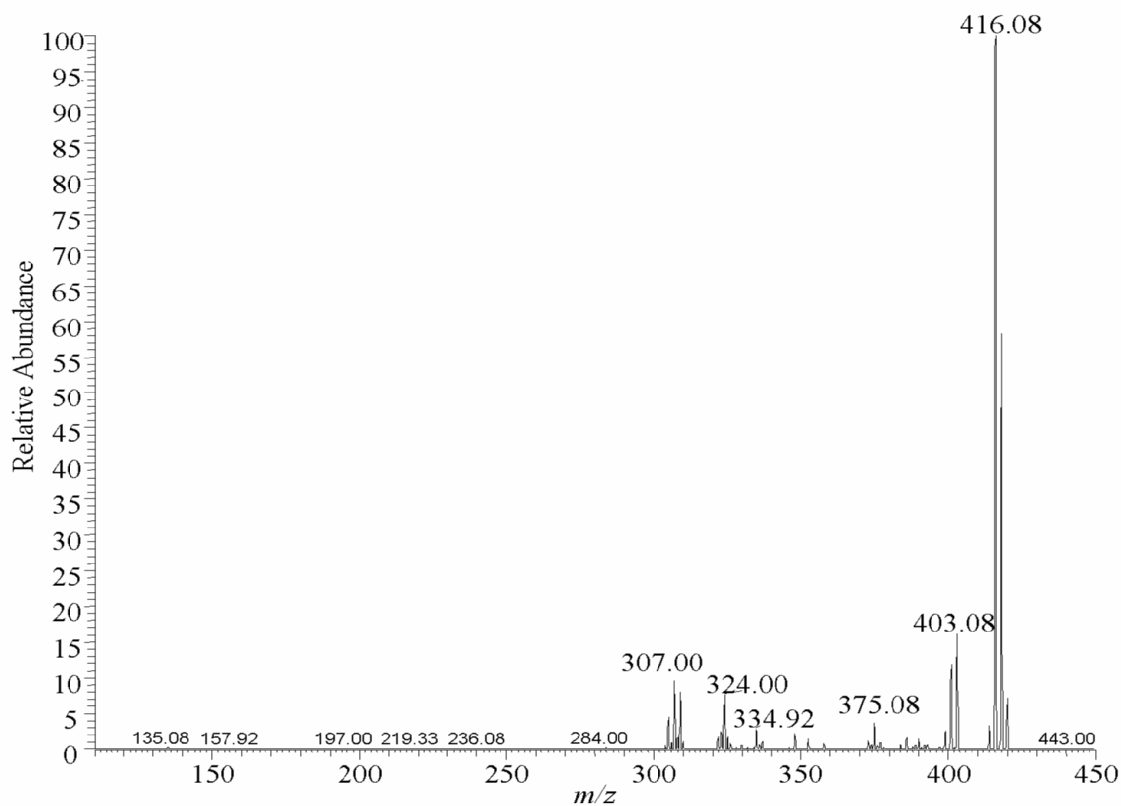


**Figure 9:42:** MS/MS spectrum of product ions obtained by CID of the  $^{196}\text{Pt}$ -C adduct at  $m/z$  420 to yield the free Pt drug at  $m/z$  307. Collision energy = 20 eV and isolation width =1 Da.

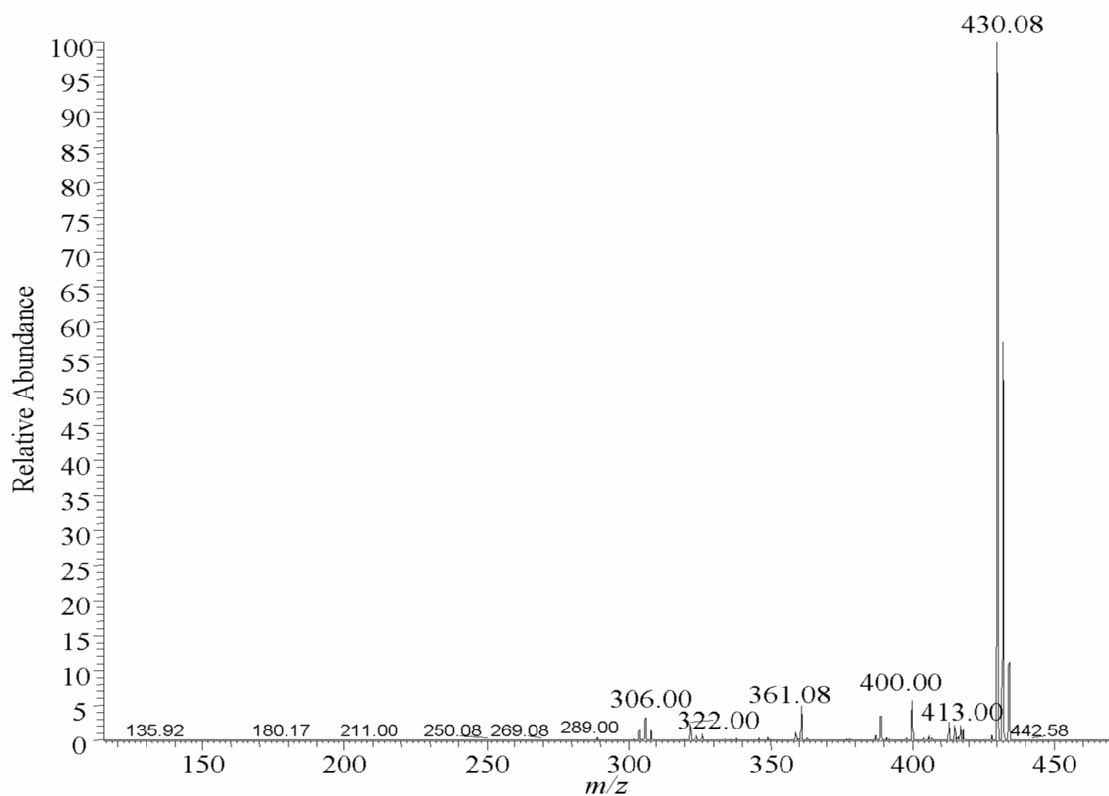


**Figure 9:43:** MS/MS spectrum of product ions obtained by CID of the  $^{195}\text{Pt-T}$  adduct at  $m/z$  434 to yield the free Pt drug at  $m/z$  306. Collision energy = 20 eV and isolation width =1 Da.

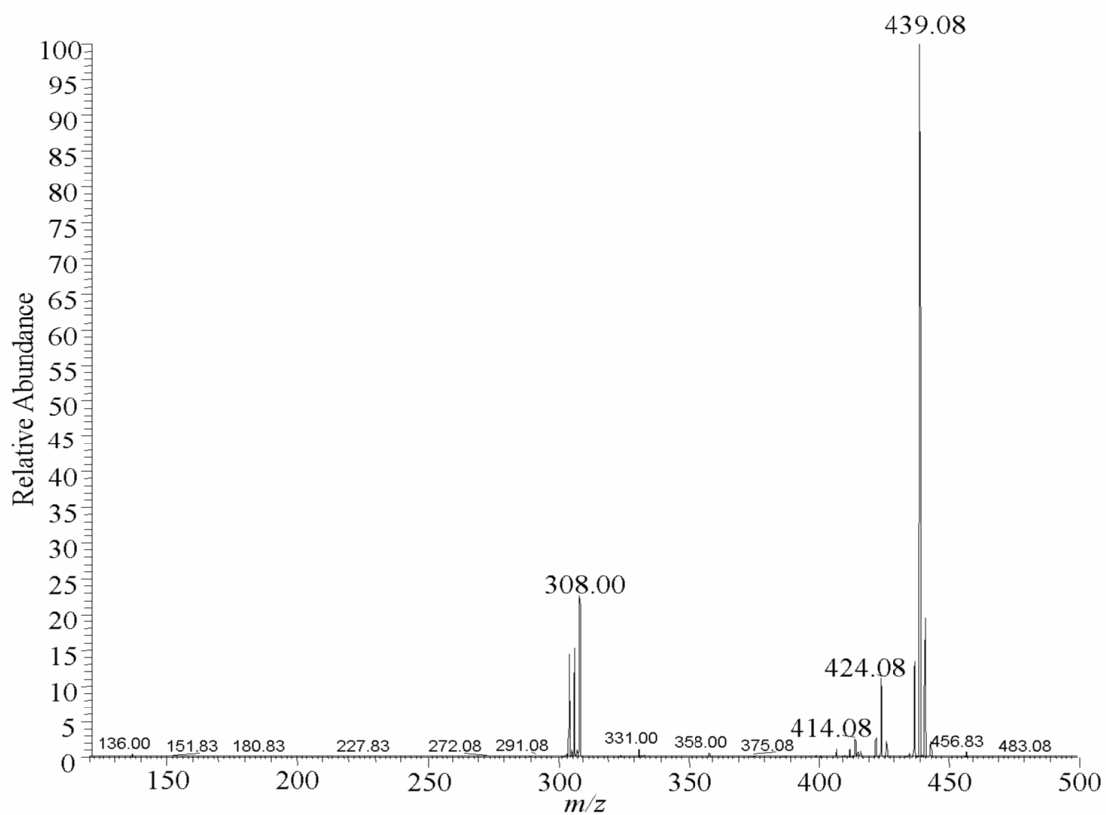


**Figure 9:44:** MS/MS spectrum of product ions obtained by CID of the  $^{195}\text{Pt-A}$  adduct at  $m/z$  443 to obtain the free Pt drug at  $m/z$  308 and free adenine base at  $m/z$  136. Collision energy =20 eV and isolation width =1 Da.

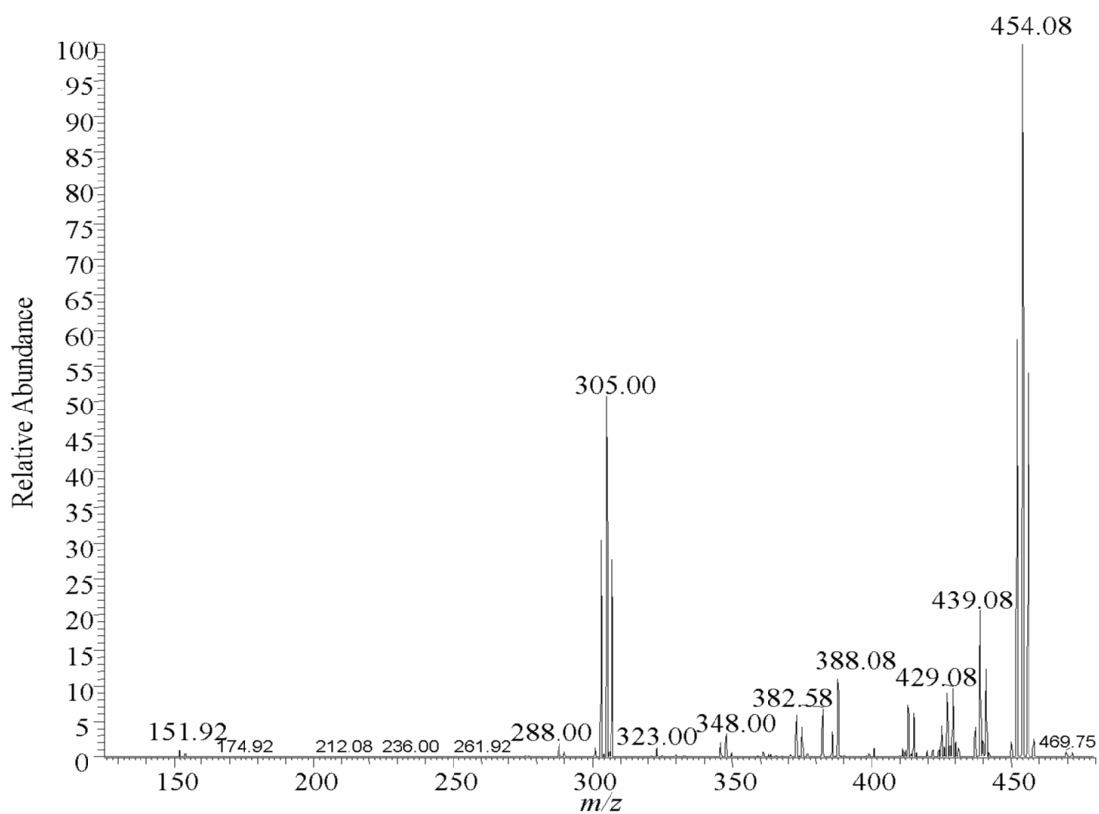


**Figure 9:45:** MS/MS spectrum of product ions obtained by CID of the  $^{194}\text{Pt-G}$  adduct at  $m/z$  458 to yield the free Pt drug at  $m/z$  305 and free guanine base at  $m/z$  152. Collision energy = 20 eV and isolation width = 1 Da.

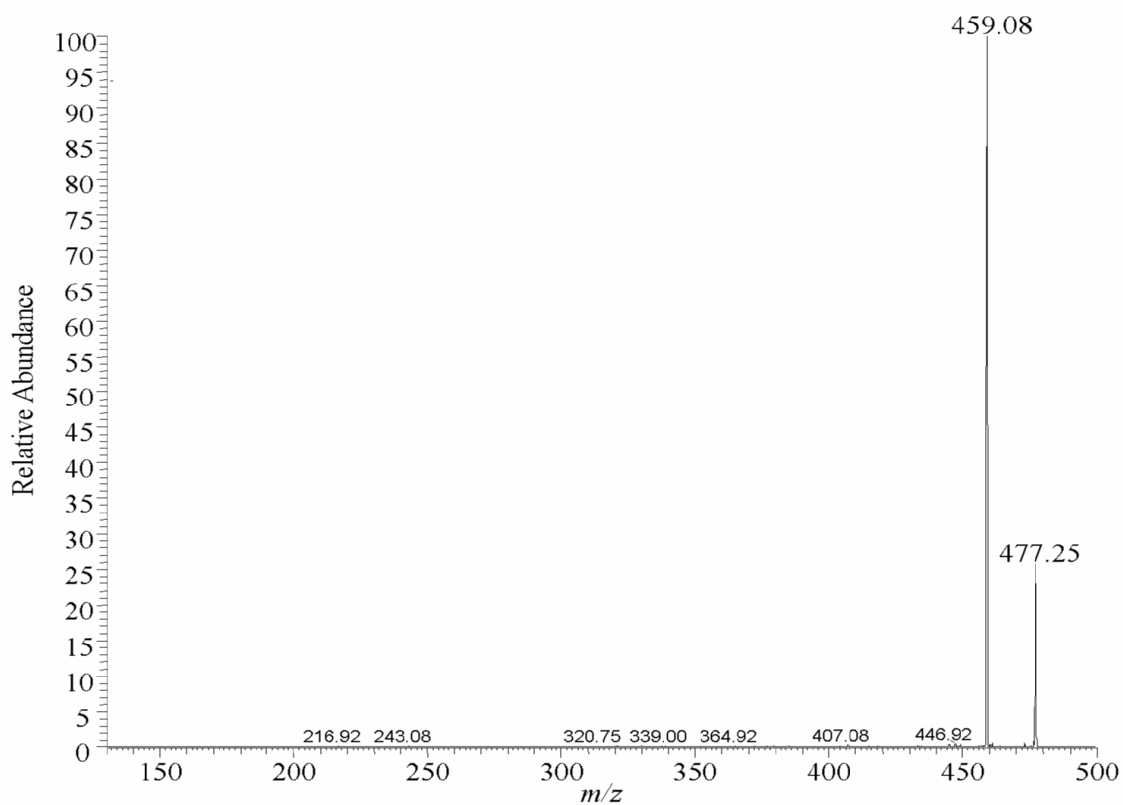


**Figure 9:46:** MS/MS spectrum of product ions obtained by CID of  $^{195}\text{Pt-G}(\text{H}_2\text{O})$  adduct at  $m/z$  477 to obtain the  $^{195}\text{Pt-G}$  adduct at  $m/z$  459. Collision energy = 20 eV and isolation width = 1 Da.



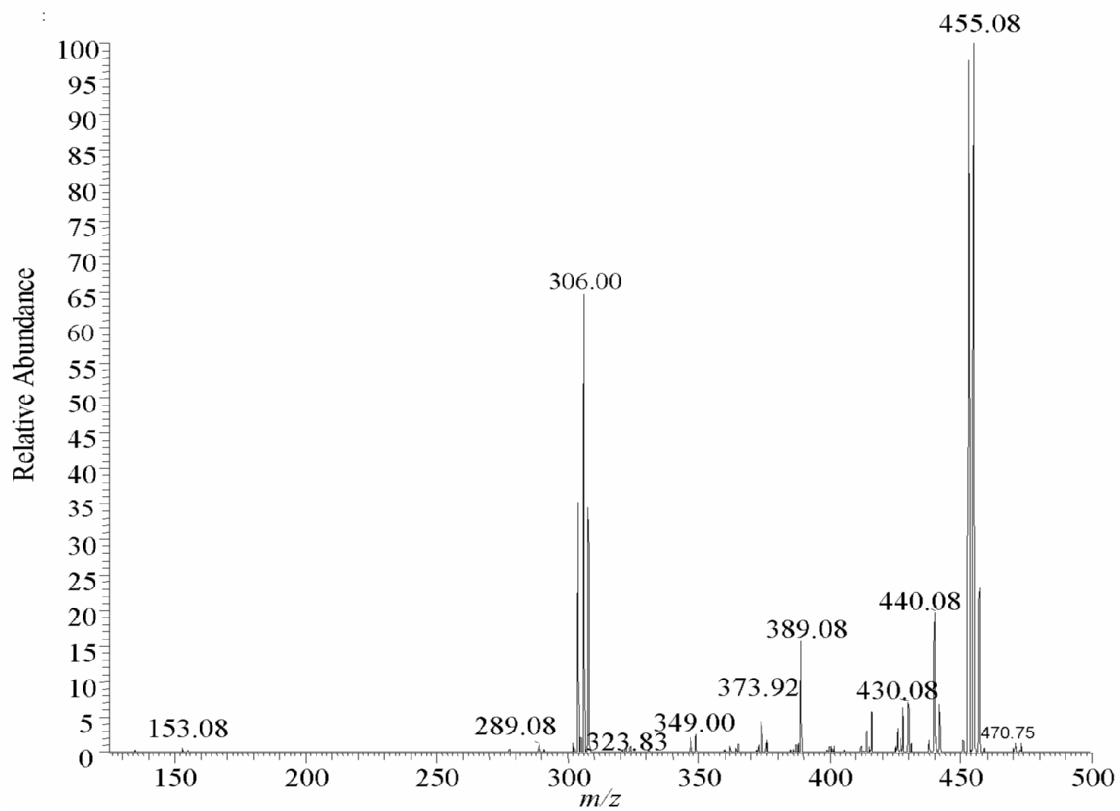


**Figure 9:47:** MS<sup>3</sup> spectrum of product ions formed by CID of the <sup>195</sup>Pt-G adduct at *m/z* 459 (collision energy = 20 eV), which was obtained by CID of the <sup>195</sup>Pt-G(H<sub>2</sub>O) adduct at *m/z* 477 (collision energy = 20 eV and isolation width = 1).

## 9.5 Appendix 2.5: Fragmentation of the Pt-AG adduct

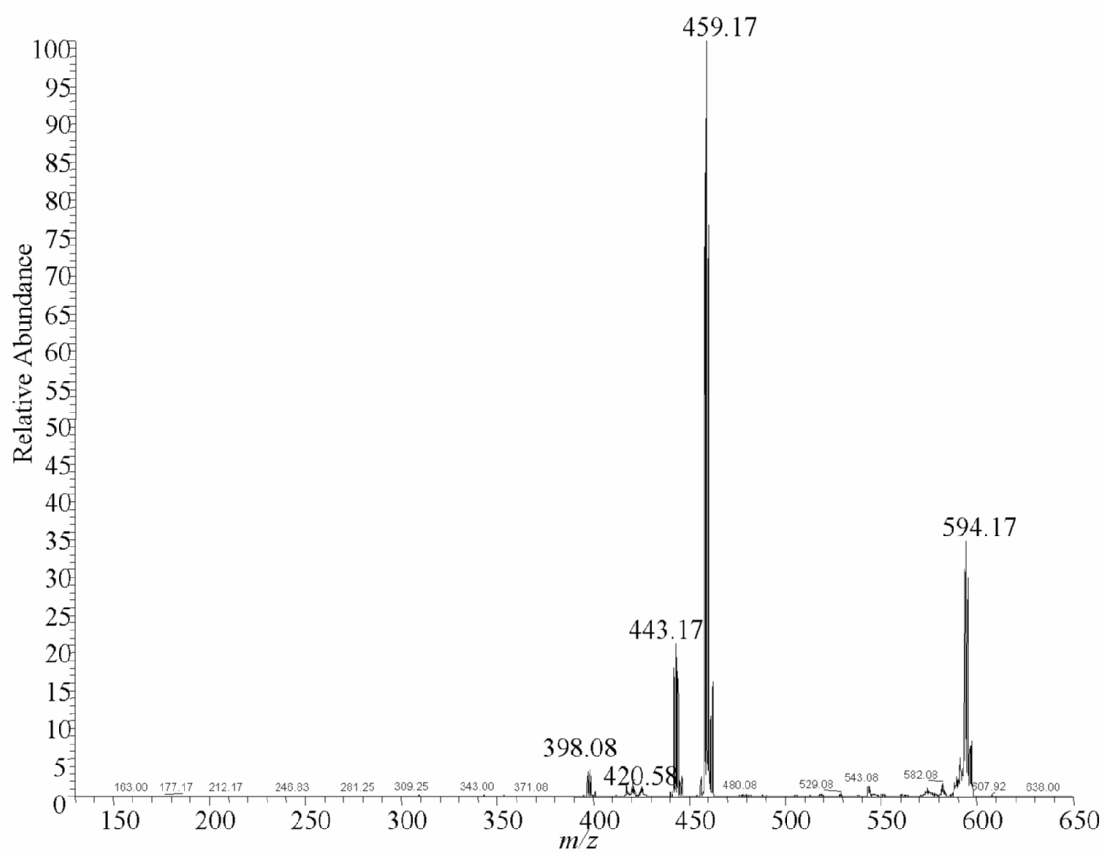


**Figure 9:48:** MS/MS spectrum of product ions obtained by CID of the Pt-AG adduct at  $m/z$  594 to yield the Pt-G and Pt-A adducts at  $m/z$  459 and 443 respectively. Collision energy = 20 eV and isolation width = 10 Da.

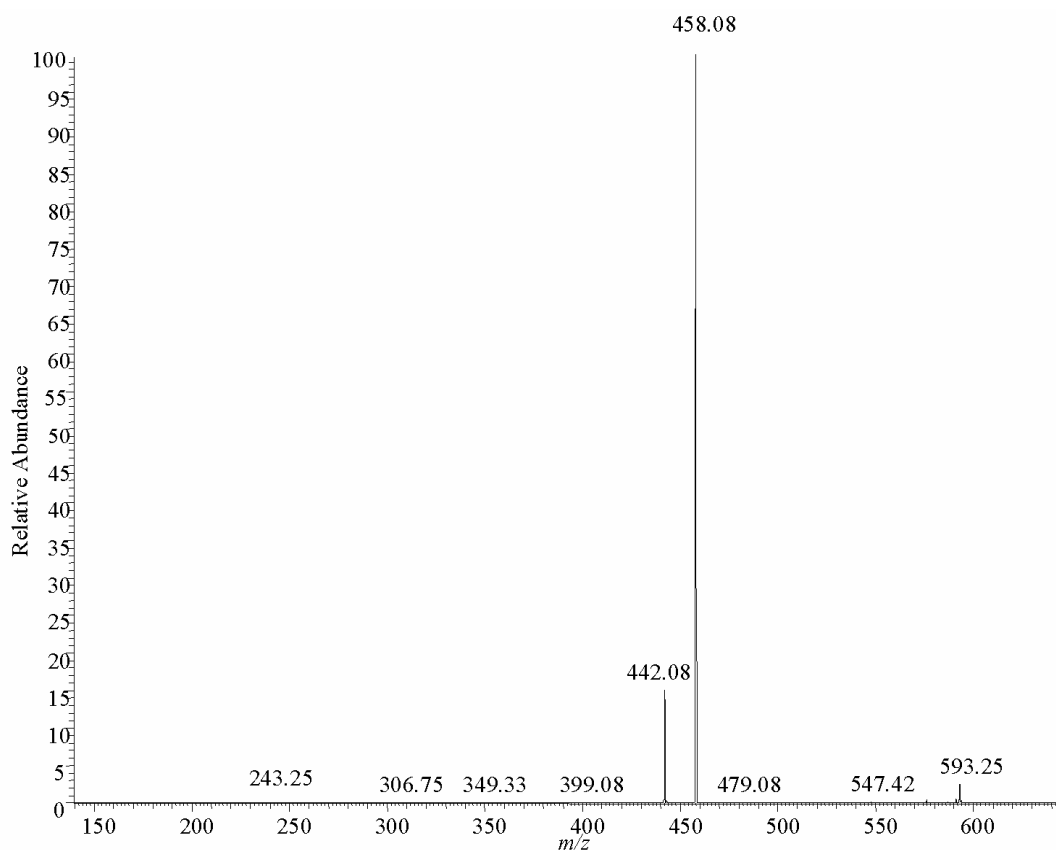


**Figure 9:49:** MS/MS spectrum of product ions obtained by CID of the  $^{194}\text{Pt}$ -AG adduct at  $m/z$  593 to yield the  $^{194}\text{Pt}$ -A adduct and  $^{194}\text{Pt}$ -G adduct at  $m/z$  442 and 458 respectively. Collision energy = 20 eV and isolation width = 1 Da.

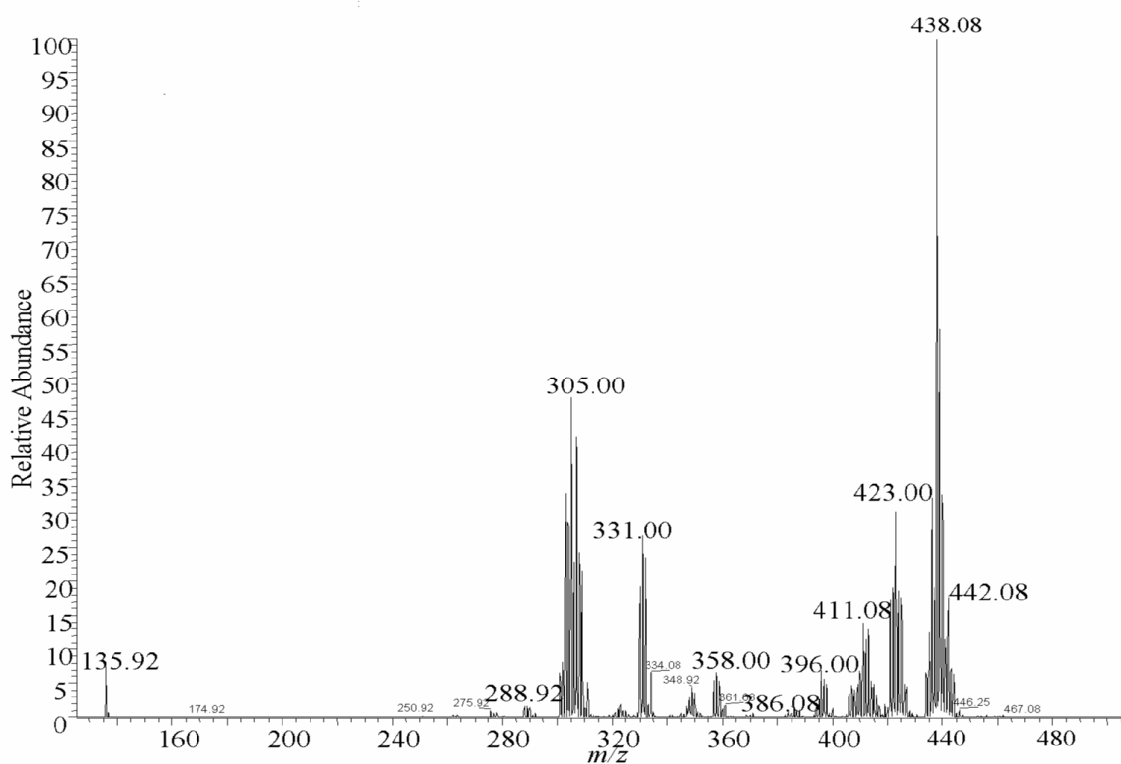


**Figure 9:50:** MS<sup>3</sup> spectrum of product ions obtained by CID of the Pt-A adduct at  $m/z$  443 (collision energy = 20 eV and isolation width = 10 Da), which were obtained by CID of Pt-AG adduct at  $m/z$  593 (collision energy = 20 eV and isolation width = 10 Da).

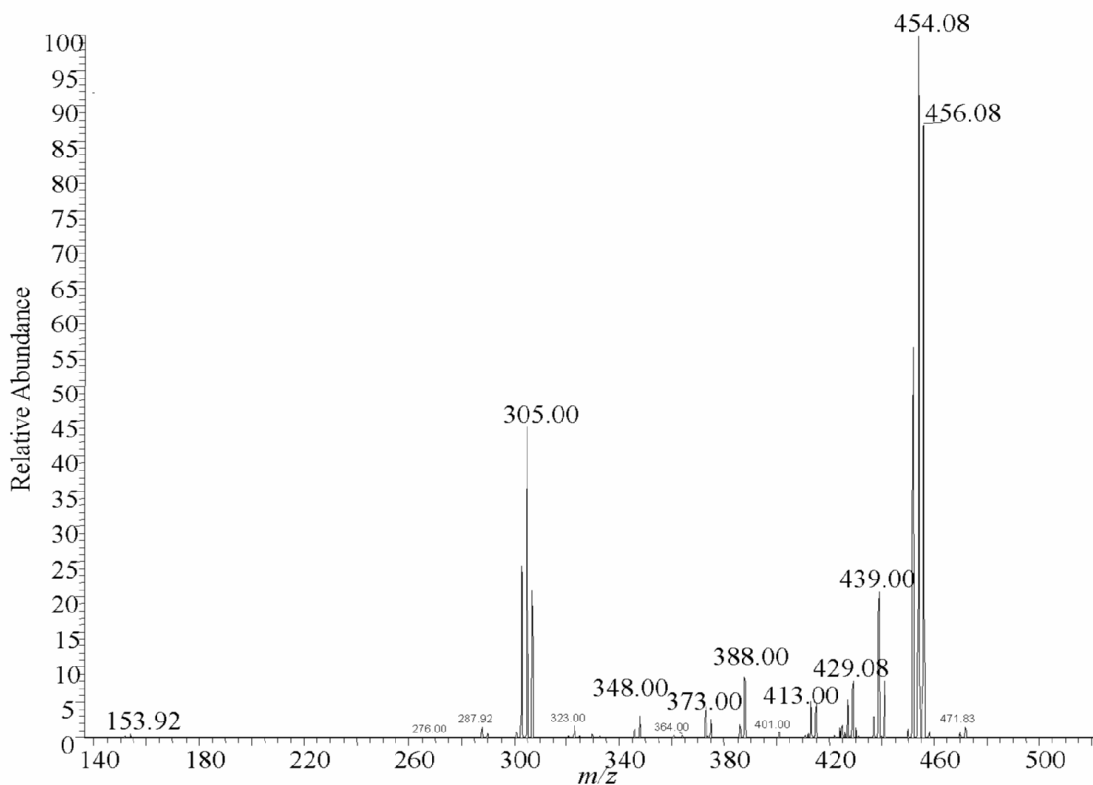


**Figure 9:51:** MS<sup>3</sup> spectrum of product ions obtained by CID of the Pt-G adduct at  $m/z$  458 (collision energy = 20 eV and isolation width = 10), which were obtained by CID of the Pt-AG adduct at  $m/z$  593 (collision energy = 20 eV and isolation width = 10 Da).

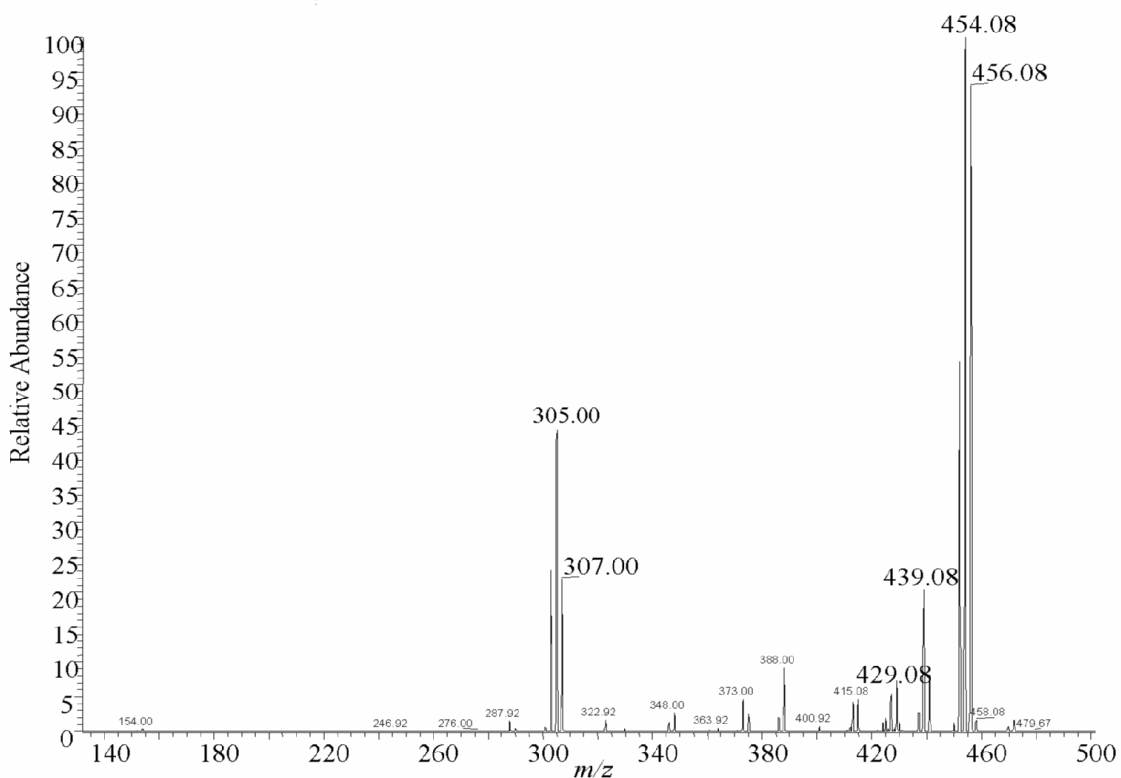


**Figure 9:52:** MS<sup>3</sup> spectrum of product ions obtained by CID of the <sup>194</sup>Pt-G adduct at  $m/z$  458 (collision energy = 20 eV and isolation width = 1 Da), which was obtained by CID of the <sup>194</sup>Pt-AG adduct at  $m/z$  593 (collision energy = 20 eV and isolation width = 1 Da).

## 10 Appendix 3: Continued Professional Development Record

Event	Organisation/Department	Date Attended	Duration
Statistics and Chemometrics Short Course	Professor Miller, Chemistry	October 2004	2 days
PhD. Induction	Professional Development	October 2004	½ day
Proteomics Seminar	Waters Corporation	November 2004	1 day
Raman Spectroscopy Course	Loughborough University, Physics Department	11 <sup>th</sup> -12 <sup>th</sup> Nov 2004	2 days
Preparing to Teach	Professional Development	19/11/04	½ day
Promoting Learning	Professional Development	25/11/04	½ day
Supervising Practical Activities	Professional Development	30/11/04	½ day
Laser Safety Training	John Tyler, Physics	8 <sup>th</sup> December	½ day
Leicester University, Cancer Biomarkers and Prevention Group	Dr. R. Le Pla, Leicester University	13-14/09/05	2 days
Waters Proteomics Seminar	Waters Corporation	19/10/05	1 day
Keeping your Research up-to Date	Professional Development	17/11/05	½ day
Conference Presentation Skills (Parts A and B)	Professional Development	24/01/06 & 7/02/06	1 day
Presentation at Leicester University on the application of ICP-MS to Pt drug research.	Leicester /Loughborough collaboration	8/02/06	½ day
Biological Applications of Elemental and Molecular Mass Spectrometry	RSC	16/03/06	1 day
Reading for Research	Professional Development	13/03/06	½ day
Personal Organisation and Time Management	Professional Development	22/05/06	½ day
Career Management	Professional Development	12/05/06	½ day
Getting the Most out of Supervision	Professional Development	13/06/06	½ day
Managing Projects for PG and RA	Professional Development	27/06/06	½ day
BNASS Conference, Glasgow Caledonian University. Presentation on the ICP-MS analysis of Au labelled nucleic acids.	RSC	10-12 <sup>th</sup> July 2006	3 days

Continued Professional Development continued:

Event	Organisation/Department	Date Attended	Duration
Cricket Secretary Role: Taking and distributing minutes at monthly committee meetings. Issuing correspondence to club members. Organising end of season presentation evening		Nov 2005- July 2007	15 days
Viva - What Happens?	Professional Development	5/10/06	½ day
Visit to Loughborough High School (career management)		02/10/06	1 day
Visit to Burleigh College (career management)		09/10/06	1 day
Intellectual Property	Professional Development	14/12/06	½ day
Successful Applications	Professional Development	31/01/07	½ day
Toarmina Plasma Winter conference Oral presentation given on the analysis of Au labelled nucleic acids by HPLC-ICP-MS		Feb 2007	6 days
Emerging Young Professionals Conference: Presentation given on the analysis of Au labelled nucleic acids by ICP-MS. Also attended team building exercises	RSC – Analytical Science Network	29-31/05/07	2 days
Presentation given to MSc. students on the biological applications of ICP-MS, followed by instrument demonstrations	Chemistry		½ day

## 11 Published Material

Two journal articles were produced from this thesis; the first article detailed the enhancement of nucleic acid signal by nano-particle labelling, whilst the second publication discussed the study of oxaliplatin-nucleobase interactions by linear ion trap ESI-MS. These two research areas were outlined in Chapter 2 and 4 respectively. The full journal citations are shown below and the full published versions are shown on the following pages.

S. L. Kerr and B. L. Sharp, Nano-particle labelling of nucleic acids for enhanced detection by inductively coupled plasma-mass spectrometry (ICP-MS), *Chem. Commun.*, 2007, 4537-4539.

S. L. Kerr, T. Shoeib and B. L. Sharp, A study of oxaliplatin-nucleobase interactions using ion trap, electrospray mass spectrometry, *Anal. Bioanal. Chem.*, 2008, DOI 10.1007/s00216-008-2128-3

### Publications in Preparation

S. L. Kerr, P. D. Winship, R. Le Pla, C. Harrington, H. J. Reid, G. D. D. Jones and B. L. Sharp, Determination of cisplatin and oxaliplatin adducts by ICP-MS.

P. D. Winship, S. L. Kerr and B. L. Sharp, Comparison of collision reaction cell and cold plasma methods of P detection by ICP-MS.